IAEA-TECDOC-1132

Control assembly materials for water reactors: Experience, performance and perspectives

Proceedings of a Technical Committee meeting held in Vienna, 12–15 October 1998

INTERNATIONAL ATOMIC ENERGY AGENCY IAEA

February 2000

The originating Section of this publication in the IAEA was:

Nuclear Fuel Cycle and Materials Section
International Atomic Energy Agency
Wagramer Strasse 5
P.O. Box 100
A-1400 Vienna, Austria

CONTROL ASSEMBLY MATERIALS FOR WATER REACTORS: EXPERIENCE, PERFORMANCE AND PERSPECTIVES
IAEA, VIENNA, 2000
IAEA-TECDOC-1132
ISSN 1011–4289

Printed by the IAEA in Austria
February 2000

FOREWORD

The safe, reliable and economic operation of water cooled nuclear power reactors depends to a large extent upon the reliable operation of control assemblies for the regulation and shutdown of the reactors. These consist of neutron absorbing materials clad in stainless steel or zirconium based alloys, guide tubes and guide cards, and other structural components. Current designs have worked extremely well in normal conditions, but less than ideal behaviour limits the lifetimes of control materials, imposing an economic penalty which acts as a strong incentive to produce improved materials and designs that are more reliable.

Neutron absorbing materials currently in use include the ceramic boron carbide, the high melting point metal hafnium and the low melting point complex alloy Ag-In-Cd. Other promising neutron absorbing materials, such as dysprosium titanate, are being evaluated in the Russian Federation. These control materials exhibit widely differing mechanical, physical and chemical properties, which must be understood in order to be able to predict the behaviour of control rod assemblies.

Identification of existing failure mechanisms, end of life criteria and the implications of the gradual introduction of extended burnup, mixed oxide (MOX) fuels and more complex fuel cycles constitutes the first step in a search for improved materials and designs.

In the early part of this decade, it was recognized by the International Working Group on Fuel Performance and Technology (IWGFPT) that international conferences, symposia and published reviews on the materials science aspects of control assemblies were few and far between. Consequently, the IWGFPT recommended that the IAEA should rectify this situation with a series of Technical Committee meetings (TCMs) devoted entirely to the materials aspects of reactor control assemblies. The first was held in 1993 and in the intervening five years considerable progress has been made. In bringing together experts in the materials science and materials engineering of control assembly materials, the 1993 meeting and the current one are helping to fill a gap in the information exchange opportunities in this important branch of nuclear research and development.

This second TCM, entitled Control Assembly Materials for Water Reactors: Experience, Performance and Perspectives, was held in Vienna from 12 to 15 October 1998. Thirty-one participants from fourteen different countries attended the meeting and nineteen papers were presented and are reproduced in these proceedings together with a summary of the meeting.

The IAEA wishes to thank all of the participants for their contributions to this publication, which summarizes experience to date with control materials and ongoing research in the field in the participating countries. I.G. Ritchie and M.J. Crijns, both of the Division of Nuclear Fuel Cycle and Waste Technology, were the IAEA officers responsible for the organization of the meeting and the compilation of this publication, respectively.

EDITORIAL NOTE

This publication has been prepared from the original material as submitted by the authors. The views expressed do not necessarily reflect those of the IAEA, the governments of the nominating Member States or the nominating organizations.

The use of particular designations of countries or territories does not imply any judgement by the publisher, the IAEA, as to the legal status of such countries or territories, of their authorities and institutions or of the delimitation of their boundaries.

The mention of names of specific companies or products (whether or not indicated as registered) does not imply any intention to infringe proprietary rights, nor should it be construed as an endorsement or recommendation on the part of the IAEA.

CONTENTS

Summary 1

LWR control assembly designs: A historical perspective 7
M.W. Kennard, J.E. Harbottle

PWR control rod degradation as observed in post-irradiation examinations in Studsvik 33
T. Jonsson, T. Andersson, L. Björnkvist

Status of control assembly materials in Indian water reactors 41
V.G. Date, P.G. Kulkarni

Calculation modelling of the RCCA movement through bowed FA guide tubes 57
D.V. Razoumovsky, Yu.I. Lihkachev, V.M. Troyanov

Material operating behaviour of ABB BWR control rods 65
B. Rebensdorff, G. Bart

Experience of CR and RCCA operation in Ukrainian WWER-1000:
Aspects of reliability, safety and economic efficiency 77
A. Afanasyev

Dysprosium and hafnium base absorbers for advanced WWER control rods 91
V.D. Risovaniy, A.V. Zaharov, E.P. Klochkov, E.E. Varlashova, D.N. Suslov, A.B. Ponomarenko, A.V. Scheglov

Behaviour of different boron rich solids as promising absorbers for PWR 103
D. Simeone, X. Deschanels, P. Cheminant, P. Herter

Reinforcement against crack propagation of PWR absorbers by development
of boron–carbon–hafnium composites 107
B. Provot, P. Herter

NSC KIPT's experience in production of absorber materials, composites and
products for control mechanisms of various nuclear reactor types 113
N.P. Odeychuk, V.F. Zelensky, V.A. Gurin, Yu.F. Konotop

Damage analysis of ceramic boron absorber materials in boiling water reactors
and initial model for an optimum control rod management 121
W. Schulz

Fabrication and metallurgical properties of hafnium alloys for control rods 153
J.L. Béchade, P. Parmentier

Irradiation behaviour of boron carbide in WWER-1000 167
A.V. Zakharov, V.D. Risovaniy, S.R. Fridmann, V.B. Ponomarenko, A.O. Poslavskiy

WWER-1000 control rod materials: Experience and development 175
V. Ponomarenko, A. Poslavskiy, A. Scheglov, A. Zaljetniy, V. Risovaniy

FRAMATOME control rod absorber materials: Experience and development 191
M. Monchanin, X. Thibault

Measure of 11-boron, 10-boron and 7-lithium concentrations in control rods
using the nuclear microprobe technique 203
D. Simeone, X. Deschanels, P. Herter

The role of cladding material for performance of LWR control assemblies 215
P. Dewes, A. Roppelt

BWR control blade replacement strategies 229
M.W. Kennard ,J.E. Harbottle

High temperature study of the control rod behaviour under accident conditions 245
V. Troyanov, A. Pomeschikov, V. Sougonjaev, V. Ponomarenko, A. Scheglov

List of participants 259

SUMMARY

1. INTRODUCTION

For the purposes of this meeting, "control assembly materials" included all of the solid materials used in the construction of control assemblies for the regulation or shutdown of water cooled, power reactors, i.e. neutron absorber(s), cladding, guide tubes and guide cards, and other structural components of the assembly. Liquid neutron absorbers and poisons were not considered and, with the exception of one paper comparing the behaviour of boron carbide (B_4C) and dysprosium titanate ($Dy_2O_3 \cdot TiO_2$) in severe accident conditions, the deliberations dealt with the behaviour of control materials in normal operating and shutdown conditions.

International conferences, symposia and published reviews on the materials science aspects of control assemblies have been relatively few and far between. Although the IAEA has held many meetings on the safety aspects of control rods and control systems, in both normal operating conditions and severe accident conditions, to our knowledge this is only the second meeting to focus on the materials aspects of reactor control assembly materials. The first Technical Committee meeting (TCM) entirely on this topic was held in 1993 and in the intervening five years considerable progress has been made. In bringing together experts in the materials science and materials engineering of control assembly materials, this meeting, its predecessor in 1993 and their published proceedings are helping to fill an important gap in the information exchange opportunities in this branch of nuclear research and development.

The meeting was divided into three sessions: Session 1, Past Experience and Current Performance of Control Assembly Materials", chaired by P. Dewes of Siemens AG in Germany; Session 2, Absorber Materials Currently Used and Under Development, chaired by V.G. Date of Bhabha Atomic Research Centre in India; and Session 3, Cladding Materials, Life-Limiting Criteria and Future Needs, chaired by G. Bart of the Paul Scherrer Institute in Switzerland.

The nineteen papers presented covered the control assembly materials currently used in PWRs, BWRs, WWERs and RBMKs, as well as improved materials under investigation for their replacement or for advanced water reactor designs. The technical discussions focused on the performance of absorber materials, cladding, guide-tubes and guide-cards in reactor, keeping in mind issues affecting and limiting the working lifetimes of control assemblies, and hence their economic viability.

Past and current designs of control assemblies together with the stringent criteria followed by the utilities for their safe operation, inspection and replacement, has led to an outstanding safety record. However, mechanical mechanisms (fretting and wear), corrosion mechanisms (oxidation and hydriding), radiation damage mechanisms (enhanced creep and growth), and mechanisms such as irradiation assisted stress corrosion cracking (IASCC), involving synergism between two or more fundamental mechanisms, all detract from the ideal behaviour of control assembly materials. More importantly, this less than ideal behaviour limits the lifetimes of control materials, imposing an economic penalty which acts as a strong incentive to produce improved materials and designs that are more reliable and approach closer to the ideal lifetime of a control assembly, which should depend solely on the neutronics of the chosen absorber. At the time of the last TCM, improved understanding of the damage mechanisms mentioned above was leading to improved behaviour of control assemblies through design changes, wear-resistant coatings and surface treatments, and better control over microstructures and compositions of the materials at the fabrication stage. One of the major goals of this TCM was to see if this progress has been maintained in the face of increasing demands on the combined fuel/control assemblies, such as higher burnup, MOX fuel burning and load following.

Experience with control materials in water reactors is spread over many different types of reactors in many different countries. Similarly, research, development and design of the different

types of control assemblies is carried out by several different vendors. Presentations at the meeting dealt with almost all of the currently used control materials in most of the water cooled, power reactor types operated at present, with the exception of CANDU. In addition, some of the presentations and discussions were devoted to alternative, advanced absorber materials and developments aimed at increasing the lifetimes of control assemblies.

Following the formal presentations of the papers and some preliminary discussions, the meeting split into three groups to facilitate discussions and prepare a summary, recommendations for further work in the field and conclusions of the meeting. The first group considered PWRs, the second group considered BWRs and the third group considered Soviet designed reactors (WWER-1000 and RBMK). These discussions, which focused on progress since the last TCM in 1993, the current issues in the field of control assembly materials and the recommendations of the assembled experts for further R&D, are summarized in the following sections.

2. PWRs

This group was led by P. Herter of CEA-Saclay, France. As is common practice among PWR operators, the control assemblies are referred to as RCCAs for simplicity in the following. This acronym stands for rod cluster control assembly. In addition, the neutron absorber, Ag-In-Cd alloy, is simply referred to as AIC.

2.1. Progress from 1993 to 1998

The main problems seen in 1993 were:

(1) Cladding wear and the rejection criteria linked with it;
(2) Swelling of AIC; and,
(3) Potential problems at the time, such as swelling of B_4C.

At the present time, the progress in these areas can be summarized as follows:

(1) Good wear resistant coatings on the cladding materials are now in use. However, the possible transfer of the wear to the guide cards or other components (Zircaloy guide tubes) in contact with the coated cladding may become a problem and has to be kept in mind.
(2) The mitigation of AIC swelling has been achieved by modification to the designs of RCCAs to include a larger gap between neutron absorber with gas filling, and improvement of the microstructure of the AIC itself (mainly larger grain size with improved creep resistance). These improvements stem from a better knowledge of the behaviour of AIC now than was available in 1993.
(3) A better understanding of the behaviour of B_4C shows that the problem of swelling, even though it occurs, is not as great as anticipated in 1993. Experience shows that B_4C has to be washed out to be removed from the cladding and there is an irradiation threshold for the B_4C to be decomposed by the coolant.

2.2. Current issues

- There is a need to investigate the disposal of currently stored "spent" RCCAs and to plan for the disposal of those that will arise in the future.
- There is, as mentioned above, a potential for guide cards and guide tubes to be worn out through contact with wear resistant coatings on the absorber cladding.
- There is a need to analyse the existing criteria for the life of RCCAs and sub-assemblies.
- There is a need to develop more efficient RCCAs for cores with higher MOX contents than those currently used.

2.3. Evolution in RCCA management

- Since the wear problems have been for the most part solved for the cladding, there is no further need for special constraints linked to cladding wear. This provides more freedom in the management of RCCAs.
- There is no need to change the current fluence limitations on AIC and B_4C.
- For RCCAs under development, however, it is hoped that the lifetime fluence can be extended.

2.4. Recommendations

Absorber materials:

- For B_4C in the upper part of control rods a new fluence criterion must be defined because the B_4C will experience increased irradiation in the future.
- Hafnium will have to be protected against wear and hydriding, which are linked because the Hf will hydride more rapidly if the protective oxide is removed by wear.
- Dysprosium titanate, hafnium boride (HfB_2) and other new absorber materials must undergo more extensive evaluation for use in PWRs.

Other materials:

Wear has been considered only from the point of view of the cladding material. The wear of the guide cards and guide tubes must be studied also.

Development in inspection surveillance and end-of-life criteria:

- Clad swelling measurements have to be performed with increased precision.
- Clad swelling has to be inspected on a much larger scale.

3. BWRs

This group was led by B. Rebensdorff of ABB-Atom, Sweden.

3.1. Progress 1993–1998

(1) Understanding of the impact of fast neutron irradiation on stainless steel (SS) has increased significantly. However, there are still unanswered mechanistic questions associated with irradiation assisted stress corrosion cracking (IASCC).

(2) From measurements on irradiated samples, our knowledge about the swelling and creep behaviour of control rods has increased significantly.

(3) Current experience with "all-Hf" control rods is quite encouraging.

(4) Hf tips for shut down rods are behaving as predicted.

(5) The modelling of burnup behaviour (with respect to the control rod's working life) has been developed.

3.2. Current issues

(1) There is a need to compile recent B_4C irradiation data, including its interaction with stainless steel, and to compare it with current model predictions in an attempt to validate or improve the models.

(2) There is a need to study the benefit of Hf edges (strips and end plugs) on control rod wings.

(3) There is a need to improve our knowledge about the interaction of Hf and B_4C, where both absorbers are in direct contact, within a control assembly structure.

3.3. Recommendations

(1) For control cell positions the experts recommend the investigation of control rods with less reactivity worth.

(2) Increase the number of control materials currently used in BWRs, choosing new materials, by comparing the basic physical and chemical parameters (reactivity worth, materials density, etc.) taking cost into account.

(3) Improve reactor water surveillance with respect to ^3H (possibly also boron and lithium) to improve our knowledge about control rod cracking.

(4) Improve the technical instrumentation and management acceptance of dedicated NDT of control rods in spent fuel pools (to optimize control rod management strategies and to reduce waste arisings).

(5) The experts noted that the meeting would have even been more fruitful if all the major players, control rod vendors and utilities (especially from the United States of America, Canada and the Far East), had participated. Therefore, they strongly suggest that future meetings of this type should make every effort to involve a larger selection of the major players.

4. RUSSIAN DESIGNS

This group was led by V. Troyanov, Institute of Physics and Power Engineering, Obninsk, Russian Federation.

4.1. Progress 1993–1998

Since the TCM in 1993 a considerable amount of work on various absorber materials used in WWER reactor designs has been carried out. For example, the ultimate lifetime characteristics for WWER B_4C control rods have been studied, and the lifetime is limited now to 50% ^{10}B burnup. This is 3 years operating as a control rod and 6 years as a shut down system rod.

A number of in-pile tests and pre-irradiation examinations of dysprosium titanate have been carried out. $Dy_2O_3 \cdot TiO_2$ is now ready for industrial application. The design lifetime of the $B_4C/Dy_2O_3 \cdot TiO_2$ control rods is 10 to 15 years for WWERs. The long lifetime of the dysprosium absorber is confirmed by 17 years of operation in the MIR research reactor in Dimitrovgrad.

RCCAs with hybrid hafnium/B_4C absorber have been designed, manufactured and loaded in a WWER-1000 in 1997 (Rovno NPP, Ukraine).

The cladding alloy (a form of stainless steel) with the Russian designation XHM has been developed for control rod cladding application. There is experience of 17 years of successful operation with this steel irradiated in water cooled reactors in the former USSR to high fluences.

4.2. Current issues

Control rod, high-temperature performance studies have begun for the design basis accident (DBA) and severe accident analysis. It is already clear that the high temperature behaviour of $Dy_2O_3 \cdot TiO_2$ is much better than that of B_4C.

Calculation models and computer codes for core structure mechanical analysis are being developed. Fuel assembly bowing is calculated by these codes during irradiation. Computer code DORA for analysis of RCCA movement through bent fuel assemblies has been developed and continues to be improved. RCCA drop-time excess, and possible incomplete insertion of an RCCA, may be calculated for the any RCCA in the core, for any period of operating time.

Other neutron absorber improvements are under investigation including:

- Hafnium;
- Dysprosium (hafnium)/B_4C hybrids; and,
- Dysprosium hafniate.

Out-of-pile and in-pile examination techniques are being improved with the objectives of facilitating absorber material licensing.

In the multi-sectional control rods used in RBMK reactors, B_4C is the absorber and aluminium is the cladding material. Control rods based on dysprosium for RBMKs are under development, while the basic design is being improved.

4.3. Recommendations

This group recommends that a common approach should be taken to the development of control assembly materials regardless of the reactor type. The guiding principle should be the goal of extending the lifetime of control assemblies up to reactor lifetime, while satisfying the requirements of safety in the DBA and performing well under severe accident conditions. These developments should be based on a careful comparison of the following characteristics of neutron absorbers:

- initial neutron efficiency and its evolution during operation;
- chemical and structural stability;
- nuclear density;
- specific weight;
- irradiation resistance (low swelling and growth, integrity, stability of physical and mechanical properties);
- chemical compatibility with structural materials and the coolant;
- mechanical compatibility with the core structure, including ability to move within core structures without any problems;
- thermal-physics characteristics;
- structural integrity under accident conditions (including LOCA);
- radioactivation of absorbers;
- the possibility of re-fabrication or for other useful applications (for example as gamma-sources) or relative ease of disposal.

The group strongly recommended increasing the scope of international co-operation in this field, especially collaboration in the fabrication and licensing of new or improved neutron absorbers.

5. OVERALL CONCLUSIONS

- The participants concluded that the opportunities for information exchange in the field of control materials are far too limited, and that the behaviour of control assembly materials in both normal and accident conditions should be considered.
- Vendors of CCRs are encouraged to pursue more vigorously the development of absorber materials less prone to swelling.

- The participants underlined the need to investigate the disposal of currently stored "spent" RCCAs and to plan for the disposal of those that will arise in the future. Moreover, it was agreed that ease of storage and disposal should be taken into account during the development of new materials.

- Although the current designs of control assemblies have an outstanding safety record, their reliability and economic viability can still be enhanced by improvements in design and materials behaviour that allow increased lifetimes in the core.

- Wear-resistant coatings and surface treatments of RCCAs in PWRs are performing very well, but the wear problem may just have been moved to the guide cards and guide tubes.

- Unclad hafnium has excellent properties provided that it resides in the coolant flow where its oxide coating protects it from hydrogen pick-up.

- More efficient absorber materials based on enriched boron and hafnium will probably have to be developed for advanced reactor types, for example, reactors designed to burn MOX fuels.

- Dysprosium titanate has continued to be developed for use in NPPs and shows great promise. According to the developers, it is ready for industrial application. In addition the special form of stainless steel developed for absorber cladding in The Russian Federation continues to perform well, even at high fluences.

LWR CONTROL ASSEMBLY DESIGNS: A HISTORICAL PERSPECTIVE

M.W. KENNARD
Stoller Nuclear Fuel,
NAC International,
Pleasantville, New York,
United States of America

J.E. HARBOTTLE
Stoller Nuclear Fuel,
NAC International,
Thornbury, United Kingdom

Abstract

Control rod designs and materials have evolved in response to performance problems in both PWRs and BWRs. Irradiation-assisted stress corrosion cracking (IASCC) due to absorber swelling has primarily affected BWR control rods with B_4C absorbers, but has also occurred in PWRs with Ag-In-Cd absorbers. The primary problems for some designs of PWR control rods have been wear of the rodlets against upper internal components and swelling with tip wear and cracking. Competition amongst vendors for supplying control rod reloads has also resulted in design improvements. This paper provides an historical review of PWR and BWR control rod designs, their problems and remedies.

1. PRESSURIZED WATER REACTORS (PWRs)

1.1. Introduction

Vendors use different names to refer to their neutron absorbing components - Rod Cluster Control Assembly (RCCA) by Westinghouse (W), Fragema (FGA) and Siemens/KWU; Control Rod Assembly (CRA) by Framatome Cogema Fuels (formerly Babcock & Wilcox Fuel Company, BWFC) and Control Element Assembly (CEA) by Combustion Engineering (ABB-CE). For simplicity in this part of the review, one term only has been adopted for use when referring to all vendors: Control Element Assembly (CEA).

1.2. Summary of designs

1.2.1. Introduction

The various vendors' CEA designs are reviewed in this section. Each vendor has one general design; however, different models exist to match the various rod arrays and fuel designs. The reloading of CEAs by one vendor in another's nuclear steam supply system (NSSS) has also produced new designs.

1.2.2. Mechanical design

1.2.2.1. ABB-COMBUSTION ENGINEERING

The basic CEA design offered for both 14x14 and 16x16 standard lattice CE-NSSS plants are similar with respect to the large diameter absorber rodlets or 'fingers'. In the CE fuel design, each guide tube displaces four cell locations in the fuel lattice as opposed to a single cell as in the other vendors' fuel designs. Typically, the CEAs have four or five fingers which are attached by a threaded joint to a central hub or spider as illustrated in Figure 1a. A pin in the connection prevents rotation of the finger. The 16x16 System 80 plants (Palo Verde and Yonggwang) have a 12 finger CEA which is illustrated in Figure 1b. The fingers are attached to the spider by a bayonet-type fitting.

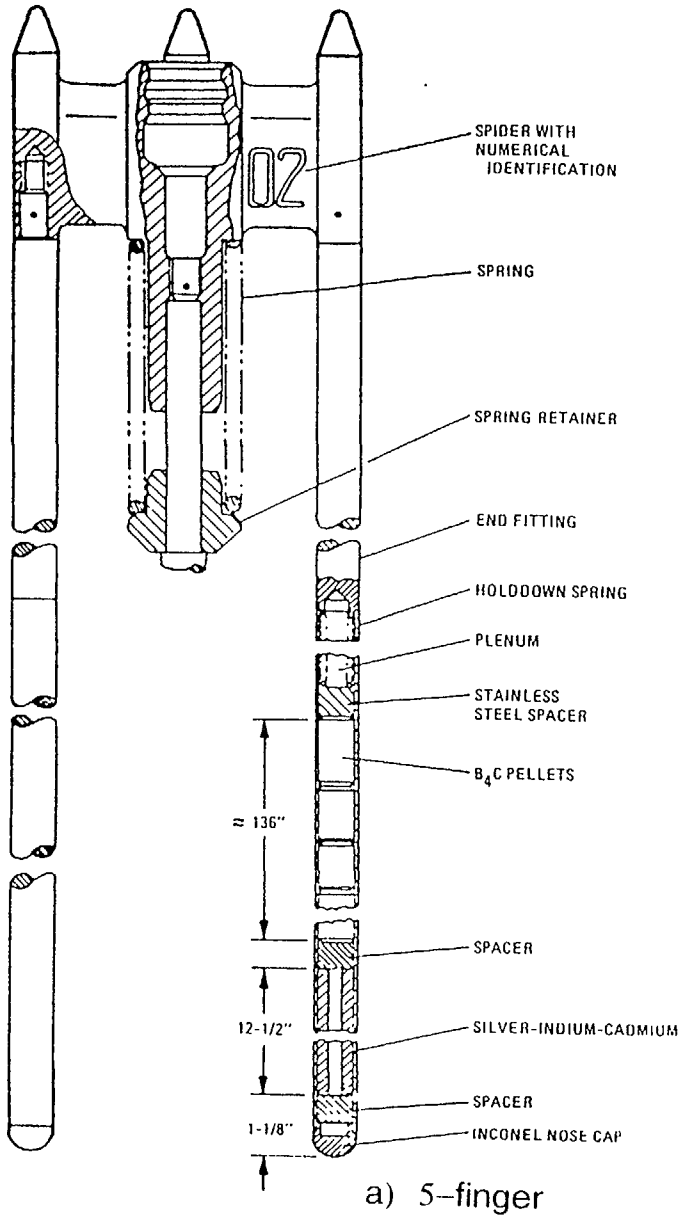

a) 5–finger

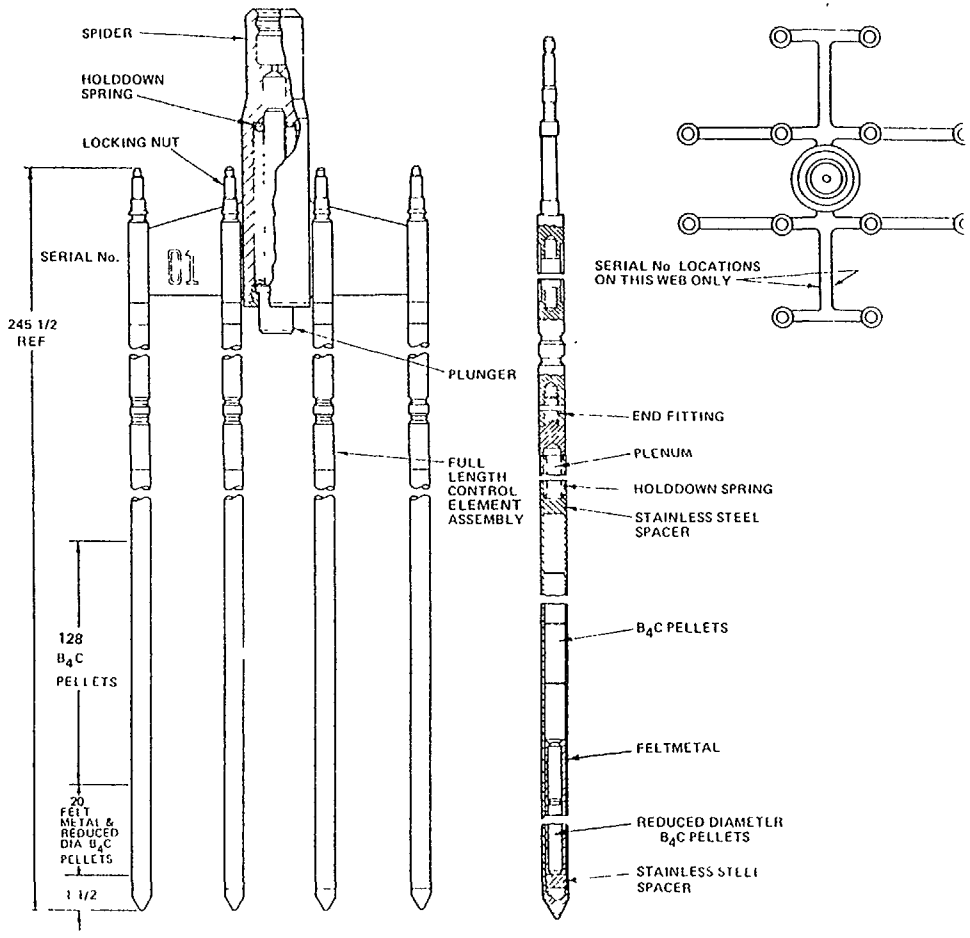

b) 12–finger

FIG. 1. Full length CEAs from ABB-CE for a) Standard 16x16 reactors and b) System 80 16x16 reactors (Reference: ABB-CE)

The cladding and upper and lower end-fittings for all fingers are made from Inconel 625. With some exceptions, both B_4C and Ag-In-Cd absorbers are used. In the original designs for 14x14 plants, the center finger was all B_4C and the outer fingers had Ag-In-Cd in the tips with the remainder B_4C. In all replacement CEAs for 14x14 plants and original CEAs for 16x16 plants, all fingers use B_4C with Ag-In-Cd tips. One exception is an ANO-2 CEA design in which the tip of the center finger contains Inconel 625 in place of the Ag-In-Cd absorber. In another exception, the fingers of the System 80 CEAs contain all B_4C. The tip has reduced diameter pellets surrounded by a low density (~20% TD) 347 SS liner (Feltmetal). The purpose of the Feltmetal liner is to accommodate swelling of the absorber.

1.2.2.2. FRAMATOME COGEMA FUEL (BWFC)

BWFC manufactured CEAs for its own NSSS plants as well as for Westinghouse NSSS plants. With respect to the BWFC NSSS plants, the 15x15 plants utilize sixteen 'fingers' or rods fastened to a central cast spider assembly. The rods are attached to the spider using a threaded nut which provides a stiff connecting joint. The standard full length control rods in BWFC plants are 304SS clad rods with type 304 or 308SS end plugs. The absorber material in the rods is Ag-In-Cd alloy. The designs for 15x15 plants are illustrated in Figure 2.

Full length control rods are offered with Inconel 625 cladding to reduce wear and an increased absorber/cladding gap to reduce rod swelling. This design is designated as 'Plant Life' control rods. More recently, two further design modifications have been offered:

- Hybrid absorbers consisting of a 36-40 inch (914-1020mm) region of Ag-In-Cd in the high flux region of the rod and B_4C pellets to reduce gas release;
- Cladding hardened with wear-resistant coatings:
  - 304SS with Armoloy chrome plating;
  - Inconel 625 cladding coated with chromium carbide Cr_3C_2;
  - 316SS hardened with ion-nitriding.

BWFC offers 'black' and 'grey' axial power stepping rods (APSRs) with reduced absorber lengths. The black rod contains a 36 inch (914 mm) section of Ag-In-Cd whereas the 'gray' rod contains a 63 inch (1600 mm) section of Inconel 600.

The CEAs offered by BWFC to Westinghouse NSSS plants contain all of the design permutations discussed above. The principal differences are that the control rod diameter, length and location in the fuel assembly are altered to be compatible with Westinghouse 15x15 or 17x17 fuel assemblies and Control Rod Drive Mechanisms (CRDMs).

1.2.2.3. WESTINGHOUSE

Westinghouse manufactures control rod assemblies for their 17x17, 15x15 and 14x14 NSSS plants. All designs are based on a central cast spider to which individual sleeves are brazed. The control rods are attached to the sleeves. This connection of rods to the spider is common to all W CEA designs and allows some additional flexure in the connection during operation. Mitsubishi, under a license with Westinghouse, offers a similar product.

The standard 17x17 CEA contains twenty-four rodlets. All rodlets are clad in high purity Type 304SS and use Type 308SS end plugs. Absorber material is available in two configurations. Full length standard rods utilize Ag-In-Cd absorber. Hybrid rods are also offered in which the lower 40 inches (102cm) of the absorber is Ag-In-Cd and the remaining 102 inches (259cm) is B_4C. The standard and hybrid designs are shown in Figure 3.

There are 20 rodlets in the 15x15 fuel assembly array and 16 rodlets in the 14x14 array. Both cladding and absorber material, as well as construction, are identical to the 17x17 designs offered.

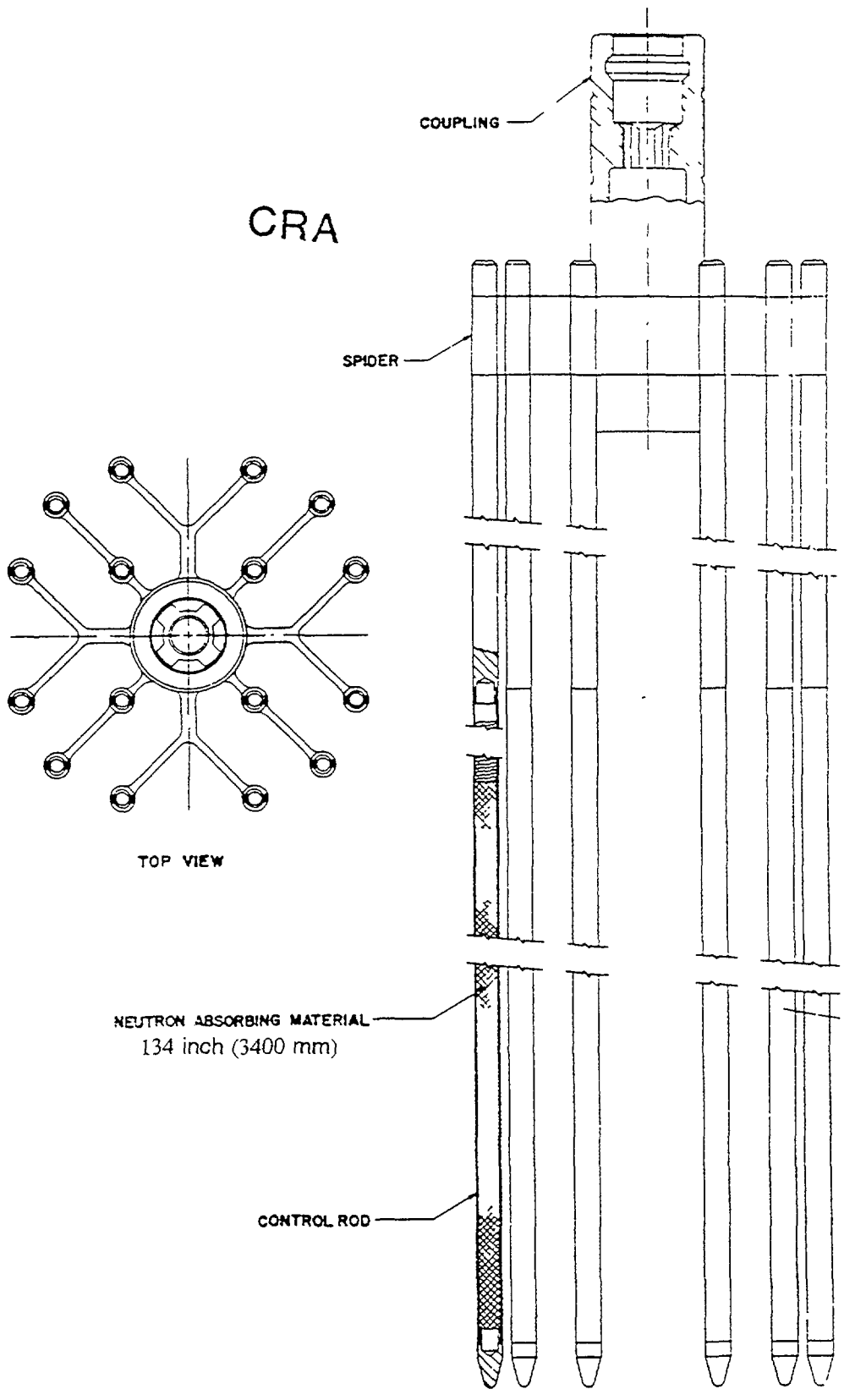

FIG. 2. BWFC control rod assembly for 15x15 plants

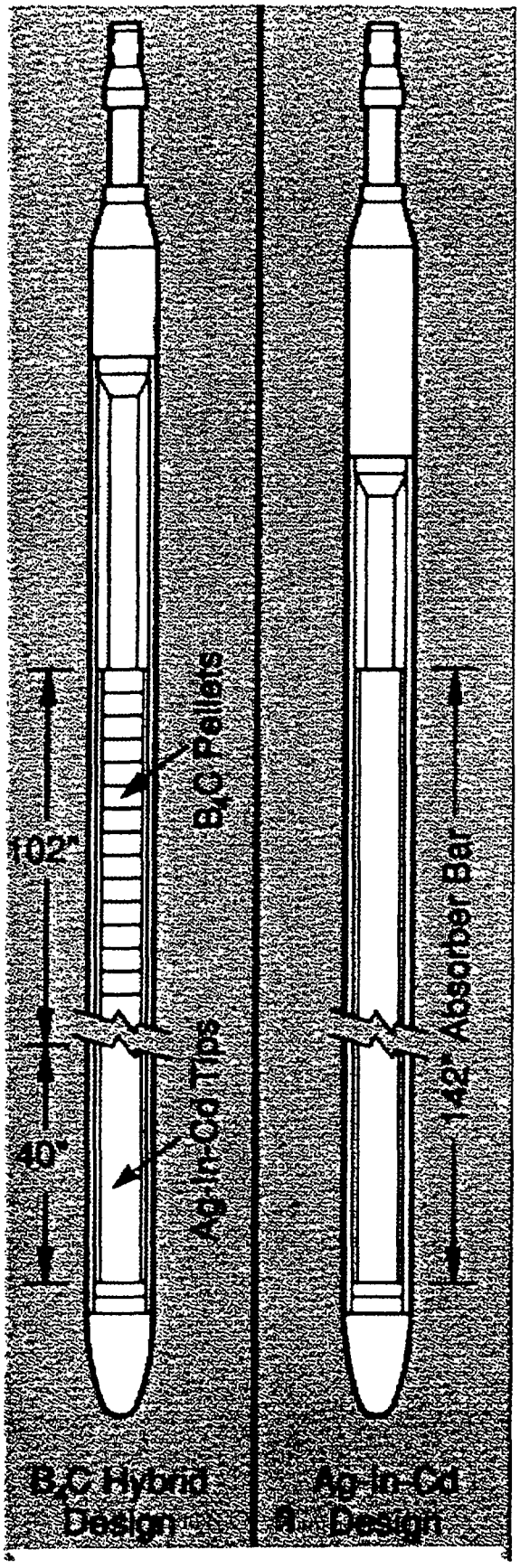

FIG. 3. Westinghouse standard and hybrid control rods

Hybrid absorber rods are not currently manufactured for either the 14x14 or 15x15 designs. Some hybrid absorber rods were placed in service in the early 1980's in Westinghouse 17x17 plants. In 1987, Westinghouse introduced the Enhanced Performance Rod Cluster Control Assemblies (EP-RCCAs). The EP-RCCAs differ from the standard control rods in the following respects:

- Hard chrome, Armoloy-coated cladding to mitigate wear;
- High purity 304SS cladding with increased resistance to irradiation assisted stress corrosion cracking (IASCC);
- Increased diametral gap between the absorber material and the cladding in the highest neutron flux location to accommodate absorber swelling. (See Figure 4).

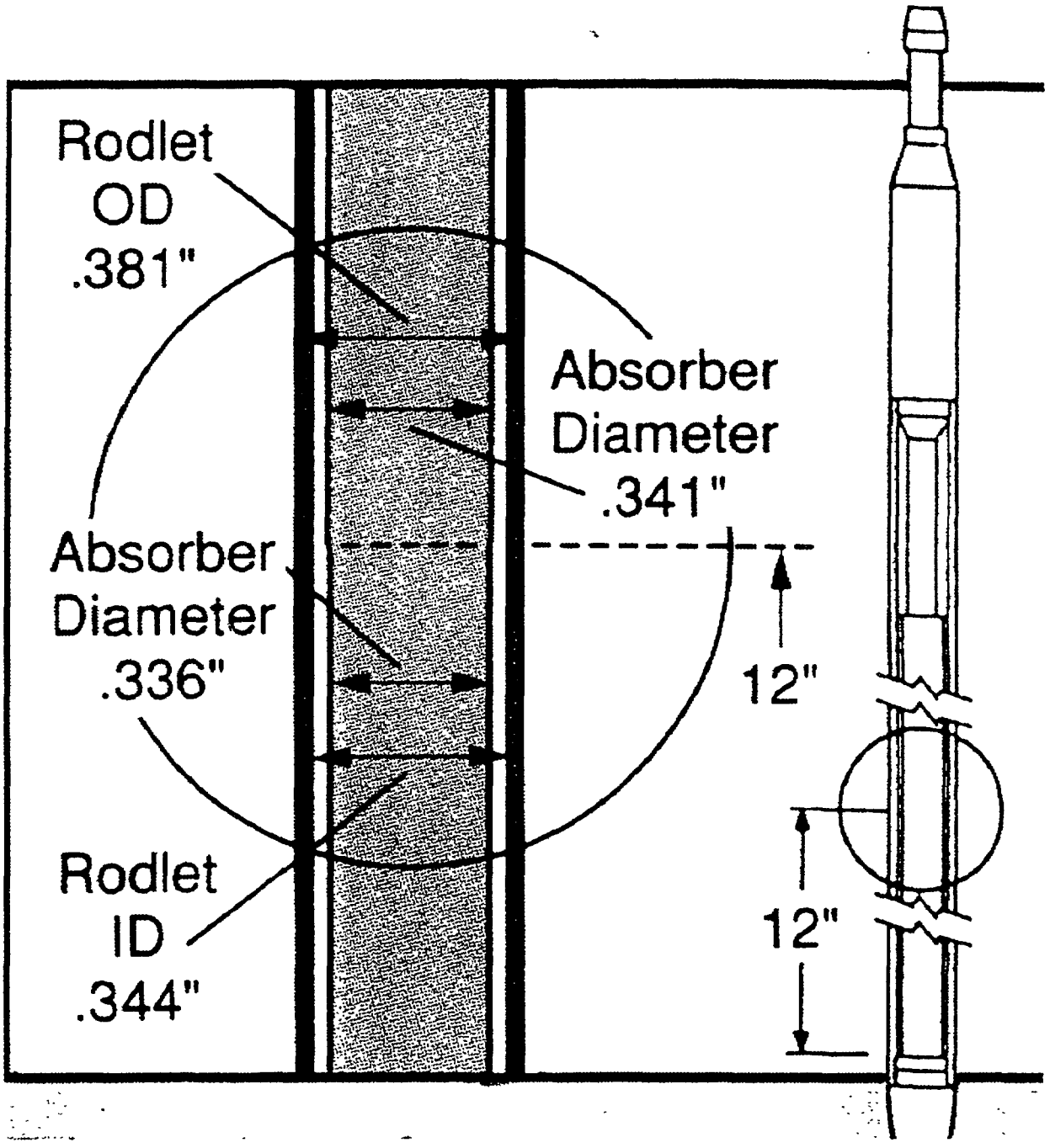

FIG. 4. Westinghouse increased gap design

EP-RCCAs have been in service in many reactors ranging from 14x14 to 17x17 core design in Europe and the U.S., as well as in Japan. All 14x14 and 15x15 units are considered to be low-to-moderate wear environments. The 17x17 units are classified as T_{cold}, i.e. are high wear environments, and coincidentally all have had Hf-RCCAs replaced by the EP-RCCAs. A similarly improved control rod design offered by Mitsubishi is operating in most Japanese PWRs.

1.2.2.4. FRAGEMA (FGA)

The CEAs in EdF's 900 and 1300 MW plants in France are similar to the W 17x17 core CEAs. The 900 MW units have all Ag-In-Cd and the 1300 MW units have hybrid B_4C/Ag-In-Cd absorbers. The Ag-In-Cd length is 40 in. (about 1 meter) at the rodlet tip, identical to the W design.

Differences between the FGA and W are in the new Harmoni™ FGA designs:

- Type 316 L cladding tubing;
- Ion-nitrided tube surface;
- Increased Ag-In-Cd absorber-to-cladding gaps with decreased absorber diameter.

Type 316 L stainless steel has better mechanical properties, IASCC resistance, and forms better nitride coatings than Type 304 used previously. Some BWR control rods have also switched to Type 316. The ion-nitrided tube surface provides added wear-resistance and is discussed later in this paper. The increased absorber-clad gap is to delay mechanical interaction, clad diameter swelling and potential cracking due to IASCC.

1.2.2.5. SIEMENS

Siemens/KWU manufactured CEAs for their standard 14x14, 15x15, 16x16 and 18x18 reactor cores. The design of the rodlets and assemblies varies between the different plants. The layout of the rodlets within the spider for the 18x18 fuel is shown in Figure 5. By comparison the CEA for the 15x15 fuel, which has been the subject of the most significant wear, has 16 fingers, 12 of which have one rodlet at the end and 4 have two rodlets per finger as also shown on Figure 5.

Siemens is the only vendor that uses stabilized stainless steel cladding (Titanium stabilized type 321) and no B_4C in any of their rods. The Cr_3C_2 coating is offered as an option for wear resistance since the wear problem was first observed in the late 1970s, and is discussed later.

1.2.3. Nuclear design

In general, the nuclear design objectives for the control rod system of all PWR vendors are equivalent. That is, the control rod system must compensate for the reactivity effects of the fuel and water temperature changes that accompany power level changes over the range from full-load to no-load. In addition, the control rod system must provide at least the minimum shutdown margin under Condition 1 events (normal operation events) and must be capable of making the core sub-critical rapidly enough to prevent it exceeding acceptable fuel damage limits, assuming that the highest worth control rod is withdrawn at the time of a trip.

All PWR control rod (cluster) systems whether they contain Ag-In-Cd, B_4C, or combinations of both absorbers are designed to meet the above objectives. Unlike BWR control blades, the loss of total control rod worth (for safe shutdown) due to material irradiation is negligible, since only a small number of control clusters (e.g. D-bank in W reactor), and part length rods (in some cases, e.g., BWFC cores) may be in the core under normal operating conditions. There are no nuclear lifetime limits for PWR control rods.

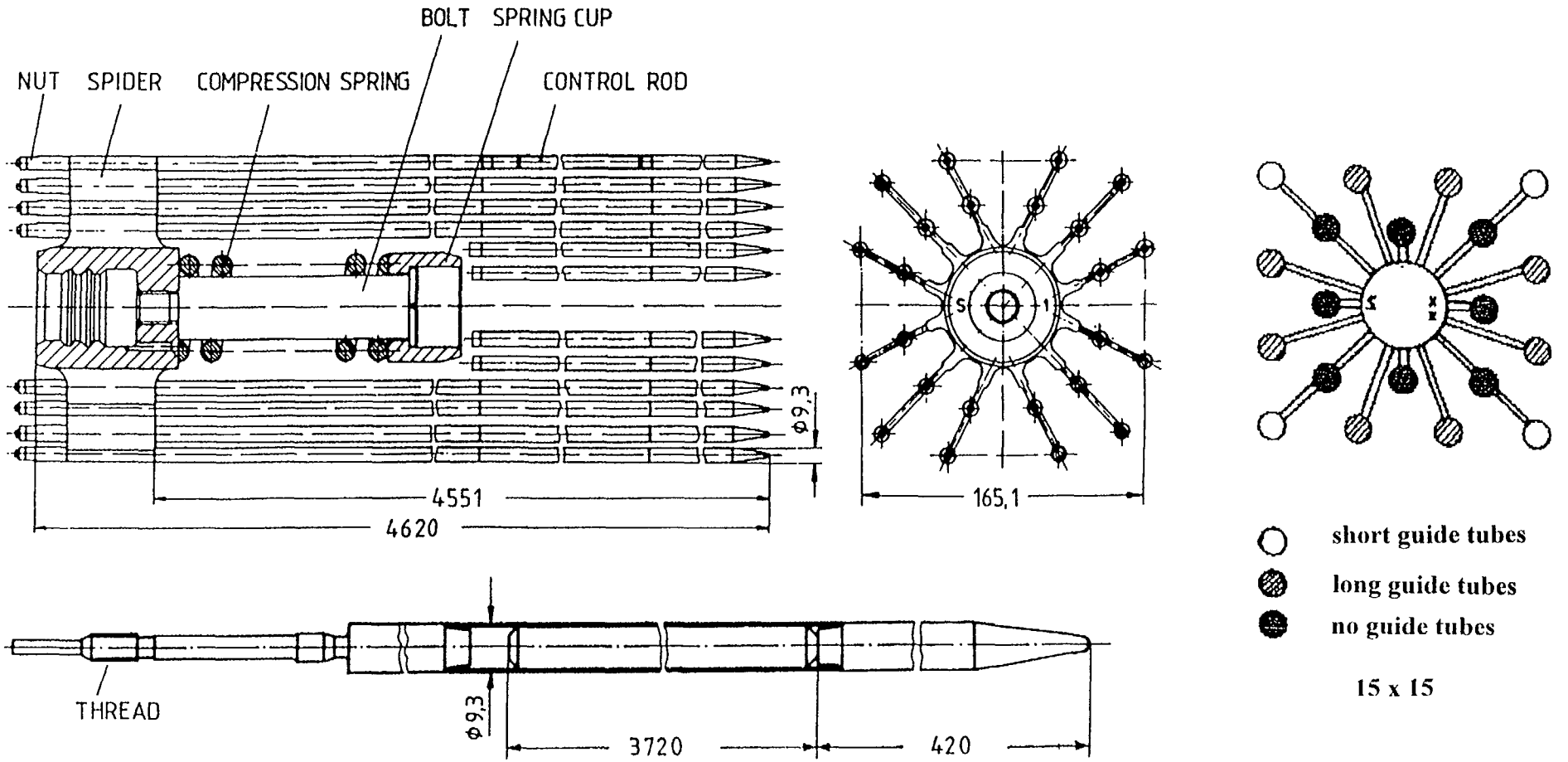

FIG. 5. PWR RCCA and control rod for Siemens Convoy plants (18x18)

1.3. Problem areas and remedies

1.3.1. Wear

The wear of control rods by rubbing against upper internal components, specifically guide cards, is a well known phenomenon today. Control rod wear is caused by several mechanisms. The predominant mechanism is rodlet vibrational contact against upper internal guide cards when control rods are parked in their fully withdrawn position. With the exception of the control rods in W control bank D, or in the case of FGA also bank L, many utilities operate their control rods in the fully withdrawn position during 100% reactor power operation.

Secondary mechanisms such as sliding wear and rodlet tip wear can also contribute to the reduction of control rod lifetimes. Sliding wear occurs as a result of rodlet contact with fixed upper internal surfaces during control rod movements into and out of the core. Tip wear occurs as result of rodlet vibrational contact with fuel assembly guide tubes when control rods are parked in their fully withdrawn position.

Figure 6 shows a distribution of wear patterns typical of a FGA or W CEA. The wear at the rodlet tip is crescent-shape and is due to contact with the fuel element guide tube. The wear in the continuous guide zone is due to stepping-induced friction and is spread axially over a fairly large span. Local discontinuous wear can occur there also from CEAs that are relatively stationary. The wear at the tip is against the fuel assembly guide tube and is generally crescent-shape.

Control rod clad wear can lead to clad failures and consequently to absorber leaching. Clad failures can occur as a result of the high stresses imposed by differential pressure at localized wear scars. The differential pressure across the clad is caused by a combination of the external reactor coolant and internal gas pressures. These high stresses will either result in clad ovalization, which increases the possibility of a stuck rod, or brittle fracture which can lead to a dropped rodlet. Fatigue fracture during frequent load follow operation with rods could also occur at the wear location.

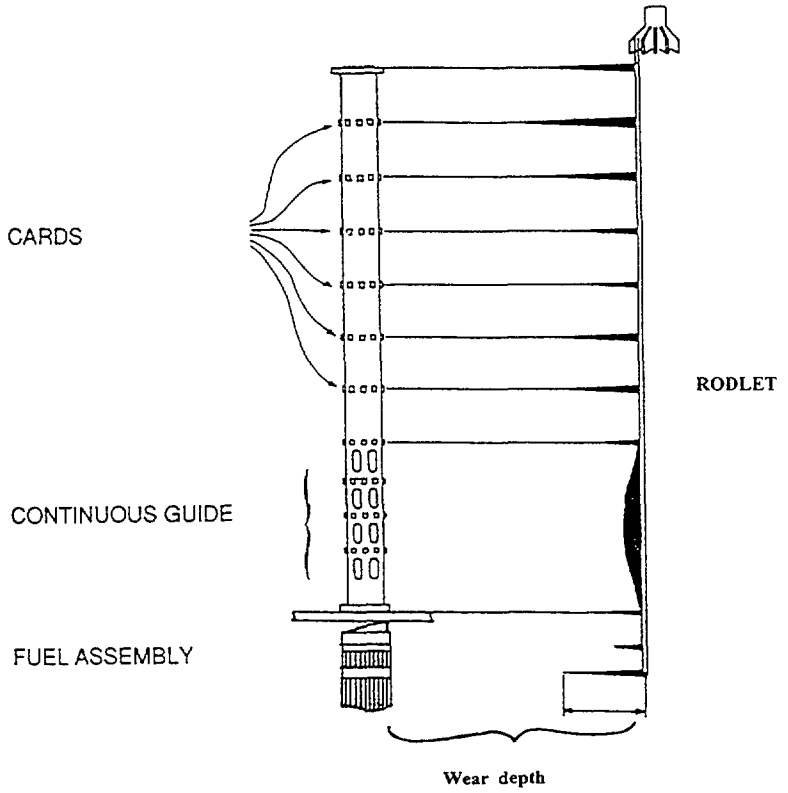

FIG. 6. Typical Recorded Wear for a Low-Mobility RCCA (Reference: Framatome)

Absorber leaching occurs when through-wall wear exposes the absorber material of B_4C control rods to the coolant. In this configuration, leaching leads to a loss of shutdown margin. Although leaching does not occur in control rods that utilize Ag-In-Cd as the absorber material, mechanical erosion can lead to an introduction of undesirable isotopes into the coolant (e.g., Ag^{110m}).

The variables that determine the amount and type of wear are:

- hydraulic forces in the upper guide structure;
- dimensions and weight of the rodlets;
- dimensions and configuration of the structure designed to guide the control rodlets;
- control rod motion related to operational mode.

All of these variables can have a significant effect on the extent, and type, of wear and account for differences between vendors and between various plants of the same vendor.

The hydraulic forces are the most complex and difficult to characterize of all these variables. In the W type guide structures for instance there is both downward flow from the top and upward flow from the bottom with cross-flow in the middle, while in Siemens' plants all of the coolant is upflow. The rodlets in W type and Siemens plants are guided by intermediate cards, while in B & W plants they are enclosed in continuous tubes for their entire length.

1.3.2. Wear remedies: Development of wear resistant coatings

1.3.2.1. Introduction

Several options exist to reduce or eliminate wear:

- modify the hydraulics
- modify the upper internal structures
- modify the absorber rodlets to provide a wear resistant surface for Type 304 steel
- replace Type 304 with a more wear resistant material.

The easiest of these options is to put a wear-resistant coating on the rodlet surface or use a different cladding. All of the vendors now provide improved, or enhanced designs, and to date most of them have performed satisfactorily. A hard wear-resistant coating on the rodlet may transfer the wear problem to the guide cards or guide tubes. Increased monitoring of the coating surfaces is needed as coatings are introduced. Another consideration is the mechanical integrity and corrosion resistance of the coating in the reactor. The various types of coatings are discussed below.

1.3.2.2. Chromium carbide Cr_3C_2

Coatings of Cr_3C_2 are applied either by plasma spray gun or by detonation gun (LC1C), a process patented by Union Carbide. The carbide is in a NiCr binder and applied at a 150 °C tubing temperature. This type of coating is favored primarily by BWFC and Siemens. The coatings used are about 40-50 μm thick. There is concern that the very hard surface of a Cr_3C_2 coated rod could result in increased guide card wear (Cr_3C_2 is harder than chrome-plated or ion-nitrided surfaces) but early measurements in USA after two cycles showed no evidence of this. Siemens has not detected wear or flaking in plasma-sprayed Cr_3C_2 coated rods in many years of service in a lead assembly in Germany and in more than 250 accumulated cycles of lower duration on about 40 CEAs. To date Cr_3C_2 is the only coating which has had no reported performance problems. Its high cost is its major disadvantage; the current process requires that each tube be coated individually.

1.3.2.3. Chromium plating

Two Cr-plated (Armoloy) CEAs fabricated by BWFC were irradiated in a US reactor. After one cycle of irradiation, the maximum wear depths of 2.3 mils (58 μm) and 2.9 mils (74 μm) exceeded the complete coating thickness of 0.05 mil (13 μm). In the next cycle standard CEAs replaced these two. The wear in these standard CEAs were, after one cycle, 14.7 mils (370 μm) in the location where the Cr-plated rod had 2.3 mils (58 μm), and the wear was not significant in the other location. It is not clear why the BWFC chrome plate is not as effective as the W application (W experience is less than 0.5 mil (13 μm) wear in up to three cycles). This experience led BWFC to conclude that chrome plating is not very effective. The W EP-RCCA, described above, uses a chromium plated (Armoloy) SS 304 clad. The nominal thickness of the plating is 0.5 mil (13 μm). The first of these rods were delivered in 1987.

1.3.2.4. Nickel plating

The Framatome tests showed that this performed well. However, nickel solution and activation in the coolant could have a negative effect on activity transfer. This is of course true of Ni alloys for cladding as well.

1.3.2.5. Nitriding

Nitrides are extremely hard and the commercial nitriding of stainless steel surfaces by a variety of processes for improved wear and fatigue resistance is common. One of the potential disadvantages is poor corrosion resistance.

The Framatome have selected the ion-nitriding process for nitrogen enrichment of the steel surface of their Harmoni™ design CEAs. Electrical discharge in a nitrogen atmosphere produces a plasma which depassivates and heats the surface and converts molecular nitrogen to ionic nitrogen. The nitrogen can then diffuse into the steel surface.

The nitrogen resides interstitially in a surface layer in the range 12 to 20 μm thick (Figure 7). Chromium nitrides (CrN or Cr_2N) may form with excess nitrogen or thicker coatings (35 μm) and degrade the corrosion resistance of the coating. This was a problem with earlier coatings until the process and final product were optimized.

Ion-nitriding is performed in a furnace as shown in Figure 7. Tubes with their tips welded on are suspended and sealed at the top in the furnace. After vacuum evacuation a mixture of nitrogen and hydrogen is introduced and a high voltage generator (300 - 1000 volts) forms the plasma. The corrosion resistance is closely related to the process temperature and after evaluation of several process conditions, the current low temperature treatment was found to prevent nitride formation and also provide good corrosion resistance.

1.3.3. Absorber swelling and IASCC

1.3.3.1. Introduction

Mechanical interaction between the absorber and the cladding, which results in cracking of the clad, is one of the mechanisms which governs the service life of control rods. The phenomenon can occur, in slightly different forms, with all absorber materials: Ag-In-Cd, B_4C or Hf. In the case of the first two the cause of the intergranular cracking of the clad is a combination of some or all of the following:

- absorber 'swelling', which stresses the clad;
- clad wall thinning, due to wear;
- irradiation effects on the clad mechanical properties;
- coolant chemistry.

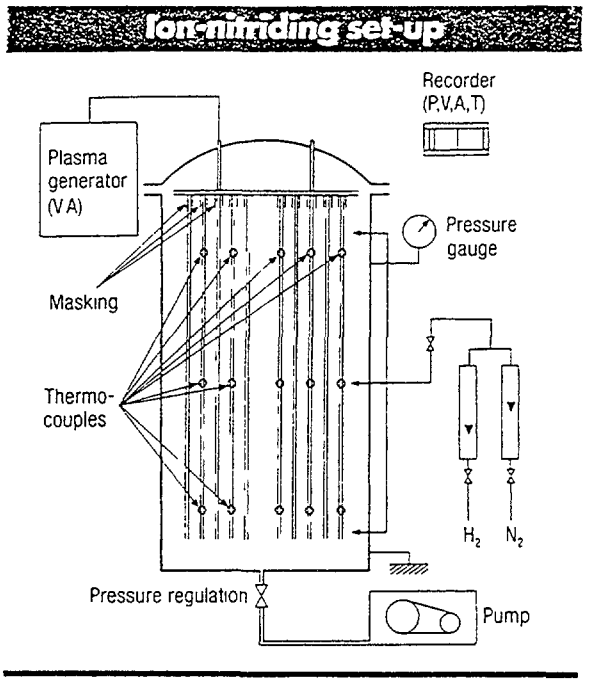

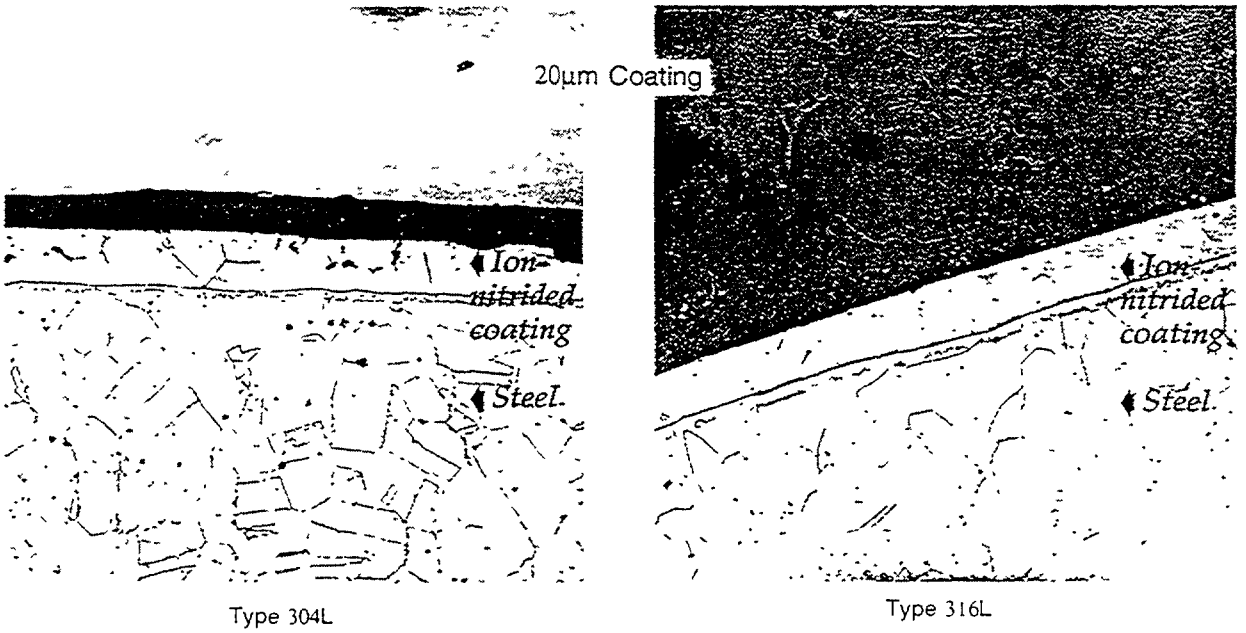

FIG 7. Ion nitrided control rodlet coatings by Framatome

The problem generally occurs in the region of highest neutron fluence, near the rod tip, which is also vulnerable to sliding wear against the guide tube. In some instances the cracks remain hairline (i.e. very tight) and continued operation is possible. This is particularly true of Ag-In-Cd rods. Deterioration of the cracked condition can lead to leaching of soluble B_4C into the coolant and, in severe cases, to complete failure of the rod resulting in the loss of absorber pellets. In the case of low solubility Ag-In-Cd, the combination of exposure of the absorber and erosion processes can result in the isotope Ag^{110m} appearing as a contaminant in the primary coolant.

The problems with Hf absorber rods fabricated by W are related to hydrogen diffusion through the cladding wall causing primary hydriding of the Hf. The manufacture of this design has been discontinued by W but some of the originally supplied Hf CEAs may still be operational.

1.3.3.2. Ag-In-Cd

The swelling of Ag-In-Cd is due to the transformation of indium (In) into tin (Sn) by neutron capture. The change in chemical composition and the basic transmutations are shown in Figure 8. The mechanism leading to IASCC clad cracking in Ag-In-Cd rodlet tips is as follows:

- Absorber - clad gap closure due to creep and slump of Ag-In-Cd under its own weight, and compression by rodlet spring (if present);
- Increased creep rate if absorber temperature is increased;
- Swelling of Ag-In-Cd;
- After gap closure, swelling continues;
- The clad fracture strength, or ductility limit, is reached and the cladding cracks longitudinally;
- Stresses are relieved and swelling continues.

The main operational effect of swelling is the potential interference within the dashpot region, leading to incomplete or slow rod insertion.

2. BOILING WATER REACTORS

2.1. Introduction

The primary mechanical life limit of BWR control rods has been due to IASCC cracking of containers for the B_4C absorber. The B_4C irradiation induced swelling is the source of stresses and the coolant the source of corrosion. Stress due to crud accumulations have also contributed to IASCC. Improved designs and materials have been introduced periodically since the discovery of the B_4C swelling problem in 1978 and the life limit of the designs has been extended. The improved mechanical and nuclear designs and the current performance problems are discussed for the three current BWR control rod vendors: ABBA, GE and Siemens.

2.2. Summary of designs

2.2.1. Introduction

All BWR control rods are cruciform in shape and the four wings fit between the channeled fuel assemblies. Three types of control rods are in use:

- GE and Siemens: each of the 4 wings has 18 - 21 tubes filled with vibro compacted B_4C powder and bundled together using a U-shaped stainless steel sheath. The U-shaped sheaths are welded to a center post, to a lower casting and to a handle to form the housing for the B_4C absorber rods;
- GE: the newer 'Marathon' blade wings are composed of longitudinally welded tubes with a square outer envelope filled with encapsulated, vibratory-compacted B_4C powder or Hf-rods and sealed at the ends;
- ABB: The wings of the ABB control rods are solid pieces of stainless steel with gun-drilled horizontal holes that are filled with B_4C powder by vibratory compaction. The holes are covered with a stainless steel bar and the wing is seal welded. The B_4C columns are also connected by a vertical gas plenum along the outer edge of each wing.

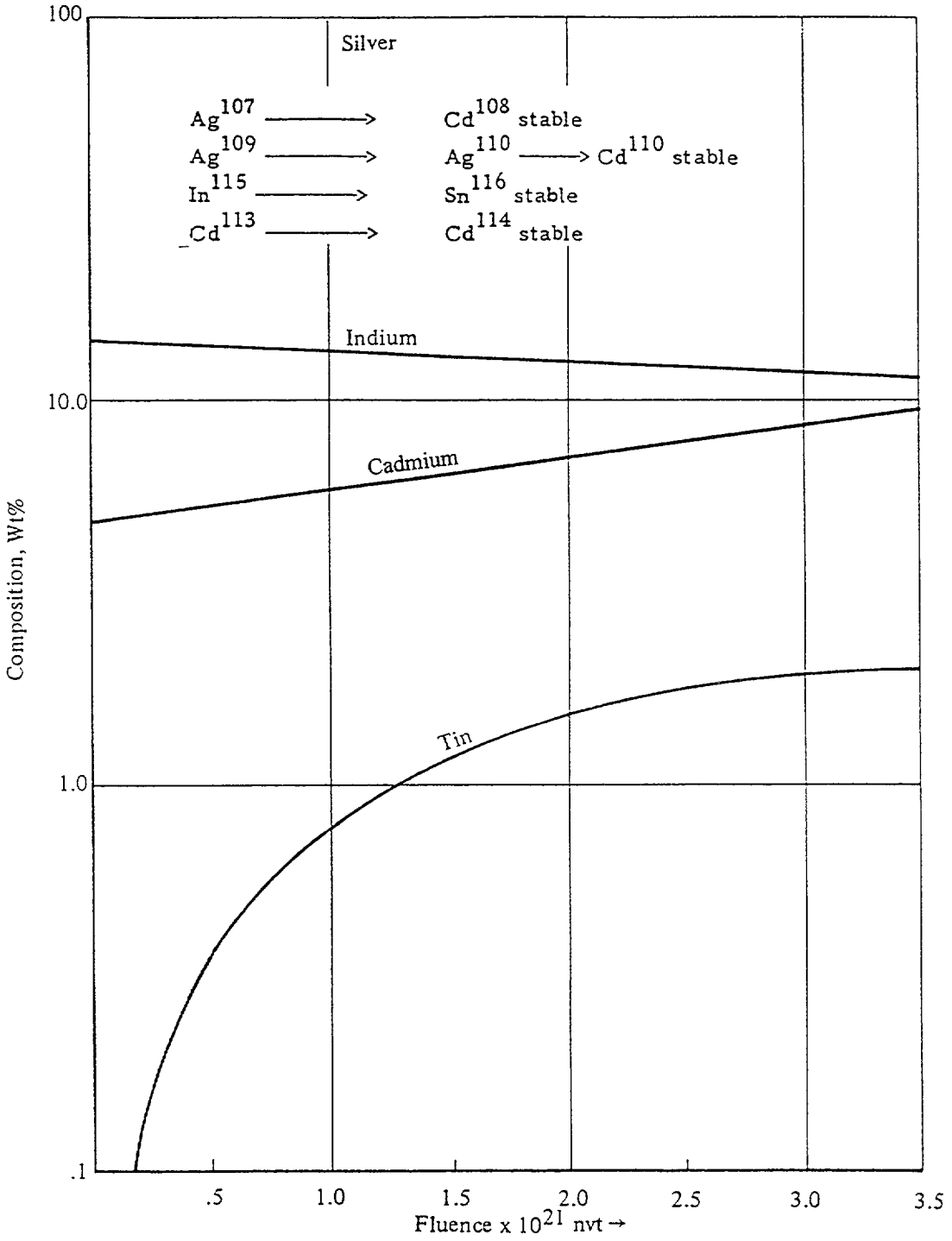

FIG. 8. Calculated changes in composition of AgIn-Cd alloy as a function of fluence (Reference: WAPD-214, December 1959)

In order to extend the mechanical lifetime of the blade, each vendor has developed hybrid absorber control rods which use Hf in the high exposure sections and IASCC resistant steel absorber tubes. Almost all control rods currently supplied are of this type.

2.2.2. Mechanical design

2.2.2.1. ABB ATOM

The currently offered control rod designs are all of the general type described in the previous section and differ primarily in the absorber design as listed below with the commercial designation in parenthesis:

- All B_4C absorber (CR-70);
- Hf rods in holes at the tip, standard diameter absorbers (CR-82);
- Same as the CR-82, but smaller diameter absorbers (CR-82M);
- Hf rods in holes at tip and plugs at rim, standard diameter absorbers (CR-85).

The designs are shown schematically in Figure 9 and the reasons for the differences discussed below.

CR-70, the all B_4C control rod, is the original supply to ABB plants. Sales of this model essentially stopped in 1984 because it was superseded by the hybrid designs with improved mechanical lifetimes.

The CR-82 control rod design was ABB's first progression from the basic CR-70 all B_4C containing rod. The top 152 mm (6 inches) or 22 holes of the absorber region in each of the four absorber wings were filled with hafnium pins. The remainder of the absorber region is all B_4C. As in all the ABB control rods the four wings are a solid piece of stainless steel with gun-drilled horizontal holes that are filled with B_4C powder, by vibratory compaction. The CR-82 blade material was until recently high purity 304L stainless steel with control of P to <0.025%, Si to <0,3%, S to <0,02%, B to <5 ppm and C to <0,03%.

Early irradiation results indicated that further mechanical life extension would be desirable which lead to the development of the modified CR-82, or CR-82M. The CR-82 is recommended for shutdown rod applications. The material change from Type 304L to Type 316L stainless steel, made for the CR-82M, has been applied to this as well as all other control rods.

The CR-82M has two features designed to extend the mechanical lifetime:

- A modified absorber configuration to minimize strain at the blade outer surface achieved by:
  - smaller absorber holes;
  - thinner ligaments between holes;
  - thicker outer wall;
- more IASCC resistant steel:
  - Type 316L instead of high purity Type 304L (L = low carbon).

The comparison of absorber configurations is shown on Figure 10. Finite stress analysis comparison showed a 40% decrease in strain for the modified design as shown in Figure 11. Ex-reactor materials tests have shown that Type 316L stainless steel has better IASCC resistance than Type 304L. The difference between the two steels is 3% molybdenum contained in Type 316.

The CR-85 control rod design has hafnium plugs at the wing tips of the horizontal absorber holes. The remainder of those holes contain the standard vibro compacted powder. The extensive cracking found in the initial lead assemblies was associated with secondary hydriding and swelling of the hafnium. The CR-85 had the standard diameter absorber holes and Type 304 L structural steel. Currently there is no further interest in this design.

The CR-85M was then marketed as the improved version which has the same design modifications as the CR-82M. This design has been used by Japanese utilities, however since the absorber diameter change would require a licensing change, they opted for the standard absorber diameter and only the material change to Type 316L steel. The design is identified as CR-85M-1.

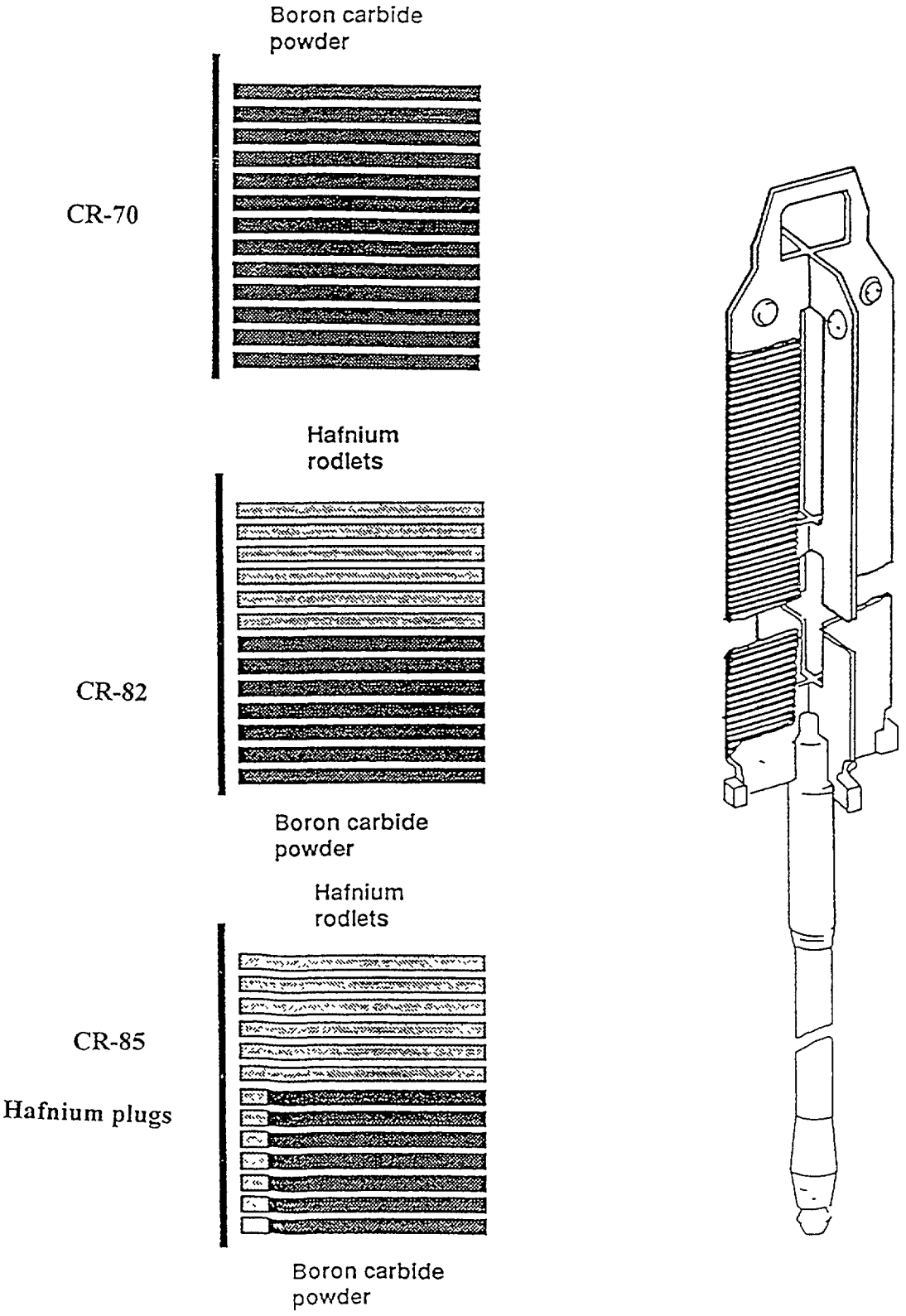

FIG. 9. ABB control blade types

High worth control rod versions of the above designs have also been produced. The higher worth is achieved by increasing the diameter and the length of the absorber holes, but at the potential cost of higher stresses at the blade surface. With the trends in fuel development towards higher burnup, longer cycles and higher power densities, control rods with an increased control rod worth compared with the original equipment rods are desirable for:

- Improved shutdown margin
- Flexibility in reload pattern designs
- Possibility to extend fuel cycle length and burnup
- Operational flexibility.

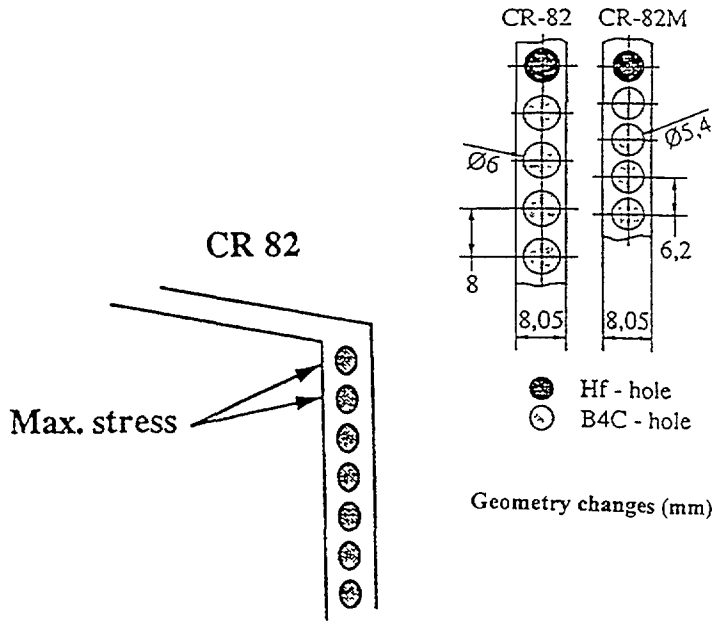

FIG. 10. Modifications of ABB's CR-82 control blade

ABB control rods are called 'high worth' (HW) control rods if they have 5-15% (relative) higher rod worth than the original equipment rods. The CR-82 HW design has a larger diameter absorber (0.217 in., 5.5 mm) and a longer length absorber (4.09 in., 103.9 mm).

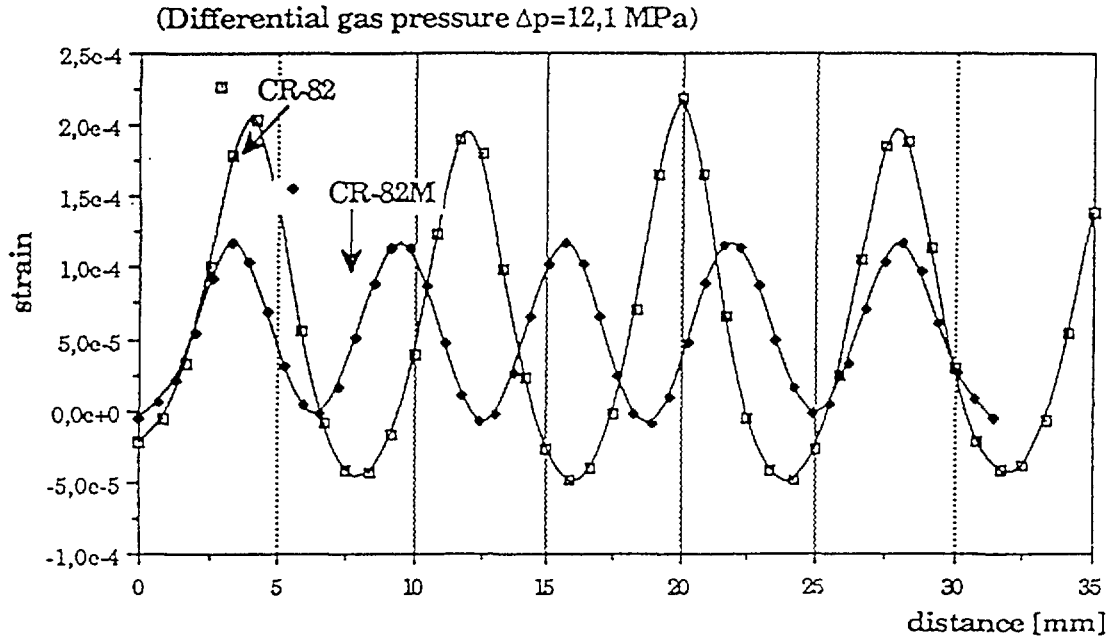

FIG. 11. Outer wall strain analysis

2.2.2.2. GENERAL ELECTRIC

GE produces two general types of advanced control rod designs. The first type is the Duralife Series of control rods which primarily differ from the original equipment design by the use of low cobalt alloys and high purity 304SS tubing. In addition, later designs in the Duralife series contain hafnium in various high exposure portions of the rod.

The second, mechanically dissimilar design is the Marathon control blade which uses square tubing welded to form each blade wing. Hafnium absorber is also used in high exposure regions, such as the edge tubes, and if necessary can be added as plate material at the blade tip. Individual blade hafnium loading may be varied with control rod requirements.

The distinguishing design features of each Duralife control blade type are summarized below:

- Duralife 120 - All B_4C-absorber design utilizing high purity 304SS and non-cobalt pins and rollers.
- Duralife 140 - All of the features of the Duralife 120 with the addition of hafnium at the top of one absorber section.
- Duralife 160 - All of the features of the Duralife 120 with the addition of hafnium absorber rods in the highest burnup locations (outside edge of each wing).
- Duralife 190 - All of the features of the Duralife 160 with additional hafnium absorber in the second highest burnup location (top of each blade wing). In addition, a lighter weight velocity limiter is also used.
- Duralife 215 - All of the features of the Duralife 190 with additional B_4C absorber material in thicker blade wings. The Duralife 215 is specifically designed for C-lattice plants.
- Duralife 230 - Similar to the Duralife 215 but designed for D-lattice (BWR 4-6) plants.

Marathon

The Marathon control rod is a radically different concept when compared to the Duralife series. The main difference in the Marathon control rod is the replacement of the absorber tube and sheath arrangement with an array of square outer envelope tubes (Figure 12), which results in reduced weight and increased absorber volume. In addition, the full length tie rod used in previously approved designs is replaced with a tie rod segment, which also reduces weight (Figure 13). The outer corner sections of the individual tubes are used as wear surfaces against the channels. They are fabricated from a high purity Rad Resist Type-304 stainless steel that provides resistance to irradiation-assisted stress corrosion cracking. Each wing is comprised of either 14 or 17 absorber tubes. If needed for enhanced life, provision is made for the incorporation of a hafnium plate in a rectangular section (pocket) below the handle at the top of the control rod, with the tip being variable in length dependent upon individual customer requirements.

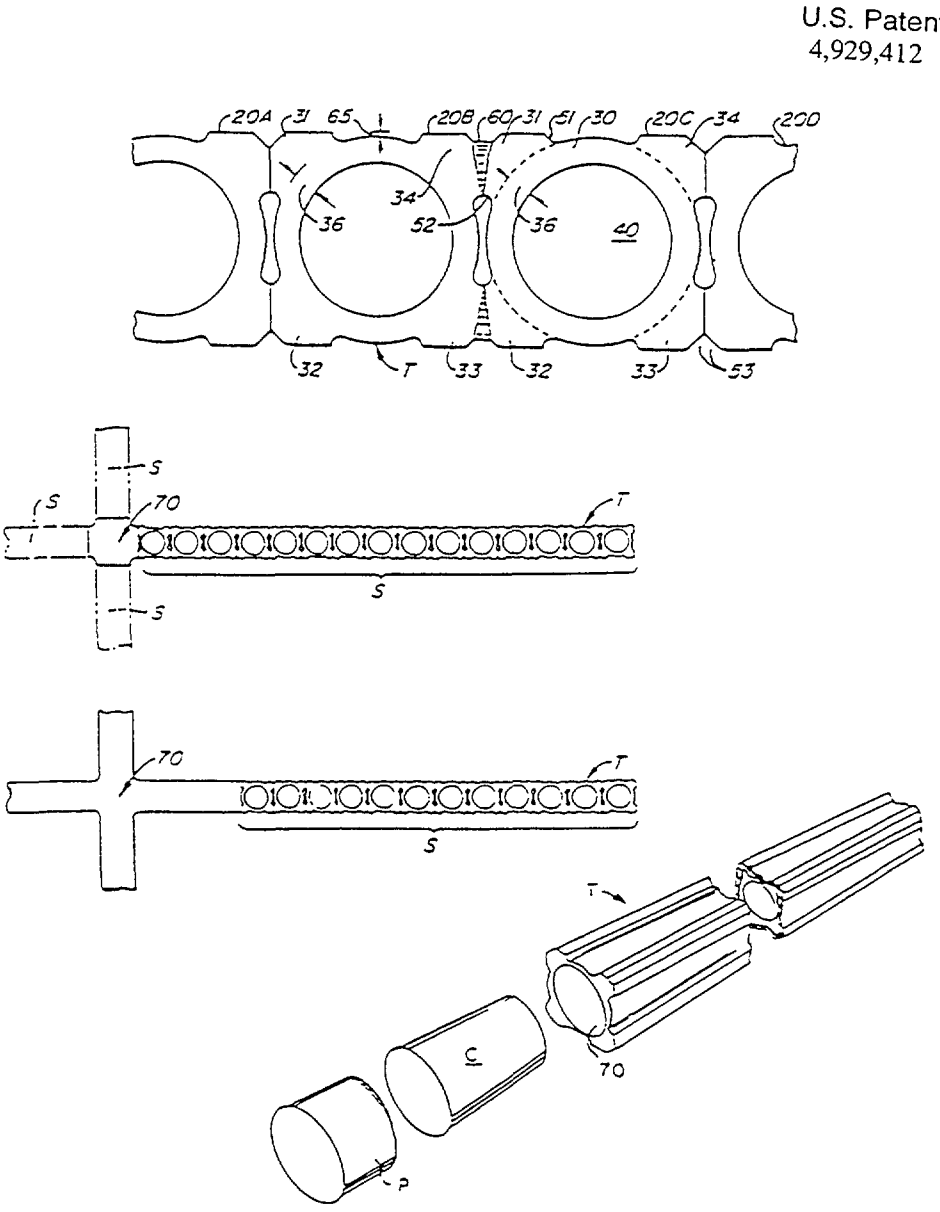

FIG. 12. Internal features of the Marathon control blade (U.S. Patent 4,929,412)

Hafnium blade

In co-operation with GE, Hitachi and Toshiba have introduced two all-hafnium absorber control blade designs for use in BWR control cell locations. The two designs, one with Hf-plates and the other with Hf-rods, are shown in Figures 14 and 15 respectively. With both designs, the control rod drop rate is approximately 0.85 m/sec, or less than the maximum allowable rate of 0.95 m/sec, and the time to 90% of full-in position is approximately 2.6 seconds, or less than the maximum allowable time of 3.6 seconds.

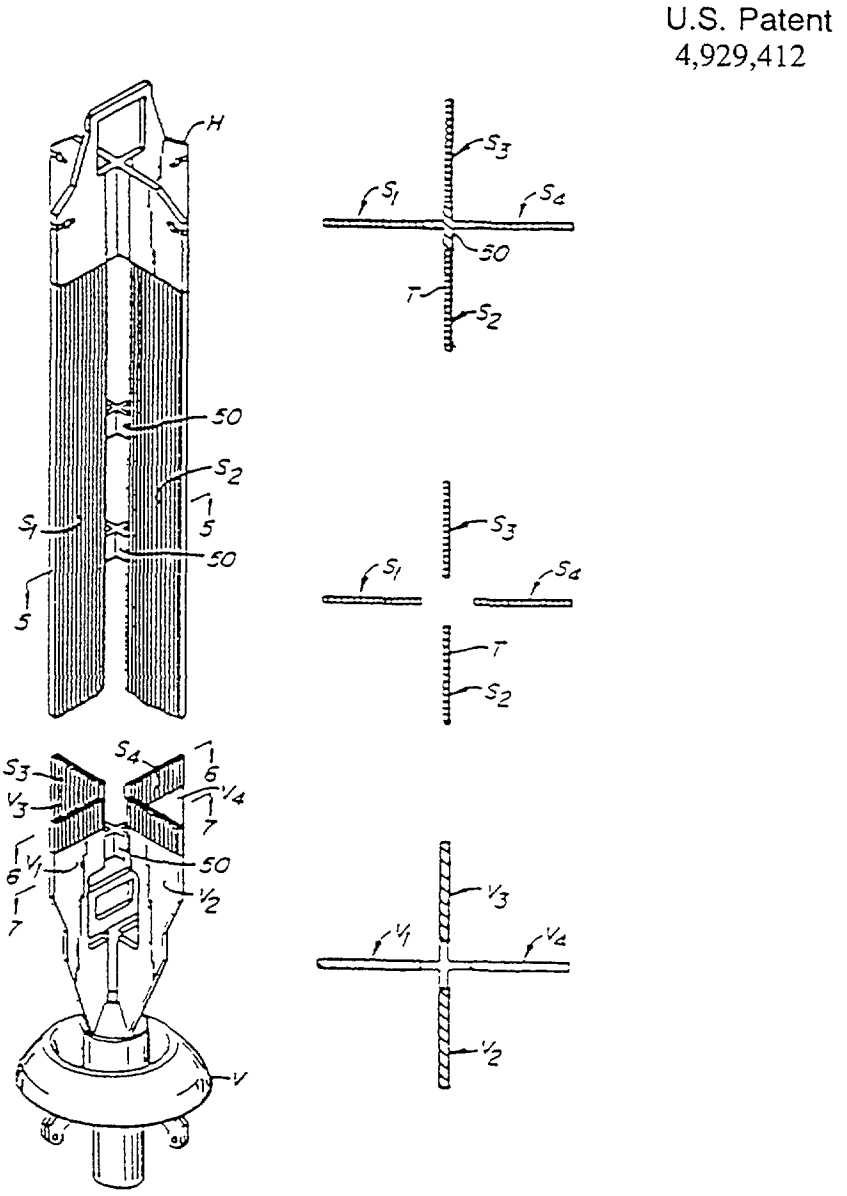

FIG. 13. Marathon control blade (U.S. Patent 4,929,412)

As with the early GE version, the plate design utilizes two hafnium plates on each face of the wing of the cruciform blade. The absorber plates are fixed to the sheath by stainless steel pins which also provide separation of the plates. The water-filled gap between the absorber plates forms a flux trap in which epithermal and fast neutrons are moderated and absorbed. To save weight but provide the required shutdown margin, four hafnium plates with different thickness are used with the plates at the top of the blade (most likely the peak exposure location) having the maximum width of approximately (0.08 inch) 2 mm. Proceeding down the blade, the thickness is reduced in three stages to approximately (0.04 inch) 1 mm.

In the rod-type blade, the structure is essentially identical to the B_4C design (Duralife 120) with the hafnium absorber rods replacing the B_4C tubes. The absorber rods are suspended from the top of each wing. The rods are thicker (5 mm) in the top half of the wing and thinner (3 mm) in the bottom half. The all-hafnium designs have been in service since 1989.

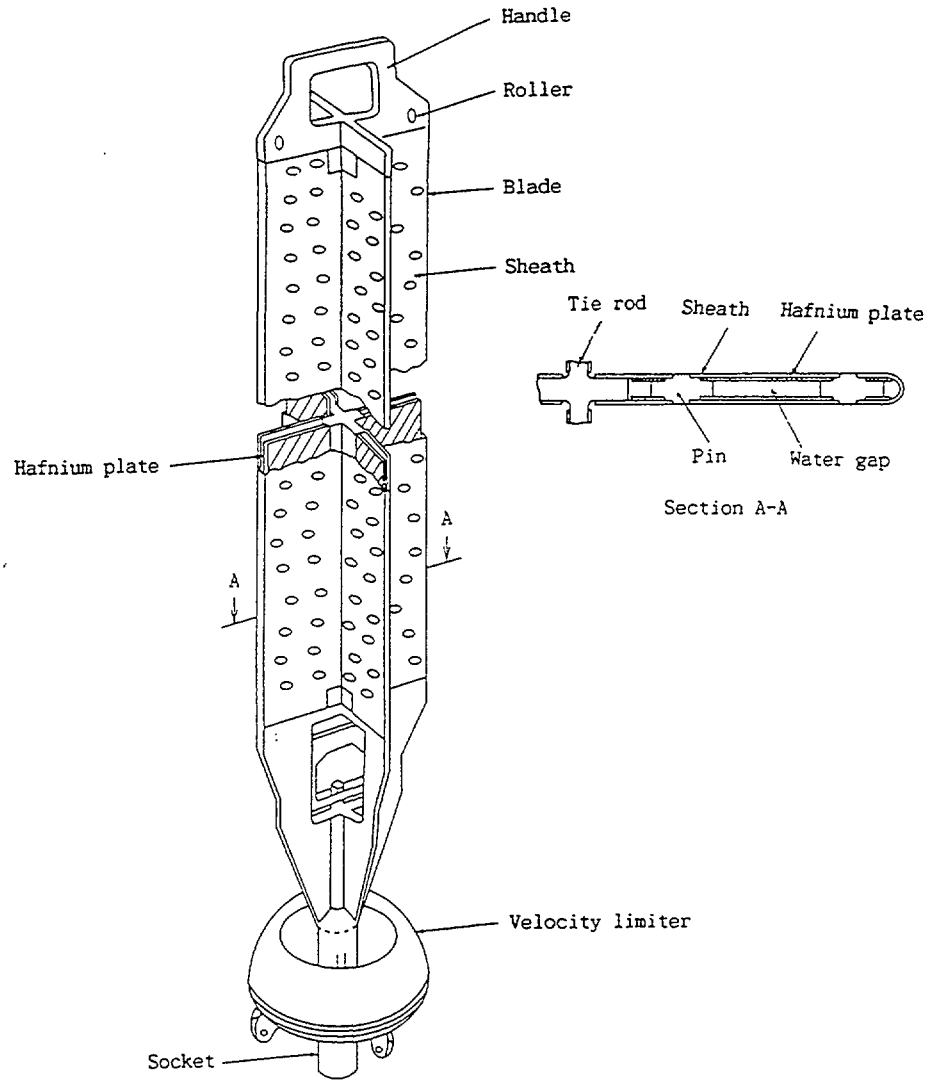

FIG. 14. Plate type Hafnium control blade

2.2.2.3. SIEMENS

The Siemens Hybrid 4 control rod design is similar to the Duralife type GE control rods. The earlier Hybrid 1 design had Hf edge rods only. There has been no change in the design of these rods as Siemens no longer manufactures BWR control rods.

2.2.3. Nuclear design

The key nuclear criterion governing the nuclear design of a core's worth of BWR control blades is the cold shutdown margin specified in the Technical Specification, with the most worthy blade stuck out of the core at any point in a fuel cycle. A second criterion for replacement blades is to maintain or improve the scram reactivity function as defined by the Technical Specifications. Meeting the scram reactivity criterion is primarily a mechanical design concern (blade weight) since blades are generally designed to have a reactivity hold down characteristic at least equivalent to those they are replacing.

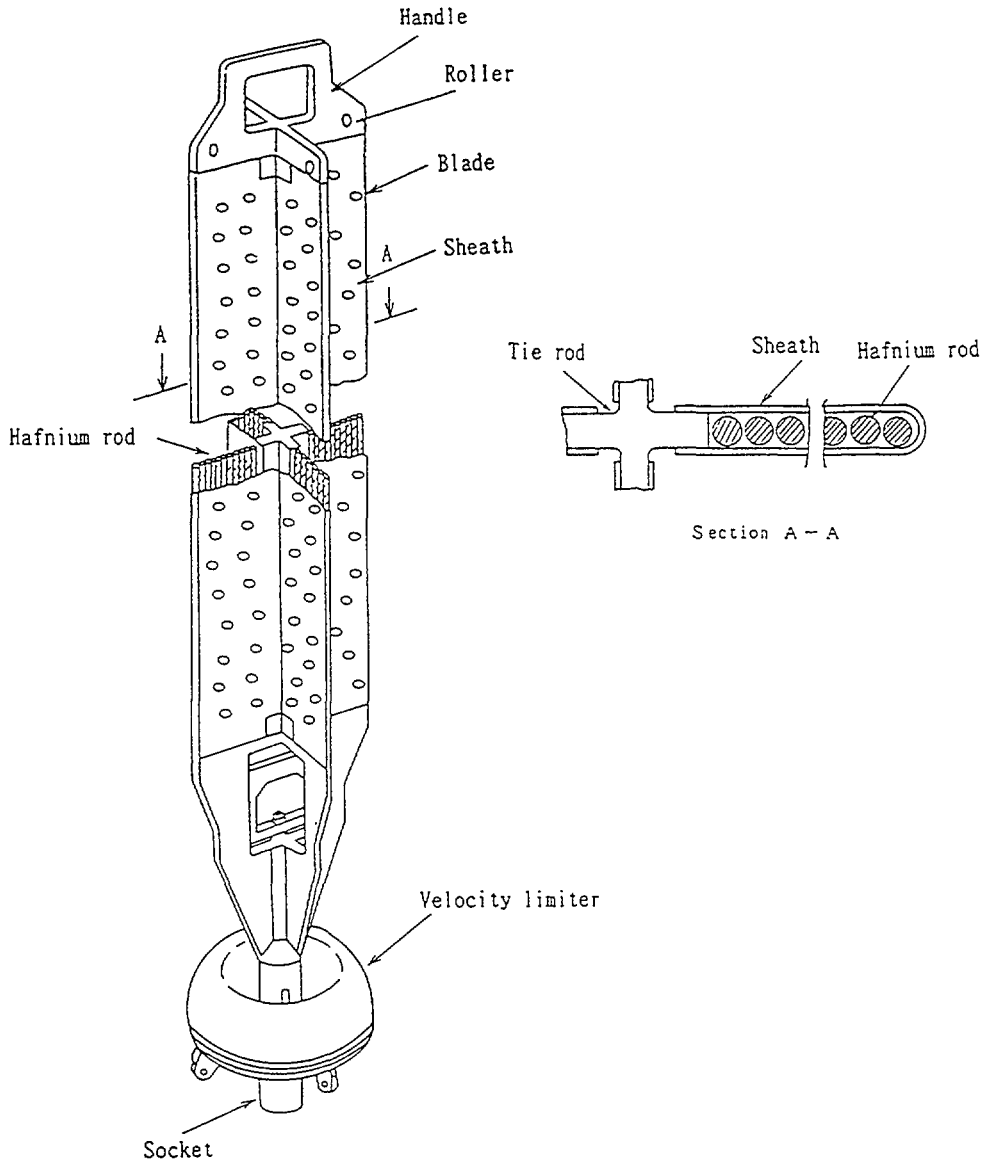

FIG. 15. Rod type Hafnium control blade

BWR control blades normally operate in the core for a good portion of their history and therefore the absorber material is subject to depletion, and loss of worth. The end of nuclear life is defined as a 10% relative reduction in cold reactivity worth in any highest exposed axial quarter segment. The relative worth reduction is taken from the cold initial worth of the control blade design. The 10% value most probably evolved from use in conservative core design analysis. In BWRs a significant axial segment is defined as a quarter axial segment (generally the top quarter controls). In GE and Siemens plants the quarter axial segment criterion is also compatible with the original plant process computer tracking the control rod fluence. In modern process computer systems the control rod tip is also tracked for fully withdrawn control rods.

Worth reduction and quarter segment average depletion are determined through detailed neutronic analysis of a blade as mechanically designed. If Hf is present in the blade design, an equivalent average depletion expressed in terms of ^{10}B, is used:

$$\text{Equivalent Avg. Depletion} = \frac{\text{Total absorptions in } B_4C + Hf}{\text{Total Boron atoms if entire blade were } B_4C}$$

This allows the plant process computer control blade tracking to be used directly with multiple absorber control blade designs.

BWR control blades generally can be designed with extended nuclear life (more snvt[1] to reach 10% worth loss) by increasing the number of absorber atoms per unit volume. If this is done by increasing the absorber surface density (absorber surface per unit volume of absorber), initial worth will increase, so that lifetime increases could be limited by the 'matched worth' criteria if applicable.

3.3. Problem areas and remedies

3.3.1. B_4C swelling and irradiated assisted stress corrosion cracking

The B^{10} isotope in boron carbide (B_4C) reacts with neutrons to form He and Li in equal proportions. As an example 30% B^{10} depletion produces 3 w/o Li. The B_4C lattice accommodates the He and Li, but bulk swelling of the B_4C occurs as a result as shown in Figure 16. The B_4C has good high temperature strength, and since it operates at relatively low temperatures, the swelling results in significant stresses in the B_4C container. In addition a portion of the He is released producing additional gas pressure as depicted in Figure 17. The combination of these stresses with the oxygenated coolant and irradiation result in the irradiation assisted stress corrosion cracking (IASCC) of the stainless steel container. The B_4C is slowly washed out through the crack by the coolant.

The effect was first discovered during the examination of GE blades from a German BWR in 1978 and since then has been established as the mechanical life limit of BWR blades. The development of improved blades focused on better IASCC resistant steels and alloys as well as substitution of the much lower swelling rate Hf for B_4C.

3.3.1.1. ABB remedies

For mechanical life extension ABB is relying primarily on the current improved features of:

- smaller, more closely spaced absorber holes to reduce blade surface stresses
- Type 316 L steel for improved IASCC resistance.

More advanced remedies are being irradiated in assemblies to test high density (99% of theoretical) B_4C pellets as a substitute for powder.

ABB believes that standard Type 316 is satisfactory to $9x10^{21}$ nvt, which is beyond the nuclear life of $6x10^{21}$ nvt. Nevertheless, a testing program was initiated on high purity versions of Type 316 as well as various heats of the same composition. Grain boundary segregation has been studied for evidence of embrittling elements Fe, Cr, Ni, Mo, Si, O, S, and P. Work on Type 304 has shown the presence of Ni, S, and P peaks, as well as Cr depletion , at the grain boundaries. The latter effect is believed to accelerate IASCC.

3.3.1.2. GE remedies

Substitution of Hf for B_4C in high exposure positions in the Duralife series eliminates some of the B_4C swelling. This also extends nuclear lifetime. In addition, encapsulating the B_4C in the Marathon design reduces the impact of B_4C swelling on the square tubes. Increased void volume in the square tubes of the Marathon design accommodates B_4C gas release at higher exposure. Substituting Hf for B_4C obviously reduces the problems associated with B_4C.

---

[1] snvt – smeared thermal neutron fluence based on the exposure of the four fuel assemblies adjacent to the control blade of interest, units of 10^{21} n/cm^2

Crevice corrosion was believed to be the cause of cracking in original GE control blade designs, because a relatively stagnant crevice is formed in the space between the sheath and the handle. In combination with a relatively high impurity content in the coolant, the concentration factor in the crevice will accelerate corrosion. Subsequently GE revised all of their designs to eliminate locations with stagnant coolant by the modification and addition of flow holes near the sheath-to-handle weld, as well as modifying the top weld configuration. Modified lead control rods have been operating since 1986 and these changes have largely eliminated the crevice corrosion problem.

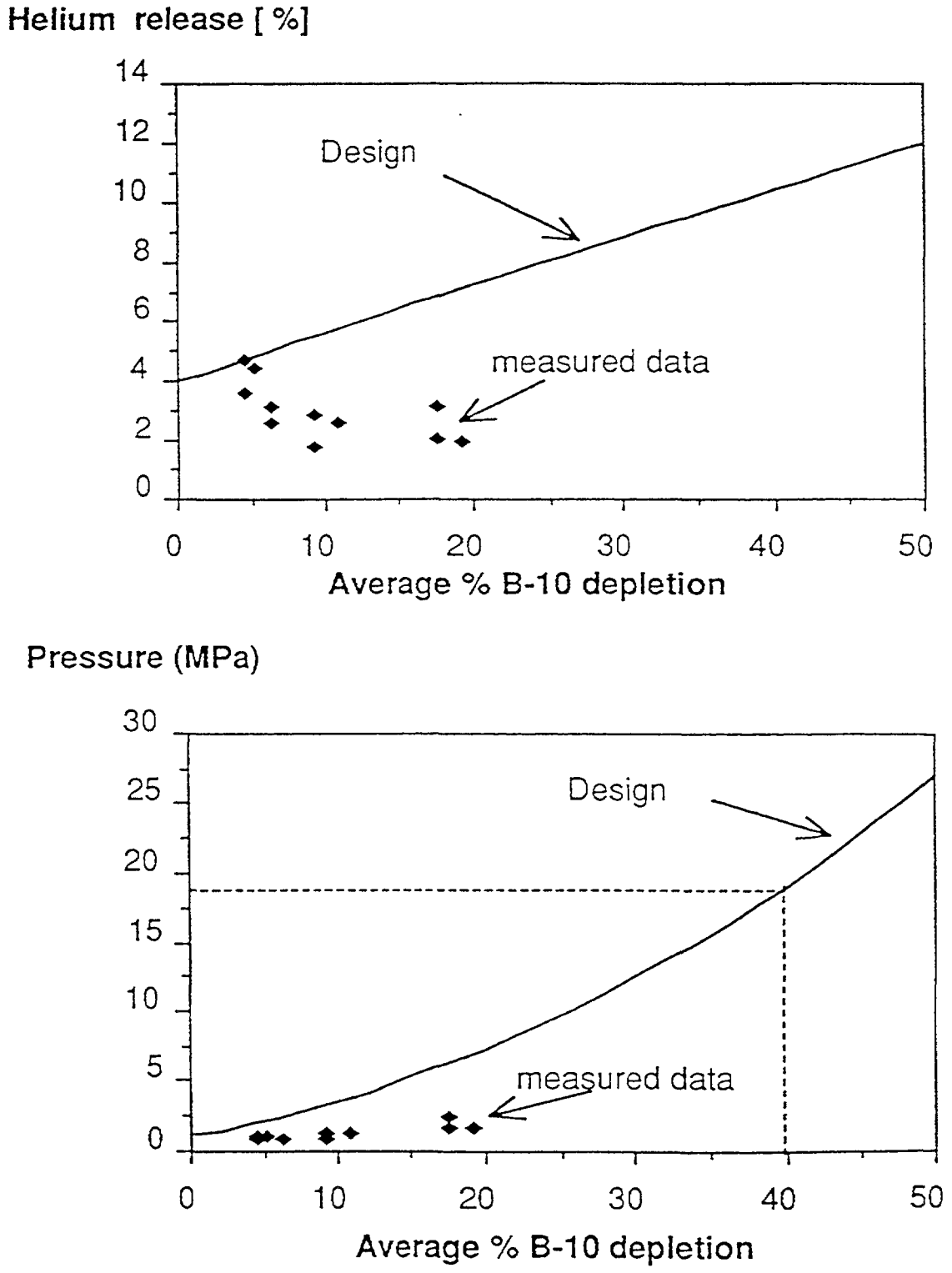

FIG. 16. ABB-Atom helium release and control blade pressure data (Reference: ABB)

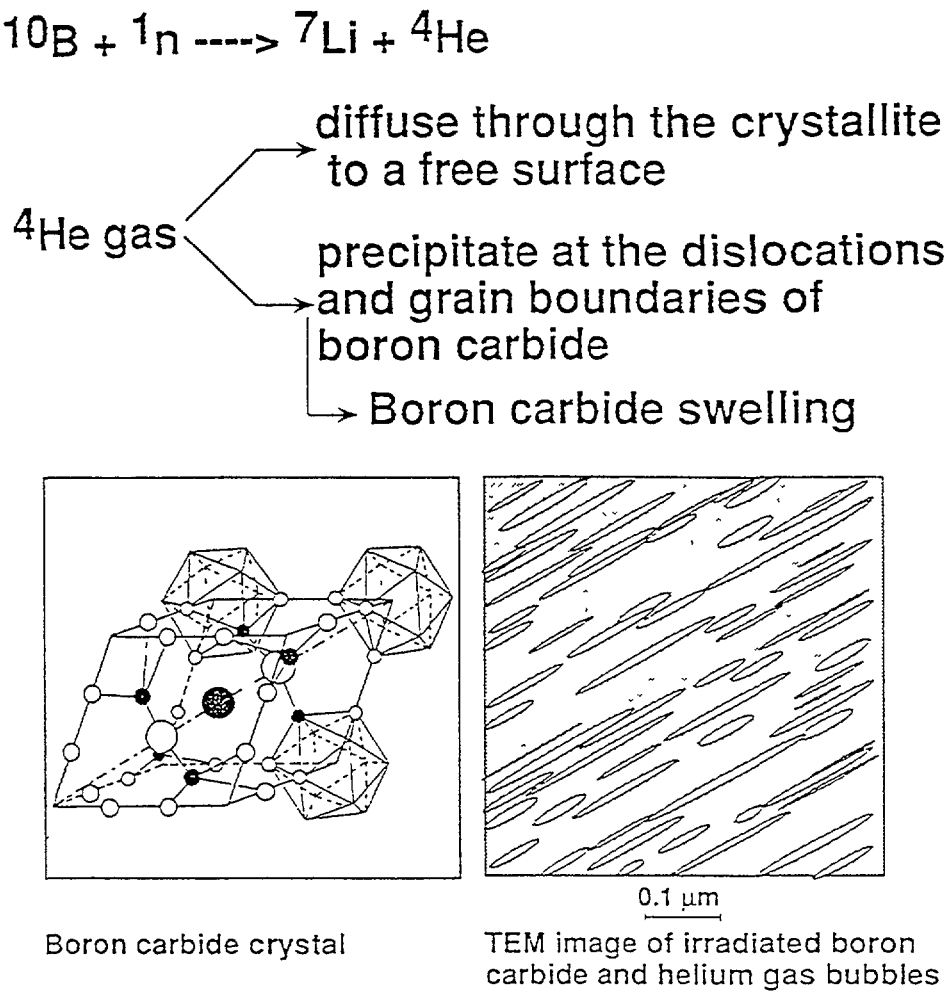

FIG. 17. Helium migration in B_4C (Reference: ABB)

REFERENCES

[1] K. Goto and Y. Sasaki, 'Countermeasures for PWR Control Rod Degradation in Japan', to be published.

[2] H. Shirayanagi, T. Fukumoto and S. Shiga, 'Advanced Control Rods for Japanese BWR Plants', to be published.

[3] Kodama et al. 'IASCC Susceptibility of Austenitic Steels Irradiated to High Neutron Fluence'. Sixth International Symposium on Degradation of Materials in Nuclear Power Systems - Water Reactors. San Diego, CA, August '93 (A Publication of TMs).

[4] S. Bruemmer et al. 'Grain Boundary Chromium Concentration Effects on the IGSCC and IASCC of Austenitic Stainless Steels'. Ibid.

[5] H. Chung et al. 'Grain Boundary Microchemistry and Intergranular Cracking of Irradiated Austenitic Stainless Steels'. Ibid.

[6] S. Kasahara et al. 'The Effects of Minor Elements on IASCC Susceptibility in Austenitic Stainless Steels Irradiated with Neutrons'. Ibid.

[7] R. Katsura et al. 'Effect of Stress on IASCC in Irradiated Austenitic Stainless Steels'. Ibid.

[8] J. Cookson et al. 'The Role of Microchemical and Microstructural Effects in the IASCC of High Purity Austenitic Stainless Steels'. Ibid.

[9] A. Jacobs et al. 'The Correlation of Grain Boundary Composition in Irradiated Stainless Steel with IASCC Resistance'. Ibid.

[10] F. Garzarolli et al. 'Deformability of High Purity Stainless Steels and Ni-Base Alloys in the Core of a PWR'. Ibid.

[11] C. Vitanza 'In Pile Test Programme in the Halden Reactor'. Ibid.

NEXT PAGE(S) left BLANK

PWR CONTROL ROD DEGRADATION AS OBSERVED IN POST-IRRADIATION EXAMINATIONS IN STUDSVIK

T. JONSSON
Studsvik AB,
Nyköping

T. ANDERSSON, L. BJÖRNKVIST
Vattenfall AB,
Ringhals, Väröbacka

Sweden

Abstract

The PWR control rodlets examined in Studsvik are of the common type with Ag-Cd-In alloy as absorber in stainless steel cladding. The main degradation mechanisms for this type of control rods are diameter increase due to absorber swelling and wear of the cladding against the components, which guide the rodlets above the core. Some examples of degradation due to these mechanisms are shown and discussed. The consumption of neutron capturing isotopes is not life-limiting for this type of control rods.

1. INTRODUCTION

Totally 19 rodlets from PWR control rod assemblies from Ringhals 2, 3 and 4 have undergone hot cell examinations to varying extents in Studsvik. The main purpose of the examinations has been to study the degradation of rodlets due to long term exposure to the reactor environment.

2. WEAR OF CONTROL ROD ABSORBER

The control rods are withdrawn from the reactor core during the main part of the reactor operation. Only the lower ends of the rodlets are exposed to a high neutron flux. The complete length of a rodlet is however exposed to the water coolant above the core. This will cause some vibration of the rodlets and wear against the different components. The observations of wear agree essentially with previously reported observations e.g. [1].

The lower ends of the rodlets are supported by the guide tubes in the top end of the fuel assemblies. Some wear of the bullet nose is normally observed in hot cell examinations (Figure 1). The wear at the lower end often extends irregularly around the complete circumference. The depth of the wear can be observed in dimensional measurements (spiral profilometry in Figure 2). The depth and extent of the wear near the lower end has in no observed case been large enough to threaten the integrity of the rodlets. It should however be observed that the wear makes the bullet nose less suitable for calibration of equipment, when dimensional measurements of rodlets are performed at a power station.

A guide region above the core also supports the rodlets. Wear occurs also in this region. A quantification of this wear can be disturbed by interference with a diameter increase in the same region due to absorber swelling. The spiral profilometry curve in Figure 3 shows wear in the lower part of a rodlet with very small diameter increase due to absorber swelling. The wear at the guide cards higher up along the rodlets is often localised to small regions and the depth of the marks can amount to a large part of the clad thickness. In one case it has been observed that the fretting at such a location has resulted in a penetrating defect (Figure 4). The spiral profilometry in Figure 5 shows the axial extension of wear at guide cards. The fretting can in some cases have a peculiar appearance, which is not easily explained by pure fretting (Figure 6). The mechanism is unknown to the examiners, but some kind of contact corrosion is suspected. The wear of the corresponding guide card has not been examined.

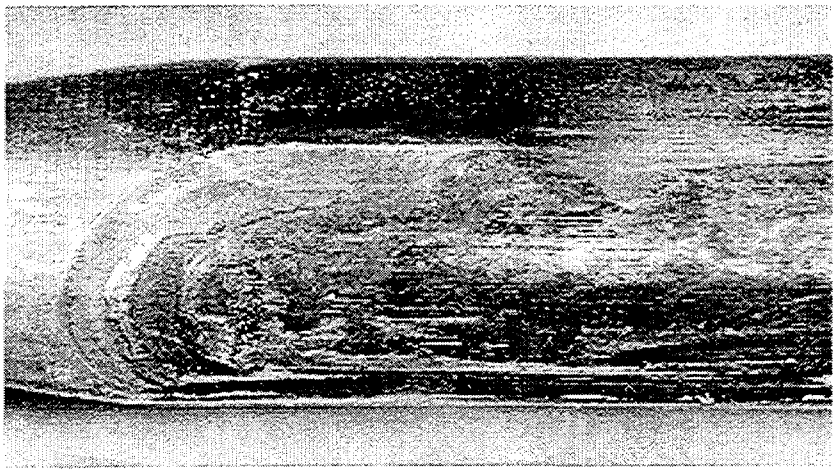

FIG. 1. Lower end of rodlet with wear

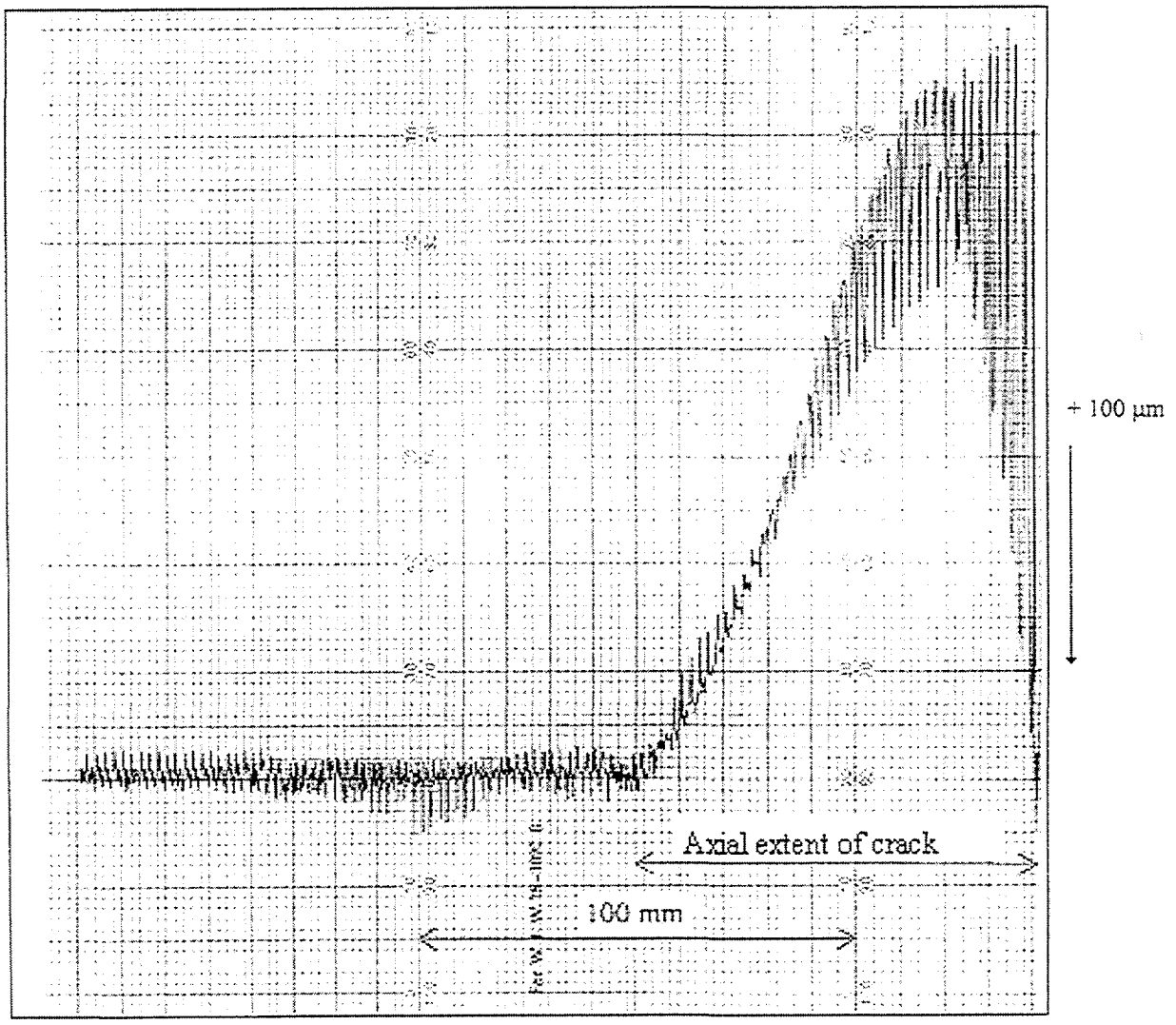

FIG. 2. Spiral profilometry of lower end of rodlet with axial crack, swelling and wear

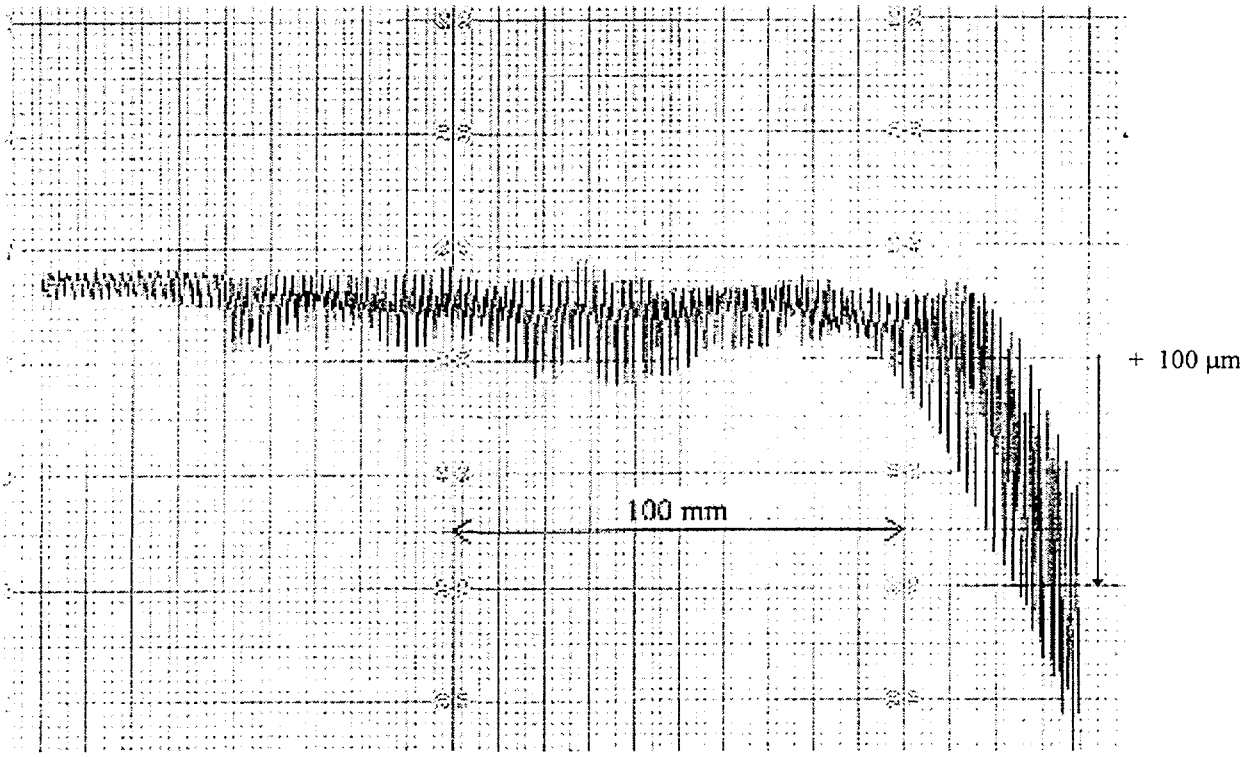

FIG. 3. Spiral profilometry of lower end of rodlet with wear but no axial crack or swelling

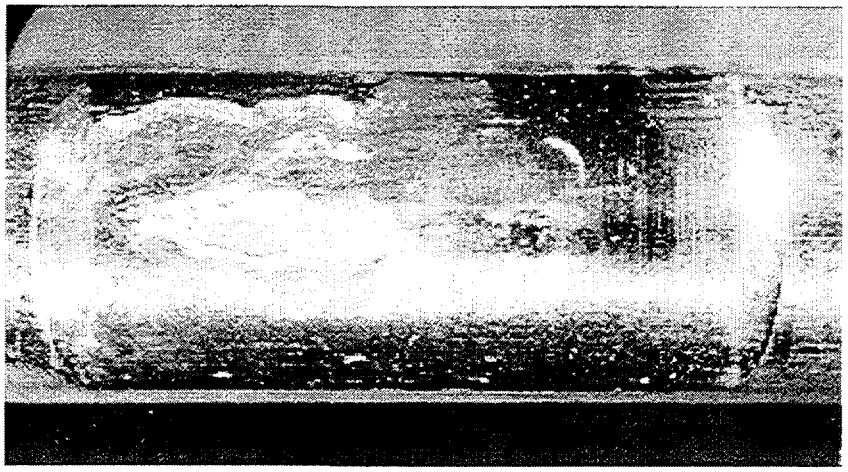

FIG. 4. Penetrating fretting due to wear against a guide card

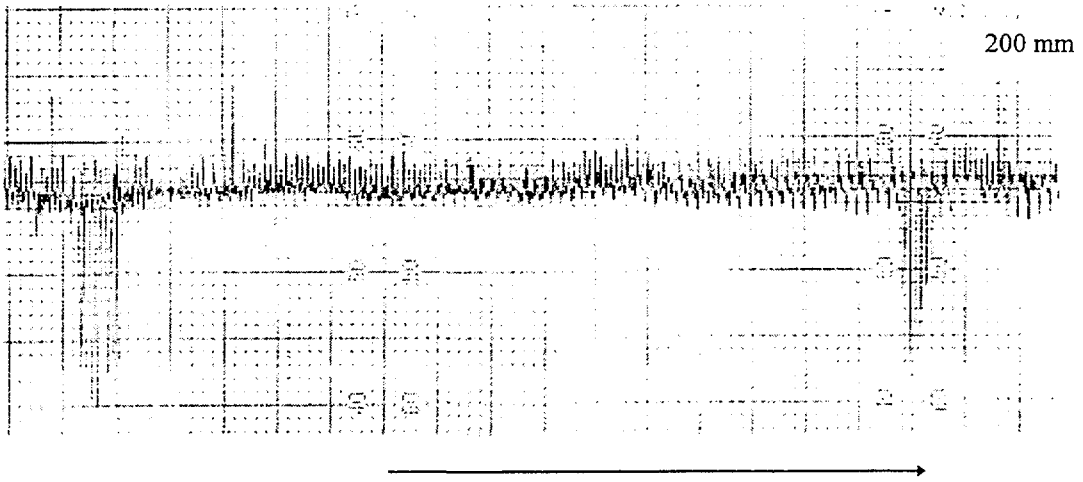

FIG. 5. Spiral profilometry showing wear against guide cards

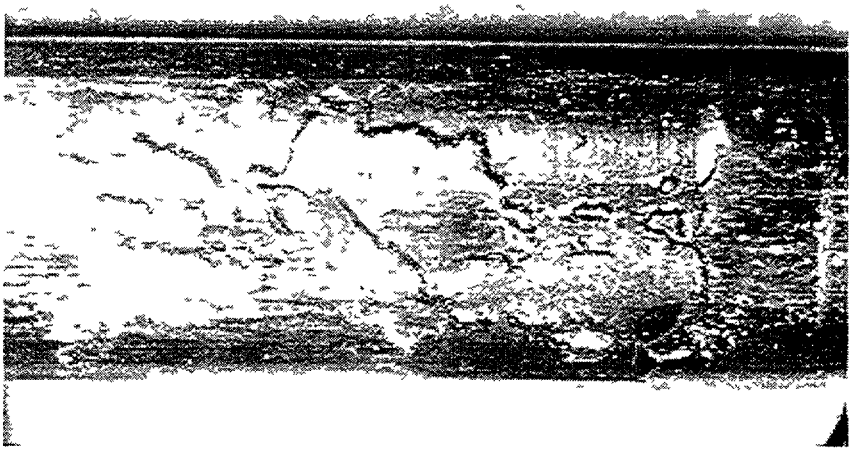

FIG. 6 Fretting due to wear against a guide card, irregular shapes due to contact corrosion and/or material loss in both rodlet and guide card

3. SWELLING OF ABSORBER

Gamma spectrometry measurements confirm that the neutron dose received by the control rodlets has a very steep axial gradient (Figure 7). The swelling of the absorber increases with increasing dose. The swelling should consequently be largest at the end of the absorber. The maximum diameters however, occur about 30-60 mm from the ends of the rodlets. An important factor for an explanation of this phenomenon is the plasticity of the absorber. The axial cut shown in Figure 8 shows that plastic deformation of a swelling Ag-Cd-In absorber can occur The Ag-Cd-In absorber has been extruded out into the open space between the end plug and the cladding The free space in the lower end of the rodlet and the deformation of the absorber will result in a delayed increase of the outer diameter of the rodlet. More free space in the lower end of the rodlet will therefore increase this delay

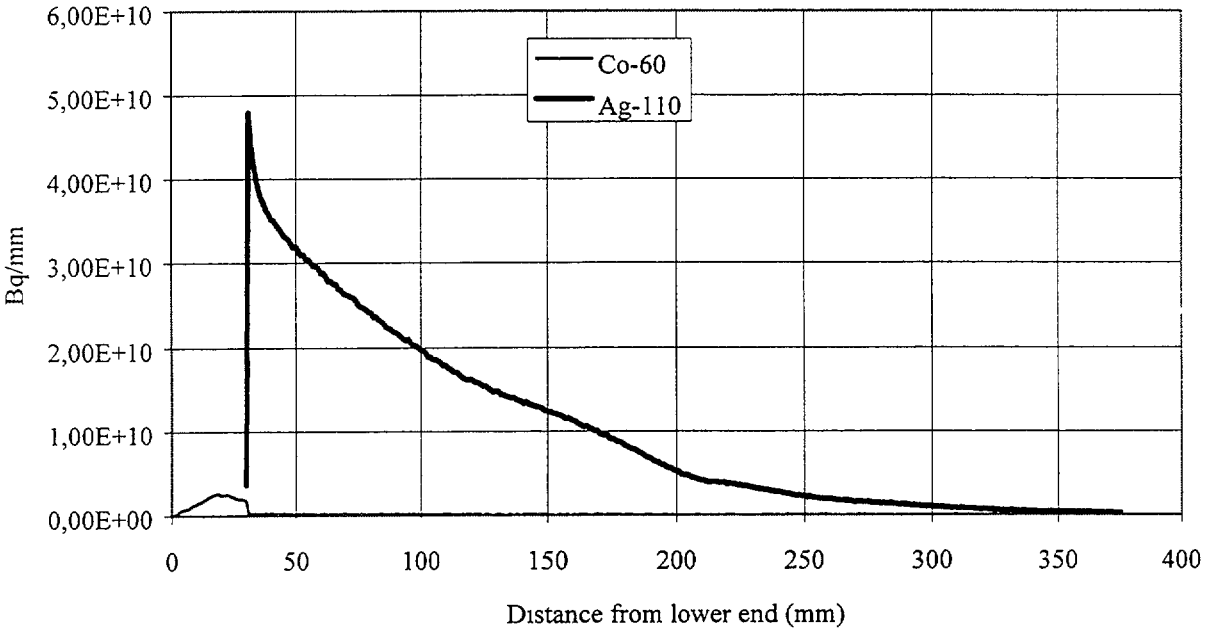

FIG 7 Gamma measurement showing Co-60 activity in end plug and Ag-110 activity in absorber

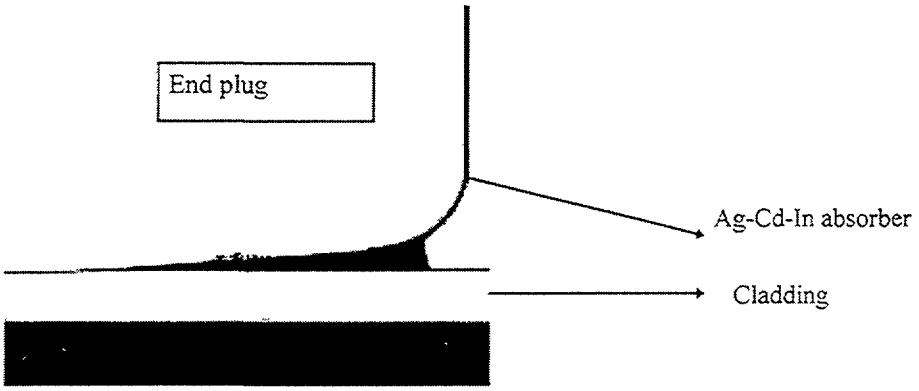

FIG. 8. Metallography; Axial cut through end plug and absorber

4. DIAMETER INCREASE OF RODLETS

Significant diameter increases of rodlets have only been measured for rods with axial cracks in the cladding. Typical examined defect rodlets have axial cracks only on one side of the rodlets. It is evident that a starting crack will decrease the stress in other parts of the circumference. In most cases there is only one axial crack. Inspection of the outside of the rodlets shows in some cases irregularities in the propagation of the axial cracks (Figure 9). The propagation fronts of the axial cracks extend further on the inner than on the outer side of the cladding. The observed short interruptions in the cracks can be interpreted as due to branching during axial growth of the cracks. Without evident experimental proof it is suspected however, due to the environmental conditions, that the cracks start from the outer side of the cladding. The observations but not the conclusions agree with published data [2]. The geometry of the crack in Fig. 10 supports that the crack at that axial position has propagated inwards. Examinations of the propagation of cracks has been performed within an EPRI project [3]. The presented results illustrate the axial variation of the cracks, but the authors of the EPRI report do not conclude whether the cracks start from the inner or outer surface of the cladding.

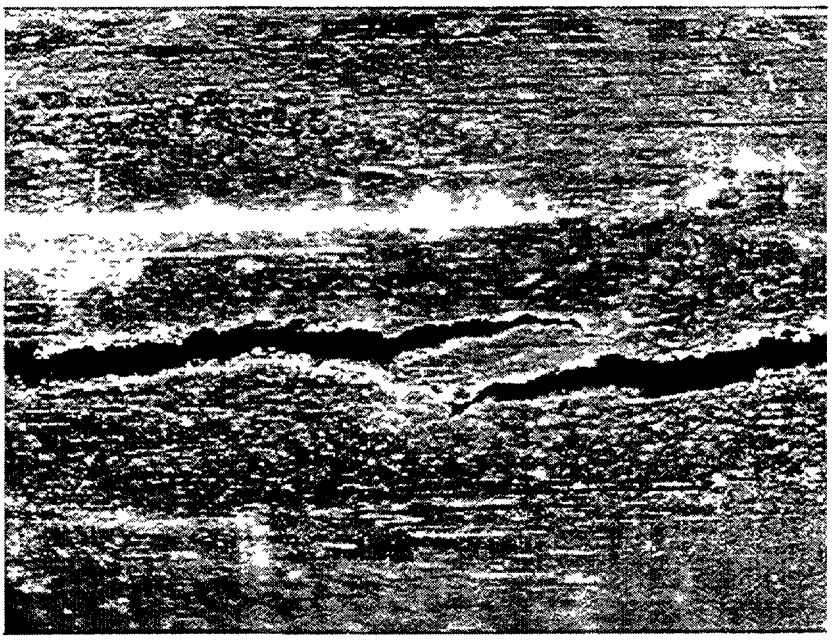

FIG. 9. Optical photo of rodlet, showing irregularity in axial crack

The diameter increases can be estimated with reasonable accuracy from the size of the opening of the cracks. The difference between measured diameter increase and diameter increase calculated

from the crack width corresponds to a uniform strain of 0,1-0,6 %[1]. The cross section in Figure 10 shows thinner cladding at the position of the crack. This may be caused either by local deformation or by thinning due to wear. Wear of the cladding may be a mechanism for localising axial cracks to one part of the circumference of the cladding.

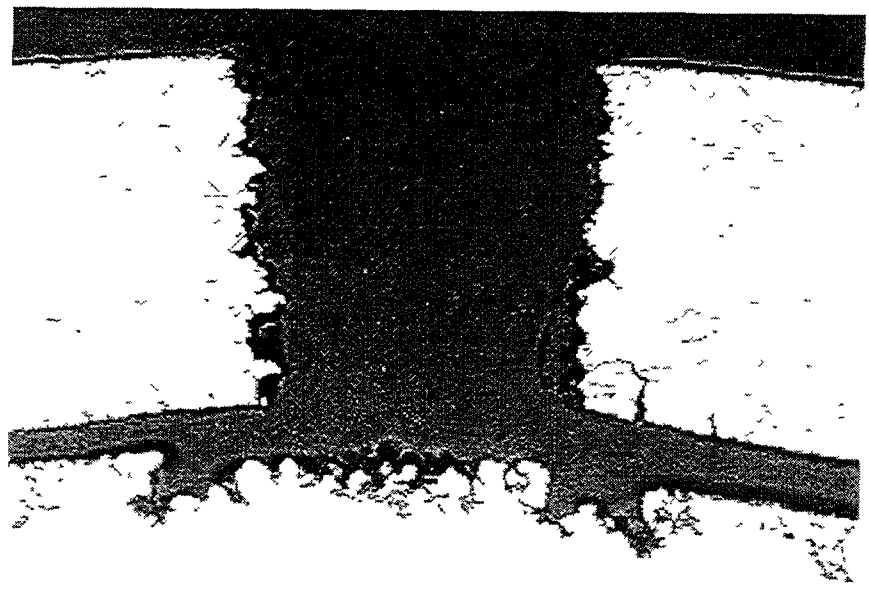

FIG 10. Metallography; Transverse cut through axial crack in the cladding

The content of hydrogen can influence the mechanical properties of stainless steel. The composition and amount of gas was measured inside one intact rodlet. The gas pressure at room temperature was 1.4 bar and 86 % of the gas was hydrogen. It seems likely that hydrogen diffuses fairly quickly through the cladding material at reactor temperature and that the measured hydrogen content corresponds to an equilibrium pressure with the reactor coolant.

The correlation between the axial extent of the cracks and the diameter increase is weak. Among the rodlets examined in 1997, there were several rodlets where the axial cracks extended downwards below the Ag-Cd-In absorber. The axial cracks were in several of these cases divided into two branches at the lower end (Figures 11 and 12). The increases of the diameter were also larger in these cases and it is evident that the resistance of the cladding will be smaller in such cases The fast swelling at the tip of the absorber results more directly into a diameter increase with less plastic deformation of the absorber. The branching of the crack will consequently result in a larger diameter increase of the rodlets per reactor cycle.

5 CORROSION OF ABSORBER

One cross section of a defect rodlet was examined. The material loss from the absorber was small in the studied cross section. There was some material loss close to the crack in the cladding and some intergranular corrosion at the surface of the absorber (Figure 10). A microprobe examination showed that Sn, which is formed by transmutation from In, is inhomogeneously distributed in the material and Sn is probably concentrated to grain boundaries in the absorber.

6. DISCUSSION

From the examinations it is concluded that the diameter increase of control rodlets without cracks is very small. The swelling of the absorber results in cracks in the cladding starting about 40-

[1] The calculation assumes that all deviations from the maximum diameter are due to wear and that the maximum diameter is unaffected by wear. The strain may be smaller than calculated if the ovalisation is mainly caused by deformation and not by wear.

50 mm from the lower end of the rodlets. The rate of the diameter increase is probably determined by the average swelling along some cm length of the absorber. If the irradiation of the rodlet continues there is some danger that the crack propagates below the lower end of the absorber and divides into two branches. The resistance of the cladding against absorber swelling will then be much smaller and the continued diameter increase is probably determined by an average swelling rate of only some mm of length at the tip of the absorber.

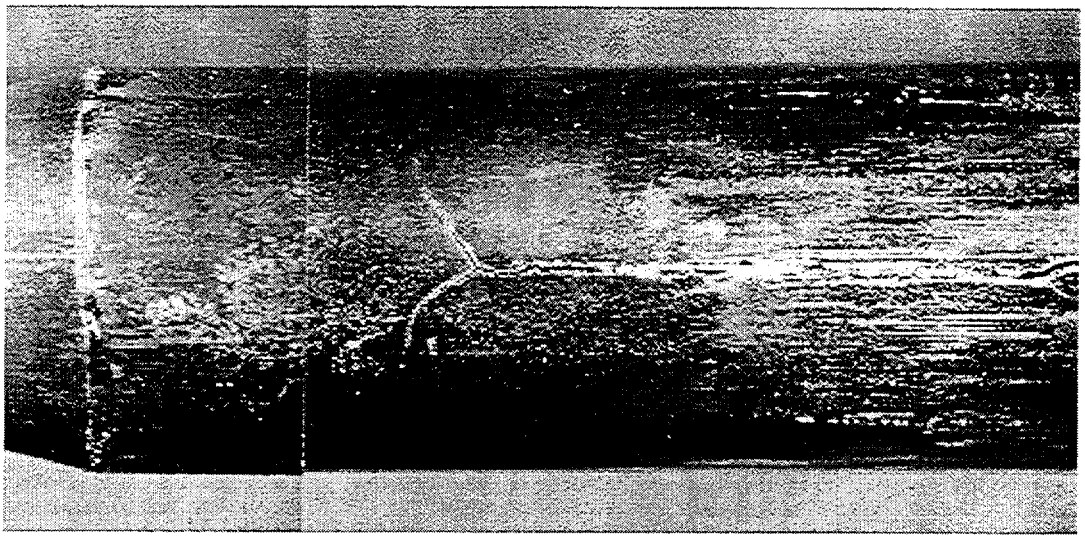

FIG. 11. Axial crack with branches in the lower end

FIG. 12. Axial crack with branches in the lower end

REFERENCES

[1] DE PERTHUIS, S., RCCA's Life Limiting Phenomena: Causes and Remedies, (Proc. Technical Committee Meeting on Advances in Control Materials for Water Reactors, Vienna, 29 Nov. to 2 Dec. 1993), IAEA-TECDOC-813, Vienna (1995) 61-78.

[2] MATSUOKA, T., et al., J. Nucl. Sci. Technol., **35**, (August 1998) 564-578.

[3] SIPUSH, P. J., et al., Lifetime of PWR Silver-Indium-Cadmium Control Rods, NP-4512, (March 1986).

STATUS OF CONTROL ASSEMBLY MATERIALS IN INDIAN WATER REACTORS

V.G. DATE, P.G. KULKARNI
Bhabha Atomic Research Centre,
Trombay, Mumbai,
India

ABSTRACT

India's present operating water cooled power reactors comprise boiling water reactors of Tarapur Atomic Power Station (TAPS) and pressurized heavy water reactors (PHWRs) at Kota (RAPS), Kalpakkam (MAPS), Narora (NAPS) and Kakrapara (KAPS). Boiling water reactors of TAPS use boron carbide control blades for control of power as well as for shut down (scram). PHWRs use boron steel and cobalt absorber rods for power control and Cd sandwiched shut off rods (primary shut down system) and liquid poison rods (secondary shut down system) for shut down. In TAPS, Gadolinium rods (burnable poison rods) are also incorporated in fuel assembly for flux flattening. Boron carbide control blades and Gadolinium rods for TAPS, cobalt absorber rods and shut down assemblies for PHWRs are fabricated indigenously. Considerable development work was carried out for evolving material specifications, component & assembly drawings, and fabrication processes. Details of various control and shut off assemblies being fabricated currently are highlighted in the paper.

1. INTRODUCTION

Reactor control systems and reactor shut down systems are the most important engineering safety systems of any reactor. The first man made reactor CP-1, in 1942, had the manual shut down system called SCRAM-Safety Control Rod Accelerated Movement – to protect the reactor from over power [1]. The 1st generation of pressurized heavy water power reactors (PHWRs) use moderator level control and moderator dumping for control and shut down of reactor. Since then lot of technological developments have taken place to improve the reactor control and shut down systems. New and improved designs, materials, fabrication techniques, advancements in reliability analysis, instrumentation and control all have contributed to the present reliable and safe control and shut down systems in various power reactors.

The current meeting is aimed at reviewing mainly the material aspects of control and shut down assemblies used in water-cooled power reactors and the behaviour of the materials under normal operating conditions. An attempt is made in the following paragraphs to present a status of the control assemblies used in Indian water cooled reactors with respect to materials used, fabrication techniques used in assemblies and operational experience. The absorber materials used in these assemblies are B_4C, Cd sandwiched tubes, boron steel, Co absorbers and gadolinium rods.

2.1. Control blades used in Tarapur Atomic Power Station (TAPS)

Tarapur Atomic Power Station (TAPS) consists of two General Electric (GE) BWR units, which are one of the oldest operating in the world. TAPS went into commercial operation in 1969 and has so far completed 29 years of safe and economic commercial operation logging 58 years of valuable reactor operation experience.

Manoeuvring of the reactor power and reactor shut down is carried out by inserting/withdrawing control blades from reactor core with the help of control rod drive (CRD) mechanism. There are 69 control blades, which are still operative, in each of the TAPS reactor. All control blades enter the core from the bottom. Bottom entry of the control rod has the following advantages:

(a) It provides axial flux shaping for greater fuel economy;

(b) The drives do not interfere with off-line refuelling operation in which the reactor vessel is to be removed for the access of the core.

2.2. Description of control blade

Control blade is 4 M long assembly and consists of sheathed cruciform array of stainless steel tubes filled with Boron carbide (B_4C) powder. The main structural members of the blade (Fig.1) consist of the two end castings of 304L grade stainless steel; the top incorporating a handle and the bottom incorporating drive connecting hub, a central hollow cruciform bar and 4 U shaped tube sheaths. There are 17 poison rods containing B_4C powder, in each wing of the cruciform and they are encased in U shaped stainless steel sheaths. The TIG welding of the end castings to the central cruciform bar and the spot welding of the U sheaths onto the arms of the cruciform bar provide a rigid structure to the blade. Spherical rollers are provided in the top castings, for movement of the blade in between fuel channels and disc shaped rollers are provided in the bottom casting for movement inside the guide tube.

A shaft passes through the central hole in cruciform bar to the bottom of which a spring loaded lock plug is attached. By means of the handle in the top casting the lock plug can be operated from the top of the reactor for latching and delatching of the blade from the control blade drive.

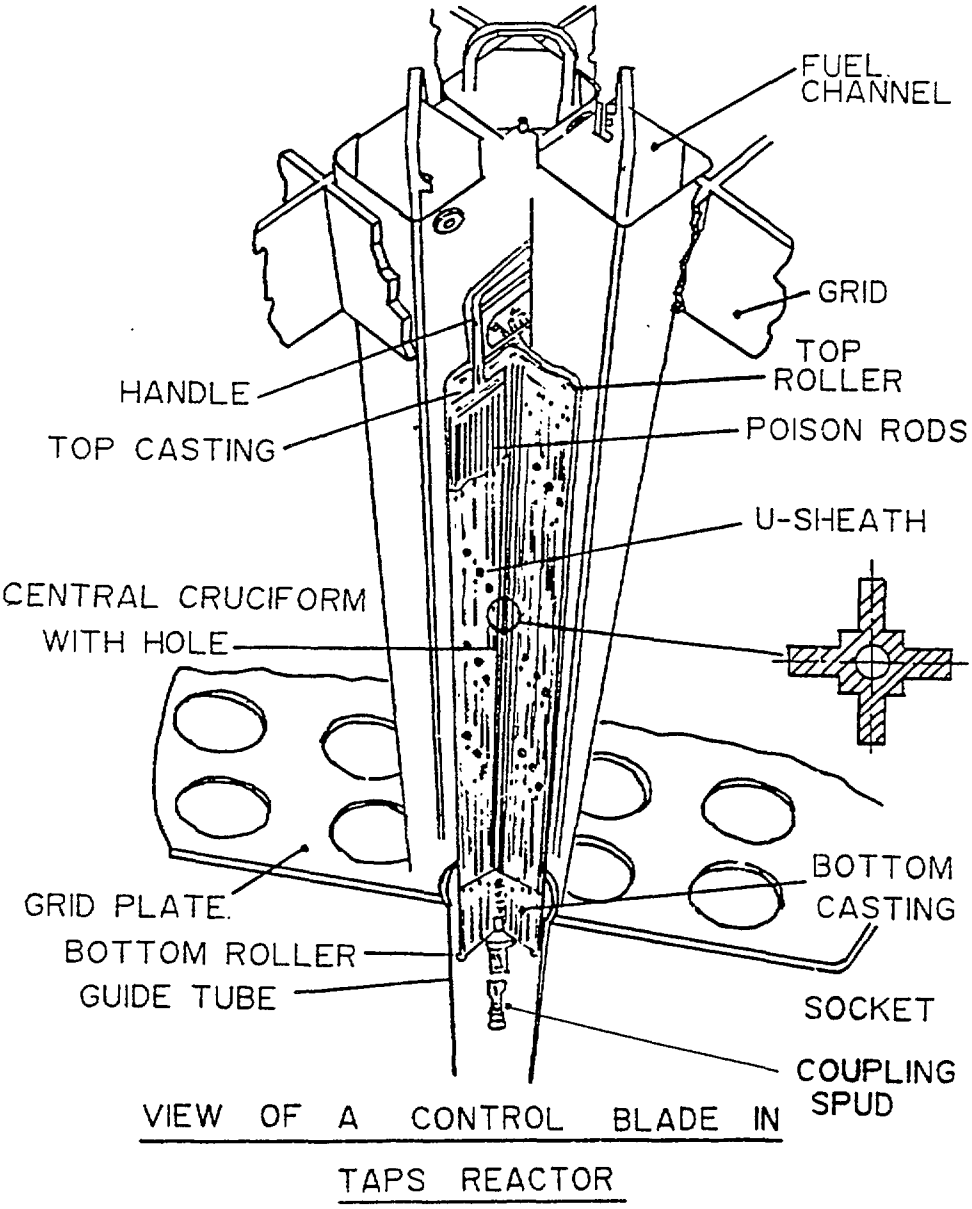

FIG. 1. View of a of control blade in TAPS reactor

2.2.1. Poison rod

Each poison rod is a small diameter (4.7 mm OD x 3800 mm L x 0.63 mm WT) stainless steel 304 L grade tube containing boron carbide powder and welded with end plugs at both ends. Fig. 2 shows a typical poison rod. Boron carbide powder is packed to the required density (65 to 75% of T.D) by vibro compaction. The powder is confined longitudinally into several independent compartments by crimping over steel balls located inside the tubes at regular intervals. The purpose of this compartmentalization is to avoid the densification of B_4C in bottom due to vibrations in operation and avoiding forcing of B_4C to top by deceleration forces. Fig. 3 gives flow-sheet for the fabrication of poison rods.

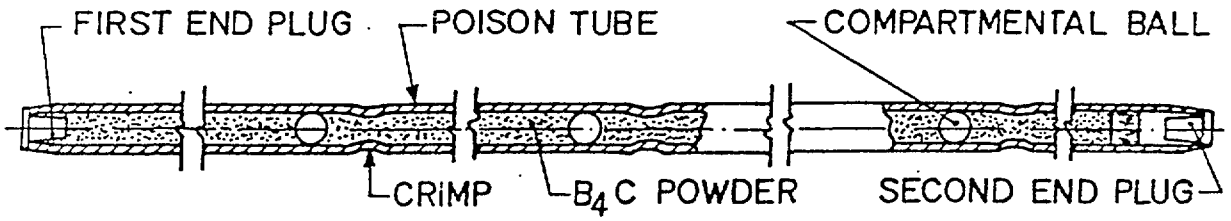

FIG. 2. Poison rod

2.3. Development of materials & fabrication technology

Considerable development effort had been put in for the indigenous fabrication of control blades. The most important task was to generate detailed specifications and fabrication drawings for the components. Extensive development work has also been carried out for standardizing fabrication parameters like vibro compaction of B_4C, TIG welding of end plugs in Argon & Helium, spot welding of sheaths and assembly of blade. Special fixtures were designed and fabricated for B_4C filling and welding of assembly. Fig. 4 shows a flow-sheet for the fabrication of control blade. The prototype blades were tested successfully in out-of-pile tests and then loaded in reactor. Subsequently about 35 blades have been made so far towards requirements of replacement of blades in TAPS reactors.

2.3.1. Boron Carbide Powder

Natural Boron Carbide powder is used in the blades. The main specification for the powder are given in Table I. The boron carbide powder is prepared by reacting boron anhydride with carbon at high temperature in a graphite resistor furnace [2]. Boron carbide is formed as dense crystalline chunks which are subsequently ground to powder and graded into different size fractions. A special leaching treatment is given to the powder to control the B_2O_3 and moisture content within specified limits. The powder of 3 size fractions viz. – -16 + 20 mesh, -60 + 80 mesh and –200 + 325 mesh in the proportion of 40:20:40 gives the required tap density of 1.7 gm/cc. Fig. 5 gives a sketch of graphite resistor furnace used for production of Boron carbide and Fig. 6 gives flow sheet for the production of Boron Carbide. B_4C is capable of soaking large volumes of hydrogen which can be released upon irradiation. It is therefore prudent to prevent absorption of H_2 by B_4C. B_4C powder is dried at 200 C for 2 h before filling into tubes and B_4C filled tubes are degassed at 200 C for 8 h before II end plug welding.

2.3.2. Other materials in control blades

The majority of components of the blade except the rollers and pins in top and bottom castings are made out of stainless steel grade 304L. L grade is used to avoid sensitization during welding. For rollers, so far stellite-3 alloy was used and for pins Haynes alloy-25 was used. It is now proposed to

TABLE I. MATERIALS SPECIFICATION FOR BORON CARBIDE POWDER

1. Chemical analyses	boron	76.5% minimum
	boric anhydride	0.1% maximum
	iron	0.8% maximum
	titanium	0.1% maximum
	total chlorine and fluorine	100 ppm maximum
	cobalt	50 ppm maximum
	copper	100 ppm maximum
	manganese	100 ppm maximum
	sodium	100 ppm maximum
	carbon	remainder
2. Boron isotopic content	the boron shall be of natural isotopic content, i.e. 19.6 ± 0.3 at. % B^{10}	
3. Particle density	the material shall have an average particle density of not less than 2.38 g/cm^3 (95% of the theoretical density)	

change to inconel X-750 alloy for rollers and PH-13.8 Mo alloy in H-1100 condition, for pins, in view of the high radioactivity build up due to Co-60 while using of Co base stellite & Haynes alloys. Similar replacements have been incorported by GE [3].

2.4. Control rod drive mechanism

The basic drive mechanism is a double acting mechanically latched, hydraulic cylinder using reactor feed water as operating fluid. The use of reactor feed water as operating fluid eliminates the need for special hydraulic system. The drive uses simple piston seals with leakage into the reactor

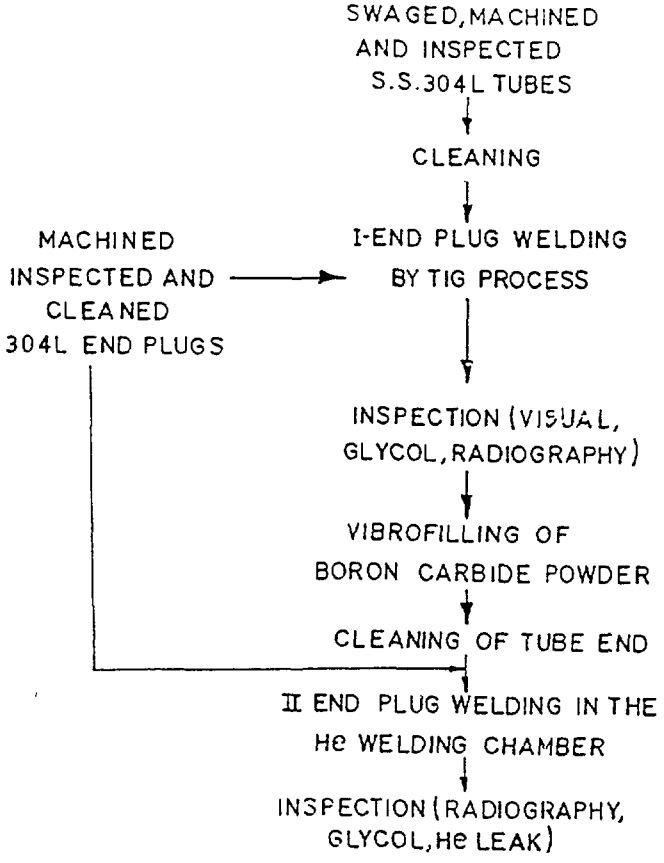

FIG. 3. Flow sheet for fabrication of poison rod

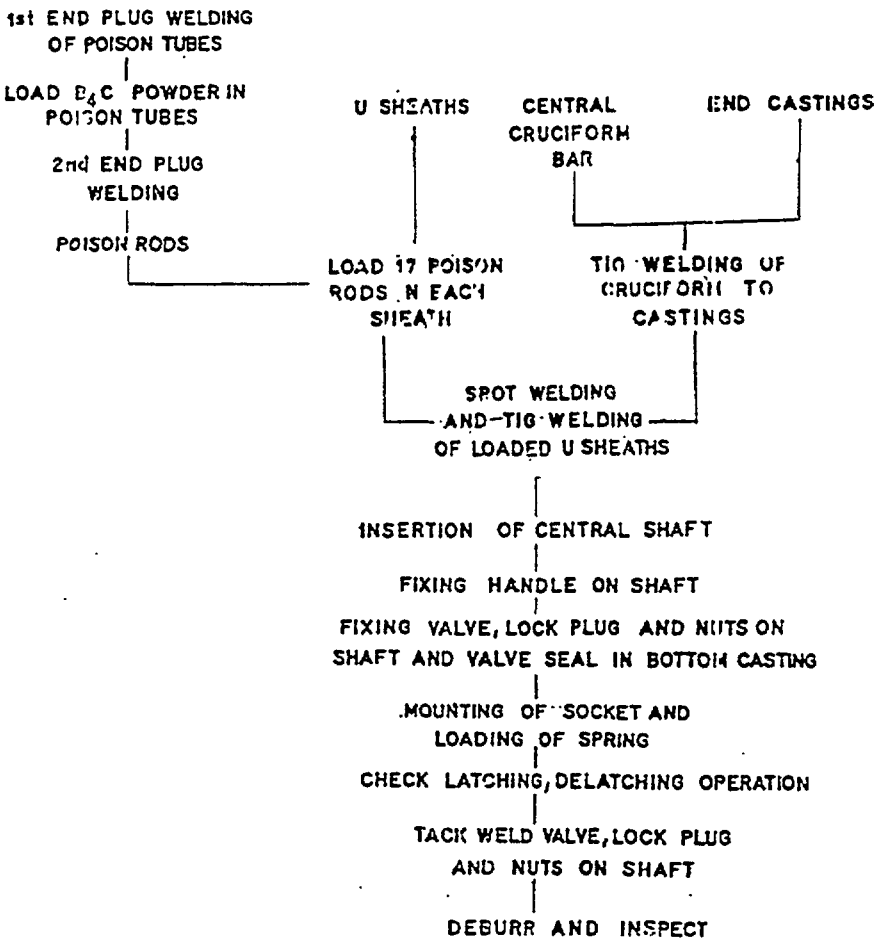

FIG. 4. Flow sheet for control blade fabrication

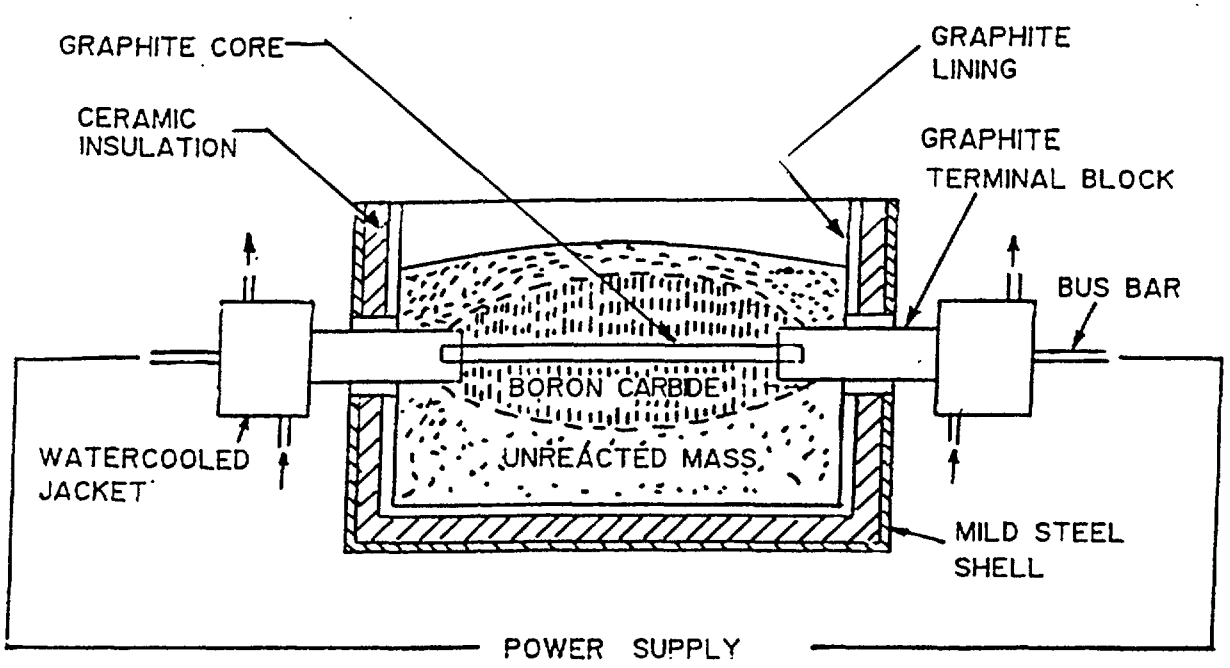

FIG. 5. Graphite resistance furnace used for the production of boron carbide

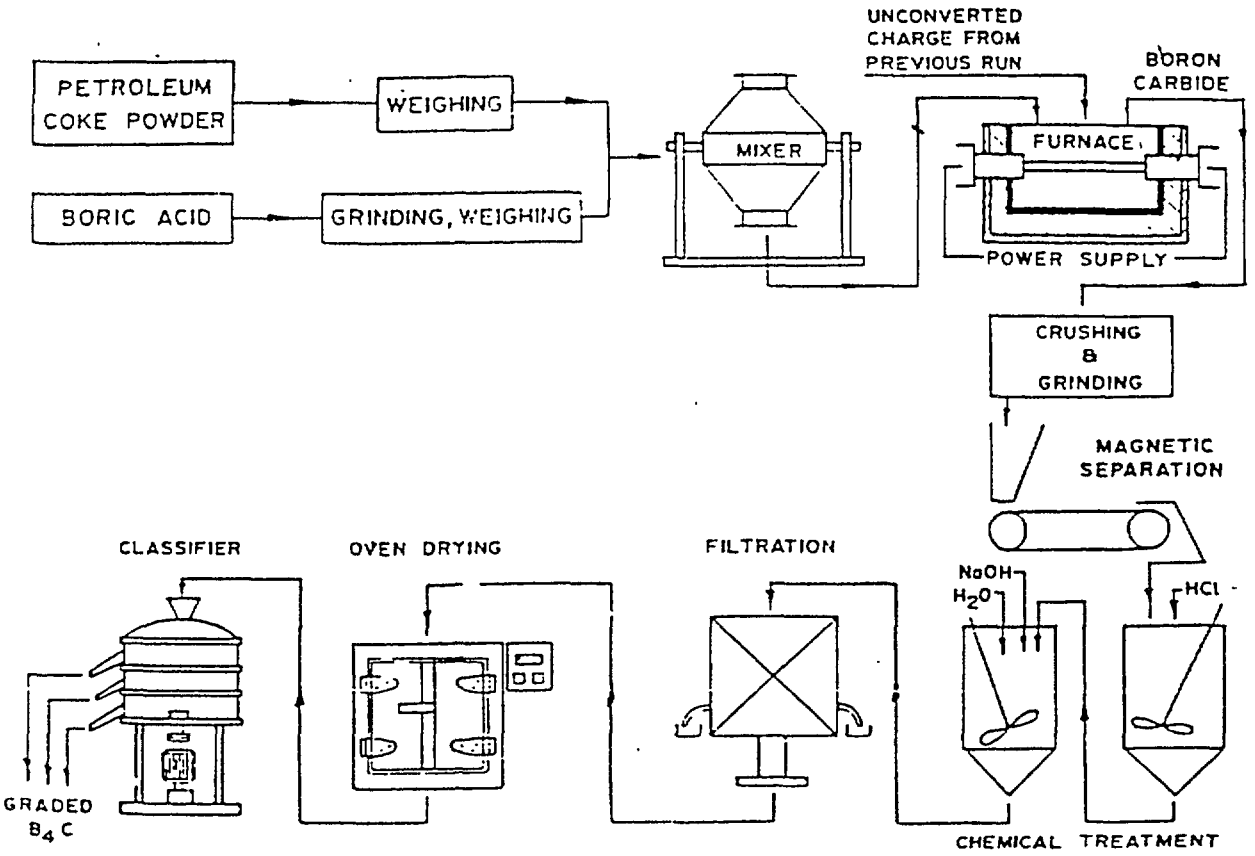

FIG. 6. Flow sheet for the production of boron carbide

minimizing contamination and helping to cool the mechanism. The drive is capable of inserting and withdrawing the control rod at a slow, controlled rate as well as providing rapid insertion in an emergency condition. The hydraulic fluid to control rod drive system for its rapid insertion on a scram signal is supplied from three redundant sources:

- The stored energy in the accumulator;
- High pressure CRD hydraulic system; and
- Reactor pressure itself.

With this arrangement, during total loss of power (TLOP) to the station all the 69 control blades get inserted into the reactor core within the required time by stored energy in the accumulators, failing which by the reactor pressure itself. Control rod drives are replaced in following conditions:

- After 10 years of service;
- When the drive is having persistent high temperature problem;
- When the drive is not moving on application of normal hydraulic pressure.

2.5. Operational experience with boron carbide control blades

Right from the commissioning of TAPS units in 1969 till 1996 TAPS Unit I has experienced 152 scrams and unit 2 has experienced 109 scrams, because of system transients and loss of power to the station. It was seen that the reactor could be brought to safe shut down sub-critical state by fast acting shut down mechanism alone, without necessitating slow acting liquid poison system to actuate [4]. For cooling control rod drive seals continuous cooling water of highest purity is maintained through mini-filters of 25 microns with 99% efficiency. This is to prevent damage of seals due to high background temperatures. During the operation of the reactor, control rod high temperature, problem

appears to be due to clogging of the mini-filters. Rectification of high temperature problems is carried out by isolating the drive and replacing the mini-filters. Clogging of the mini-filters also poses problems in controlled movement of the control blades in/out of the core. It may be noteworthy that the design of CRD system does not jeopardize the fast acting reactor shut down mechanism function even with a clogged mini-filters.

During the operation of last 28 years no failures have been observed with regard to materials of control blades. Problems such as swelling under irradiation and reaction with stainless steel at high temperatures have been reported for boron carbide in literature [5]. No boron contamination has been observed in water samples taken at regular intervals confirming that there are no gross defects in any of the poison rods.

No PIE has been carried out so far for any of the control blades removed from reactors after completing design life which is based on 10% reduction in control worth or 34% reduction in boron[10] content.

3.0. CONTROL & SHUT DOWN ASSEMBLIES FOR PHWRs

3.1. Control assemblies

India has operating pressurised heavy water power reactors each of 220 Mw(e) capacity at Kota (RAPS), Kalpakkam (MAPS), Narora (NAPS) & Kakrapara (KAPS).

Basically for the control of reactivity in PHWRs three types of devices are provided (Fig. 7). Regulating rods (RRs) or central adjusters for adding and removing reactivity quickly (± P), the absorber rods or corner adjusters (ARs) which are provided to add positive reactivity (+P) for

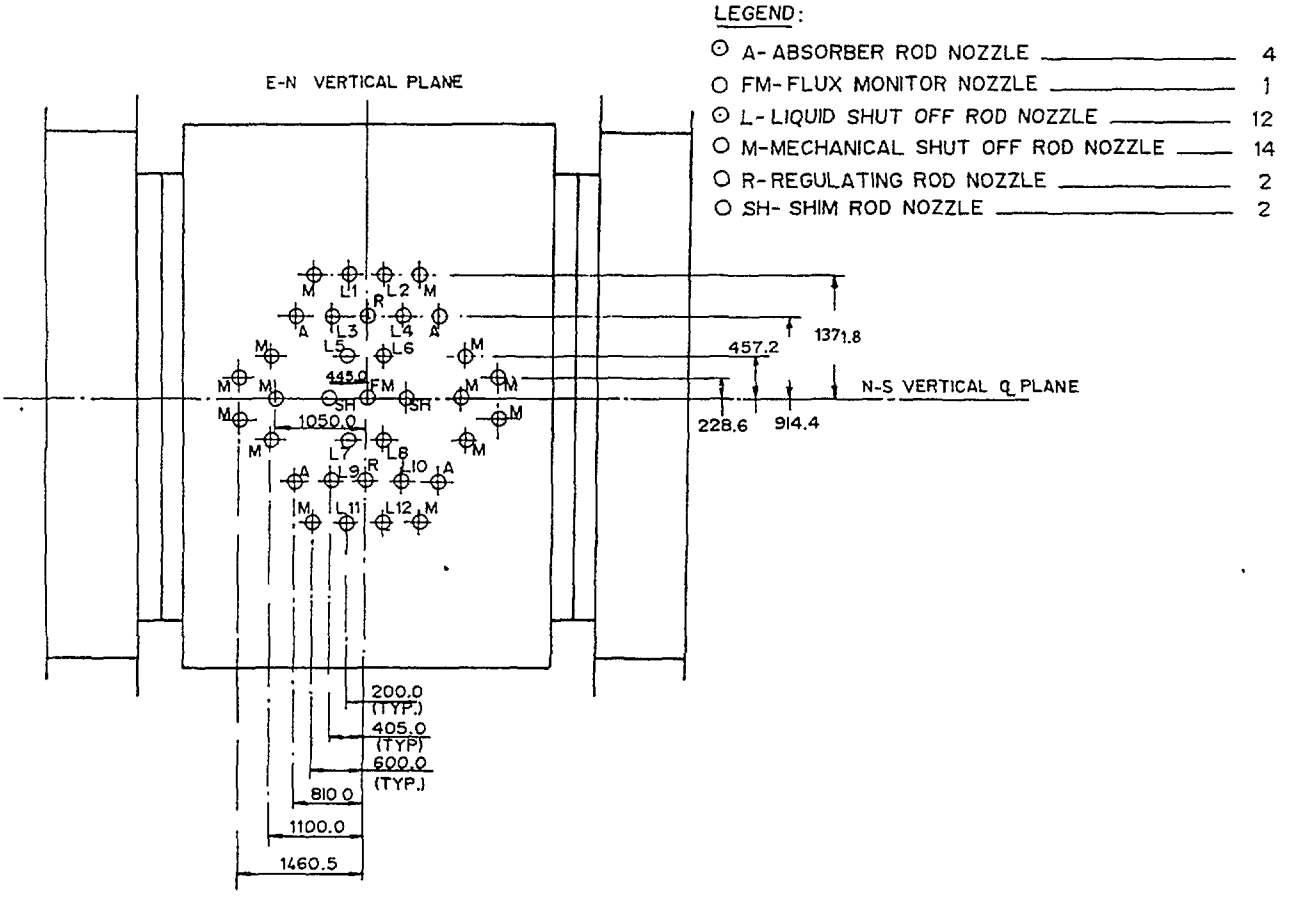

FIG. 7. Location of reactivity control devices in PHWR

providing xenon override following a trip or to compensate the daily burn-up load in the case of non availability of fuelling machine and shim rods (SRs) for providing backup to regulating rods in bringing negative reactivity (-P) for power set back or step back [6]. In RAPS & MAPS the set back action is done by moderator level control while in other PHWRs it is done by shim rods (SRs). Normally RRs are kept partially IN (about 80% IN) and on AUTO control. The ARs are kept fully IN on manual control with a mechanical stopper called ratchet which prohibits withdrawal. The SRs are always kept on auto control outside the core. If they enter the core for any set back action for more than 10 seconds they are pushed back by addition of about 1 mk equivalent of boron added by the chemical boron addition system [Control Addition Mode (CAM) system]. All these control devices are fully inserted on any trip signal.

In 500 MWe PHWRs the first units of which are coming up at Tarapur, the three control actions are respectively done by the Light water zonal power control system consisting of 14 zonal control compartments (ZCCs), 17 adjuster rods and four control rods (CRs).

3.1.1. Control assembly materials & fabrication

3.1.1.0. Absorber rods or corner adjuster rods

Cobalt assemblies are used as absorber rods at corner locations of the regulating system of PHWRs. However stainless steel assemblies can also be used at these locations. Eight absorber assemblies, 2 each in the 4 corner positions, provide about 11 mk reactivity increment to override xenon for approximately 30 minutes after shut down from full power equilibrium operation of the reactor. Another purpose of the cobalt absorbers is to produce Co-60 isotope in the form of Co slugs of specific activity 50 curies/gram or in the form of pellets of specific activity 200 curies/gram.

Each absorber assembly consists of 4 sub assemblies mounted on a central support tube with retention support assembly at top. There are 6 elements per slug sub assembly and 8 elements per pellet sub assembly. Each element contains 15 cobalt slug or 3 pellet capsules encapsulated in aluminium.

3.1.1.1. Encapsulation

Considering the end use and design requirements, Co slugs and pellets are to be encapsulated with Al as cladding. The stringent specifications stipulated for slug/pellet capsules are:

i. The capsule should be made as per close dimensions;
ii. Seal welds should be defect free;
iii. There should be intimate mechanical contact between the cobalt slug and the cladding material;
iv. The space in the pellet capsules should be filled with He gas. Specifications for cobalt & aluminium to be used in absorber assemblies are given in Table II.

After several trials encapsulation routes were standardised to get acceptable slug/pellet capsules. The main steps in fabrication of these assemblies are given in Figures 7 & 8.

3.1.1.2. Cobalt elements

A slug element contains 15 Co slug capsules and pellet element contains 3 pellet capsules clad in zircalloy-2 tubes. The capsule-element inter-space contains He gas. For the fabrication of Co elements, resistance welding technique under He cover gas proved successful.

After fabricating the elements, the elements were autoclaved in steam at about 400°C and 53 Kg/cm^2 pr. for 10 hrs. Radiographic examination of these elements revealed collapsing of pellet capsules and the analysis of fill gas showed hydrogen as the major content in pellet capsules and also in element/capsule inter-space.

TABLE II. SPECIFICATIONS FOR COBALT AND ALUMINIUM USED IN COBALT ABSORBER ASSEMBLIES

Cobalt	Cobalt material for the manufacture of slugs and pellets shall be of a high quality suitable for irradiation	
	Chemical composition shall be as follows	99.8% minimum
	cobalt	0.15 maximum
	nickel & iron	0.01 maximum
	other impurities	0.15 maximum
	gases	
	Material density shall be	8.4 g/cc minimum
Aluminium	The aluminium alloy material to be used for the encapsulation of cobalt pellets and slugs shall be indal-is or equivalent having the following mechanical properties	
	U.T.S.	63 Mpa minimum
	% elongation (in 50 mm)	25% minimum
	Material shall be	
	aluminium	99.5% minimum
	copper	0.05% maximum
	iron	0.4% maximum
	silicium	0.3% maximum
	manganese	0.05% maximum

After close examination of all the fabrication procedures and elaborate checking it was found that the H_2 was released from Ni plated Co pellets during autoclaving of the elements and the pellet capsules collapsed due to pressure built up in the elements as a result of differential – expansion of Al & zircaloy-2 during autoclaving. Release of H_2 was eliminated by baking the cobalt pellets in vacuum and the collapsing of pellet capsules was eliminated by increasing the free space in the elements.

3.1.1.3. Co assemblies

The design of assembly was finalised after several trials, out of pile testing, and also performance trials in the reactor. The initial design, caused a severe spinning effect resulting in element rotation and subsequent severe wear/fretting – wear on end plugs, spacers, anti torque pins and central support tubes. A new design was found to be satisfactory which incorporated modifications like:

- Improved latch body;
- Provision of holes in central support tube;
- Tapered end spacers;
- Provision of spring at the bottom to give a compressive force of 100 lbs. on the sub-assembly;
- Anti torque pins of different designs.

3.1.2. Regulating rods and Shim rods

There are two regulating rods made in stainless steel 304 grade and two shim rods made of borated stainless steel per PHWR reactor. Borated stainless steel rods containing about 2% boron are hollow rods with 60 mm OD and 30 mm ID.

3.2. Operational experience of control assemblies of PHWR

The adjuster rods of RAPS offered trouble free operation till 1986 when one of the central adjuster rod got struck due to ball screw failure. During the rehabilitation of adjuster rods that had failed during 1986, it was noticed that the coolant flow provided to the adjusters is inadequate and

consequently these mechanism are running dry. The ball screws thus were deprived of water lubrication. The failure of the ball screws was attributed to lack of lubrication.

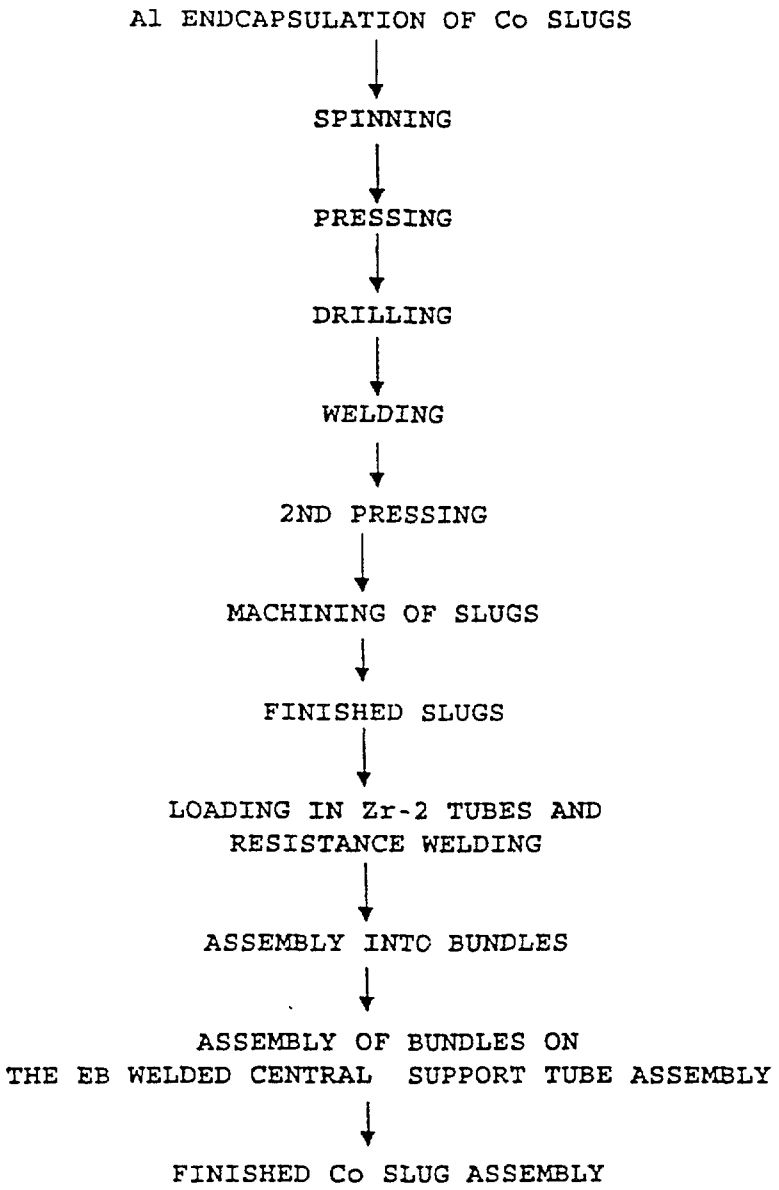

FIG. 8. Steps in fabrication of Co slug absorber assembly

A typical problem of NAPS moderator system is a high Co-60 activity coming from adjuster rod ball screws [7]. The stellite-3 balls of the ball screw assemblies have been found heavily eroded. The Co-59 of the balls travel to the reactor core with coolant and gets activated and leads to contaminate the equipment and piping and increased activity of entire moderator system.

3.3. Shut down assemblies

The first four units at RAPS & MAPS have only one shut down system (SDs) viz. moderator dump system. It is engineered to have high reliability & it has a large depth of negative reactivity. But it has a slow initial insertion rate of negative reactivity. Further mechanically the dump action puts a lot of stress on the core components. More importantly the moderator which provides a large heat sink would be absent after shut down action. These lead to the concept of two independently fast acting

systems in the standard PHWRs designs from NAPS onwards. These two independently operating fast acting systems are -- primary shutdown system (PSS) and secondary shut down (SSS). PSS consists of 14 stainless steel clad cadmium shut off rods, which get inserted from top of the core in about 2.2 seconds and has a worth of about 35 Mk. SSS consists of 12 zircaloy empty tubes through which Lithium pentaborate solution is inserted from the bottom of the reactor under the action of high pressure helium gas. It is grouped into 4 banks having a total worth of about 32 Mk.

The 500 MWe PHWRS have two independent SDS in line with the CANDU philosophy. The first SDS, SDS-1 consist of 28 stainless steel clad cadmium shut off rods having a total worth of about 72 Mk. The second system, SDS-2 consists of 6 poison injection nozzles which inject curtains of gadolinium nitrate solution under high pressure gas action directly into the moderator providing greater than 300 Mk of negative reactivity.

3.3.1. Materials and fabrication of shut down and assemblies

The primary shut down system of Indian PHWRs, from NAPS onwards, is also called as mechanical shut off rod system (MSRs). The system consists of 14 shut off rods located at 14 location on top of the reactor vessel (Fig. 7). The arrangement of at location consists of a vertical tubular Cd shut off element sandwiched between austenitic stainless steel tubes. The element is hung from the drum in the drive mechanism with the help of a 316 type austenitic stainless steel wire rope. The rope from the drum runs to pulleys to locate the shut off element centrally at its site. The schematic sketch of a typical MSR is given in Fig. 9. The shut off rod movement in reactor is guided by a zircaloy-2 guide tube (Fig. 10). The thermal neutron absorbing material in the shut off element is the reactor grade cadmium. The cadmium is contained between two co-axial stainless steel tubes. (Fig. 11).

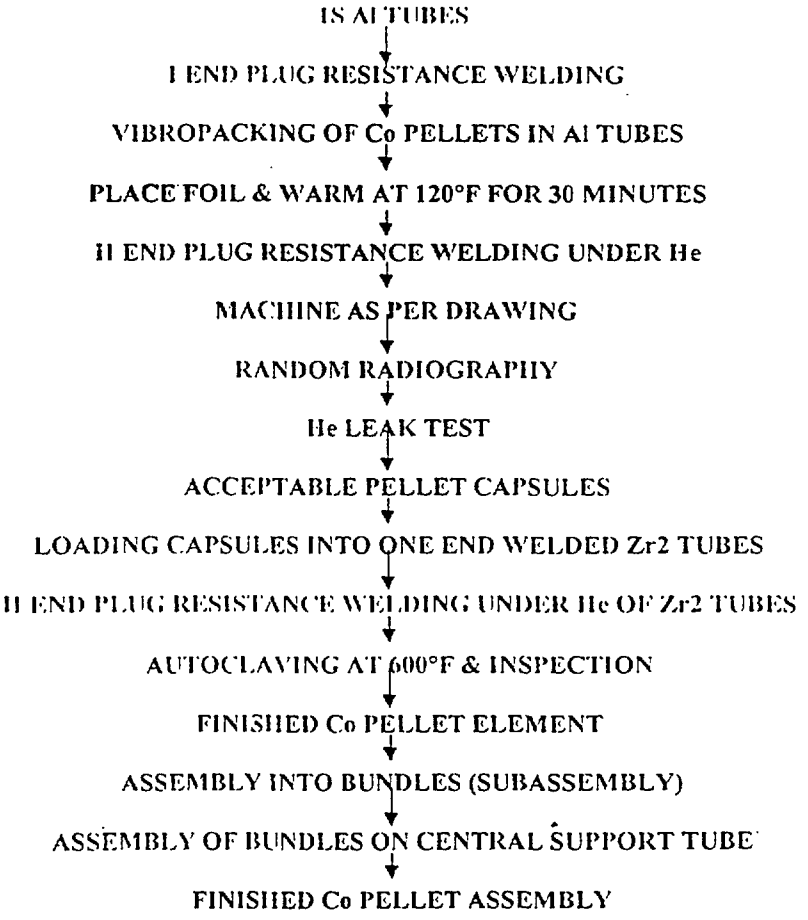

FIG. 9. Steps in fabrication of Co pellet absorber assembly

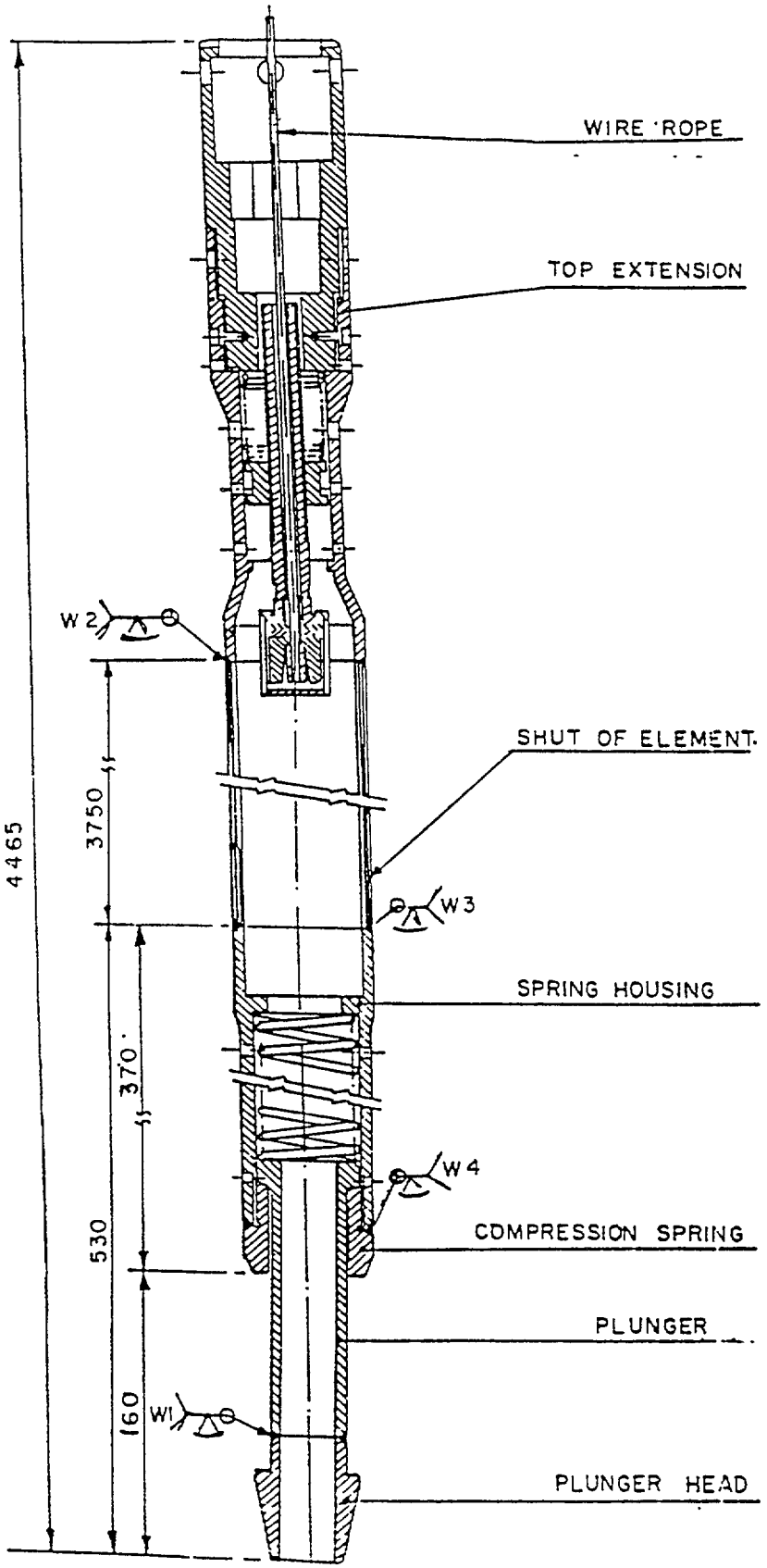

FIG. 10. Mechanical shut-off rod for PHWR

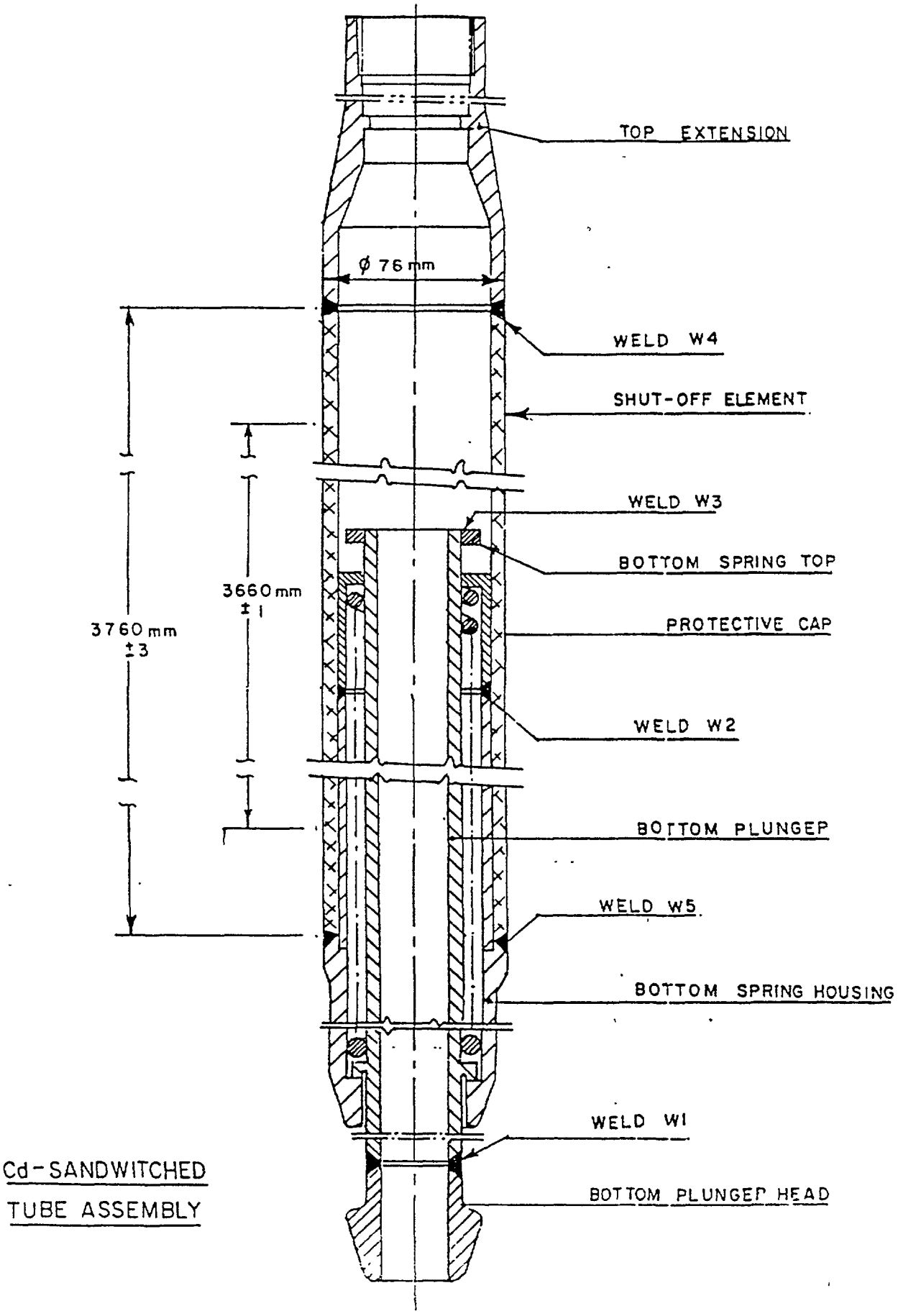

FIG. 11. Cd sandwiched tube assembly

Cadmium sandwiched with stainless steel was chosen as neutron absorbing element due to high neutron absorption cross section, ease of fabrication and low vapour pressure. Sandwiching is required for augmenting strength. Cd sandwiched absorber element is further welded to other SS components. MSR has bottom spring which absorbs kinetic energy when rod touches "stop plate" of guide tube. Upper end of MSR has wire rope fixing arrangement. Fabrication of zircaloy-2 guide tube assembly (Fig. 12) for MSRs involves intricate machining and EB welding of components 5-6 meters long. The fabrication of MSRs involves TIG welding of components using special fixtures.

3.4. Operational experience of shut off rod assemblies in PHWRs

The performance of shut-off rod assemblies is reported to be smooth and good till date, as far as shut off elements are concerned. Some minor problems were faced during commissioning due to mechanical design deficiencies such as

- Rope snapped during partial element drop in many mechanisms during commissioning period.
- Malfunctioning of position indicating micro-switches during commissioning & operations.
- He leakage from the flange joints to the stand pipe lower body

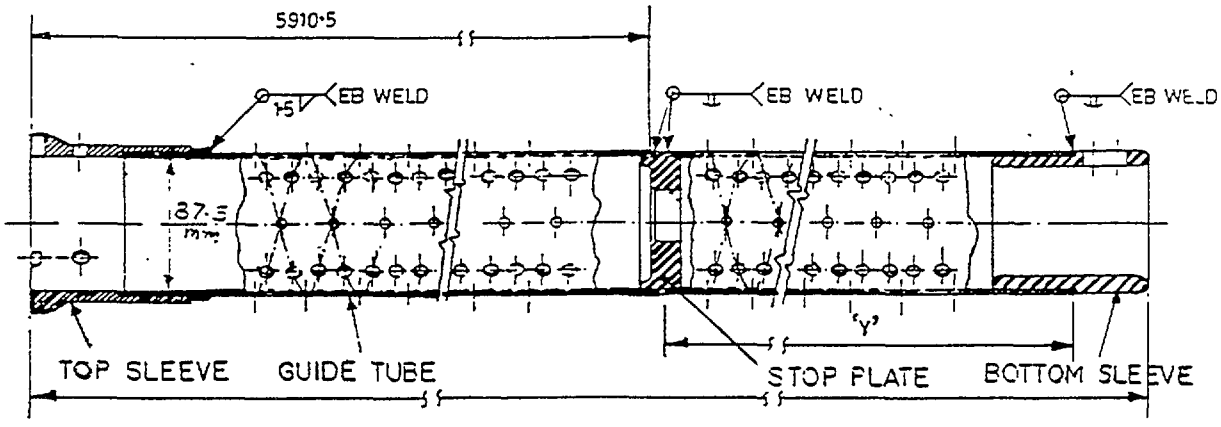

FIG. 12. Zircaloy-2 guide tube assembly for PHWR

4.0. BURNABLE ABSORBER RODS IN TAPS

4.1. Gadolinium rods used as burnable poison rods in TAPS

1.5% Gd_2O_3 is added to UO_2(2.66% enriched) and these UO_2 – 1.5% Gd_2O_3 pellets are used in 2 rods of the 6 x 6 fuel bundles of TAPS . These burnable poison rods help in reducing flux peaking and in obtaining flux flattening in fuel assemblies in the core.

The general processing scheme for the preparation of UO_2 –1.5% Gd_2O_3 pellets is given in Fig. 13. Gadolinium rods are made and used regularly in the fuel bundles manufactured by NFC (Nuclear Fuel Complex), Hyderabad for TAPS. Operational experience of TAPS shows that gadolinium rods are giving the desired performance and no problems have been faced.

5.0. OTHER MATERIALS UNDER DEVELOPMENT

Development work is planned to be taken up on control rod materials like Cr-Hf borides, mixtures of B_4C & ceramics, Gadolinium compounds, in view of their potential applications in water reactors.

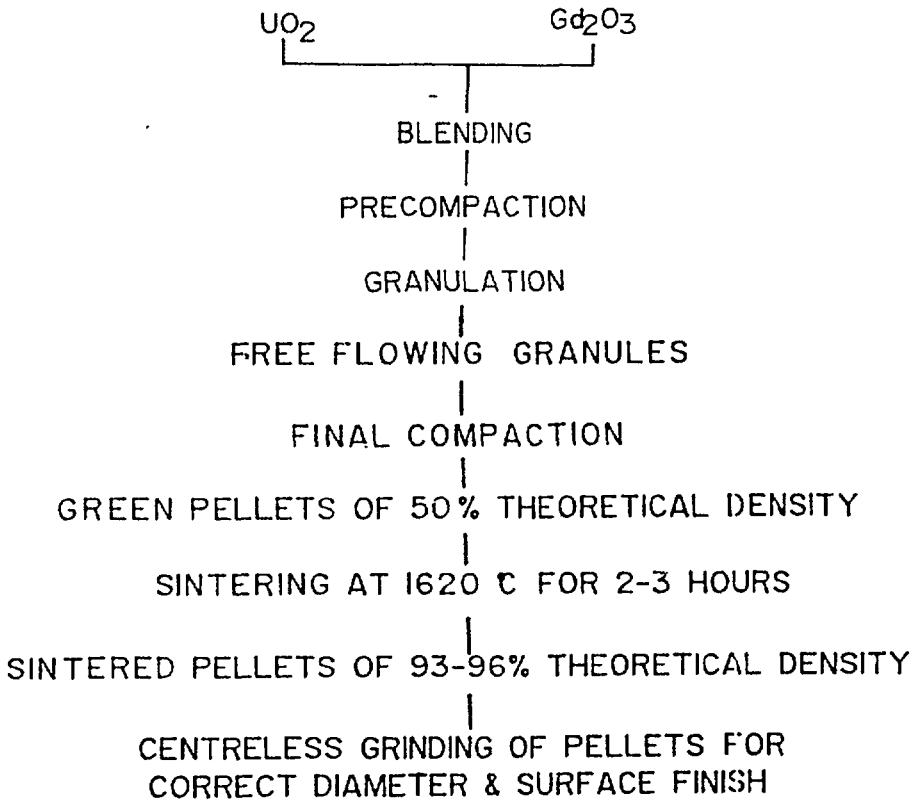

FIG. 13. Flow sheet for UO_2-Gd_2O_3 pellets

6.0. CONCLUSIONS

The indigenous capabilities have enabled us to cater to the requirement of control and shut down assemblies of the operating water cooled power reactors. The performance of the assemblies in the reactors has been reported to be satisfactory. However, this has to be substantiated by poolside inspection and PIE on few discharged assemblies. Use of MOX fuel and setting-up of PWR & AHWR reactors envisaged in our programme will require control assemblies with improved design, materials, fabrication and hence improved performance. Efforts are hence required to be put in this direction.

REFERENCES

[1] Reactor shutdown system (Proc. Workshop, Kalpakkam, 1997), IGCAR, Kalpakkam.
[2] BOSE, D.K., et al., Production of high purity boron carbide high temperature materials & processes, Vol.7, Nos 2 & 3, (1986) 133-140.
[3] BWR Control Rod Cobalt Alloy Replacement, EPRI NP-2329, (March 1982).
[4] BHASIN, B.K., et al., "Control & shutdown mechanism, operating experience of TAPS" (VI.1.1., Proc. Workshop on reactor shutdown system, Kalpakkam, 1997) IGCAR, Kalpakkam.
[5] BART, G., "High temperature boron carbide interaction with stainless steel in control rods" (Proc. TCM Advances in control assembly materials for water reactors, Vienna, Dec 1993) IAEA. TECDOC-813, Vienna, (1995) 177-186.
[6] SRIVENKATESAN, R., et al., "Physics requirements of shutdown systems for Indian PHWR" (I.2.1, Proc. Workshop on Reactor shutdown system, Kalpakkam, 1996) IGCAR, Kalpakkam.
[7] JAIN, A.K., et al., "Malfunction and failure in regulation and protective systems of PHWRs" (VI.8, Proc. Workshop on Reactor shutdown system, Kalpakkam, 1997), IGCAR, Kalpakkam.

CALCULATION MODELLING OF THE RCCA MOVEMENT THROUGH BOWED FA GUIDE TUBES

D.V. RAZOUMOVSKY, Yu.I. LIHKACHEV, V.M. TROYANOV
State Research Centre IPPE,
Atomic Energy Ministry,
Obninsk, Kaluga Region,
Russian Federation

Abstract

Rod control cluster assembly movement through the bowed guide tubes is considered. The movement equation is presented with some of the assumptions and special attention is paid to the determination of the mechanical friction force. The numerical algorithm is described and some results of parametric studies are presented.

1. INTRODUCTION

The number of operational and technological factors influences on a coverless fuel assembly (FA) and results in FA deflection in a core. This fact is proved to be true at the NPP with WWER-type reactors. Sometimes this phenomenon produces Safety and Control System (SCS) malfunction, that is not suitable for the safe NPP operation. The facts of the same kind are reported at a number of PWR of US and France design [1, 2].

Both required time limit excess and rod control cluster assembly (RCCA) incomplete insertion are classyfied as SCS malfunction. In the core RCCA is affected by the two types of resistance forces. That are the hydrodynamic forces (namely viscous friction on the rod walls, the back flow of the displaced water, the coolant flow, the spider hub flow separation) and the mechanical friction between the guide tubes (GT) walls and rods. The last force is brought into existence after FA deflects at the value of the difference between inner GT calibre and rod diameter. Time limit excess may be accounted for the hydrodynamic forces increase, but it is not true for incomplete RCCA insertion.

The paper [3] deals with the problem. The slide friction force is said to be a principal cause of incomplete insertion. But they suggested simplyfied approach for the force determination, also it was necessary to carry out the rod drop experiment in the concrete core. This paper offers more universal technique to predict RCCA behavior on the only base of the FA bended axis.

2. RCCA DROP DYNAMICS MODEL

In a core RCCA is affected by the gravity, the viscous friction, the spider hub resistance and the mechanical friction. The RCCA acceleration is defined by these forces sum:

$$M\frac{d^2x}{dt^2} = g\,M - k\,x\frac{dx}{dt} - k_1\left(\frac{dx}{dt}\right)^2 - \mu N(x) \qquad (1)$$

M is the RCCA mass, g is gravity constant, k is viscous friction coefficient, x is the RCCA mass centre coordinate ($x \in [0, L]$, L is the length of the GT), k_1 is the spider hub resistance coefficient, μ is the friction coefficient, N(x) the normal force between the RCCA and GT.

The initial conditions look like: $t = 0: x = 0; \quad t = 0: \frac{dx}{dt} = 0.$ (2)

In the equation (1) is ignored: the pressure reduction due to the coolant flow across the FA, the back flow of the displaced water, the pressuresation of the water ahead of the RCCA and the damping devices affection after the bottom design position is reached.

Both incomplete RCCA insertion ($X_{V=0} < L$) and required time limit excess ($t'_{X=L} > \Delta T_{np}$) will be assumed as a malfunction. Then the SCS failure function will be the following:

$$f(x,t) = (x_{V=0} < L) \vee (t_{X=L} > \Delta T_{np}).$$

3. MECHANICAL FRICTION DETERMINATION

The main resistance cause was said to be the friction force, that is proportional to the normal force between RCCA and GT. Let us apply the relationships:

$$N(x) = \int_0^x q(x)\,dx \tag{3}$$

$$q(x) = E\,J\frac{d^4 y(x)}{dx^4} \tag{4}$$

q(x) is the rod lateral load, y(x) is the rod axis deflection, E is the Young modulus, J is the moment of inertia for the rod (it is assumed the fixed characteristics along the rod length).

Let us roughly suppose the abscence of the annulus between inner GT wall and the rod, that is equal to the situation when rod is deflected according to the GT form.

For the two-dimensional solution FA axis is described with the (X, Y) set, Y is the deflection in point X, X ∈ [0, L]. To define the lateral load the analytical representation y*(x) (y*(X) = Y) is necessary. The general solution of the equation (4) is the sum of its particular solution $y_p(x)$ and a general solution of the congruent homogeneous equation $y_g(x)$:

$$y(x) = y_g(x) + y_p(x) \tag{5}$$

$$y_g(x) = C_0 + C_1 x + C_2 x^2 + C_3 x^3; \quad y_p(x) = C_4 x^4 + C_5 x^5 + C_6 x^6 + C_7 \cos(x) + C_8 \sin(x)$$

Due to the absence of the forces and the moments of forces across the rod it is necessary for the function y(x) to be continuous and to possess its continuous derivation up to the fifth one. At the ends of interval the conditions y'(0) = const è y'(L) = const are added. Let us divide all the FA length at a number of steps, so any of them to be relied on the adjacent spacer grids. The solution of the equation (5) will be represented by the set of functions $y_j(x)$, which describe FA axis at the proper step. The function $y_j(x)$ must be equal to the two inner point axis deflections and equal to the both step end deflections. Moreover, at the step ends this function must have continuous derivations up to the fifth one.

Coefficients in the equation (5) are strictly defined from the system of these conditions. The system is solved by the Gaussian method modification. This technique allows to increase the number of steps in order to refine the FA bended axis without complication of the algorithm.

It is necessary to define the lateral load q_x è q_y that are applied to the rods in two orthogonal planes OXZ, OYZ for three-dimensional solution. The total friction force will be equal to their sum:

$$F_{fr} = \mu \int_0^z \sqrt{q_x^2 + q_y^2}\,dz.$$

Text continued on page 63.

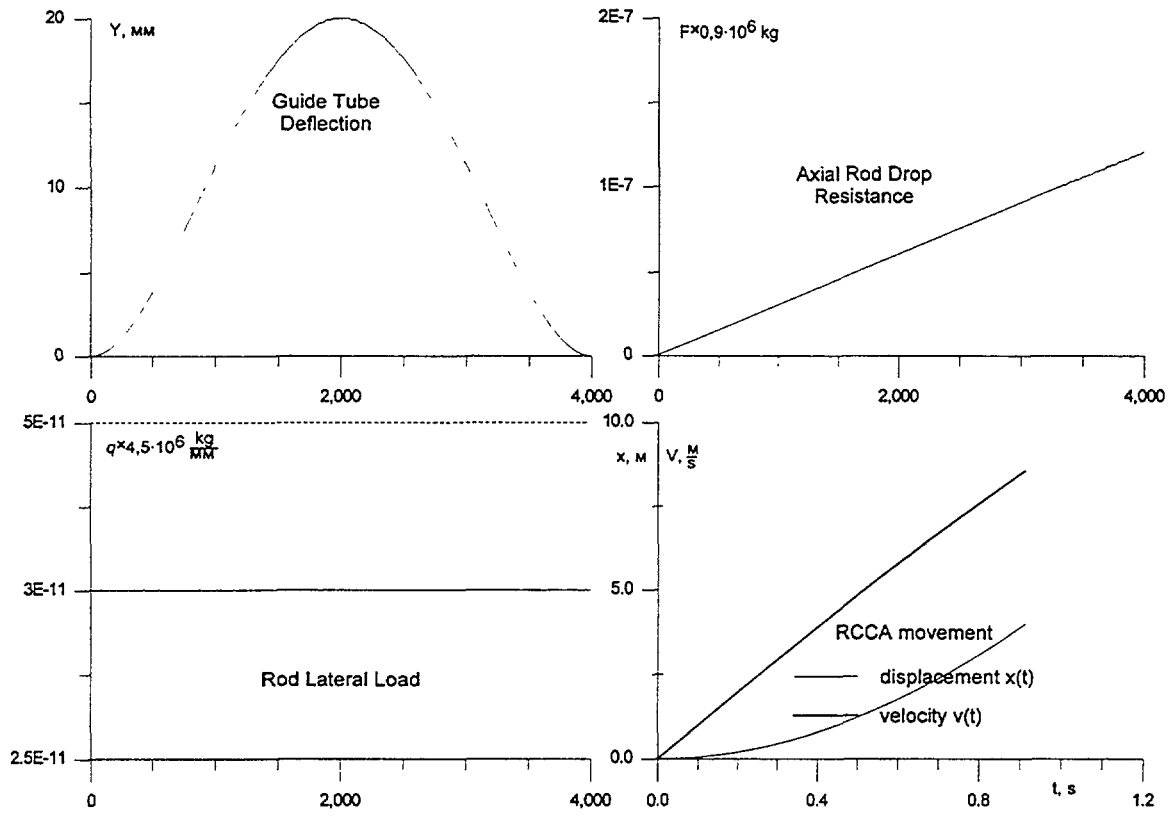

FIG. 1. RCCA insertion in "cosine"--shaped FA

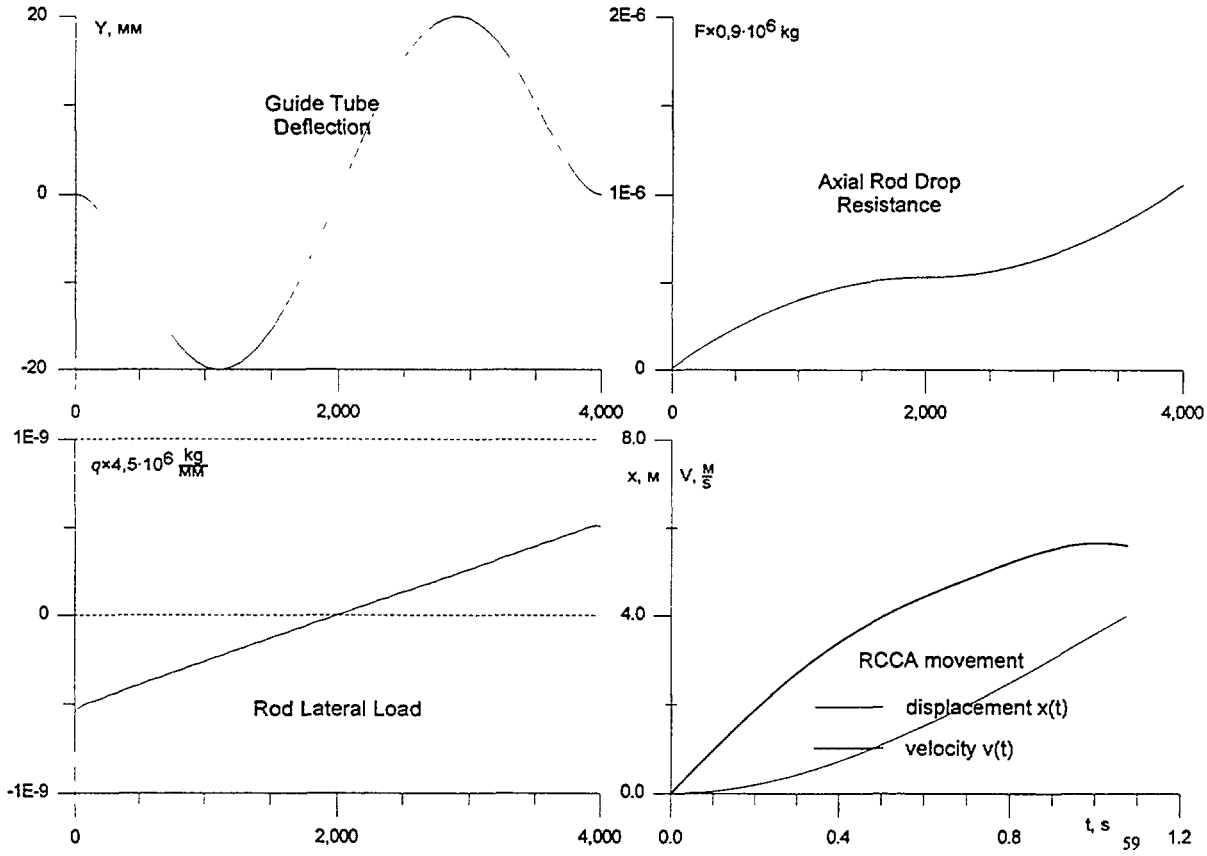

FIG. 2. RCCA insertion in "dollar"--shaped FA

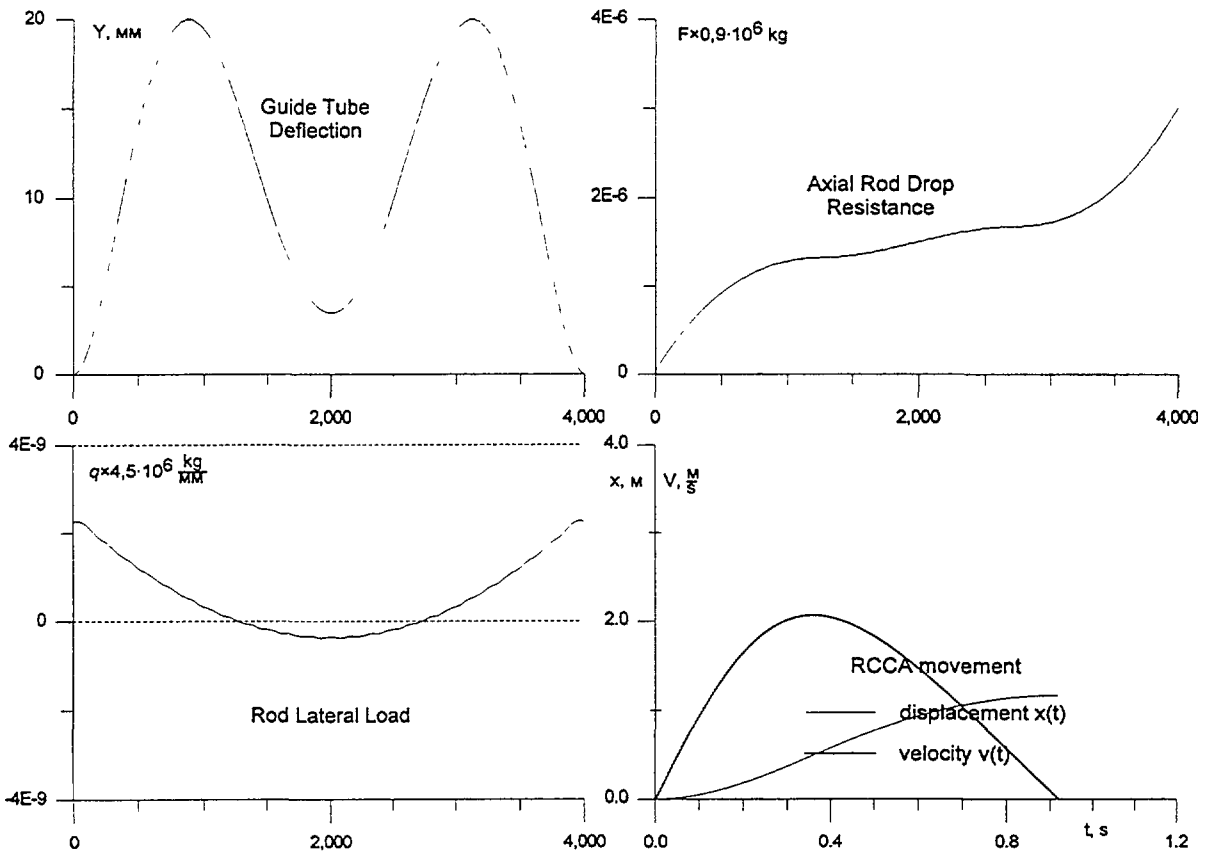

FIG. 3. RCCA insertion in "bow"--shaped FA

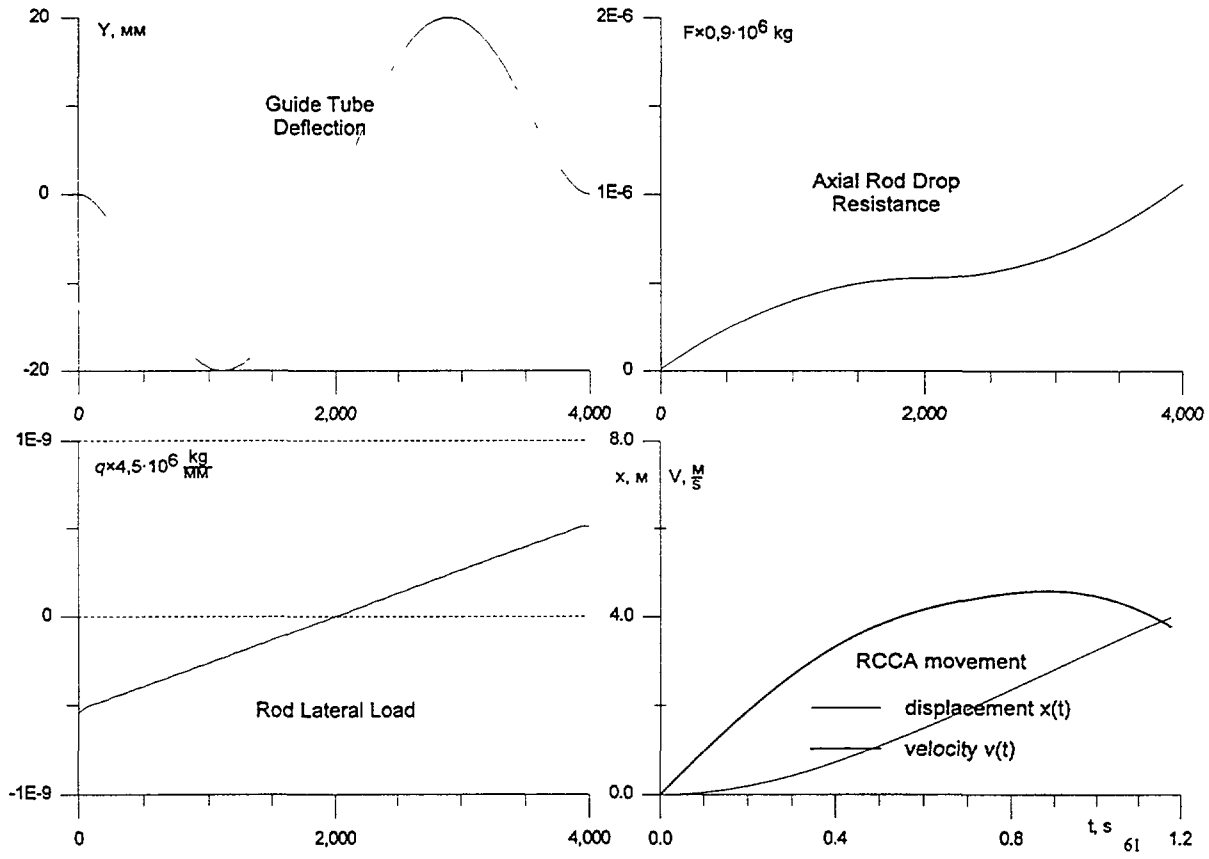

FIG. 4. RCCA drop. Viscous & mechanical friction influence

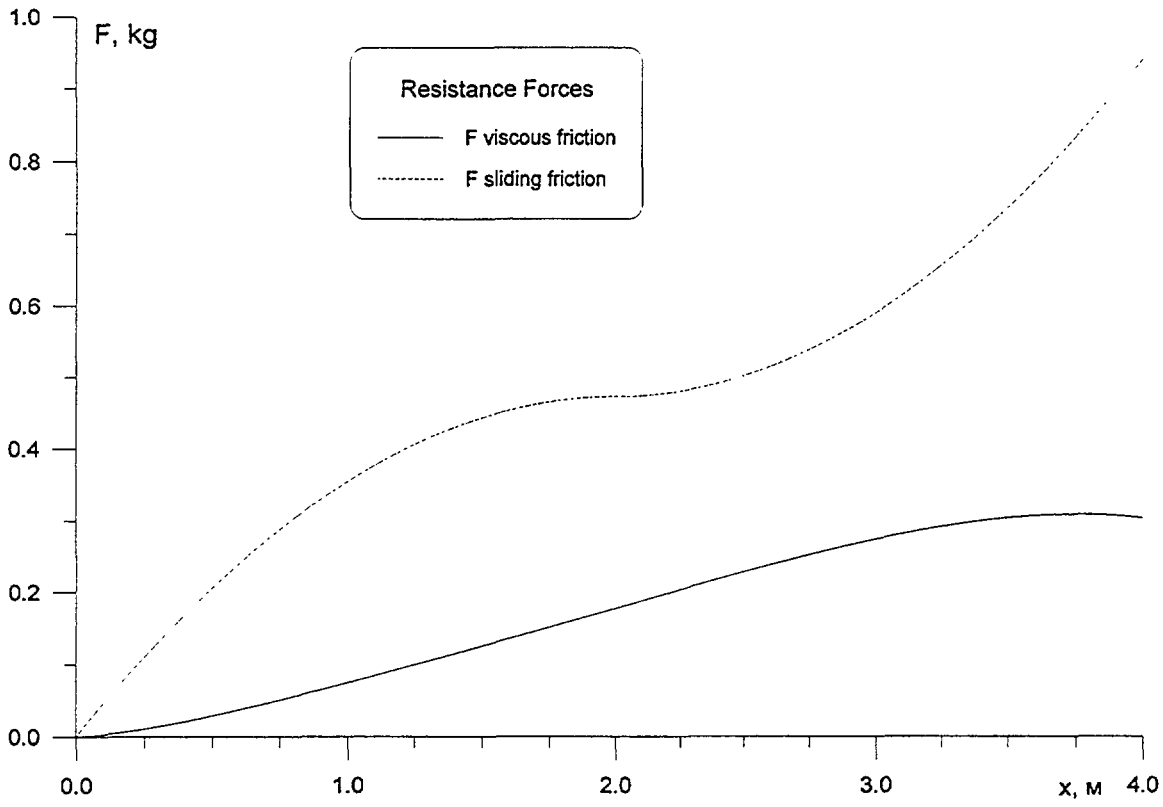

FIG. 5. Mechanical & viscous friction forces comparison

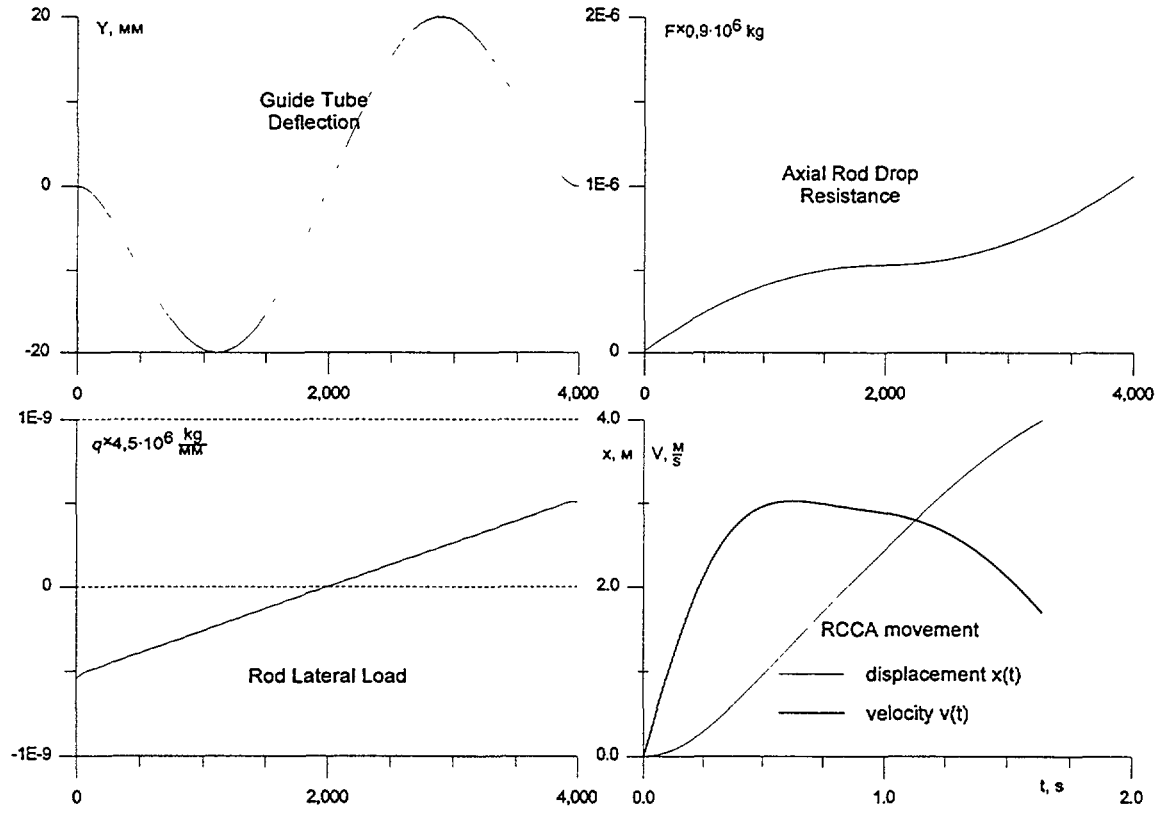

FIG. 6. RCCA drop. Hub resistance & friction influence

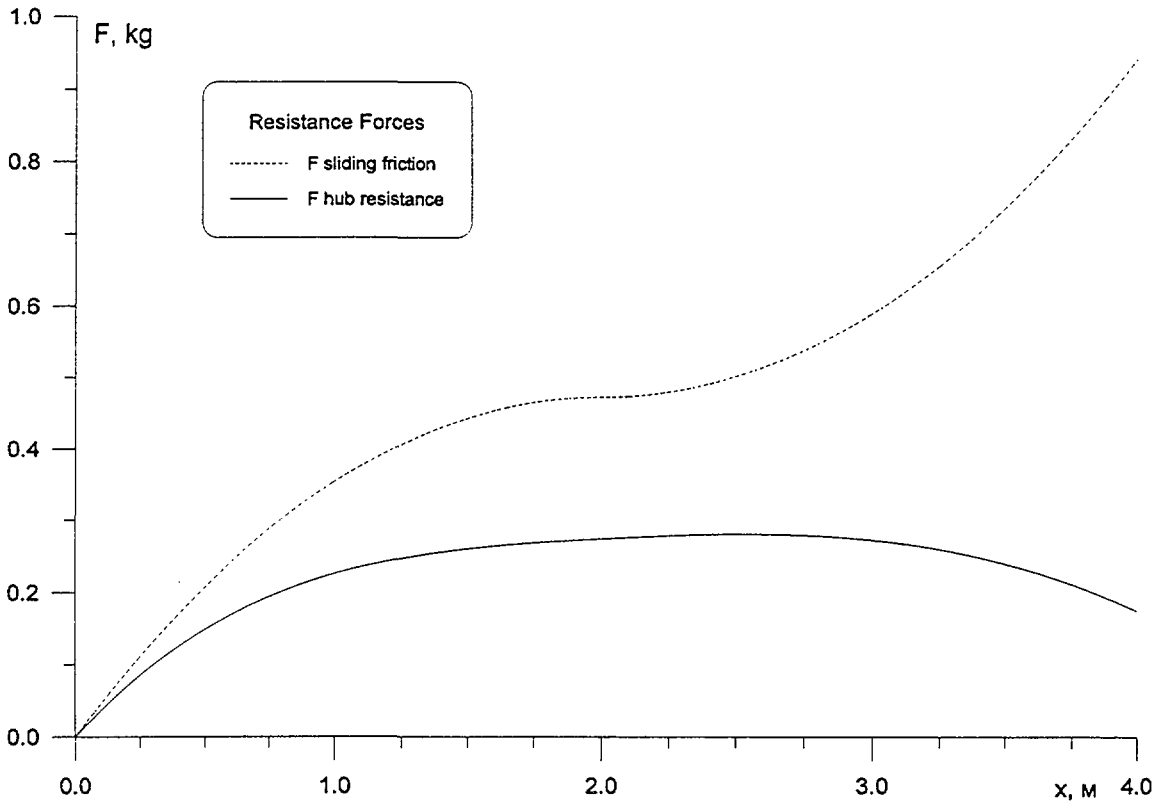

FIG. 7. Hub resistance & friction comparison

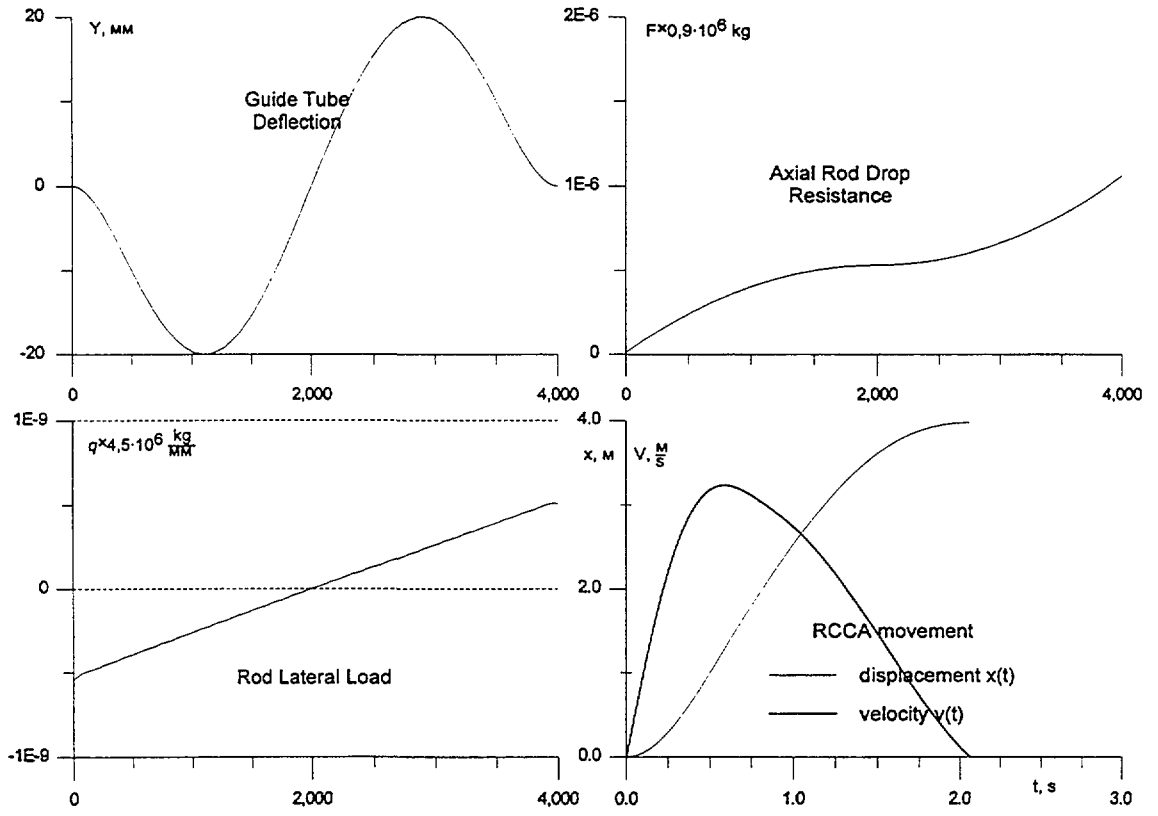

FIG. 8. RCCA drop. All forces influence

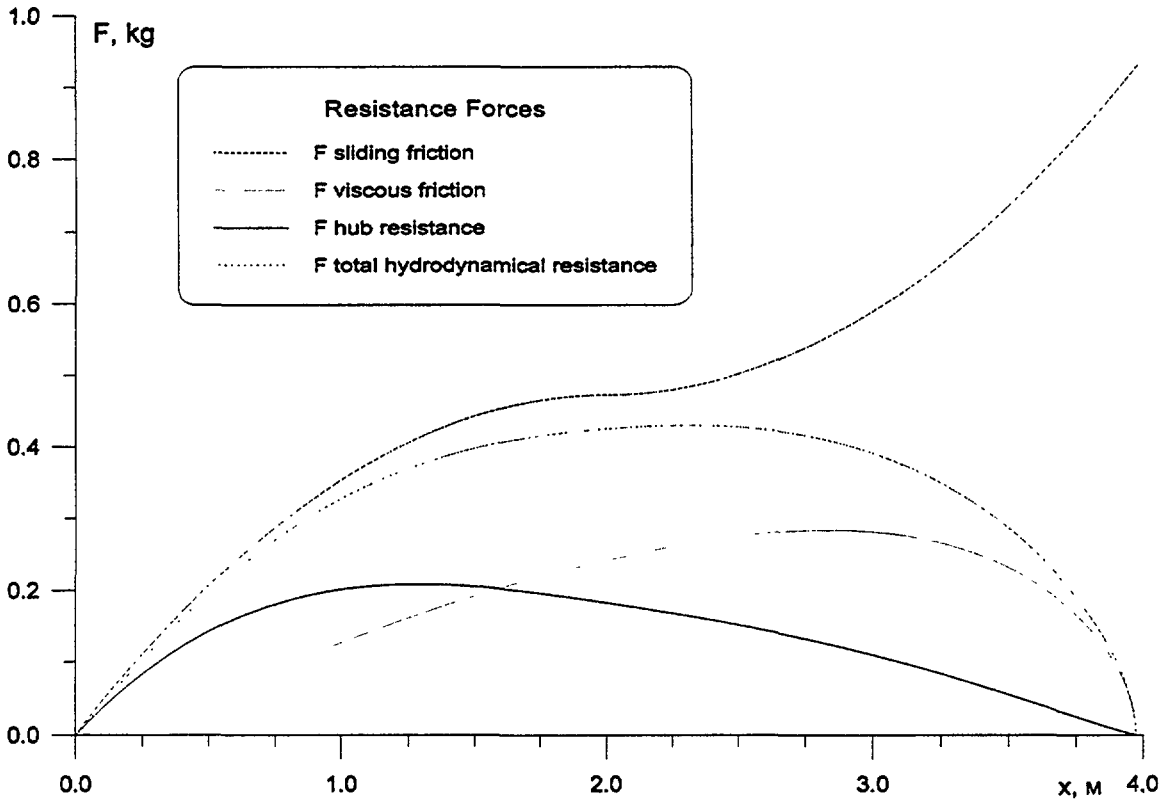

FIG. 9. All forces comparison

4. APPLICATION AND RESULTS

This algorithm was realised in the computer code "DORA", that is a part of a program complex "RANDEVU-3" - "TEREMOK" - "DORA", intended for prediction of FA axis bowing and SCS behaviour (drop time and insertion depth is determined) for the WWER-type core at the arbitrary moment of fuel cycle.

A number of parametric results are listed below. The influence of FA form, friction coefficient and hydrodynamic forces on the RCCA drop was investigated. The mass center velocity v(t) and insertion depth was calculated.

The study of FA shape influence on RCCA movement has been carried out on the three basic variants (Fig. 1, 2, 3), namely so-called "cosine", "dollar" and "bow". The Figures represent GT deflection, rod lateral load, axial rod drop resistance, rod displacement and velocity. The "bow" shape seems to be the most inclined for the RCCA sticking.

In the case study of friction force influence the incomplete insertion arose while the doubling of its value had happened over the initial one.

The investigation of the hydrodynamic viscous friction was also carried out (Fig. 4, 5). This force does not affect the RCCA movement very much. In general it became valuable in the second half way, when rods are almost inserted at full length. In comparison, the spider hub resistance force produces the specific velocity profile (Fig. 6, 7). It tends to influence at the beginning, when the RCCA gets its velocity maximum.

Under the influence of all forces (Fig. 8, 9) the hydrodynamic RCCA resistance is composed of the approximately equal impacts of both viscous friction and hub resistance. In the beginning the hub resistance affects more, but in the end the viscous friction magnitude exceeds the hub one.

REFERENCES

[1] Specialist Meeting on Nuclear Fuel and Control Rods: Operating Experience, Design Evolution and Safety Aspects, Madrid, 5 -- 7 November 1996.

[2] International Topical Meeting on Light Water Reactor Fuel Performance, Portland, Oregon, 2 - 6 March 1997.

[3] BJÖRNKVIST, L., KEE, E., Application of a semi-empirical rod drop model for studying rod insertion anomalies at South Texas Project and Ringhals unit 4. International Topical Meeting on Light Water Reactor Fuel Performance, Portland, Oregon, 2 - 6 March 1997, 81-89.

MATERIAL OPERATING BEHAVIOUR OF ABB BWR CONTROL RODS

B REBENSDORFF
ABB Atom AB,
Vàsteras,
Sweden

G. BART
Paul Scherrer Institute,
Villigen PSI,
Switzerland

Abstract

The BWR control rods made by ABB use boron carbide (B4C) and hafnium as absorber material within a cladding of stainless steel The general behaviour under operation has proven to be very good ABB and many of their control rod customers have performed extensive inspection programs of control rod behaviour However, due to changes in the material properties under fast and thermal neutron irradiation defects may occur in the control rods at high neutron fluences Examinations of irradiated control rod materials have been performed in hot cell laboratories The examinations have revealed the defect mechanism Irradiation Assisted Stress Corrosion Cracking (IASCC) to appear in the stainless steel cladding For IASCC to occur three factors have to act simultaneously Stress, material sensitization and an oxidising environment Stress may be obtained from boron carbide swelling due to irradiation Stainless steel may be sensitized to intergranular stress corrosion cracking under irradiation Normally the reactor environment in a BWR is oxidising The presentation focuses on findings from hot cell laboratory work on irradiated ABB BWR control rods and studies of irradiated control rod materials in the hot cells at PSI Apart from physical, mechanical and microstructural examinations, isotope analyses were performed to describe the local isotopic burnup of boron Consequences (such as possible B4C wash-out) of a under operation in a ABB BWR, after the occurrence of a crack is discussed based on neutron radiographic examinations of control rods operated with cracks

1 INTRODUCTION

ABB Atom has delivered almost 4000 control rods to Boiling Water Reactors (BWRs) around the world. More than 1000 of these rods have been inspected after varying time of operation and at varying levels of neutron exposure. Besides the visual pool-side inspections, control rod wings with cracks have been analysed by neutron radiography to reveal the behaviour of irradiated boron carbide behaviour in case of cracking and water intrusion. Irradiated control rods and irradiated control rod material samples have been examined in hot cell laboratories to understand the materials behaviour and properties due to fast and thermal neutron irradiation.

2 ABB BWR CONTROL ROD DESIGN

The basic design of ABB BWR control rods is shown in Figure 1 Four stainless steel plates are forming a cruciform shaped rod. The steel quality initially used from start was AISI 304L SS which has in later manufacturing been replaced by AISI 316L SS. Boron carbide (B_4C) powder with a void volume of 30% is used as absorber material together with hafnium.

3 NEUTRON IRRADIATION OF CONTROL ROD MATERIALS

Neutron irradiation is known to the change properties of the materials used in control rods Some of these changes have an influence on the control rod behaviour.

3.1. Stainless steel

Neutrons of energies above 1 MeV cause hardening, increase in yield and ultimate strength, segregation etc. in the stainless steels used. Segregation of chromium from the grain boundaries of the steel means that the material becomes sensitized for stress corrosion attack in the grain boundaries. The impact, for the operational behaviour, of other changes in the stainless steel material structure and properties is under investigation since not yet fully understood.

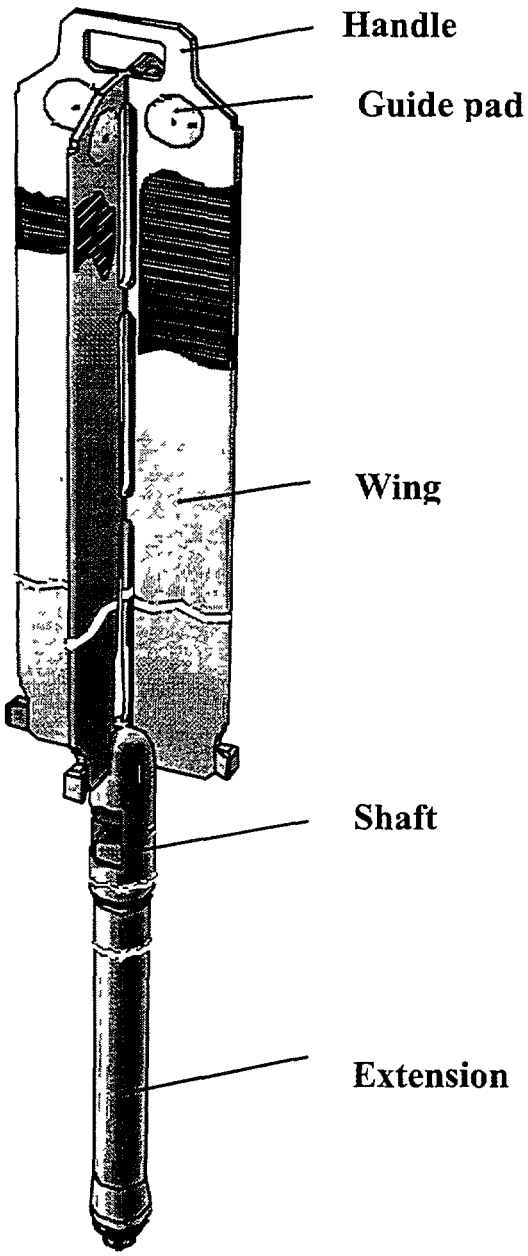

FIG 1. Basic design of the ABB BWR control rod

The environmental assisted cracking occuring in control rods is intergranular and called Irradiation Assisted Stress Corrosion Cracking (IASCC). IASCC needs three simultaneous factors to occur:

1. Stresses - in a control rod, these can be caused by the swelling boron carbide,
2. Material sensitization - chromium depletion in grain boundaries is such a factor caused by neutron irradiation, there might be others not yet understood;
3 Oxidising environment - IASCC due to chromium depletion in the grain boundaries requires an oxidising environment There seems, however, to be other factors at higher irradiation eliminating the requirement of oxidising conditions.

The crack mode has been observed in several investigations and the picture in Figure 2 is from a Post Irradiation Examination (PIE) of a ABB BWR control rod at the Paul Scherrer Institute (PSI). The material is Type 304L stainless steel. In Figure 3, a grain boundary STEM analysis (made by Magnox Electric) of element profiles, from the same material shows the depletion of chromium from the grain boundary. The neutron fluence was 3 10^{21} n/cm^2 (E>1MeV).

FIG 2 Intergranular crack mode in irradiated type 304L SS, 3 10^{21} n/cm^2 (E>1MeV)

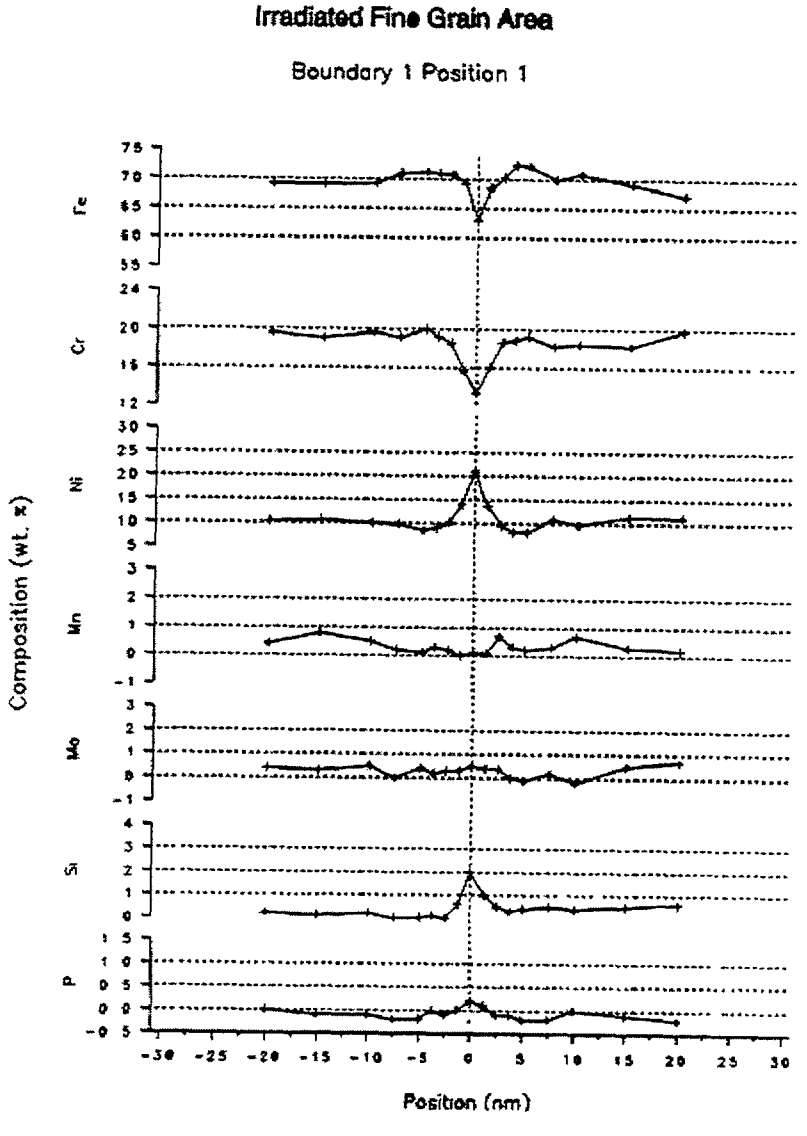

FIG 3 Concentration profiles of elements in type 304L SS. irradiated to 3 10^{21} n/cm^2 (E>1MeV)

Figure 4 shows the chromium profile of the material before irradiation. In this non-irradiated condition there is an enrichment of chromium to the grain boundary. The material was in a solution heat treated condition prior to irradiation.

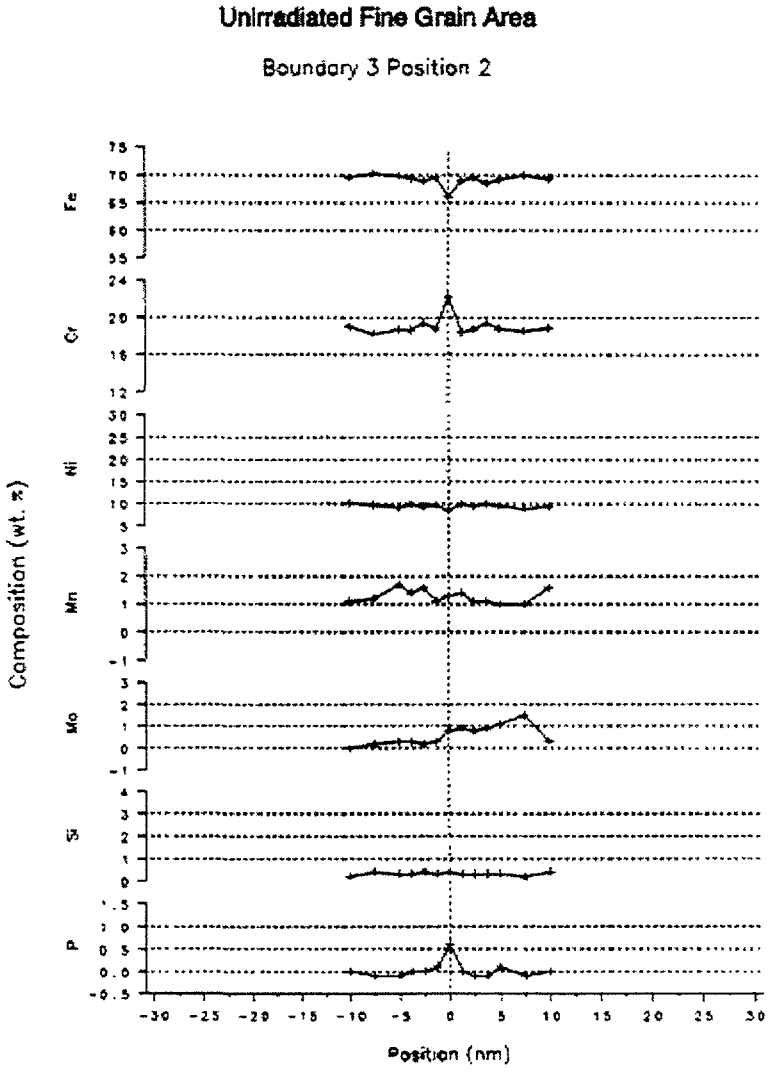

FIG. 4. Concentration profiles of elements in non-irradiated type 304L SS

Studies by Ljungberg and Jenssen [1] have shown that Type 316L SS material is less susceptible to IASCC after irradiation to relevant BWR neutron exposure levels, $10^{21} - 10^{22}$ n/cm^2 (E>1MeV), see Figure 5.

Control rod experiences with this material show a significant delay in IASCC susceptibility for Type 316L SS compared to Type 304L SS. However, immunity against IASCC seems to be best obtained by avoiding high stresses in the steel.

3.2. Boron Carbide (B_4C)

By absorption of thermal neutrons, the ^{10}B isotope in the B_4C gets transmuted to helium and lithium according to the reaction:

$$^{10}B + n \rightarrow {}^{7}Li + {}^{4}He + 2{,}8 \text{ MeV}$$

This means that B_4C is swelling due to neutron irradiation since most of the helium atoms formed by the neutron absorption reaction are trapped in the boron carbide crystals.

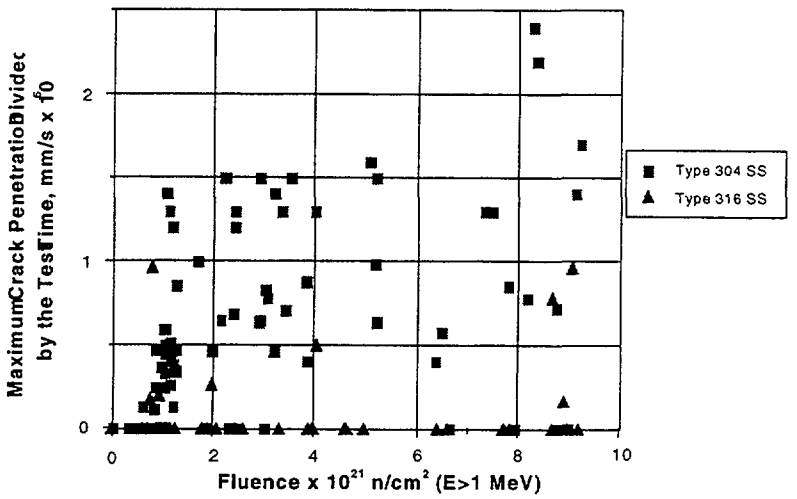

FIG. 5. Comparison of susceptibility to IASCC of type 316L SS and type 304L SS

Secondly the chemical properties may be changed when the B_4C structure is disturbed by formation of Li and He in the crystals, replacing some boron atoms. Smaller amounts of tritium (^3H) are also formed during irradiation by other, less frequent transmutation reactions. This has no impact on the control rod behaviour but it can be used to monitor the status of the control rod inventory in the reactor core, as discussed later in this paper.

Swelling of the boron carbide as well as the helium gas release are important parameters when designing the control rod. Experiences from control rod operation has shown that swelling has been the service lifetime determining parameter but not the helium release. A hot cell examination of boron carbide samples, irradiated under relevant conditions in the Forsmark 1 BWR, has been performed at PSI [2]. The study showed that the fraction released helium from the irradiated boron carbide was much lower than the helium release curve presented in [3].

3.3. Hafnium

Hafnium in BWR control rods is used in locations with high local neutron exposure. Hafnium is heavy and expensive which explains the limited use of the material in the rods. The benefit of using hafnium is the absence of swelling during irradiation. This behaviour has been verified by a PIE on an irradiated ABB BWR control rod with hafnium tip at PSI, [4]. The same study revealed that that hydrogen content of hafnium in a BWR control rod is low even after operation, as long as the control rod is free from cracking. This result is in agreement with calculations made by ABB [5]. Thus it is shown, that the hydrogen concentration in the BWR environment, also in case of hydrogen water chemistry operation, is too low to cause significant concentration of hydrogen within the control rod although the stainless steel cladding has high permeability for hydrogen. Tritium formed in the boron carbide during irradiation is retained in the boron carbide structure [3] and does not influence the hafnium. The latter has also been proven by inspection of hundreds of intact control rods with hafnium, showing no swelling.

If a crack occurs that leads to water intrusion hydrogen may be formed by corrosion reactions as well as by reaction between lithium and water. In such cases hydriding of hafnium has been experienced as shown in Figures 6 and 7. Experiences by use of hafnium in ABB BWR control rods show that no significant hydrogen concentrations are obtained in the hafnium of an intact control rod. Water intrusion after rod cracking is hence the only possible source to hafnium hydride formation.

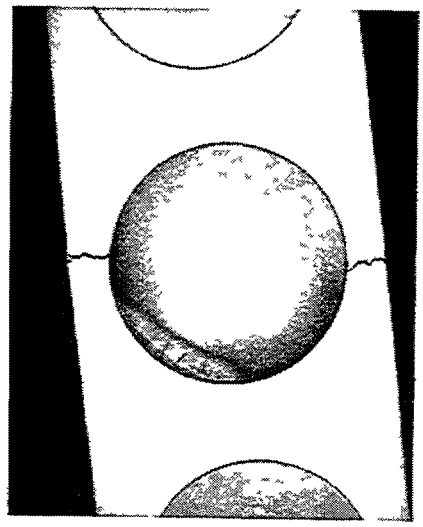

FIG 6 Hafnium plug with hydride formation

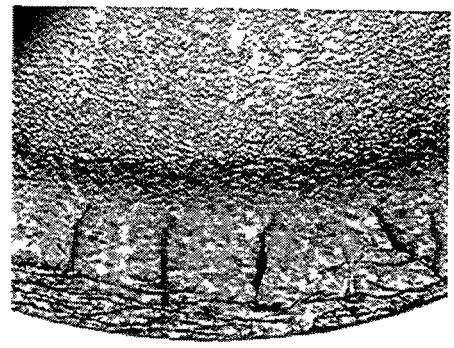

FIG 7 Magnification of hafnium hydrides

4. CONTROL ROD MANAGEMENT

Guidelines for control rod management must be based on experience data from inspections and PIEs. More than thousand control rods of ABB BWR design have been inspected after irradiation. Many have also been subject for PIEs such as neutron radiography and hot cell examinations. Guidelines are formulated for each different design by frequent inspections of leading rods of that particular design. By inspections, the general appearance of the rod after operation as well as possible crack appearance is observed.

4.1. Neutron radiography

In the case of water intrusion into a control rod, by crack occurrence, the consequences for the boron carbide absorber material is of vital importance For this reason an extensive work by neutron radiography has been performed especially in Swedish BWRs. Control rods from shut-down operation and control cell operation, with cracks, have been analysed in this way, see Table I.

TABLE I. RESULTS OF NEUTRON RADIOGRAPHY

Reactor	Type	Year	No of Wings	Estimated Tip* exposure (snvt)	B_4C Leach-out
A	CR70	1985	2	6,6 – 7,1	No
A	CR70	1986	2	6,8 – 7,3	No
B	CR70	1986	13	6,8 – 7,7	limited loss in 2 blades
C	CR70	1986	10	7,6 – 7,7	limited loss in 4 blades
B	CR70	1987	13	7,2 – 8,1	limited loss in 2 blades
B	CR85	1991	1	5,0	limited loss in 1 blade
D	CR85	1992	2	4,4**	limited loss in 2 blades
E	CR82	1993	1	4,8	limited loss in 1 blade

* Tip means the uppermost absorber hole
** Top quarter exposure

By exposing a control rod wing to a neutron source and detecting the non-absorbed neutrons a clear picture of the boron carbide content can be obtained. An example of such a picture is shown in Figure 8. The lighter areas in the upper absorber bores reveal some B_4C loss.

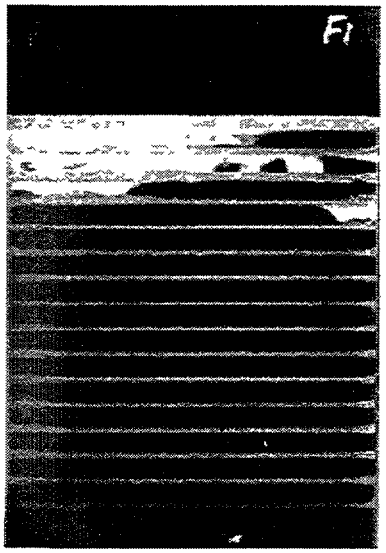

FIG. 8. Neutron Radiography picture of an ABB BWR control rod wing tip

In the cases where losses of B_4C has been detected it has been very limited, which means that there has been no influence on the shut-down margin. The conclusions from these studies are that a control rod can be operated with cracks that appear during a operating cycle. The recommendation of ABB is nevertheless not to start up a reactor with known cracks in the rod wings.

4.2. Tritium

Tritium (^3H) is produced in the B_4C absorber by several reactions with fast and thermal neutrons. Other sources for tritium production are:

- neutron activation of deuterium in the reactor water;
- neutron activation of lithium contamination in the reactor water;
- ternary fission of the fuel.

The reactor water content of tritium will reach a stable level during operation. The level is determined by the tritium production in the reactor water and the reactor water exchange under normal conditions. It has been shown that a control rod with cracks may contribute to the tritium content of the reactor water in case of water intrusion. This intrusion leads to formation of THO. The tritiated water may then be mixed with the reactor water. For a plant where the basic tritium level under normal operating conditions is known, increased tritium levels probably indicate control rods with cracking. This means that the planning of control rod inspections can be made more efficient by following the tritium content in the reactor water. A method for using tritium analysis in the control rod management work is now under development by ABB.

5 DEVELOPMENT

Experiences from operation of ABB BWR control rods has led to the conclusion that avoiding stresses in the stainless steel clad material is the best way to extend the mechanical service life time of control rods.

Normally boron carbide is used as a powder within a stainless steel cladding. To avoid stresses in the steel from swelling boron carbide, the void volume of the powder must accommodate the increasing volume of the grains. If we assume that this would be the case we receive a decreasing void in boron carbide powder with irradiation. Our experiences indicate that a large variation prevails between control rods regarding the behaviour of the powder. Modelling the behaviour of the swelling powder is hence a difficult task.

By using boron carbide without internal void, several advantages are obtained:

- The behaviour of a theoretical dense body is much easier to model;
- By allocating the void outside the dense body, the use of the void for accommodation of swelling is ensured;
- Designing a control rod to avoid stresses is more readily done.

A concept to use almost theoretically (>99%) dense boron carbide pins instead of powder has been developed by ABB. The concept, that includes boron carbide compositions in the range of B_4C to $B_{8.5}C$, has been studied by irradiation of pins in the Forsmark 1 BWR and a PIE of the pins at PSI. From this study swelling has been determined as a function of ^{10}B depletion in the pins. The accuracy in the modelling of the swelling behaviour of the pin can be improved by determining the ^{10}B depletion profile through the body. Such a work was performed at PSI by using the SIMS technique.

5.1. Isotopic analysis of a theoretically dense boron carbide pins with SIMS technique

Due to the large thermal neutron capture cross section of ^{10}B, its burnup and helium production within a boron carbide absorber body is inhomogeneous. The developed SIMS technique now offers a direct measure of the radial burnup of ^{10}B in a $B_{8.5}C$ neutron absorber test sample with almost theoretical density. The sample, previously mounted like a ceramographic specimen is bombarded within an ultra-high vacuum chamber with a focused ^{133}Cs primary ion beam and the secondary ions emitted from the sample surface are detected and separated according to their ion mass. The technique allows to measure quantitatively the radial boron burnup.

5.1.1. Experimental

The test sample selected for radial boron burnup analysis was a cylindrical $B_{8.5}C$ sample of 1.75 mm diameter and (initially) natural isotopic content, brought to an estimated burnup of 55 %. The sample was mounted in araldite, (wet) ground with diamond discs (125, 40, 20 and 10 μm) and polished with 3 μm diamond paste, see Figure 9. The formation of cracks at the specimen periphery is clearly visible.

After an ultrasonic cleaning in alcohol, the sample was introduced into an ATOMICA-4000 SIMS and sputtered with a ^{133}Cs primary ion beam of ≅ 30 μm diameter at 11 kV energy and 120 nA current. For each analysis a shallow 50x50 μm^2 crater was eroded away from the sample surface before performing the isotopic measurements in order to get stable secondary ion count rates. The secondary ion optics was (individually) tuned for ^{3}H, ^{7}Li ^{10}B and ^{11}B analysis (the tuning was set the same for the latter two nuclides).

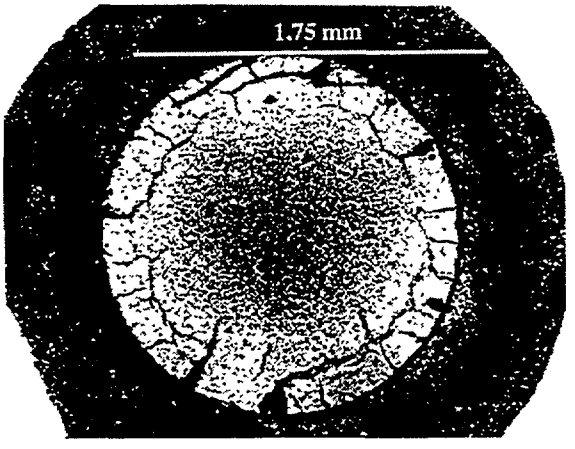

FIG. 9. Macrography of the hipped, irradiated $B_{8.5}C$ specimen after preparation

A "checker board" area scan of 50 by 50 measurement points was then performed across the sample surface with steps of 50 µm. A direct (non-corrected non-normalized) area scan of the ^{10}B and ^{11}B count rates is presented in Figure 10. This direct information had to be corrected because of problems with the sample holder movement (which simulates an oval sample shape) and normalized (presently with ^{11}B) because a direct individual secondary ion count rate conversion to an isotopic surface concentration requires a careful calibrations. The isotopic distribution of the two boron isotopes after irradiation can be extracted from the SIMS measurement and is presented on Figure 11. The ^{11}B count rate was used to quantify the variation of the ^{10}B content after the irradiation with the assumption that the ^{11}B content has not changed during the irradiation. The ^{10}B content in the specimen after irradiation in % of the initial content as well as the burnup are presented in Figure 12. From this curve an area averaged ^{10}B burnup value was calculated and compared with the value measured by (classical) inductively coupled plasma mass spectrometry (ICP-MS) from a neighbouring sample after dissolution, see Table II.

TABLE II. ^{10}B BURNUP DETERMINATION BY SIMS AND ICP-MS

	Isotopic concentration (atom%)		**^{10}B burnup (%)**
	^{10}B	**^{11}B**	
SIMS based ^{10}B burnup analysis	-	-	47 ± 2
ICP-MS burnup analysis on neighbouring sample	9.77	90.23	51 ± 0.5

5.2. Discussion

The applied SIMS analysis technique requests sample holder movements in front of the (stationary) secondary ion optical, electrostatical energy filter. The movement leads to variations in the electrical field strength and secondary ion extraction conditions, resulting in (with respect to the area) tilted count rate distributions. The ^{11}B normalization removes this problem and shows a symmetrical (cylindrical) ^{10}B distribution. Further secondary ion peaks of ^{3}H, ^{7}Li, ^{12}C and possibly also ^{4}He can be identified but are not discussed in this presentation.
The data presented in Figure 12 and Table 2 show that the technique leads to quantitative, local (and averaged) boron burnup results which can indeed be used to validate burnup models. The value of the technique is not limited to boron analysis as has been demonstrated by PSI in hafnium burnup and actinide distribution analyses on burnable poison and UO_2 and MOX fuel rods respectively [Ref 6 and 7]. Obviously such analyses could be introduced also for new absorber isotopes in discussion. Presently the error assessment is only qualitative and needs to be improved (e.g. by comparing in the future a ^{11}B normalization with a ^{12}C normalization). As indicated above, the distribution of lithium and tritium can be assessed as well. This analysis however makes sense only after improved (dry) sample preparation which will be tested next on full size dense boron carbide absorber samples.

6. SUMMARY

Several studies of failures in control rods have shown that the mechanism of cracks in stainless steel is IASCC. To avoid IASCC the most efficient way seems to be to remove causes for stresses in the component. If the absorber material can be designed not to strain the steel cladding, cracks will not appear in control rods under the nuclear life. Such an concept is to create a boron carbide pin of almost theoretical density where boron carbide densification is accomplished prior to operation. Modelling of the operational behaviour of pins is much easier then modelling of powder. By post irradiation isotope analysis in a cross section of the pins with techniques like SIMS, the modelling is improved. By using boron carbide pins without internal void it is ensured that the void,

now allocated outside the body, is ensured for accommodation of swelling. Designing a control rod to avoid stresses is more readily done this way.

Management of control rods must be based on experiences from inspection programs. Examinations such as neutron radiography have been a valueble help to reveal the consequences of absorber material behaviour in case of water intrusion after cracks in the stainless steel cladding. Data shows that the B_4C losses are neglible in rods with cracks. Cracks can be allowed to appear under operation. Knowledge of the base-line tritium levels in the reactor under operation makes it possible to interpret peaks in the tritium levels, which can be used in the planning of control rod handling. A concept is studied at ABB Atom.

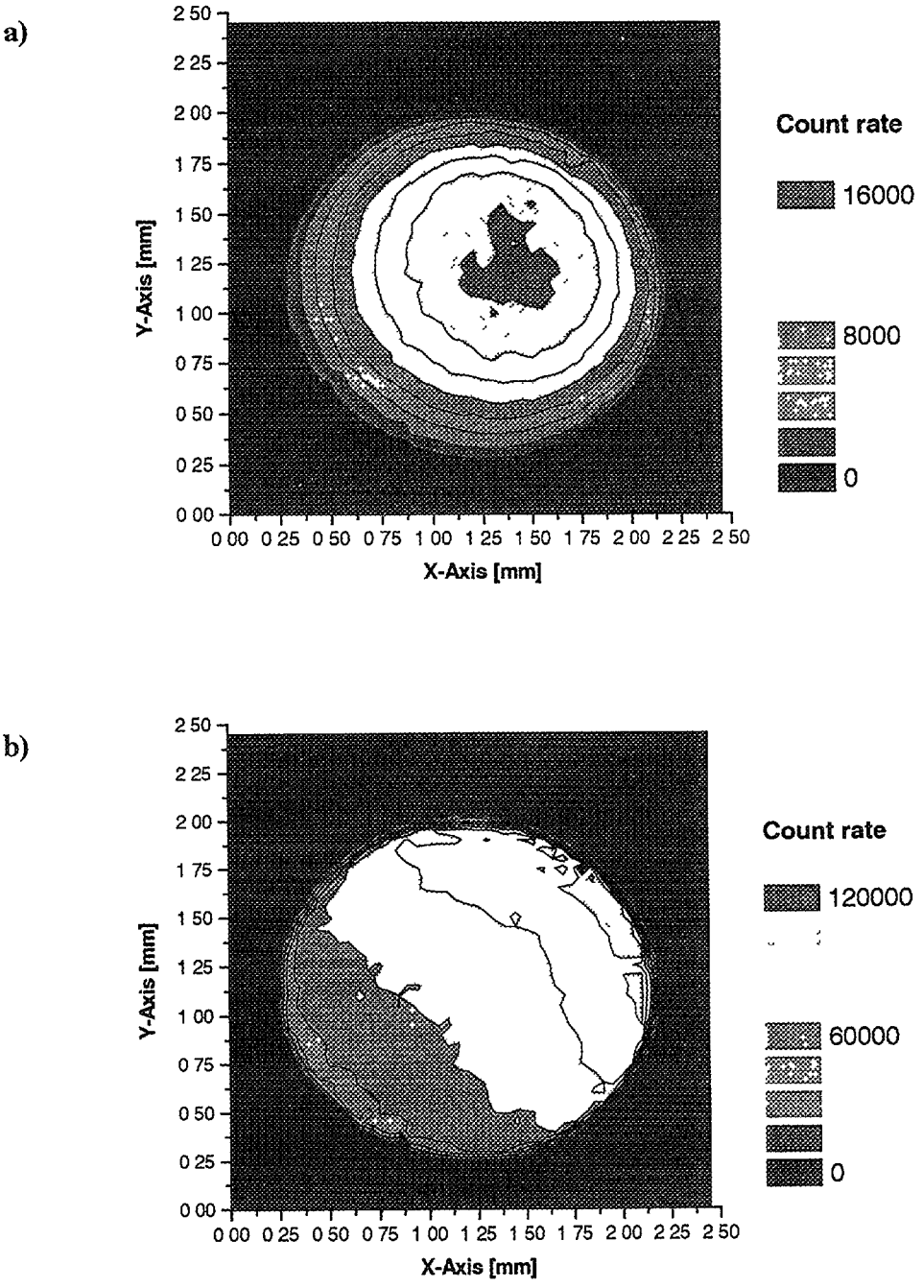

FIG. 10. SIMS area scan of the $B_{8\,5}C$ absorber specimen (Raw data, not corrected, not normalised). a) ^{10}B count rate distribution, b) ^{11}B count rate distribution

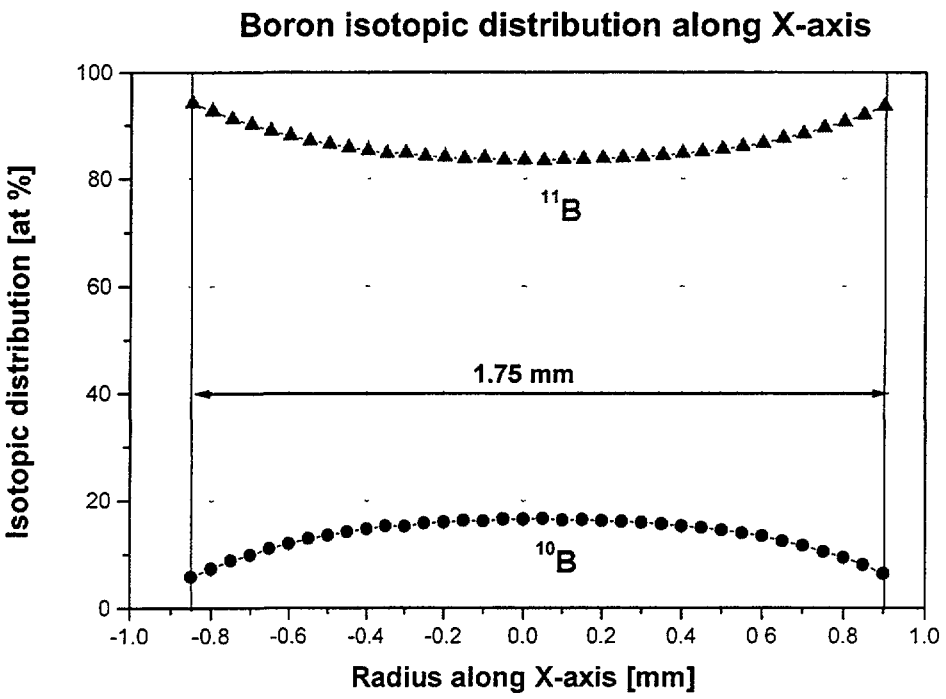

FIG. 11. Boron isotopic distribution along the X-axis of the specimen

(calculation : $Iso^{10}B(r) = \frac{cr^{10}B(r)}{cr^{10}B(r) + cr^{11}B(r)}$, $Iso^{11}B(r) = 1 - Iso^{10}B(r)$)

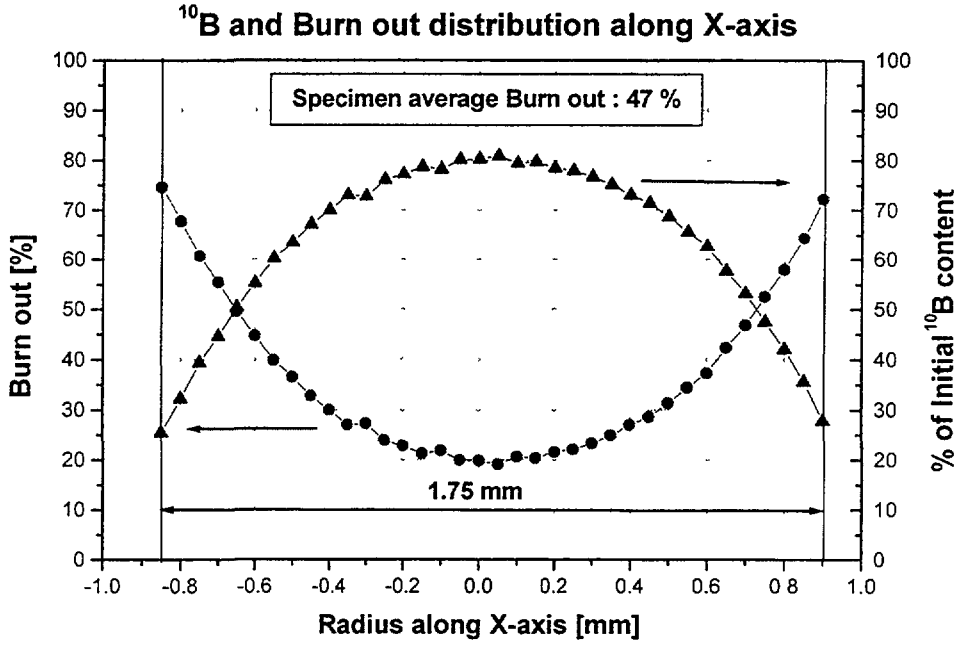

FIG. 12. ^{10}B content and burnup distribution along the X-axis of the specimen

(calculation : $^{10}B(r) = \frac{cr^{10}B(r)}{cr^{11}B(r)} \cdot \frac{^{11}B_{initial}}{^{10}B_{initial}}$, $BU^{10}B(r) = 1 - ^{10}B(r)$)

REFERENCES

[1] JENSSEN, A., LJUNGBERG, L., Sixth Int. Symp. on Environmental Degradation of Materials in Nuclear Power Systems – Water Reactors, Breckenridge, CO, 7-10 August, 1995, p.1043.

[2] Non published data.

[3] STRASSER, A., YARIO, W., Control Rod Materials and Burnable Poisons, EPRI TPS 79-708 (1980).

[4] BART, G., et al, Hf Control Rod Analysis for ABB – Final Report, PSI report TM 43 90-41 (Sept 1990).

[5] MASSIH, A.,"Hydrogen Uptake in Hafnium in ABB Atom Control Rods: Model Calculations", ABB Atom Report, UK 89-441.

[6] ZWICKY, H.U., et al., "Evaluation of the Radial Distribution of Gadolinium Isotopes in Nuclear Fuel Pins by Secondary Ion Mass Spectrometry (SIMS)", Radiochimica Acta 47, 9-12 (1989).

[7] Radial Plutonium and Fission Product Isotope Profiles in Mixed Oxide Fuel Pins Evaluated by Secondary Ion Mass Spectrometry (SIMS), JNM 202 (1993) 65-69.

EXPERIENCE OF CR AND RCCA OPERATION IN UKRAINIAN WWER-1000: ASPECTS OF RELIABILITY, SAFETY AND ECONOMIC EFFICIENCY

A. AFANASYEV
Ministry of Energy on Ukraine,
Ukrainian State Department of Nuclear Power,
Kiev,
Ukraine

XA0053632

Abstract

The next topics are represented in the paper

- A brief history of WWER-1000 control rod (CR) and WWER-1000 rod cluster control assembly (RCCA) design,
- Evolution of WWER-1000 CR manufacturing technology and design,
- Experience of RCCA operation,
- Lifetime extension of WWER-1000 boron carbide CR,
- WWER-1000 reactor core operation problems due to partial RCCA insertion,
- Designing and licensing procedures and first operational experience of WWER-1000 RCCA (CR) with a combined absorber "boron carbide-hafnium" and a chromium-nickel alloy cladding

The main conclusions are

- Fuel assembly (FA) bow is the main reason of partial RCCA insertion during reactor core operation However, the use of the RCCA and its driver bar with increased dead load, alongside with other measures, allow to reduce the probability of incomplete RCCA insertion,
- The materials used in CRs of RCCA in existing reactor operating modes have been working reliably,
- The use of hafnium under an appropriate price policy can give certain economic advantages for the Ukrainian NPPs, however, additional research is needed in order to confirm the specific CR physical characteristics and reliability

1. INTRODUCTION

The RCCAs of a reactor control protection system (CPS) are the most important elements of maintaining the safe reactor operation, ensuring control and distribution of reactor core power level and fast reactor core transfer from initial to subcritical condition during an accident. The share of RCCAs in fuel reloading cost is 1-1.2%. However, for CR materials choice it is necessary to take into account the possibility of inexpensive RCCA recovery or disposal.

2. THE SELECTION OF MATERIALS AND RCCA DESIGN, DEVELOPMENT OF RCCA

In the former USSR, the Moscow manufacturing plant of polymetals (MPP) was the designer and manufacturer of CR for almost all reactor types. The boron carbide (B_4C, with a natural mixture of isotopes) was selected as an absorber material because of it's accessible, cheap and quite effective material Stainless steel 06 X18 N10T was selected as CR clad material. The design of the WWER-1000 RCCA is shown in a Figure 1.

Up to 1985, CRs were produced by a joint drawing method. An initial pipe with a diameter of 11 mm and wall thickness of 0.7 mm, was filled with B_4C having a density of 1.65 g/cm^3 Then it was extended through some dies. Drawing was performed till the moment when the sizes of the pipe became equal to 8.2×0.6 mm, so that the average density of the absorber became equal to 1.95 g/cm^3 The B_4C density in the central part of the pipe was 1.6 - 1.65 g/cm^3 and on the rim layer 2 - 2.1 g/cm^3.

From late1985 until now, the RCCAs are produced by a method of vibro compaction of an initial pipe 8.2 × 0.6 mm with boron carbide of 1.75 g/cm^3 density. The initial pipe is not subject to deformation [1]. The advantages of this technology are the following:

- Less absorber material is needed;
- Some technological operations are eliminated from the process,
- The smaller the density of the boron carbide (1.75 g/cm^3) in the rim (external) layer, the smaller the swelling of B_4C particles is in the layer under the same neutron flux.

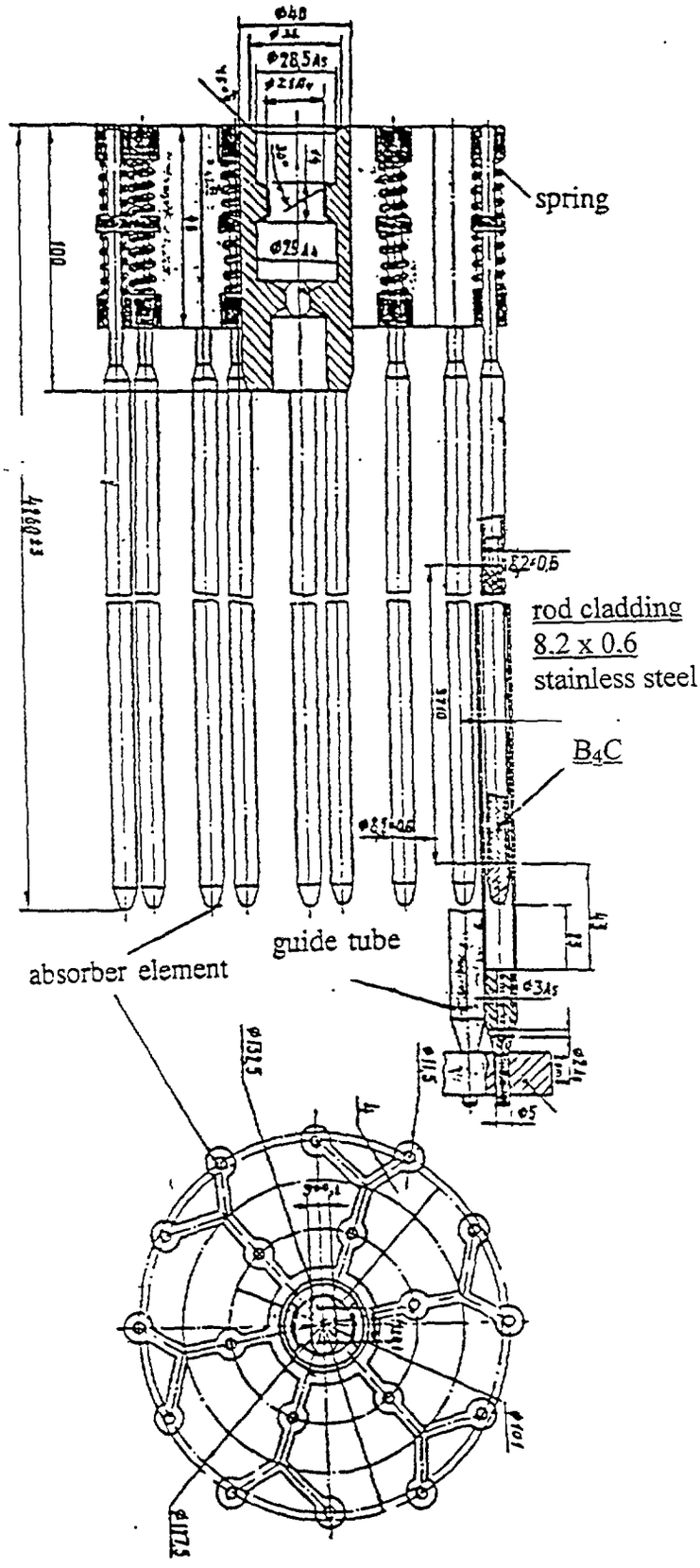

FIG. 1. WWER-1000 Rod cluster control assembly (RCCA) design

The change of B_4C density from 1.95 g/cm^3 up to 1.75 g/cm^3 has not reduced the efficiency of the RCCA. The RCCA efficiency measurements, with respect to various B_4C densities, have been made by using WWER-1000 critical assemblies. In the first case, the critical assembly was the fuel assembly (FA) from the first loading of unit-1 of the South Ukrainian NPP (49 RCCAs). In the second experiment, the critical assembly was the FA from the first loading of unit-1 of the Kalinin NPP (61 RCCAs). The results of the measurements [3] are shown in Table I.

TABLE I. RCCA EFFICIENCY MEASUREMENTS

Number	B_4C density in CR g/cm^3	Efficiency of RCCA %	RCCA relative efficiency (%)	Comments
1	1.80	9.8×10^{-2}	100%	
2	1.67	9.8×10^{-2}	100%	
3	1.14	9.4×10^{-2}	96%	there corresponds to burnup ^{10}B 33% for initial density B_4C - 1.75 g/cm^3
4	0.95	9.2×10^{-2}	93,7%	there corresponds to burnup ^{10}B 45% for initial density B_4C - 1.75 g/cm^3
5	0.69	8.6×10^{-2}	87.6%	there corresponds to burnup ^{10}B 60% for initial density B_4C - 1.75 g/cm^3

The initially RCCA lifetime was determined to be 1 year for control (regulating) groups (CGs) and 5 years for shut down (scram) groups (SGs).

3. EXTENDED RCCA OPERATION AND POST-IRRADIATION EXAMINATION

The results of high flux tests of an RCCA model in a material test reactor and commercial operation experience have created premises for RCCA lifetime extension. In order to provide lifetime extension, the RCCAs of unit-5 of the Novovoronezh NPP had been operated for longer time comparing with the period given by the project. After irradiation, these RCCAs have been examined at the Research Institute of Atomic Reactors (RIAR) and the Novovoronezh NPP hot cells. The research was performed and paid by the Russian and Ukrainian utilities (ROZENERGOATOM and GOSKOMATOM) [1-3].

The value of the neutron flux was checked up by means of ^{10}B burnup and accumulation of activation products (^{60}Co). The main results are given in Table II [1-3]. Completed tests and further research on CRs from CG have confirmed the expected outcome. Vibre compacted CRs have the best operating performances in comparison with joint drawn CRs.

The divergence in maximum thermal neutron flux (F^{max}) in CRs between calculated data (2.1×10^{21} by the Kurchatov Institute and OKB GP) based on ^{10}B burnup (4.5×10^{21}) and data based on ^{60}Co accumulation in the steel cladding of the CR (6.0×10^{21}) has been determined through SG CR research. The calculated results appeared to be underestimated.

The analysis of all research, resulted in establishing the values for several parameters, i.e. the maximum allowable ^{10}B burnup for vibro compacted CRs was 57.5%, the CR swelling ($\Delta\Phi$) was less than 1.2 % (implying that there were safety and plasticity margins of the cladding material) and the relative thermal neutron flux was 3.6×10^{21}.

TABLE II. RESULTS OF RCCA RESEARCH

Characteristic, parameter	**CR vibrating filling mode (Absorber of vibrating packed type)**		**CR joint drawing mode**
Time of operation, maximal neutron fluence, $F^{max} \times 10^{21}$	CG 2 y, 491 eff. days, neutron energy: E>08MeV ~3.3 E>01MeV ~5.4 thermal ~1.5	CG 3 y, 819 eff. days, neutron energy: E>08MeV ~7.6 E>01MeV ~12.5 thermal ~3.2	SG 7 y, 2028 eff. days, neutron energy: E>08MeV ~4.5 E>01MeV ~6.1 thermal ~4.5
General state of the CR	All of CR have saved the form and tightness. There is black dense oxide film the thickness of which 4 - 7 microns on a surface		Longitudinal cracks (L=10mm) are detected at the bottom CR
CR swelling in the area of F^{max} ($\Delta\varnothing$)[mm, /%]	0	0.02 - 0.06 0.24 - 0.72	0.11 - 0.16 1.35 - 2.0
Burnup of ^{10}B, %	max. ~32.5	max. ~53.2	max. ~72 - 77
Helium release under cladding	70-130 [cm^3]	260-350 [cm^3]	~100[cm^3], part of gas has left through cracks
Pressure of gas under cladding	at 20°C 2-4 bar at 333°C 4-8 bar	at 20°C 15-25 bar at 333°C 35-56 bar	2-9 bar, ,Part of gas has left through cracks
Absorbing material B_4C state	Powder B_4C freely hailed down under cutting of cladding on samples	At the CR bottom there was a sintering of a powder, which densely adjoins to the cladding. Change of cladding diameter + 0.2 - 0.7%	swelling of the CR bottom B_4C lead to the open cracks
Mechanical properties of cladding in the area of F^{max} σ_b[MPa] σ_{02}[MPa] δ_0 [%]	σ_b at 20°C - 820 σ_b at 350°C - 520 σ_{02} at 20°C - 500 σ_{02} at 350°C- 290 δ_0 at 20°C - 14.2 δ_0 at 350°C - 7.1	σ_b at 20°C - 893 σ_b at 350°C - 630 σ_{02} at 20°C - 670 σ_{02} at 350°C - 580 δ_0 at 20°C - 18.6 δ_0 at 350°C - 1.1	σ_b at 20°C - 830 σ_b at 350°C - 580 σ_{02}at 20°C - 640 σ_{02} at 350°C - 480 δ_0 at 20°C - 26,4 δ_0 at 350°C - 3.9
General conclusion on spent CR state	CR condition is satisfactory. It is probable to continue their operation within one more year (fuel cycle)	CR are close to extreme allowable condition. CR swelling makes 0.24-0.72 % in the area of F^{max}	Actual duration of operation has exceeded allowable time for this CR type, that has caused the excessive swelling of B_4C and cladding, of cracks, washing away of B_4C

4. EXPERIENCE OF RCCA LIFETIME EXTENSION

4.1. Operation time

The operation time of RCCAs for CG was enlarged from 1 to 2 fuel cycles [3].

4.2. Life extension

The unconditional specification of the RCCA lifetime extension for SG from 5 to 6 years (and even to 7 years) was not possible, based on the results of the research, as the calculated thermal neutron flux density above the reactor core was lower than the actual value.

In order to be able to specify the SG RCCA lifetime extension, the exact position of the RCCA lower flat end above the reactor core for each unit in each fuel cycle is needed. The lower flat end of RCCA would be within the 0.9 - 14.9 cm above the core in serial WWERs-1000 (e.g. for unit-5 of Novovoronezh NPP - 7.7-8.7 cm). The thermal neutron flux density within the same range should not be a constant value. The dependence of the allowable time of SG RCCA operation according to the position of the lower flat end is given in Table III [2].

TABLE III. ALLOWABLE OPERATING TIME OF RCCAs

Position of the lower flat end B_4C above the core h (cm)	**^{10}B burnup for 1 year of operation (300 eff. days) (%)**	**allowable time of SG RCCA operation (eff. days/years)**
0.9 - 8	11.4	1530\5
9	11.1	1570/5
10	10.7	1630/5
11	10.0	1735/5
12	9.3	1870/6
13	8.7	2000/6
14	7.85	2210/7
14.9	7.23	2400/8

Approximately 10 - 15 % of Ukrainian WWER-1000 SG RCCAs have been operated during the 6 fuel cycles. The total duration of operation did not exceed 1700 -1790 effective days. The experience of SG RCCA lifetime extension to 6 and more years has not received broad attention for the reason of difficulties related to monitoring of the RCCA lower flat end position. During the whole period of operating WWERs-1000 in the Ukraine, there occurred no RCCA damage. The materials used in the RCCAs performed reliably.

5. RESULTS OF IMPROVED RCCAs BASED ON A COMBINATION OF Hf AND B_4C

The cost, allowable time of operation, and possibility of inexpensive disposal are the main consumer features of RCCAs. In order to increase the RCCA lifetime, it is required to replace the bottom (300-500 mm) n/α absorber B_4C by an n/γ absorber (Hf, Dy_2TiO_5or In-Ag-Cd, which doenot swell) and to use cladding material that will be more stable to radiation embrittlement.

12 RCCAs with combined Hf-B_4C absorber were designed, manufactured and accepted by an interdepartmental commission. In 1997, they were loaded in the WWER-1000 of the Rovno NPP for the operation according to a joint decision of GOSKOMATOM and MPP (with participation of Kurchatov institute, RIAR, OKB GP). The CR cladding was made from Cr-Ni alloy EP-630Y. The design of the combined absorber CR is shown in Figure 2. It was decided to use the new designed RCCA in SG.

The ingots made in the Ukrainian zirconium plant, based on the calcium-thermal recovery technology and further double electronic radial remelting, were used as raw Hf source material. Further processing and manufacturing of Hf rods for CRs were carried out in Russia. Samples of Hf pipes with a diameter (⌀) 9.6 mm, wall thickness of 2 mm, length 100 mm (9.6×2 mm) and rods with a diameter of 8.2 mm, length 10 mm were stage by stage irradiated and investigated in RIAR for the period 1993 - 1997.

Irradiation of samples located in ampoules were made in the material test reactors (BOR-60, in a sodium environment at a temperature of 340 - 360°C, and in CM-2, in water at 60 - 80°C). At the first stage, the irradiation was performed in BOR-60 by a fast neutron flux of (E>1 MeV) 1×10^{22}.

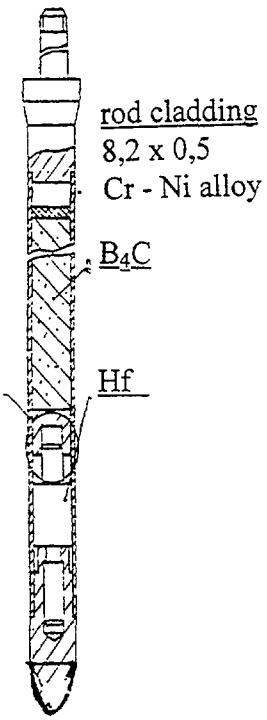

FIG. 2. Combined absorber rod design (Hf + B_4C)

The diameter of the pipe decreased by 0.3% and that of the rod by 0.8%. The lengths of the pipe and rod were increased by 0.3% and 1%, respectively after the irradiation. The densities of the pipe and rod have decreased by 0.42% and 0.55%, respectively. The pipe has plasticity at the level of 1-2% and there was no damage. Two longitudinal radial cracks, which could have occurred at the rod manufacturing stage, were detected. The Hf rod was damaged (an = 4 kgm/cm^2) [4] by shock tests. For that reason the Hf rod has been located inside the cladding. As cladding material, the Cr-Ni alloy (Cr-42%, Ni-56%, Mo-1%) was used. This material named as EP-630Y has a high plasticity after long irradiation and a high corrosion stability (resistance) in a water environment. At the second stage, the irradiation was performed in BOR-60 and CM-2 by a fast neutron flux of (E>1 MeV) 3.4×10^{22}. The average radiation growth of the sample was 3%. After the first stage of irradiation, cracks of the same form and size were detected in the rods [5]. The mechanical properties of EP-630Y are given in Table IV [6].

TABLE IV. MECHANICAL PROPERTIES OF EP-630Y

Temperature [°C]	Neutron fluence$\times10^{22}$ E>8MeV [cm^{-2}]	σ_{02} [MPa]	σ_b [MPa]	δ_p [%]
20	0	360	770	53
	0.7	640	840	50
	2.7	750	870	44
	6.8	820	910	22
300	0	250	640	52
	0.7	480	800	40
	2.7	540	660	39
	6.8	660	680	16

The behaviour of modelled CR was investigated under accident conditions:

- B_4C, Hf, Dy_2TiO_5 absorbers do not affect the EP-630Y cladding at temperatures between 350 and 500°C during 1000 hours;
- The CR research under simulated cladding leakage conditions (temperature of overheated steam of 1150°C) has shown, that there is reliable compatibility of Hf and Dy_2TiO_5. The Hf modelled CR surface damage was revealed at a level of 400μm. The melting occurred in the Hf cladding contact area under a vapour temperature of 1250°C [10].

6. SOME LICENSING REQUESTS

In order to obtain the licence of the nuclear regulatory administration (NRA) for CR test performance, it should be shown that, at the time of the RCCA insertion, the reactivity derivative ($\partial\rho/\partial\tau$) will be negative (the accident factor of the Chernobyl NPP). This condition is always required if the CR lower part has the lowest differential efficiency.

7. EXPERIMENTAL RESULTS OF THE COMBINED Hf-B_4C ABSORBER EFFICIENCY.

The Hf efficiency has been calculated and is 80% of the B_4C efficiency. The use of more durable cladding material allows to decrease the wall thickness from 0.6 mm down to 0.5 mm and consequently to increase the absorber diameter from 7 mm to 7.2 mm. The calculated combined Hf-B_4C RCCA efficiency is equal to 1.025 of the ordinary RCCA [6, 7].

Efficiency measurements have been made in the beginning of cycle (BOC) at a level of 1-2% of $N_{nominal}$, with a temperature of 280°C and a pressure of 160 bar. The location of the RCCA groups, including the combined groups (#2 and #7), is shown on Figure 3. The Rovno WWER-1000 reactor core parameters in the BOC (for the 11^{th} fuel cycle) are presented in Table V.

TABLE V. ROVNO REACTOR CORE PARAMETERS

Date of experiment	**Effective days**	**CG position %**	**H_3BO_3 concentration g/kg**	**Xe**
6 Nov. 97	0	0 - 90	8.5 - 9.3	no
17 Nov. 97	7	55 - 57	7.7	yes
18 Nov. 97	7	36 -50	7.7 - 8.0	yes

On 6 November 1997, differential and integral RCCA efficiencies were measured at the time of RCCA insertion by means of a reactivity meter. The inserted reactivity was compensated by CG (#10) movement. Separated RCCA movement, combined groups (#2 & #7) movement, and groups (#1 and #8) movement have been made step by step (in turn) from upper position (H=100%) down to lower position (H=0%) by steps of 5%. The reactor criticality was maintained constant, as well as the coolant pressure, temperature and H_3BO_3 concentration. The measurement results are presented in Figures 4 and 5.

On 18 November 1997, differential and integral RCCA efficiencies were measured at the time of RCCA insertion by means of a reactivity meter. Inserted reactivity was compensated by H_3BO_3 concentration change. Separated RCCA movement, combined groups (#2 & #7) movement, and groups #1 and #8 movement have been made step by step (in turn) from upper position (H=100%) down to lower position (H=0%) by step of 5%. The reactor criticality was maintained constant, as well as the coolant pressure and temperature, and the CG position was at the level of H=55%.

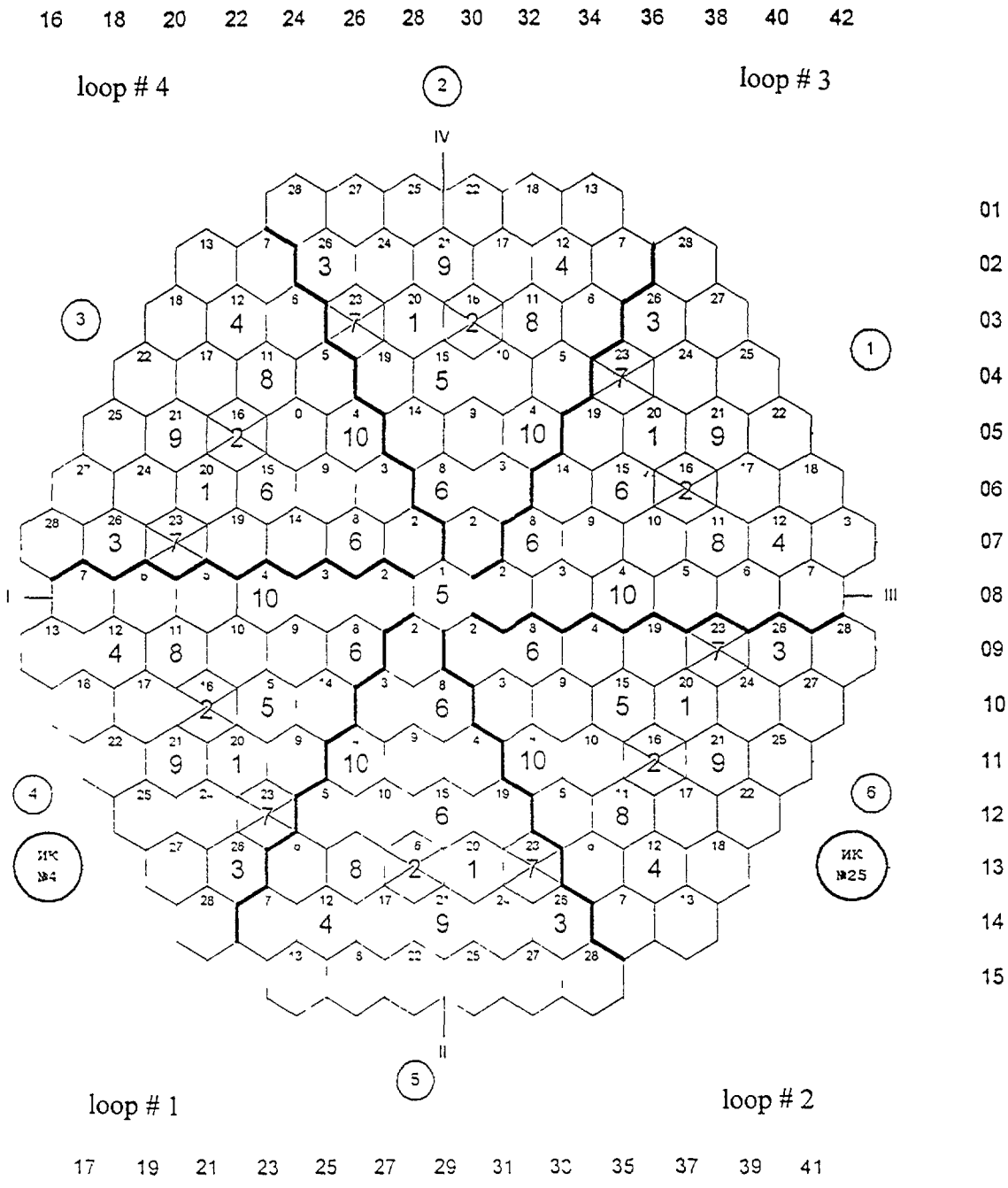

FA Number in 60^0 symmetry sector
- Number of RCCA group (X - Hf RCCA)

FIG 3 Reactor core of the Rovno unit-3, 11th fuel cycle

In addition, the measurements of combined group (#2 & #7) 10% insertion efficiency (that corresponds to the height of Hf absorber) alongside with insertion of groups #1 and #8 were completed The same was done for 20% of separate RCCA insertion The results are shown on Figures 6 and 7.

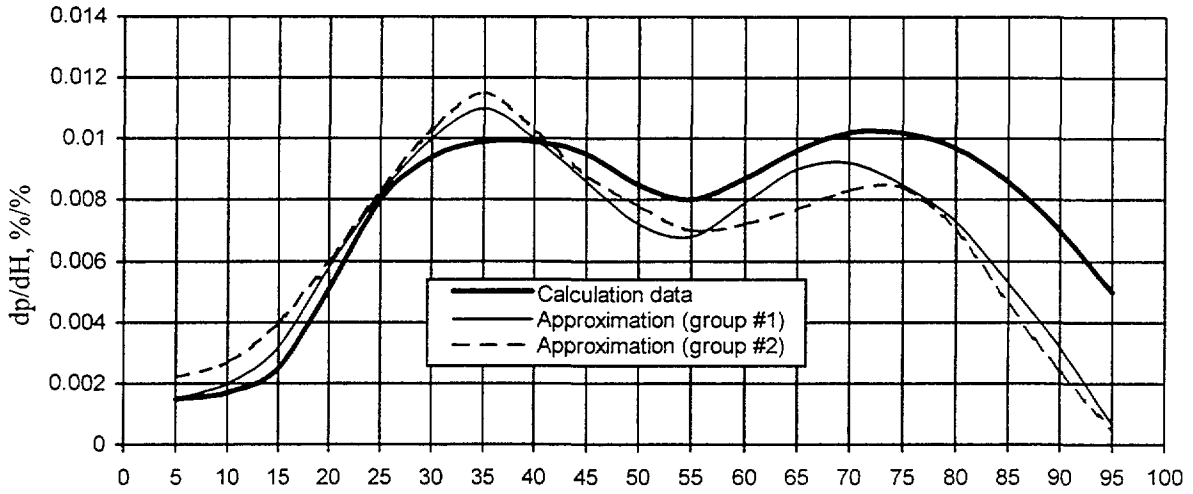

FIG. 4. Differential characteristics of RCCA group (#1 and #2 (Hf)), The reactivity was compensated by control group (CG)

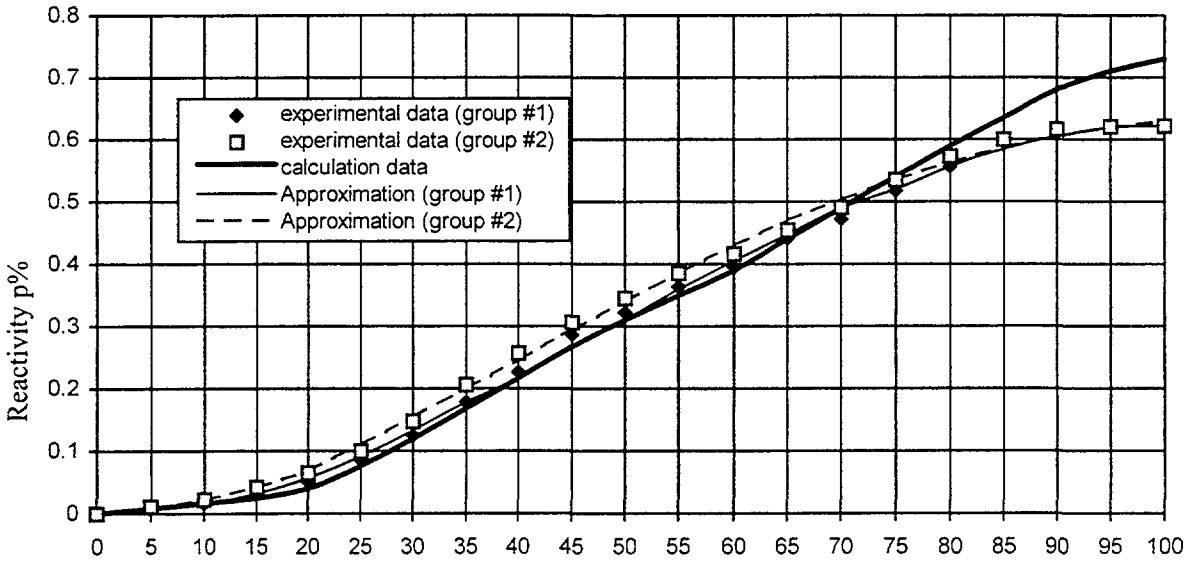

FIG. 5. Integrated characteristic of RCCA group (#1 and #2 (Hf)), The reactivity was compensated by control group (CG)

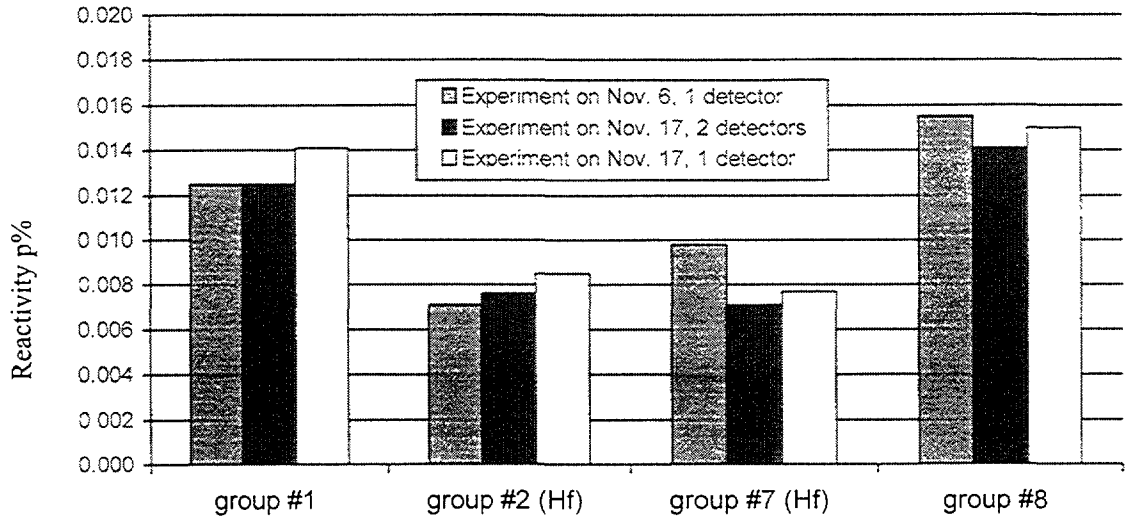

FIG. 6. Integrated efficiency of 10 % of groups RCCA (groups #1, #2(Hf), #7(Hf), #8), the RCCA lower flat end position in core (H%) was changed from 100% up to 90%

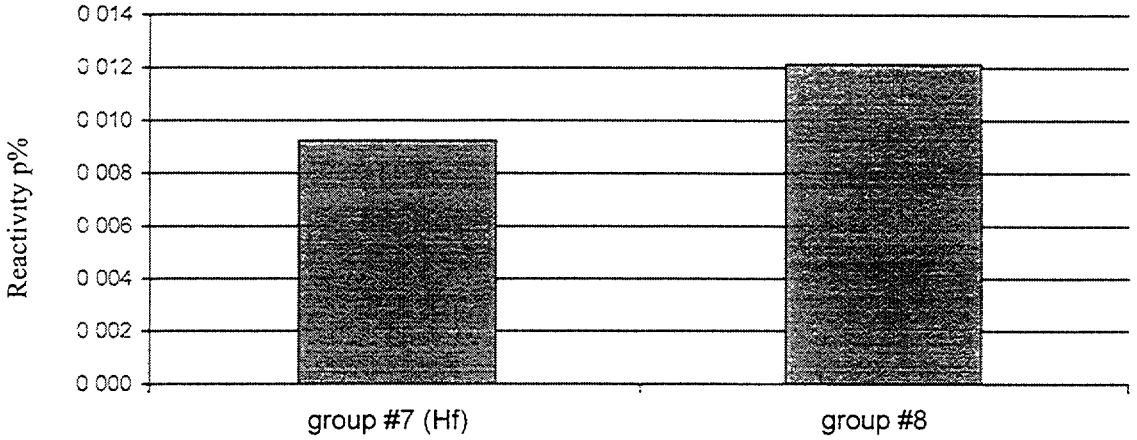

FIG. 7. Integrated efficiency of 20% separate (one) of RCCA in group (group #7(Hf), #8), the RCCA lower flat end position in core (H%) was changed from 100% up to 80% (experimental data)

By the 13th of September 1998 at the end of cycle (EOC), the measurements have been made at the power level of 50% $N_{nominal}$. According to the preliminary data, the results were similar to those obtained earlier. The results allow to conclude:

- integral characteristics of RCCA with and without Hf are almost the same (Figure 8);
- at the moment of 20% insertion, the integral efficiency of the lower part of the RCCA with Hf was 24% less then the ordinary RCCA;
- at the moment of 10% insertion, the efficiency of the RCCA with Hf was equal to 0.53-0.58 against the ordinary RCCA efficiency (the calculated value was 0.8);
- at the moment of reactor scram, the summary efficiency of the RCCA was equal to 8.7% and exceeded the calculated value (7.5%).

In order to clarify the reasons of low Hf efficiency in existing RCCAs, it is useful to perform calculation of:

- burnup effect (neutron spectrum influence);
- research on geometry effect on the RCCA lower part efficiency;
- safety analysis of RCCA with Hf as CG.

When RCCA with Hf are used as SG all safety requirements are met.

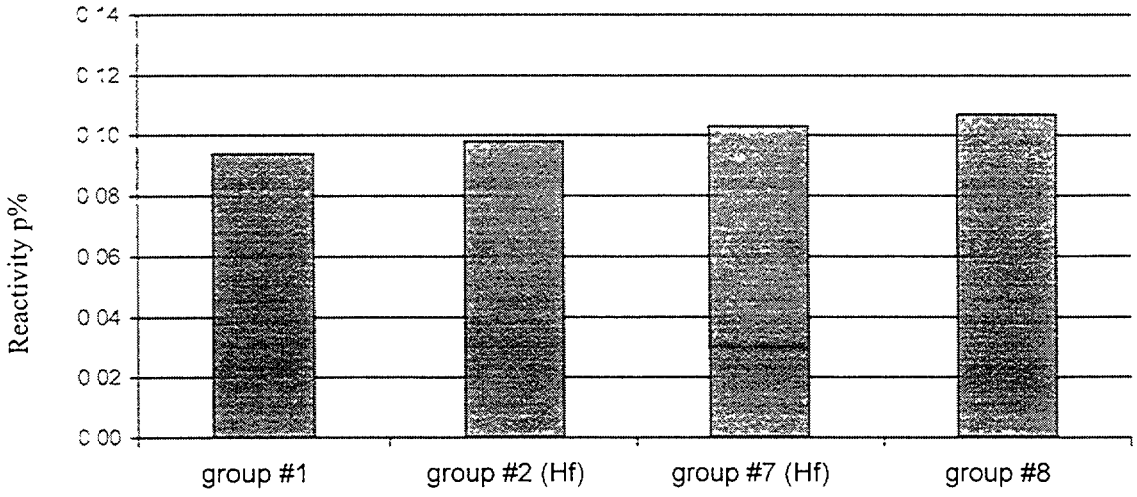

FIG 8. Integrated efficiency of separate (one) RCCA in groups (groups #1, #2 (Hf), #7 (Hf), #8) (experimental data)

8. SAFETY PROBLEMS OF REACTOR OPERATION WITH INCOMPLETE RCCA INSERTION

During 1992 and 1993, almost at all WWER-1000 in Ukraine, Russia and Bulgaria incomplete RCCA insertion occurred, i.e. an RCCA stuck in an intermediate position and RCCA drop time exceeding 4 s (design time). A programme of additional quarterly measurements of RCCA drop time was developed and implemented. In the case of RCCA operation violation (and when there was no chance to cease one) the unit had been transferred to the operational mode with three loop coolant circulation and with preliminary power reduction to 67% of $N_{nominal}$.

The following Ukrainian units were transferred to the 3 loop operational mode:

- Zaporozye NPP unit 1; fuel cycle # 7 and 8; Generation loss- $2,1\times10^9$ kWh;
- Zaporozye NPP unit 3; fuel cycle # 7 , 8 and 9; Generation loss-$3,3\times10^9$ kWh;
- South Ukraine NPP unit 2; fuel cycle # 7; Generation loss-$1,0\times10^9$ kWh.

In 1993, the chief reactor designer had calculated the neutron physical and thermal hydraulic characteristics of the reactor core for the RCCA drop time up to 10 s, keeping in mind the case when all RCCA are inserted except the most effective RCCA. It was shown that the design safety criteria were met. However, the results obtained were not used to cancel operational restrictions according to the conservative principle. Fuel assembly (FA) bow is the main reason of incomplete RCCA insertion during reactor core operation. Complicated form of FA bow results in:

- appearance of additional friction force between CR and guide thimble clad;
- either RCCA drop time increase in scram mode or RCCA jam in intermediate position;

In order to reduce the probability of incomplete RCCA insertion, to decrease the size of FA bow and to ensure the reactor's safe operation, the following compensatory measures have been performed during the scheduled repairs in 1993-1997:

1) New designed heavier RCCAs with gafnium or titanat of dysprosium were used in the Rovno and Zaporozye NPP;
2) The dead load of the RCCA driver bar was increased;
3) In order to decrease losses of the RCCA kinetic energy during RCCA insertion (the pump effect), holes in the RCCA driver bar have been drilled;
4) The position of the bundle safety tube (BST) was updated with the purpose of maintaining the spring block of the FA, without exceeding the compress maximum (axial compression of FA head).

Figure 9 shows the curves of RCCAs (both of original and advanced design) drop speed [9].

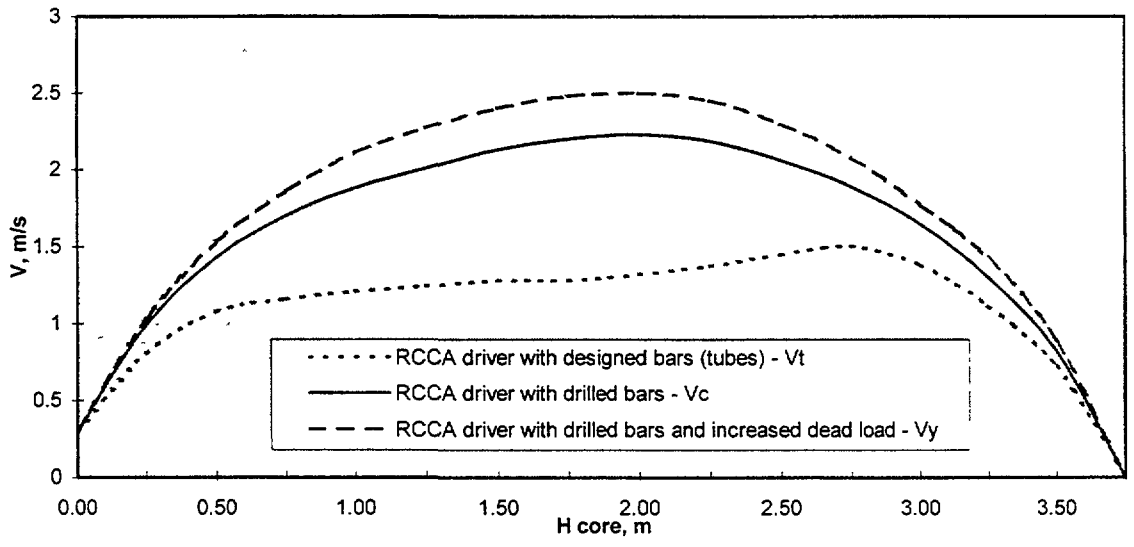

FIG. 9. Curve of average speed of RCCA drop

In Figure 10, the curves of the RCCA drop time change for the period 1993 - first quarter of 1998 are represented as an example for Zaporozhe NPP-2. Before the implementation of compensatory measures for Ukrainian WWERs-1000, the average RCCA drop time (τ average) was 3.3 s, 200 RCCAs had a drop time larger than 4 s and 28 RCCAs were jammed After implementation of measures, the average RCCA drop time was 2 5 s, whilst 11 RCCAs had a drop time larger than 4 s and only 1 RCCA was jammed.

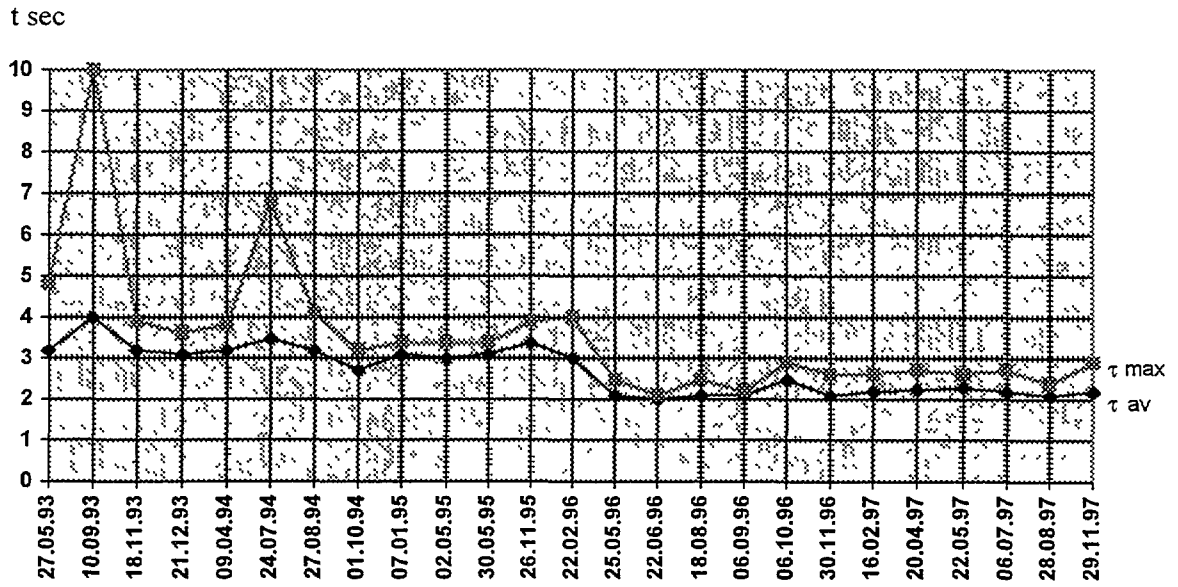

FIG 10 Measurement of RCCA drop time on ZNPP-2

Only after the beginning of the implementation of compensatory measures for the period 1995 - first quarter of 1998, 140 RCCA drop tests have been performed, from which 18 have been performed at 40-50% $N_{nominal}$ power level, some measurements have been done at power level of 20-30% $N_{nominal}$ and the rest was performed under "hot shutdown" conditions The results of "under power" tests have complied with the design requirements The average results of the RCCA drop time measurements on all Ukrainian WWER-1000 units before and after compensatory measures are presented in Table VI.

TABLE VI SUMMARIZED RESULTS OF RCCA DROP TEST

NPP/UNIT	**τ average (s)/Number of RCCAs with τ > 4s/Number of jammed RCCAs**	
	For the period before compensatory measures were applied (1993-1995)	For the period after compensatory measures were applied (1995 - first quarter of year 1998)
Zaporozhe NPP 1	3 22 / 34 / 8	2 31 / 0 / 0
Zaporozhe NPP 2	3 18 / 30 / 0	2 18 / 0 / 0
Zaporozhe NPP 3	3 17 / 29 / 6	2 61 / 0 / 0
Zaporozhe NPP 4	3 21 / 11 / 0	2.52 / 0 / 0
Zaporozhe NPP 5	3 28 / 9 / 8	2 85/ 2 / 1
Zaporozhe NPP 6	3 15 / 1 / 0	2.68 / 2 / 0
South Ukraine NPP 1	3 5 / 0 / 0	2.51/ 0 / 0
South Ukraine NPP 2	3 72 / 32 / 1	2 48 / 0 / 0
South Ukraine NPP 3	3 55 / 19 / 0	2 35 / 3 / 0
Rovno NPP 3	3 465 / 35 / 5	2 74/ 3 / 0
Khmelnitski NPP 1	3 72 / 12 / 0	2 53 / 1 / 0

REFERENCES

[1] PONOMARENKO, V., RISOVANY, V., SHMELEV, V., KONDRATYEV, V., et al., "Control rod and burnable absorber rod of reactor and paths of their perfecting", Problems of Atom Science and Engineering, Series: Radiation Damaging Physics and Radiation Materials Science, issues 2/63 and 3/63, Kharkov, (1994).

[2] CHERNYSHOV, V., RISOVANY, V., KOSOUROV, K., VASILCHENKO, I., et al., "The substantiation of WWER-1000 SG RCCA lifetime extension", Moscow, (1994).

[3] PONOMARENKO , V., CHERNYSHOV, V., RISOVANY, V., OSADCHIJ, A., VASILCHENKO, I., et al., "The substantiation of WWER-1000 CG RCCA lifetime extension up to 2 years" , Moscow, MPP, (1992).

[4] CHERNYSHOV, V., RISOVANY, V., PONOMARENKO, V., et al., "Research of hafnium control rod models irradiated in the reactor BOR-60 up to a fluence of fast neutrons (E>1MeV) equal 1×10^{22} cm^{-2}", Dimitrovgrad, (1994).

[5] HUDJAKOV, A., KLOCHKOV, Å., RISOVANY, V., et al., "Dimensional and structural stability of a hafnium sample irradiated up to high dose", Problems of Atom Science and Engineering, Series: Radiation Damaging Physics and Radiation Materials Science, issue 2/68, Kharkov, (1998).

[6] RJAHOVSKIH, V., SHMELEV, S., et al., "State of WWER-1000 RCCA development and production, Problems of Atom Science and Engineering, Series: Radiation Damaging Physics and Radiation Materials Science, issue2/66, Kharkov, (1997).

[7] Report # 32/1-89-97, Kurchatov Institute.

[8] SOKOLOV, D., BORIS, V., GRABKO, V., KOLISNICHENKO, M., et al., "Results of RCCA neutron physical characteristic measurements in WWER-1000 at the BOC (fuel cycle #11)", Report, Rovno, (1998).

[9] AFANASYEV, A., "Comparison of WWER-1000 and PWR cores with fuel assembly bow operational experience and problems", Problems of a Atom Science and Engineering, Series: Radiation Damaging Physics and Radiation Materials Science, issue 2/68, Kharkov, (1998).

[10] CHERNYSHOV, V., TROYANOV, V., "Lessons learned from control rod irradiation experience; development of advanced absorbers and their refractory properties under accident condition", (Proc. Int. Top. Meeting on Light Water Reactors, Portland, Oregon, 1997).

DYSPROSIUM AND HAFNIUM BASE ABSORBERS FOR ADVANCED WWER CONTROL RODS

V.D. RISOVANIY, A V. ZAHAROV, E.P. KLOCHKOV,
E.E. VARLASHOVA, D.N. SUSLOV
State Scientific Center of the Russian Federation
"Research Institute of Atomic Reactors" (SSC RF RIAR),
Dimitrovgrad

A.B. PONOMARENKO, A.V. SCHEGLOV
Moscow Polimetal Plant (MPP),
Moscow

Russian Federation

Abstract

Disprosium titanate is an attractive control rod material for thermal neutron nuclear reactors such as WWER and RBMK Its main advantages are almost non-swelling, no out-gassing under neutron irradiation, quit high neutron efficiency, a high melting point (~1870°C), non-interaction with the cladding at temperatures above 1000°C, simple fabrication, non-radioactive waste and easy to reprocess The disprosium titanate control rods have worked without operating problems in the reactor MIR during 17 years and in WWER-1000 4 years After post-irradiation examinations, this long-life control rod type was recommended for using in the nuclear reactors Dysprosium hafnate is a promising absorber ceramic material The research results confirmed that it has a large radiation damage resistance The examination results of hafnium dummies (GFE-1) irradiated in BOR-60 are presented The maximum accumulated neutron fluence was 3 $4x10^{22}cm^{-2}$ (E>0 1 MeV) and the temperature range was 340 to 360°C Due to high radiation growth (3-4 %) and the absence of an axial gap between the dummy and the upper capsule tip the dummies were bent The irradiated dummies have high mechanical properties Other aspects of the expected hafnium irradiation behaviour and the use of hafnium in control rods are discussed This report presents some experimental data on Dy_2O_3 TiO_2, Hf, Dy_2O_3 HfO_2 and possibilities of their use in WWER control rods

1. INTRODUCTION

At present, boron carbide (WWER-1000) and boron steel (WWER-1, -2, -3M, WWER-440) are the most widely used in control rods of Russian water reactors. These absorber materials have large radiation damages owing to (n,α)-reaction on ^{10}B isotopes, helium formation and swelling. The first damage of WWER-1000 Rod Cluster Control Assembly (RCCA) due to B_4C swelling and cladding cracking was noticed in the Novovoronezh Nuclear Power Plant.

Long before this accident, the State Scientific Center of the Russian Federation "Research Institute of Atomic Reactor" (SSC RF RIAR) (together with the Moscow Polimetal Plant (MPP)) carried out research on (n,γ) absorbers, which do not swell. More than 60 ceramic absorber materials based on Dy, Eu, Sm, Gd, Hf, Cd, pure Hf and Hf-alloys were investigated.

Post-irradiation examinations have shown that lanthanide oxides ($Ln_2O_3 \cdot MO_2$) with fluorite structure have the largest radiation damage resistance among the ceramic absorber materials. Dysprosium titanate ($Dy_2 \cdot TiO_5$) was selected for WWER-1000 RCCA. It is used in commercial reactors since 1995. Dysprosium hafnate ($Dy_2O_3 \cdot HfO_2$) has attractive properties too. It is characterized by a more stable fluorite structure, larger efficiency and less swelling in comparison with $Dy_2O_3 \cdot TiO_2$. Now dysprosium hafnate research is continued. Hafnium has attractive properties too, especially when it is used simultaneously as absorber and cladding material [1].

2. DYSPROSIUM TITANATE

Natural dysprosium has 5 stable isotopes which have comparatively high absorption cross-sections for thermal neutrons (Fig. 1). Decay products are Ho and Er. All produced radionuclides have small γ-activity and small half-life time. Some results of the γ activity of irradiated $Dy_2O_3 \cdot TiO_2$ are shown in Table I.

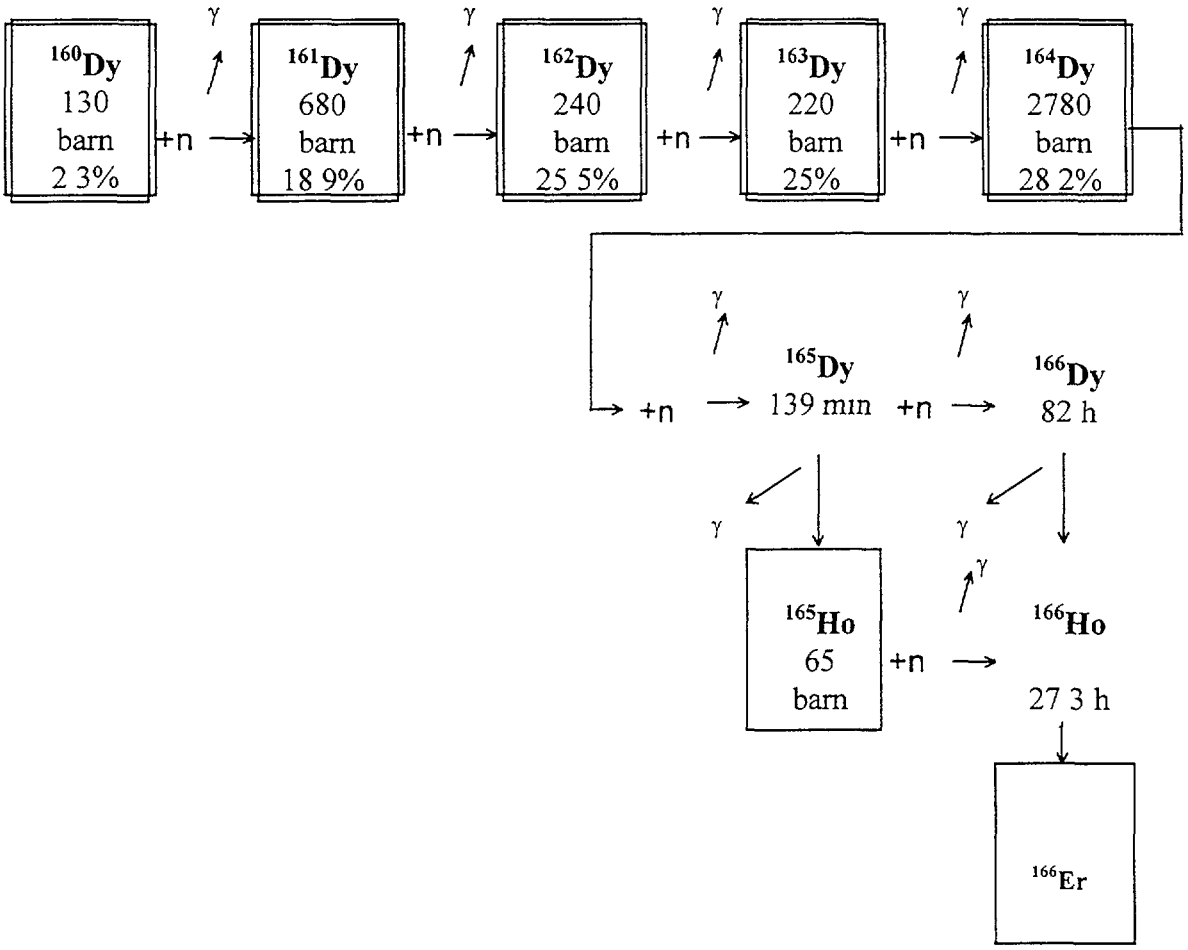

FIG 1 Transformation of irradiated disprosium

TABLE I γ ACTIVITY OF Dy_2O_3 TiO_2

Sample	Fluence, $\times 10^{22}$ cm ^{2} (E>0 1 MeV)	Time after irradiation day	Distance m	γ activity μR/s
Pellets of Dy_2O_3 TiO_5 m=2 5 g	0 9	380	0	200±20
			0 35	100±10
			0 80	15±15

According to the Dy_2O_3 TiO_2 phase diagram (Fig 2), an interaction between Dy_2O_3 and TiO_2 can result in formation of two compounds They are dysprosium dititanate (Dy_2 Ti_2O_7) and dysprosium titanate (Dy_2 TiO_5), the last is polymorphous (at low temperature it has a the rhombic lattice, with rising temperature it transforms into a hexagonal lattice (~1350°C) and then into a fluoride (~1680°C)) The melting point of Dy_2 TiO_5 is 1870°C It is possible to obtain Dy_2 TiO_5 with different initial crystal structures verifying heating and cooling regimes The fluorite structure of Dy_2 TiO_5 has less swelling under irradiation and is more promising to be used as a control rod absorber material During irradiation the pyrochlore structure can transmute into the fluorite (Fig 3)

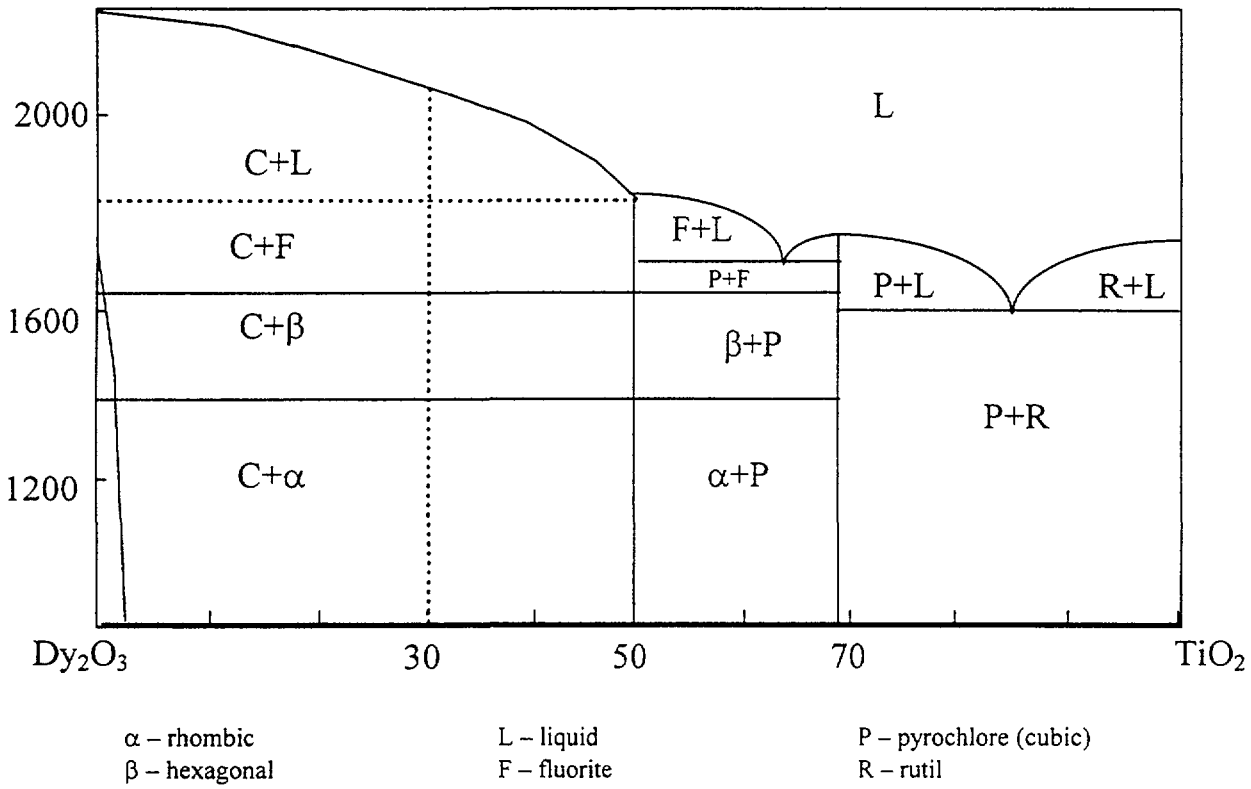

FIG. 2. Dy_2O_3·TiO_2 phase diagram

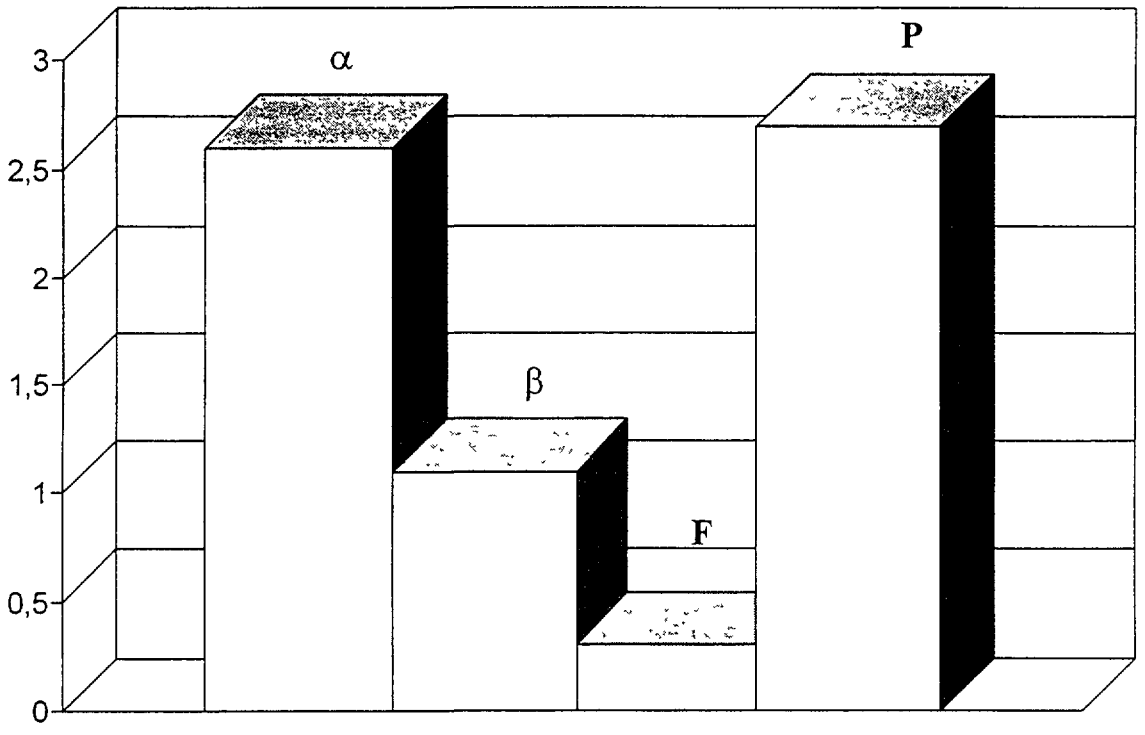

FIG. 3. Volume variation of phase components of dysprosium titanate after irradiation ($F=1\times10^{22}$ n/cm^{-2}, T=250-450°C)

The initial physical efficiency of $Dy_2 \cdot TiO_5$ ($\rho \sim 5$ g/cm^3) in WWER-1000 environment is 15% smaller than that of natural B_4C ($\rho \sim 1.7$ g/cm^3). On the other hand, $Dy_2 \cdot TiO_5$ has a higher life-time (Fig. 4) due to existence of daughter isotopes characterized by high absorption cross-sections. It makes $Dy_2 \cdot TiO_5$ very attractive for use in control rods. The physical efficiency of $Dy_2 \cdot TiO_5$ control rod decreased only by 5-6 % within 17 years of operation in the research reactor MIR (RIAR) ($F = 2.2 \times 10^{22}$ cm^{-2} (E>0.1 MeV))

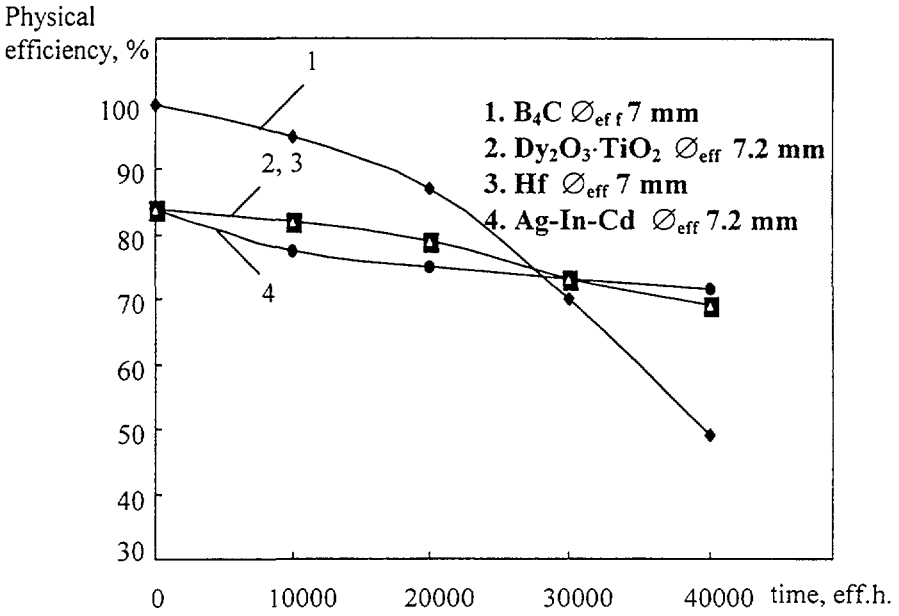

FIG. 4. Dependence of efficiency of absorbing materials during irradiation in WWER-1000

Some thermo-physical properties of $Dy_2 \cdot TiO_5$ are given in Figs. 5 - 7 and the lattice volume increase upon radiation in Fig. 8. At a temperature of 350°C, the heat capacity (Cp) is equal to 0.441 J/gK, the thermal conductivity (λ) of powder ($\rho = 4.8$ g/cm^3) is 0.33 W/mK, the thermal expansion coefficient (α) of pellets ($\rho = 6.2$ g/cm^3) is equal to $(8.52 \pm 0.15) \times 10^{-6}$ K^{-1}. $Dy_2 \cdot TiO_5$ is characterized by a good chemical inertness. Dysprosium titanate does not interact with the austenitic steel cladding at temperatures between 280 and 320°C during 146 000 h and at 1000°C during 1 h.

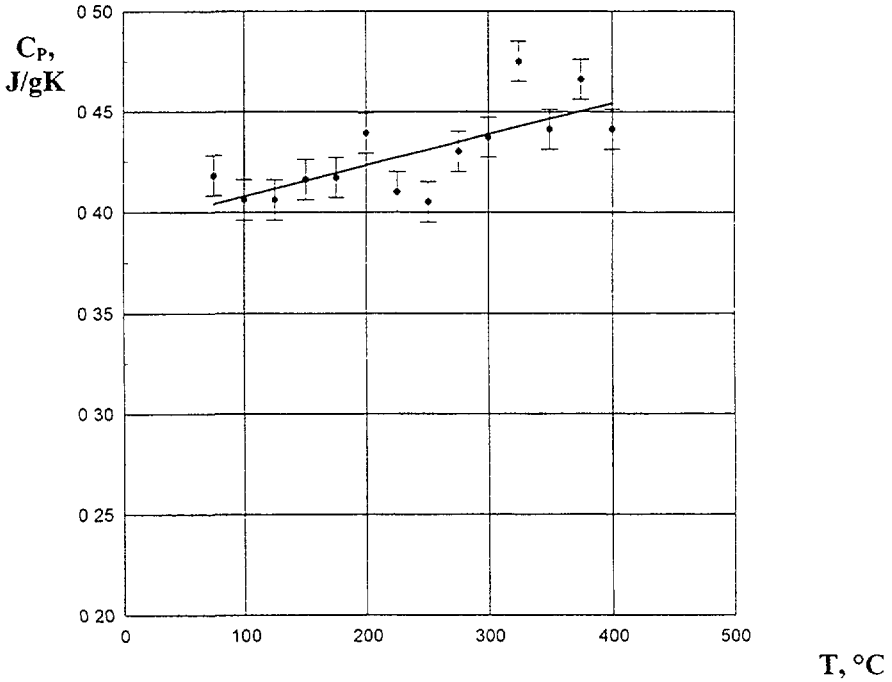

FIG 5. Dependence of $Dy_2O_3 \cdot TiO_2$ heat capacity (C_P) upon temperature

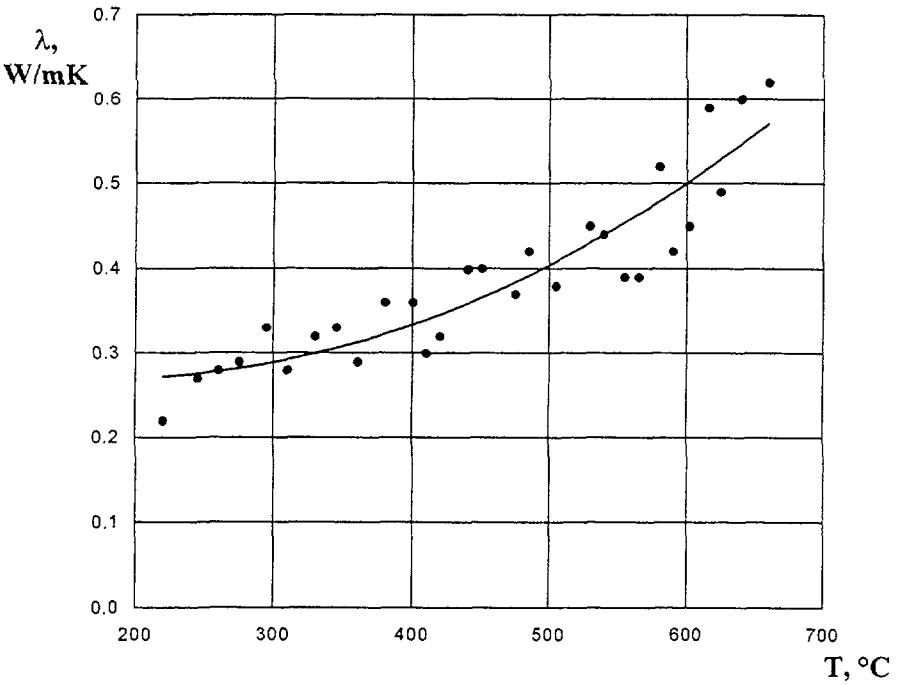

FIG. 6. Dependence of $Dy_2O_3 \cdot TiO_2$ thermal conductivity (λ) upon temperature (ρ_{POWDER}=4.8 g/cm^3, P_{He}=0.1 MPa)

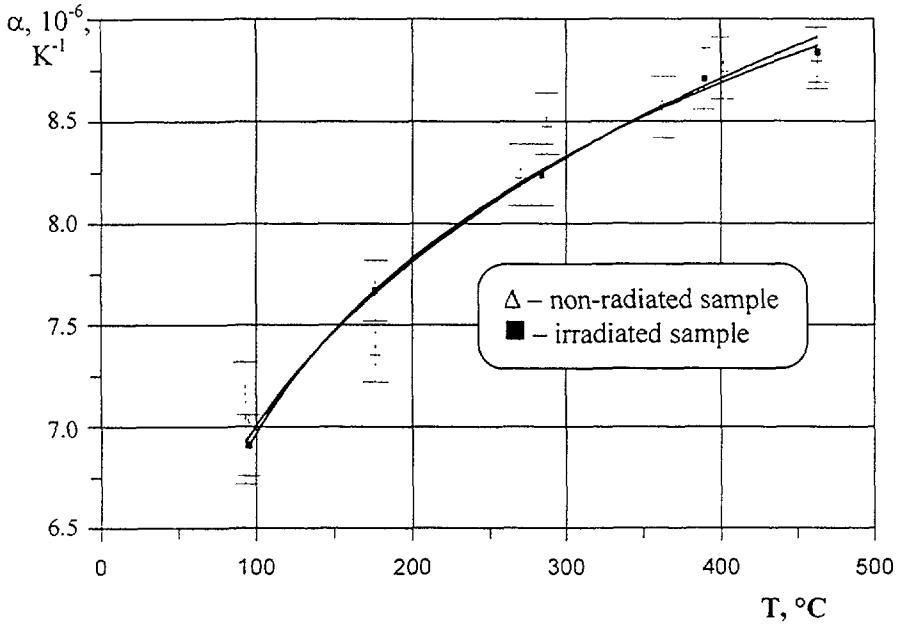

FIG. 7. Temperature dependence of thermal coefficient (α) of $Dy_2O_3 \cdot TiO_2$ (ρ=6.2 g/cm^3)

$Dy_2 \cdot TiO_5$ ($D_2 \cdot Ti_2O_7$) could be used in control rods as powder or in pellet form. In the first case, as a rule, its density is equal to 4 - 5 g/cm^3, in the second case, it is more than 6 g/cm^3. Some results of $Dy_2 \cdot TiO_5$ pellets and powder dimension stability after irradiation by neutron fluence 3.4×10^{22} cm^{-2} (E>0.1 MeV) are given in Table II. These results show that $Dy_2 \cdot TiO_5$ is characterized by the low swelling rate. The powder does not sinter and freely extract from the cladding, the lattice volume, pellet diameters, lengths and volumes increased (due to micro-cracking (Fig. 9)) at 1.7%, 0.5÷0.7%, 0.2÷0.7 % and 1.2÷2.3 %, accordingly. Dysprosium titanate pellets were cracked and fragmented on pieces of 1 - 5 mm at a temperature gradient of more than $\Delta T \geq 60$°C/mm. It is a ceramic material characterized by brittleness and low plasticity. But it is not a large problem because these absorber pellets do not interact with the cladding and do not deform it (as is with $Dy_2 \cdot TiO_5$ powder). The out-gassing absence and good corrosion properties in water at a temperature of 300°C are very important advantages of dysprosium titanate too.

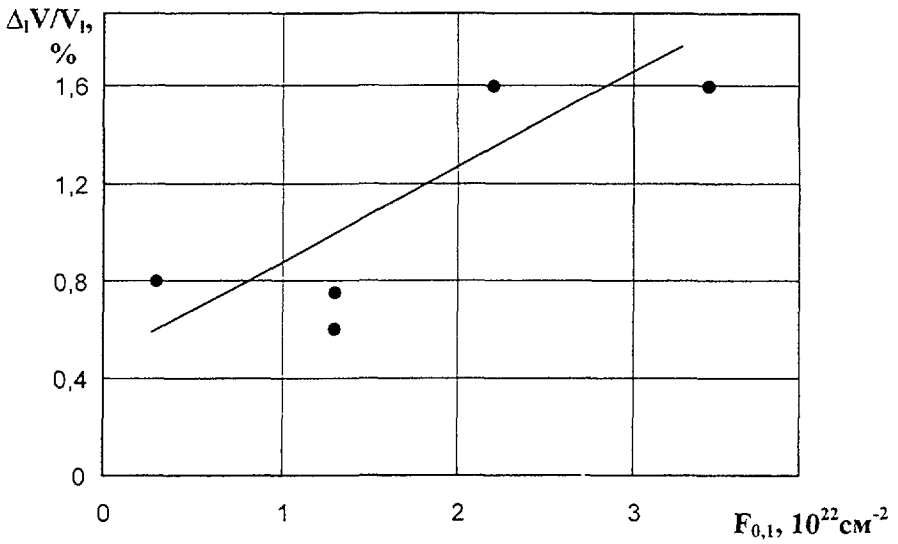

FIG. 8. Dependence of lattice volume ($\Delta V_l/V_l$) increase of fluorite $Dy_2O_3 \cdot TiO_2$ upon irradiation

TABLE II. DIMENSION STABILITY OF $Dy_2O_3 \cdot TiO_2$
($F_{max}=3.4\times10^{22}$ cm^{-2}, E>0.1 MeV)

Test	Powder	Pellets
Visual observation	freely emptied, sintering is absent	a) at the t=345-360°C, Δt=(3-5)°C/mm pellets are not destroyed, press on cladding is absent; b) at the t=150-500°C, Δt>60°C/mm pellets are destroyed on fragments due to thermal stress, press of cladding is absent
Size dimension	–	at temperature =345-360°C Δd/d=(0.5-0.7)%, ΔH/H=(0.2-0.7)%, ΔV/V=(1.2-2.3)%.
X-ray picture	a = 5.1692±0.003 Å ΔV/V=1.7%	–

3. HAFNIUM

Hafnium is used in the world (e.g. in the USA) as absorber and cladding material from the end of the seventies. Many attractive properties of hafnium were already discussed and published. Nevertheless, there are some factors restraining the more widely use of hafnium in control rods. These are the relatively high cost, the absence of reliable experimental results on radiation behaviour and hydrogenation, sometimes low mechanical properties, the absence of industrial production in Russia, etc. From our point of view, hafnium remains one of the most promising materials for using in water reactor control rods, especially it is used as absorber and cladding simultaneously.

Hafnium investigations on various fabrication, technology and composition are carried out in Russia more than 20 years. The main results received up to 1993, were published in the book "Hafnium in Atomic Technics" [1]. Pure hafnium really possesses unique nuclear, physical, mechanical and corrosion properties. Most essential demands made to hafnium control rods without cladding are presented in Table III.

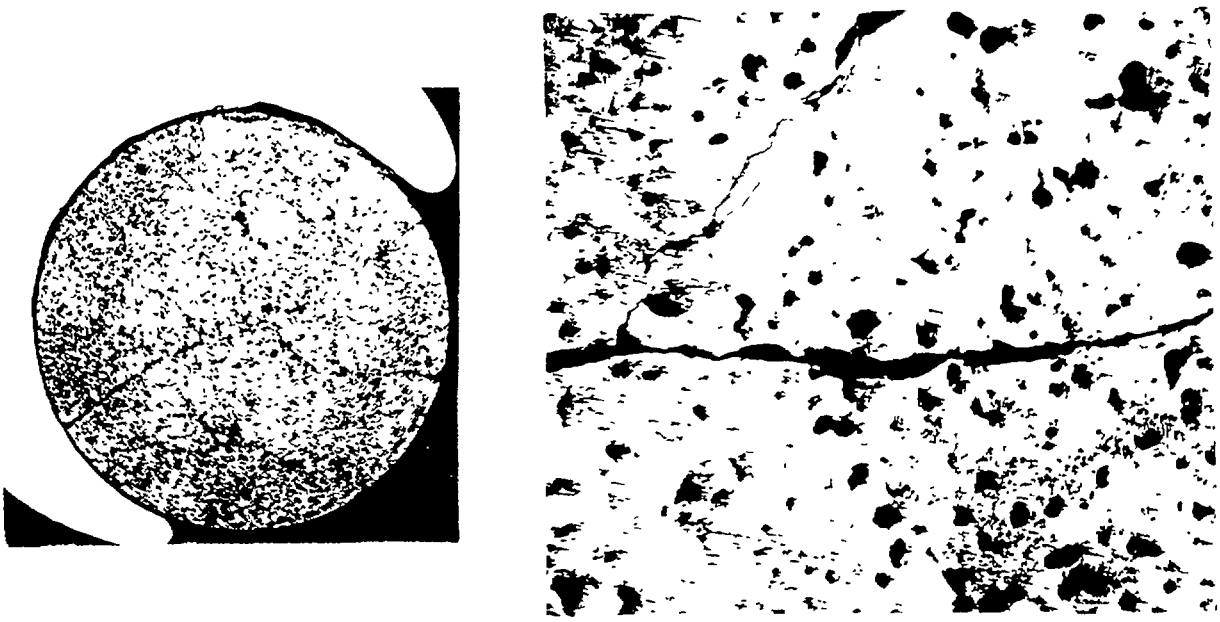

FIG. 9. Structure of Dy_2TiO_5 pellets after irradiation by neutron fluence $F=3.4\times10^{22}$ cm^{-2} (E>0.1 MeV) at the temperature 340 - 460°C, ×200

TABLE III. MAIN REQUIREMENTS PRESENTING TO HAFNIUM CONTROL RODS

Chemical contents	O – 0.03	Cr – 0.01	Mo – 0.02
	H – 0.003	Fe – 0.03	Al – 0.01
	N – 0.01	W – 0.01	Co – 0.005
	C – 0.01	Ta – 0.02	Pb – 0.005
	Cu – 0.005	Nb – 0.01	Zr – 1.0
	Ni – 0.005	Ti – 0.01	Hf – base
	V – 0.005	^{235}U – 7×10^{-6}	
Hf+Zr	> 99.8%		
Contents of gas additions	min		
Grain dimension	< 10 mkm		
Texture	not		
Mechanical properties	H_μ<1900 MPa σ_B=420 - 560 MPa σ_{02}=270 - 310 MPa δ_p>30%		
Metal	Absence of internal cracks and blisters		
Surface of control rods	Absence of micro-cracks after mechanical treatment and absence of Cu, N, Ni and W on the rod surface		

The use of hafnium control rods without cladding is more expedient. There exist many positive experimental operation results of such water reactor control rods. For instance, these control rods worked without any problems off more than 15 years in the Shippingport reactor [2]. Since 1991,

control rods without cladding were used in the research reactor RBT-6 (RIAR). Their planned lifetime is more than 20 years.

The physical efficiency of hafnium, as well as that of dysprosium, slowly decreases during operation (Fig. 4). Hafnium does not swell too. Its dimensional changes are connected with a radiation growth, as its crystal lattice is hexagonal close packed (hcp). The radiation growth deformation can change in a large range, it depends on the fabrication method and the thermo-mechanical treatment (Fig. 10). The lengths of some hafnium samples increased by 3-4% after irradiation by a neutron fluence of 3.4×10^{22} cm^{-2} (E>0.1 MeV) at temperatures between 320 - 360°C and their diameters decreased by 2-3%. Because of the absence of an axial gap in the radiation equipment some of them were curved (Fig. 11).

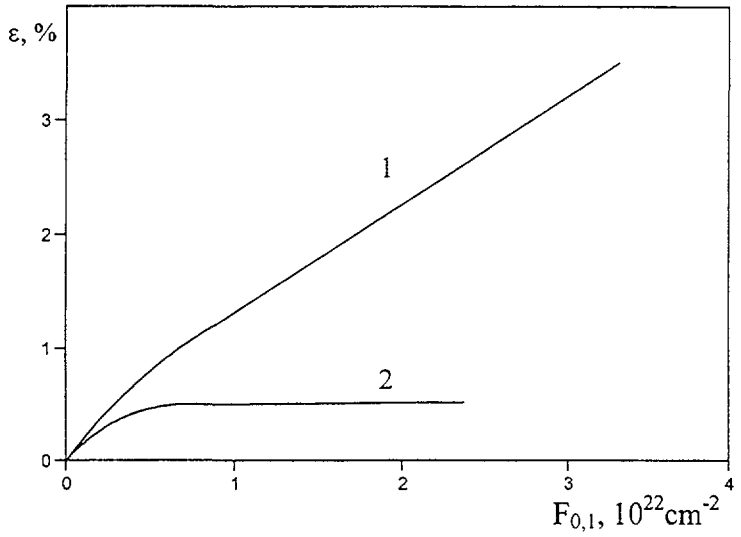

FIG. 10. Radiation growth of hafnium
1 – GPhA-1 (t=340 - 360°C); 2 – GPhI-1 (t=280 - 320°C)

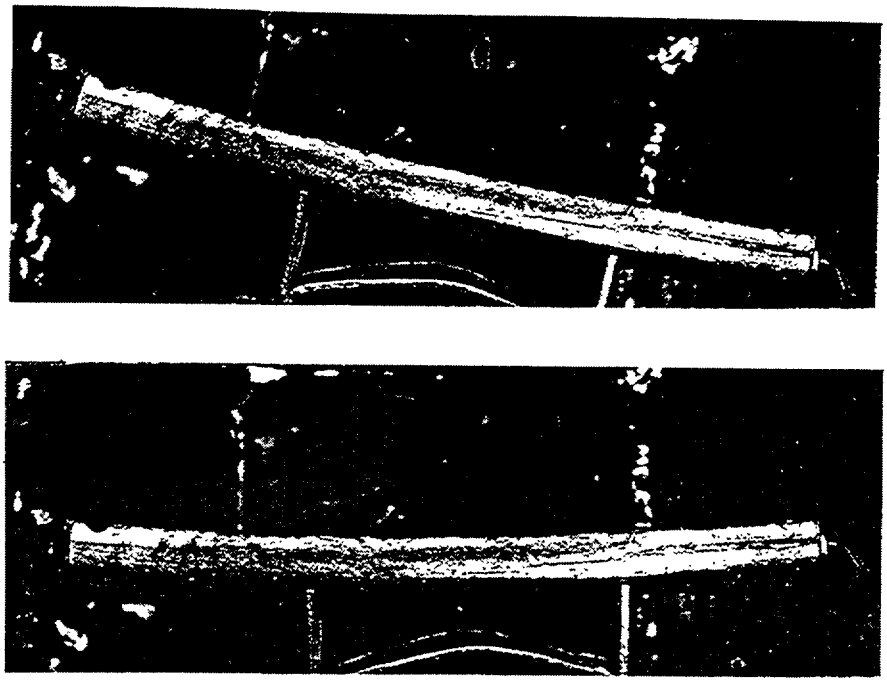

FIG. 11. View of Hf rodlets (GPhA-1) after irradiation by neutron fluence $F=3.4 \times 10^{22}$ cm^{-2} (E>0.1 MeV) at the temperature 340 - 460°C

Hafnium structural damage appears in changes of its dislocation structure (mainly dislocation loops) due to an accumulation of nuclear reaction products (transmutants), e.g. tantalum (Ta) and lutetium (Lu), and hydrogenation. More than 2% of Ta is contained in hafnium after irradiation by a neutron fluence of $2\text{-}3\times10^{22}$ cm^{-2} (E>0.1 MeV). It is necessary to take into account at the development of hafnium alloys. We suppose that only pure unalloyed hafnium must be used in control rods.

There is a good correlation between the dislocation loop concentration and the hafnium microhardness (Fig. 12). Dimensions of loops are equal to 25 - 50 Å after irradiation by a neutron fluence of 2×10^{22} cm^{-2} (E>0.1 MeV) at temperatures between 230 - 340°C, density is 5×10^{16} cm^{-3}.

The hafnium mechanical properties depend widely on a hydrogen absorption and the hydride phase appearance. At the oxidation film thickness 3 - 20 mm, hydrogen contents in irradiated hafnium is not more than 2×10^{-2}%. Relative lengthening of irradiated hafnium samples, as a rule, is 2 - 4%. The view of the ring samples of irradiated hafnium after mechanical tests are shown in Fig. 13.

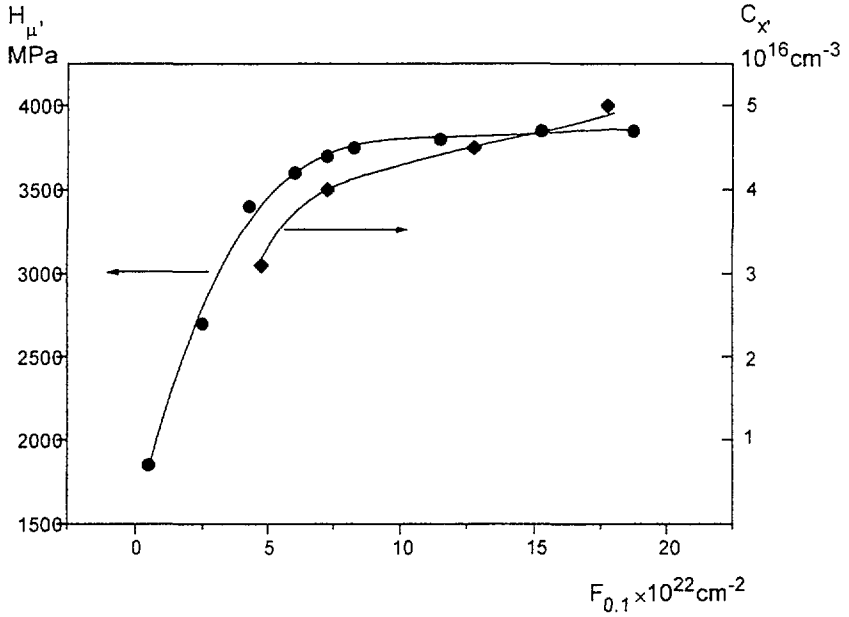

FIG. 12. Dependence of microhardness and dislocation loops upon neutron fluence (E>0.1 MeV) an temperatures between 280 - 340°C

4. DYSPROSIUM HAFNATE

Dysprosium hafnate is considered as a possible material for water reactor control rods. It has a higher neutron absorbing ability and lifetime, in comparison with $Dy_2O_3{\cdot}TiO_2$, since Ti atoms are replaced by the second absorber Hf. Hafnate disprosium has also a stable fluorite structure and a higher radiation resistance.

$Dy_2O_3{\cdot}HfO_2$ pellets (∅6×10 mm, ρ=6,2 g/cm^3) were irradiated by a fast neutron fluence 1×10^{22} ñm^{-2} (E>0.1 MeV) in helium in the BOR-60 (RIAR) at temperatures between 360 - 480°C. All pellets saved their shapes and the initial structure after irradiation (Fig. 14). The pellet diameter increased by 0.3%. The fluorite crystal structure did not change and the lattice volume increased by 0.6%. There is good agreement with the results of the volume measurements of the $Dy_2O_3{\cdot}HfO_2$ pellets. Some dimension stability results of irradiated B_4C, in comparison with (n,γ)-absorber materials based on Dy and Hf, are given in Fig. 15.

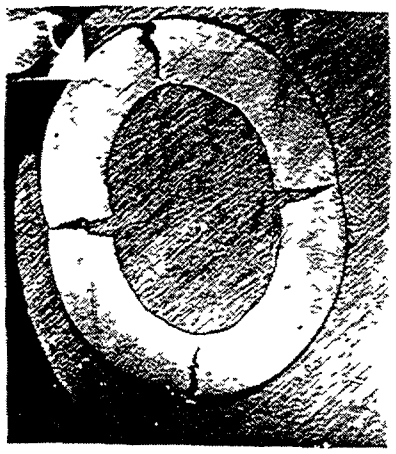

20°C

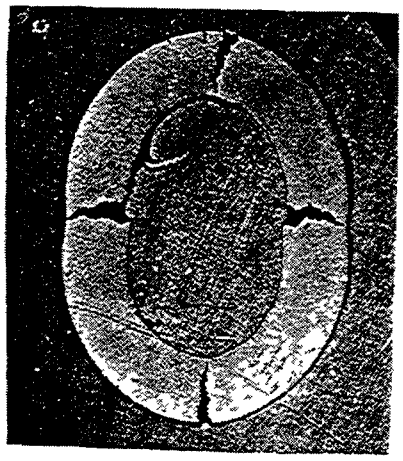

150°C

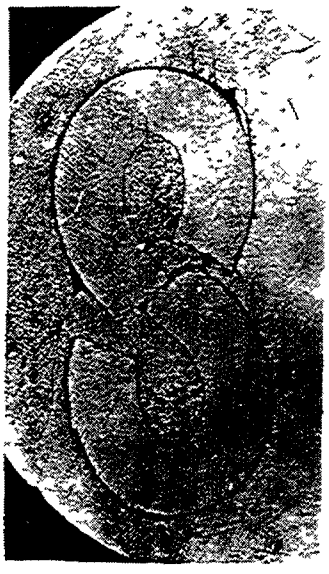

250°C

300°C

FIG 13 View of irradiated hafnium samples after mechanical tests

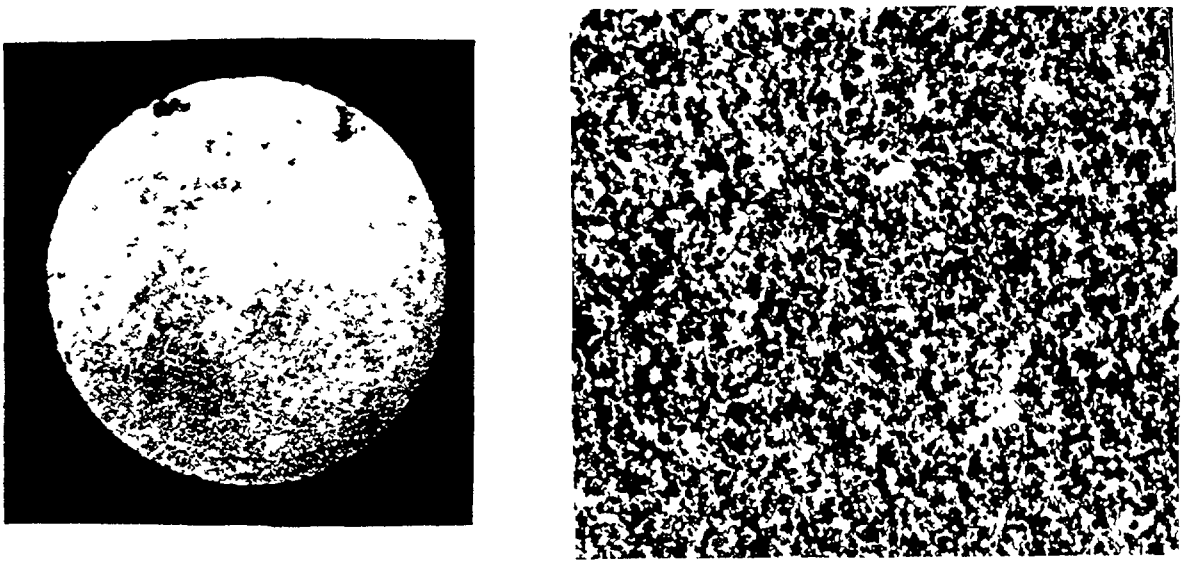

FIG 14 Structure of irradiated pellets of Dy_2O_3 HfO_2 ($F=1\times10^{22}$ cm^{-2}, $E>0$ 1 MeV, $t=360$ - 480°C), ×200

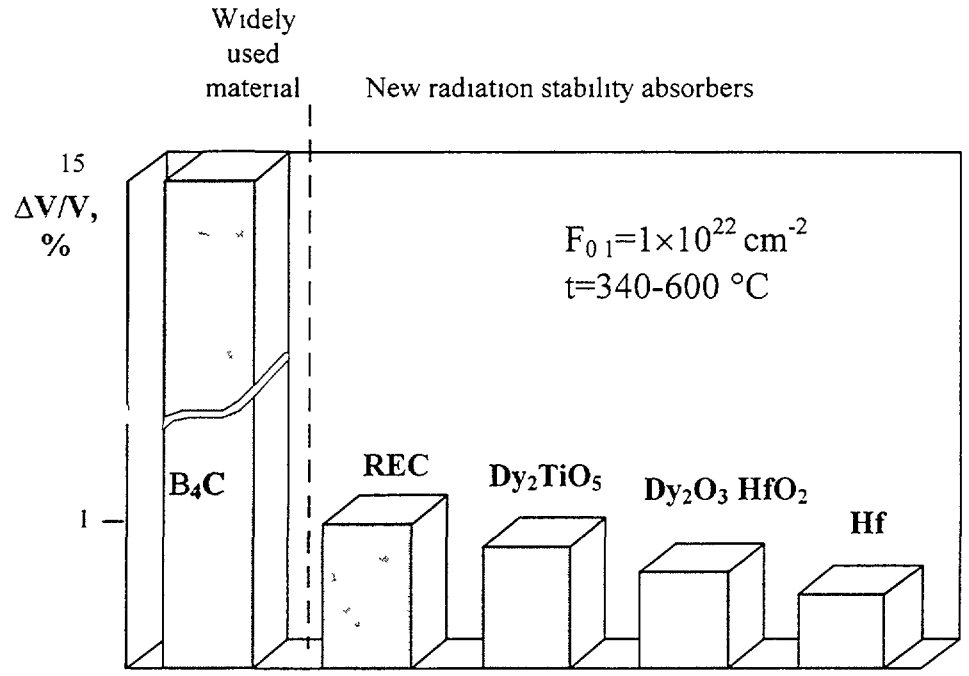

FIG 15 Dimension stability of absorber materials after irradiation in WWER-1000 RCCA (REC-Ln_2O_3 TiO_2 Ln -Dy, Gd, Eu Sm)

5 (n, γ) ABSORBER MATERIALS IN WWER CONTROL RODS

At present time the main reasons of WWER control rod degradation and their small life-time in reactors are cladding deformations due to absorber pin swelling and losses of cladding mechanical properties during irradiation Claddings, for instance, from X18H10T and SS304 steels, crack and distract, as a rule, at the deformation more than 0 5% (Fig 16) In using absorber pins which do not swell, the WWER-1000 control rod resource may be increased from 2 - 5 years, for B_4C, to 15 - 20 years

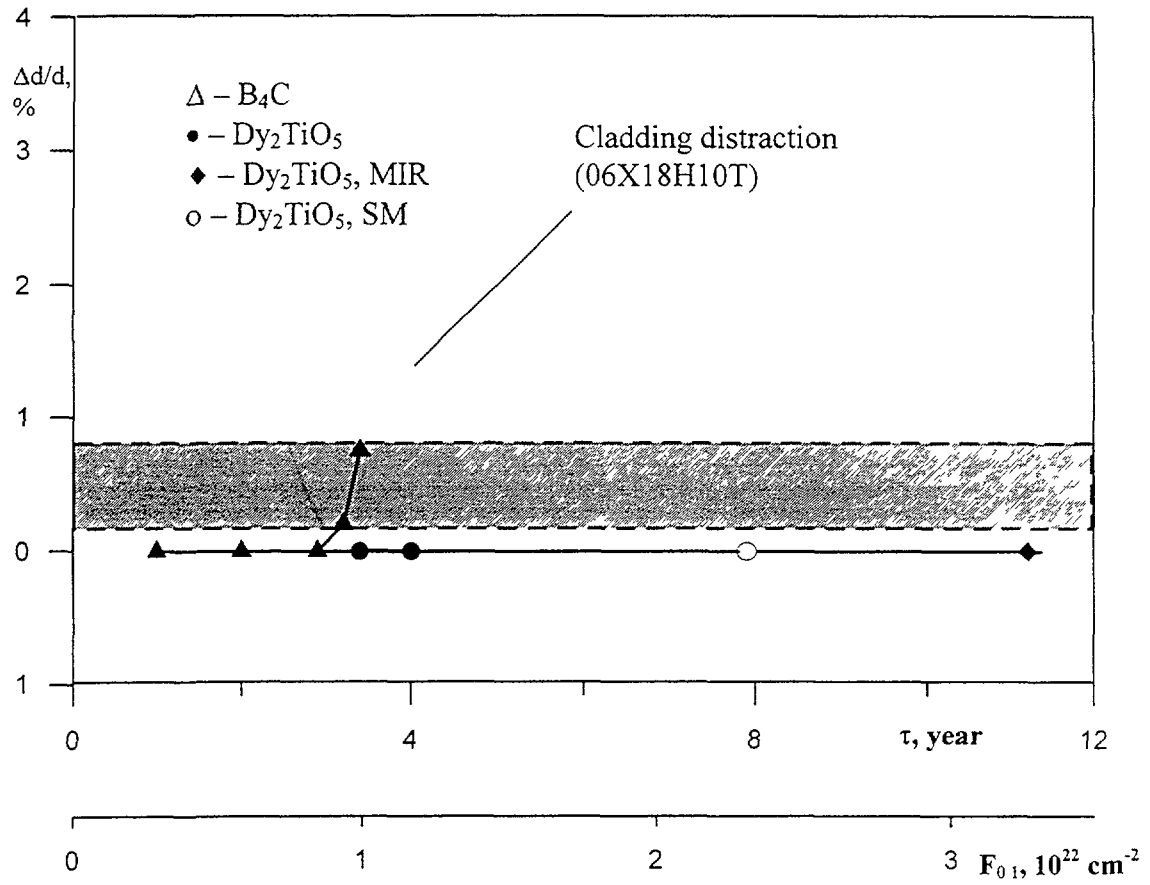

FIG 16 Dependence of diameter cladding change (Δd/d) with Dy_2O_3 TiO_2 upon fluence ($F_{0\,1}$) and operating time (τ)

From 1995, RCCAs containing $Dy_2 \cdot TiO_5$ powder (the bottom part) and B_4C powder (the upper part) are used in Russian WWERs-1000 and, from 1997, RCCAs containing Hf and B_4C are used in Ukrainian reactors.

6. CONCLUSION

New (n,γ) absorber ceramic materials of $Dy_2O_3 \cdot TiO_2$, $Dy_2O_3 \cdot HfO_2$ and Hf for WWER control rods were investigated. The use of these materials allow to raise the reliability and the safety of operation and, also, to increase the lifetime of control rods in comparison with rods containing B_4C The use of RCCAs containing Dy_2 TiO_5 and Hf in WWER-1000 has taken place. Tests and research on $Dy_2O_3 \cdot HfO_2$ are continued.

REFERENCES

[1] RISOVANY, V.D., KLOCHKOV, E.P , PONOMARENKO, V B., Hafnium in Nuclear Technique, Dimitrovgrad, SSC RF RIAR, (1993) 143 pp (In Russian)

[2] BECTON, I.M., Post irradiation examination and performance of hafnium as control rod material, Trans American Nuclear Soc , V 39, (1981) 399 pp.

BEHAVIOUR OF DIFFERENT BORON RICH SOLIDS AS PROMISING ABSORBERS FOR PWR

D. SIMEONE, X. DESCHANELS, P. CHEMINANT, P. HERTER
Centre d'Etudes de Saclay,
Laboratoire d'Etudes des Matériaux Absorbants,
Gif-sur-Yvette,
France

Abstract

Absorbing materials are used to control the reactivity of nuclear reactors by taking advantage of nuclear reactions (e g $^{10}B(n,\alpha)^{7}Li$) where neutrons are absorbed During such reactions, energetic recoils are produced As a result, radiation damage in absorbing materials originates both from these nuclear reactions, and from elastic collisions between neutrons and atoms This damage eventually leads to a partial destruction of the materials, and this is the main limitation on their lifetime in nuclear reactors Using different techniques, elementary mechanisms responsible of these ceramic destruction are studied The knowledge of such mechanism will help to improve the lifetime of these materials

1. INTRODUCTION

Among pressurized water reactors (PWR) control rods, many of them are made of two kinds of absorbers, an alloy of silver, indium and cadmium, and boron carbide B_4C. The isotope ^{10}B can efficiently absorb low and fast neutrons (Fig. 1). This is why boron carbide is also used in Fast Breeder Reactors (FBR). With the future generation of PWR, absorber pins will need to be able to capture more neutrons. Hafnium diboride HfB_2 could then be an attractive material for these reactors, because of the high neutron absorption cross sections of both hafnium and 10-boron. In addition, their low cost of fabrication, their high melting point (T_m=2400°C for B_4C, and T_m=3380°C for HfB_2), and their low neutron activity after irradiation, makes them attractive materials for the nuclear industry. The evolution of such materials under irradiation is however not enough understood. It is observed that after a typical burnup of 5%, B_4C pellets fall apart [1]. The most likely explanation proposed so far is that this destruction is purely caused by the high stresses built up around micrometric penny-shaped He bubbles [1], He coming from the $^{10}B(n,\alpha)^{7}Li$ capture reaction. However, radiation damages may also play a role in this degradation process but few calculations of radiation damages have been done for materials undergoing nuclear reactions [2]. In addition to the damage produced by elastic collisions between neutrons and target atoms, energetic recoils are a second source of damage. the $^{10}B(n,\alpha)^{7}Li$ reaction generates helium and lithium atoms with an average kinetic energy of 1.48 MeV and 0.83 MeV, respectively.

Two different techniques were used to study the evolution of B_4C and HfB_2 under a neutron irradiation: the Raman spectroscopy permitted to study the B_4C [3] and the "Transmittion Electronic Microscopy" was used to analyse the HfB_2 [4].

2. DAMAGE STUDY OF B_4C AND HfB_2

2.1 Raman study of irradiated B_4C

To better understand the degradation mechanisms of irradiated B_4C, some samples have been submitted to beams like of 1.2 MeV electrons or 180 keV He^+. In these experiments, the only damages in the B_4C structure are due to the recoil of the boron and carbon atoms knocked out of their equilibrium positions, or the presence of He inside the matrix. Other samples have been irradiated by neutrons, and the damages do not only come from to the recoil of B and C, and the presence of He, but also from the disappearance of boron isotopes from the structure, due to the $^{10}B(n,\alpha)^{7}Li$ capture reaction.

Arguments for using Raman are provided by comparing peaks between B_4C and α-boron. The two structures are identical (the same 12-atoms icosahedron structures) but a C-B-C median chain

exists in B_4C and is absent in α-boron (Figure 2a). The Raman spectrum differences between B_4C and α-boron is precisely due to the presence or not of this chain. This associated with some modelization allowed to identify precisely two peaks, located at 480 cm^{-1} and 530 cm^{-1}, associated with the C-B-C chain.

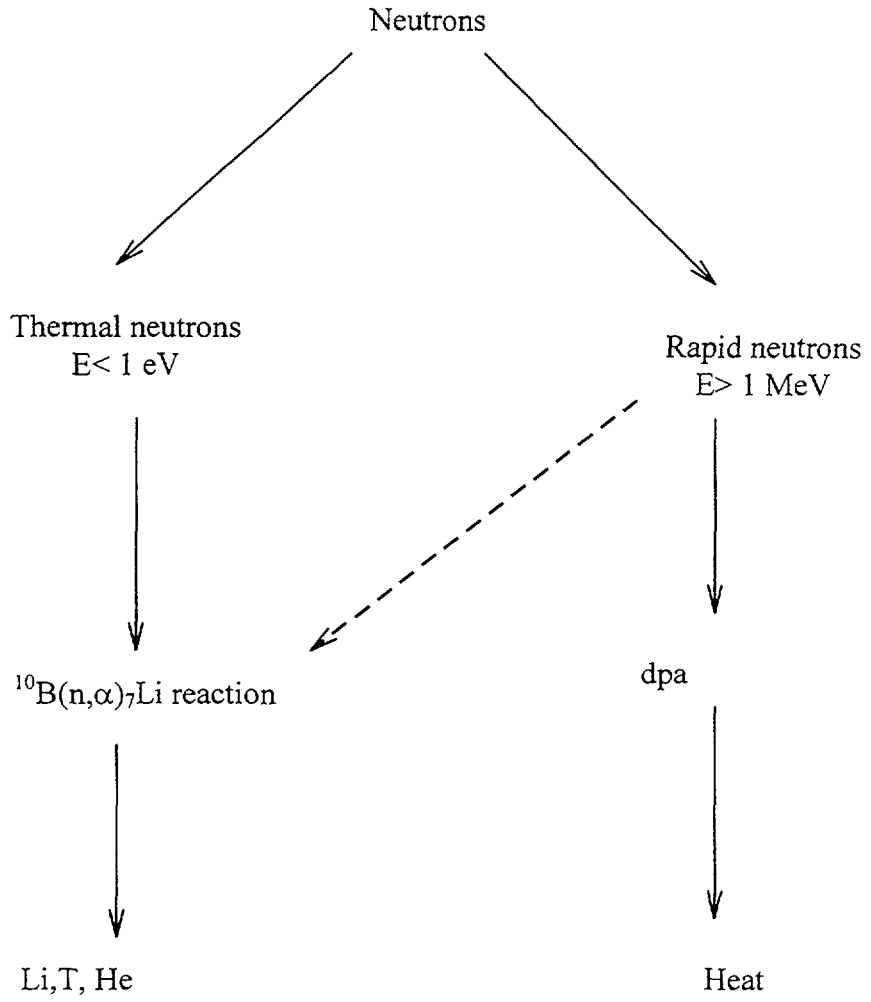

FIG. 1. Neutron absorption by 10 boron

Comparison of the C-B-C Raman peaks between B_4C samples irradiated only with electrons or He^+ (no disappearance of B), and B_4C irradiated by neutrons (disappearance of B) shows the material's capacity to restore its structure (C-B-C peaks) when damaged by electrons or He^+. This is due to the extraordinary self-healing ability of the icosaedrons which are able to "pump" atoms from the less stable C-B-C chain, to complete their structures. Thus Raman peaks of B_4C irradiated by electrons or He^+ are not degraded or promptly restored.

Neutron irradiation is accompanied by boron isotopes disappearance (Figure 3). To complete their structure, icosaedrons "pump" boron and carbon atoms from the C-B-C chain whose structure disappears (and the Raman peaks too) for lack of atoms. During a neutron irradiation, B_4C move progressively to an α-boron structure without C-B-C chain. Only the presence of this chain could enable formation and migration of point defects through the structure, thus its absence would block any defect transfer and consequently the possibility for penny-shaped bubbles in irradiated B_4C to relax their surrounding stress field by a defect inflow.

To conclude, arguments have been brought to explain the B_4C degradation during a neutron irradiation: the initial damage is due to the building of penny-shaped helium bubbles, associated with

high local stress fields. At the same time an aggravation is occurring inside the matrix, the materials becoming progressively unable to release these stresses, due to the disappearance of point defects and/or their mobility.

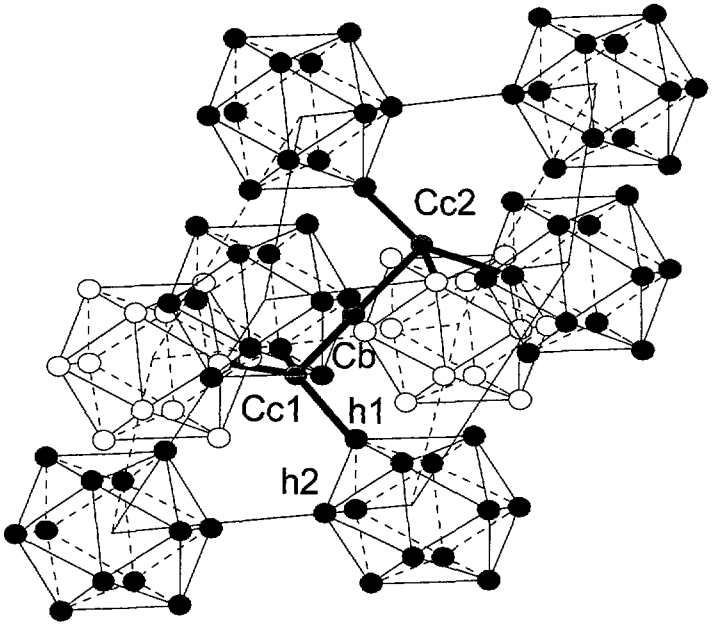

FIG. 2a. Crystallographic structure of B_4C

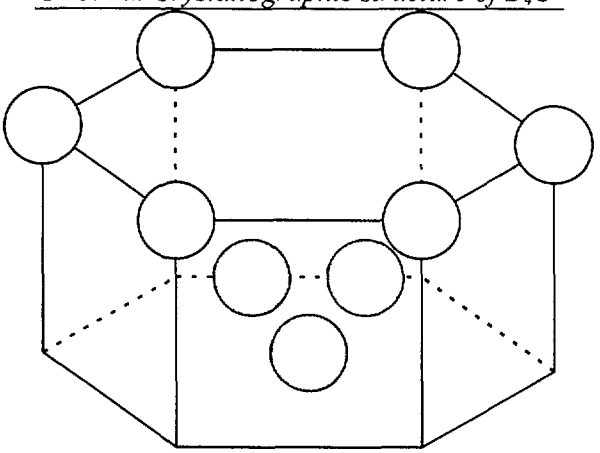

FIG. 2b. Crystallographic structure of HfB_2

Figure 2a shows a schematic description of the rhomboidal unit cell of B_4C. C sites refer to carbon atoms of the linear C-B-C chain, B site refers to the inversion center occupied by a boron atom. h1 refer to polar sites occupied by boron atoms and h2 sites refer to boron and carbon atoms occupying the equatorial sites.

Figure 2b presents a schematic representation of the HfB_2 unit cell. Hafnium atoms are whites dots situated at each vertex of the hexagon, and three boron atoms over six are drawn in the hexagon in interstitial positions.

FIG. 2. Crystalographic structures of B_4C and HfB_2

2.2. MET study of irradiated HfB_2

The symmetry group of HfB_2 is P6/mmm (Figure 2b). The unit cell is an hexagone possessing hafnium atoms at each vertex of the structure. Boron atoms occupy vacancies positions inside the hexagon. TEM photographies of HfB_2 irradiated under 1073°K at low ^{10}B burnup (about 10^{20} captures/cm^3) show clearly dislocation loops in the basal plans [4]. For high temperature values (above 1073°K) and similar ^{10}B burnup, helium bubbles appear in the grain boundaries of the material. Therefore, helium bubbles are not penny-shaped like in B_4C but spherical like in UO_2. No

strain fields are associated to these bubbles in HfB_2. The destruction of the material is due to the agglomeration of basal dislocation loops (vacancies loops) which meet each other near the grain boundaries forming micro cracking.

As a conclusion for HfB_2, in this material helium bubbles are not damaging thanks to the defects mobility. But the anisotropy of relocation of these defects induces anisotropy of the elementary grain's strain thus a thread to the material's integrity.

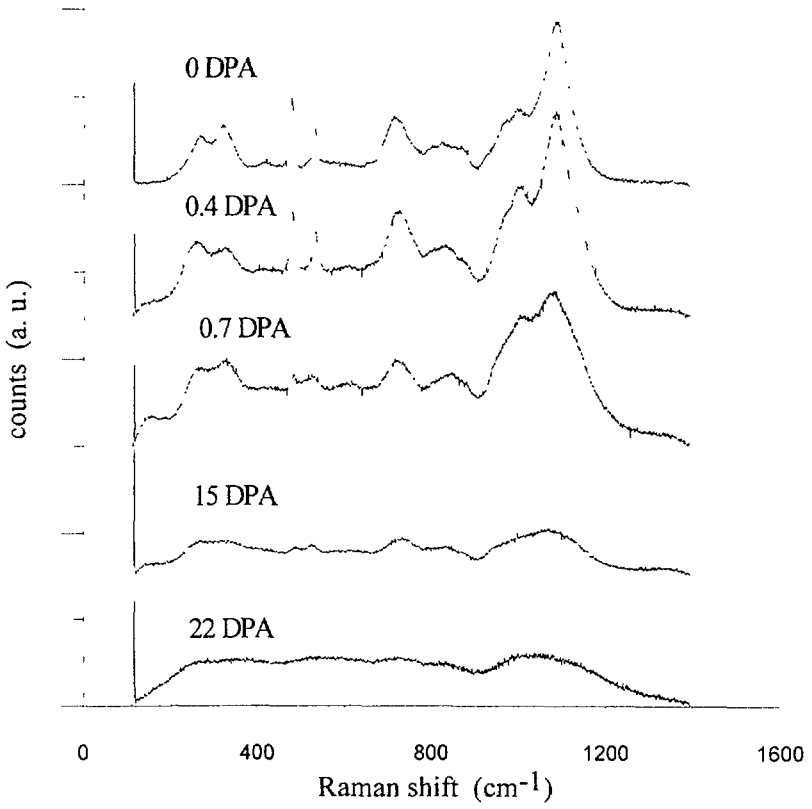

FIG. 3. Evolution of Raman spectra of irradiated B_4C samples at different dpa values

3. CONCLUSION

The different unit cell symmetry ($R\bar{3}m$ for B_4C and P6/mmm for HfB_2) and the different nature of the chemical bonds leads to opposite behaviour under neutron irradiation of these two materials :

- In B_4C, the B_{12} icosaedric clusters do not permit the appearing of vacancies to diminish strain fields around helium bubbles, which remain damaging for the material.
- In HfB_2, many vacancies are present and allow helium bubbles to relax in the material. At low irradiation temperatures (under 1073°K), the high number of vacancies loops (basal loops) are responsible of microcracking apparition in the material.

REFERENCES

[1] T. STOTO, L. ZUPPIROLI, J. PELLISSIER, Radiation Effects, **90**, (1985) 160-170.

[2] A. ALBERMANN, D. LESUEUR, Am. Soc. for Test. and Mat., PA 19103, (1989).

[3] D. SIMEONE, C. MALLET, X. DESCHANELS, G. BALDINOZZI, O. KAITASOV, Study of B_4C unit cell evolution under neutron irradiation by Raman spectroscopy, submitted in Phys. Rev. B, (1998).

[4] P. CHEMINANT, PhD Thesis, Orsay, (1997).

REINFORCEMENT AGAINST CRACK PROPAGATION OF PWR ABSORBERS BY DEVELOPMENT OF BORON-CARBON–HAFNIUM COMPOSITES

B. PROVOT, P. HERTER
Laboratoire d'Etudes des Matériaux Absorbants,
CEA,
Saclay, Gif-sur-Yvette,
France

XA0053635

Abstract

In order to improve the mechanical behaviour of materials used as neutron absorbers in nuclear reactors, we have developed CERCER or CERMET composites with boron and hafnium. Thus a new composite B_4C/HfB_2 has been especially studied. We have identified three kinds of degradation under irradiation (thermal gradient, swelling due to fission products and accidental corrosion) that induce imposed deformations cracking phenomena. Mechanical behaviour and crack propagation resistance have been studied by ball-on-three-balls and double torsion tests. A special device was developed to enable crack propagation and associated stress intensity factor measurements. Effects of structure and of a second phase are underline. First results show that these materials present crack initiation and propagation resistance much higher than pure boron carbide or hafnium diboride. We observe R-Curves effects, crack bridging or branching, crack arrests, and toughness increases that we can relate respectively to the composite structures.

1. INTRODUCTION: DAMAGES IN NEUTRON ABSORBERS DURING IRRADIATION

Neutron absorbers in nuclear control rods consist in boron compounds in metallic cladding. The neutron capture by boron atoms leads to the creation of helium atoms which cause an important swelling of the materials (~0,15 vol. % per 10^{20} captures.cm^{-3} corresponding to 80 cm^3 He/cm^{-3} B_4C) [1] according to the reaction:

$$^{10}B + n \rightarrow {}^4He + {}^7Li + 2{,}6\ MeV.$$

This reaction causes material damage due to atom recoil, swelling and thermal stresses. In pressurized water reactors (PWRs), a high flux depression involves a differential irradiation induced swelling along the pellets radius and thus induces high stresses at the pellet's periphery, but no thermal stresses. Associated with neutron damage, this leads to fragmentation starting from the surface of the material.

In Fast Breeder Reactors (FBRs), contrary to PWRs, neutrons penetrate the bulk of the pellets. This leads to an homogeneous volume heat release, a temperature gradient of about 1000°C between pellet's centre and surface and tangential stresses, which largely overcome material's strength, causing premature rupture of the absorbers (radial cracks). Associated with bulk neutron damage, this leads to a complete fragmentation [2].

In both type of reactors, absorber fragments may segregate by gravity to the bottom of the rods or stick between pellet and clad. Associated with irradiation induced He swelling, this can induce a significant damage to the absorber's cladding. In PWRs, if a seal loss of the clad occurs, pellets may be corroded by the primary coolant. Corrosion pits induce then crack initiations leading to premature failure [3].

All these absorber phenomena involve imposed deformation cracking mechanisms: thermal dilatation (FBR), oxide phase dilatation (PWR corrosion) and irradiation induced swelling (creation of helium in PWR and FBR pellets) (see Figure 1).

This work displays the mechanical study of several composites based on boron carbide or hafnium diboride matrixes. The purpose is to characterize the materials (strength, rupture modes and crack propagation resistance) and to identify reinforcement modes towards cracking in comparison with associated single phase materials.

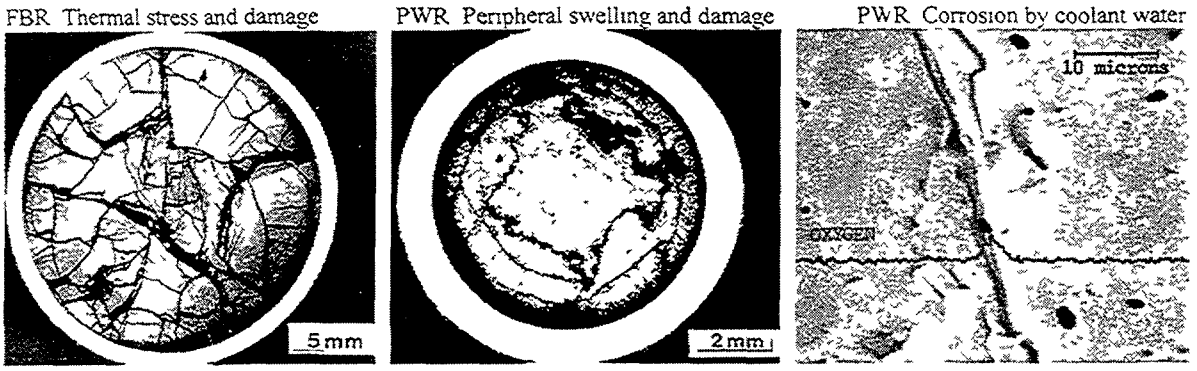

FIG 1. Damage modes of pellets during irradiation

2. DEVELOPMENT OF MATERIALS

The aim is to give to our materials sufficient reinforcement to stop or minimize crack propagation and to enable them to conserve a sufficient cohesion though a high mechanical damage. The reinforcement of a ceramic can take different routes. Most frequently, a second phase is introduced (metal or ceramic) and different mechanisms are taken into account [4]. In a cermet, the metallic component (continuous or dispersed in a matrix) confers globally some ductility. In the case of a reinforcement by ceramic inclusions, we try to create a network in which cracks will propagate with difficulty A process zone can develop in the vicinity of the crack tip leading to a significant decrease of the crack driving force. The more frequent mechanisms acting in a process zone are residual stresses due to differential thermal expansion coefficient or phase transformation, or micro-cracking due to differential elastic constants.

Several composite materials have been fabricated by hot uniaxial pressing of mixed ceramic and/or metallic powders. Fine micrometric HfB_2 or B_4C powders have been mixed with fine powders like metallic hafnium [4] or ceramic hafnium oxide, or particles of hafnium diboride [5, 6]or metallic hafnium. Table I shows the different studied materials. We obtained two main grades of materials: fine grained homogeneous composites named "microdispersed" and heterogeneous composites in which reinforcement is constituted by large secondary phase aggregates or inclusions named, "macrodispersed" (by adjusting the hot pressing parameters, macrodispersed materials are obtained by coalescence from microdispersed powders).

TABLE I. DIFFERENT TYPES OF MATERIALS AND COMPOSITES STUDIED

Matrix	**Symbol**	**Additive**	**Second phase after sintering**
HfB_2	A		
	A1	Hf micrometric powder	microdispersed HfB, HfB_2, HfC
	A2	HfO_2 micrometric powder	microdispersed HfO_2
B_4C	B		
	B1	micrometric HfB_2 powder	macrodispersed $HfB_{2\text{-}d}$
	B2	HfB_2 submillimetric agglomerates	HfB_2 submillimetric agglomerates macrodispersed
	B3	Hf submillimetric agglomerates	Hf submillimetric agglomerates macrodispersed

3. EXPERIMENTAL PROCEDURE

3.1 Ball-on-three-balls biaxial bending test [7, 8]]

The load is applied thanks to a central ball on the upper side of a thin disc (Figure 2). The disc is supported on its lower side periphery by three balls regularly distributed on a concentric ring. In this case, radial and tangential stresses are equal and maximal at the centre of the sample, and are expressed by an analytical simple plate theory formula of the form:

$$\sigma_{rr}^{max} = \sigma_{\theta\theta}^{max} = P \times F(\nu, geometry)$$

P being the load and ν the Poisson's ratio. An estimation of the Young modulus is also obtained from the central deflection w. Thus measurement of the critical load at the sample's collapsing enables to calculate material strength.

This test is particularly well adapted to characterization of very hard and brittle ceramic materials as boron carbide or hafnium diboride, and gives better results than 3-points or 4-points bending tests (These tests are however kept for samples with strain gauges for measurement of Poisson's ratio).

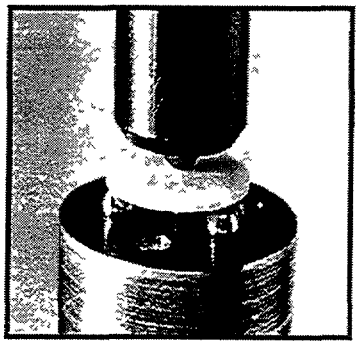

FIG. 2 Ball-on-three-balls bending test

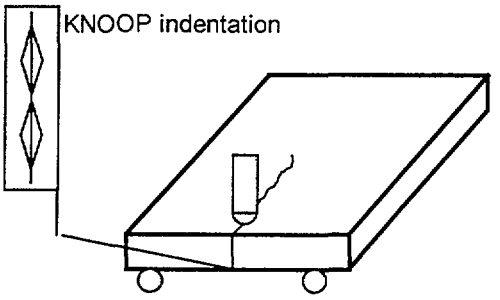

FIG. 3. Double torsion test

3.2. Double torsion test [9]

Double torsion test allows to measure ceramic toughness K_{IC}. Samples are thin rectangular plates in which a notch is prepared (Figure 3). The notch is submitted to bending and the crack propagates from the tip of the notch. The sample in supported by four balls and the load is also applied with a ball on the beginning of the notch. The stress intensity factor is proportional to the load P and depends on geometry and elastic constants. It is expressed by analytical formula:

The critical value K_{IC}, where the crack propagates, is then obtained by a formula like:

$K_{IC} = P_c \times G(elastic\_constants,\ geometry)$, where P_c is the critical load (Figure 4).

Thus we can determine the evolution of stress intensity factor as a function of crack length via the load. In the case of a brittle homogeneous material, crack propagates for a constant value of critical load (Figure 5). If crack shielding occurs (deflection, bridging, arrest), the deflection-load curve is perturbed, with (Figure 6) or without (Figure 7) global reinforcement. In this second case, material demonstrate a R-Curve effect i.e. an increasing toughness as crack propagates in the material.

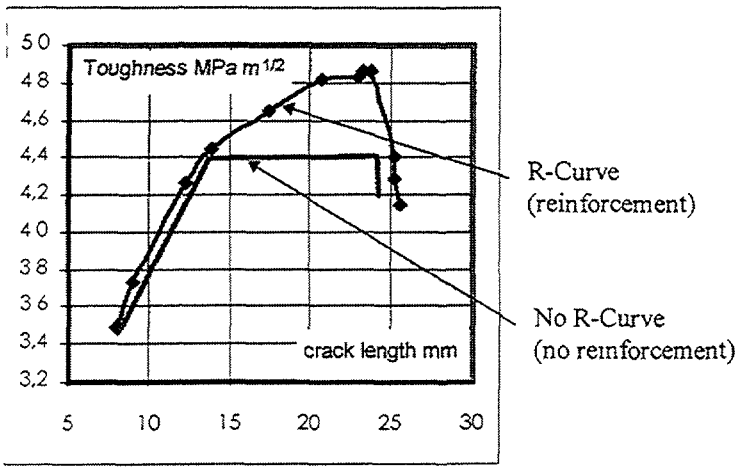

FIG 4. R-Curve effect

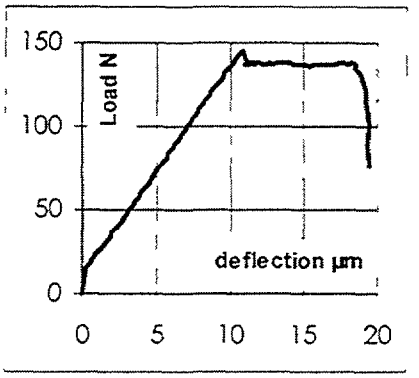

FIG 5 Brittle homogeneous material

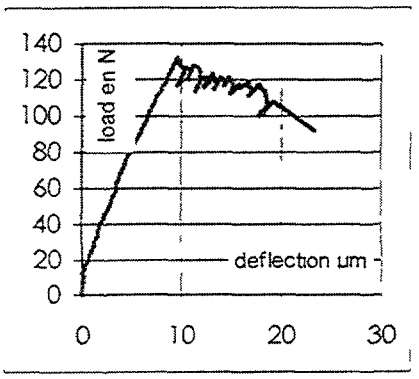

FIG 6 Crack shielding without reinforcement

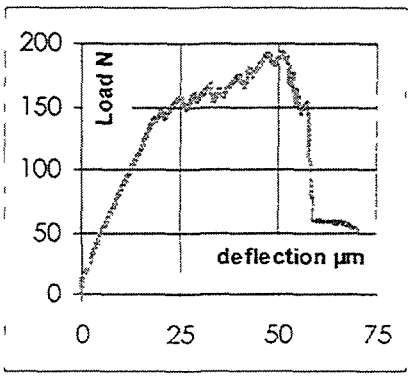

FIG. 7. Crack shielding with reinforcement

3.3 Thermal gradient crack test

This test consist in applying to a ceramic thin disc a thermal gradient by focusing with two elliptic reflectors high power halogen bulb light at the centre of the sides of the sample which is cooled at its periphery. The parabolic like temperature of the pellet's surface is measured by thermocouples and the light power is measured with a power meter.

Testing no-notched discs leads to thermal strength determination. The materials are submitted to increasing thermal gradient, so far as they crack and/or break. Measurement of thermal gradient leads to thermal gradient strength according to classical 1-D radial analytical formula.

Testing notched discs leads to thermal gradient toughness. An analytical method based on superposition principle in mechanics leads to toughness calculation via a Gauss-Chebychev resolution. Thus at crack start, toughness K_{IC} is obtained through an analytical formula depending on crack length, geometry, material's thermo-mechanical properties, and lamp power. The toughness calculations is confirmed by a finite element calculation (CASTEM 2000). Finite elements are later used for crack propagation calculation.

This test offers the possibility to proceed to a step by step propagation experiment, where the sample is removed and examined by scanning electron microscopy (SEM) at each step. Items obtained are: crack length, reinforcement mechanisms (crack arrest before, inside or after an inclusion or at an to interface inclusion-matrix), calculation of toughness at crack start and crack arrest in order to quantify reinforcement mechanism like:

$$K_{IC}^{composite} = K_{IC}^{matrix} + \Delta K^{inclusion}$$

At last, we can obtain a curve describing a global reinforcement as a function direct measurement of crack length identifying each respective reinforcement mechanisms (see Figure 8).

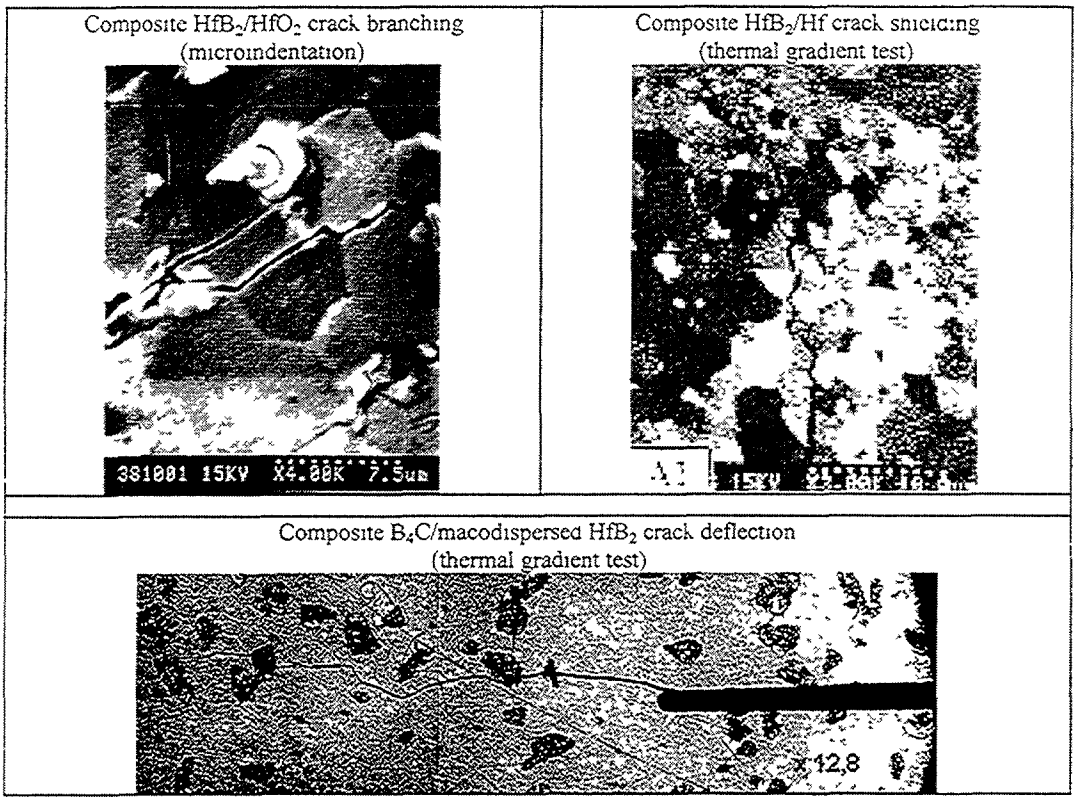

FIG. 8. Different crack morphologies obtained

4 RESULTS AND DISCUSSION

Strengths and toughness have been respectively measured by ball-on-three-balls [10] and double-torsion [11] tests. Results of these experiments are reported in Table II . The strength can be strongly affected, especially in the case of "macrodispersed" composites because of the change in critical flaw size. However, strength is not a critical material parameter versus the loading conditions during pellets irradiation. The aim is not to avoid crack initiation but to avoid fragmentation. Toughness or crack arrest are certainly more relevant parameters for the considered application.

Optical and SEM observations, on polished or fractured surfaces reported in Figure 8, allow the mechanisms of crack propagation and of crack arrest to be understood. In all composites, A1 excepted, the crack propagation is disturbed by the second phase. Deflection by the inclusions, shielding by the particles and branching of the crack can be observed. Inclusions, hafnium-rich phases, residual stressed areas and microcracked particles [12] play a role. The composite inclusions delay or sometimes stop simple intragranular brittle cracking of HfB_2 or B_4C matrix. The efficiency of these reinforcement phenomena is confirmed by the measurements of the mechanical properties Compared with single-phased materials, the fracture toughness increases from 31 up to 62 %. An R-curve is also sometimes observed, probably because of crack bridging by particles. Only A2 composite does not present a R-curve effect because of the small size of inclusions. B2 composite exhibits moreover a dissipative behaviour during strength measurements probably due to the presence of microcracked aggregates.

In all cases, these results confirm the possibility to delay complete and premature collapse of ceramics

TABLE II. TEST RESULTS OBTAINED BY BALL-ON-THREE-BALLS BIAXIAL BENDING, DOUBLE TORSION AND THERMAL GRADIENT TESTS

Symbol	Brittle (B) or Dissipative (D) rupture	R-Curve effect	Young modulus (MPa)	Strength (MPa)	Weibull coefficient m	K_{IC} (MPa.m$^{-1/2}$)
A	B	no	418	398	10	3,1
A1	B	yes	416	688	7	4,8
A2	B	no	405	527	16	5,1
B	B	no	310	497	7	3,6
B1	D	yes	242	264	17	5
B2	D	yes	207	176	10	5
B3	D	yes	147	120	5	

REFERENCES

[1] ZUPPIROLLI, L., et al., Phil. Mag. A, 60-5 (1989) 539-551.
[2] STOTO, T., et al., J. Appl. Phys., 68-2 (1990) 3198-3206.
[3] DESCHANELS, X., Key Eng. Mat., Vol. 13 (1996) 189-198.
[4] EVANS, A.G., J. Am. Ceram. Soc., 73-2 (1990) 187-206.
[5] GOSSET D., et al., JJAP, Series 10 (1994) 216-219.
[6] CHEMINANT, P., et al., Key Eng. Mat., Vols 132-136 (1997) pp.643-646.
[7] KIRSTEIN, A.F., J. of research of the Nat. Bur. of Stand. - C Eng. and Instrumentation, Vol. 70C, N°4, (Oct.-Dec. 1966).
[8] DE WITH, G., J. Am. Ceram. Soc., 72 [8] (1989) 1538-41.
[9] BOUSSUGE, M., PhD Thesis ENSMP, Paris, (1984).
[10] DE WITH, G., et al., J. Am. Ceram. Soc., 72-8 (1989) 1538-1541.
[11] FOURNEL, B., PhD Phesis, Ecole Nationale Supérieure des Mines de Paris, Paris, (1991).
[12] FABER, K.T., et al., Proc. Int. Conf. Fract., 4th, (1977) I 529-56.

NSC KIPT'S EXPERIENCE IN PRODUCTION OF ABSORBER MATERIALS, COMPOSITES AND PRODUCTS FOR CONTROL MECHANISMS OF VARIOUS NUCLEAR REACTOR TYPES

N.P. ODEYCHUK, V.F. ZELENSKY, V.A. GURIN, YU.F. KONOTOP
National Science Center,
Kharkov Institute of Physics and Technology,
Kharkov, Ukraine

XA0053636

Abstract

Data on NSC KIPT developments of absorber composites B_4C-PyC and B_4C-SiC are reported. Results of prereactor studies and reactor tests of absorber composites developed are given. It is shown that the B_4C-PyC composites have a high radiation resistance at temperatures up to 1250°C.

1. INTRODUCTION

The NSC KIPT has been engaged in the development of absorber composites and products based on them for reactivity compensation system elements of high-temperature gas-cooled reactors and fast reactors since the sixties. The processes developed to produce absorbing composites and items rely on the original technology making use of the methods of volumetric gas phase densification of porous media with pyrocarbon [1-6]. This paper reports the results from studies into basic characteristics of B_4C-PyC and B_4C-SiC produced by the gas phase technology, and also, their behaviour under neutron irradiation conditions.

2. B_4C-SiC COMPOSITE

Potential corrosion-resistant materials, capable of operating in an oxidizing environment under reactor radiation conditions at temperatures between 800 and 1300°C, are the composites based on silicon carbide (fast reactor design with a dissociating coolant N_2O_4) [4].

The NSC KIPT group has developed absorber composites comprising a dispersion of boron particles in a carbide-silicon matrix (B_4C-SiC composite) for nuclear reactor control rods. The absorber materials of this type are produced in the process of binding a mixture of silicon and boron carbide powders with pyrocarbon. After binding and mechanical treatment up to the required parameters, the products obtained undergo heat treatment in vacuum at a temperature of about 1500°C. In the process, silicon interacts with a pyrocarbon binder to form a carbide-silicon matrix which comprises boron carbide particles as inclusions.

The corrosion resistance of B_4C-SiC composites was studied for several thousand hours at temperatures up to 1300°C in air, water vapour environments and other reactive gas media. With time, the oxidation rate decreases and the weight of specimens becomes invariant. No carry-over of boron and failure of specimens were observed in the course of corrosion tests. Table I gives the reactor test results for absorber composites B_4C-SiC [4]. The results bear witness to a high radiation resistance of the B_4C-SiC composite.

The method devised to manufacture B_4C-SiC products makes it possible to make intricately-shaped control rod elements, including units with threaded joints. Figure 1 shows some products made on the basis of B_4C-SiC composite [4].

TABLE I. REACTOR TEST RESULTS FOR B_4C-SIC ABSORBER COMPOSITES [4]

Description of specimens				**Irradiation conditions**			**Variations in size and volume after irradiation**			**Variations in strength**
Dimensions	B_4C content (natural)	B_4C particle size	Total density	Temperature	Fluence	^{10}B burnup	Diameter	Length	Volume	
	%	mm	g/cm^3	°C	n/cm^2	%	%	%	%	%
1	2	3	4	5	6	7	8	9	10	11
4×4×40 mm	0	80	1.65	270-300	7.10^{20}	-	-	+0.360	-	-
	9		1.72					+0.317		
	16		1.82					+0.242		
	32		1.80					+0.242		
	47		1.87					+0.262		
	58		1.84					-0.015		
2×6×24 mm	46	80-120	1.75	550-650	$1.2.10^{21}$					
	50	~ 5	1.75		(thermal)					
∅ 20 mm	45	80-120	1.95	760-1070	$3.6.10^{20}$	6.5	+0.22	-0.28	-0.15	- 10 (σ_{cp})
l=30 mm	45	~ 5	1.95		(thermal)	10	+0.28	-0.26	+0.31	
∅ 10 mm	45	80-120	1.95	740-1250	$2.3.10^{21}$	71	+0.43	-0.04	+0.82	- 9 (σ_{cp})
l=15 mm	45	~ 5	1.95		(thermal)	68	+0.38	-0.32	+0.47	

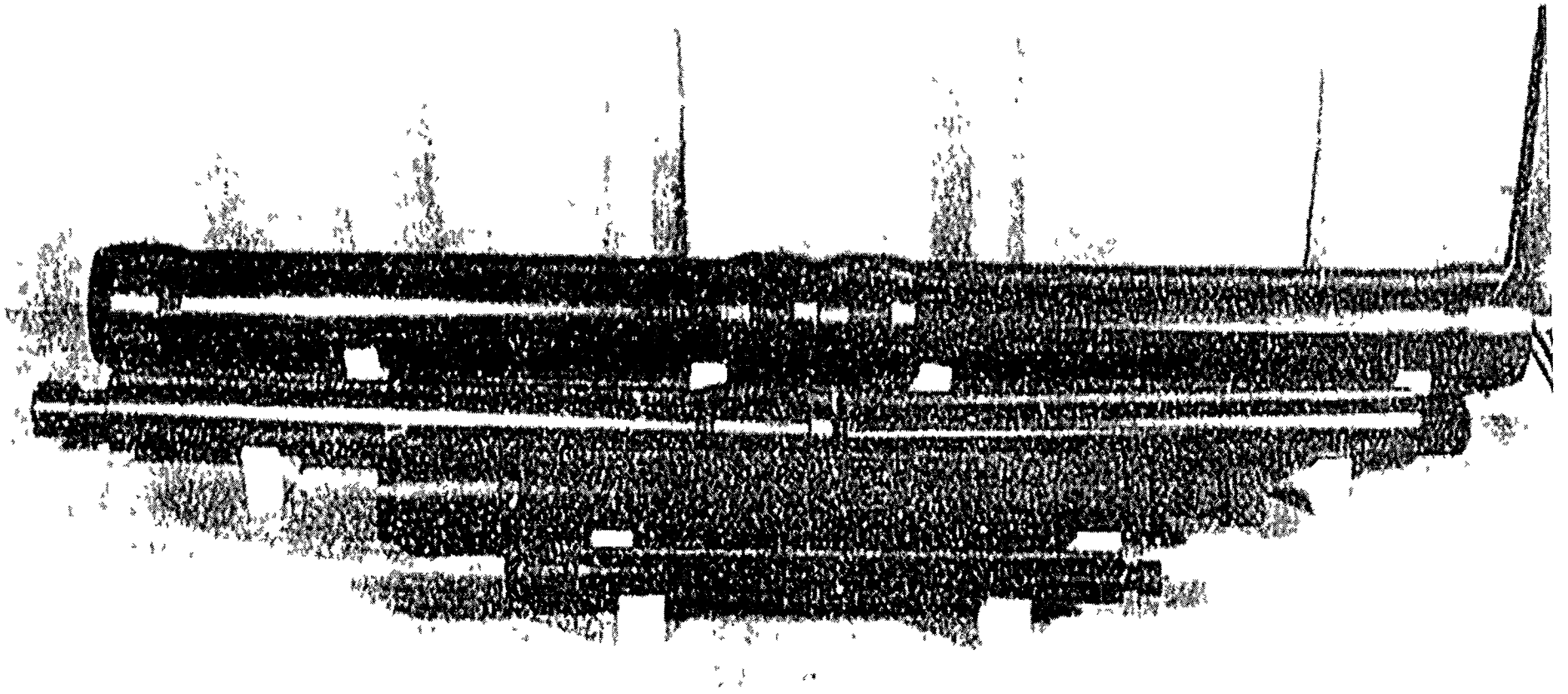

FIG 1 Rod-like absorber elements manufactured through the process of hydrocarbon pyrolysis [4]

3. B_4C-PyC COMPOSITE

The B_4C-PyC absorber composite and the products on its basis were developed at NSC KIPT for application in highly stressed reactivity compensation systems, mainly, in high temperature gas-cooled reactors (HTGR) [2, 4-6]. In particular, the VGM facility, designed in the former SU with the pebble-bed HTGR as the basis, provided for three independent reactivity compensation systems (RCS): a) control and shield rods (CSR) that can shut down the reactor and maintain it in a subcritical state in case of the worst possible accident [6]; b) for emergency shutdown an additional independent ball RCS was designed, it was based on filling special channels in the lateral reflector with absorber elements, $\leq$ 10 mm in diameter; c) at the initial phase and when the reactor is brought to the equilibrium operating conditions the excessive reactivity is compensated by spherical absorber elements (SAE) with an outer diameter of 60 mm; these SAE are placed directly in the core together with spherical fuel elements and empty (fuel free) elements.

As an absorbing material, the absorber elements of all three systems make use of B_4C with natural composition in boron, yet the specific content of absorber being different. Thus, for example, the B_4C content in the SAE matrix graphite is about 4.10^{-3} g/cm^3, and in small diameter SAE and in CSR rings is $\geq$ 1.3 g/cm^3. The NSC KIPT technology of manufacturing the B_4C-PyC absorber composite and its products, relies on the methods of volumetric gas phase saturation of porous media with pyrocarbon [1-5], namely, binding the B_4C powder with pyrocarbon (or mixing the graphite powder with the required content of B_4C). During the process development, both pilot specimens of materials and products for research purposes and pilot SAE batches (2500 pieces for critical stand "Astra") as well as ball RCS (2000 pieces for OKBM stands) were manufactured.

The metallographic sections of materials with increased absorber contents clearly exhibit the B_4C particles bound with pyrocarbon into a monolith (B_4C-PyC composite, see Fig. 2) [6]. The pyrocarbon binder has high strength characteristics [6], that eventually ensures a high mechanical strength of the composite. The main characteristics of B_4C-PyC absorber composites are presented in Table II (1.6 g/cm^3 B_4C content) [2].

FIG. 2. Microstructure of B_4C-PyC absorber composite with a specific B_4C content $\geq$ 1.5 g/cm^3, x 75 [6].

TABLE II. MAIN CHARACTERISTICS OF B_4C-PyC ABSORBER COMPOSITES (1.6 G/CM^3 B_4C)

Characteristic	γ	$\sigma_{cp.}$	σ_{bend}	λ	α
	g/cm^3	MPa	MPa	W/m 7	10^{-6} 7^{-1}
Value	2.1-2.2	300-330	80-100	10-17	4.8-5.3

It is seen from the Table that the strength of the B_4C-PyC composite is rather high. As the annealing temperature rises, the thermal coefficient of linear expansion and the electrical resistance values decrease, and the heat conduction of B_4C-PyC is nearly doubled (Figs. 3 and 4).

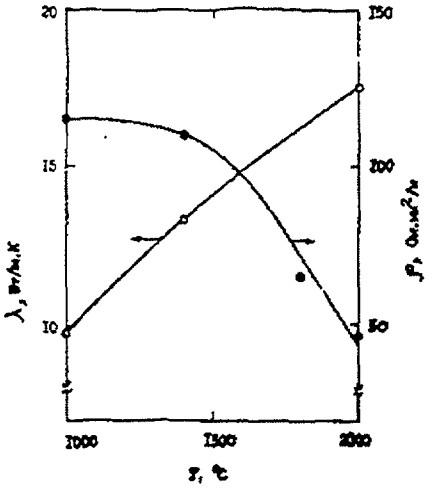

FIG. 3. Effect of annealing temperature on thermal conduction (l) and electrical resistance (r) of B_4C-PyC composite [6]

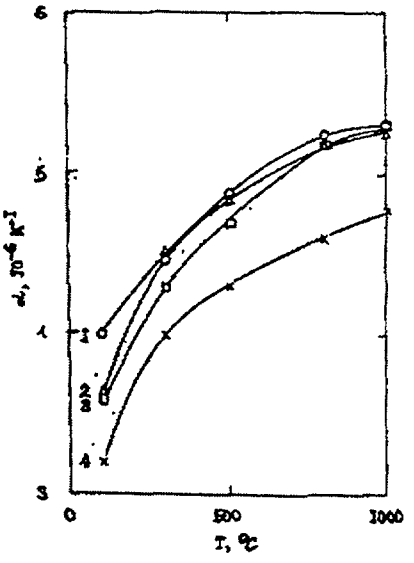

FIG. 4. Thermal coefficient of linear expansion (a) of B_4C-PyC with B_4C content of 1.6 g/cm^3 versus measurement temperature [6]:
1 - initial sample;
2 - annealing at 1400°C;
3 - annealing at 1300°C;
4 - annealing at 2000°C

The specimens of products were irradiated in a high flux reactor SM-2 [4, 6]. The model SAE diameter varied between 45 and 49 mm and the loading of their ∅ 40mm kernels with boron carbide was 3.9×10^{-3}, 3.6×10^{-2} and 1.9×10^{-1} g/cm^3, i.e. it varied by a factor of about 50.

The specimens with an increased B_4C content (≥ 1.3 g/cm^3) were of three types:
- cylindrical: ∅ 6 x 40 mm;
- bushings: ∅ = 45 mm, ∅ = 25 mm, H = 40 - 48 mm;
- sectors cut from the bushings at an angle of 120°.

Cylindrical specimens of matrix graphite GSP and of industrially made hot-sintered B_4C (produced by pressing the powder followed by sintering) were used as reference specimens.

To study the effect of heat treatment on the radiation deformation of B_4C absorbers, part of the specimens were annealed at temperatures between 1600 and 2000°C. The post-reactor examination revealed that the SAE underwent isotropic shrinkage, the value of which was independent of B_4C content (ranging from 3.9×10^{-3} to 1.9×10^{-1} g/cm^3), irradiation temperature and burnup of ^{10}B. All

experimental points showing relative diameter variations (ΔD/D) lie within the range of scatter presented in Fig. 5 [6]. The variations of ΔD/D = f(F) for SAE are in good agreement with the variations of Δl/l = f(F) for matrix GSP graphite specimens (see the curve in Fig. 5).

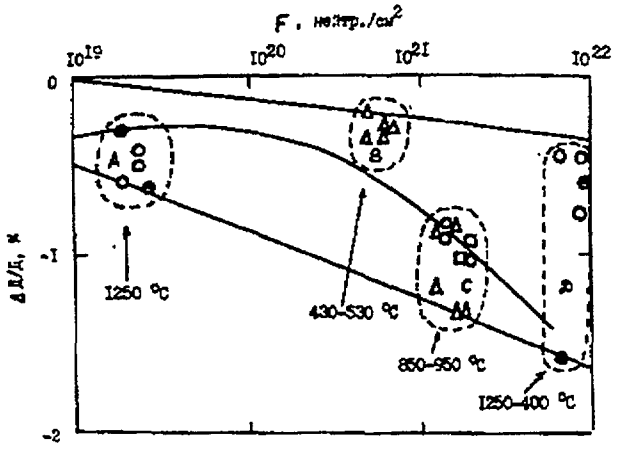

FIG. 5. Radiation deformation (ΔD/D) of spherical absorber elements with B_4C content of 0.004 g/cm³ (O, ◗, ●); 0.036 g/cm³ (Δ) and 0.19 g/cm³ (□) versus fast neutron fluence [6]
O, Δ, □ - initial spheres;
™ - annealing at 1600°C, 6 hours;
• - annealing at 2000°C, 6 hours.
(Figures near the encircled regions denote the irradiation temperatures; the curve shows deformation of matrix graphite GSP specimens irradiated at 1100 - 1200°C)

It should be noted that the ^{10}B burnup in SAE relating to region C in Fig. 5 was found to be 55 and 21% for SAE with B_4C content of $3.9.10^{-3}$ and 0.19 g/cm³, respectively. In SAE irradiated to a high fluence of neutrons (see region D in Fig. 5), practically a complete burnup of ^{10}B nuclei took place. The annealing of SAE at 1600 and 2000°C for 6 hours has no appreciable effect on the ΔD/D value, and the scatter of experimental data can be due to both the structural peculiarities (density, pyrocarbon content) of individual SAE and their irradiation conditions.

The SAE, absorber composites based on B_4C dispersions in GSP with B_4C (natural) content up to 1.6 g/cm³ were also tested in wide ranges of temperatures (300 to 1250°C) and fluences [1, 2, 4, 6]. All the materials have exhibited an extremely high radiation resistance. Even for the materials with a B_4C content of 1.6 g/cm³, irradiated at 1200 to 1250°C to 90% burnup in ^{10}B, the dimensional changes were no more than 1%. After irradiation, the B_4C-PyC specimens remained intact, no spalling, cracks or other defects were observed. At the same time, at similar irradiation conditions the hot-sintered B_4C specimens showed swelling: ΔV/V - 0.75 - 1.5% [6].

It is known [6] that the specimens of hot-pressed or hot-sintered B_4C exhibit swelling under irradiation, and the swelling value drastically increases with increasing irradiation temperature and burnup depth. In particular, with a ^{10}B burnup of about 5% at irradiation temperature of 900°C the ΔV/V ratio reaches 30%. Therefore, the results of investigations into radiation deformation of type B_4C-PyC absorber composites, reported here and in [6], are in a way unique. The near- zero deformation of the composites under study can be attributed to a competing action of two factors: swelling of B_4C particles and shrinkage of the pyrocarbon matrix [6].

The present results suggest that further studies are needed to clarify the applicability of B_4C-PyC absorber composite instead of a vibro compacted B_4C powder in the end part of CSR of the WWER-1000 reactor (Fig. 6).

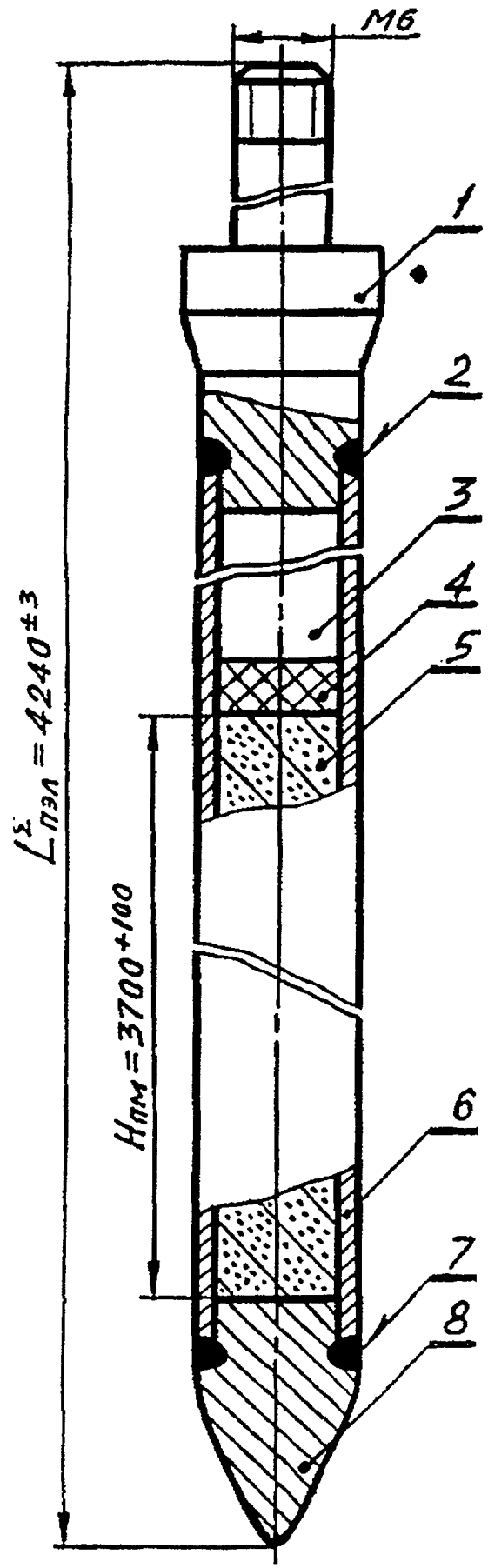

1 - upper end part;
2 - upper weld;
3 - compensation volume;
4 - plug - fixing catch of absorber material;
5 - B_4C-PyC absorber composite;
6 - absorber element cladding:
∅8.2 × 0.6; 08X18H10T;
7 - lower weld;
8 - lower end part

FIG. 6. Design of WWER-1000 absorber element proposed for further studies

4. CONCLUSION

So, the bench and reactor tests undertaken here allow us to draw the following conclusions:

1. The B_4C-PyC and B_4C-SiC absorber composites have high strength characteristics;
2. Radiation deformation of B_4C-PyC absorber composites with an increased B_4C content ($\geq$ 1.3 g/cm^3), irradiated at temperatures between 1200 and 1250°C to a 90% burnup in ^{10}B, was no more than 1%;
3. Irrespective of a high damaging of the matrix, estimated in some experiments to be about 30 dpa [6], the absorber composites under study show an extremely high radiation resistance and this makes them promising not only for HTGR but also for the reactors of other types;
4. It is recommended to investigate the possibility of using the B_4C-PyC absorber composite instead of the vibration-densified B_4C powder in the end part of the CSR of the WWER-1000 reactor.

REFERENCES

[1]. GURIN, V.A., ZELENSKY, V.F., "Gas-phase methods of producing carbon and carbon-carbon materials", Voprosy At. Nauki i Tekhniki, Ser. Fiz. Rad. Povrezhden. i Rad. Materialoved., Kharkov, NSC KIPT publ., is. 3(69), 4(70), (1998) 83-85 (in Russian).

[2]. ZELENSKY, V.F., GURIN, V.A., KONOTOP, YU.F., ODEYCHUK, N.P., et al., "Spherical fuel and absorber elements for HTGR", Vopr. At. Nauki i Tekhn. Ser., Fiz. Rad. Povrezhden. i Rad. Materialoved., Kharkov, NNTs KhFTI publ., is. 5(71), (1998) p.40 (in Russian).

[3]. ZELENSKY, V.F., GURIN, V.A., KONOTOP, YU.F., ODEYCHUK, N.P., et al., "GSP graphite", Voprosy At. Nauki i Tekhniki. Ser. Fiz. Rad. Povrezhden. i Rad. Materialoved., Kharkov, NSC KIPT publ., is. 3(69), 4(70), (1998) 86-87 (in Russian).

[4]. IVANOV, V.E., ZELENSKY, V.F., TSYKANOV, V.A., et al., "Dispersive fuel and absorber elements based on pyrocarbon-bound graphite for high temperature gas-cooled reactors", book: Reaktorn. Materialoved. (Proc. of Reactor Materials Science Conf., Alushta, 29 May - 1 June, 1978), V.6, Moscow, TsNIIAtominform publ., (1978) 308-325 (in Russian).

[5]. GURIN, V.A., ZELENSKY, V.F., EVSEEV, V.M. et al., "Development of monolithic-type pyrocarbon-bound fuel and absorber elements for HTGR", book: Nuclear hydrogen energetics and technology, Moscow, Ehnergoatomizdat publ., is. 5, (1983) 213-225 (in Russian).

[6]. ZELENSKY, V.F., GURIN, V.A., KONOTOP, YU.F., et al., "Radiation resistance of absorber composites with a pyrocarbon binder", (Proc. of the Int. Conf. on Radiation Materials Science, Alushta, 22-25 May, 1990), Kharkov, KIPT publ., v.8, (1991) 68-76, (in Russian).

DAMAGE ANALYSIS OF CERAMIC BORON ABSORBER MATERIALS IN BOILING WATER REACTORS AND INITIAL MODEL FOR AN OPTIMUM CONTROL ROD MANAGEMENT[1]

XA0053637

W. SCHULZ
Preussen Elektra Aktiengesellschaft,
Hannover,
Germany

Abstract

Operating experience has proved so far that BWR control rods cannot be used for the total reactor life time as originally presumed, but instead has to be considered as a consumable article After only few operating cycles, the mechanism of absorber failure has been shown to be neutron induced boron carbide swelling and stress cracking of the absorber tubes, followed by erosion of the absorber material In the case that operation of such a control rod is continued in control cells, this can lead to an increase of the local power density distribution in the core and, under certain conditions, can even cause fuel rod damage A non destructive testing method has been developed called "UNDERWATER NEUTRON RADIOGRAPHY" applicable for any BWR control rod "Lead-control rods" being radiographed are used to evaluate their actual nuclear worth by the help of a special analytical procedure developed and verified by the author Nuclear worth data plotted against burn up history data will allow to create an "EMPIRIC MODEL" This model includes the basic idea of *operating control rods of a certain design first in a control position up to a target fluence limited to an amount just below the appearance of control rod washout Afterwards they have to be moved in a shut down position to work there for the total remaining holding period* The initial model is applicable to any CR-design as long as sufficient measuring-data and thus data about the nuclear worth are available The results of these experiences are extrapolated to the whole reactor holding period After modelling no further measurements of this particular control rod type are necessary in any reactor The second focal point is to provide an APPROXIMATION EQUATION By knowing the absorber radius, B_4C density and absorber enclosure data an engineer will *calculate reliably the working life of any control rod design* on control position, indicated as maximum allowable neutron fluence margin until absorber wash-out starts **This concept - to calculate the control rod's working life both in the control position and the shut-down position - will automatically lead to an optimization of the control rod strategy** Control rod optimisation is demonstrated by accumulating the total amount of control rods required in a medium-sized BWR up to the total reactor holding period At least 60% of the first core inventory - for this control rod type an existing EMPIRICAL MODEL is already available - may be used up to the total operating period without any safety loss Looking to the present disposal situation this concept represents a practical way to reduce all high level waste In addition benefit of utilizing this concept is that it minimizes tritium emission Control-rods utilized within Boiling Water Reactors (BWR) are designed for the purpose to control and shape the neutron flux profile in the reactor, to adjust the range of regulation referring to the weight rate of the reactor coolant and thirdly by- shutting down the reactor at any time and under any conditions with regard to nuclear aspects, mechanical integrity and control rod history The designation control- or shut down rod characterize the particular field of activity for a given control rod The focal point of my work had shown to be a calculation of the nuclear working life of any control rod design as well as an optimisation method with reference to the holding period for a given control rod inventory as a result of measuring data and a theoretical analysis describing the parameters in a general validity form

1. DESIGN VARIATIONS

The control rods typically used in boiling water type reactors (see Figure 1) are provided with a cruciform shape and pass in the interstices between fuel channels. The typical basic product line of the GE control rod (standard control rod) is shown in the Figure 1 Four absorber blades are arranged in order to form the required cruciform shape. Every blade is filled with up to 21 small absorber tubes placed in side by side relation along the axis of the cruciform shaped control rod containing B_4C powder inside, compressed to a theoretical density of 70 % by vibro compacting. B_4C is preferably used in most of all reactor types because of the high reactivity worth reduction capability and its low price compared to other absorber materials

The mechanical integrity of those control-rods is safely fixed by a sheath metal jacket surrounding the absorber tubes and welded to the upper and lower end fittings of the control rod and to a connecting rod arranged at the centre of the absorber cross Design variations have been performed in order to extend the service life limit by using high purity steel, different absorber

[1] Summary report of thesis including some additional aspects to the actual problem by using B_4C and Hf within a control-rod in general

volumes and Hf located at the higher burn up zones. The latest GE control rod version called marathon shows a new basic control blade structure consisting of vertically extending square tubes welded together in a long line (about 450m) to form solid stainless steel blades filled up with absorber segments.

In another prior art configuration, it has been known to provide a solid stainless steel member with drilled holes, the ABB basic design (CR 70) [1, 2]. This solid steel member has the same length and width of the prior sheath metal jacket. Every solid blade has a plurality of accurately drilled holes extending horizontally from the side edges of the rod to and towards the centre of the required cruciform shape. The solid stainless steel sheets designed with a thickness of about 8 mm are welded together at the centre. Depending from different design variations the B4C powder in each wing is filled by vibro compacting in horizontally drilled holes of about 6mm diameter and spaced at a pitch of about 7.5 mm. Regarding to newer design variations the holes are additionally filled with hafnium pins (the uppermost 19 holes) at the top of the wing (CR 82) or additionally filled together with Hf end plugs (CR85) at the outer section of the blade wing. To balance the gas pressure between different absorber holes the border in front of the absorber wing is equipped with a communication channel to balance the gas pressure between different exposed absorber sections. The nuclear worth is adjustable by varying the depth of the holes, the absorber cross section and the space between two holes.

At the moment the latest ABB control rod versions CR82m and CR85 m are tested all over the world to extend the nuclear data base. This particular control rod design shows up to 4 significant variations [2] by using:

- B_4C pellets instead of B_4C powder (partly)
- smaller hole diameter
- closer hole to hole separation

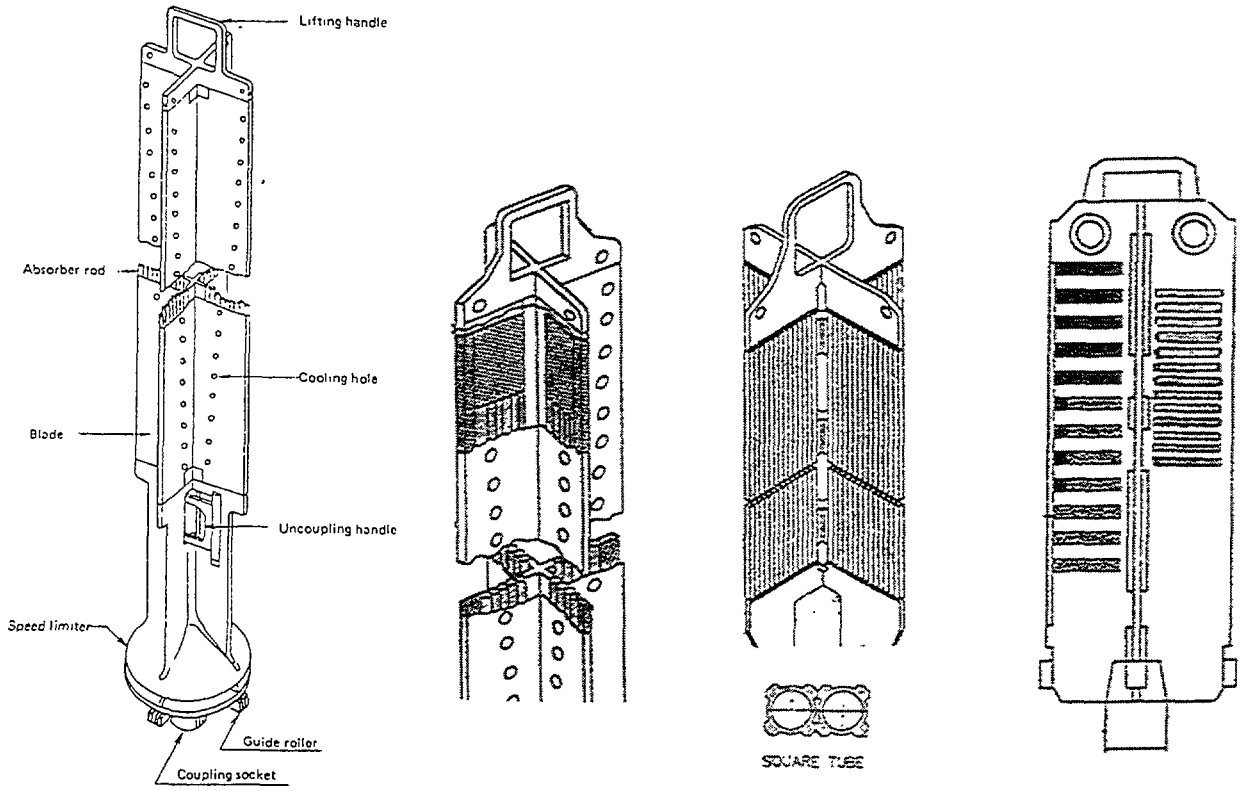

FIG. 1. Different basic design variations of BWR control rods

2. OPERATING EXPERIENCE

Operating experience has proved so far that this reactor component cannot be used for the total reactor life time as originally presumed, but instead has to be considered as a consumable article [3-11]. After only few operating cycles, the mechanism of absorber failure has been shown to be neutron induced boron carbide swelling up to 16% compared to unirradiated B_4C powder, density reduction of the absorber material at the same magnitude and stress cracking of the absorber tubes (enclosure) followed by erosion of the absorber material. The occurrence of absorber gaps will start at a local-burn up between a range of 50 to 55% boron 10 depletion in the case by exposing the GE standard control rod design [12, 13]. Eddy current testing of the rods showed defect signals, i.e. longitudinal cracks, corresponding to a slight diameter increase up to 0.2% (Stainless steel 304).

The mechanism during absorber exposure with neutrons has to be pictured as follows. During irradiation a solid ring is formed (Figure 2a) as a result of the ^{10}B reaction with neutrons, starting from the outer surface of the absorber area to grow up to the axial centre line of the absorber tube by following an exponential burnup expression. This means the density reduction will start directly at the inner wall of the tube to indicate massive circumferential stress. Those forces are necessarily needed to move small particles of absorber product forcibly to the gaps (free volume) available. The original free volume of 30% (B_4C 70% at theoretical density) is not completely available for swelling accommodation, since the forces needed to move small particles of absorber product will pass the mostly intergranular (see Figures 2b and 2c) and longitudinal in view of the tube axis (see Figure 2d) to allow a wash out mechanism through the crack (see Figure 3) during exposure ultimate strength of the absorber enclosure which is actually used. From this it may be concluded that the cracks could only arise in connection with mechanical steady state stress to the inner surface

a) B_4C cake [4]

c) crack (more older) [3]

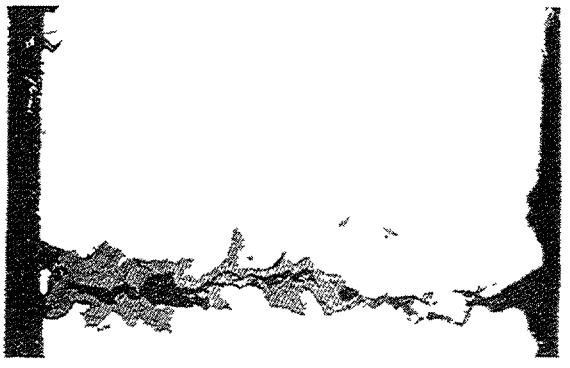

b) Intergranular young crack [3]

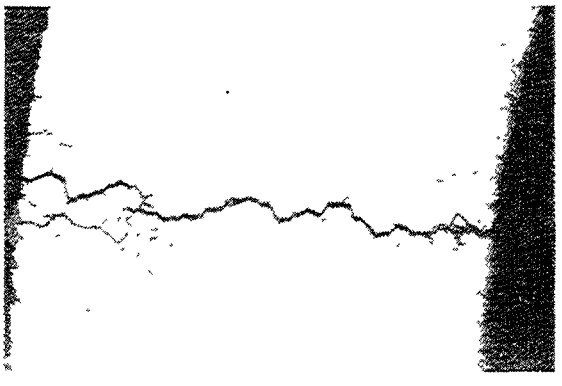

d) View through the coolant hole to absorber tube (segment) showing a longitudinal crack [4]

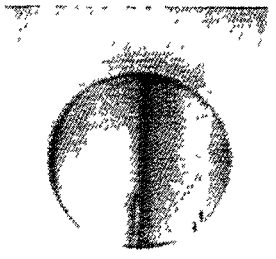

FIG. 2. B_4C cake and cracking behaviour within the absorber tube

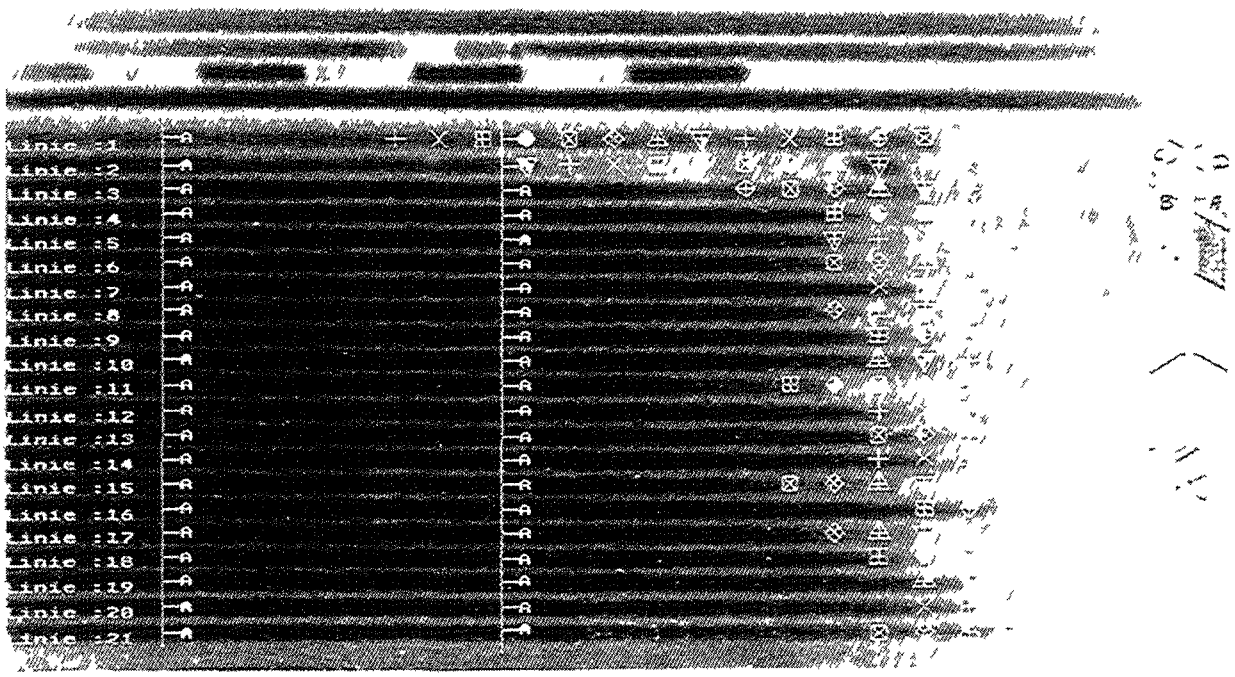

FIG 3 Radiography of the upper section of an absorber blade showing absorber loss (marked)

In the case that operation of a control rod showing massive absorber gaps is continued in control cells, this can lead to an increase of the local power density distribution in the core and under certain conditions, can even cause fuel rod damage (PCI) (e g see Figure 4, where a loss of about 73% regarding to the original ^{10}B content due to burnup and wash-out occurred [15], the thermal accumulated neutron fluence in the absorber was $\Phi(CR/4)$ = 2 46 snvt, whereas 1 snvt ≡ 1×10^{21} n/cm^2) Depending from the axial power distribution in the core the relative worth reduction of a quarter control rod like this has been calculated to be 22% corresponding to a local amount of even 35% [15]

Figure 5 illustrates the core loading scheme of NPP Wurgassen cycle 4 showing locations of defect fuel elements (fuel array) and defect fuel rods (marked dots) including all control positions (cruciforms) being inserted during the fourth cycle

The nuclear behaviour of ABB control rods is basically comparable to those of the GE-design Destroying investigations performed at the first core control rod CR70 design verified that the damage mechanism has to be exactly the same neutron induced intergranular stress cracking of the absorber blade resulting in absorber loss at high burn up zones Figure 6 shows a radiograph of the uppermost part of two CR70 control rod wings [16] The gaps located at the outer ends of the horizontal fillings indicate, that the cracks must have a longitudinal shape (horizontally cracks) and every hole has to be calculated separately in view of "critical" neutron fluence (defined as beginning of absorber loss)

As part of a research program 8 ABB lead control rods were tested One of 4 CR70 type control rods showed cracks after 3x18 months cycles (Φ_{cnt} = 2-2 3 × snvt) [17] The accumulated operating experience with all B_4C control rods (CR70) showed, that more than 90 % of the replaced rods were found to be cracked in the uppermost top section [18] The reason is explained by G Vesterlund (ABB) to be a very strong axial gradient of absorption Same results has been observed by the author regarding to GE type control rods

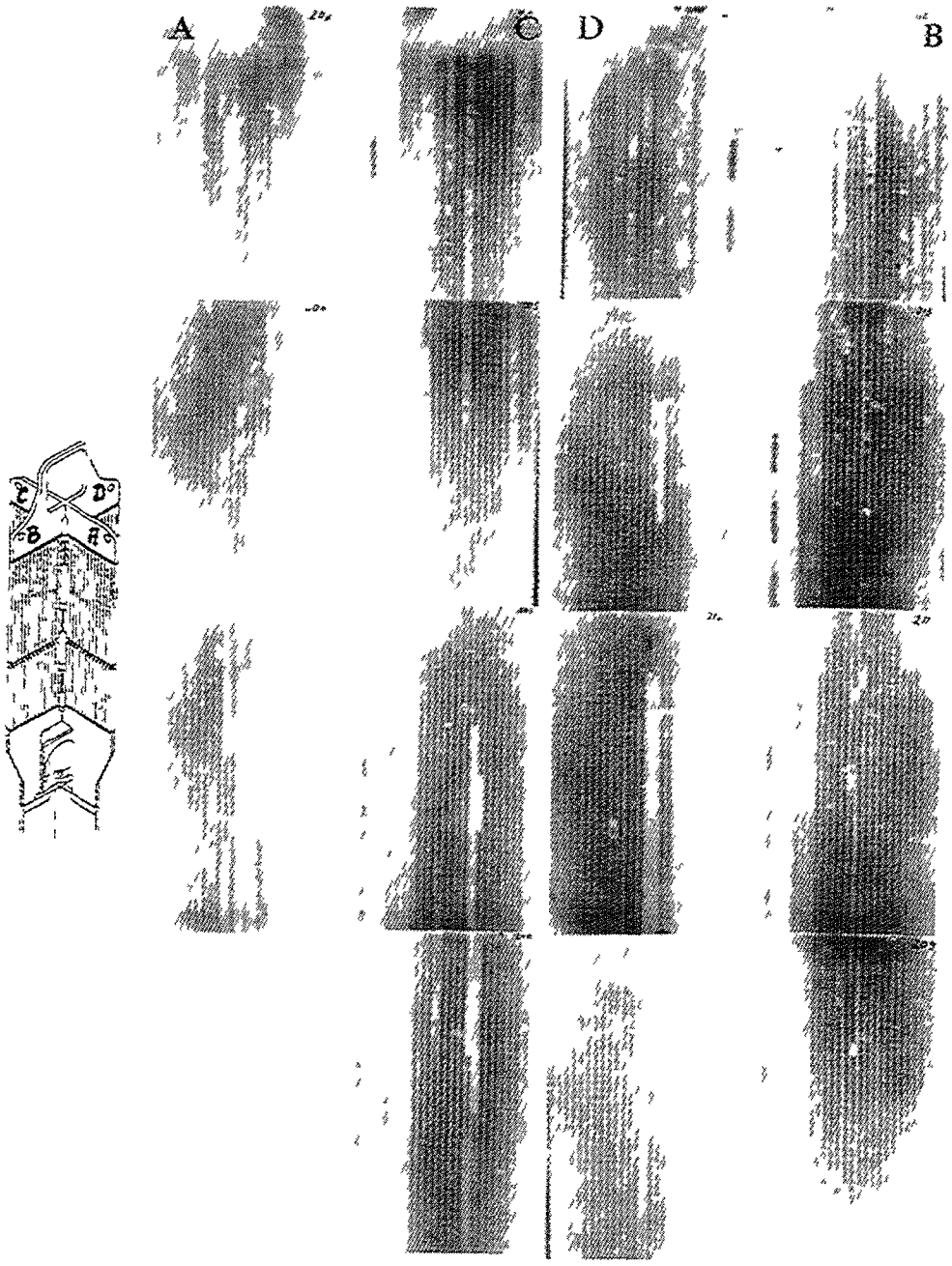

FIG 4 Radiograph of the upper quarter of a high burnup control rod (GE standard design) showing massive absorber gaps

A Johnson [2] reports about two CR85 control rods operating in deeply inserted control positions during all cycles from 1985 to 1990 One of the rods was found to be cracked during the inspection in 1990 The crack was positioned above hole number 20 from the top, i e the uppermost hole containing boron carbide

A Huttmann [19] reports about 2 "Ultimate" control rods (type CR85) operating in deeply inserted control positions up to a neutron fluence of 3 3 snvt (quarter segment) They were also found to be cracked The author came to the result, that CRs of this particular type will not loose their shutdown and scram capabilities, if defects of the described nature are present (I give proof of the incorrectness of this conclusion in [15])

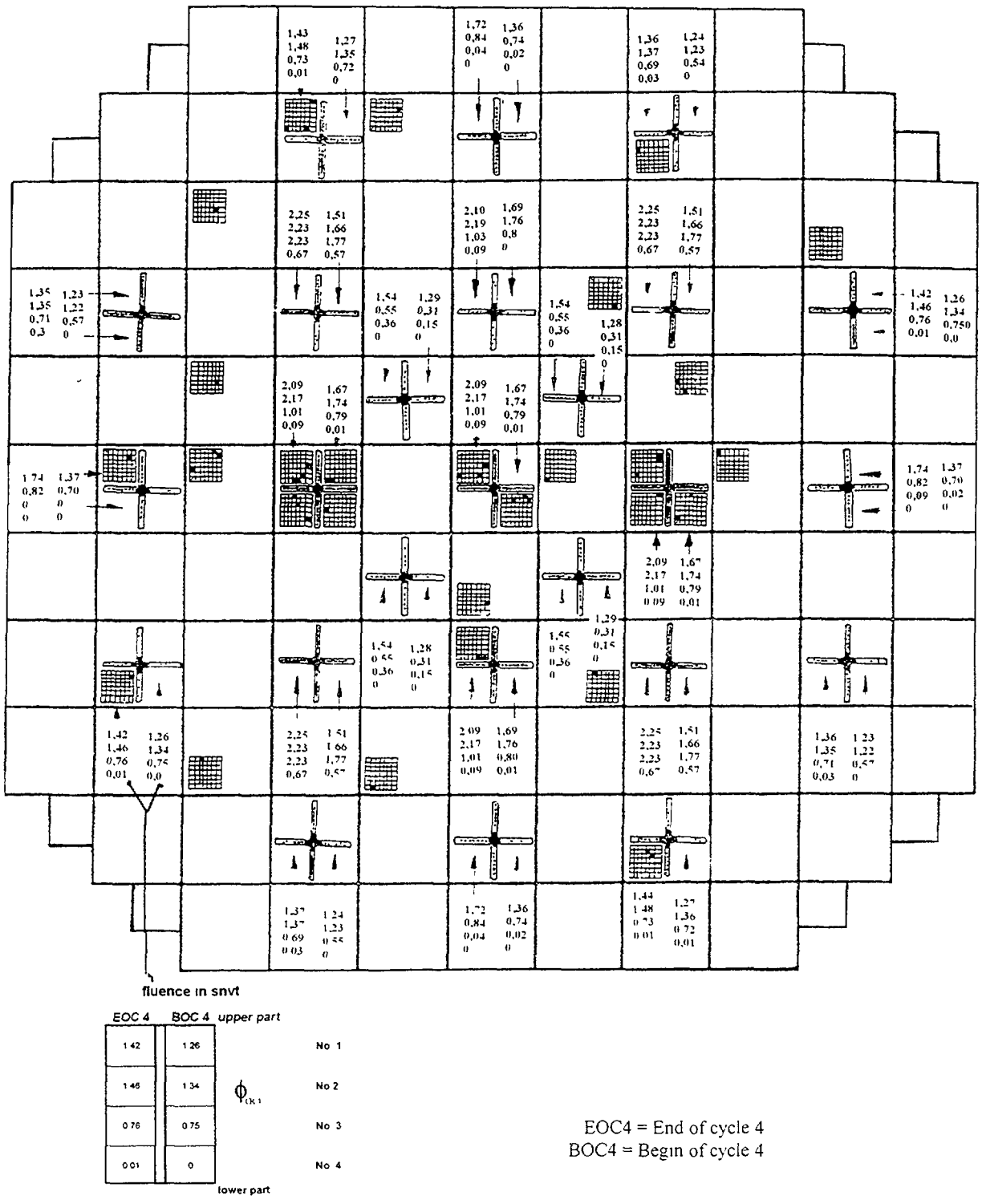

FIG. 5. Core loading scheme of NPP Wurgassen cycle 4 showing all locations of defect fuel elements (yellow) and defect fuel rods (marked red) including all control positions (blue) being moved (inserted) during the fourth cycle

Introducing those high worth control rods (110% relative worth), the gadolinium concentration can be reduced significantly up to 3% by using a control rod management to exchange all control rods up to the outermost located core row against CR85 CRs (type 110%) within 3 cycles (ABB patent). This strategy must include that all control rods have to hold the relative effectiveness at 110% any time and during each cycle! Own investigations for a given example showed, that the number of

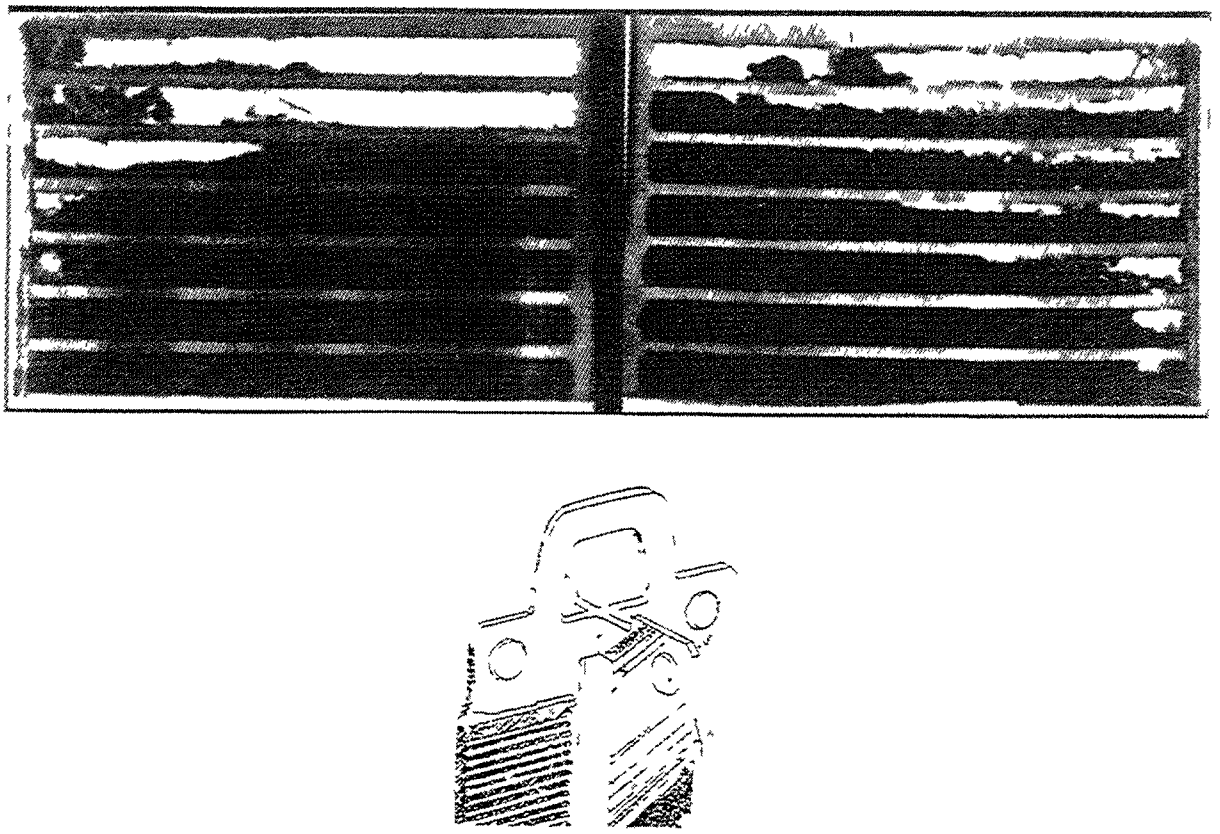

FIG 6 Radiograph of the uppermost part of CR70 control rod wings [16]

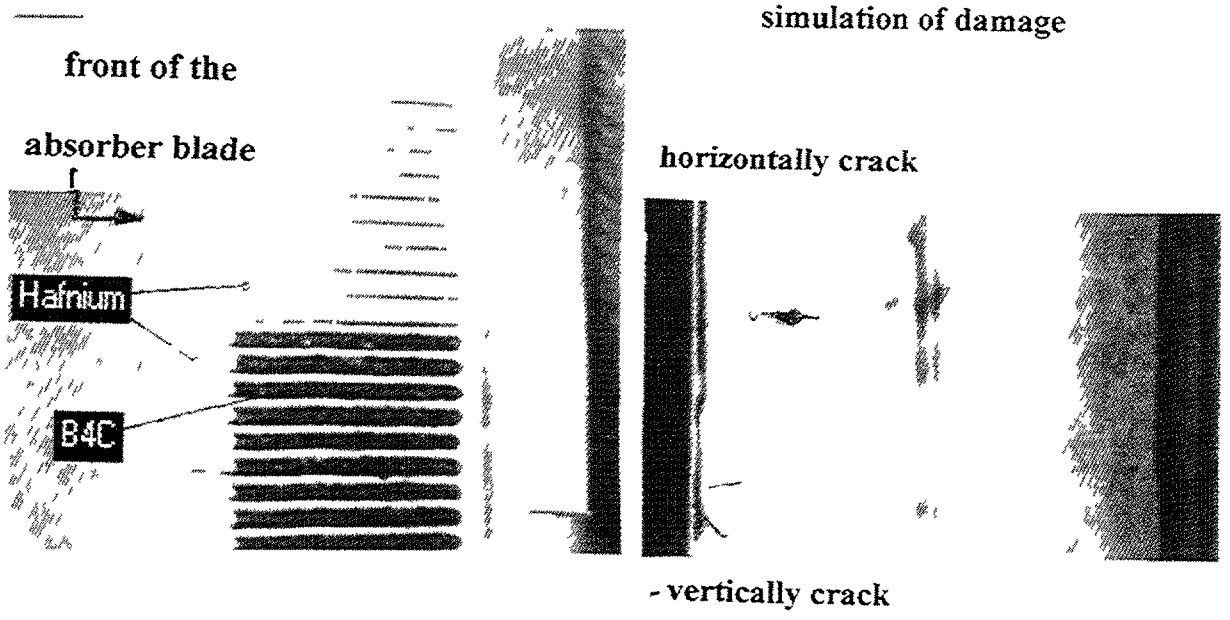

FIG 7 Schematic representation of an ABB control rod segment and mechanism of damage randomly designed by digital image processing to get a visual impression (any resemblance to an existing blade section is purely coincidental)

control rods per cycle will raise up to 200% by reducing the gadolinium concentration only at a quarter fuel loading. This fact should explain enough! According to the latest reports [20], it may be concluded that control rods, additionally filled with hafnium pins at the top of the wing, will show horizontally as well as vertically cracks (Figure 7).

By combining both absorber materials within one absorber enclosure, **two different damage mechanism** will work together. The **cracks having a longitudinal shape** will only arise in connection with mechanical steady state stress as a function of the accumulated neutron fluence. The **vertically shaped cracks** must have another cause.

At ABB control rods (CR82, CR85) first cracks were preferably found at the upper part of the control rod, the hafnium/boron carbide area. For this reason the boron burnup reaction should be investigated with respect to the reaction B_4C with Hf during exposure to neutrons. Control rods containing B_4C and Hf material which are directly located close together do not need any H_2 pick up mechanism through stainless steel clad. The nuclear reactions building tritium within the control rods containing ^{10}B are as follows:

$$^{10}B + n \rightarrow {}^{7}Li + {}^{4}He + 2,79\,MeV \qquad \text{(thermal)} \qquad (1)$$

$$^{7}Li + n \rightarrow {}^{4}He + {}^{3}H + n$$

$$^{10}B + n \rightarrow 2\,{}^{4}He + {}^{3}H + 0,23\,MeV \qquad (2)$$

$$^{10}B + n \rightarrow {}^{9}Be + {}^{3}H \qquad \text{(fast)} \qquad (3)$$

$$^{2}H + n \rightarrow {}^{3}H \qquad (4)$$

They might act excellent as supplier for the hydrating process to form Hf $H_{1\,7}$ bulges. The kinetic energy (see eq. (1)) resulting from different reactions during neutron capture probably works as a moderator with respect to the tritium to react with hafnium to form a metallic gas mixture. Hf hydride precipitates in producing Hf hydride bulges. The following formula describes the chemical mechanism

$$10\,\mathrm{Hf} + 17\,\mathrm{H} \Rightarrow 10\,\mathrm{Hf\,H_{1\,7}} \qquad (5)$$

(6)

$$m(H) = \frac{n(H) \times M(H)}{n(Hf\ H_{1\,7}) \times M(Hf\ H_{1\,7})} = \frac{1.7 \times 1.008}{1 \times 180.314} \approx 0.0095 \approx 9500\ \text{ppm}$$

Figure 8 represents the H Hf phase diagram which is based on the isothermal equilibrium hydrogen vapour pressure measurements of R.K. Edwards and E. Veleckis [18]. For a different pressure (the pressure adjusting during exposure) the principle phase line to be expected is marked in red. Figure 8 shows that at locations of lower temperatures Hf hydride precipitates due to thermal diffusion. Local volume extension by 14.7 % (Hf $H_{1\,7}$) obviously reacts in removing the metallic border from the front of the absorber wing (vertically crack).

The two different mechanism of damage might be the reason to the **longitudinal and vertically shaped cracks found in the ABB control rods.**

Additionally swelling deformation of several absorber holes side by side (ballooning), as it has been observed recently in different BWRs in Japan [20], is probably only possible by using the latest ABB control rod design CR82m/CR85m (Figure 9). The following reasons should be responsible to this event:

- reduction of the absorber diameter in comparison to the CR70/82/85/ control rod design and in this way reduction of the nuclear life limit (described later);
- distance "b" is reduced (closer hole to hole separation) in comparison with distance "a" to claim the way the cracks should follow;
- new steel with higher strain capability (creeping) does not bring any advantage in view of the nuclear life limit (described later).

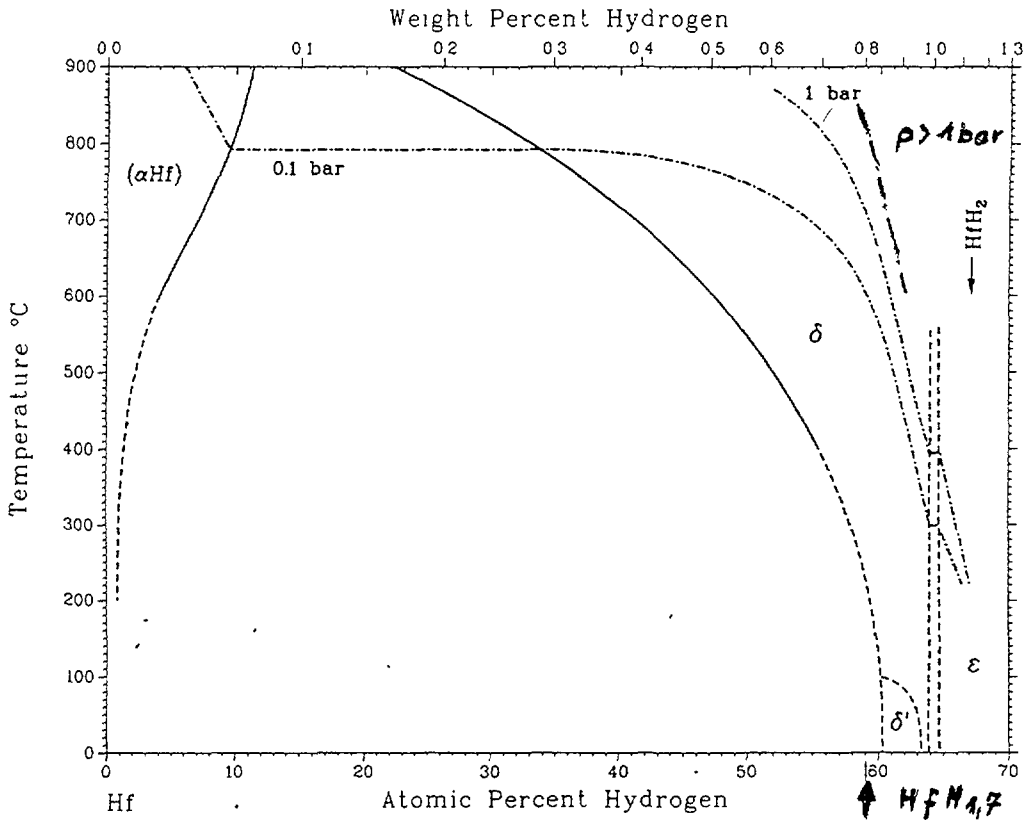

FIG. 8. H-Hf phase diagram

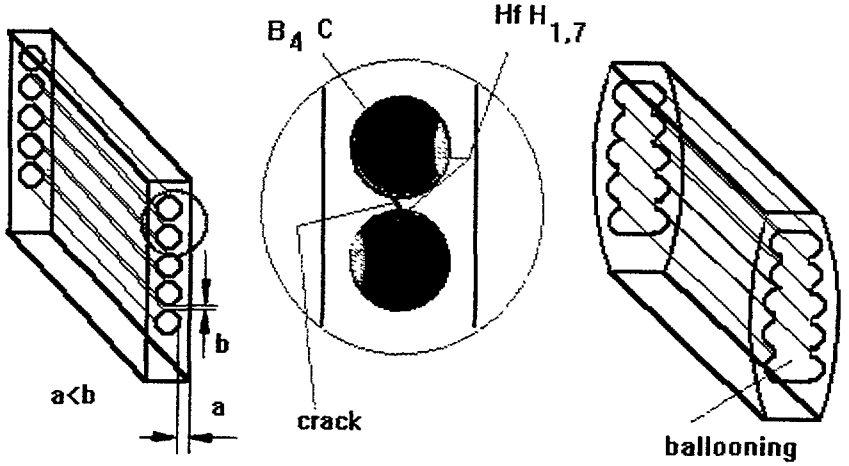

FIG. 9. Schematic representation of the new ABB control rod concept and mechanism of ballooning (which will lead to "stuck rod")

3. MANAGEMENT FOR AN OPTIMUM CONTROL ROD STRATEGY

The limited service life of this important core component requires carefully planned strategies in order to minimize the number of control rods to be exchanged. For this reason the author developed a non-destructive testing method to systematically study the operating behaviour of control rods since 1983 and to optimize the control rod management with regard to their life expectancy.

The present work demonstrates the measuring results of different BWR control rod design variations evaluated with the help of a non-destructive testing method utilizing neutrons - referred to as ***underwater neutron radiography***. This particular testing method is comparable to the X-ray examination method and was developed by the author specifically for this application. The evaluation of all neutron radiography results including a re-analysis of results from destructive tests of B_4C absorber samples, led to two basic findings.

First: An **approximation equation to calculate reliably the control rod's working life on control position, indicated as neutron fluence as a function of different construction features like absorber radius, theoretical density and absorber tube parameters** until absorber washout starts.

The second focal point of this work is to provide an **empirical model application to be used for control rods in the shutdown positions** for the total remaining holding period corresponding to the safety-related evaluation criteria required. By using both instruments to calculate the control rod's working life, users can optimize their control rod strategy to save 60% of the control rod inventory during the reactor period.

Figure 10 illustrates how **the method generally works to achieve an optimized control rod management**. All new results based on the authors thesis work are shaded. To get a surveillance of the control rods working life, generally **4 different methods** are available:

- Monitoring of the tritium activity in the reactor coolant;
- Monitoring of the neutron fluence in substitution for the reactivity control;
- Optical inspection method;
- The submarine neutron radiography.

3.1. Monitoring of the tritium activity in the reactor coolant

Tritium is produced in a remarkable amount during reactor operation. It shows a long half life and is difficult to detect, because of its low radiation energy level. It is often to be found as HTO or T_2O in steamy or liquid form. Because of this great expenditure would be necessary to separate this element from natural water. Storage of ^3H for a longer time period in the reactor coolant is unsuccessful, because of the long half-life of 12.3 years [21].

So the ^3H has to be disposed to the waste water treatment and additionally to the waste air. In contrast to German regulations, where the tritium release [22] is fixed to different amounts depending on reactor type and federal authority of the respective federal state, in the USA the tritium release is generally fixed to a maximum limit of 10 curies at any one time or to 100 curies in any one calendar year [23].

The nuclear reactions building tritium within the control rods are as described in equation (1) to (4). So monitoring the tritium activity in the reactor coolant is generally a good tool to get information about control rod behaviour. The method works by comparing the measuring results of the tritium transmission rate into the reactor coolant of cycle A and B being existent as an equilibrium concentration. The balance equation referring to a BWR working with leaking control rods (see Figure 11) is based on the following expression:

$$\frac{dN_T}{dt} = r_T - \lambda_T \ N_T - \beta_1 \cdot N_1 \tag{7}$$

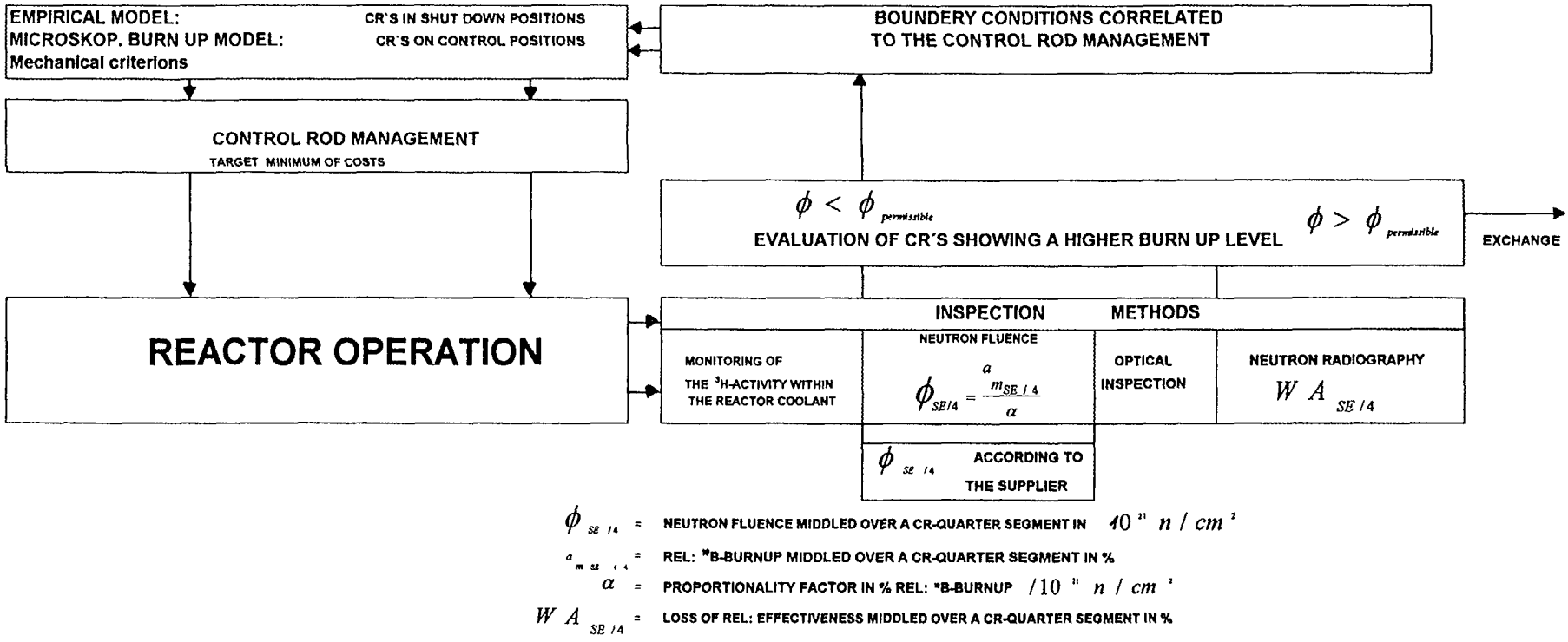

FIG 10 Strategy for an optimized control rod management

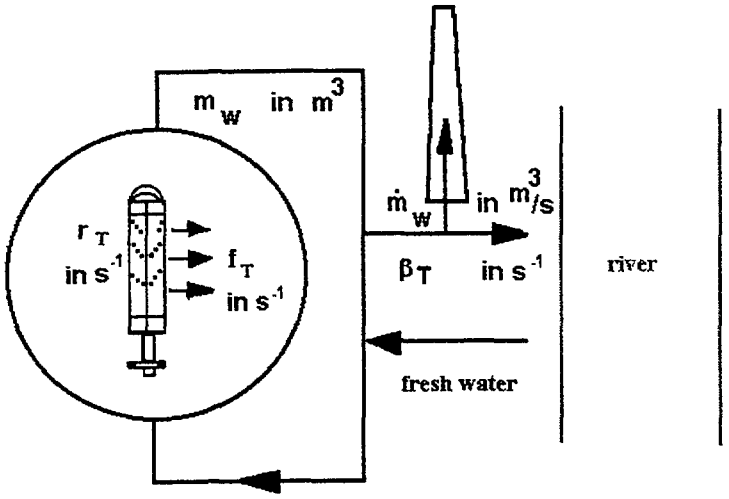

FIG. 11. Schematic representation of the reactor circulation including leakage of coolant

The tritium release in the absorber, described as function of the inventory, will be:

$$f_T = \beta_T \cdot N_T \tag{8}$$

whereas f_T = tritium release in1/s

$\beta_T = \frac{\dot{m}_W}{m_W}$

N_T = number of tritium atoms

β_1 = proportionally factor in 1/s

r_1 = tritium production rate in s^{-1}.

The **tritium transmission rate R_T** finally will be derived as:

$$R_T = A_{T(m_W)} \cdot \left(\lambda_T \cdot m_W + \dot{m}_W\right), \tag{9}$$

whereas $A_{T(m_W)}$ in $\frac{\mu Ci}{m^3}$ specific tritium activity per m^3 coolant (as to be measured)

A_T in μCi

$\dot{m}_W$ in m^3/s = reactor coolant loss rate (out of the circulation)

m_W in m^3 = reactor coolant inventory

λ_T in $1/s$ = constant of radioactive transformation with respect to tritium

This analytical study of a balance equation, shown in Figure 12, generally only permits to get an integral answer about leaking control rods in the core. Figure 12 shows that comparing cycle A and B, the tritium transmission rate into the reactor coolant will be reduced significant by shuffling (48) high burnup control rods at the end of cycle A from control positions to shut down positions during the following cycle B ("effect 48U"). This fact is important regarding to the "Empirical Model" applicable for control rods on a shut down position showing low burnup until end of reactor life (this will be described later). Same effect occurs if (8) high burnup control rods on control positions are going to be replaced at the end of any cycle ("effect 8E").

As a second important fact regarding to Figure 12, it may be concluded that the tritium release will only be a function of the control rod leakage itself. Defect fuel elements may not show

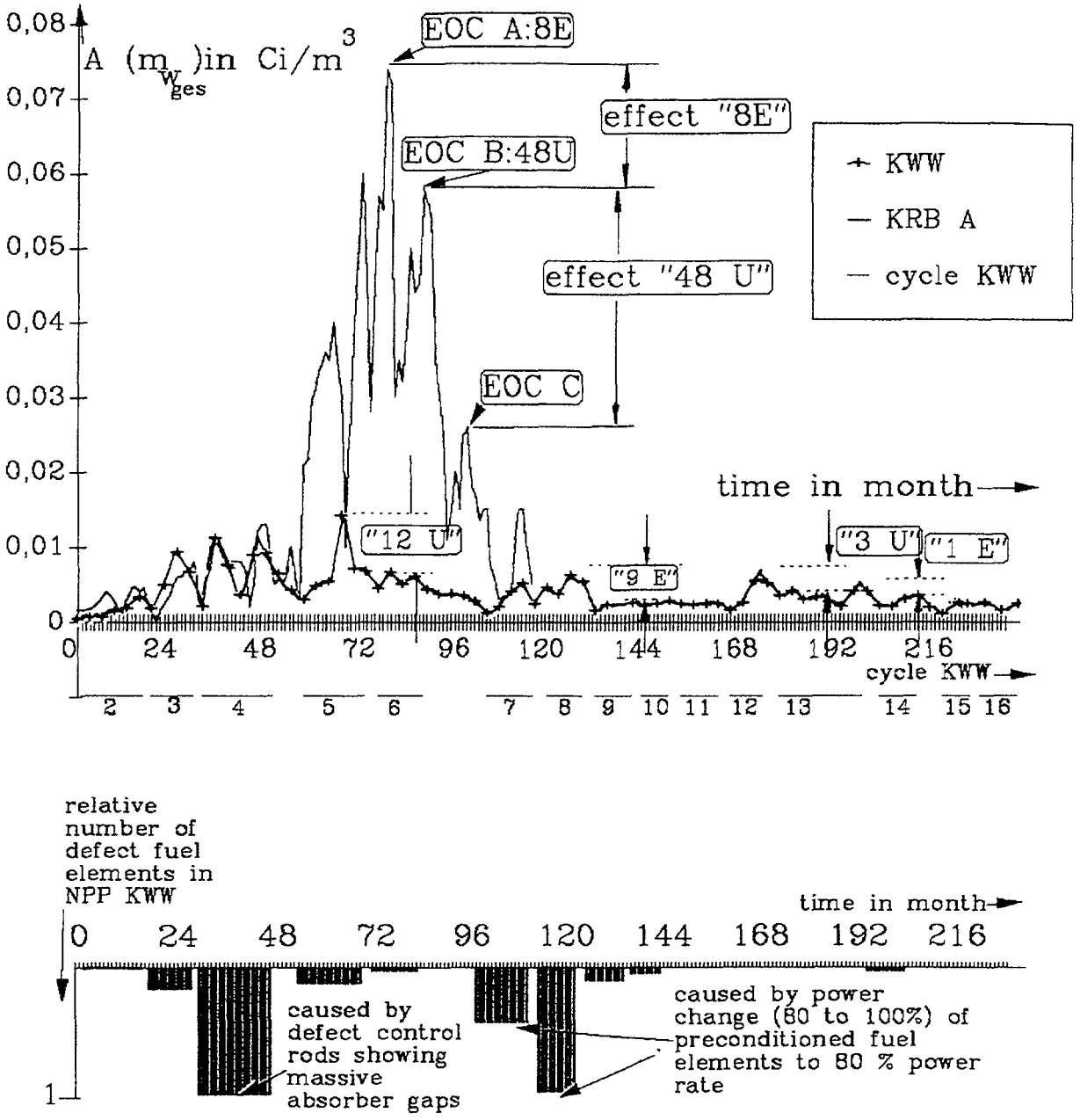

FIG. 12. Change of the specific tritium activity $A_{T(m_W)}$ per m³ reactor coolant by shuffling or unloading of high burnup control rods in NPP KRBA [4] and in NPP Würgassen

remarkable tritium release by comparing the time periods from cycle 3 to 10 and cycle 11 to 16 of NPP Würgassen: after cycle 10 in principle no fuel defect occurred. The tritium activity measured after cycle 10 had been verified by the help of neutron radiographic investigations only to be a result of leaking control rods (3 of „high purity steel" version and one of a prototype version).

3.2. Monitoring of the neutron fluence in substitution for the reactivity control

The process computer accumulates the fuel exposure adjacent to each quarter axial segment of every control rod and converts the exposure to a neutron fluence $\Phi_{CR/4}$ respectively to a ^{10}B burnup $a_{m_{CR/4}}$. Generally the reactivity worth of a given control rod is determined by the initial amount and individual type of control rod, his irradiation depletion and last not least the total reactivity inserted

into the core. The accumulated neutron fluence $\Phi_{CR/4}$ basically being proportional to an equivalent ^{10}B burnup $a_{m_{CR4}}$ is convertible to a burnup by the help of a proportionality factor α.

$$\phi_{CR\,4} = \frac{a_{m_{CR4}}}{\alpha} \tag{10}$$

whereas

$$\phi = \int_t \Phi(r,z,t)dt \quad in\ snvt \equiv 10^{21} n/cm^2 \tag{11}$$

$\phi_{CR\,4}$ = average neutron fluence over a control rod quarter segment in 10^{21} n/cm^2

$a_{CR\,4}$ = relative average ^{10}B burnup over a control rod quarter segment in %

a = relative ^{10}B burnup in % = $\frac{A}{A_{max}}$ $\quad A, A_{max}\ in\ (n,\alpha)/cm^3$

α= proportionality factorα in $\frac{\%burnup}{10^{21} n/cm^2}$

So, **if the relative ^{10}B burnup a has not been indicated as a correct neutron fluence value Φ in the past, the proportionality factor α has to be modified for any control rod design as well as the relative worth**. A realistic forecast of the service life only based on quarter segment fluences $\Phi_{CR/4}$ currently indicated by the designer will not be possible, but will lead to the mentioned effects described before. Figure 13 shows the basic relation between the local fluence/burnup (Φ/a) with corresponding averaged (over a quarter segment) values $\Phi_{CR/4}/a_{CR/4}$ to be explained by the help of local factors f_{ax}, f_{rad}.

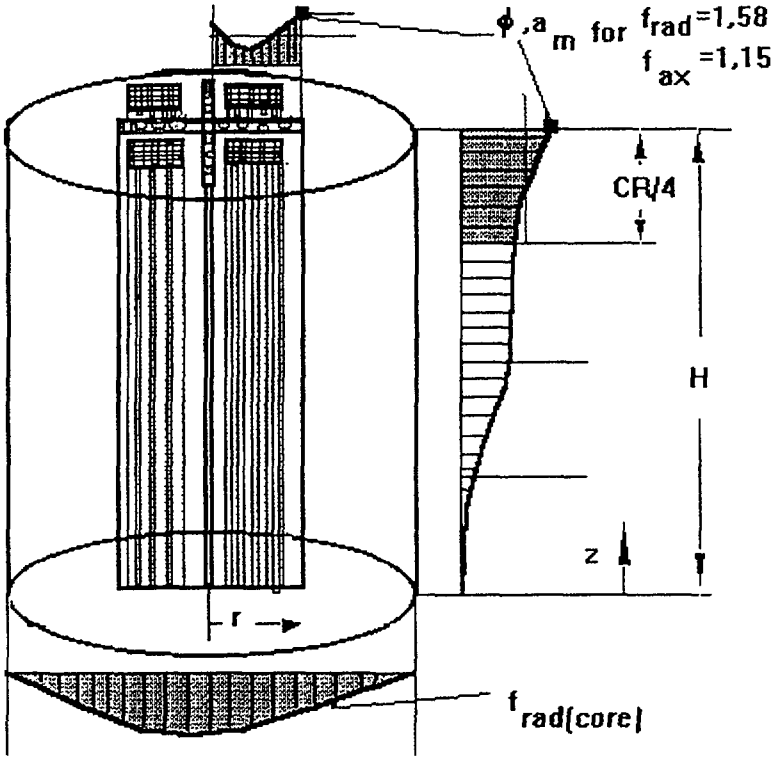

FIG. 13. Basic connection between the local fluence Φ and burnup a with corresponding averaged values $\Phi_{CR\,4}$ respectively $a_{CR\,4}$

3.3. Optical inspection method

The **optical inspection method** (see Figure 14) performed during an outage by using an underwater camera permits to get an visual impression about metallography (corrosion characteristics), mechanical properties and in case of a prototypical control rod version information about dimensional changes (dimensional measurements) But this method is not suitable to give any answer about absorber behaviour (burnup condition, boron loss) described before

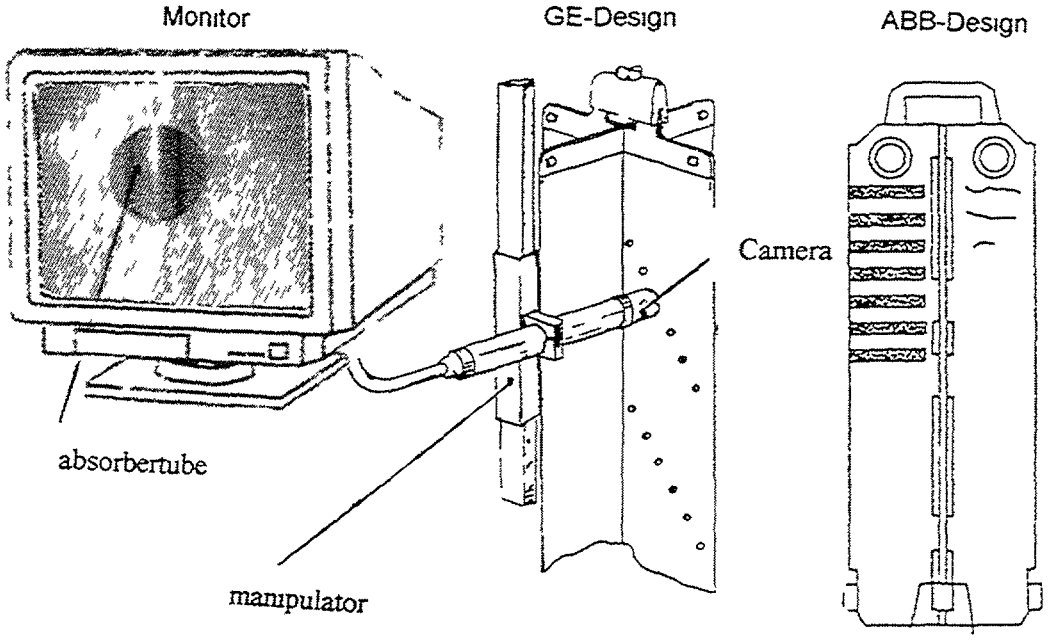

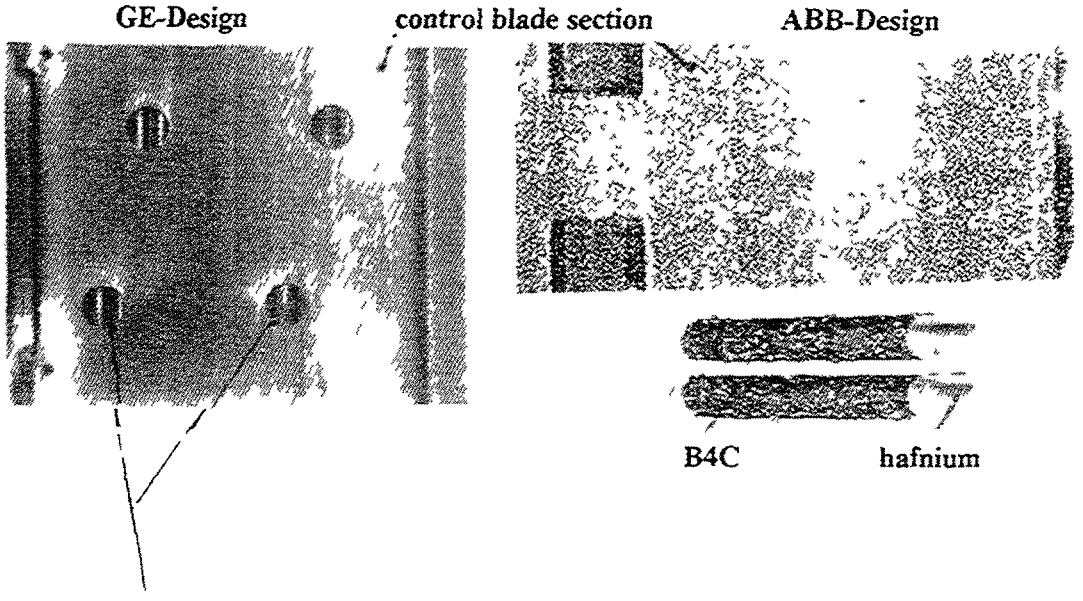

coolant hole in the cover sheet
and visible parts of the absorbertubes
(longitudinal to the axis of
the control rod)

blade segment with 2 Absorberholes
filled up with B4C and hafnium
(transvers to the axis of the control
rod)

FIG 14 Optical inspection of control rods in the fuel storage pool

3.4. The neutron radiography

The neutron radiographic inspection system shown in Figure 15 consist of an inspection station, which safety retains the control rod to be inspected, an inspection hood with collimator and reference rods, film cassettes, a 500 μg Cf-252 neutron source ($Q_{(t=0)}$ = 1.2×10^9 n/cm^2), nuclear tracer films (approximately 5.9 × 9.84 in) and a film development and evaluation device.

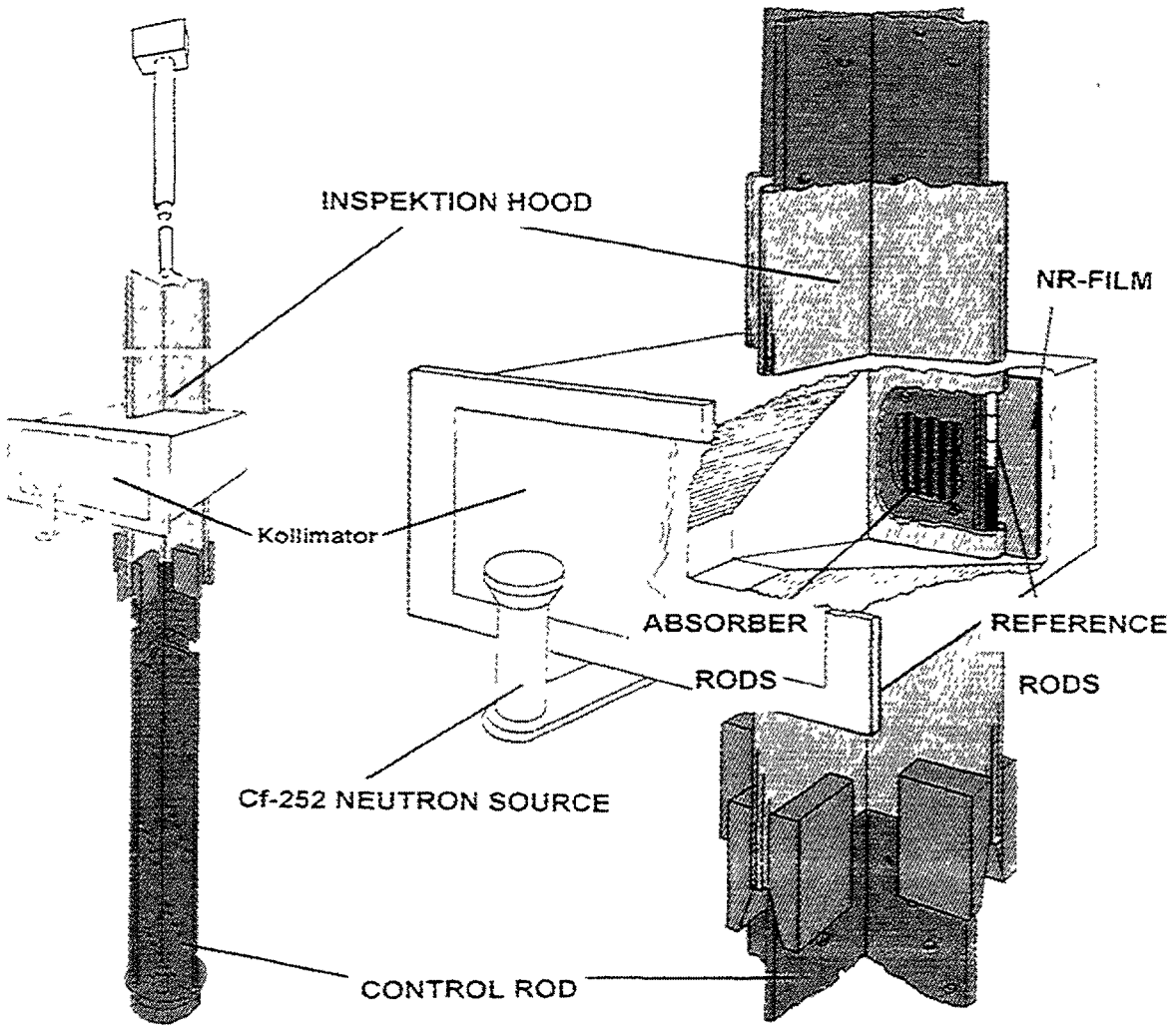

FIG. 15. Neutron radiographic inspection system

3.4.1. Measuring principle

The control blade segments are exposed to a low energy, parallel neutron flux in the fuel storage pool. The measuring principle is based on the absorption of these neutrons by the ^{10}B present in the absorber rods and the irradiation of a nuclear tracer film by the neutrons which were not absorbed. To calibrate the measurement segmented reference rods filled with B_4C of different theoretical densities simulating different ^{10}B burn-up as well as water and air. The reference rods are exposed together with every radiograph of a particular control blade section.

Those neutrons not being absorbed will react with the ^{10}B converter located behind the film foil to indicate invisible small nuclear traces in the foil as a result of recoil protons and α particles (see Figure 16).

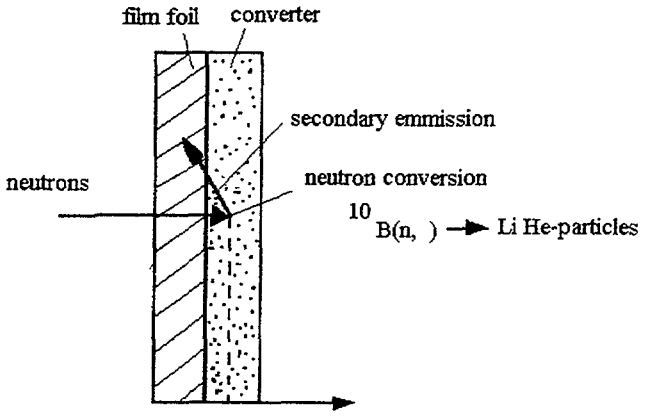

FIG 16. Illustration of the film/foil arrangement showing nuclear traces to form a picture

The invisible traces have to be etched in an alkine solution (10% NaOH) at about 60°C for at least 1.5 to 3 hours (see Figure 17).

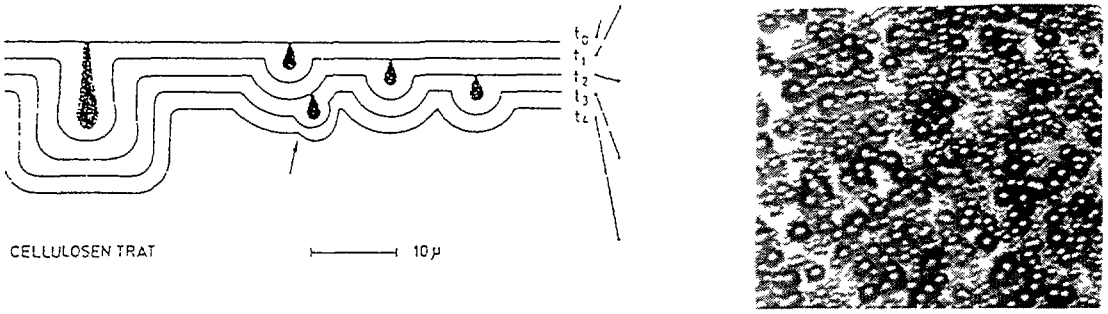

FIG. 17 Film developing mechanism and part of a track-etch foil after exposure

The weak contrast is amplified by means of diffused light to convert the trace density to different points of brightness as follows (Fig. 18):

- a high trace density results in bright field illumination;
- a weak trace density will form a weak illuminated picture.

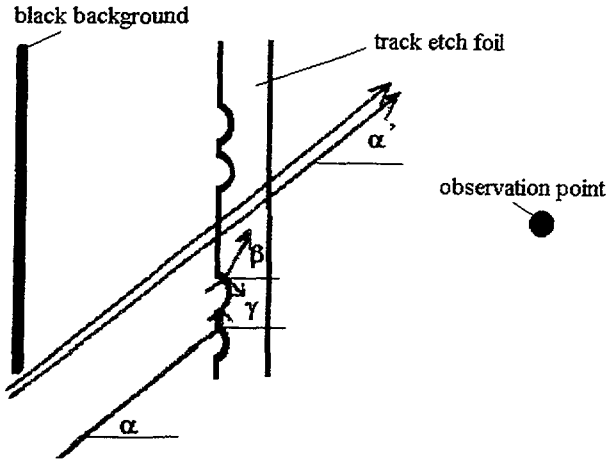

FIG. 18. Principle to convert the trace density on the track-etch foil to an image

3 4.2. Method to evaluate "loss in relative control rod worth - WA" for a particular control rod quarter segment

To evaluate loss in relative control rod worth for a quarter segment first the neutron radiography results of 16 track etch films have to be digitized (see Figure 19) and converted to the actually burnup by the help of an image analyzing system. Using a high level CCD-camera, a real time digital image processing system, the video input signals (image) are digitized and converted (A/D-converter) into 1024 × 1024 × 8 bit pixel values with a range of 256 grey levels or RGB false colours.

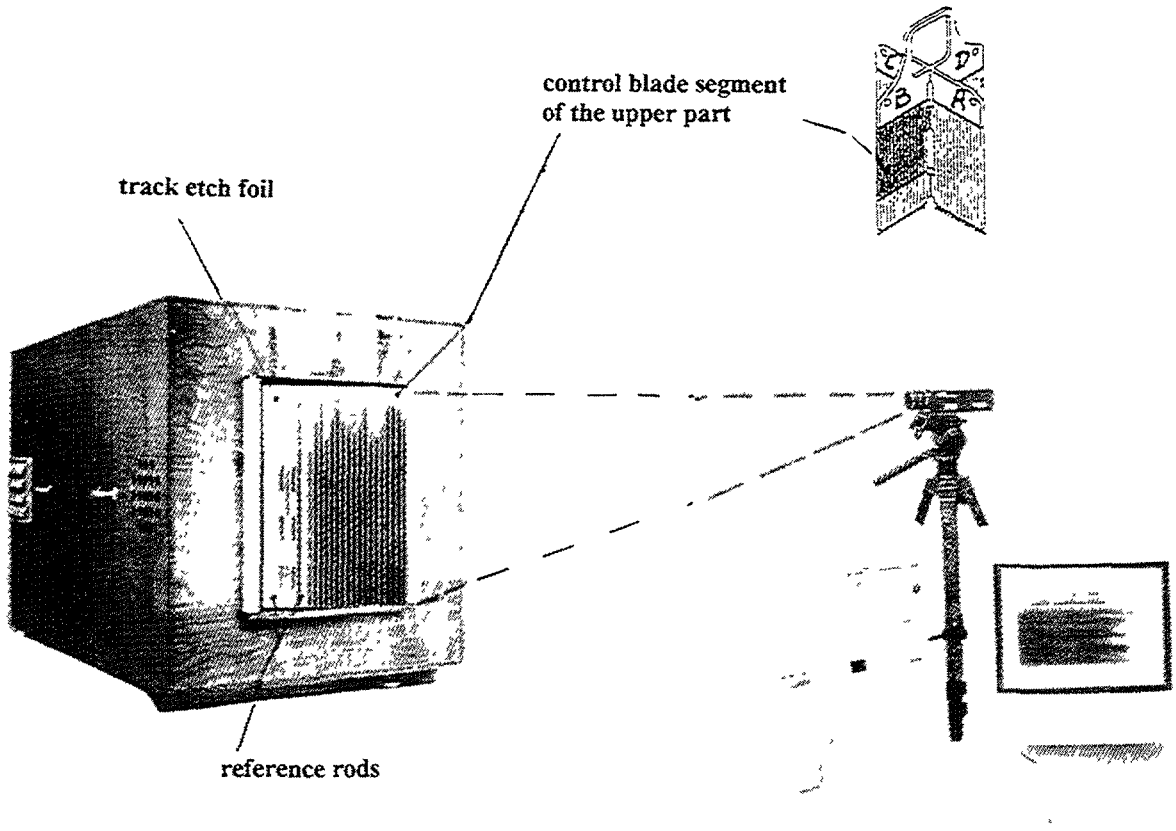

FIG 19 Digitisation of track-etch foils

To realize an automatic analysis in relation to the ^{10}B content of 16 stored images in each image first the centre lines of the absorber tubes have to be detected. After drawing two lines from C to D and from E to F (see Figure 20) marker flags are automatically generated from a line luminance profile. The straight line connecting the two "valleys"- each automatically created from the same absorber tube, but from different axial positions- represents the unknown centre line from A to B.

After digitizing the boron content of a control rod quarter segment this part has to be divided virtually in 92 horizontally cross shaped slices of 1 cm length (see Figure 21) or 92 B_4C arrangements (equivalent to a control rod quarter segment length). Those arrangements are used as an input for k-infinity calculations (KMC). The geometry model includes heterogeneous core geometric, fuel rods, absorber rod dimensions, boron fillings and fuel channels of a particular core cell. So different radial boron fillings detected by neutron radiography inspection will be taken into account.

To reduce the time for expensive k-infinity calculations a correlation has been developed to calculate loss of relative control rod worth as a function of different empty absorber tubes. This linear function allows to calculate loss of relative control rod worth "WA_{KMC}" for every of the 92 "axially homogenized" control rod slices in a simplified way. However, to evaluate a realistic loss of relative control rod worth WA in a particular core each of the 92 WA_{KMC} results have to be modified by using correcting factors.

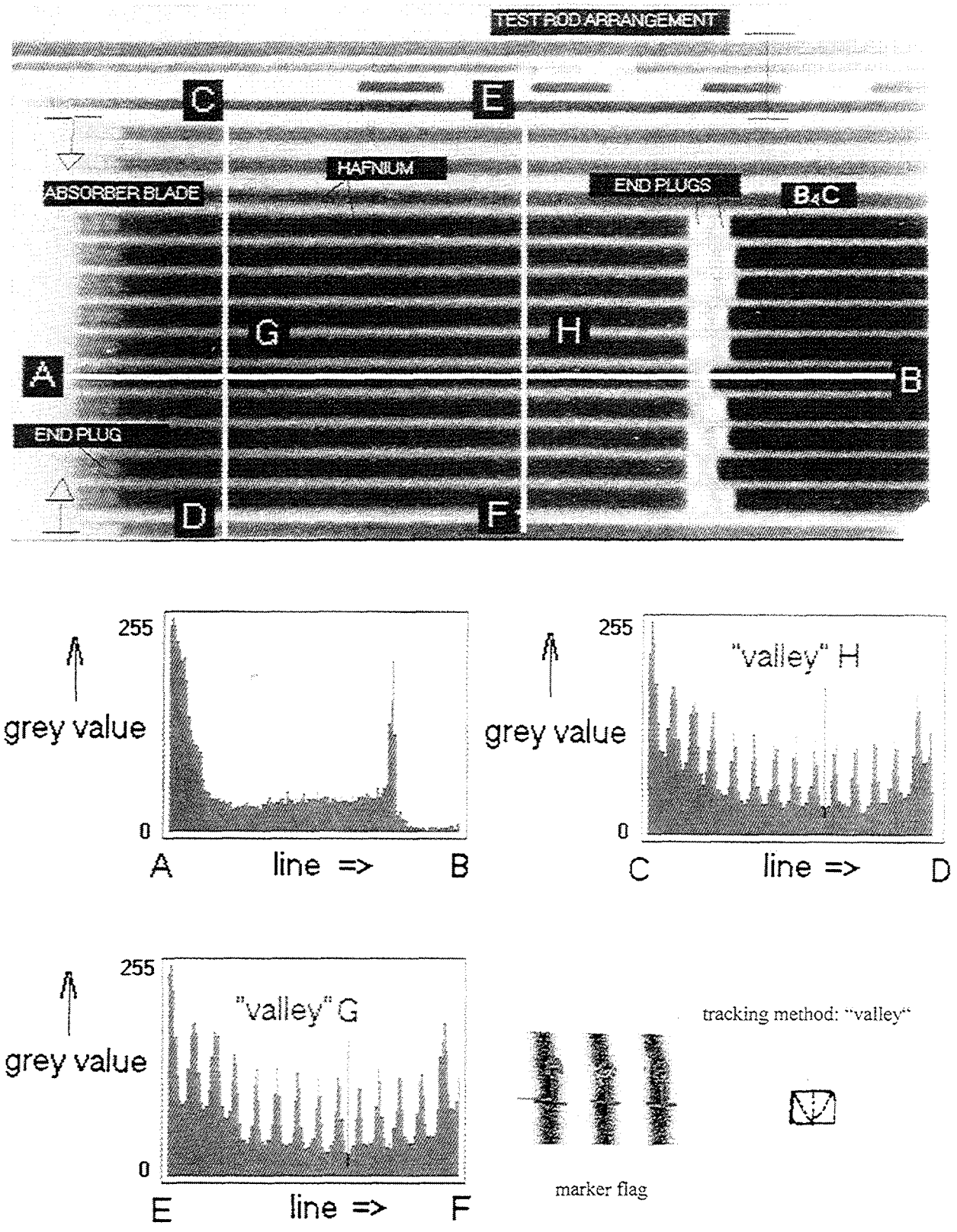

FIG. 20. Principle of auto-tracing

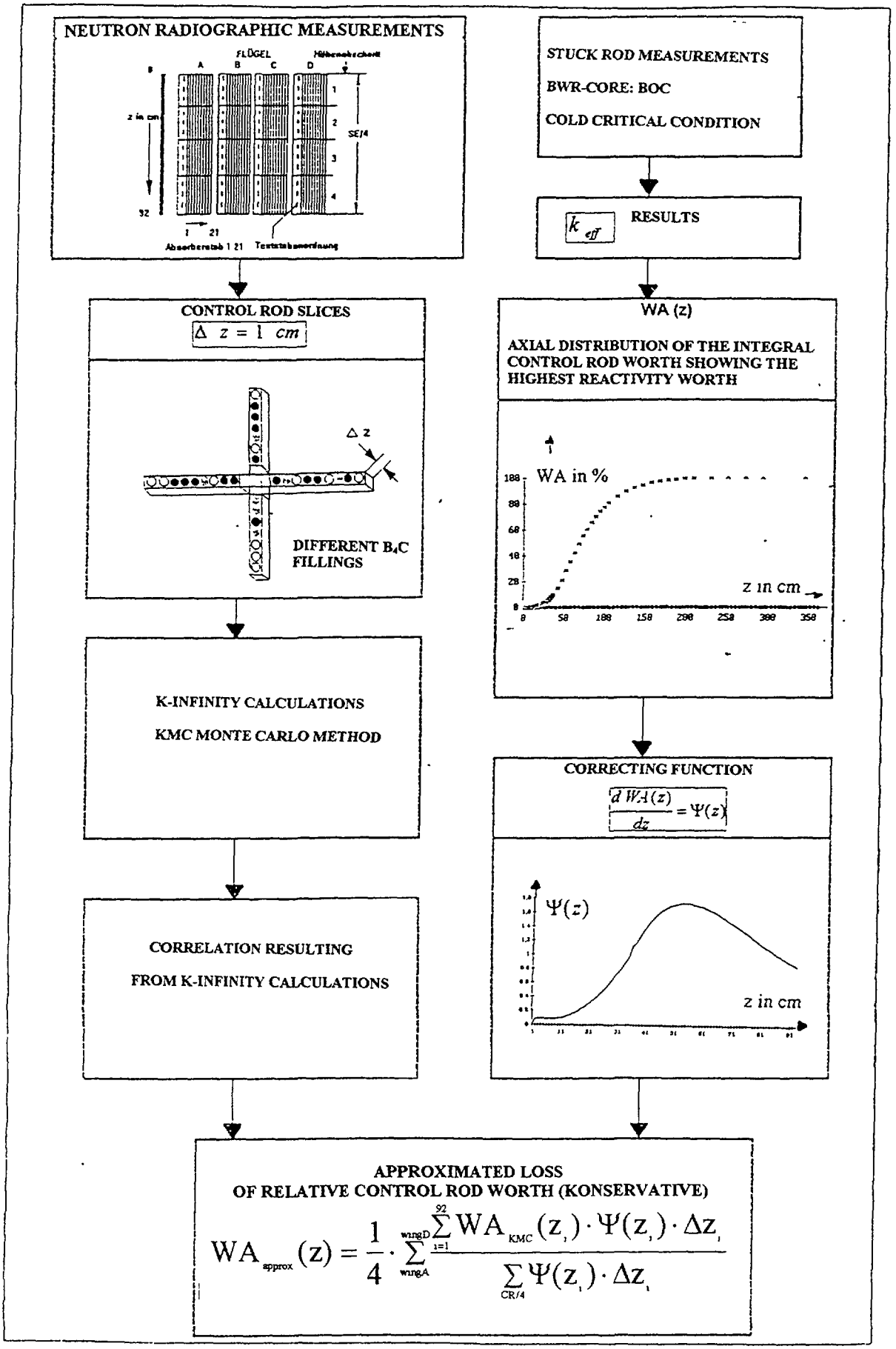

FIG. 21. Method to evaluate a realistic loss of relative control rod worth Wa_{approx}

Those correcting factors will be easy derivable from reactivity worth analyses (cold worth condition) generally performed in each BWR at the begin of any cycle to find the control rod with the highest reactivity worth in the particular core. Based on the axial distribution of the integral (total) control rod worth here defined as WA in % versus the core height the correcting factors will be easily derived by differentiating each cm of the mentioned control rod worth function along the quarter rod length to provide 92 correcting factors. Each of those correcting factors will calibrate the corresponding (same core position) 92 k -infinity results described in flow chart 2 as WA_{approx}. By simulating conservative conditions a realistic loss of relative control rod worth WA_{approx} is available.

4. THE EMPIRICAL MODEL

The ***empirical model*** applicable to used control rods in the shut down positions includes the basic idea of operating control rods of a certain design first in a control position up to a target fluence (Figure 22, horizontal front axis) in order to move them afterwards in a shut down position (Figure 22, left horizontal axis), where they may work for the total remaining holding period corresponding to the safety-related evaluation criteria required (diagram 3, vertically axis). The control rods are still only required for start-up and shut-down procedures and are no longer exposed to steady neutron irradiation. The initial model - in this case primarily used for BWR control rods of the type "first core load" - in principal is applicable to any design as long as sufficient measuring data is available about the behaviour of the corresponding control rod type as a function of their burn-up history. The present model, calibrated to neutron radiographic measuring data and gathered by the author during the past 12 operating years, includes a total operating experience of 16 reactor cycles. The results of these measurements are transformed to data representing loss of relative control rod worth WA_{approx} and are extrapolated to the whole reactor holding period (see Figure 22).

5. THE MICROSCOPIC BURNUP MODEL

In the microscopic burn-up model basic influences of the single design related parameters are described which are important to the nuclear burn-up behaviour of cylindrical ^{10}B absorbers in general. An approximation equation has been developed to calculate reliably, the working life of any control rod design, indicated as neutron fluence Φ_{crit} in snvt until absorber wash out starts - and as a function of different construction features such as absorber radius R, influence of the absorber-tube F(s) (-enclosure) as well as the absorber density ρ_{th} in g/cm³. Measurements, destructive investigations of absorber tubes and results from irradiation tests conducted in the Hanford thermal reactors in Washington (USA) are basically used to create the microscopic burn-up model. Different burn-up distributions of B_4C absorber pellets (ρ_{th} = 100 %) will demonstrate the main differences of the shell model depicted in [24] in comparison to the microscopic burn-up model developed by the author. In both diagrams exemplary 4 different local burn-up profiles $a(\Phi)$ as well as the corresponding specimen averaged ^{10}B burnup $a_m(\Phi)$ are depicted as a function of the applied neutron fluence (see Figures 23 and 24).

The relationship between irradiation exposure and averaged ^{10}B burn-up $a_m(\Phi)$ had been established in [24] by mass spectroscopy analysis of the $^{10}B/^{11}B$ ratio and represents the basic expression $(\Phi) = a_m/\alpha$ which is already described in equation (10). However, a re-analysis of those investigations showed that the relationship between specimen averaged burn-up $a_m(\Phi)$ and local burnup $a(\Phi)$, calculated by the help of the shell model has to be modified. This modification has been successfully verified by using the theory of functions.

By comparing the local burnup profiles in both diagrams each corresponding to the same specimen averaged burn-up (same colour) its obvious, that **the local profiles show divergence preferably within the outer absorber zones, where the burnup shows a steep angle of gradient.** Therefor it may be assumed, that mass spectroscopic analysis conducted at those locations generally will contain a large margin of error.

Based on the local burn-up equation

$$a(r,\phi), \tag{12}$$

where r= absorberradius and ϕ = applicated neutron fluence follows, that a_m, the specimen averaged burn-up is a function of

$$a_m = f(R,\phi,a_{max}) \tag{13}$$

where a_{max} = the maximum of the local burnup profile

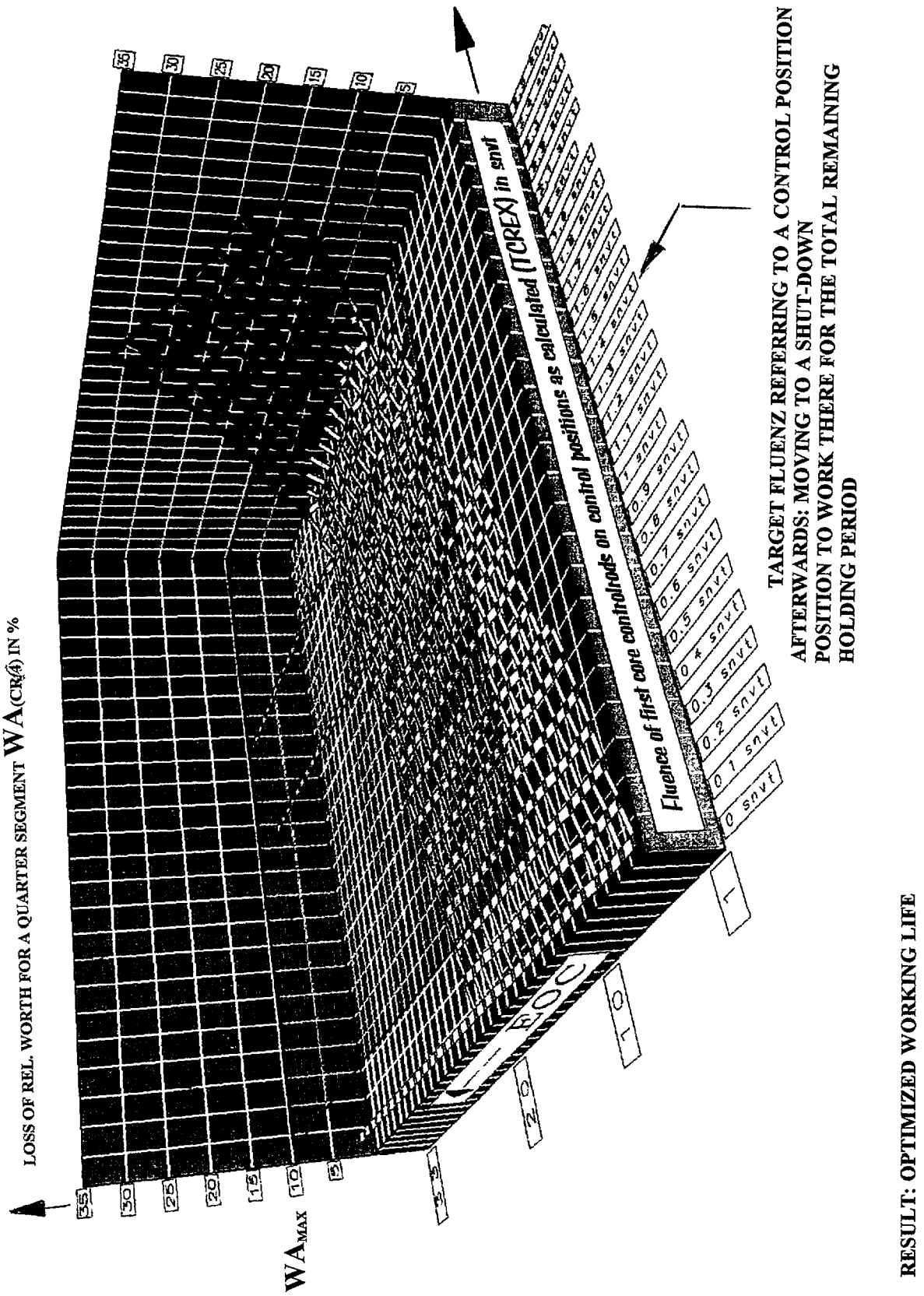

FIG. 22. Relative cold worth reduction of a control rod quarter segment in % (vertical axis) \resulting from neutron radiographic measurements of standard control rods depicted as a function of the applied neutron fluence in snvt (horizontal front axis) and as a function of cycles in shut down positions (left horizontal axis)

resultig from the boudary condition of the critical fractional radius change $\frac{\Delta R_{knt}}{R}$ of the absorber tube indicated as to be time proportional to absorber tube cracking follows, that

$$a_{m_{knt}} = f(\frac{\Delta R_{krit}}{R}, a_{max}) \tag{14}$$

That means, $a_{m_{knt}}$ will only be dependent as a function of the material properties of the particular absorber tube and not as a function of the tube radius itself.

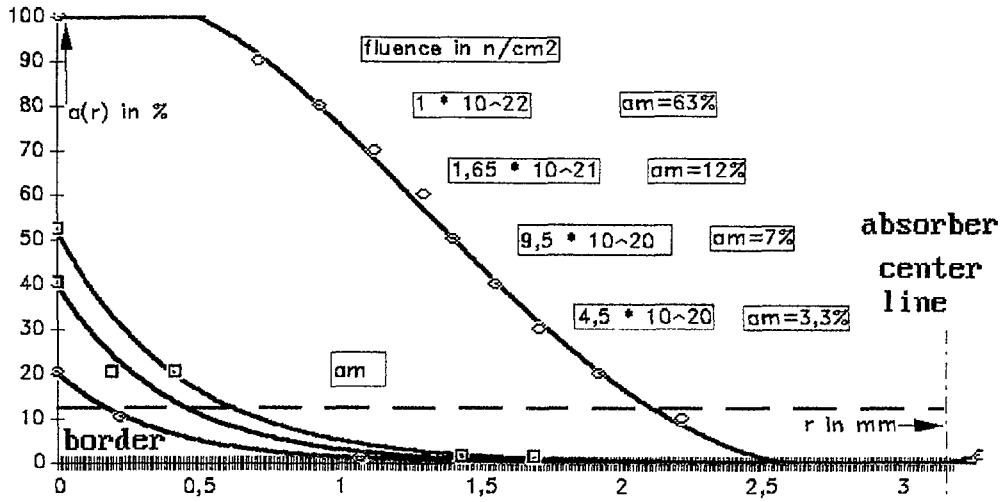

FIG. 23. Local a(r) and average burnup a_m distribution in 0.25 inch cylinders of 100% TD B_4C as a function of the applied neutron fluence based on measurements and calculations by the shell model in [24]; logically false relation between a(r) and a_m

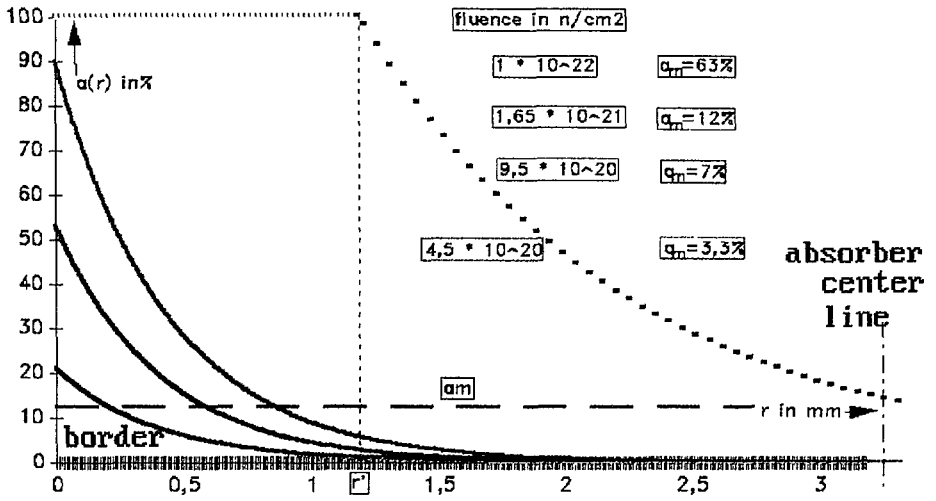

FIG. 24. Local a(r) and average burn-up a_m distribution in 0.25 inch cylinders of 100% TD B_4C as a function of the applied neutron fluence based on the microscopic burnup model in [15]; logically corrected function of $a_m = f(a(r))$

Figures 25 - 27 show exemplary the „critical[1] local burn-up distribution $a(\Phi_{crit})$ (Fig. 25) as well as the critical density distribution (Fig. 26) and in addition the distribution of the critical free volume (Fig. 27) as a function of the absorber radius referring to the standard control rod design basically calculated by the help of the microscopic burnup theory.

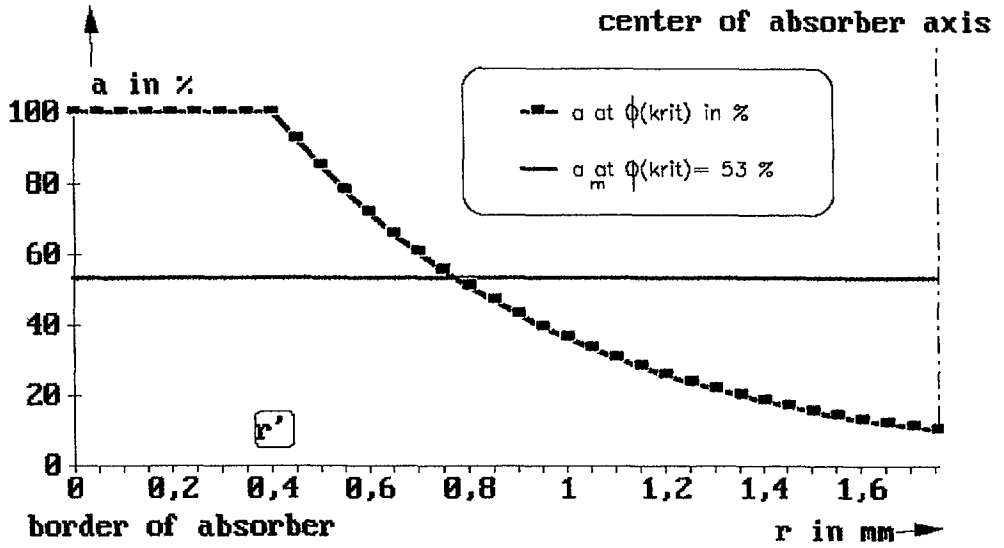

FIG. 25. Critical local burn-up distribution $a(\Phi_{crit})$ in % and averaged relative burnup $a_m(\Phi_{crit})$ in % as a function of the absorber radius r in mm (standard control rod design) calculated by the help of the microscopic burn-up theory

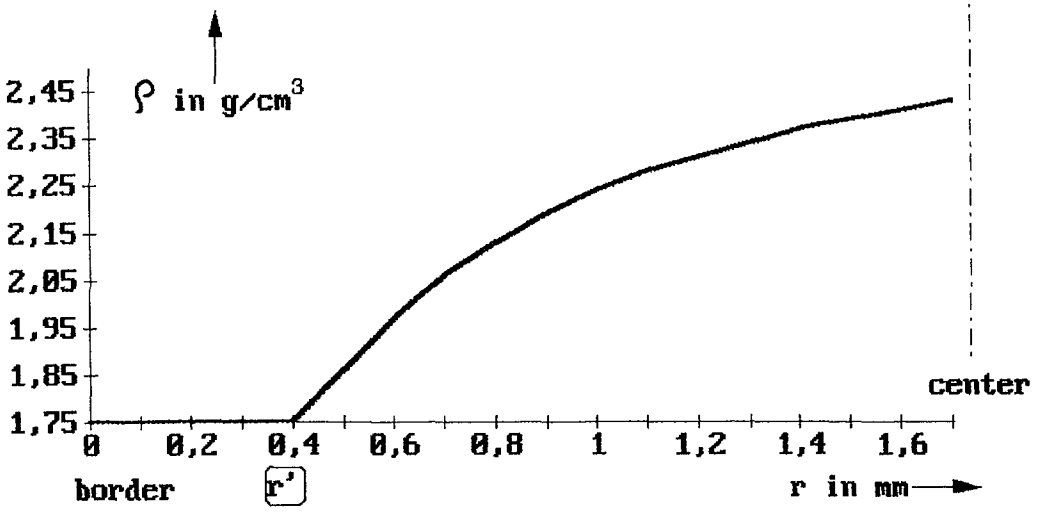

FIG. 26. Critical local density distribution $\rho(\Phi_{crit})$ as a function of the absorber radius r (standard control rod design) calculated by the help of the microscopic burn-up theory

[1] defined as beginning of washout mechanism

After passing the "critical" fluence a solid ring of absorber material is formed to a solid ceramic cake(100% burnup zone). At this area the original free volume of 30% existing at the beginning of the exposure event is completely used up to zero %. For illustration, Figure 28 shows the cross section (polished section) of an exposed original B_4C absorber tube just after passing the critical burnup margin of about 50% as measured by the help of a secondary ion mass spectrometer (SIMS) in the GKSS Forschungszentrum Geesthacht.

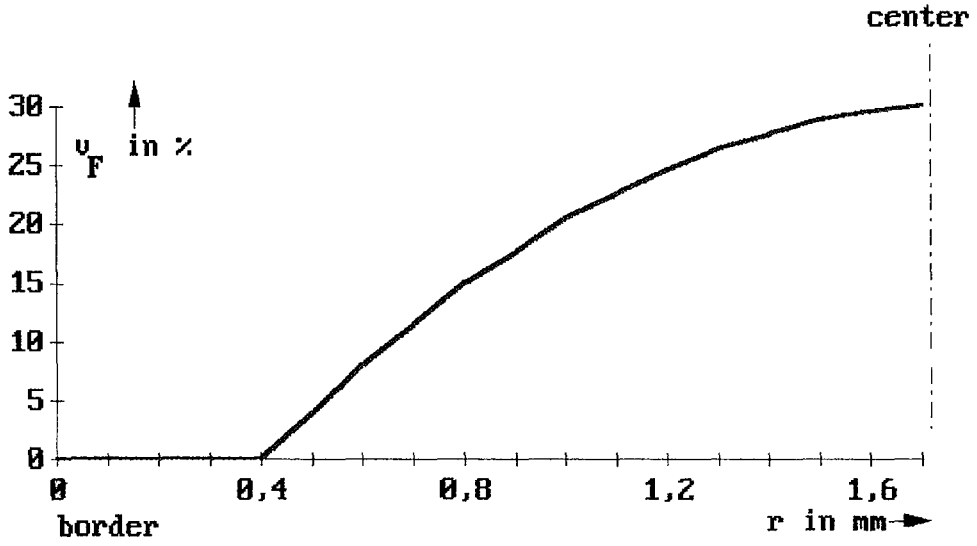

FIG. 27. Critical local free volume distribution $V_F\Phi_{crit}$ as a function of the absorber radius r (standard control rod design) calculated by the help of the microscopic burn-up theory

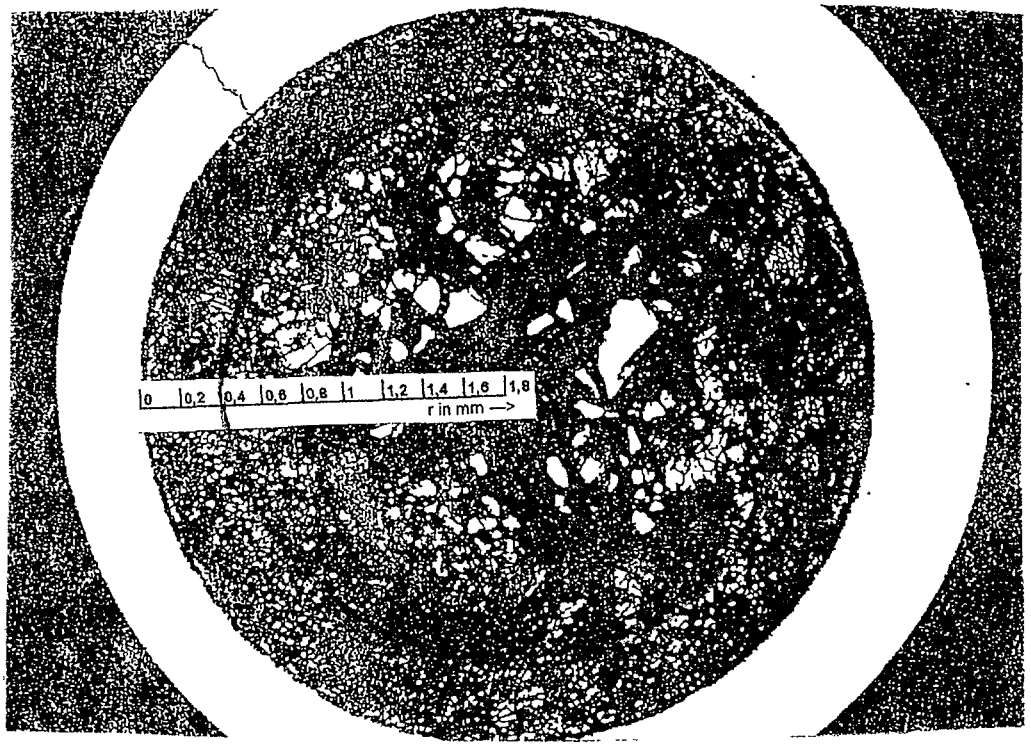

FIG. 28. Absorber tube Nr.3, section located 340 mm from the upper end; burnup $a_m(\Phi_{crit}) \approx 50\%$ (averaged over the cross section) [15]

The marked line illustrates r', where the free volume of 0 at % is left to raise up by smoothing to the shape of an exponential function (see Fig. 27) in direction to the centreline of the absorber affected. Evaluation of all neutron radiographic measurements results and a re-analysis from destructive tests of B_4C samples finally lead to a master equation describing the nuclear working life of any particular BWR control rod as a neutron fluence margin Φ_{cnt} until absorber washout starts:

$$\phi_{krt\,(CRquartersegment)} = \phi(R, \rho_{th}, F_{(s)}) \tag{15}$$

whereas R = radius of the absorber tube
ρ_{th} = theoretical density (B_4C)
$F(s)$ = factor representing the influence of absorber tube properties

$$\phi_{knt}(CR/4) = \frac{(\rho_{th} - B)\cdot R}{f_{ax}\cdot f_{rad}\cdot(C_0 + C_1\cdot\rho_{th})\cdot R_p \cdot A} \cdot \frac{R_a^2 - R_i^2}{(s_1 + R_i)^2 - R_i^2} \cdot \frac{1 - \frac{(s_1 + R_i)^2}{\left(R_i + \frac{s_1}{2}\right)^2}}{1 - \frac{R_a^2}{\left(R_i + \frac{R_a - R_i}{2}\right)^2}} \tag{16}$$

where

f_{ax}	= axial burnup factor (available data accumulated with process computer (TCREX))		
f_{rad}	= radial burnup factor (available by the help of KMC Monte Carlo analysis)		
R	= absorber radius		in mm
R_a	= outer radius of the absorber tube	in mm	
R_i	= inner radius of the absorber tube	in mm	
s_1	= 0.635	wall thickness referring to the standard absorber tube	in mm
ρ_{th}	= B_4C	theoretical density	in %
B	= 101.28	constant	in %
A	= - 0.5902	constant	in %
R_p	= 3.175	absorber radius of the test specimen as reported in [24]	in mm
C_0	= 17.152	constant	in % / snvt
C_1	= - 0,1 constant		in 1 / snvt

Equation (15) involves different construction features which are responsible to the nuclear working life in general. This will be shown in Figures 29 -31.

5.1. Influence of the absorber radius

The nuclear working life of a particular control rod will increase as the absorberradius increases by following a linear function (see Figure 29).

5.2. Effects with respect to the wall thickness of an absorber tube

To get information about influences to the nuclear working life of absorber tubes showing different wall thicknesses, neutron radiography results have been compared to calculations based on the elasticity law as well as on the plasticity method, see Table I.

An influence referring to the wall thickness of an absorber tube - verified to be a calculation based on the elasticity method - showed not to be a predominant factor regarding to the nuclear life time as presumed before (see Figure 30).

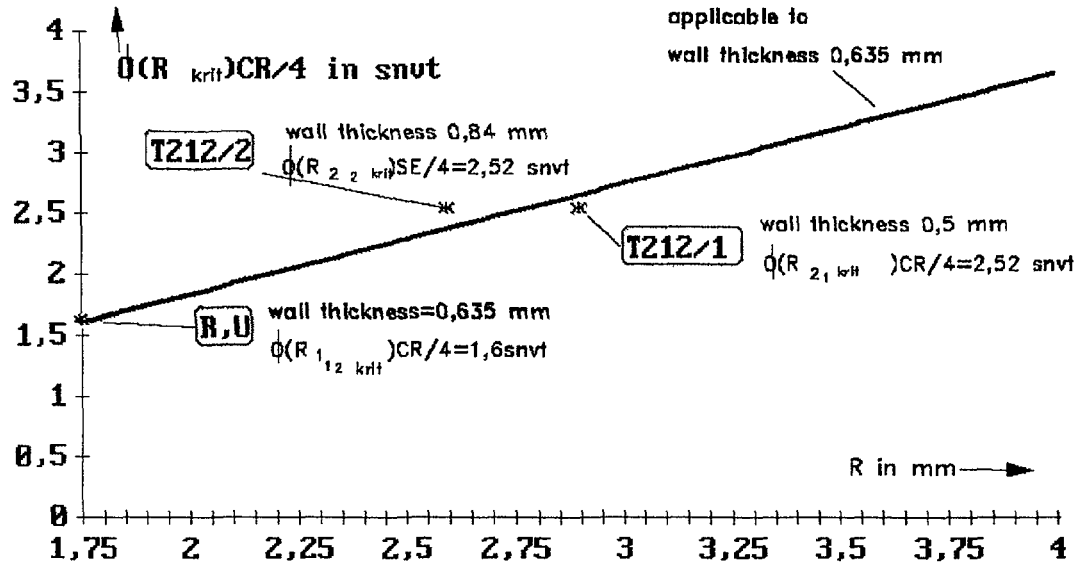

FIG. 29. Critical fluences $\Phi(R)_{CR/4\,crit}$ of BWR control rods as a function of the absorber radius R resulting from neutron radiographic measurements. (ρ_{th} = 70%)

TABLE I. FACTOR OF INFLUENCE REFERRING TO THE WALL THICKNESS OF AN ABSORBER TUBE F(S) RESULTING FROM MEASUREMENTS (NEUTRON RADIOGRAPHY) COMPARED TO CALCULATIONS BY FOLLOWING THE ELASTICITY-PLASTICITY METHOD

	F(s) in %			
	neutron radiographic measurements	calculations based on the elasticity method	calculations based on the plasticity method	
			Variant A	Variant B
T212/1 = case 1	- 5.6	- 3.3	- 17	- 20
T212/2 = case 2	+ 6.8	+ 5.7	+ 21	+ 28

5.3. The steel selection

The steel selection of an absorber enclosure showing a large creeping capability used to obtain a large volume for swelling accommodation of the absorber material will not lead automatically to a longer working life, since it had been demonstrated, that the radial creeping velocity of the absorber tube material defined as $\Delta\varepsilon / \Delta t$ shows small values in comparison to the absorber growing capability (velocity) defined as $\Delta r / \Delta t$. The swelling behaviour of the absorber described in principal by the help of the applied neutron fluence $\phi = \int_t \Phi dt$ is basically controlled by the forces acting to the absorber tube after exposure.

5.4. Variation of the theoretical density

The capability to use the original free volume within an absorber for swelling accommodation will basically grow up by reducing the theoretical density from 70% to a lower margin (Figure 31). The Figure shows that by using a reduced density for better swelling accommodation this have to be optimized in relation to the number of ^{10}B atoms required to held the relative reactivity worth during the whole operation period.

The working life determined by using the master equation is in line with the operating experience and is compared to the values currently indicated by the designer which are higher by the factor of about 2. The reason may be explained by comparing the local burnup profiles a(r) in Figures 23 and 24 showing divergences within the outer absorber zones.

The literature does not offer any comparable studies concerning these problems. According to the present research, **it has to be concluded that the control rod design of all reactors using B_4C as neutron poison have to be revised in order to predetermine the real holding periods.**

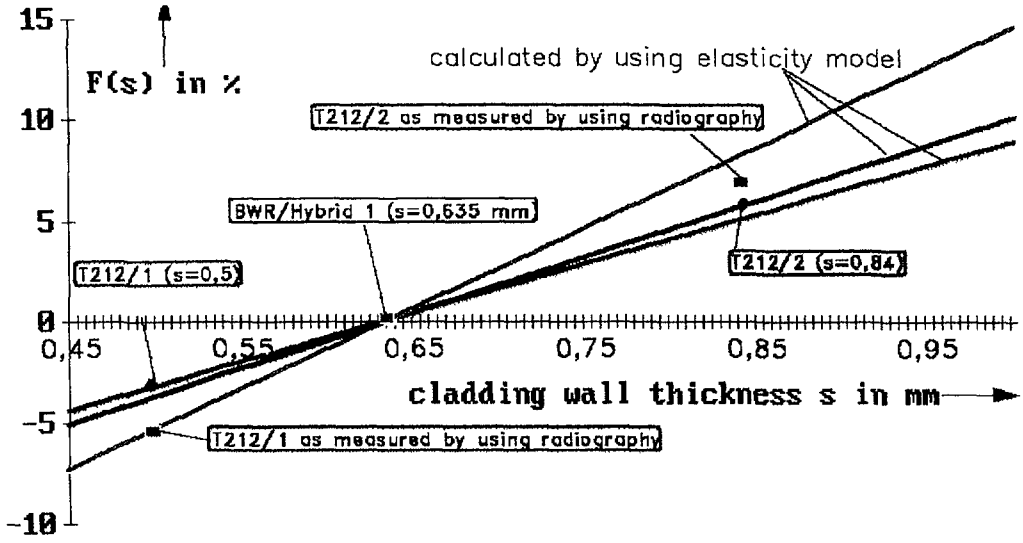

FIG. 30. Factor of influence referring to the wall thickness of an absorber tube F(s) (same steel selection) as a function of the wall thickness s in mm normalized to the wall thickness of the standard absorber tube s = 0.635 mm

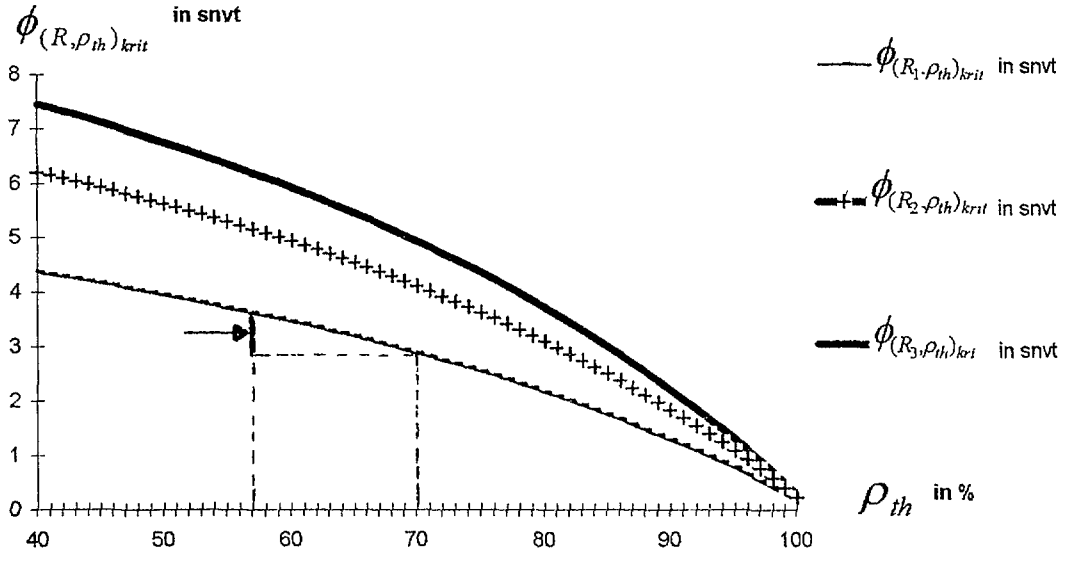

FIG. 31. $\Phi_{(r,TD)\,crit}$ in snvt as a function of the theoretical density ρ_{th} in % until absorber wash out starts depicted for absorber radius- R_1 = 1.75 mm; R_2 = 2.5 mm; R_3 = 3 mm - normalized to the wall thickness of the standard absorber tube s = 0,635 mm

Coming back to Fig. 10, both models - the **EMPIRICAL MODEL** applied to used control rods on the shut-down positions and the approximation equation to calculate the control rod's working life on control position based on the **MICROSCOPIC BURNUP MODEL** will preset how an optimized control rod management will be handled (see Figure 32).

The different coloured square boxes shown in Figure 32 will simulate control cells of a mid-sized BWR core. All yellow square boxes are shown as typical shut down positions whereas the other coloured square boxes will simulate the control positions. Based on the calculated nuclear working life (equation (16)) of any different control rod version being inserted, the "long life" control rods will be positioned firstly on a control position up to a maximum allowable neutron fluence margin (below the „critical value" until absorber wash-out starts) to move them afterwards in a shut down position where they may work for the total remaining holding period. At least 60% of the first core inventory may be used up to the total operating period without any safety loss.

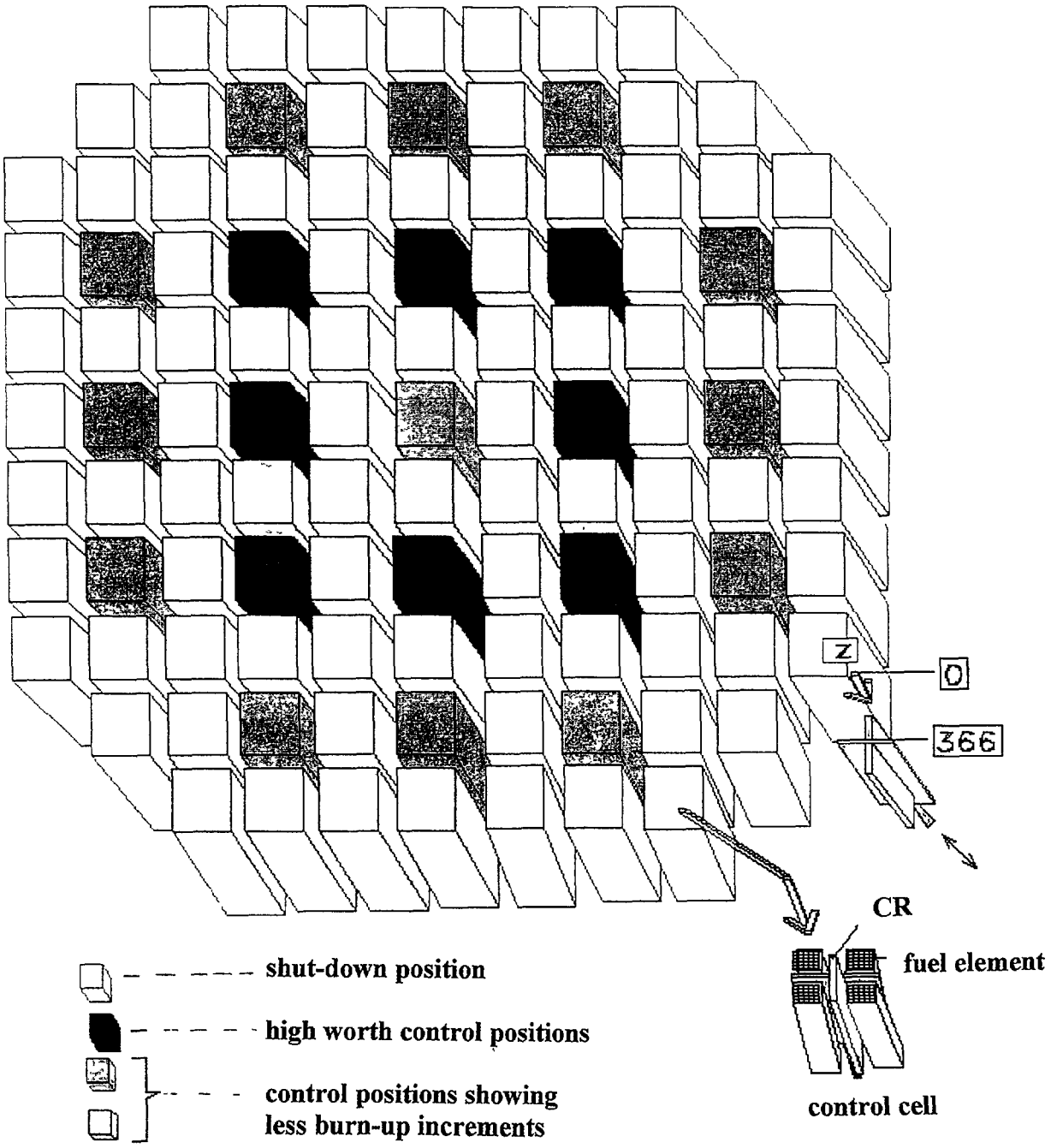

FIG. 32. Typical control rod loading pattern

An existing EMPIRICAL MODEL - is already available for BWR control rods of the type "first core load" - but in principal such a model is applicable to any design. Some measuring data (radiographic inspection) about the behaviour of the corresponding control rod type must be available as a function of their burn-up history and working life in a shut down position. After modelling no further measurements of this particular control rod type are necessary in any reactor.

REFERENCES

[1] VESTERLUND, G., HALLSTADIUS, L., HOFFMANN, H., CORSETTI, L., Development of ABB control rods and operational experience, Kerntechnik, Vol. 57 No. 2, (April 1992) 102-106.

[2] JONSSON, Å., "Control rod performance at Oskarshamn" in Kerntechnik, Vol. 57 No. 2, (April 1992) 113-115.

[3] EICKELPASCH, N., MÜLLAUER, J., SEEPOLT, R., SPALTHOFF, W., "Erfahrungen mit SWR-Steuerelementen", Tagungsbericht, Jahrestagung Kerntechnik, 1980.

[4] EICKELPASCH, N., MÜLLAUER, J., SEEPOLT, R., SPALTHOFF, W., "Operational Experience with and Postirradiation Examinations on Boiling Water Reactor Control Rods", Nuclear Technology, Vol. 60, (March 1983) 362-366.

[5] SCHULZ, W., "In-Pool Neutron Radiography of BWR-Control Rods within the Scope of a Routine Refuelling Operation", Neutron Radiography, Proc. of the Second World Conference, Paris (1986) 359-366.

[6] SCHULZ, W., "Neutron Radiography of BWR Control Rods during Outages", ANS Topical Meeting on LWR Fuel, Performances, Williamsburg, Virginia (1988) 364-369.

[7] SCHULZ, W., "Betriebserfahrungen mit SWR Steuerelementen", Jahrestagung Kerntechnik (1990).

[8] HOFFMANN, H., BÄRO, G., SCHULZ, W., RYTER, H., "Neutronenradiographie an SWR Steuerelementen", Jahrestagung Kerntechnik (1990).

[9] SCHULZ, W., "In-Pool Neutron Radiography of BWR Control Rods", Eighth Int. Conf. on NDE in the Nuclear Industry, 17-20 November 1986, Orlando, Florida.

[10] SCHULZ W., "Neutron Radiography of BWR Control Rods in European NPPs", BWR Owners' Group (BWROG), General Meeting, San Jose, Dec. 1990.

[11] ABB Reaktor GmbH, Nuclear Services "Neutron Radiography of BWR Control Rods in European NPPs", Firmenbroschüre.

[12] GIDARAKOS, E., SPALTHOFF, W., "Tritium Untersuchungen an einem Hochabgebrannten SWR Steuerelement", GKSS Forschungszentrum Geesthacht GmbH, Jahrestagung Kerntechnik (1983) 581-558.

[13] BEAVEN, P.A., GIDARAKOS, E., GREIM, M., MÜLLAUER, J., NIELSEN I., SCHMELZER, F., SPALTHOFF, W., STAHLENBRECHER, L., WILHELM, H., WITTSTOCK, D., "Untersuchungen an einem hochabgebrannten Siedewasserreaktor-Steuerlement (Abschlußbericht)", GKSS 86/V/1 mit freundlicher Genehmigung des Auftraggebers.

[14] SE T212-Inspektion, Kopie der Videoaufzeichnungen von 1991, Siemens-KWU BA43 mit freundlicher Genehmigung der Fa. Siemens.

[15] SCHULZ, W., Schadensanalyse von keramischen Bor-Absorberstoffen in Siedewasser-reaktoren und Ansätze für eine optimale Steuerstabeinsatzstrategie, Dissertation, TU, Berlin, (1998).

[16] Kopien von neutronenradiographischen Untersuchungen an ABB CR 72 SE in Studsvik, SE Blatt 938 und 1029 obere SE-Spitze, mit freundlicher Genehmigung der ABB Atom AB.

[17] ÅDIN, S., "Summary of Dresden 3 Control Rod Experiences", Asea Brown Boveri, MB 250/90, (1990) (mit freundlicher Genehmigung der ABB Atom AB).

[18] EDWARDS, R.K., VELECKIS, E., Binary Alloy Phase-diagrams, Second edition, Volume 2, Journal of Phys., Chem. 66, (1962) 1657-1661.

[19] HÜTTMANN, A., KETTELER, M., "Operation of High Worth Control Rods in Boiling Water Reactors", Kerntechnik 57, No. 2, (Apr. 1992) 116-117.
[20] Press Release Information Nuclear Power Safety Administration Division, ANRE/MITI, (24 October 1997).
[21] SCHRÜFER, E., "Strahlung und Strahlungsmeßtechnik in Kernkraftwerken", Elitera-Verlag, Berlin 33 (1974).
[22] KTA 1504, Sicherheitstechnische Regel des KTA, Fassung 6/78, Messung flüssiger radioaktiver Stoffe zur Überwachung der radioaktiven Ableitungen.
[23] Office of the Federal Register National Archives and Records Administration: Code of federal regulations, Part 10, (Revised as of 1 January 1991) §30.55.
[24] PITNER, A.L., RUSSCHER, G.E., "IRRADIATION OF BORON CARBIDE PELLETS AND POWDERS IN HANFORD THERMAL REACTORS", Wadco Corporation, Richland, Washington, Dec. 1970, UC-25, Metals, Ceramics and Materials.

FABRICATION AND METALLURGICAL PROPERTIES OF HAFNIUM ALLOYS FOR CONTROL RODS

J.L. BÉCHADE
Service de Recherches Métallurgiques Appliquées, SRMA

P. PARMENTIER
CE2M/LETRAM

CEA-CEREM, CEA-Saclay,
Gif-sur-Yvette, France

Abstract

Due to its high thermal neutron absorption cross section and excellent steam corrosion resistance, hafnium has been used in the nuclear reactors as control rods (solid hafnium rods) since the late 1950's. However, the high cost of the material and also the high density of Hf in solid rod shape have ruled out its wide application in commercial reactors. But at the present time, Hf is beginning to be a potential candidate for use as neutron absorbing material in control rods of the pressurised water reactors of the next generation. An important research programme has been carried out at the CEA in order to propose a new type of control rod which would replace the steel cladded Ag-In-Cd, currently used by HfB_2 pellets in a small diameter thin wall Hf cladding tube. The purpose of this paper is to present the metallurgical studies performed on Hf alloys in our laboratories to obtain Hf tubes with optimised properties. The first part relates to the metallurgical (grain size, chemical composition, texture, etc.) and mechanical (tension and creep) tests, which were performed on two different tubes elaborated by Sumitomo Metal Industry (Ltd, Tokyo Japan) and by CEA (CE2M/LETRAM). The wide difference in the mechanical behaviour and metallurgical parameters of these tubes have led us to acquire a better knowledge of the metallurgical and functional properties of Hf. In particular, the contents in oxygen and other alloying elements, the grain size and the deformation level appeared to be key parameters to avoid cracking during the route process and especially the cold-rolling phases. The second part of this paper deals with the results of the ongoing programme pursuing the following objectives to produce Hf alloys plates with different compositions in order to have a better transformability of Hf, to improve the process of rolling and the associated heat treatments in order to obtain thin plates with small grains and no heterogeneities, and finally to optimise the material (composition, coating, etc.) in order to obtain a good wear resistance of Hf to restrict attrition in operating conditions in reactor.

1. INTRODUCTION

An important research programme is carried out at the CEA since the early 1990's for Pressurised Water Reactors (PWRs) of the next generation, in order to propose a new type of control rod to replace the steel cladded Ag-In-Cd (AIC), mainly to improve the neutron efficiency and also to increase the longevity and safety of control rods. The use of HfB_2 pellets in small diameter thin wall Hf cladding is the solution proposed.

Hf is used because of its high thermal neutron absorption cross section and excellent water corrosion resistance. Solid hafnium rods have been used in US naval nuclear reactors (submarine 571 Nautilus) since the late 1950's and in American PWR commercial power reactors (Shippingport-1 Indian Point Unit-1 and Yankee Rowe) in the early 1960's as control rods [1]. Hf has also been used as control rods in Russian reactors [2]. But the high cost of this material has been an obstacle to its wide application. At the present time, Hf seems to be a good solution for control rods as its availability has improved with the increased production of Zr, especially when the drawback of its high density is balanced out by the use of small diameter thin wall tubes.

The purpose of this work made at CEREM/SRMA in collaboration with CEREM/CE2M, both from CEA, is to study the fabrication and metallurgical properties of Hf alloys for control rods. First, we have performed a comparison between two different tubes (CEREM/CE2M and industrial processes) which have led us to make a bibliographic study of Hf to improve our knowledge on metallurgical and functional properties of Hf. Secondly, we have tried to optimise Hf alloys especially to improve their fabrication process and their wear resistance.

2. COMPARISON BETWEEN TWO Hf TUBES

2.1. Chemical composition

The first tube has been elaborated by CEREM/CE2M from a CEZUS ingot (referred to as LETRAM tube) The second one has been elaborated industrially by a tube manufacturer (henceforth referred to as INDUSTRIAL tube) from a WAH-CHANG ingot Both tubes have nearly the same external diameter (9.8 mm) and thickness (1 mm), but the chemical compositions are quite different. The INDUSTRIAL tube has a higher Zr and Fe content and a lower O content (~ 3 or 4 times for each element) in comparison to the LETRAM tube (Table I). As will be seen later, these composition differences have a great influence on the metallurgical properties.

TABLE I. CHEMICAL COMPOSITION OF THE LETRAM Hf TUBE

Tube	Ingot	Position	Zr	Fe	O	H	N
			%	ppm	ppm	ppm	ppm
		1	1.06	31	310	11	14
LETRAM	CEZUS	2	0.87	26	285	12.5	15
		3	0 97	<20	300	<3	<10

2.2. Metallographic analysis

The characterisation of the microstructures by optical metallography has shown a wide difference in grain size between the tubes (Fig. 1). Although both tubes are in a fully annealed condition with equiaxed grains, the LETRAM tube (grain size from 40 to 50 μm) exhibits larger grains than the INDUSTRIAL tube (grain size from 4 to 8 μm). Similarly to Zr alloys [3], this fact could be explained by the fabrication route and also by the composition.

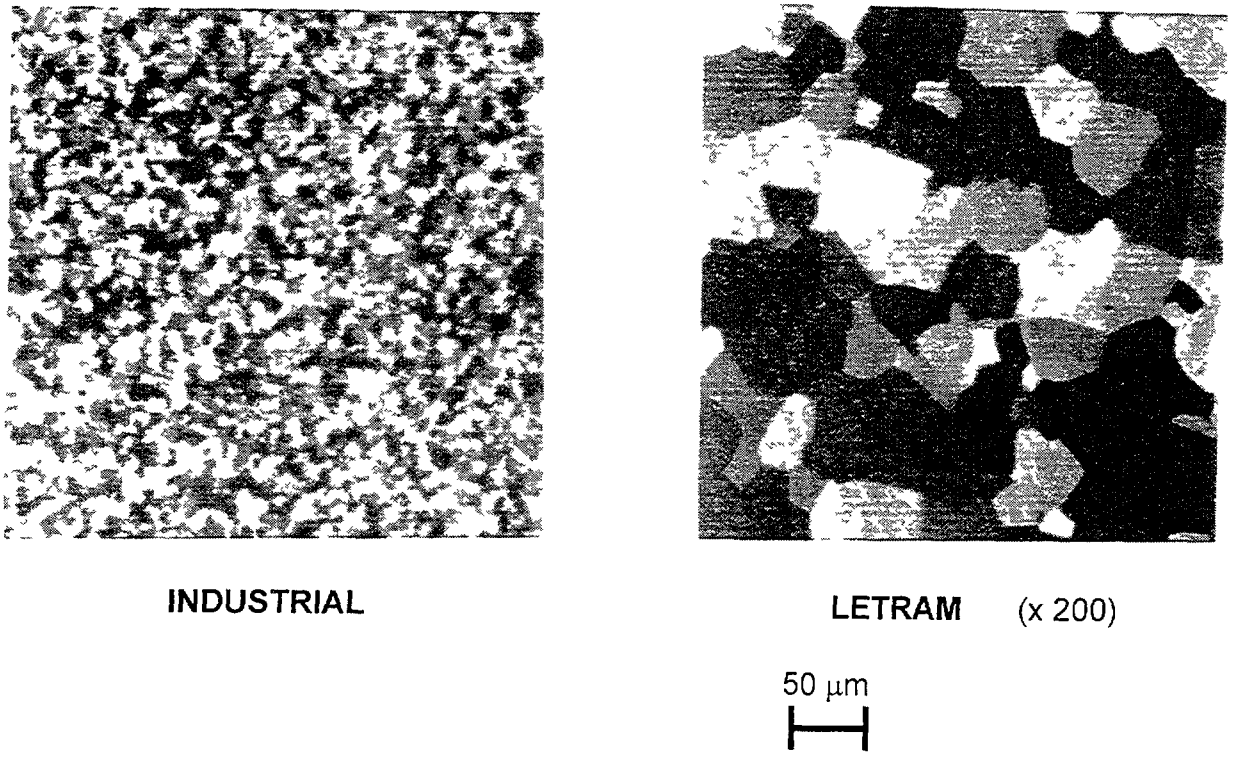

FIG 1 Microstructure of the INDUSTRIAL and LETRAM Hf tubes

2.3. Texture analysis

Texture analyses of the tubes have been performed by using X-Ray diffraction. The (10.0), (00.2), (10.1), (10.2) and (11.0) pole figures have been determined with a SIEMENS D500 Texture Goniometer and analysed with the Orientation Distribution Function. As can be seen from Figure 2, the <c> axes (normal to (00.2) pole figure) are mainly orientated along the hoop direction for the LETRAM tube, where their main orientation is at 40° from the radial direction in the hoop-radial plane for the INDUSTRIAL tube. This strong difference is linked to the fabrication route, as previously observed in Zr alloys [4].

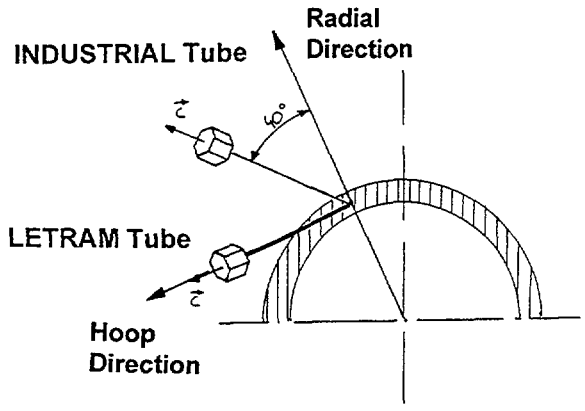

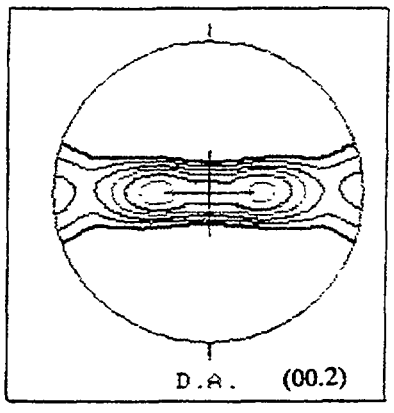

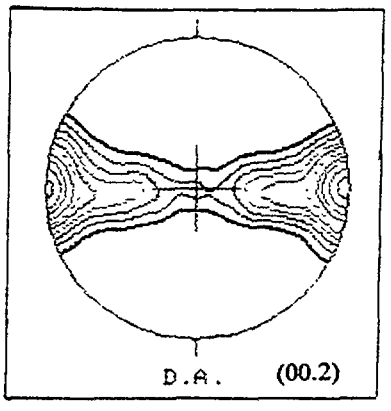

INDUSTRIAL LETRAM

FIG. 2. Texture analysis of the INDUSTRIAL and LETRAM Hf tubes

2.4. Mechanical behaviour

2.4.1. Tensile and burst test

The mechanical properties of the tubes have also been examined. Tensile tests at 20°C along the axial direction of the tube and burst tests at 20 and 320°C have been performed. From the stress/strain curves obtained at 20°C, it is noticed that the LETRAM tube has a small total elongation compared to the INDUSTRIAL tube, this difference disappearing at 320°C (Figures 3 and 4). To

understand the early rupture of the LETRAM tube we have used Scanning Electron Microscopy (SEM) on the rupture surface after the tension test at 20°C. As can be seen from Figure 5, the rupture surface of the INDUSTRIAL tube is ductile with dimples, when the rupture surface of the LETRAM tube is nearly brittle with some intergranular cracks. This type of brittle fracture is certainly due to the chemical composition, perhaps to the high oxygen content. This demonstrates that the LETRAM tube can not accept a very high level of deformation and presents early cracking to accommodate the deformation.

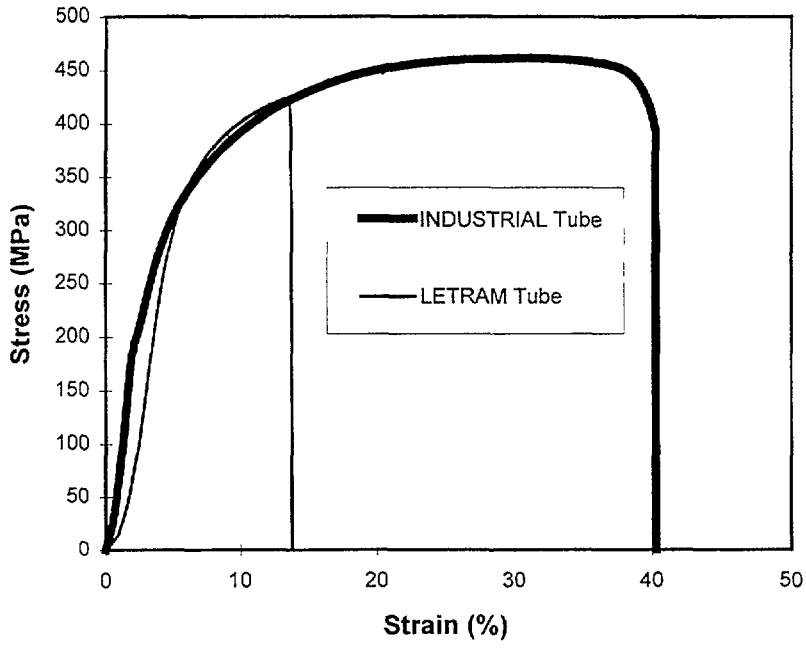

FIG. 3. Tensile test at 20°C

2.4.2. Creep test

At last, we have performed internal pressure creep tests at 320 and 350°C for different stress levels (from 50 to 160 MPa) and compared the behaviour of Hf tubes with that of Zy-4 guide thimbles. We can see from Figure 6 that after 240 hours of deformation the INDUSTRIAL tube has a very low hoop strain, whereas the LETRAM tube has a higher hoop strain than the Zy-4 tube, which could be explained mainly by the microstructure (texture, grain size, etc.) and perhaps by the chemical composition of the LETRAM tube.

3. BIBLIOGRAPHIC STUDY

The wide differences of these tubes (metallurgical parameters and mechanical behaviour) have led us to acquire a better knowledge of the metallurgical and functional properties. We have mostly focused our study on the transformation of the product to obtain a thin material with fine grains and no cracks and also on the mechanical wear resistance. In this paper we will give only the main results of our study. Using this bibliographic study we have now better understanding of the differences between INDUSTRIAL and LETRAM tubes and we can now propose an optimised Hf alloy taking into account the parameters of transformation and controlling the mechanical and wear properties of each Hf alloy elaborated.

3.1. Elaboration and route process

To avoid cracking during the transformation of the product (tube/plate), it is essential to have:

- a low oxygen content;
- an addition of other alloying elements which help obtaining high deformation levels such as Zr (3 to 5%) or Nb (higher content 35%) [5];

- a small grain size which is in contradiction with a low oxygen content for Hf alloys but can be obtained by an addition of Fe and Si;
- a high level of deformation during the hot rolling process which is essential to obtain small grain especially when the oxygen content is low.

These conditions seem to be the key parameters to have a good product especially during the cold rolling phases. But, in comparison to Zr alloys, Hf alloys are much more difficult to transform.

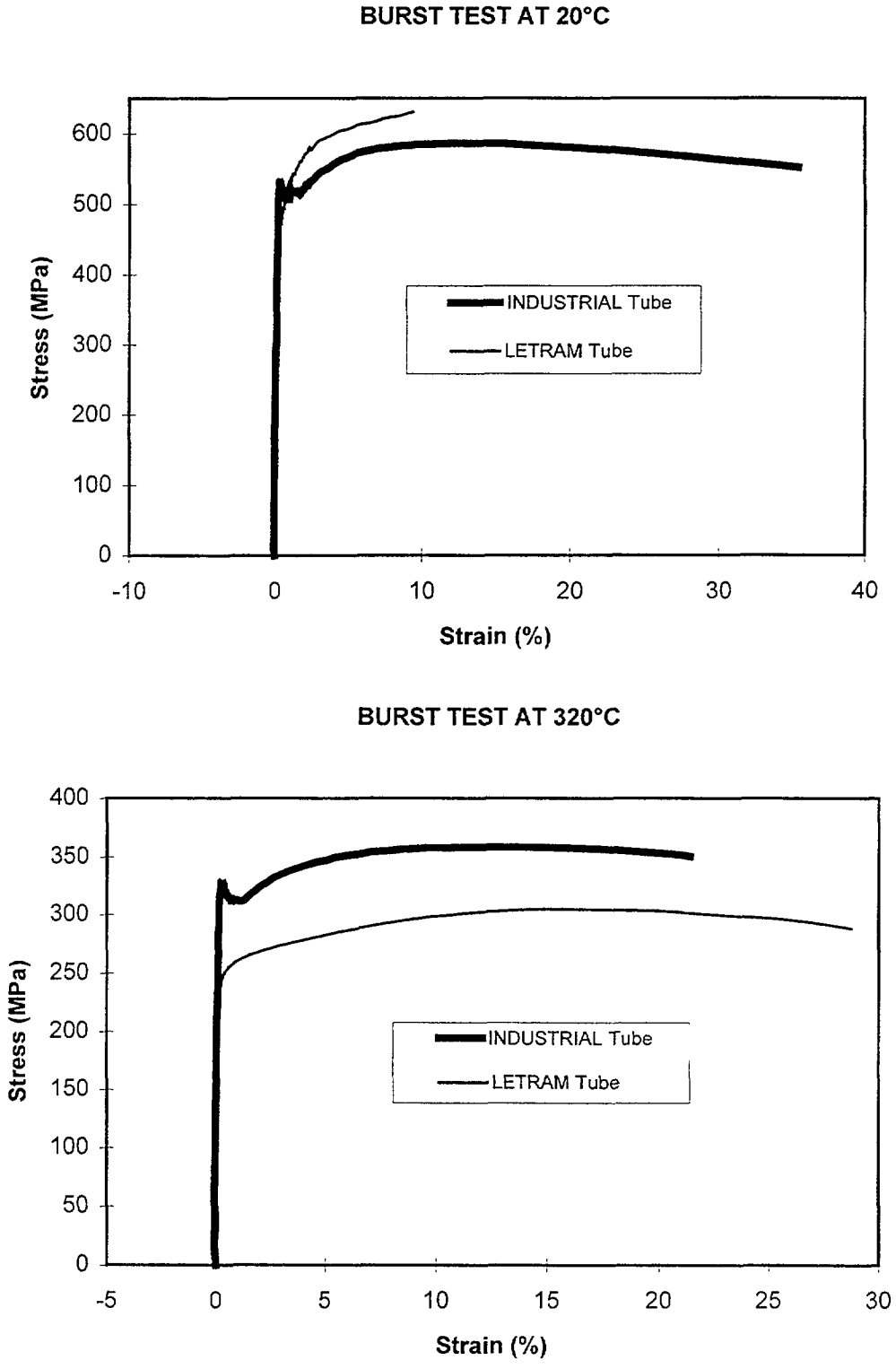

FIG. 4. Burst test at 20 and 320°C

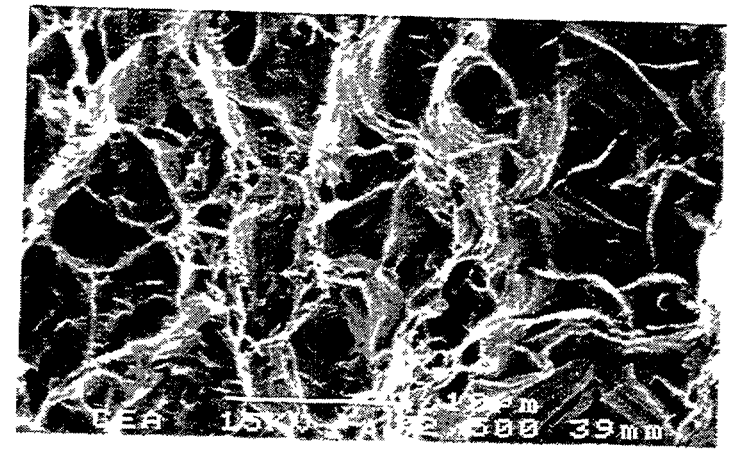

INDUSTRIAL

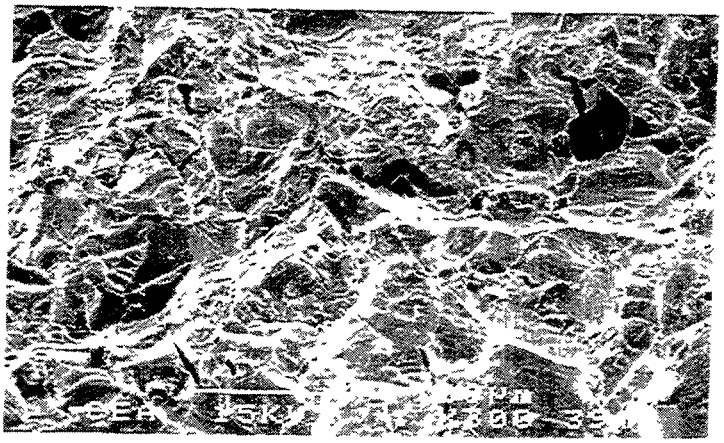

LETRAM

FIG. 5. Fracture surface of the INDUSTRIAL and LETRAM Hf tubes after tensile test at 20°C

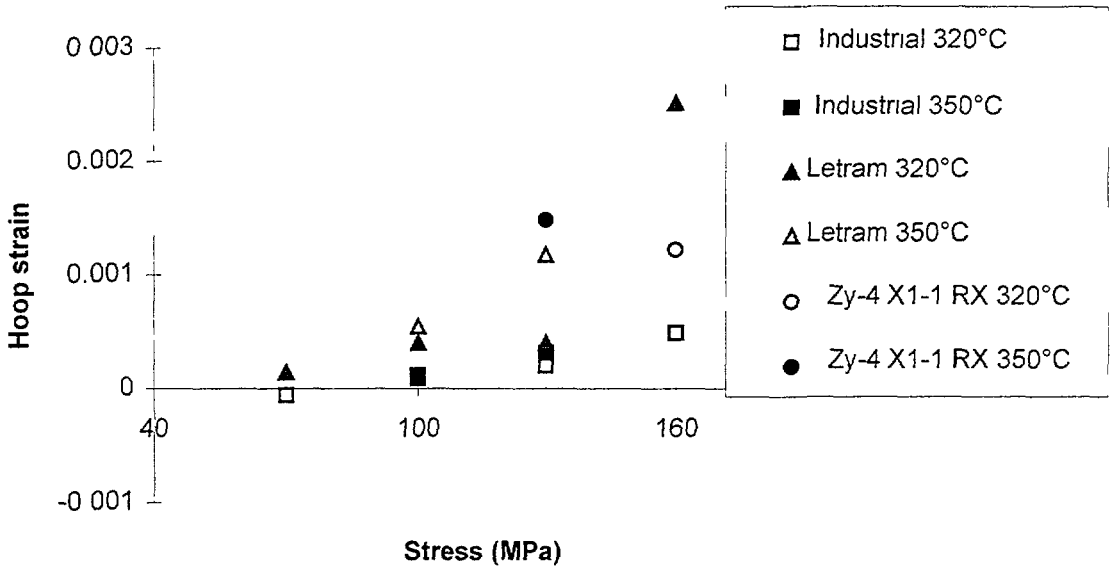

FIG. 6 Internal pressure creep test at 320 and 350°C

3.2. Functional properties

3.2.1. Mechanical properties

There is a very strong influence of small additions of alloying elements (such as O, Fe) and impurities (such as C, N) on the mechanical properties of Hf alloys. Cold working also has a strong effect on the hardening of the material. In comparison to Zr alloys, the effect of oxygen content for example is increased by a factor 4 or 5 [5].

3.2.2. Corrosion and hydrating

Hf has a very good behaviour in water corrosion, much better than that of Zr alloys and HfO2 is a very good barrier against hydrogen diffusion. Hydrating can become a real problem if hydrogen penetrates inside the material by cracks. Therefore, the material must be crack free.

3.2.3. Irradiation

Except for Russians studies [6], very few results are available about irradiation effects on Hf especially about creep under irradiation. As for Zr alloys, irradiation strengthens the material and decreases the elongation (total and uniform). Irradiation growth which is mainly linked to texture is quite limited (1% in diameter after 6×10^{25} n/m^2). During irradiation, there is also appearance of new products linked to the transmutation of Hf, i.e. formation of a second phase rich in tantalum.

3.2.4. Wear resistance

Hf seems to have a very bad behaviour in wear resistance in comparison to steels. This result has been shown by tests performed at CEA in the 1980s at 320°C in PWR water.

4. OPTIMISATION OF AN Hf ALLOY

4.1. Provisioning and fabrication programme

An ingot of very good purity has been provisioned from Wah-Chang. The chemical composition is given in Table II. There is especially a very low content of O (63 ppm). Metallurgical analyses of the initial product have been performed: grain size hardness and tension test.

TABLE II. COMPOSITION OF THE INITIAL PRODUCT

Ingot	**Zr** %	**FE** ppm	**O** ppm	**H** ppm	**N** ppm
Wah-Chang	0.47	51	63	3	5

Starting from this product we have planned a programme of optimisation for Hf plates of different composition (addition of principal elements, Table III) and we will deal only with Hf-3.5%Zr.

TABLE III. OPTIMIZATION PROGRAMME FOR Hf PLATES

Composition	**Objective**
+ 3% Zr	to improve the fabrication process
+ 3% Zr (250-500 ppm Fe)	to obtain a small grain size and to improve the wear resistance
+ Ti (3%, 25%)	to lighten the tube and to improve the wear resistance
+ Nb (8%, 50%)	to improve the fabrication process and the wear resistance

4.2. Elaboration and route fabrication of Hf-3.5%Zr plate

The final chemical composition of the alloy elaborated by CEREM/CE2M is given in Table IV. The main difference is the addition of 3% Zr and a slight oxygen pollution (O content increases from 63 to 140 ppm) can also be observed. The fabrication process is:

- Hot rolling at 930°C, the plate thickness goes from 10.5 to 1.8 mm;
- Annealing at 930°C during 30 mn;
- Cold rolling, the plate thickness goes from 1.8 to 1.2 mm (thickness reduction: 33%)
- Determination of the optimised heat treatment after cold working, following the evolution of hardness test and grain size as a function of the temperature (Fig. 7). Finally, a good compromise is obtained after 2 hours at 800°C, which gives a 30 μm grain size;
- Cold rolling. The plate thickness goes from 1.2 to 0.82 mm (thickness reduction: 32%);
- Annealing at 800°C during 2 hours in vacuum which gives a 22 μm grain size (Fig. 8).

TABLE IV. COMPOSITION OF THE Hf ALLOY Hf-3.5%Zr

Plate 1	Zr %	Fe ppm	O ppm	H ppm	N ppm
Hf-3.5%Zr	3.5	60	140	5	15

At this point of the fabrication process we have obtained a quality product with no cracks and with a fine grain size: we refer to it as **sample A.** As the material can accept a higher level of deformation, we have tried to cold work the product further:

- Cold rolling. The plate thickness goes from 0.82 to 0.33 mm (thickness reduction: 72%);
- Annealing at 800°C during 2 hours in vacuum which gives a 16 μm grain size (Fig. 9).

The product obtained at this point, **sample B,** can not be cold worked further because we have reached the limit of the tools used for this fabrication.

4.3. Texture analysis

The texture analysis performed in the same conditions as the ones given in Section 2.3, has shown that the sample B has a very marked texture with the <c> axes mainly orientated along the normal direction of the plate (Fig. 10). This type of texture is close to the texture observed in the INDUSTRIAL tube. The prismatic planes (11.0) are orientated along the rolling direction which is characteristic of a fully recrystallized product.

4.4. Mechanical properties

4.4.1. Tensile test at 20°C

Tensile tests have been performed on samples A and B at 20°C with the tensile axis along the rolling direction of the samples. We found a high resistance for both samples with an ultimate tensile strength of nearly 400 MPa which decreases slightly with cold work (Fig. 11), but the most interesting feature is that the plastic elongation (uniform and total) increases with cold work (at 72% of cold work, the total elongation reaches 35%).

4.5. Wear resistance

This study has been performed in collaboration with M. Jandin from the *Ecole Supérieure des Mines de Paris, Centre des matériaux EVRY.* The first part of this study was to carry out a wear test which could help us to rank the different Hf alloys.

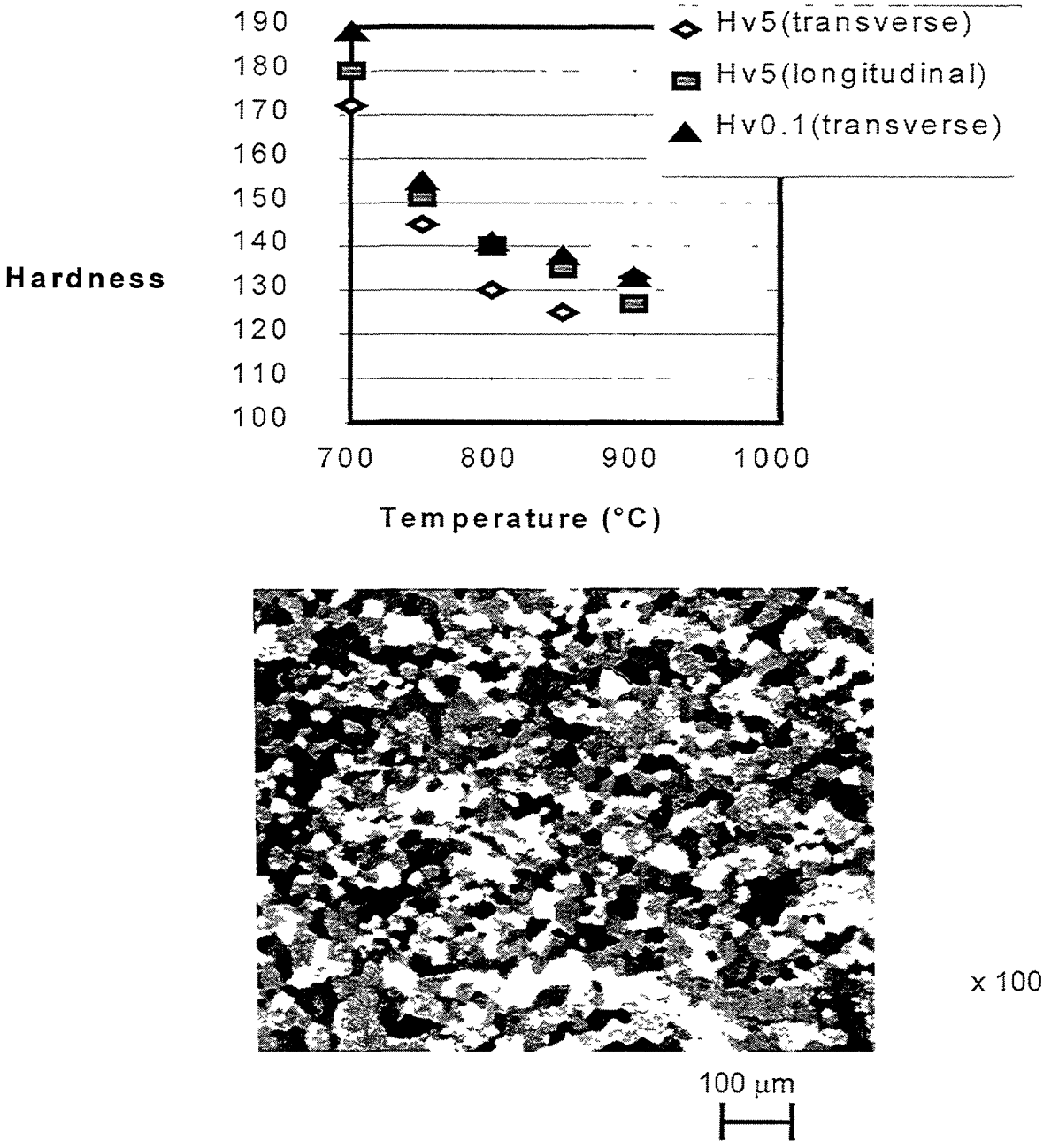

FIG. 7. Determination of the heat treatment conditions

The testing conditions are detailed below:

- pin-on-disk apparatus;
- disk on Hf alloys (diameter 30 mm);
- alumina ball;
- normal load of 1 to 10 N;
- constant sliding velocity of 0.1 m/s;
- test were carried out up to 10 000 laps,
- room temperature;
- relative humidity 25% (one test with 50%).

One can see from Figure 12 that only one mechanism of attrition is observed. We found also that, for this test, the dispersion is small The attrition coefficient μ, obtained after 10 000 laps and calculated from the disk rotation couple, has been measured This coefficient, which is independent of the load (Fig. 13) increases rapidly for the first few laps and is then constant. The specific wear rate k ~m^2/N) has also been calculated (k = material loss (m^3)/normal load (N) × sliding distance (m)) This coefficient is equal to 5.3×10^{-13} m^2/N which is less than the coefficient obtained for steels ($6.1 - 7\times10^{-13}$ m^2/N) This result seems to be in contradiction with the bibliographic result, but the differences can be attributed to the fact that the wear resistance test is very dependant of the composition of the alloys and the testing conditions.

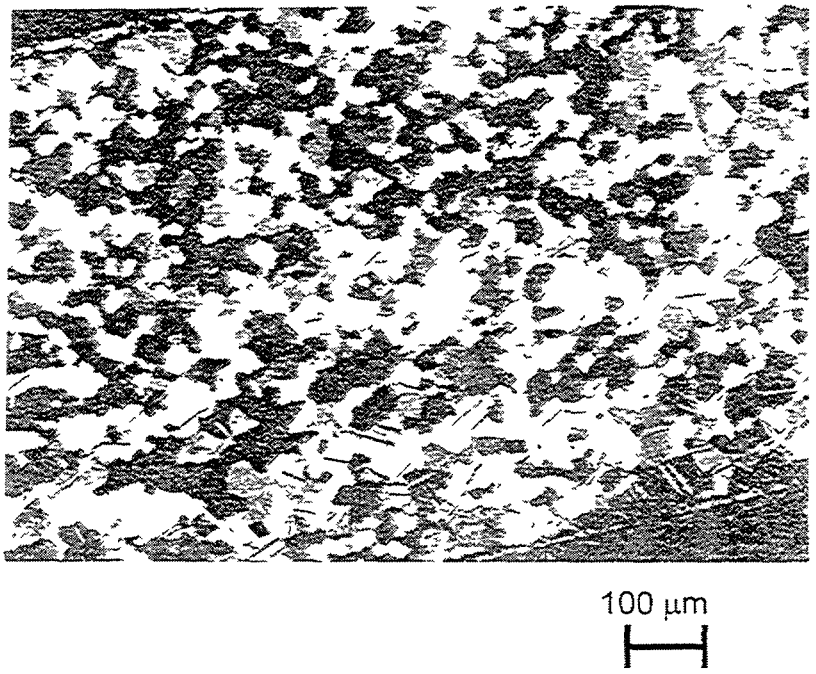

FIG 8 Microstructure of sample A

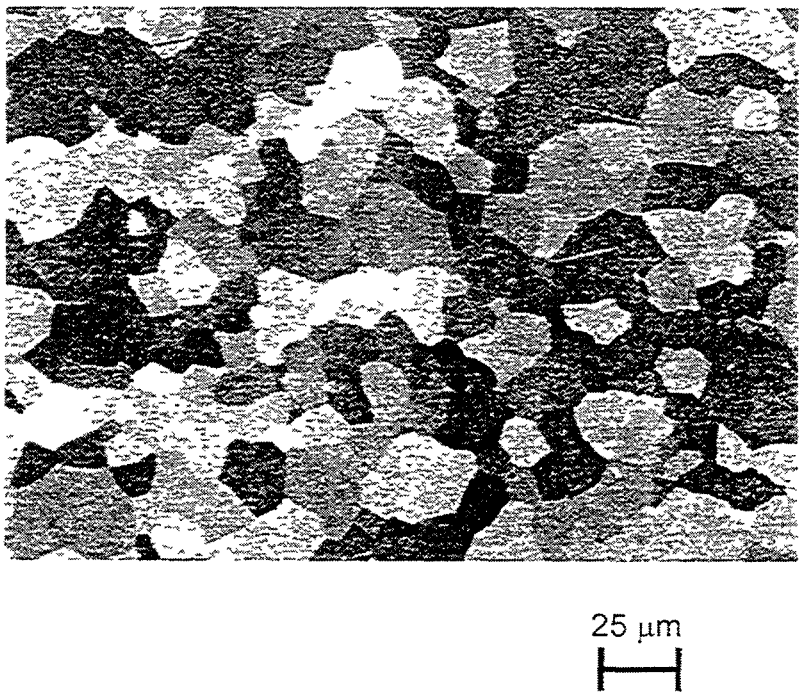

FIG 9 Microstructure of sample B

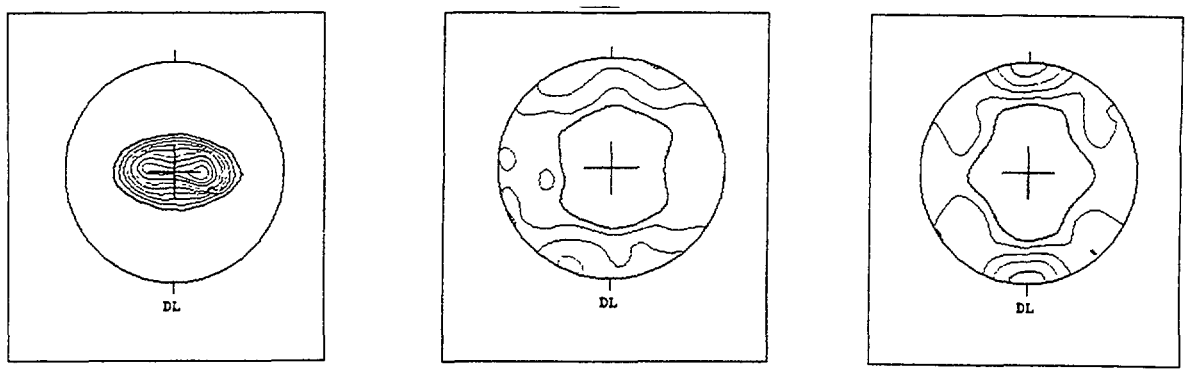

(00.2) (10.0) (11.0)

FIG. 10. Texture analysis of sample B (DL: rolling direction)

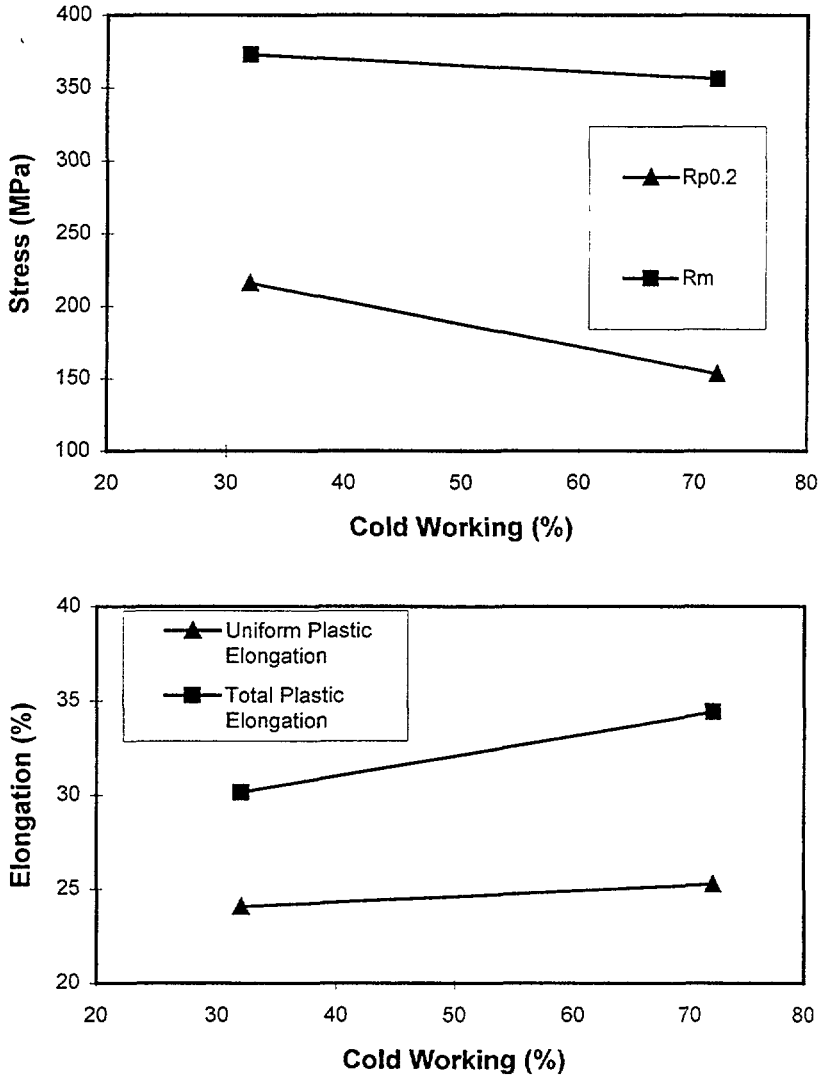

FIG. 11. Tensile test at 20°C on samples A and B

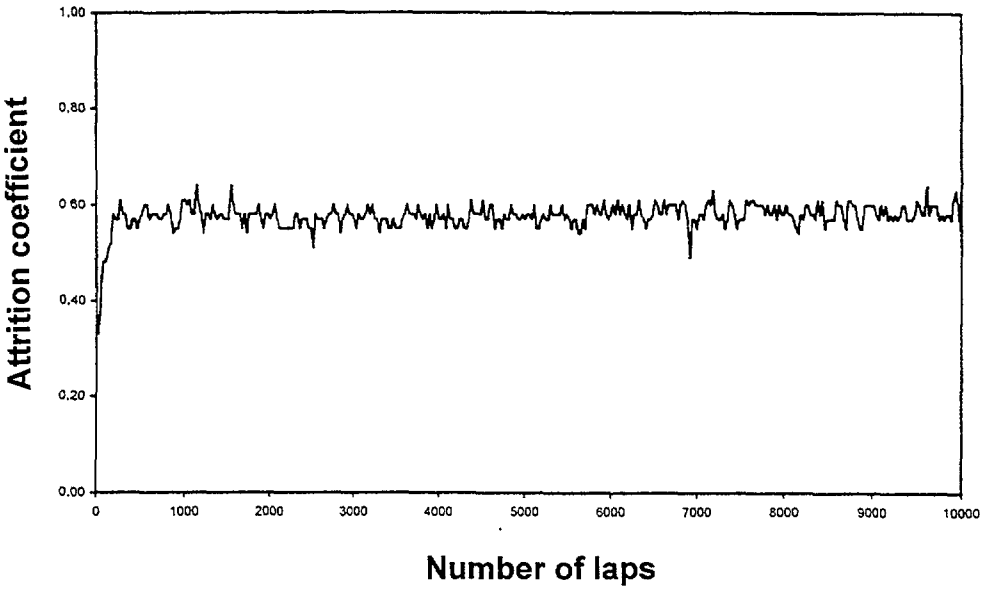

FIG. 12. Attrition coefficient as a function of number of laps (F = 1 N, v = 0.1 m/s, 25%R. H.)

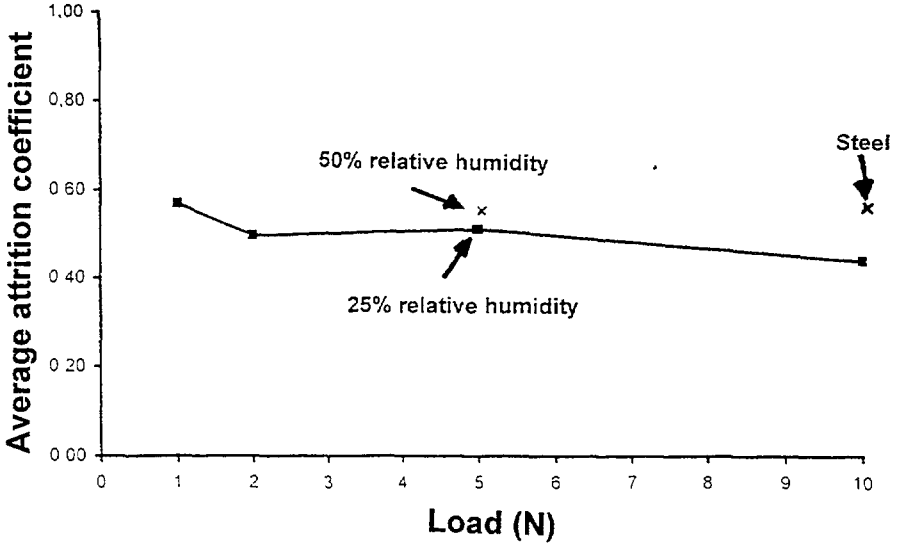

FIG. 13. Specific wear rate as a function of the load

5. CONCLUSION

First, this metallurgical study about Hf has shown, from two different fabrications (LETRAM and INDUSTRIAL tubes), the noticeable influence of the metallurgical parameters (grain size, alloying element contents, etc.) on the fabrication process and on the Hf tubes properties.

A bibliographic study has confirmed these preliminary experiments on tubes and has helped us to propose an optimised Hf alloy product for the fabrication process and for a specific use in reactor, i.e. a low oxygen content with iron an essentially zirconium addition (3-5% Zr), hardly hot rolled, needed to improve the wear resistance.

Secondly, a first optimised Hf plate has been elaborated and characterised. This Hf-3.5%Zr plate alloy has been cold rolled up to 72% then annealed at 800°C for 2 hours. The plate exhibits no cracks and a fine grain size of 15 μm. This Hf alloy presents also a good mechanical behaviour with a marked cold rolling texture. Finally, pin-on-disk wear testing has been carried out and has shown a good behaviour of this alloy in comparison to steel.

As a perspective, other alloys have to be elaborated and characterised and, concerning the wear resistance, surface treatments on Hf alloys have also to be developed (oxidation and nitrogen hardening). At last, the transposition to the tube geometry (thick tubes of 1.5 mm) should be made.

REFERENCES

[1] HERBERT, KELLER, W., et al., Development of hafnium and comparison with other pressurised water reactor control rod materials, Nuclear Technology, Vol. 59, (1982) 476-482.

[2] RISOVANIY, V.D., et al., Hafnium in nuclear engineering, Third Int. Conf. on Reactor Material Science, Dimitrovgrad, Russian Federation, 27-30 October 1992.

[3] DOUGLASS, D.L., The metallurgy of zirconium, IAEA, Vienna, (1971).

[4] TENCKHOFF, E., Deformation mechanisms, texture and anisotropy in Zr and Zircaloy, ASTM, STP 966, (1988).

[5] THOMAS, D.E., HAYES, E.T., The metallurgy of hafnium, Naval Reactors Division U.S. AEC, (1960).

[6] RISOVANIY, V.D., et al., Structural damages of metal hafnium during reactor irradiation, Int. Conf. on Radiation Material Science, Alushta, Russian Federation, 22-25 May 1990.

IRRADIATION BEHAVIOUR OF BORON CARBIDE IN WWER-1000

A.V. ZAKHAROV, V.D. RISOVANIY, S.R. FRIDMANN
Research Institute of Atomic Reactors,
Dimitrovgrad, Ulyanovsk Region

V.B. PONOMARENKO, A.O. POSLAVSKIY
Moscow Polimenal Plant,
Moscow

Russian Federation

Abstract

Rod Cluster Control Assemblies (RCCAs) with rodlets made from vibropacked boron carbide powder are used in WWERs-1000 They are used as automatic control rods (CRs) and safety rods (SRs) RCCA CRs and SRs have been examined after operation periods of 2-4 years and 2-7 years, respectively The examination of the rodlets shows absence of the corrosion effects, external mechanical influences and cladding wear The ^{10}B burnup was uneven along height and radius of the rodlets This is a typical characteristic of RCCAs used as SRs Considerable values of ^{10}B burnup are observed at a length of 1000-1500 mm for CRs and, at 300-400 mm for SRs Not more than 5% of released gas penetrates to the rodlet gas plenum and its work is inefficient The main part of the produced helium is located in the bottom part of the rodlets as a free gas or inside the boron carbide grains The gas pressure under the cladding was 1 0-1 7 MPa Under irradiation the plasticity of the cladding decreases according with fast neutron fluence along the rodlets At a burnup of 20-25%, the powder core forms coagulated sintered substance filling the cladding, but its deformation is not observed yet Appreciable values of rodlet cladding swelling are observed at burnup of about 45-50% The rate of ^{10}B burnup in RCCAs varies in the different reactors The SRs of the Zaporozhe Nuclear Power Plant and the Kalinin Nuclear Power Plant have an average burnup for one year accordingly 2 5 and 5% after ending operation The similar distinctions are characteristic for CR Carried out investigations allow to consider the main criterion of resource opportunities of the RCCAs based on a boron carbide is maximal average on section burnup of isotope ^{10}B, which should not exceed 45-50% There are methods to increase the lifetime of RCCAs based on boron carbide up to 20-25 years

1 INTRODUCTION

Boron carbide has many unique properties, a high neutron worth, chemical stability, high melting temperature, low density and low cost. It has caused extensive use of boron carbide in RCCAs of various nuclear reactor types. Boron carbide powder containing natural isotopes is at present applied as absorber material in the RCCAs of WWERs-1000. Its behaviour during irradiation determines in a decisive degree the capacity for work of the rodlets and the RCCA's lifetime

Research on WWER-1000 RCCAs with various operation times is presently carried out in the nuclear power plants (NPPs) at Novovoronezh, Zaporozhe and Kalinin. Based on the results of this research, it was recommended to increase the operation time from 1 year to 3 years for control rods (CRs) and to 5 years for safety rods (SRs).

To maintain the growing requirements on lifetime extension and reliable operation of the RCCAs, the Moscow Polimetal Plant (MPP), as the developer and the manufacturer of the rodlets, has accepted that not less than one WWER-1000 RCCA will be rexamined at the State Scientific Centre of the Russian Federation «Research Institute of Atomic Reactors» (SSC RF RIAR) annual research. Some results and recommendations of the research carried out is produced with their help and is submitted in this report.

2. BORON CARBIDE RCCAs AND THEIR WORKING CONDITION IN WWERs-1000

WWER-1000 RCCAs are unified and can be used as CRs or as SRs. During their operation a change in operation mode is possible The WWER-1000 has 61 RCCAs, of which 10 are used as CRs and the other 51as SRs

WWER-1000 RCCAs (Fig. 1) have 18 rodlets with a length of 4 240 mm. The rodlets are made of a 06X18H10T steel tubes with a diameter of 8.2 mm and a wall thickness of 0.6 mm, and are filled with vibropacked powder of boron carbide with natural isotopic composition up to a density of 1.7 g/cm^3. The ends of the cladding tube are sealed with tip details by means of argon-arc welding. The length of the absorber column is 3 710 mm and above the absorber column, there is a gas plenum filled with helium at atmospheric pressure.

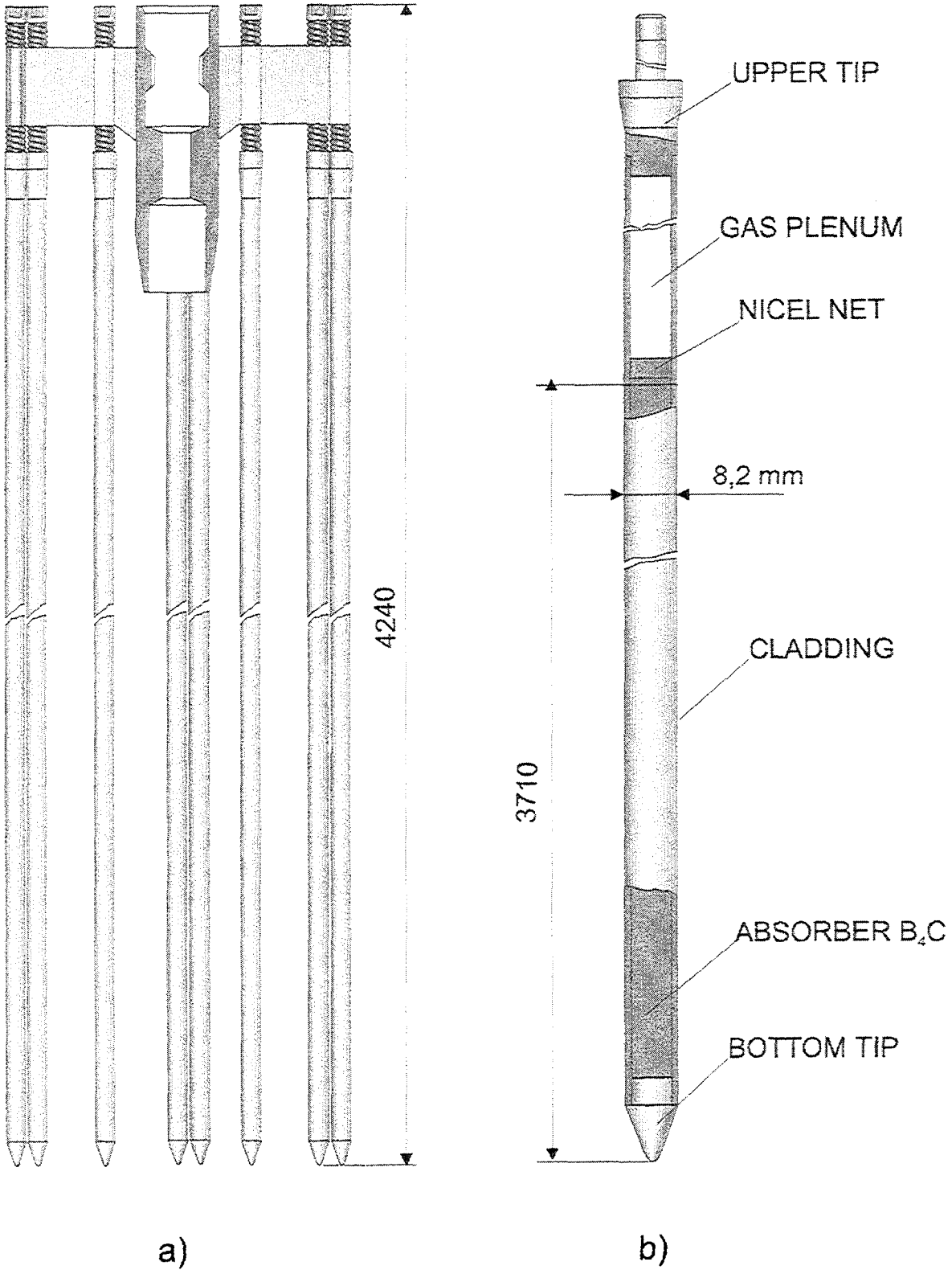

FIG. 1 Design of WWER-1000 RCCA (a) and rodlet (b)

The rodlets are moving inside guide tubes, made from 06X18H10T steel with a diameter of 12.6 mm and a wall thickness of 0.8 mm, in the fuel assembly. The internal diameter of the guide tubes is 11 mm, and the radial gap with the rodlets is 2.8 mm. Coolant (water) flows through the channel with a speed of 2 m/s, the water pressure is 15 MPa and the temperature is 300°C.

The bottom ends of the rodlets of RCCAs working as SR are approximately positioned 80-100 mm above of the upper edge of reactor core. At reactor shut off they fall down under their own weight with a speed of about 1 m/s. For RCCAs operating as CR, only the bottom ends of the rodlets are inserted in the reactor core at a depth of 300-700 mm.

3. RESEARCH ON REGULAR RCCAs AFTER OPERATION IN WWERs-1000

WWER-1000 RCCA CRs and SRs were examined in the nuclear power plants (NPPs) at Novovoronezh, Zaporozhe and Kalinin, after an operation period of 2-4 years and 2-7 years, respectively. The assessment of the rodlets exterior condition indicates that, among the possible damaging phenomena, there are no corrosion effects, external mechanical effects and wear of the cladding. These conclusions have been confirmed by eddy current non-destructive testing and metallographic research of cladding. Some diameter increase of rodlets cladding was observed in RCCAs from the Novovoronezh NPP after being used as CR during 3 years (0.7%) and as SR during 7 years (2% with cracking of cladding).

The ^{10}B burnup is very uneven amongst the rodlets. It is most typical for the RCCAs used as SRs. A considerable burnup of the isotope ^{10}B is observed at the bottom end of CR rodlets at a length of 1000-1500 mm and at 300-400 mm for SRs (Fig. 2). A high uneven distribution of the radial burnup is noted in the absorber. For example in RCCA rodlets of the Kalinin NPP, the ^{10}B burnup on the outer rim (about 1 mm) of the absorber core was just about 50%, in the centre it was 3-8% and the average radial burnup was 25-30% (Fig. 3). Thus the maximum average yearly rate of ^{10}B burnup did not exceed 5%.

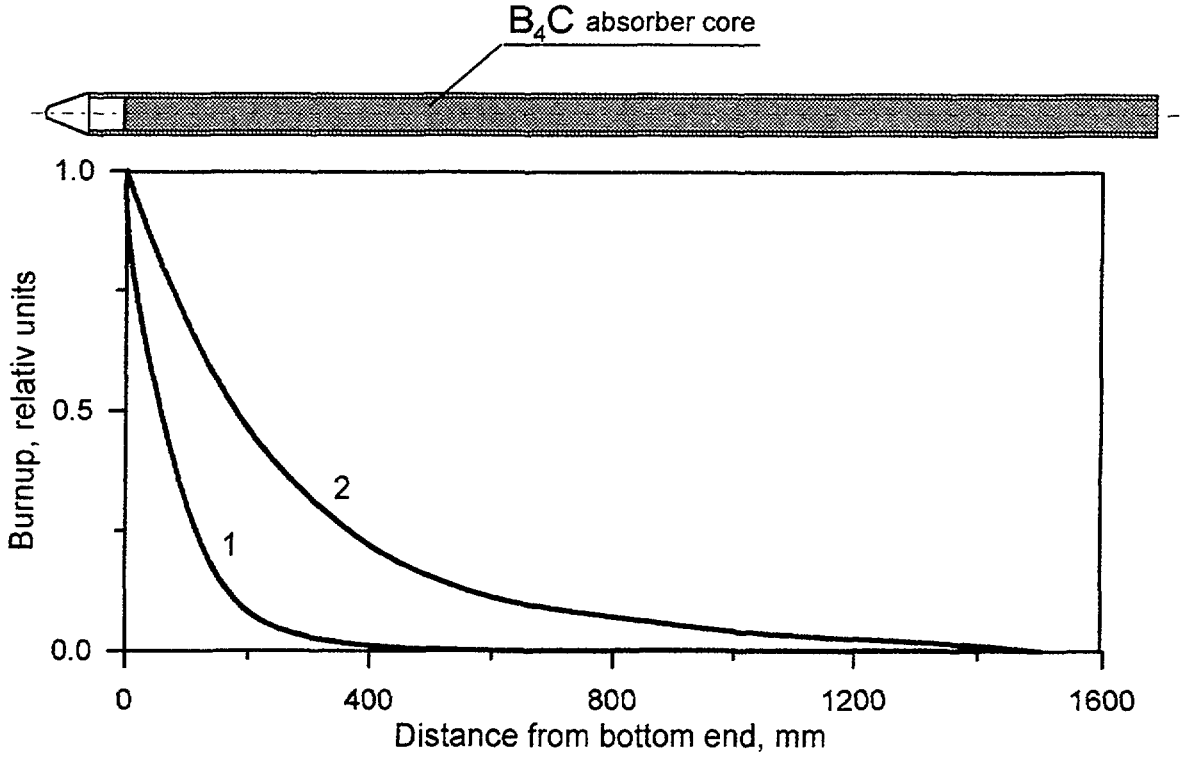

FIG. 2. Relative ^{10}B burnup distribution in the B_4C core of WWER-1000 RCCAs after operation as SR (1) and as CR (2)

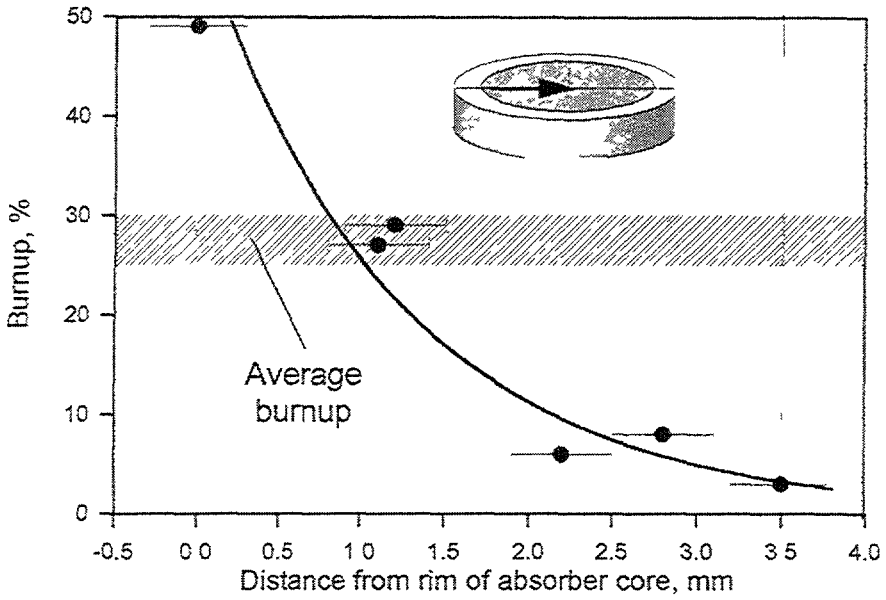

FIG. 3 Radial ^{10}B burnup in B_4C rodlet after 6 years operation as SR (Kalinin NPP)

The measurements of the maximum radial averaged ^{10}B burnup of the absorber core of the rodlets used as SR in different NPPs, have shown, that the rate of burnup essentially differs: from 2.5%/year (at Zaporozhe NPP, for 2 years operation) and 5%/year (at Kalinin NPP, during 6 years) up to 11%/year (at Novovoronezh NPP, during 7 years) (Table I).

TABLE I. SOME OPERATION CHARACTERISTICS OF EXAMINED BORON CARBIDE RCCAs

NPP	**Operation Mode**	**Calendar time of operation**	**Effective time of operation**	**Maximum radial averaged ^{10}B burnup of rodlet**	**Maximum increase of rodlet cladding diameter**
		Years	Effective days	%	%
Novovoronezh	CR	2	491	32.5	0
	CR	3	793	42.6	0
	CR	3	819	53.2	0.7
	SR	7	2030	77	2, destruction of cladding
Zaporozhe	SR	2		3.5	0
Kalinin	SR	6		25-30	0

The absorber material changes with increasing ^{10}B burnup. At a burnup of 20-25%, the absorber material remains a powder and at higher burnup it will form a coagulated sintered substance. This was observed at cuts on the bottom ends of RCCA rodlets of the Kalinin and Novovoronezh NPP after being used as CR and SR at a burnup of more than 25%.

The helium produced due to neutron interaction, partly is released from grains B_4C, filling empty spaces, and partly remains in pores of grains B_4C. Results of gas pressure measurements under the cladding have shown that only up to 5% of the released helium moves to the gas plenum on top of the rodlets. The main share of a helium stays in the bottom part of the rodlets under the cladding. The

calculated maximum internal pressure in the gas plenum did not exceed 0.3 MPa under normal conditions and 0.6 MPa at an operation temperature of 350°C with an outside coolant pressure of 15.3 MPa.

Properties of the cladding material (steel 06X18H10T) testifies the appreciable decrease of plasticity at the bottom ends of rodlets. However, plasticity of the cladding has not decreased to critical values. The minimum values of uniform relative lengthening at temperatures 20°C and 350°C were 17-20% and 5-6%, respectively. The maximum increase of microhardness in the bottom part of the rodlets was 30% (from 1800 MPa up to 2380 MPa). There is no interaction of the cladding with the boron carbide absorber.

There is a strong correlation between changes of the cladding and the absorber properties and the length of the rodlets with distribution of induced gamma-activity, fast and thermal neutrons fluence and ^{10}B burnup in the absorbing core.

4. TESTS OF BORON CARBIDE RODLETS DUMMIES IN THE REACTOR SM

More detailed research on boron carbide absorber material properties in the rodlets was carried out through tests of short rodlets dummies, made with application of nominal materials in the research reactor SM. The dummy design is shown in Fig. 4b and c. The boron carbide in the dummy was used both as a powder and as pellet made by cold compacting with subsequent sintering. The density of the absorbing core was 1.7-1.8 g/cm^3. The length of the rodlet dummies is about 100 mm. A demountable irradiation device was used for carrying out the tests (see Fig. 4a), allowing to periodically replace and inspect the dummies. Simultaneously, 24 rodlet dummies can be loaded in the irradiation device.

Irradiation was carried out in a fast neutron flux of 3.3×10^{14} cm^{-2} (E > 0,1 MeV) and a thermal neutron flux (without the account of depression) of 8.9×10^{14} cm^{-2} (E < 0.46 eV). The temperature of the coolant was 290 ± 20°C, the pressure 14 ± 0.5 MPa and the water flow 1.7 ±0.3 m/s. After each 20-30 day of irradiation, inspection of the dummies condition was carried out. A maximum ^{10}B burnup of about 40% was achieved. All dummies have kept their form and integrity. The maximum increase of cladding diameters did not exceed 0.3%. With increase of the neutron fluence and ^{10}B burnup, the He release increased (Fig. 5). For pellets, the He release was more than twice higher than that for powder, because of the higher temperature caused by the irradiation.

Irradiation results to swelling, cracking and destruction of B_4C pellets in fragments up to 2-5 mm at a ^{10}B burnup of 10-15%. The linear swelling rate of B_4C pellets was approximately 0.3% at 1% of ^{10}B burnup. The B_4C powder practically does not change its structure up to ^{10}B burnup of 20-25%. Above this burnup sintering was observed, as well as in nominal rodlets. In its structure there are no cracks and the porosity decreases.

At average radial ^{10}B burnup of 35-40%, there is no essential difference between pellet and powder with densities of 1.7-1.8 g/cm^3. For a final conclusion about the advantage of various rodlet designs, reactor tests should be continued to higher burnup.

5. ANALYSIS OF RESULTS

In practice, for safe and reliable operation of RCCAs, it is necessary to supervise one or two operational parameter, which determine the condition of the rodlets to a maximum degree. The research on nominal RCCA and boron carbide rodlet dummies after irradiation unequivocally indicates that the main parameter determining the operating lifetime of the RCCAs is the ^{10}B burnup. Safe and risky limits of operation can be specified depending on the ^{10}B burnup (Fig. 6).

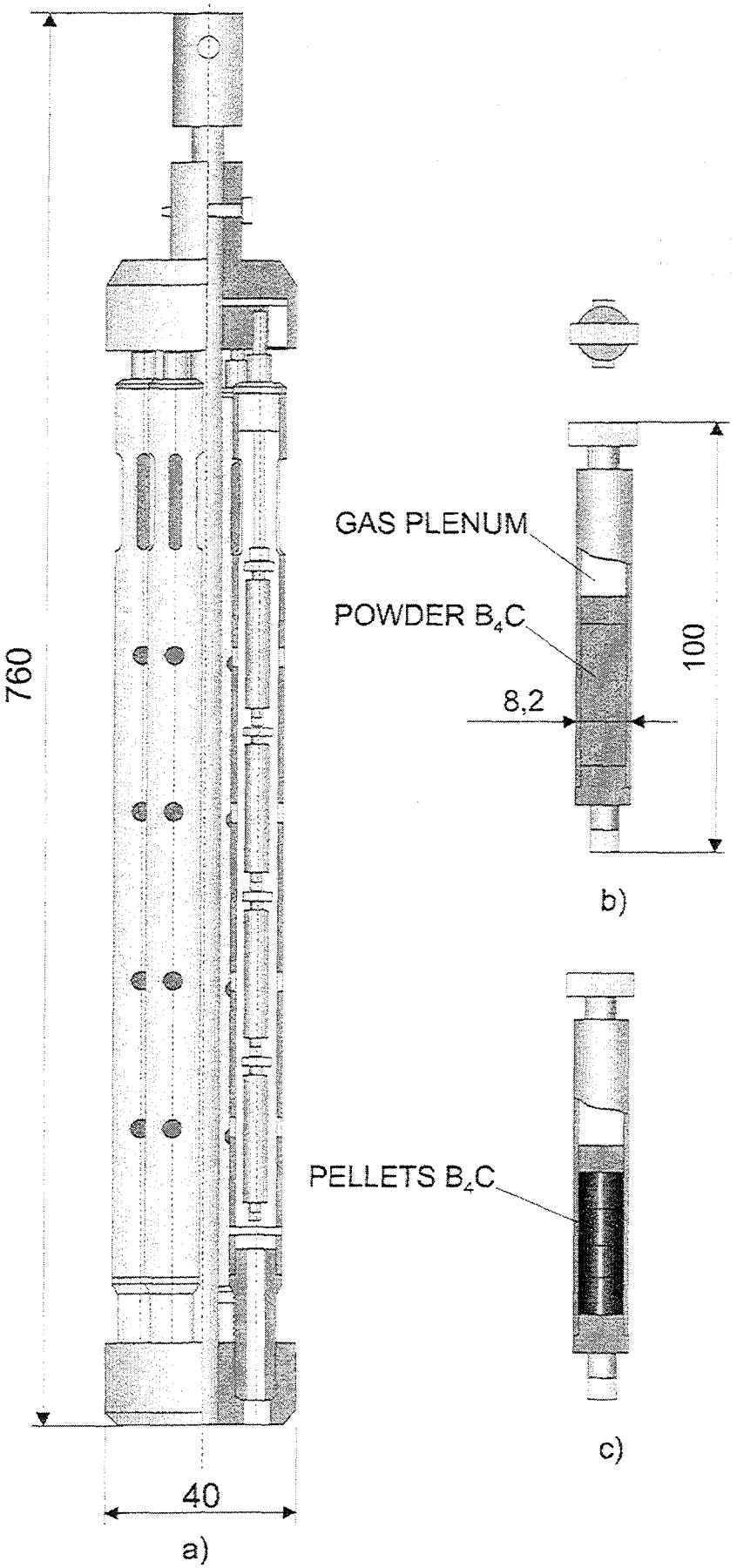

FIG. 4. Design of sectional irradiation device (a), dummy with powder (b) and pellets (c) of boron carbide

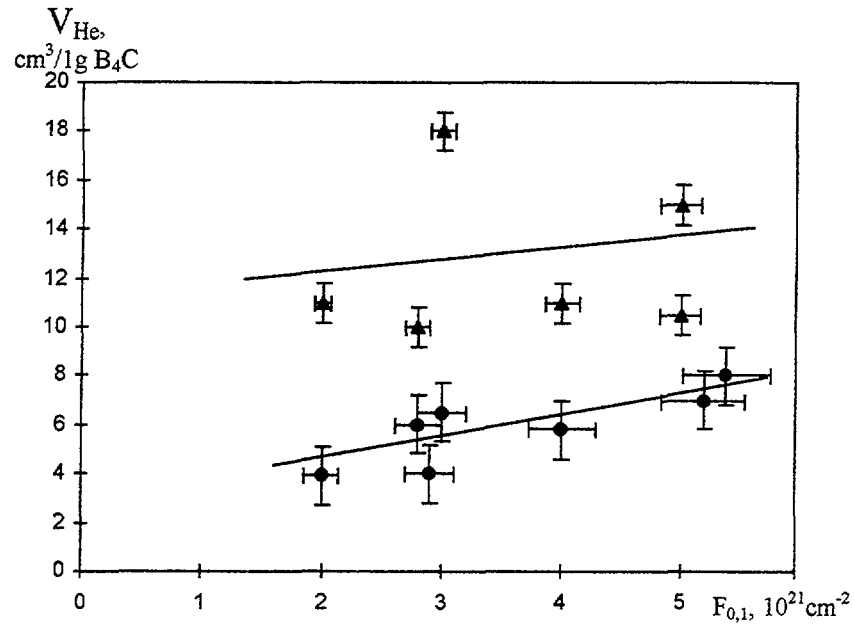

FIG. 5. Dependence of He release from B_4C at thermal neutron fluence E < 0.465eV; (1) pellets; (2) powder

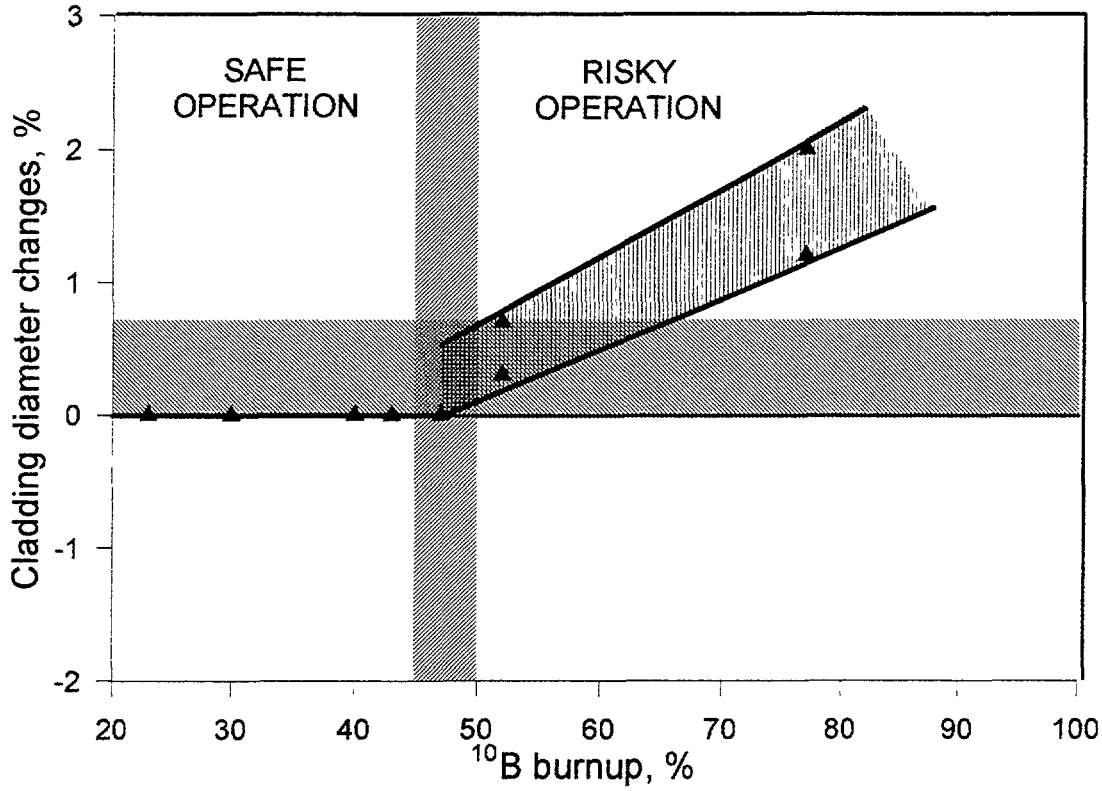

FIG. 6. Dependence of diameter changes of rodlet cladding with B_4C from ^{10}B burnup at operation in WWER-1000

At operation of RCCAs in WWERs-1000, different conditions of burnup rates are realized. Therefore, their lifetime cannot be determined as a calendar service life. It is expediently to fix dynamics of burnup change for each RCCA by computational or experimental methods. Criterion of achievement of a limiting condition should be the average radial ^{10}B burnup of about 50%. Above this burnup, the deformation of the cladding and its destruction is observed at linear swelling rates of 0.5-0.7% in case 06X18H10T steel is used as cladding material. The lower burnup provides safe and reliable operation of RCCAs.

From research results follows, that there are simple solutions for increasing the lifetime of the boron carbide RCCAs, especially when used as SRs. For example, change of the position of the bottom ends of rodlets so that the bottom edge of the absorbing column is placed at a distance of about 150 mm from the upper margin of the reactor core, will lower the average ^{10}B burnup rate up to 2%/year and in such mode, the RCCA can safe work up to 20-25 years (Fig. 7b).

There is a Russian patent for rodlets with the gas plenum in the lower part, which provides not only a decrease of the ^{10}B burnup rate, but also reduces the internal gas pressure under the cladding (Fig. 7c) and thus increases the RCCAs lifetime up to 20-25 year.

6. SUMMARY

The lifetime of boron carbide RCCAs used in the WWERs-1000, directly depends on the ^{10}B burnup, achieved at their operation. An average radial ^{10}B burnup approximately up to 50% is the limiting factor for safe operation of such RCCAs. Lifetime possibilities of B_4C RCCAs is not complete. Actions reducing the burnup can increase the lifetime of such RCCAs up to 20-25 years.

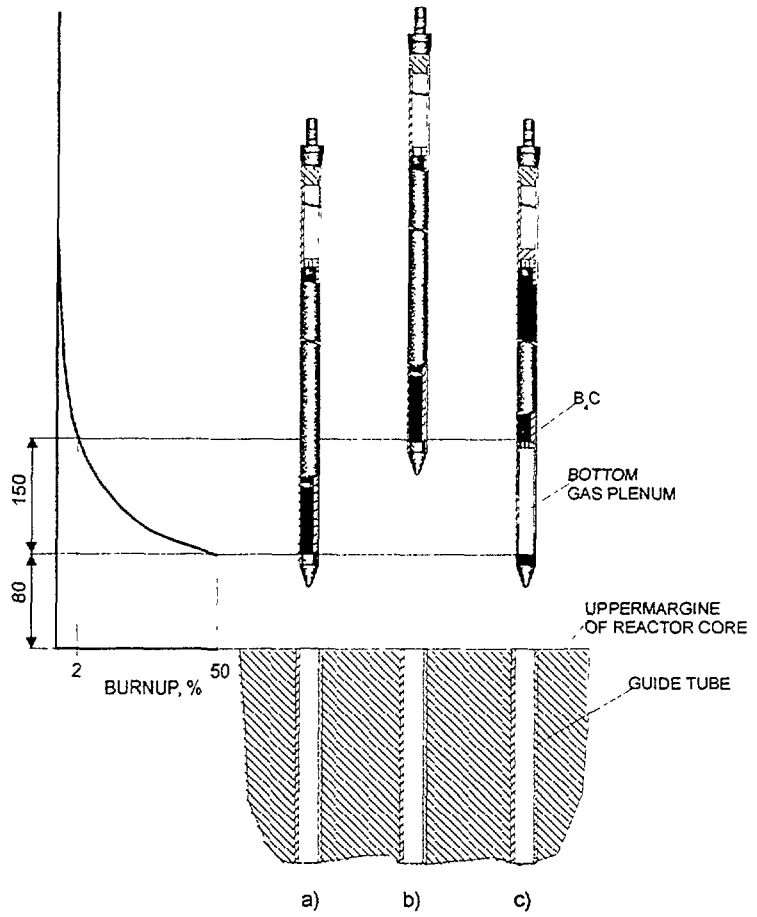

FIG. 7. ^{10}B burnup in rodlets (a) and change of their position relatively of reactor core (b) and design (c) to increase safe operation time

WWER-1000 CONTROL ROD MATERIALS: EXPERIENCE AND DEVELOPMENT

V. PONOMARENKO, A. POSLAVSKIY, A. SCHEGLOV
Moscow Polimenal Plant,
Moscow

A. ZALJETNIY
Novovoronezh NPP,
Novovoronezh

V. RISOVANIY
State Scientific Centre "Research Institute
of Atomic Reactors",
Dimitrovgrad, Ulyanovsk Region

Russian Federation

Abstract

The Moscow Polimetal Plant (MPP) is the senior designer and producer of native nuclear reactor control rods of various types and purposes since 1966 year (Table I) The standard requirements of Russian nuclear reactor control rods and absorber materials are given in Table II During 1962 and 1998, the Moscow Polimetal Plant mastered the production of various absorber materials meeting the different requirements (Table III) As a rule, the Moscow Polimetal Plant uses the same construction materials in fuel assemblies, fuel elements, fuel rods, etc These are austenitic and martenstate stainless steel, alloys based on Zr, Al and Ti and heat-resistant and high-temperature alloys based on Ni and Cr The control rods are made in accordance to safety guides of the Russian Federation (e g OPB-88, PBJa RO AS-89) and meet high standards The Moscow Polimetal Plant carries out its work together with other commercial enterprises and research institutes Some of them are presented in Table IV In this paper we consider different aspects of experience design, testing and operation of WWER-1000 RCCAs and, also, their development

1. DESIGN AND SERVICE CONDITIONS OF WWER-1000 RCCA

Since 1971, the Moscow Polimetal Plant has produced RCCAs for WWERs-1000. The main operation characteristics of the WWER-1000 are given in Tables V and VI and Figs 1-5. The main absorber material requirements are·

- the physical effectivity of absorber materials is not less than 80% of B_4C physical effectivity (natural contents of ^{10}B is ~18.9%),
- the rodlet cladding must be produced from a stainless steel able to be in the water of the first reactor circuit during long time (P=160 to 180 atm., $T \leq 350°C$);
- the work resort must be as much as possible ($\tau \geq 5...7$ years).

A WWER-1000 RCCA contains 18 rodlets A commercial WWER-1000 has 61 RCCAs. Six of them are used as regulation control rods (CRs), the rest are shut-down rods (SRs). RCCA characteristics are given in Table VII There exist four primary modifications of commercial WWER-1000 RCCAs, i.e. CR-71, CR-85, CR-95 and CR-97, with different absorber and cladding materials (the CR's number corresponds to the first year of operation). Designs of these rodlets are shown in Figs. 6 and 7.

TABLE I. CONTROL RODS FABRICATED BY MOSCOW POLIMETAL PLANT

Reactor	Control rod
WWER-1, WWER-2, WWER-3M, WWER-440, VC-50	• cast hexahedral shell of ACA from boron steel • burnable poison rods
WWER-1000	• absorbers of RCCA • burnable poison rods
RBMK-1000 (1500)	• automatic and manual control rods, scram rods • additional absorber rods
AM-1, AMB-I, AMB-II, EGP-6	• automatic and manual control rods, scram rods
BN-600, BN-350	• automatic control rods, scram rods, shim rods
Research reactors e.g. SM-2, MIR, BOR-60, IRT-2000, IW-2, MR	• automatic and manual control rods, scram rods, burnable poison rods
Military reactors	• automatic control rods, scram rods, shim rods, burnable poison rods

TABLE II. MAIN STANDARD REQUIREMENTS OF CONTROL RODS

1.	Large physical efficiency
2.	Low decrease of burn-up rate of absorber
3.	High resistance to radiation damage (undesirable changes in a shape, dimensions, a structure and properties of materials during irradiation)
4.	Comparability absorber materials with cladding and cladding with coolant
5.	Low depth of deterioration
6.	Good movement in the reactor core
7.	Good behaviour at LOCA and other accident conditions
8.	Low prime cost
9.	Technological effectiveness of production
10.	Good utilizable waste, absence of long-lived high-radioactive isotopes

TABLE III. ABSORBER MATERIALS FABRICATED AT THE MOSCOW POLIMETAL PLANT DURING 1962 - 1998

Type of rods	Type of absorption	Materials
Automatic control rods, manual control rods, shut-down rods	n, α	B_4C (natural) B_4C (enriched ^{10}B) Me B_2 Me B_6 including enriched ^{10}B Boron steel (SBA-2, SB-2, SB-2M)
	n, γ	Eu_2O_3, Gd_2O_3, Dy_2O_3, Sm_2O_3, Er_2O_3, Ho_2O_3
		Dy_2TiO_5, $Dy_2Ti_2O_7$, Eu_2TiO_5, $Dy_2O_3 \cdot HfO_2$, et al.
		Eu_2O_3+Mo, Eu_2O_3+Al, Eu_2O_3+(Ni, Cr), Dy_2O_3+Cu, Dy_2O_3+Mo, et al.
		Hf, Hf+Nb, Hf+Ta
Burnable poison rods	n, α	$B_4C+Al_2O_3$, $CrB_2+Al_2O_3$, et al.
		B_4C+Al, CrB_2+Al, B+Zr, et al.
	n, γ	$Gd_2O_3+Al_2O_3$, $GdAlO_3$, $Gd_2O_3 \cdot ZrO_2 \cdot Nb_2O_5$, et al.
		Gd_2O_3+Al, Gd–Zr–Nb, et al.

TABLE IV. CO-OPERATION SCHEME OF THE MOSCOW POLIMETAL PLANT WITH OTHER COMMERCIAL ENTERPRISES AND RESEARCH INSTITUTES DURING FABRICATION OF CONTROL RODS

Technical task	The Chief Designer of a reactor
Project development	Moscow Polimetal Plant
1. Selection of absorber and composite materials, development of a construction and fabrication method of rods.	MPP
2. Physical efficiency research.	RSC CI, IPPE, EMBB
3. Compatibility research of absorber and composite materials.	MPP, IPPE
4. Research of corrosion resistance.	IPPE, RINM
5. Radiation stability research of absorber materials, rodlet model, RCCA in research reactors and their post-irradiation examination in hot cells.	SSC RIAR
6. Special testing (?, vibro-, thermo-, wear stability et. al.).	MPP, EMP, RCIET, RDO HP,EMBB,
7. The final calculations, produce of technical documents, interdepartmental tests	MPP
Production of control rods	MPP
Post-irradiation investigation of used control rods	SSC RIAR, RSC CI, IPPE, NV NPP
Serial production of control rods	MPP

TABLE V. OPERATION FEATURES OF WWERS-1000

Parameters	Unit	Condition or value
Coolant		water
Coolant pressure	MPa	16
Inlet coolant temperature	°C	129
Outlet coolant temperature • average • maximal	°C	 320 335
Max. temperature of coolant surface • outside • inside	°C	 345 375
Max. flux • thermal • E > 0.1 MeV	$\times 10^{14}$ n/cm^{2}s	 ~0.6 ~2.2
Max. RCCA drop time	s	< 4

TABLE VI. AVERAGE GROUP NEUTRON FLUX OF WWERS-1000
(IN REACTOR CORE VOLUME)

Group number	E MeV	Ft n/cm^{2}s
1.	15	2.09×10^{10}
2.	12.2	1.11×10^{11}
3.	10.0	4.34×10^{11}
4.	8.18	1.75×10^{12}
5.	6.36	4.24×10^{12}
6.	4.96	5.69×10^{12}
7.	4.06	1.18×10^{13}
8.	3.01	1.17×10^{13}
9.	2.46	3.34×10^{13}
10.	2.35	1.46×10^{13}
11.	1.83	3.10×10^{13}
12.	1.11	4.27×10^{13}
13.	0.55	6.03×10^{13}
14.	0.111	6.32×10^{13}
15.	3.35×10^{-3}	2.54×10^{13}
16.	583×10^{-6}	2.08×10^{13}
17.	101×10^{-6}	1.01×10^{13}
18.	29×10^{-6}	5.49×10^{12}
19.	10.7×10^{-6}	4.90×10^{12}
20.	3.06×10^{-6}	4.64×10^{12}
21.	1.12×10^{-6}	2.59×10^{12}
22.	0.0625×10^{-6}	6.00×10^{13}
	>0.8	~1.33×10^{14}
	>0.55	~1.54×10^{14}
	>0.11	~2.19×10^{14}
	thermal	~0.6×10^{14}

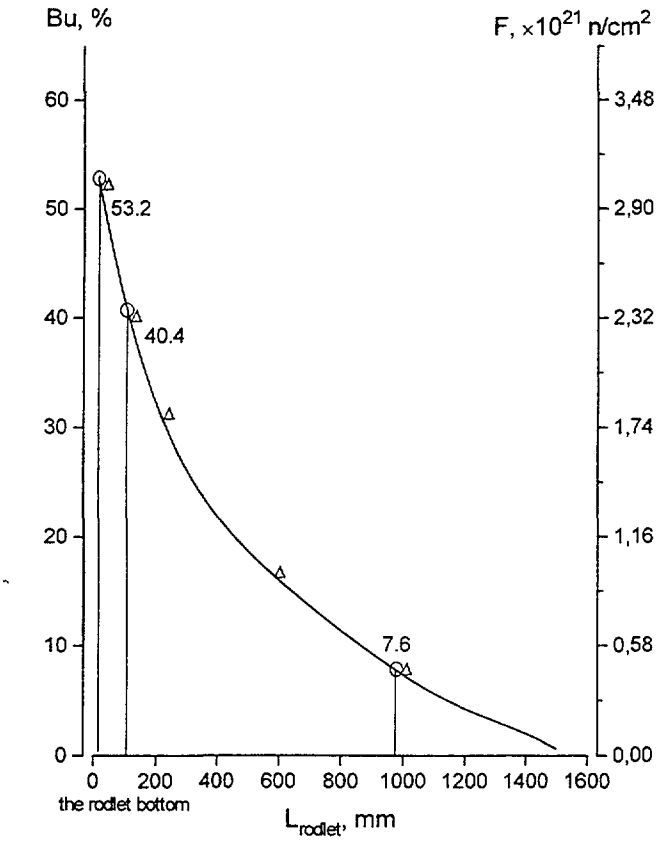

FIG. 1. Distribution of thermal neutron fluence (Δ) and ^{10}B burn-up (O) along the length of a rodlet

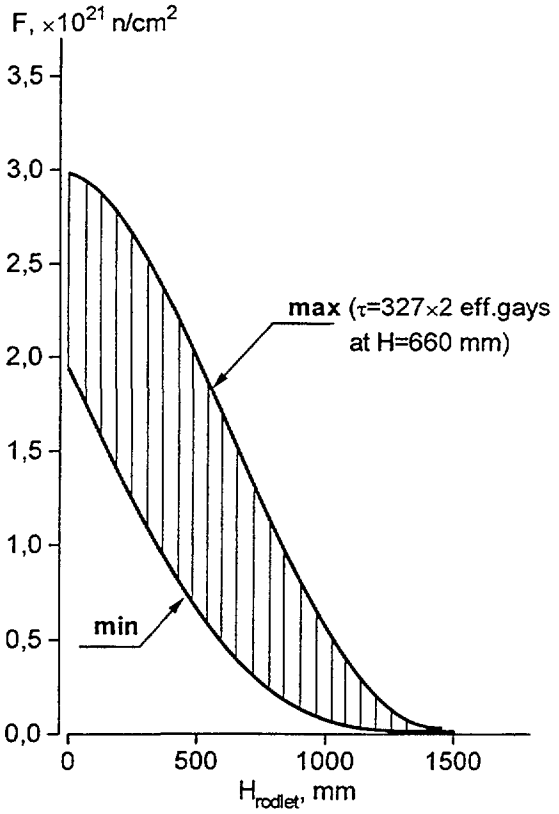

FIG. 2. Thermal neutron fluence on the lower part of a rodlet; operation time in WWER-1000 is 2 years; operation regime is regulation

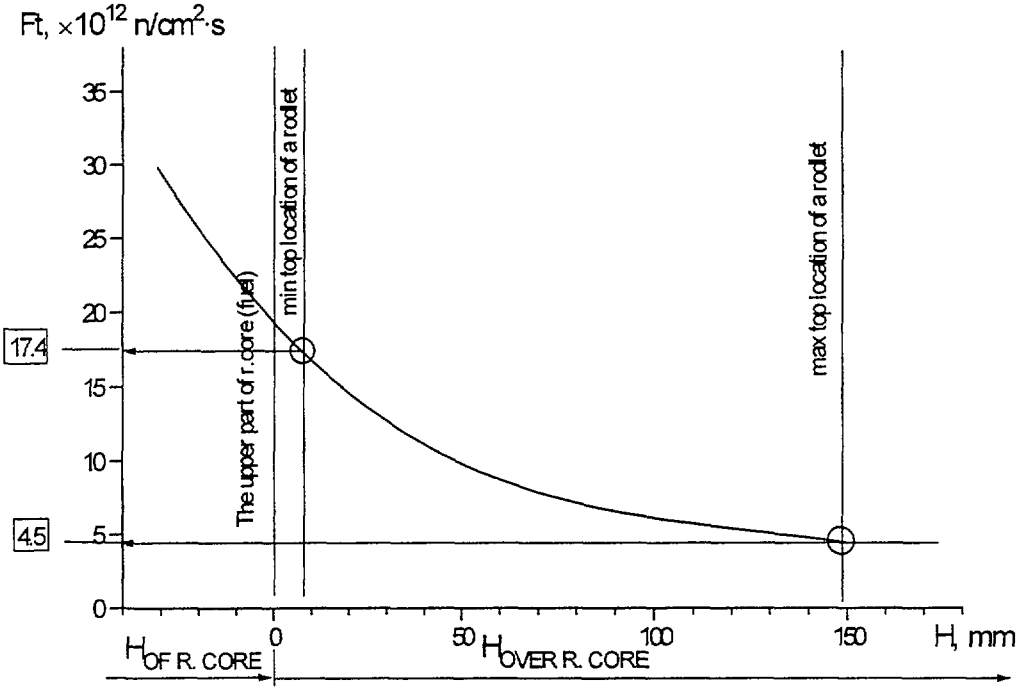

FIG. 3. The density of fast neutron flux (E≥1.11 MeV) in the upper and bottom parts of reactor core of a commercial WWER-1000

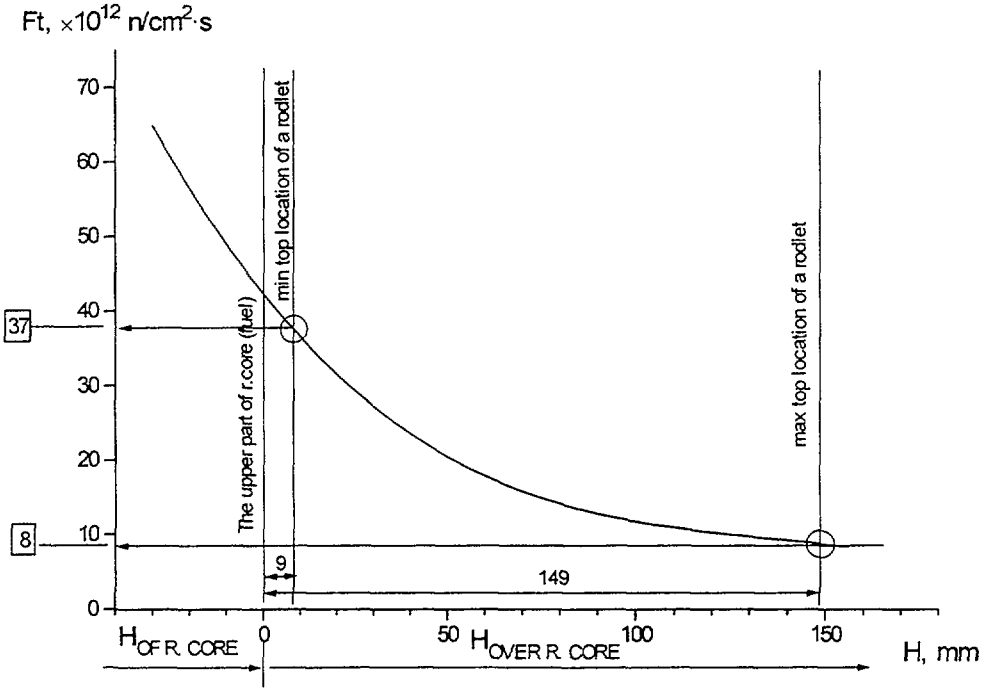

FIG. 4. The density of fast neutron flux (E≥0.111 MeV) in the upper and bottom parts of reactor core of a commercial WWER-1000

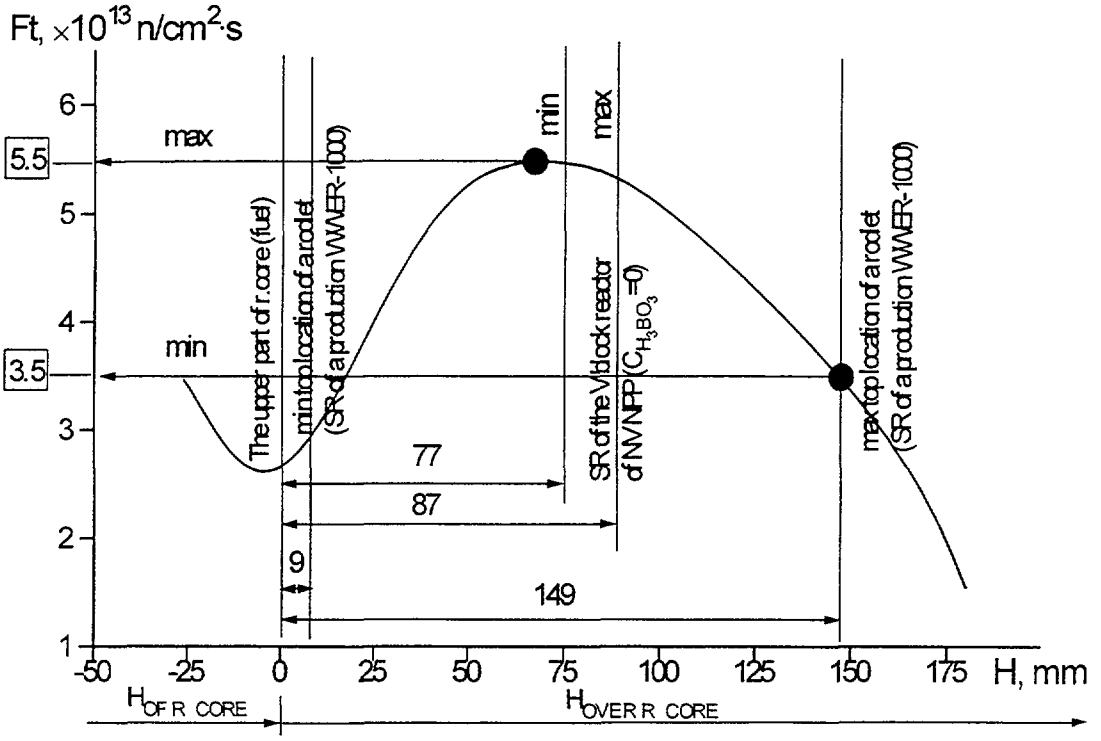

FIG. 5 The density of fast neutron flux (E≥0.111 MeV) in the upper and bottom parts of reactor core of WWER-1000 and the V block reactor of NV NPP

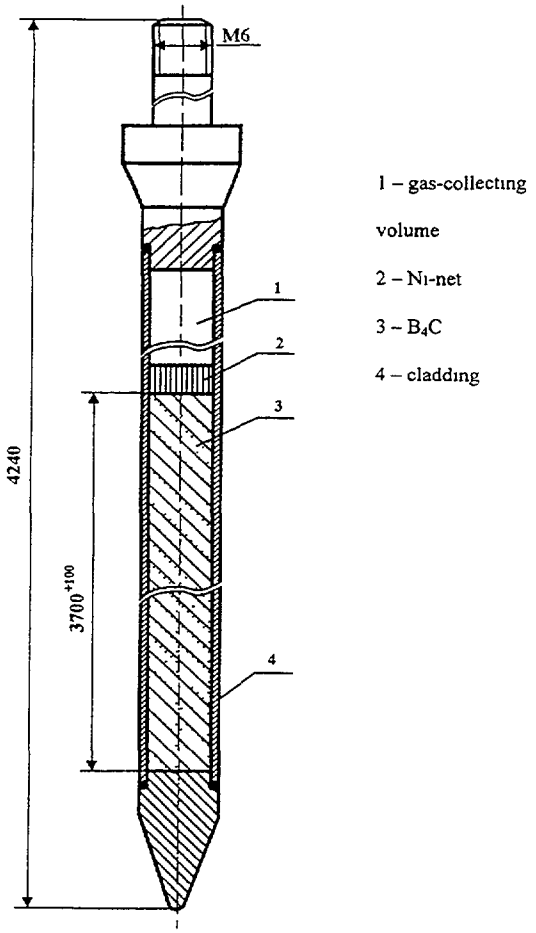

FIG 6. The first generation rodlet of WWER-1000 RCCA

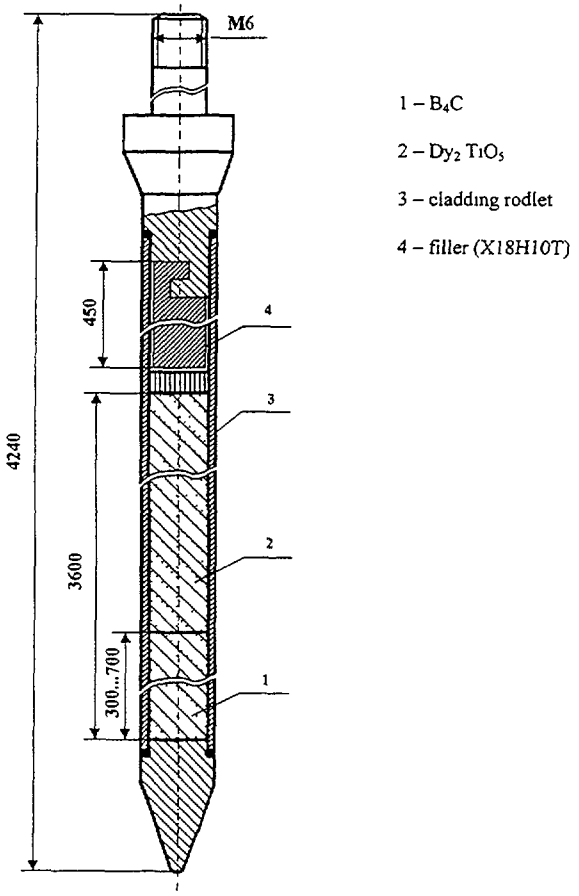

FIG 7. The second generation rodlet of WWER-1000 RCCA

TABLE VII. MAIN SPECIFICATIONS OF WWER-1000 RCCAs

Parameter	Unit	Type			
		CR-71	CR-85	CR-95	CR-97
Total length	mm	4240			
Number of rodlets		16			
Absorber material		Eu_2O_3+Al	B_4C	B_4C [a] $Dy_2O_3 \cdot TiO_2$ [b]	B_4C [a] Hf [b]
Cladding tube material		OX18H10T	OX18H10T	OX18H10T (EP-630V)	EP-630V
Tube external diameter	mm	8.2			
Tube thickness	mm	0.6	0.6	0.6 (0 5)	0.5

[a] upper part [b] bottom part

2. RODLETS REACTOR TESTS AND POST-IRRADIATION RESEARCH

At the rodlets designing of WWER-1000 RCCA rodlet, tests were carried out in the SM-2 reactor and in a WWER-1000 (NPP "Rheinsberg"). The main characteristics of the absorber and cladding materials are given in Table VIII and the main characteristics of the irradiated rodlets in Table-IX. Post-irradiation tests were carried out in the hot cells of the State Scientific Centre of the Russian Federation "Research Institute of Atomic Reactor" (SSC RF RIAR, Dimitrovgrad, RF), the NPP "Rheinsberg" (Rheinsberg, GDR) and the Central Institute of Nuclear Investigation (Dresden, GDR). All designed rodlets had high stability, their shape and dimensions did not change. Swelling of $Dy_2O_3 \cdot TiO_2$, $\Sigma R_2O_3 \cdot TiO_2$ and B_4C pellets were 0.5%, 2 3% and 3.5%, respectively (Table X).

TABLE VIII. MAIN SPECIFICATIONS OF RODLETS IRRADIATED AT NPP "RHEINSBERG" WWER-2

Absorber	1. B_4C powder extruded together with cladding, ρ=1.99 g/cm^3.
	2. B_4C pellets, cold pressing, ρ=1.75 g/cm^3.
	3. $Dy_2O_3 \cdot 2TiO_2$ pellets, hot pressing, ρ=5.49 g/cm^3.
	4. R_2TiO_5 pellets, R=Dy+(5-8 %) Ho, hot pressing, ρ=6 g/cm^3.
	5. Eu_2O_3+Al powder extruded together with cladding, ρ=2 g/cm^3.
	6. Ni – Hf – Sm – In rods, Ni – 70 %, Hf – 10 %, Sm – 10 %, In – 10 %
Cladding	1. X20H40, ∅ 8.0×0.5 mm
	2. 06X18H10T, ∅ 8.2×0.6 mm

TABLE IX. MAIN CHARACTERISTICS OF RODLETS IRRADIATED AT NPP "RHEINSBERG" WWER-2
(F=(2.2-9.1)×10^{21} cm^{-2}, water loop – P=10 MPa, T=270°C)

Characteristic	**Rodlet**					
	B_4C powder	**B_4C pellets**	**$Dy_2O_3 \cdot 2TiO_2$ pellets**	**R_2TiO_2 pellets**	**Eu_2O_3+Al powder**	**Ni-Hf-Sm-In rods**
$\frac{\Delta d}{d}$,% cladding	0	0	0	0	0	0
$\frac{\Delta d}{d}$,% absorber	–	1.35÷3.50	< 0.5	< 2.3	–	–
^{10}B burnup, %	11.8	8.8	–	–	–	–

TABLE X. MAIN CHARACTERISTICS OF RODLETS IRRADIATED AT SM-2 REACTOR
(F=1.7×10^{21} ñm^{-2}, water loop – P=19 MPa, T=350°C)

Characteristic	**Rodlet**				
	Extruded type		**Pellet type**		
Absorber	B_4C	Eu_2O_3+Al	B_4C	$Dy_2O_3 \cdot 2TiO_2$	Ni-Hf-Sm-In
Cladding	X20H40, ∅ 8.0×0.5 mm				
ρ, g/cm^3 (common)	1.93	3.63	1.72	4.85	9.82
ρ, g/cm^3 (absorber)	B – 1.53	Eu – 1.85	B – 1.35	Dy – 2.93	Hf – 0.9 Sm – 0.4 In – 0.4
$\frac{\Delta d}{d}$,% (cladding)	0.5	0	1.5	0	0
He release, cm^3	1.8	0	3.0	0	0
$\frac{\Delta d}{d}$,% (absorber)	0.5	0	3.0	0	0

3. RESORT TESTS OF WWER-1000 RCCA AT NOVOVORONEZH NPP

Two designs of rodlets were selected for the first WWER-1000 of Novovoronezh NPP. They contained $Al+Eu_2O_3$ and B_4C powder accordingly. $Al+Eu_2O_3$ rodlets have a very long life-time (> 20 years) and were replaced because of the following main reasons:

- low efficiency (80% from natural B_4C);
- high cost;
- high radioactive ^{152}Eu and ^{154}Eu isotopes with long half-life (13.4 years and 8.8 years respectively).

Large experience of RCCA operation with natural B_4C powder showed some problems. The life-time is limited, first of all, by ^{10}B burnup (Fig. 8). At a burnup of more than 30-35%, the B_4C powder sinters in a solid column due to high temperature, produces and releases helium and forms lithium (Table XI). At a burnup of 50-55%, the rodlet cladding begins to deform. These conditions are achieved during 2-3 years in regulation regime and 5-8 years in shut-down regime.

Since 1983, test with $Dy_2O_3 \cdot TiO_2$ powder filled RCCAs were started at the Novovoronezh WWER-1000. After 4 operation years in regulation regime, there were no problems. The main results of the post-irradiation investigations are:

- the absence of rodlet shape and dimension changes;
- no swelling of $Dy_2O_3 \cdot TiO_2$;
- no sintering of $Dy_2O_3 \cdot TiO_2$;
- no out-gassing during irradiation;
- $Dy_2O_3 \cdot TiO_2$ powder was freely extracted at the cladding cut;
- low γ-activity of radioactive isotopes with short half-time.

These tests and investigations showed that these RCCAs have a very high resistance to radiation damages. The main defects of this design are the relatively low efficiency (85% from natural B_4C) and burnup of Dy-isotopes (Figs. 9-12).

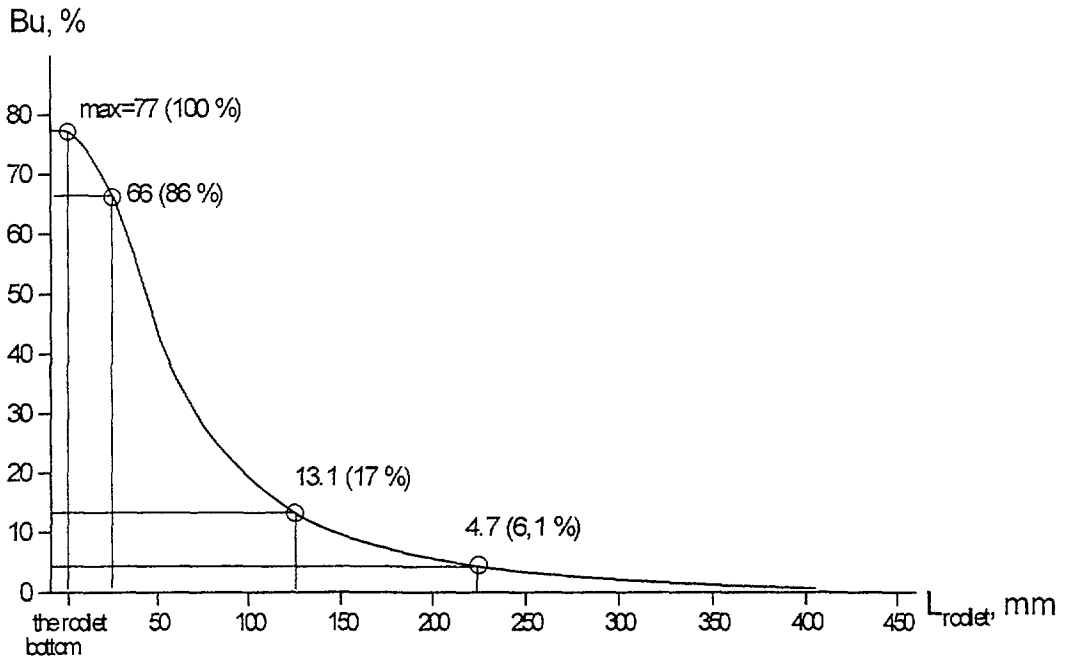

FIG. 8. ^{10}B burnup in B_4C powder of RCCA after irradiation during 7 years in Novovoronezh NPP unit-5

TABLE XI. POST-IRRADIATION EXAMINATION RESULTS OF CONTROL RODS WITH VIBROPACKED B_4C AFTER 2 AND 3 YEARS OPERATION IN POWER CONTROL MODE AT THE NOVOVORONEZH NPP UNIT-5 (WWER-1000)

Irradiation time, eff. year/day	2/491	3/793
Max. neutron fluence, n/cm^2 • thermal • fast (E>0.8 MeV)	 1.5×10^{21} 3.3×10^{21}	 2.4×10^{21} 5.3×10^{21}
Max. boron burn-up at the normal conditions, %	35	41 - 45
Helium release, cm^3	70 - 130	202 - 248
Gas pressure, kg/cm^2 • 20°C • 350°C	 5.0 - 9.3 10.6 - 19.8	 14.4 - 17.7 30.5 - 37.6
Condition of "B_4C-cladding" system in the bottom part	B_4C powder was freely emptied at the cutting of cladding	B_4C was sintered with cladding
Cladding diameter change, %	0	0
Oxide film thickness on the cladding surface, mm	5 - 7	5 - 7
Cladding mechanical properties in the bottom part	good	low plasticity

4. THE SECOND GENERATION OF WWER-1000 RCCA WITH COMPOSED (n, γ)- AND (n, α)-ABSORBER

Since 1995, the Moscow Polimetal Plant began to fabricate a new generation of RCCAs for WWERs-1000 with B_4C powder in the upper part of the rodlets and $Dy_2O_3{\cdot}TiO_2$ powder in the bottom part (300-800 mm) (Fig. 7). The OX18H10T cladding was changed by a Cr-Ni alloy, EP-630U. The mechanical properties of EP-630U are shown in Table XII. This material has a very high plasticity after irradiation and high resistance corrosion cracking (IASCC).

In some rodlets hafnium was used in the bottom part instead of titanate dysprosium. This RCCA design was fabricated for the Ukrainian WWER-1000. The Moscow Polimetal Plant is also designing hafnium rodlets without cladding.

TABLE XII. TYPICAL MECHANICAL PROPERTIES OF EP-630U

Fast neutron fluence (E>0.1 MeV) $\times10^{22}$ cm^{-2}	**Temperature of testing °C**	**Yield stress**	**Tensile strength**	**Elongation %**
0	20 350	520 390	800 700	47±3 42±3
1.12	20 350	660 310	820 620	55±3 49±3
2.7	20 350	750 540	870 660	50±3 41±3
6.8	20 350	820 660	910 680	33±3 28±3

Dy	160	161	162	163	164
Initial contents, %	2.34	19.0	25.0	24.9	29.1
Microscopic absorption section, barn	130	680	240	220	2780

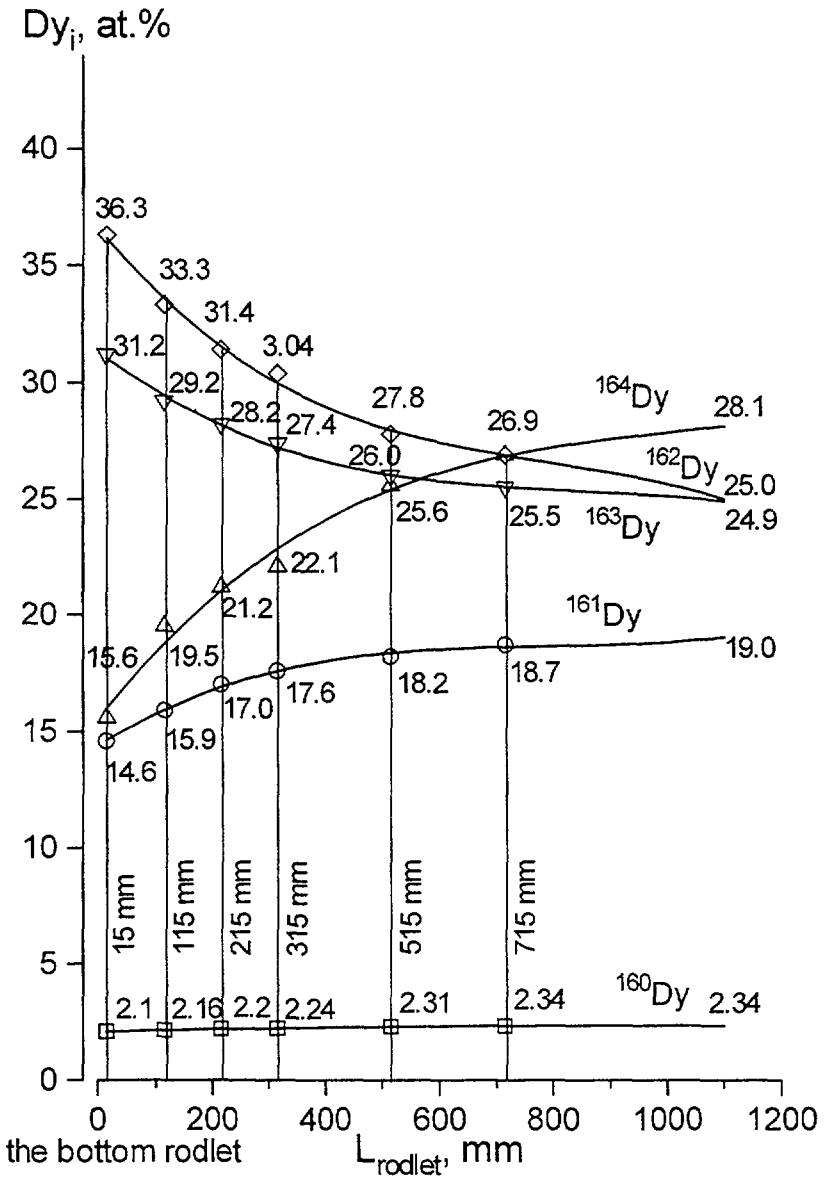

FIG. 9. Change of Dy isotopic composition along a rodlet after irradiation during 3 years in operation group of Novovoronezh NPP unit-5

5. END-OF-LIFE CRITERIA OF WWER-1000 RCCAS

The following new main criteria for the life-time of WWER-1000 RCCAs have been established:

- the efficiency decrease at the end of the operation time should be not more than 10%;
- the rodlets should have shape stability and there should be no cracks;
- the increase of the cladding diameter ($\Delta d/d$) should be not more than 0.01 mm/year (common increase is less than 0.1 mm);

the wear depth should be not more than 0.1 mm.

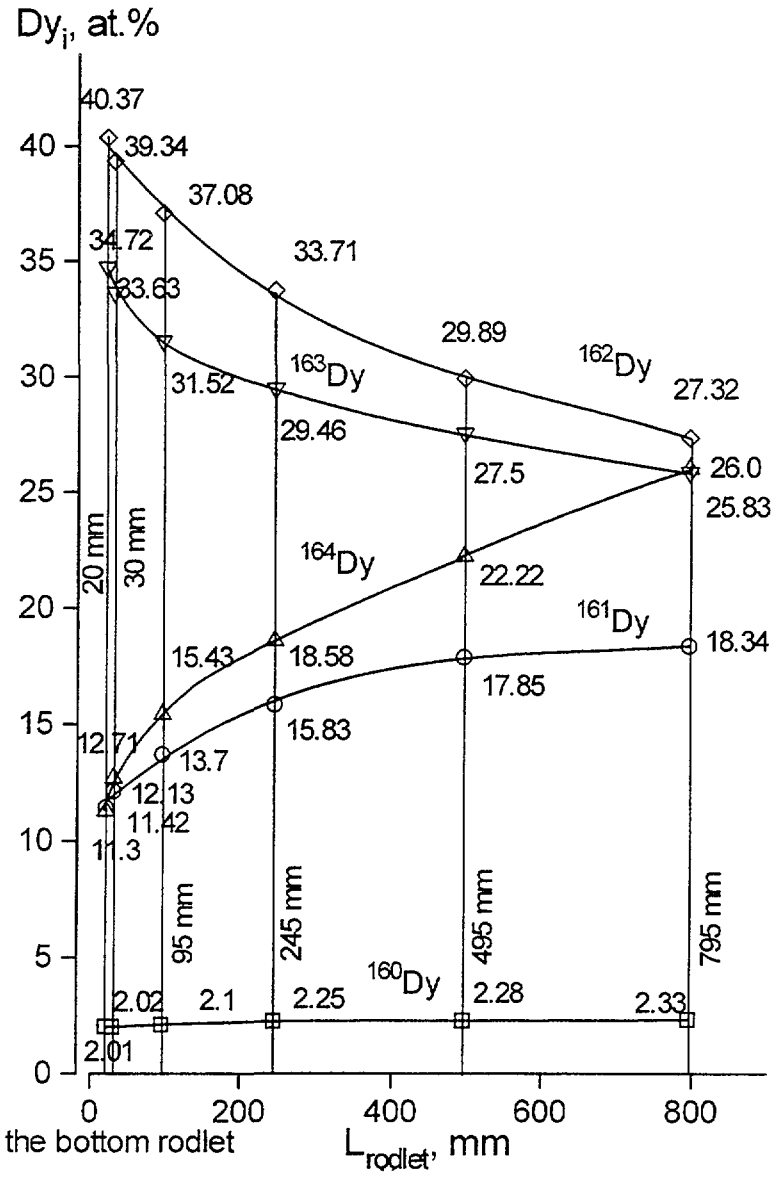

FIG. 10. Change of Dy isotopic composition along a rodlet after irradiation during 4 years in operation group of Novovoronezh NPP unit-5

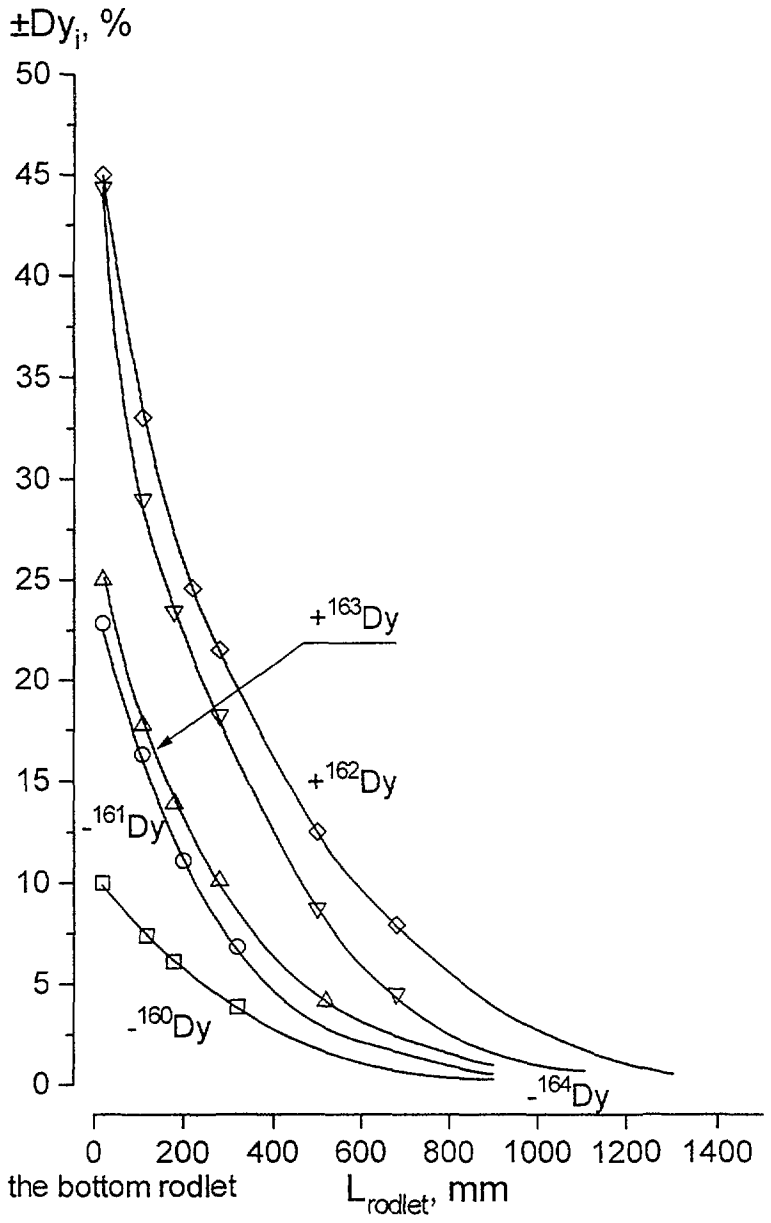

FIG. 11. Distribution of Dy isotopes burnup along the rodlet length after irradiation during 3 years

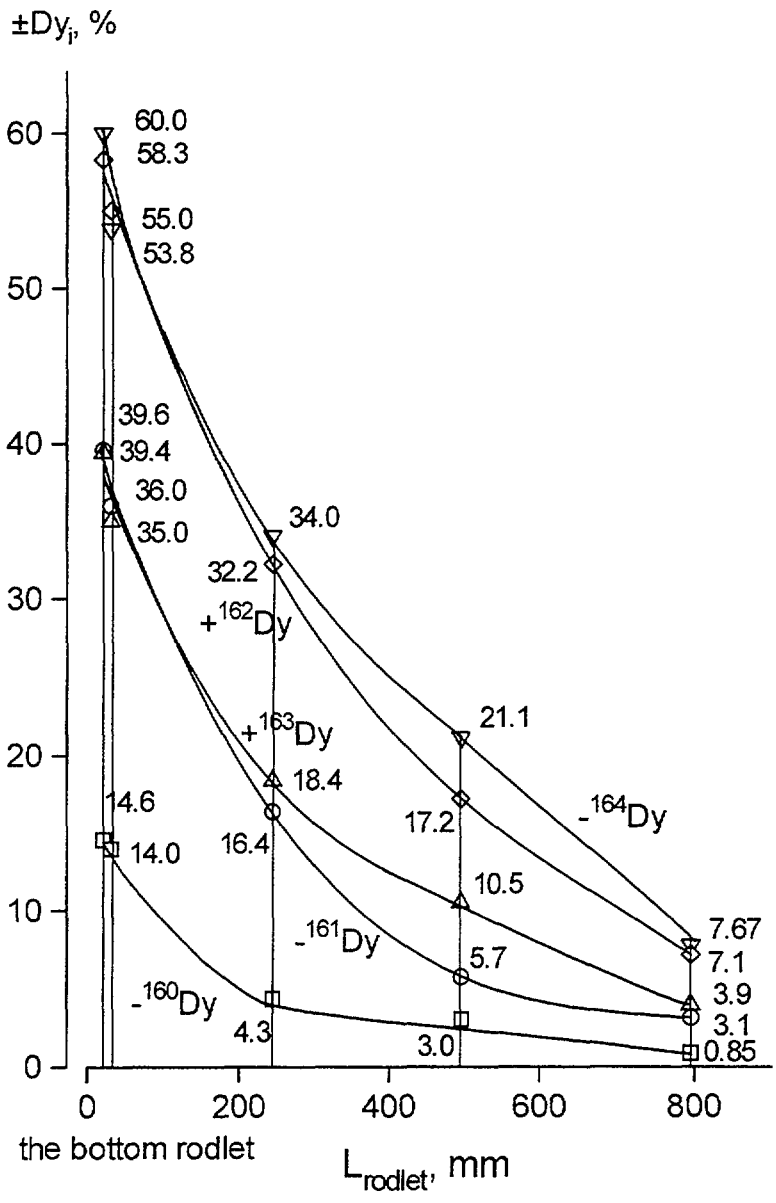

FIG. 12. Distribution of Dy isotopes burnup along the rodlet length after irradiation during 4 years

6. CONCLUSION

The experience gathered with operation of different types of RCCA in commercial WWERs-1000 at NPPs in Russia, Ukraine and Bulgaria did not show failures of components during 200 reactor-years on 17 units.

The new generation of combined RCCAs containing $Dy_2O_3 \cdot TiO_2$ (Hf) and B_4C in EP-630U cladding has a life-time of more then 20 years in accordance with the new end-of-life criteria.

FRAMATOME CONTROL ROD ABSORBER MATERIALS: EXPERIENCE AND DEVELOPMENT

M. MONCHANIN
FRAMATOME Nuclear Fuel,
Lyon

X. THIBAULT
EDF Septen,
Villeurbanne

France

Abstract

Phenomena limiting the lifetime of the RCCAs in PWRs have already been highlighted in the past Wear of the rodlet cladding and swelling in the lower tip end of the cladding arising from the structural changes in the AgInCd absorber material are the two damage mechanisms encountered wear, potentially leading first to cladding perforation secondly further later rod mechanical failure, and swelling, causing clad cracking and rod swelling possibly culminating in RCCA jamming in the fuel assembly guide thimble The upgrades applied to the new generation HARMONI™ RCCAs have provided a solution to the RCCA wear problems and delayed contact between absorber and cladding Better knowledge and prediction of AgInCd swelling in the reactor is necessary, however, as it conditions the lifetime of the RCCAs An extensive analysis programme of this AgInCd absorber was undertaken by FRAMATOME in conjunction with EDF, in order to determine the causes of its out-of-pile and in-reactor changes (creep and metallurgical changes in the material under irradiation), predict its behaviour and make structural improvements limiting its in-reactor changes The outcome of this analysis was the HARMONI™ 2G design featuring an improvement in the Ag-In-Cd material Turning to the 1300 MWe RCCAs containing boron carbide (B_4C), an experiment on the behaviour of this absorber has been conducted in an EDF reactor B_4C was inserted into claddings pre-perforated at the fabrication stage and subjected to corrosion by the reactor coolant The first lessons on the conditions of boron carbide dissolution have been drawn. The improved knowledge in the behaviour of these absorbers in the reactor and the design enhancements made are allowing prediction of a lifetime with respect to swelling which is further extended for new generation HARMONI™ RCCA relative to the first HARMONI generation A development programme on an RCCA design using hafnium absorber is also in progress The use of hafnium would completely rule out swelling in the lower tip end of the RCCAs

1. INTRODUCTION

Few years ago, FRAMATOME has developed a new RCCA product called HARMONI™ which definitively remedies cladding wear and offers a real improvement against swelling. The design of the HARMONI™ RCCA combines ion-nitriding anti-wear treatment of the cladding tube and several modifications such as reduction of absorber diameter along the lower part of each rodlet, helium backfilling of the rodlet and use of AISI 316L cladding for enhancing swelling/cracking resistance.

The accumulated in-reactor experience, under various operating conditions, confirm the adequacy of this design with respect to wear and swelling/cracking resistance. No indication of wear was detected on any rod in the ion-nitrided part on more than 1700 HARMONI™ RCCA in operation to date with approximately two thirds in EDF reactors. The maximum wear experience feedback of an ion-nitrided RCCA is seven 12 month cycles in 900 MWe and 1300 MWe EDF reactors (lead RCCA) and only four cycles regarding the clad swelling. Probably, the swelling/cracking phenomena will condition the lifetime of the HARMONI™ RCCAs design.

The HARMONI™ RCCA was the first result of a large-scale Research and Development programme undertaken to provide a second generation of HARMONI™ RCCA with higher performance regarding the phenomena limiting RCCA lifetime.

After a short recap of the swelling/cracking phenomena, this paper presents the extensive analysis programme of the AgInCd absorber behaviour under irradiation undertaken in conjunction with EDF to :

- understand the creep mechanism;
- determine the effect of AgInCd grain size on creep law;
- predict the AgInCd creep deformation rate;

- understand the swelling mechanism under irradiation (metallurgical changes in the material under irradiation);
- predict the swelling volume rate and diameter increase of AgInCd under irradiation.

The consequences of this programme on the HARMONI™ 2G design, featuring an improvement in the AgInCd material and an increase of RCCA lifetime, are detailed. The improved knowledge of boron carbide (B_4C) behaviour subjected to water corrosion is also an important safety concern. The special experiment conducted in the PALUEL 2 reactor is described and this paper gives an outline on the conditions of boron carbide dissolution.

Lastly, a general idea of the development of a lead hafnium RCCA is presented; the use of hafnium would completely rule out swelling in the lower tip of the RCCAs if it is protected against hydriding and wear.

2. GLOBAL DESCRIPTION OF THE SWELLING/CRACKING PHENOMENA

Wear inspections on RCCA absorber rods have revealed swelling on several rodlets, sometimes combined with longitudinal cracking of the cladding at the bottom of the rodlet. The interpretation of this phenomena which is based on the findings in hot cell investigations of PWR 900 and 1300 MWe rodlets presented below, demonstrates:

- diametral and longitudinal variation of the absorber caused by creep under the effect of applied static and dynamic stresses;
- diametral swelling of AgInCd absorber resulting from irradiation-induced metallurgical changes.

These findings lead to the following conclusions about the cladding strain mechanism:

- at beginning of life, axial shortening of the absorber stack occurs under the effect of thermal creep, caused by the static and dynamic stresses applied to the absorber. The direct outcome of this axial shortening is an increase in absorber diameter and gradual reduction of the absorber-cladding gap. The thermal creep mainly governs the narrowing of absorber-cladding gap and there is progressive closure of this gap. When contact has occurred, creep stresses are not sufficient to cause cladding deformation;
- at the same time, under the effect of irradiation, the chemical composition of AgInCd is modified (transmutation of Ag into Cd and In into Sn) causing the beginning of swelling and occurrence of a second phase as soon as the solubility limits of Sn are overstepped. It leads to deformation of the cladding and to a local stress increase in the cladding;
- cracking occurs along a cladding generation line if the absorber pushing leads to exceed the cladding ductility which is itself linked to irradiation;
- after cracking, absorber creep resumes and is superimposed on irradiation swelling.

Figure 1 illustrates the effect of the absorber diameter evolution versus time but in reality, the phenomenon is more complex and this variation is not fully linear since it is influenced by:

- the operating mode, which influences RCCA insertion and therefore the heat-up and the fluence seen by the materials;
- the spatial distribution of absorber-cladding gap (the off-centering of the absorber in the cladding and the progressive closure of the gap contributes to a drop in temperature);
- the changes in the absorber grain size due to temperature effect;
- the changes in mechanical properties (such as lower thermal conductivity) arising from those in the chemical composition and its structure.

Better knowledge of AgInCd creep and swelling and prediction of creep and swelling rates are however necessary as they condition the lifetime of the RCCAs.

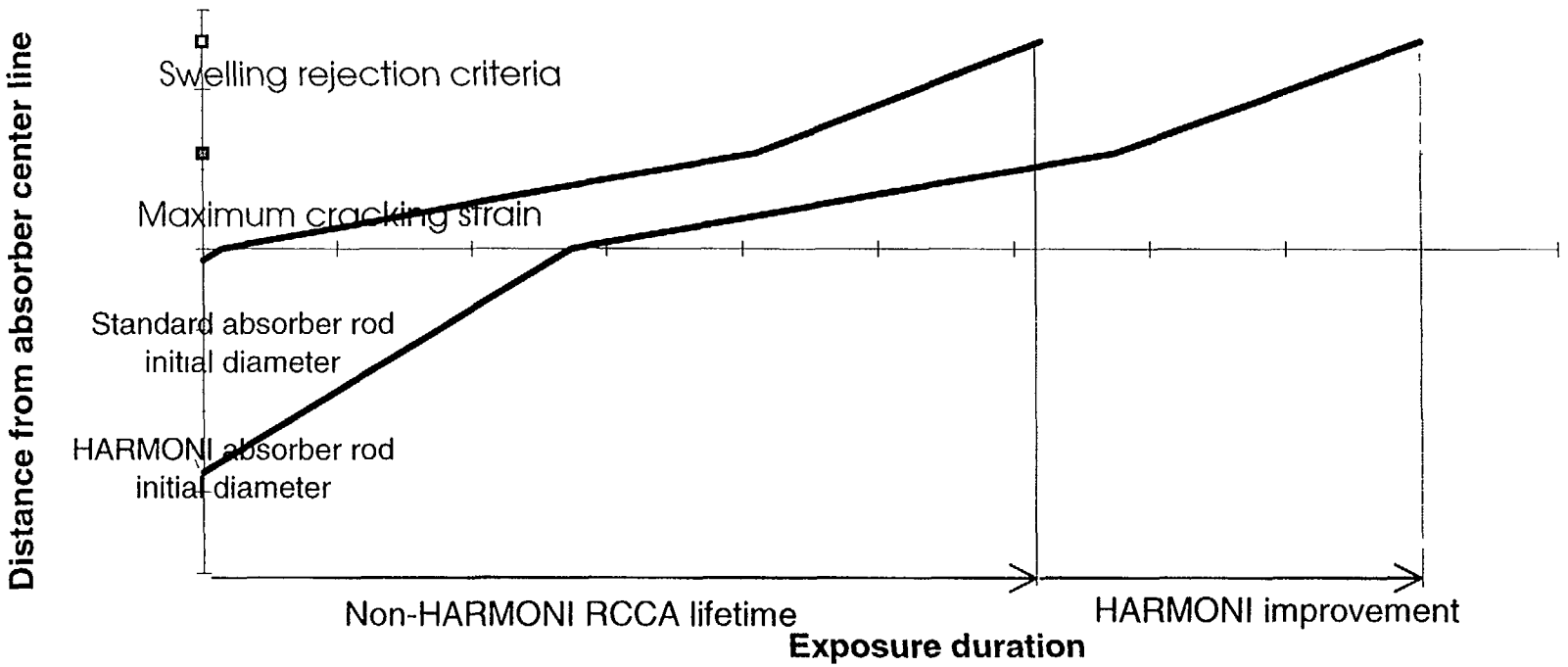

FIG 1 Absorber-clad gap evolution versus time

3. AgInCd CREEP ANALYSIS

To understand AgInCd creep and determine its thermal behaviour and creep, FRAMATOME launched an extensive programme of thermal analysis and creep tests.

3.1. Thermal behaviour of AgInCd absorber

This first phase of the investigation programme was to understand the out of pile behaviour, specially with a constant temperature. When the AgInCd material is subject to high temperature above half melting temperature (Tm/2=260 C) or recrystallization temperature (about 275 C), the grain size increases by recrystallization then the grain coarsening continues. This evolution depends on the initial grain size, the material temperature, the cold working rate and the time.

FRAMATOME ran a series of tests to measure the grain size trend for AgInCd materials which initially had a grain size included between a "small grain" size ASTM 6-8 (between 20 and 45 microns) and a "large grain" size ASTM 0-2 (between 170 and 355 microns) depending on:

- the in-reactor temperature of the material;
- the hold time.

This thermal study showed that there was no significant change of this grain size up to 350 C and for higher temperatures this change is smaller in scale with a large grain material. Grain size measurements on RCCA rodlets irradiated 8 and 9 cycles in reactors have confirmed that there was no major change in the grain size in the out-of-flux zones. As a result, the absorber-cladding gap has the time to be closed by in-reactor creep with a low grain size material before grain coarsening occurs.

3.2. Creep test programme

In order to determine both the thermal creep mechanism and a law of behaviour of the irradiated material versus the key parameters, FRAMATOME has undertaken a large-scale creep test programme on Ag-In-Cd materials in different metallurgical states and covering a wide range of initial grain sizes. 54 creep tests were run on standard specimens machined from fabrication bars for tensile creep tests or from specimens cut directly from fabrication bars for compressive creep tests more representative of the in-service loadings.

The test parameters were considered so as to be representative of the range of actual in-reactor loadings (several temperatures and stresses applied to the absorber drawn from the operating conditions) and with several grain sizes ranging from ASTM $\leq$ 0 to ASTM 8. The measurements taken on a continuous basis consisted of measurement of the axial deflection of the plates applying the force, giving a deformation/time curve and grain size measurements after testing for assessment of material changes. Figure 2 shows an example deformation/time curve obtained by creep with a temperature of 350 C and a stress of 3.5 MPa.

Irrespective of the initial grain size, all the tests show a creep rate trend which can be split up into:

- a period of 0 to 160 - 200h corresponding to primary creep;
- secondary creep at a rate diminishing in steps for test temperatures 350 C.

The grain size measurements confirmed that the secondary creep trend is dependent on the grain size growth during the test.

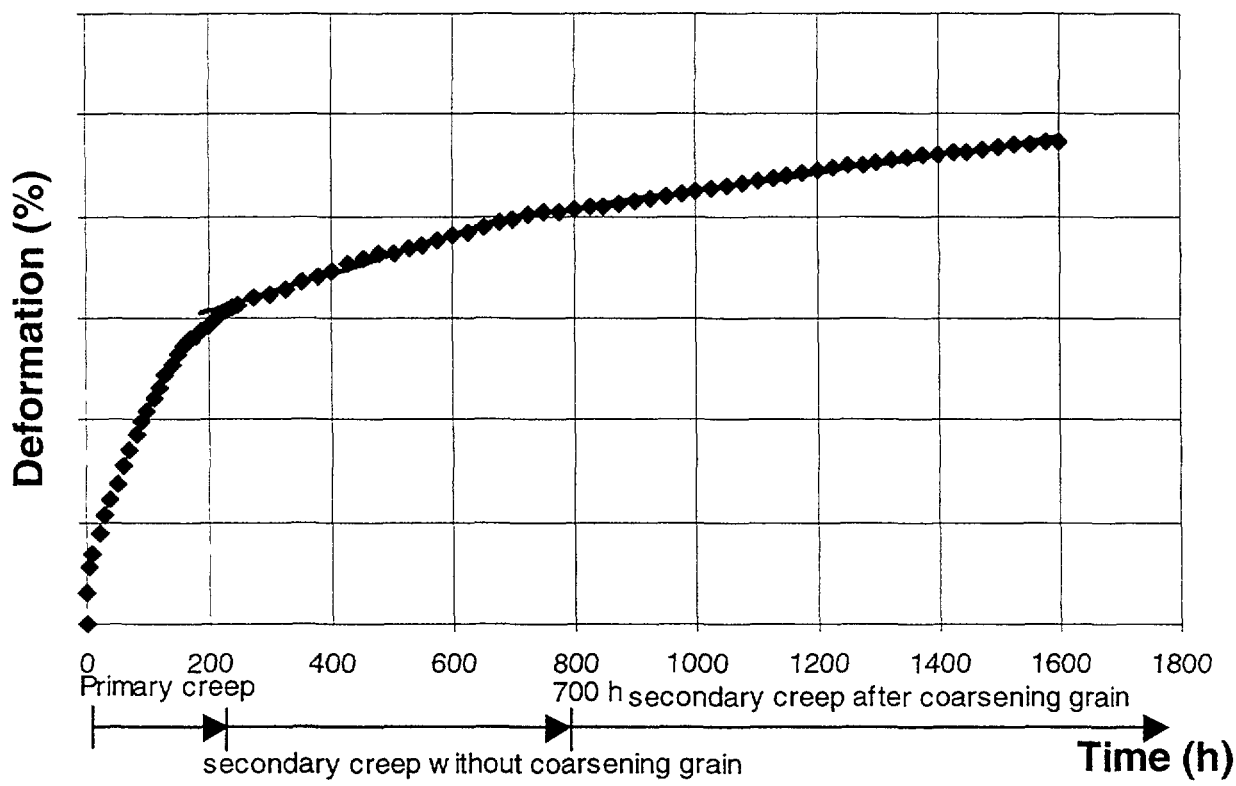

FIG. 2. Typical AgInCd thermal creep

3.3. AgInCd out of pile creep law

As primary creep is short in duration < 200h, only a formula for secondary creep rate $\dot{\varepsilon}$ measured experimentally was sought versus the parameters stress, temperature, grain size and time, in the standard form:

$$\dot{\varepsilon} = K d^{n} \sigma^{m} \exp -\frac{Q}{RT}$$

where:

$\dot{\varepsilon}$: creep rate
K, n, m : constants
d: pre-creep grain size in microns
: stress in MPa
Q: creep activation energy in Joule/mole
R: ideal gas constant
T: temperature in Kelvin.

A simplified way of taking into account grain coarsening was applied by discretizing the law into a short-term law (< 700 h - Figure 2) and a long-term law (> 700 h); the long-term law implicitly allows for growth through coefficients Q and K.

The results show creep rate dependence on stress not constant with the grain size and a creep rate inversely proportional to the initial grain size of the material. The creep activation energy is fully comparable with that of the diffusion of pure silver along the grain boundaries for the short-term law. This activation energy is drastically reduced when the test duration lengthens, showing the effect of grain growth.

3.4. Creep mechanism

The interpretation of the coefficients n, m, Q of the creep laws was performed by comparing them with the creep laws of pure silver in the domain of "high temperature" (> melting point/2) and low-stress. The coefficients obtained for a test duration shorter than 700h correspond to a plastic strain mode controlled by the diffusion of atoms along the grain boundaries (COBLE creep [1]) although Ag-In-Cd is a solid solution with major dilution.

3.5. Consequences

These tests showed that an AgInCd material with large grains (ASTM < 3) drastically reduces the creep rate (Figure 3) relative to the material previously used (ASTM 6-8) by a factor 5 to 10 and afterwards extends the absorber/cladding gap closure time in the period during which absorber creep predominates over irradiation-induced swelling.

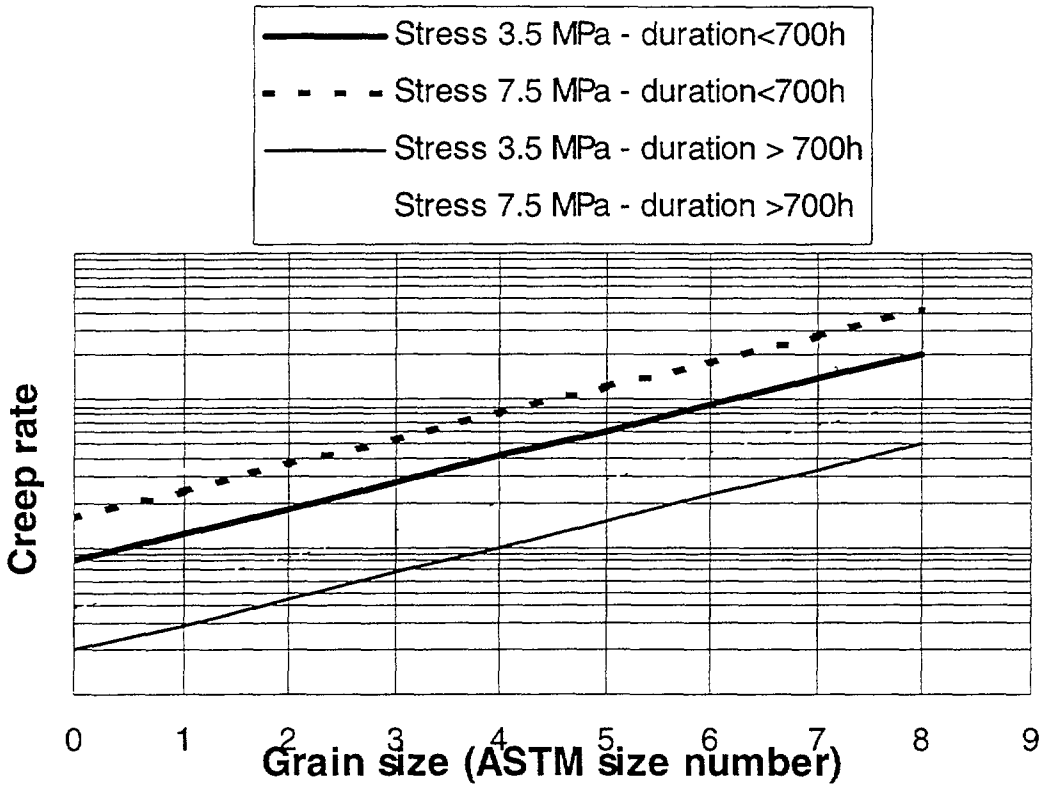

FIG 3 Grain size effect on creep rate

4. AgInCd SWELLING ANALYSIS

4.1. Examinations of irradiated AgInCd bars

To determine the swelling mechanism of absorber rods and to model the swelling kinetics, FRAMATOME and EDF co-operated in a hot cell expert assessment programme using rodlets from 900 and 1300 MWe reactors.

This programme measured the diametral swelling and absorber density trend in three 900 MWe RCCAs and four 1300 MWe RCCAs from different banks (control, shutdown, power compensation), making eleven swollen rodlets. It was supplemented by a programme characterizing the structure and the modifications made under irradiation [2] with the aid of optical microscopy, microanalysis, metallographs and X ray diffraction measurements (performed by the CEA), especially on one AgInCd bar irradiated 8 cycles in reactor.

These examinations showed in the first place that the density or volumetric swelling of the absorber changes linearly with irradiation up to a given fluence (Figure 4). Figure 4 also shows that beyond this limit fluence, the change remains linear but with a steeper slope.

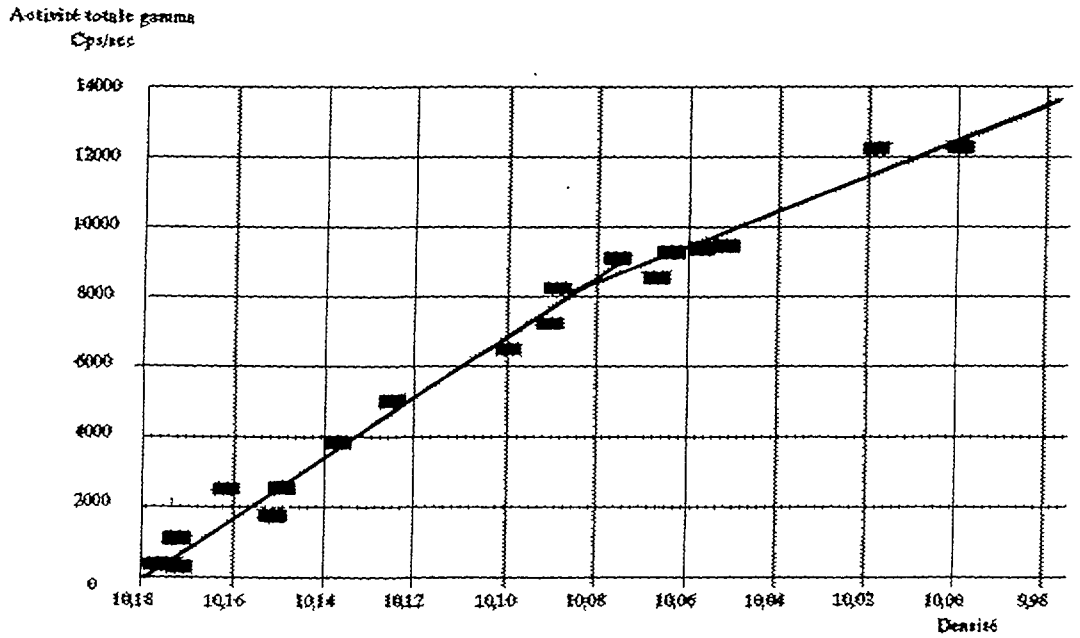

FIG. 4. Gamma rod activity versus AgInCd density

4.2. Swelling mechanism

The metallographs performed on a few samples confirm this difference in behaviour:

- up to a dose limit, the microstructure is principally single-phase face-centred cubic (fcc). During transmutations from Ag into Cd and from In into Sn, the atoms created are more voluminous and are soluble in the fcc network so there is swelling by a transmutation effect;
- beyond this dose, the solubility limit of the elements Cd, In, Sn is exceeded. There is occurrence of a close-packed hexagonal phase (hcp) more voluminous than the initial fcc phase. The structure is then principally two-phase (fcc + hcp) but at the periphery only the hcp phase can be obtained [2].

The additional analyses [2] determined a solubility limit on the order of 1.7 to 2 at.% tin in the fcc phase and a minimum 4 at.% tin in the hcp phase.

However, on a sample from a bar temporarily subjected to high flux, the X ray analyses evidenced the presence of singular zones highly enriched in tin up to 34%. These small-sized zones seem localized at the junction points of second-phase domains. This existence cannot be explained by global oversaturation of the material in tin, as the fluence received is not sufficiently high to cause such an enrichment and the micrographs reveal little hcp phase. These findings show the importance of the role of transmutations in the material structural changes and justified the need to closely investigate the AgInCd quarternary system to:

- gain greater insight into the phases forming under irradiation;
- predict the proportion of each of the phases in the material;
- simulate the development of the concentration profiles of the elements within the two phases.

This led to a joint FRAMATOME/CEA research programme as presented in 4.4. The aim of this programme is to simulate the growth of a hcp phase precipitate on an fcc phase grain boundary in the absorber and thus to finally predict the irradiation-induced swelling in the hcp phase. The swelling in the fcc phase is deduced by the Zen law [3] using the effective atomic volumes of the elements.

4.3. Swelling modelling

Based on the density measurements taken during examinations, a macroscopic model of AgInCd irradiation swelling was built, with allowance for the accelerating effect arising from the occurrence of the hcp second phase. For each examined irradiated RCCA, the volume variations along the absorber (calculated from the density measurements) were correlated with a distribution of fluences calculated on this absorber and adjusted to the values obtained from the gamma activities measured on two RCCAs. A fine fluence calculation was also carried out on a reference RCCA, for which all the insertions were recorded during the cycle.

In the case of RCCAs from temperature control bank R, the overall calculation method overpredicts by about 25% the value estimated by the measured activities. By refining the method with the reference RCCA whose every insertion is known, the accuracy of the fluence calculation improves. Should the absorber be inserted into the fuel stack, the uncertainty obtained does not exceed 11% even for an RCCA frequently in motion (power compensation bank G). The density measurement accuracy leads to an uncertainty on the volume variation measurement on the order of 10 to 20%.

A two-slope swelling model was thus determined by means of linear regressions for the experimental points lying on each side of the hcp occurrence fluence. Figure 5 shows the nominal law obtained, as defined in the neutron energy range of 0.625 - 3 eV corresponding to indium -> tin transmutations, with the experimental points. Good agreement is obtained and minimum and maximum laws bounding swelling were determined.

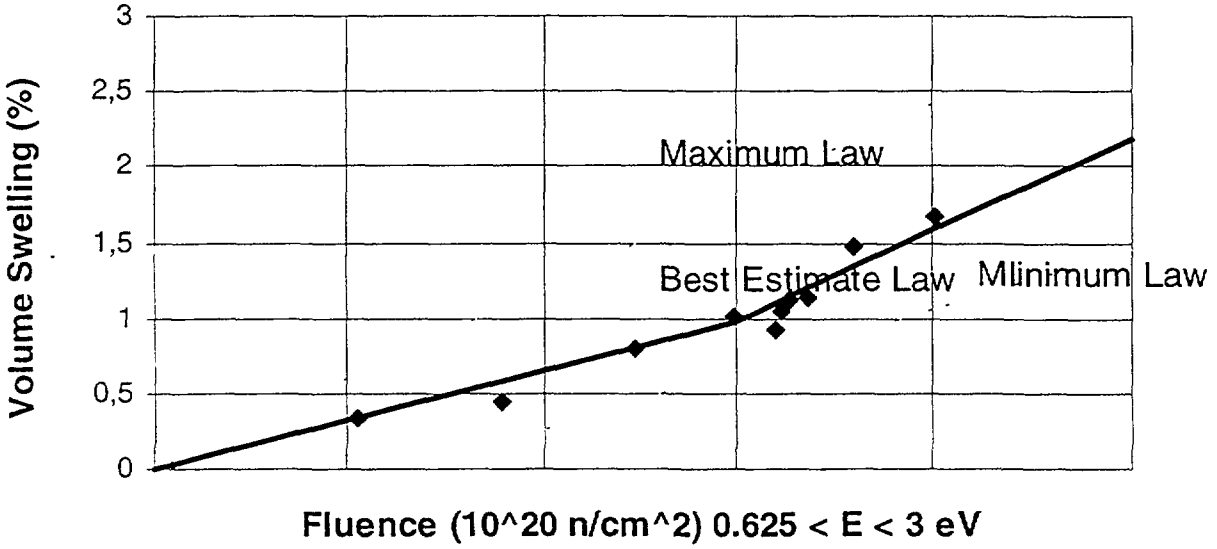

FIG 5. Swelling rate versus fluence

Application to the swelling calculation was performed by considering an isotropic swelling of the absorber as long as there is no contact with the cladding. Processing of examination results for cracked rodlets with hard contact of the absorber and cladding (absorber bar diameter change and density measurements) leads in this case to non-isotropic swelling

An evaluation of the increase in diameter of the absorber during an annual cycle was conducted with this law and compared with the experience feedback from cladding average swelling measurements determined by UT inspection. The calculated value of 21 microns/cycle for bank R is consistent with the average swelling value (19 microns/cycle) obtained for the set of measured RCCAs ; i.e more than 500 RCCAs.

The combined use of these absorber creep and swelling laws in one absorber rod thermal-mechanical computation software programme, allows prediction of the pre-contact time of the absorber and the change in clad swelling after hard contact with the absorber.

4.4. Modelling of AgInCd composition under irradiation

A wide-ranging research programme was run to understand and model the phase transformation processes in the absorber. In particular, the change under the effect of the transmutations of the concentration profiles within the two phases as soon as an hcp phase precipitate exists and the determination of the proportion of each of the phases allows evaluation of the quaternary absorber material swelling. The laws of variation of atomic volume with chemical composition in both phases was also determined from representative synthetic alloys.

For this purpose, this research relied upon two preliminary studies:

- study of the growth of a precipitate under the effect of the transmutations in the simple case of a binary alloy Ag-Cd [4];
- quantitative modelling of the phenomena of diffusion through the quarternary alloy for both phases [5].

These studies showed that the enrichment in transmuted element at the centre of the mother phase and of the precipitate occurs to the detriment of the growth of the latter as soon as the transmutation rate (neutron flux) is large compared with the mobility of the atoms. It is all the larger when the flux is high and the diffusion coefficients are small. This can give excessive oversaturation in elements at the core of the precipitate, as already experienced for tin.

The effect of increasing the absorber grain size has been looked at. As a result of the diffusion coefficients in the hcp phase which are greater by about 10 than those obtained in the fcc phase, there is no effect of increasing grain size on the second phase precipitation.

4.5. Consequences

Based on the knowledge of the neutron flux and of the axial force exerted on the absorber, the use of the full-scale swelling model in conjunction with the thermal creep model makes it possible to predict changes in absorber/cladding gap closure and subsequent clad swelling. The favourable effect of the increase in grain size on creep is maintained under irradiation. Changes in the chemical composition of the absorber were also evidenced, with the aim of supplying if necessary a further lifetime gain by delaying the occurrence of the second phase.

5. NEW HARMONI™ 2G RCCA

5.1. Description

The new RCCA generation HARMONI™ 2G incorporates an AgInCd absorber material with modified grain size. A new grain size value (ASTM < 3), i.e. a grain diameter greater than 120 microns (instead of 30 microns for the standard material) is thus obtained and it is verified, through a controlled fabrication process, that there will be no recrystallization risk during operation. The HARMONI™ 2G RCCA presents all the benefits of the HARMONI RCCA and even more regarding the AgInCd deformation which leads to an increasing of lifetime.

5.2. Absorber rod diameter evolution

The principle of Figure 1 can be retained to measure the characteristic RCCA lifetime gain supplied relative to the former design with "small grain" absorber (Figure 6) The decrease in absorber thermal creep through the increase in its grain size provides a significant reduction in the absorber/cladding gap closure kinetics at BOL at the time when the stresses and temperatures are high. The use of "large grains" has no effect on the swelling under irradiation or on the other properties and characteristics of the absorber.

During lifetime and before hard contact with the cladding, this advantage tends to diminish since the temperatures and stresses remain higher with the large grain material because of the slower change in the bar dimensions. This effect has been analyzed and is negligible compared to the gain supplied by the increase in grain size (Figure 6). After the phase of hard contact with the cladding, the time gain is therefore kept for the swelling phases (Figure 6).

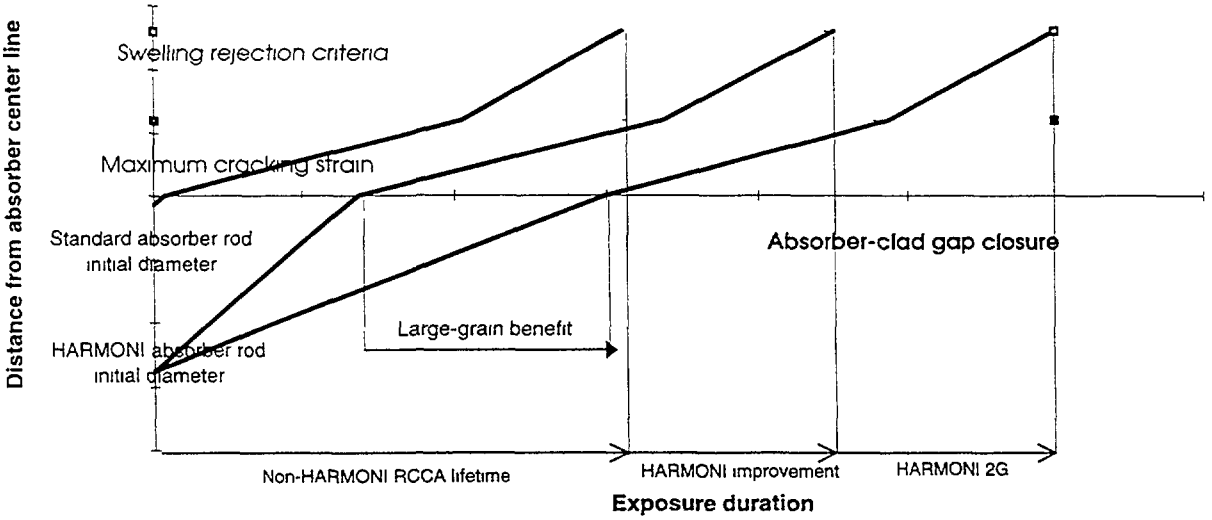

FIG 6 Grain size effect on absorber-clad gap evolution

6. BORON CARBIDE BEHAVIOUR UNDER WATER CORROSION

6.1. Experiment facility

All the experiments performed to characterize the leaching behaviour of B_4C, used in conjunction with AgInCd for the black 1300 MWe RCCAs, have been conducted in autoclave non representative of in-reactor water corrosion or with Al_2O_3- B_4C pellets different from the 1300 MWe design [6], EDF and FRAMATOME decided to launch an in-reactor experiment with two purpose-built RCCAs.

The experiment was conducted with B_4C inserted into cladding tubes pre-perforated at the fabrication stage for a few rods of two RCCAs in order to represent through-wall wear in reactor (guide card location or bottom tip wear). These two RCCAs have been inserted in PALUEL 2 plant in R bank (subjected to a constant neutron flux) The first (named A) was withdrawn after one cycle and the second (named B) after three cycles .

The RCCA A uses two pre-perforated rods, the first with an oblong hole of 3 mm width and 10 mm long positioned at the bottom of the B_4C stack made to look like guide card wear and the second rod with a 3 mm diameter hole at the bottom of the rod (25 mm above the bottom end of the cladding tube) to simulate a tip wear. The RCCA B uses the same bottom pre-perforated rod as the A one.

These purpose-built rods are designed with a special AgInCd bar of 492 mm height in place of the 1016 mm classical bar. This was performed to obtain a high B^{10} depletion rate (approximately 4.10^{20} destruction per cm^3 for a twelve month cycle). These rods have been characterized at the fabrication stage like pilot rods located symmetrically to those on each RCCAs and a complete recording of the RCCAs axial positions was carried out.

6.2. Main results

The non destructive Eddy Current inspection of RCCA A at the end of the first cycle showed a drop of the spring location and a B_4C loss of 500 mm height was measured for the perforated oblong hole rod. For the other one, no B_4C column evolution was detected.

The hot cells examinations on RCCA A confirmed this assessment and showed the damages:

a) perforated oblong rod

- loss of 523 mm of the B_4C stack;
- peripheral degradation of some B_4C pellets (decrease of the limited to 7 % of the pellets stack;

b) bottom holed - rod

- no height loss of the B_4C stack;
- peripheral degradation of 10% of the stack..

The experiment will continue in 1999 with the hot cells examinations on the RCCA B after three cycles.

6.3. Consequences

These in-reactor results show that leaching and erosion during the RCCA stepping together with the primary water media have partially affected B_4C pellets subjected to :

- a sufficient B-10 depletion (above a threshold);
- a water circulation around the pellet.

All the 1300 MWe black RCCAs are implemented with the classical 1016 mm AgInCd bar, so the B_4C pellets of RCCAs shutdown bank rods are out of irradiation or like the R bank received a small burn-up. There would be no loss of B_4C height for the usual RCCAs because the B_4C stack dimension of these classical RCCAs is in fact 524 mm greater than the tested rod stack. A prolonged irradiation exposure of bank R RCCAs could involve a small peripheral degradation of the first B_4C pellets without harmful consequence on the RCCA reactivity feedback.

7. HAFNIUM RCCA DEVELOPMENT

The design enhancements made in the HARMONI™ 2G RCCA may allow a further increase in lifetime with respect to swelling but the swelling phenomena are not ruled out. This new design allows a less frequent control of the RCCAs due to the significant reduction of the absorber-clad closure rate. The swelling lifetime of such a RCCA is not yet equivalent to the potential wear lifetime.

The hafnium absorber has a neutron worth equivalent to the AgInCd one with identical dimensions and benefit from several advantages :

- no swelling under irradiation;
- no creep behaviour (melting temperature near 2200 C);

- acceptable behaviour under accident conditions due to its high melting temperature;
- constant neutron worth during their lifetime;
- possibility to use hafnium rod without clad (owing to the fact of its excellent behaviour under primary water corrosion) and then to extend the global RCCA reactivity feedback.

FRAMATOME has decided to design hafnium RCCAs. Demonstration of new hafnium RCCAs in reactor will be implemented in EDF reactor.

8. CONCLUSION

The better knowledge of the behaviour of the absorbers present in the in-reactor designs at this time and the improvements made by the new HARMONI™ 2G generation are allowing an extension of RCCA lifetime with respect to the swelling phenomenon. The modelling of the phenomena and its comparison with experience feedback will make it possible to offer a better prediction of this swelling. This enables the RCCA maintenance strategy to be adapted and the potential risks arising from unpredicted RCCA swelling to be limited. Analysis of the clad perforation risk in the presence of B_4C also makes it possible indirectly to extend the lifetime of the RCCAs of previous designs (possibility of accepting perforation).

The use of hafnium to rule out the swelling phenomenon and to offer a substantially longer lifetime is being experimentally investigated.

REFERENCES

[1] ASHBY, M.F., A first report on deformation-mechanism maps, Acta Metallurgica, vol 20, (1972) 887.

[2] BOURGOIN, J., COUVREUR, F., GOSSET, D., DEFOORT, F., MONCHANIN, M., THIBAULT, X., The behaviour of control rod absorber under irradiation, paper proposed to Journal of Nuclear Materials.

[3] MASSALSKI, T.B., KING, H.W., Alloy phases of the noble metals, Progress in Materials Sciences, 10,1 (1963).

[4] DESGRANGES, C., DEFOORT, F., POISSONNET, S., MARTIN, G., Interdiffusion in concentrated quaternary AgInCd alloys:modelling and measurements, Defect and Diffusion Science Forum, 143-147 (1997) 603.

[5] DESGRANGES, C., MARTIN, G., DEFOORT, F., Microstructural kinetics in alloys undergoing transmutations - Application to AIC neutron absorbers, Materials Research Society Symp., Proc., (1997) 439.

[6] EPRI NP 4533LD, Research Project X101-6, Behavior of irradiated B_4C, (1986).

MEASURE OF ^{11}B, ^{10}B AND ^{7}L CONCENTRATIONS IN CONTROL RODS USING THE NUCLEAR MICROPROBE TECHNIQUE

XA0053642

D. SIMEONE, X. DESCHANELS, P. HERTER
Laboratoire d'Etudes des Matériaux Absorbants,
CEA Saclay,
Gif-sur-Yvette,
France

Abstract

The nuclear microprobe technique has been used to measure ^{10}B and ^{7}Li profiles after thermal neutron irradiation of a boron carbide absorber. The measured ^{10}B distribution along the pellet radius has been used to calculate the spatial ^{7}Li distribution with the hypothesis of no lithium migration. This result shows a discrepancy with the ^{7}Li measured distribution, indicating that up to 40% of the lithium may migrate out of the B_4C pellet.

1. INTRODUCTION

Under a neutron irradiation the $^{10}B(n,\alpha)^{7}Li$ reaction induces swelling of the boron carbide pellet [1-3]. In order to investigate a possible migration of ^{7}Li atoms out of the sample, the ^{10}boron, ^{11}boron and the ^{7}lithium concentration profiles have been measured by a technique using different nuclear reactions at the Pierre Süe Laboratory Microprobe Facility (CEA/Saclay).

2. DESCRIPTION OF THE SAMPLE ANALYSED BY THE NUCLEAR MICROPROBE

Under thermal neutron irradiation and for a mean rate of capture of 20×10^{20} capt/cm^3, usual boron carbide is partially fragmented near the surface of the pellet because of the high level of transmutation of ^{10}B in this area. To avoid measurement difficulties near the surface, a composite material constituted of B_4C fine powder (average diameter 2 μm) and an organic resin elaborated at 1000°C has been used. The porosity is nearly 25 % the most of it being open porosity. From a microstructure point of view, this material is composed of micrometric B_4C particles embedded in a carbonised resin. Some impurities like Mg and Si have been detected by a chemical analysis. This material had an initial ^{10}B enrichment corresponding to natural boron. The material obtained conserves its integrity after an irradiation at 20×10^{20} capt/cm^3.

2.1. Sample irradiation

The sample was irradiated inside a steel clad filled with ^{4}He. Two thermocouples measured the temperature on the clad's surface of the sample during the irradiation. This temperature was about 593 K. The irradiation lasted 120 days. The thermal flux was about 3×10^{12} n/cm^2/s and the fast neutron flux (> 1 MeV) was about 1×10^{14} n/cm^2/s. During the irradiation, ^{10}B is transmuted in ^{7}Li according to $^{10}B(n,\alpha)^{7}Li$. But a part of the ^{7}Li is transmuted into ^{3}H:

$$^{7}Li + {}^{1}n \rightarrow {}^{4}He + {}^{3}H + {}^{1}n'$$

This nuclear reaction occurs only with energetic neutrons (E_n> 2.8 MeV). The cross section of this nuclear reaction is about 0.4 barns. Some calculations have been done to estimate the ^{7}Li burn-up. This value is maximum at the periphery of the pellet and its value is about 10^{16} atoms of tritium per cm^3, which is about four orders of magnitude smaller than the value of the ^{7}Li at the same position. Thus the ^{7}Li burn-up can be considered as negligible.

2.2. Sample preparation

The preparation of a sample for the experiment, and more especially its polishing was difficult because of the high level of porosity which resulted in the pulling-out of many grains. For this reason, the pellet was mounted under vacuum in an epoxy resin and polished with diamond abrasive powder.

3. THE MICROPROBE EXPERIMENT

During a neutron irradiation, ^{10}B is transmuted into ^{7}Li and ^{4}He according to the reaction:

$$^{10}B + {}^{1}n \rightarrow {}^{7}Li\ (0.83\ \text{MeV}) + {}^{4}He\ (1.48\ \text{MeV}) \quad (1)$$

The recoil ranges of ^{4}He and ^{7}Li inside the pellet have been calculated by TRIM-91. These ranges are about 1.7 μm for the ^{7}Li atoms, 3.34 μm for the ^{4}He atoms and allows to conclude that ^{7}Li and ^{10}B profiles are only induced by the neutron absorption self-shielding inside the pellet. Pollard *et al* [4] have already shown ^{7}Li profiles of pellets irradiated in a fast reactors using the nuclear reaction $^{7}Li(p,\alpha)\alpha$. We have carried out a similar work using other and different nuclear reactions with boron carbide pellets irradiated in a thermal neutron flux.

3.1. Determination of ^{10}B and ^{7}Li production profiles

During a neutron irradiation, the self-shielding of the ^{10}B induces a depletion of the ^{10}B concentration along the radius of the pellet. The goal of this study is to estimate this depletion Na, $Na = N(^{10}B,t=0) - N(^{10}B,t_{irr})$, from the 10-boron measured profile using a proton beam. The number of photons detected depends on the concentration of the elements (^{10}B, ^{11}B, ^{7}Li) analysed according to the equation (2):

$$N_\gamma = k\, N_p N(X,x,t_{irr}) \int_{Es}^{E_f} \frac{d\sigma}{d\Omega}(E)\, \frac{dE}{\left(\frac{dE}{dx}\right)} \quad (2)$$

X : studied element (^{7}Li, ^{10}B or ^{11}B)
$N\gamma$: number of collected photons.
N_p : number of incident protons
$N(X,x,t_{irr})$: number of target per volume unit at the iradiation duration t_{irr} and at the reduced abscissa x.
k : numeric factor depending of the geometry and the efficiency of the detector

$d\sigma/d\Omega$: cross section for the reaction considered
dE/dx : stopping power of the matrix inside the pellet
E_f : beam energy (3.2 MeV).
E_s : cut off energy of the nuclear reaction.

The calculation of the stopping power of the matrix was done along the surface of the sample for the estimated concentration of ^{7}Li, ^{10}B and carbon using the Ziegler and Bierzack formulae [5] and the Bragg's rule. The value of the stopping power of this irradiated pellet does not differ by more than 0.5% from the stopping power of a matrix estimated with ^{10}B and carbon only. This last value of the stopping power has been used to compute dE/dx with a good accuracy in the B_4C. Under this assumption it is possible to simplify Eq. (2) to quantify the ratio $(^{10}N_B/^{11}N_B)^*$ for the sample analysed. Then the ratio $(^{10}N_B/^{11}N_B)^*$ in the irradiated pellet is given by the following relation :

$$(^{10}N_B/^{11}N_B)^* = (^{10}N_B/^{11}N_B) \times (^{10}N_\gamma/^{11}N_\gamma)^* \times (^{11}N_\gamma/^{10}N_\gamma) \quad (3)$$

The star points out data after the irradiation in the nuclear reactor.

This formula allows to obtain the ^{10}B ratio value using only the gamma ratio of the detector. Figure 1 presents the calculated and measured 10 boron profile in studied B_4C pellets. The annex shows further results of a lithium migration study inside B_4C.

3.2. Determination of the ^{7}Li concentration profiles

A reliable standard pellet of B_4C including a known concentration of ^{7}Li could not be done to determine the ^{7}Li profile using Eq. (3). For this element, we use a National Bureau of Standard ^{7}Li standard (a standard containing 500 ppm of ^{7}Li) to determine the ^{7}Li concentration in the irradiated pellet. The ^{7}Li concentration in the sample is then deduced from Eq.(4) which is a ratio of two Eq.(2) :

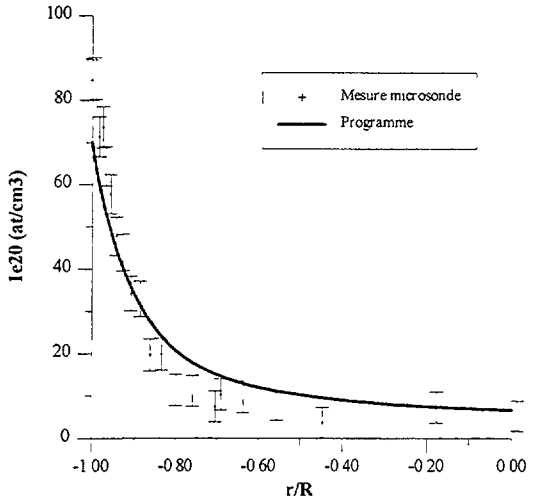

FIG. 1. Comparison between calculated and measured Na profile along the radius of a B_4C pellet (dots refer to experimental data and full line is the calculated Na profile)

The first concerning our irradiated B_4C sample, the second concerning the NBS sample also measured by the microprobe :

$$\frac{N_{Li}^{B_4C}{}_{\gamma}}{N_{Li}^{NBS}{}_{\gamma}} = \frac{N_{Li}^{B_4C} \int_{Es}^{E_f} \frac{d\sigma}{d\Omega}(E) \frac{dE}{(\frac{dE}{dx})^{B_4C}}}{N_{Li}^{NBS} \int_{Es}^{E} \frac{d\sigma}{d\Omega}(E) \frac{dE}{(\frac{dE}{dx})^{NBS}}} \tag{4}$$

E_s, the cut-off energy of the $^7Li(p,p'\gamma)^7Li$ reaction (400 keV) [6].

The ^7Li standard is a cylindrical sample with the same radius as the boron carbide pellet. The number of photons measured on the standard were separately collected in the same position as the photons of the boron carbide pellet. Therefore, the photons detector ratio and the solid angle were absolutely identical.

According to Eq.(4) we are able to determine directly ^7Li experimental concentration profile inside the irradiated pellet. The knowledge of an experimental ^{10}B profile allows also to calculate indirectly the ^7Li production. The number of ^7Li atoms generated in the irradiated pellet is given by the relation :

$$N_{7Li} = \frac{e - e^*}{e(1 - e^*)} N_{10B} \tag{5}$$

e and e* are respectively the ^{10}B enrichment $(N_{10_B}/(N_{10_B} + N_{11_B}))$ of non irradiated and irradiated material and N_{10_B} is the number of ^{10}B atoms per cm^3 referred to the unirradiated pellet. Figure 2 shows the ^7Li profile production deduced from the nuclear microprobe experimental profile of ^{10}B and ^{11}B, and the direct experimental measure of ^7Li atoms profile obtained by the nuclear microprobe.

This work shows that ^7Li profiles increase from the center to the periphery. At the center of the pellet, the calculation is in agreement with the measurement, and the ^7Li concentration seems to be measured with a good accuracy by the microprobe. But there is a large difference near the surface of

the pellet between the experimental ^{7}Li profile measured directly and the ^{7}Li calculated production. This difference may be explained by ^{7}Li diffusion out of the pellet. The recoil range of ^{7}Li atoms calculated by TRIM-91 [5], is 1.7 μm. The recoil length of ^{7}Li in the (n,α) reaction is then smaller than the grain size (≈ 2μm). That is why recoil should not be responsible for the loss of ^{7}Li near the interface between the pellet and the resin.

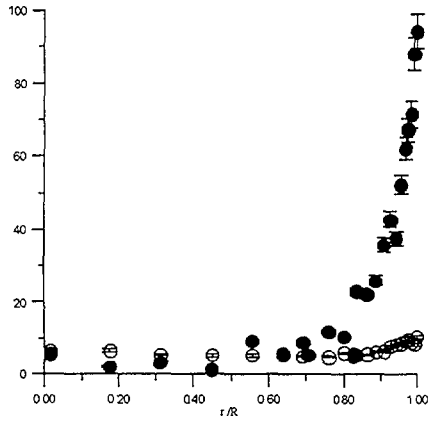

FIG. 2. Comparison between measured Na and ^{7}Li profiles along the radius of a B_4C pellet. black dots refer to Na data and white dots refer to ^{7}Li data

The ^{7}Li production provides an average value of 2.44×10^{21} atoms/cm^3 and the average value of the experimental ^{7}Li measurement is 1.4×10^{21} atoms/cm^3, indicating that approximately 40 % of the ^{7}Li produced by the nuclear reaction should diffuse out of the pellet. This loss is not due to an artefact during the sample preparation, because the value of the ^{7}Li concentration at the center of the pellet is the same for the calculated and measured ^{7}Li profiles.

4. DISCUSSION ON ^{7}LI DIFFUSION IN THE BORON CARBIDE PELLET

^{7}Li profiles obtained from the nuclear microprobe experiments indicates a possible ^{7}Li diffusion in the boron carbide absorber.

The ^{7}Li transport may occur in tree different steps [7-9]:
(i) Intragranular diffusion by a driving force (chemical potential);
(ii) Desorption on the surface of the grain of ^{7}Li;
(iii) Pore diffusion of ^{7}Li.

Such a transport mechanism may describe the loss of ^{7}Li observed in Figure 3. These phenomena have been observed in nuclear fusion problems for tritigen ceramics [10].

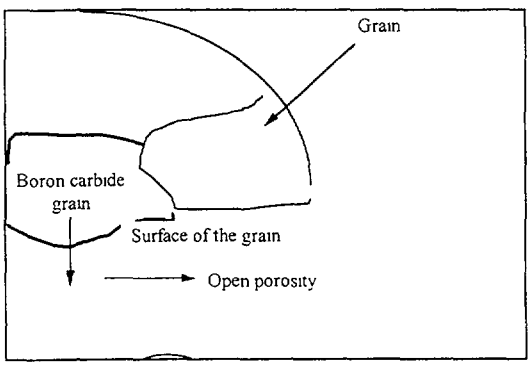

FIG. 3. Schematic of ^{7}Li transport in the boron carbide ceramic

Some authors have reported the formation of Li_2C_2[11], LiB_{10}[12], Li_4B_5[13] in the system Li-B and Li-C. Therefore it is difficult to know the chemical form of the ^7Li in the sample. We suggest that the diffusion inside the grain is due to a chemical potential gradient. At the surface of the grain, the ^7Li may desorb and goes away through the open porosity of the boron carbide pellet.

Another issue is that ^7Li may segregate at grain boundaries and could thus modify their cohesion. This hypothesis could not be verify because the grain size were too small (2 μm) to observe a segregation at the grain boundary with our size of proton beam. If we had reduced the size of the protons beam we would have had a very bad count rate of photons.

5. CONCLUSION

The comparison of the experimental and the calculated profiles of ^{10}B shows that the spatial distribution of the ^{10}B in the pellet is correctly described by a simple neutron capture calculation, which implies no diffusion of ^{10}B in the irradiated boron carbide pellet. We have experimentally shown that there is a ^7Li diffusion in this boron carbide pellet, representing a loss of about 40 % of the ^7Li atoms produced by the nuclear capture reaction. According to us, this diffusion should be essentially due to the chemical potential of ^7Li atoms.

^7Li diffusion may play a role in the brittleness of boron carbide absorber during a neutron irradiation. The ^7Li diffusion in the boron carbide pellet leads to a relative mass loss of about 6×10^{-3}. This value is not very important in our case. But in Fast Breeder Reactors or for longer irradiation times in a PWR, this relative mass variation may be much more important. Therefore, it may affect the evaluation of swelling in boron carbide absorbers, since these calculations are deduced from density measurements. Moreover, the diffusion of ^7Li atoms out of the absorber may bring these atoms in contact with the metallic sheath.

REFERENCES

[1] STOTO, T., ZUPPIROLI, L., PELISSIER, J., Radiation effects, 90, p 161-170, (1985).
[2] KRYGER, B., COLIN, M., SPECIAL MEETING ON ABSORBING PINS AND MATERIALS, CEA-CONF-6656, (1985).
[3] HOLLEMBERG, G., BASMAJIAN, J., J. Am. Cer. Soc., 65, p 179, (1982).
[4] MCMILLAN, J.W., PUMMERY, F.C.W., POLLARD, P.M., Nucl. Inst. and Meth., 197, p 171-177, (1982).
[5] ZIEGLER, J.F., Handbook of stopping power of energetic ions in all elements, 5, Pergamon Press.
[6] JARJIS, R., PhD Thesis, University of Manchester, (1979).
[7] OLIVIER, C., PEISACH, M., J. Radioanal. Chem., 98, p 389, (1986).
[8] RAFFRAY, A.R., , S., CHO ABDOU, M.A., J. Nucl. Mater., 210, p 143-160, (1994).
[9] FREDERICI, G., WU, C.H., RAFFRAY, A.R., BILLONE, M.C., J. Nucl. Mater., 177, p 1-31, (1992).
[10] RASNER, B., CEA/CEREM réf. N T 94/014 BR/FL (1994).
[11] MAHAGIN, D.E., BATES, L.L., BAKER, D.E. report HELD-TME/77-33, (1977).
[12] SECRIST, D.R., J. Am. Cer. Soc., Vol. 50, N°10, p. 520-523, (1967).
[13] WANG, F.E., MICTCHELL, M.A., SUTULA, R.A., HOLDEN, J.R., BENNETT, L.H., J. of Less-Common Metals, 61, p237-251, (1978).

ANNEX

STUDY OF LITHIUM MIGRATION INSIDE B_4C NUCLEAR CONTROL RODS USING THE NUCLEAR MICROPROBE TECHNIQUE

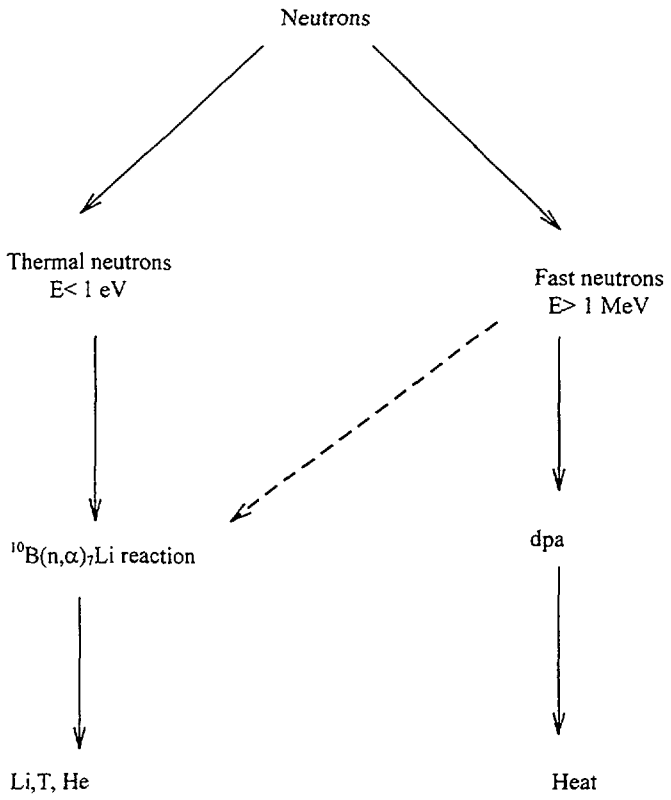

Neutron absorption by boron-10

CALCULATION OF HELIUM AND LITHIUM PROFILES

- **Physical phenomenon:**

- Self shielding of boron-10 atoms

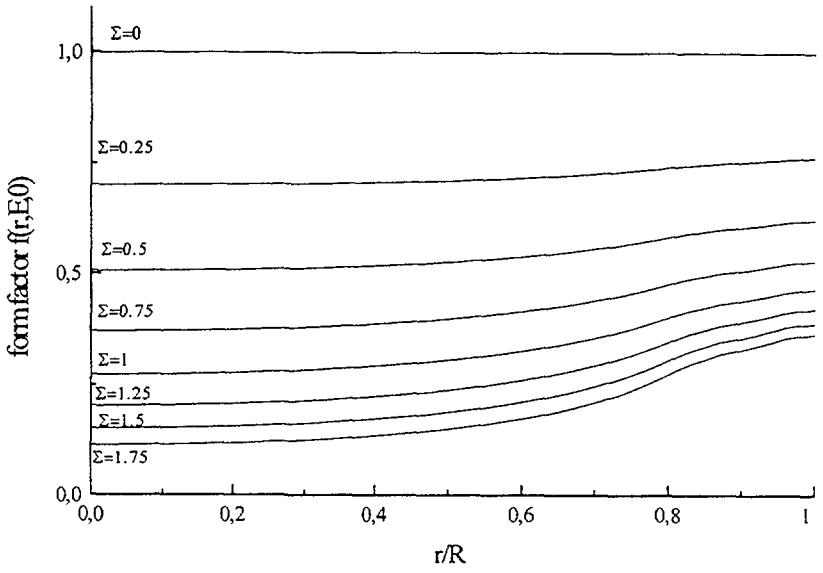

r/R is the reduced abscissa and Σ is an a-dimensional number

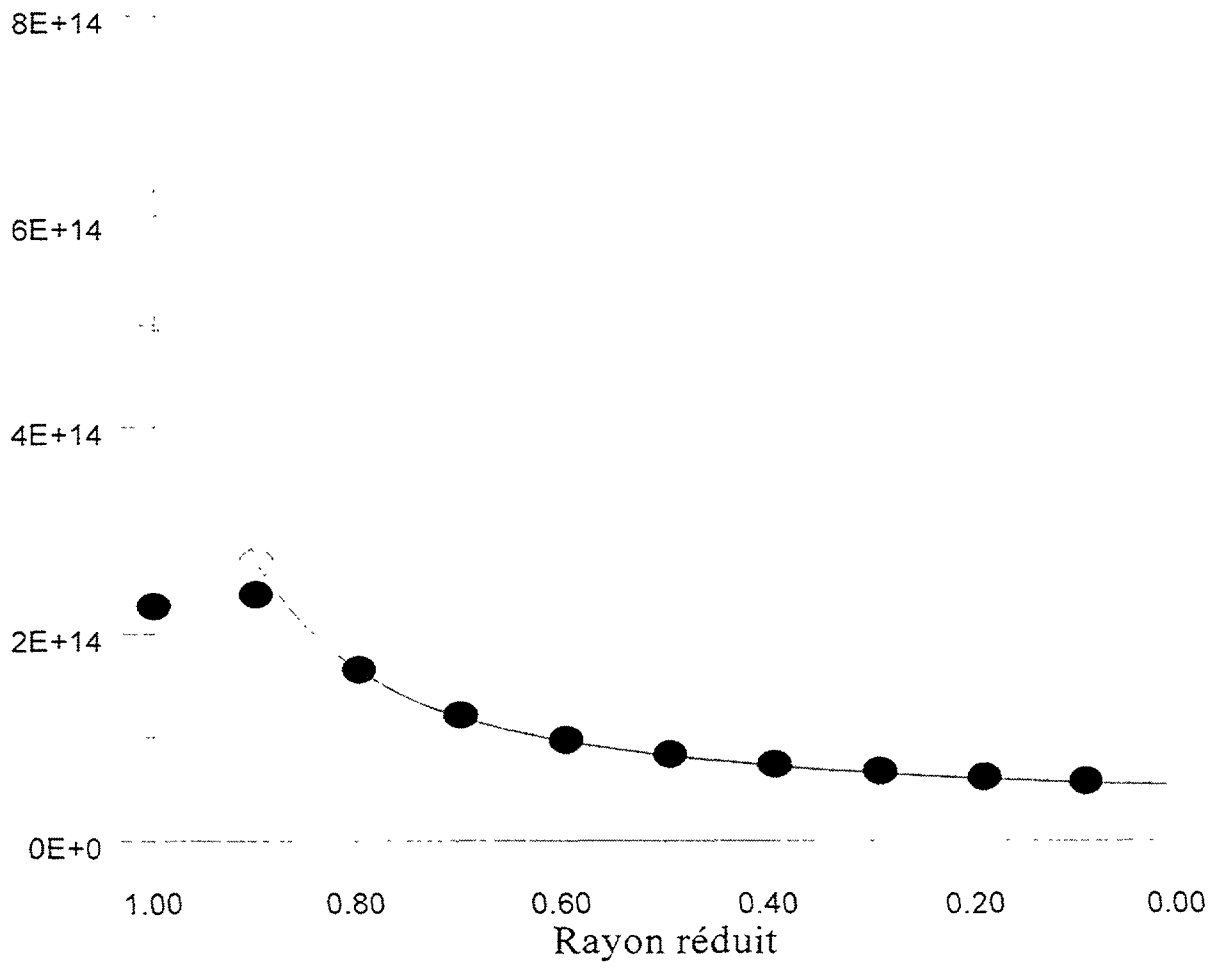

Helium profile in PWR

Helium and dpa production rates along the B_4C pellet radius

Caption :

black dots :	6.2 10^{21} ncm^{-2}
white dots :	2.1 10^{21} ncm^{-2}
white lozenges :	1 10^{19} ncm^{-2}

Choice of nuclear reaction avoiding some surface effects (rugosity).

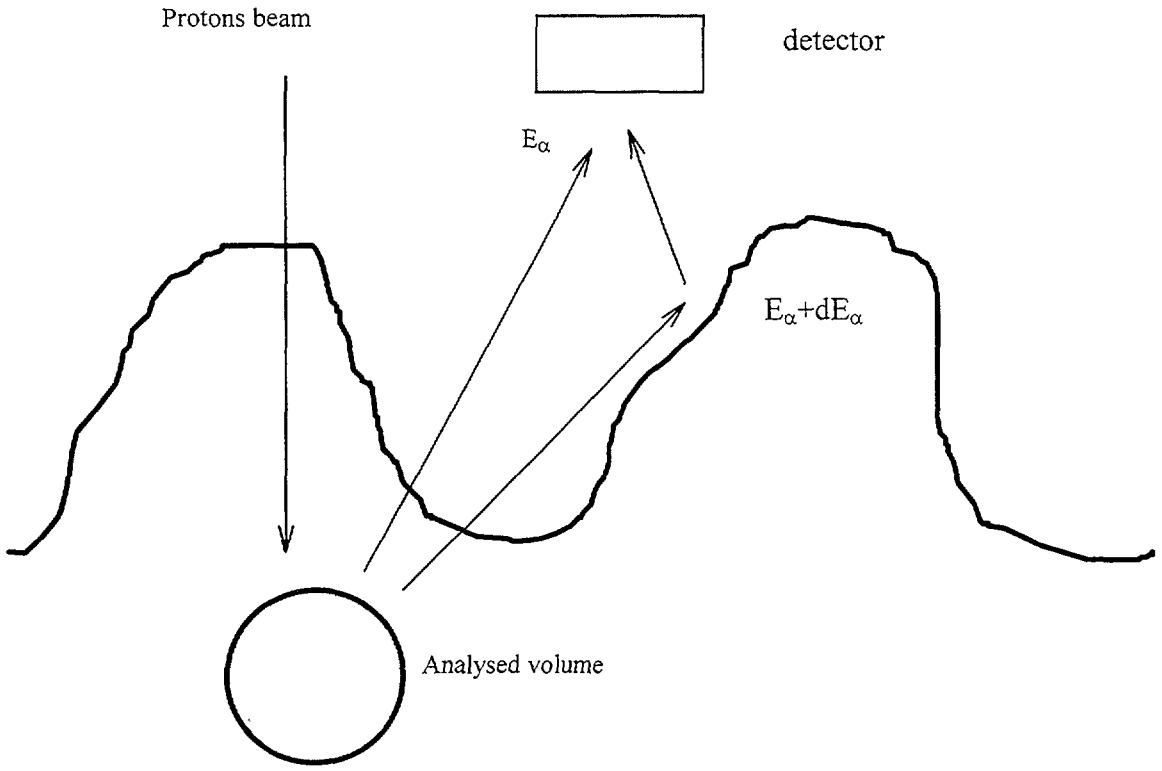

^{7}Li(p,p' γ) ^{7}Li	**E_γ = 478 keV**
^{10}B(p,α γ) ^{7}Be	**E_γ = 429 keV**
^{11}B(p,p' γ) ^{11}B	**E_γ = 2125 keV**

PWR condition (Bigarreau experiment)

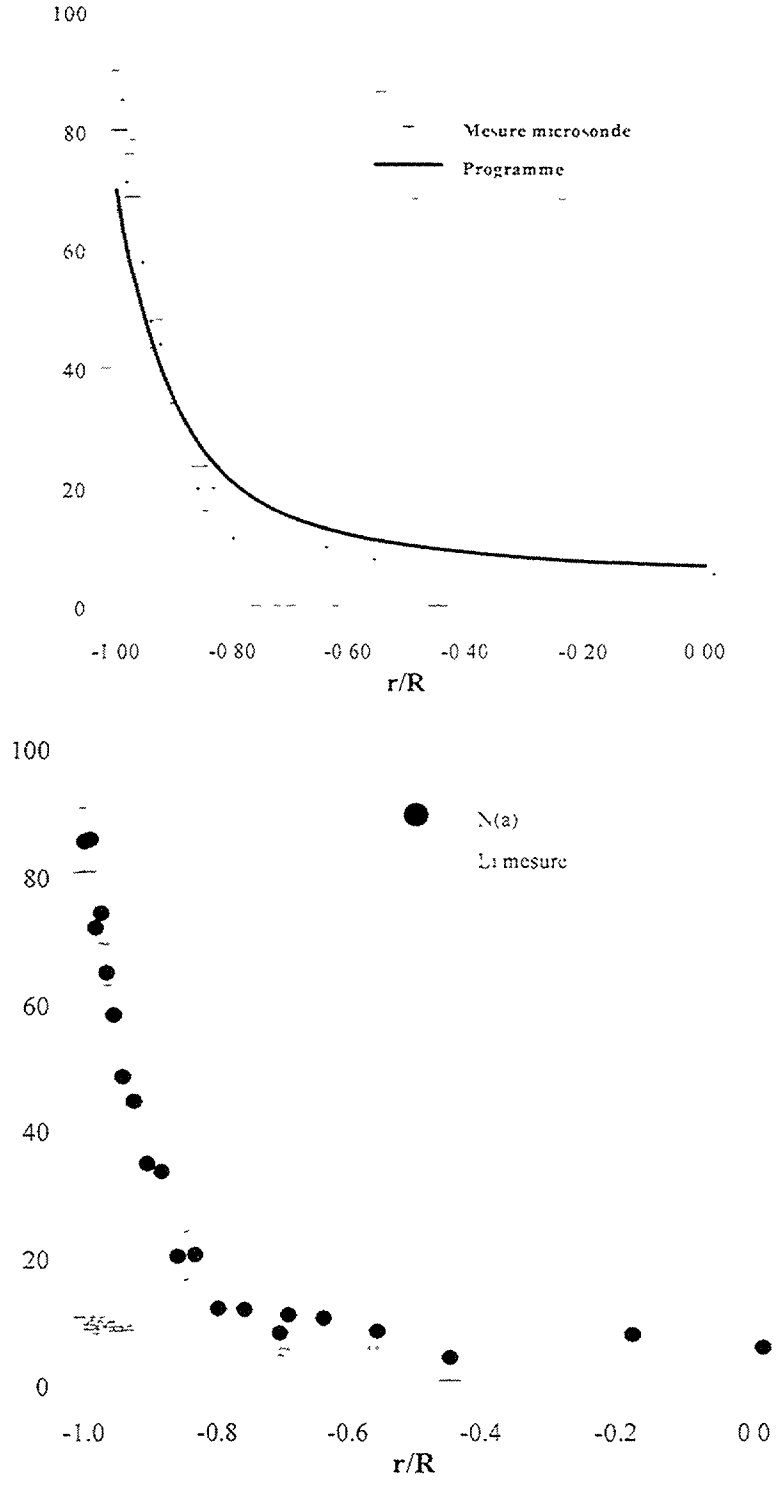

Evidence of lithium migration out of the pellet

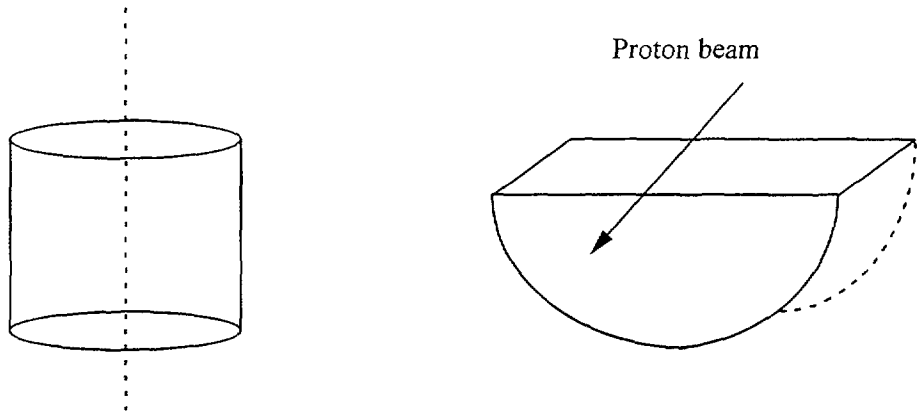

B_4C pellet irradiated in FBR

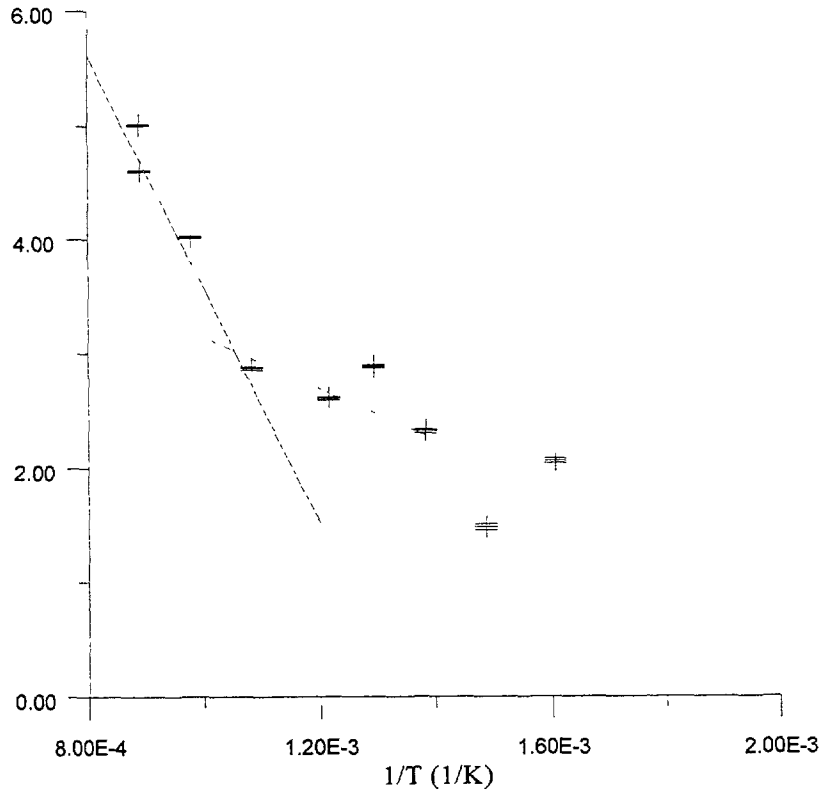

$D_0=10^{-14}$ cm^2s^{-1}

Lithium diffusion coefficient as a function of the inverse temperature

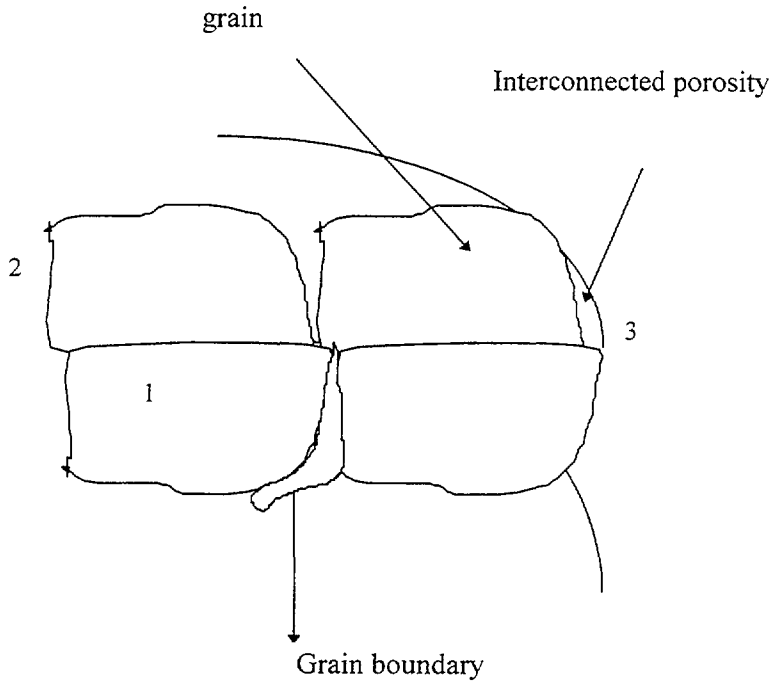

Schematic presentation of lithium migration

- intragranular diffusion of ^{7}Li atoms
- desorption of lithium atoms at the grain surfaces
- gazeous diffusion of lithium atoms in the open porosities

CONCLUSION

Interest of the nuclear microprobe technique :

- Possible validation of neutron codes by measuring the effect of the neutron flux every where inside a nuclear reactor by an indirect method;
- To obtain a better understanding of B_4C evolution under nuclear conditions;
- Experimental evidence of lithium migration outside of B_4C pellet, this may affect the corrosion of metallic sheaths.

NEXT PAGE(S) left BLANK

THE ROLE OF CLADDING MATERIAL FOR PERFORMANCE OF LWR CONTROL ASSEMBLIES

P. DEWES, A. ROPPELT
Siemens AG, Unternehmensbereich KWU,
Erlangen, Germany

Abstract

The lifetime of control assemblies in LWRs can be limited presently by mechanical failure of the absorber cladding. The major cause of failure is mechanical interaction of the absorber with the cladding due to irradiation induced dimensional changes such as absorber swelling and cladding creep, resulting in cracking of the clad. Such failures occurred in both BWRs and PWRs. Experience and in-reactor tests revealed that cracking can be avoided principally by two ways: First, if strain rates and hence, stresses in the cladding are kept low (well below the yield strength), significant strains can be tolerated. This is the case for the cladding of PWR control assemblies with slowly swelling AgInCd absorber. Recent examinations of highly exposed PWR control assemblies confirmed the design correlation up to the presently used strain limit. Second, in such cases where strongly swelling absorber material like boron carbide is still preferred, materials which are resistant against irradiation assisted stress corrosion cracking (IASCC) can be used. The influence of material composition and condition on IASCC was studied in-reactor using tubular samples of various stainless steels and Ni-base alloys stressed by swelling mandrels. In several programme steps high purity materials with special features had been identified as resistant to IASCC. Another process of cladding damage which may occur in PWRs is wear caused by friction of the control rods in the surrounding guide structure. For replacement control assemblies this problem is solved by coating of the cladding. There exists meanwhile excellent experience of up to 18 operation cycles with coated claddings.

1. INTRODUCTION

For safe operation and shutdown of nuclear reactors control assemblies (CA) are of essential importance. According to the different situation regarding design limits, operating conditions and demands in the various types of reactors different solutions were found for design of CA and choice of absorber and structural materials. Common requests to all types of CA are safe function under all normal operating conditions, tolerable behaviour in case of accidents and, for economic reasons and waste minimization, as long life time as possible.

The natural end of life is determined by reduction of the neutron worth of the CA due to depletion of the neutron absorbing isotopes. The limit, normally set to 10% reduction, would allow for very long life time; for example, in case of rod cluster control assemblies (RCCA) with AgInCd absorber widely used in PWR's the operating life is higher than 30 years. Experience, however, has shown that mechanical failures could led to premature end of life. In most cases the clad surrounding the absorber material was concerned. Either the cladding was cracked due to interaction with the absorber or it was damaged by fretting wear.

Considerable effort was spent on investigation of the root causes of such failures, on understanding of the basic mechanisms and on remedies to overcome the problems. As one consequence investigation and, at least in case of Hf, introduction of new absorber materials began and may lead to significant improvements in the future. On the other hand, the large experience with the absorbers AgInCd and B_4C, as well as certain limitations regarding e.g. weight of the CA, give rise to stick to the proven absorber materials and to rely on design modifications and improvement of cladding, instead. In this paper, the role of the cladding for CA performance will be reviewed based on Siemens' experience with CA and irradiation test samples in both PWRs and BWRs.

2. PAST EXPERIENCE WITH CLADDING FAILURES

Performance of CA in PWRs and BWRs was subject to many publications and reviews, e.g. [1-3]. Regarding cladding failure the observations can be summarized as follows:

- BWR control rods with vibro compacted B_4C powder contained in stainless steel cladding tubes or holes in blades showed cracks in the cladding and washing out of

the absorber when exposed beyond a certain limit. Cracking of the cladding is caused by irradiation assisted stress corrosion cracking (IASCC). In order not to exceed 10% reduction of neutron worth neutron dose limits for the most exposed parts of the control blades are used;

- In several PWRs, RCCA suffered from wear of the cladding caused by vibrations of the rods in the guide structure and fuel assembly guide tubes;
- At high exposures, beginning at about $0.5x10^{22}cm^{-2}$ (E > 1MeV), PWR RCCA with AgInCd absorber can have single rods with hairline cracks at the tip. The cracks are caused by diameter increase of the absorber due to swelling and deformation under axial forces.

These problems were subject to extensive investigations and improvements of design and materials. In the following results of in-reactor material test programmes relevant for CA cladding are summarized and compared to CA performance data.

3. RESULTS OF MATERIAL TEST PROGRAMMES

To investigate the behaviour of absorber and cladding materials under original irradiation conditions several material test programmes have been started since 1979 in commercial PWRs and BWRs [4-7]. The materials tested comprised:

- Stainless steels, types 304 (non-stabilized), 316, 1.4541/321 (Ti stabilized), 1.4550/348, Nb stabilized), 1.4981 (Nb stabilized);
- Ni base alloy type 625 (60%Ni/22%Cr/8%Mo/4%Nb);
- Absorbers: AgInCd, B_4C pellets and vibrated B_4C powder, Al_2O_3 with 3 or 5% B_4C addition, hafnium.

The test specimens consisted of tubes made of stainless steels or Ni base alloys and sealed with welded end plugs. They were filled with absorber materials either at large gap to allow for determination of undisturbed swelling and creep properties, or at almost zero gap to study interaction between absorber and cladding. The geometric proportions in radial direction were representative for typical absorber tubes either for PWR (OD 10.2 mm, wall thickness 0.5-0.6 mm) or for BWR application (OD 6.7 mm, wall thickness 0.5-0.84 mm). The length of the specimens ranged from 60 mm (some B_4C specimens) over 130 mm (majority) to 1700 mm (BWR absorber rods filled with B_4C powder).

The specimens were inserted into fuel assemblies and irradiated in the high flux region of PWR and BWR cores. During refuelling shutdowns examinations consisting of visual inspection, eddy current testing and diameter profilometry were performed. Irradiation lasted from one to eight operational cycles, depending on experimental objectives and performance of the specimens. Part of the specimens was taken to hot cells after irradiation for further examinations concerning especially the internal absorber materials.

3.1. Cladding creep

Whereas under LWR conditions thermal creep of stainless steels and Ni-base alloys can be neglected, measurable irradiation induced creep can occur in the high flux region of reactor cores. Creep down of cladding tubes especially at the high pressure in PWR coolant water is significant and leads to somewhat earlier interaction of absorber and cladding [8].

The results obtained from material test irradiation under PWR conditions indicated that creep is linear with fluence and no primary creep exists. An extension of the in-pile test programme which included several types of commercial and high purity austenitic stainless steels revealed similar results. Different alloy composition or differences in manufacturing process resulted in variation in creep strength by a factor of two [9].

3.2. Cladding load due to absorber dimensional change

During service absorber materials take up neutrons and thus undergo transmutations which cause severe modifications of material properties. Cladding of absorbers is mostly affected by volume increase of the absorber. Swelling can use up the internal diametrical gap between absorber and cladding and can subsequently strain the cladding. The swelling rate depends very much on the absorber material as shown in Figure 1. B_4C has by far the highest swelling rate which is in case of pellets directly transferred to the cladding when the gap has been filled. Pellets made of Al_2O_3 with small additions of B_4C show initially the same swelling rate as pure B_4C pellets. Depletion of the neutron absorbing isotope B-10 reduces the swelling rate significantly with increasing neutron fluence. B_4C powder compacted in cladding tubes to about 70% of theoretical density can use initially the internal void volume to compensate swelling of the B_4C particles. In contrast to B_4C containing ceramic materials, the ternary alloy AgInCd exhibits swelling at a constant, low rate.

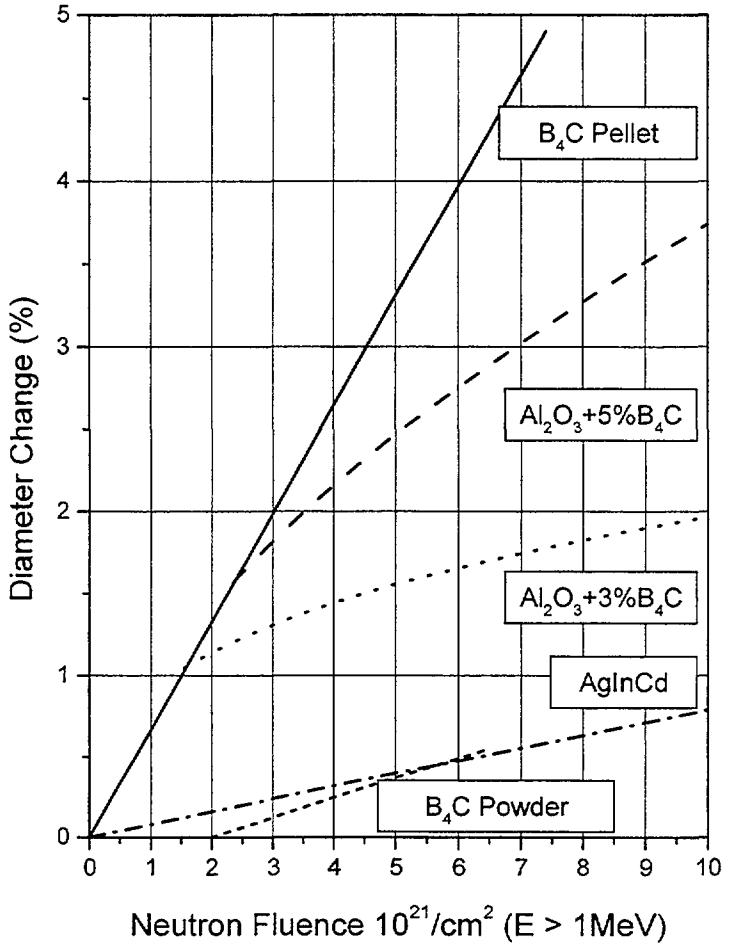

FIG. 1. Diameter change of stainless steel tubes due to swelling of various B_4C containing absorber materials compared to swelling of AgInCd rods

As a consequence of the different swelling characteristics and the mechanical properties of the ceramic B_4C and the metallic AgInCd interaction with the cladding, the stress on the cladding is different. Figure 2 shows examples of stainless steel clad samples strained by B_4C pellets (a), B_4C powder (b) and an AgInCd rodlet (c). Obviously, B_4C pellets have more strength than stainless steel cladding and are able to model the cladding according to their local modifications of the diameter. For example, enhanced diameter increase at the ends of the pellet stack indicates an end peaking effect of the neutron flux and local enhanced swelling. Despite of such local effects, however, overall straining of the cladding is isotropic in axial and tangential direction in this case.

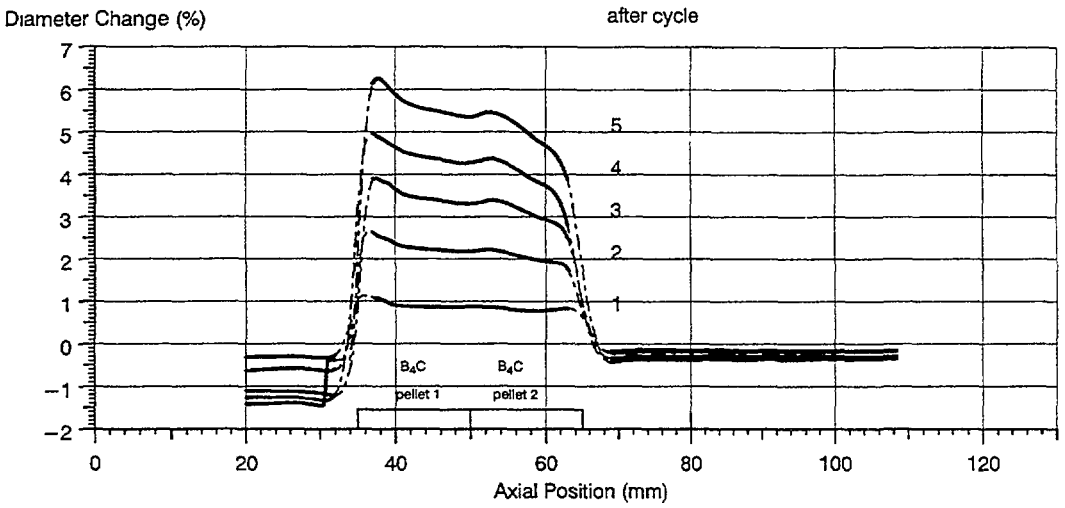

a) B_4C Pellets

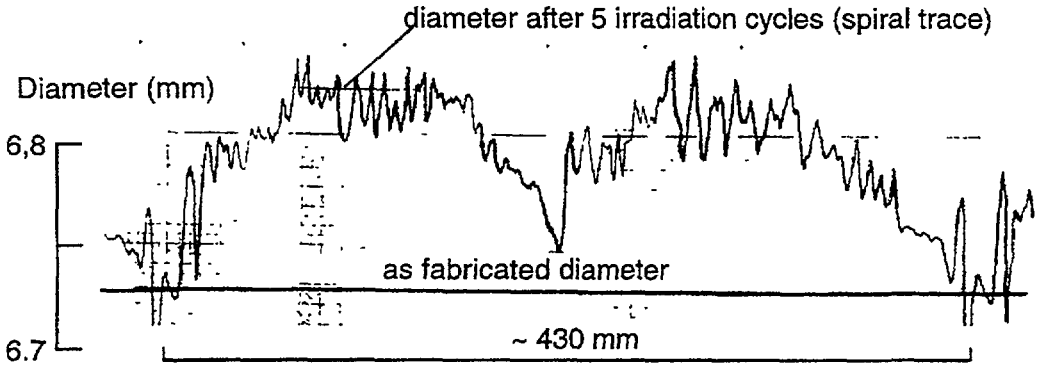

b) B_4C Powder (Compacted to 70% of Th. D.)

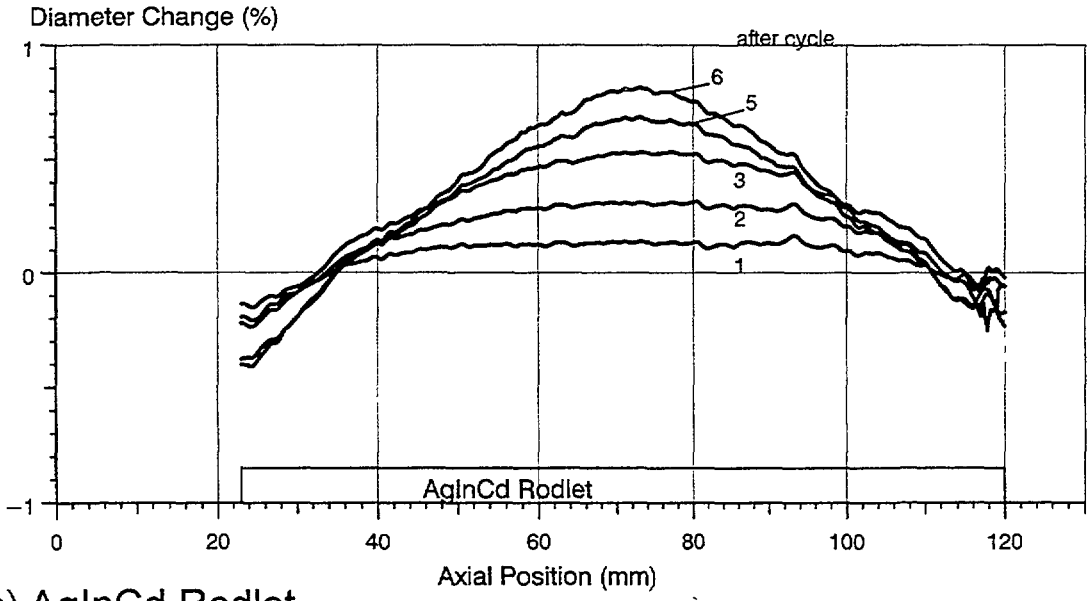

c) AgInCd Rodlet

FIG. 2. Diameter profiles of test specimens filled with different absorber materials

B_4C powder is usually filled into cladding tube sections of certain length and is compacted by vibration to reach the required average density. Due to this process some axial fluctuations in density may occur which are reflected by the diameter change profile, see Figure 2b. Maximum strains occur over considerable axial length of the rod and are higher than average strain. Measurements of rod length show an increase of rod length approximately equal to average diameter increase.

In contrast to the ceramics the metallic alloy AgInCd is rather soft. It's swelling behaviour can therefore be influenced by the retarding moment of the cladding supported by outer coolant over-pressure. This is obvious from the diameter profiles measured successively during irradiation on a short stainless steel specimen filled with AgInCd at very small gap, see Figure 2c. In the middle part of the specimen the diameter change is equivalent to that of an unrestrained AgInCd sample. Towards both ends, however, widening of the cladding decreases and about 1 cm from the ends of the AgInCd rodlet even creep down of the cladding is observed. Apparently, the AgInCd extends in axial direction filling available void volumes (chamfer of AgInCd rodlet and hollow of the end plug face at bottom side, axial gap at top side) and thus gives way to the cladding which is pressed down by the external coolant pressure. In such a case, the stress distribution in the cladding tube may differ from the isotropic state as in case of swelling ceramics and may be more pronounced in tangential direction.

3.3. Deformability of cladding materials under irradiation

To prevent cladding failures of CA in operation and to introduce improved materials for new CA it is necessary to know to what extent cladding materials can be deformed under irradiation without fracture.

In several joint EPRI/Siemens programmes, the deformability of austenitic stainless steels and Ni-base alloys under original irradiation conditions in PWRs and BWRs was studied. In the first programme phase only a low P and Si containing stainless steel was found to be resistant against IASCC in both BWR and PWR environment [4]. In the subsequent second phase of the programme these results could not be verified with other high purity material charges [5]. After the influence of Ni was ruled out in a further test run [6], the experiments finally succeeded in finding an appropriate microstructure of austenitic stainless steels which makes the alloys insensitive to IASCC. A twofold approach turned out to be successful for alloys of Types 304 and 348. First, the process temperatures during tube manufacturing were kept low resulting in materials of fine grain size. Secondly, the contents of Nb and C in Type 348 alloys were varied in three steps [7].

The specimens were tested first in a PWR. The results revealed that charges of Type 304 and 348 alloy which failed below 1% strain in the earlier test when tested in coarse-grain condition survived more than 2% strain in the fine-grain condition. High concentrations of Nb and C were found to have no effect for Type 348 alloy as long as the grain size was kept low. In such material a fine grain size can be reached with standard fabrication routines, also [7]. In these swelling mandrel tests, the stress in the cladding resulting from straining depends on the creep strength of cladding and mandrel. For ceramic mandrels the creep strength can be assumed to be considerably higher than for the cladding, so that creep of the mandrel can be neglected. Since the in-reactor creep of the cladding materials tested here has been measured also, stress histories can be calculated for several combinations of cladding and swelling mandrel materials.

Figure 3 shows for example stress histories of three Type 304 specimens. They can be compared with the yield strength of this alloy which increases with neutron fluence. Calculated stresses above yield strength are not meant real, of course, but indicate plastic deformation. In the non-failed specimen the applied stress clearly remained below yield strength during all the irradiation time. In another specimen, the calculated stress reached the yield strength early in irradiation. Inspections and examinations of the specimens could not unambiguously exhibit cladding failure. The third specimen, however, which clearly exceeded the RT yield strength, failed with long intergranular cracks. In contrast to that, alloys which are resistant to IASCC, can be deformed plastically without fracture, as shown in Fig. 4 and 5.

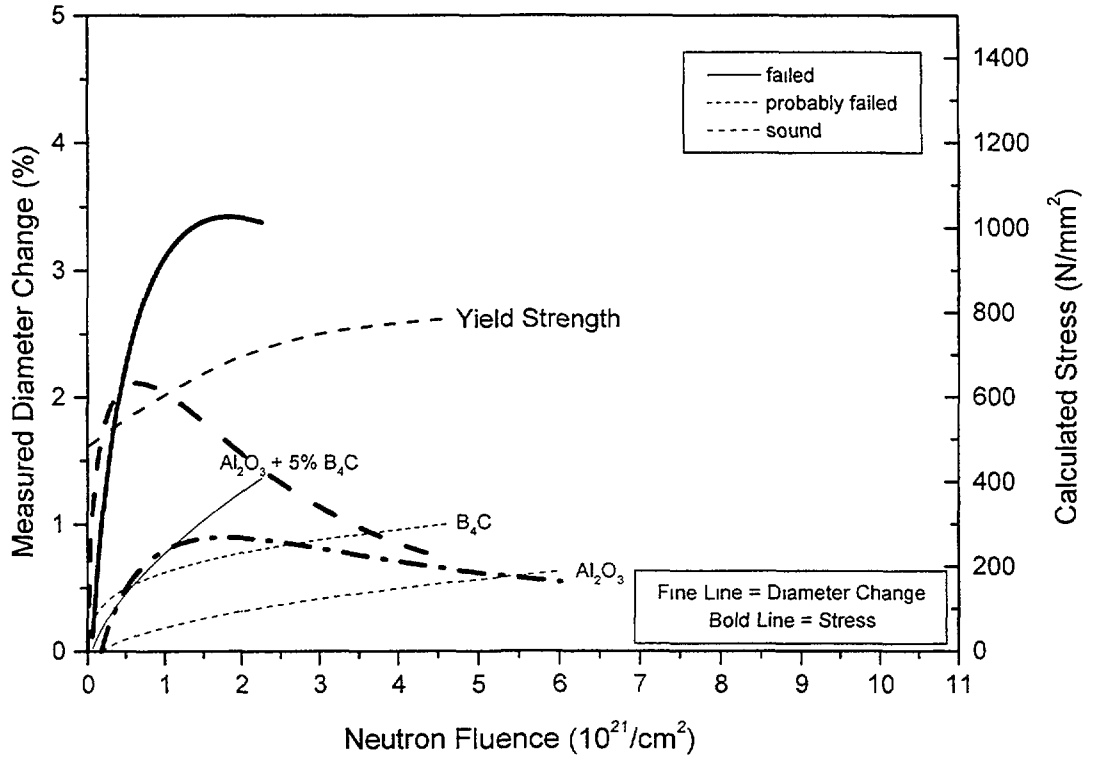

FIG. 3. Measured diameter change and calculated stress history of three type 304 tube samples with different swelling mandrels; a) rapid diameter increase of Al_2O_3+5%B_4C caused stress in cladding tube to reach yield and the sample failed; b) similar rapid stress increase caused sample probably to fail quickly, thereafter washout of B_4C slowed down further diameter increase; c) slowly swelling Al_2O_3 pellets resulted in low stress well below yield strength and the cladding remained sound

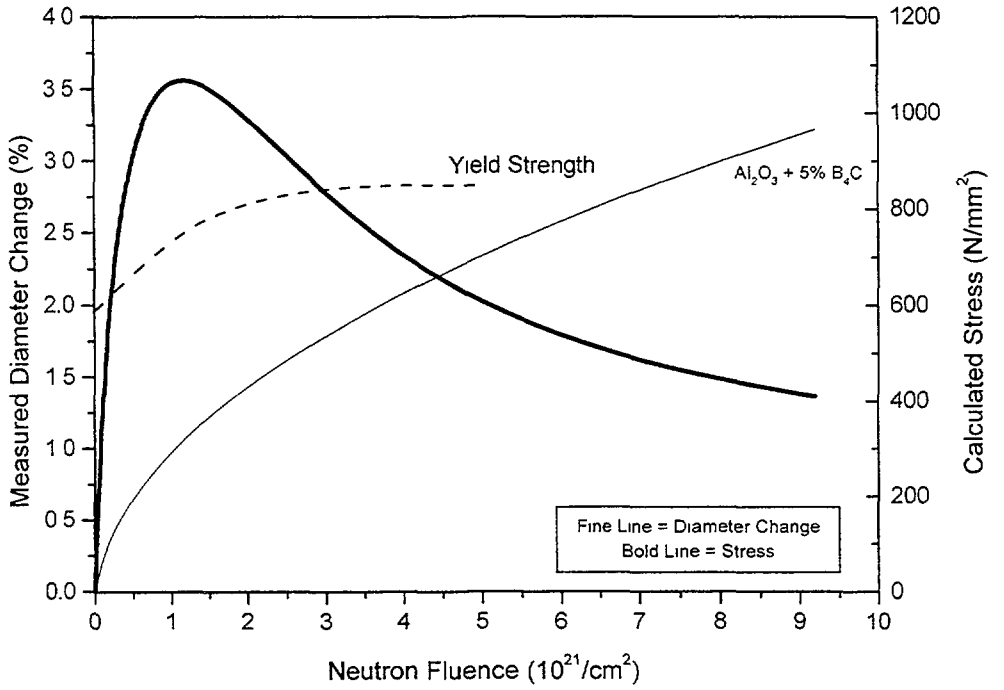

FIG. 4. Measured diameter change and calculated stress history of a type 348 tube sample with Al_2O_3+5%B_4C pellets

After the successful tests with IASCC resistant materials in the PWR environment, the same tests were repeated in a BWR. The results were about the same; the fine-grain materials again were able to reach high deformations without fracture.

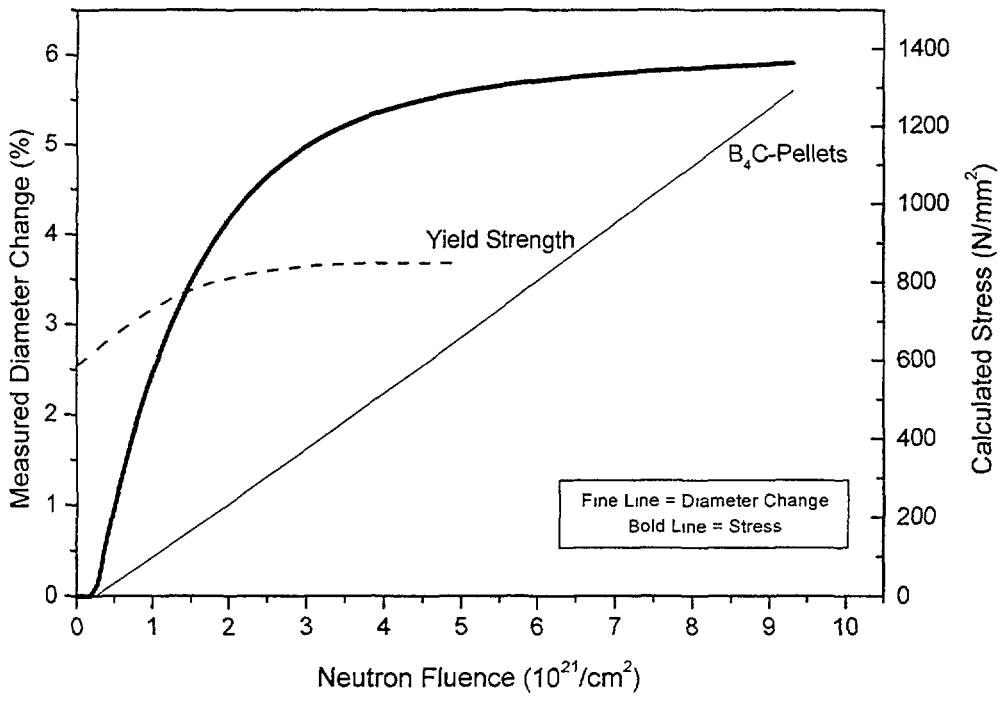

FIG. 5. Measured diameter change and calculated stress history of a type 348 tube sample with B_4C pellets

4. IRRADIATION TEST RESULTS AND CONTROL ASSEMBLY PERFORMANCE

As shown in the swelling mandrel tests, the strain rate or stress level governs the damage process. Furthermore, it is known that IASCC needs certain neutron exposure; dose threshold values of $0.05 \times 10^{22} cm^{-2}$ for BWR (non-hydrogenated water chemistry) and about $0.2 \times 10^{22} cm^{-2}$ for PWR environment have been derived [10].

An appropriate way to summarize the data and to define failure and non-failure regimes was shown in [11], where experimental results of the first irradiation tests were presented in a map of tangential strain and fast neutron fluence. In Fig. 6 this map is extended to higher neutron doses to include recent data of the irradiation tests [5-7] and of examinations of RCCAs in several PWRs. Fig. 6a shows data from commercial purity heats of type 1.4541 (321) tested in irradiation programmes and used as RCCA cladding. Data from several high purity austenitic stainless steels (types 304, 348, 316 and 1.4981) found to be susceptible to IASCC, also, are shown in Fig 6b. The critical strain at which fracture can occur decreases with increasing neutron dose to very low values below 0.2% above $0.2 \times 10^{22} cm^{-2}$ (E > 1MeV). The lower boundary curve for failures shown in Fig. 6 was derived for commercial purity alloys, The results obtained for several high purity alloys indicate in some cases a slightly higher threshold, but the general trend is the same.

As shown in [11] at lower and medium neutron doses, there exists a critical strain rate; below that the non-failure/failure threshold curve can be exceeded without failure. The data indicate that the critical strain rate may be slightly higher for high purity than for commercial purity alloys.

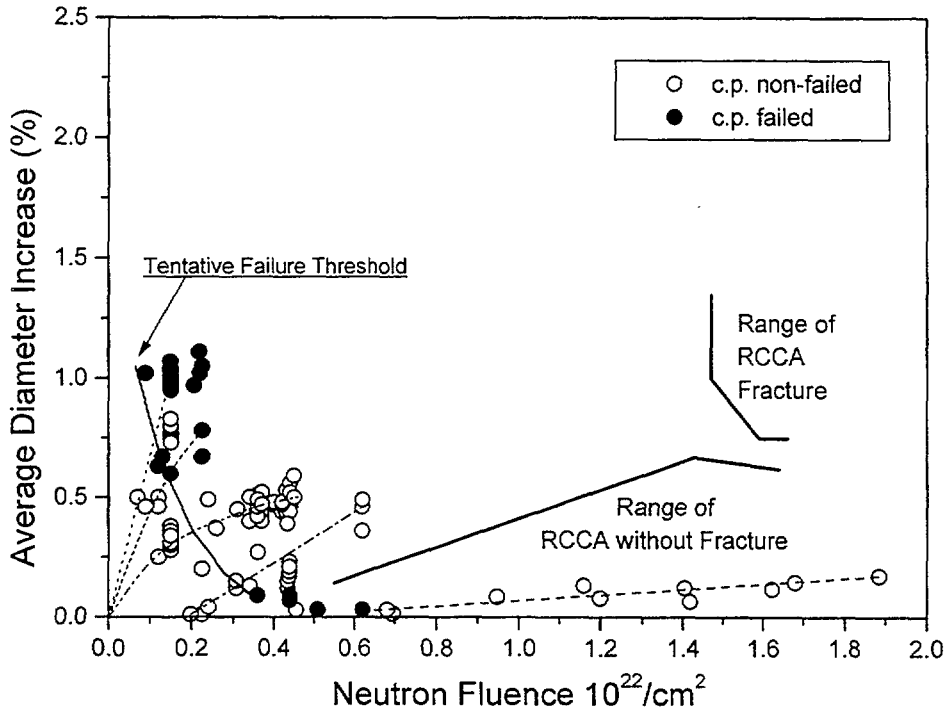

a) Commercial purity alloys

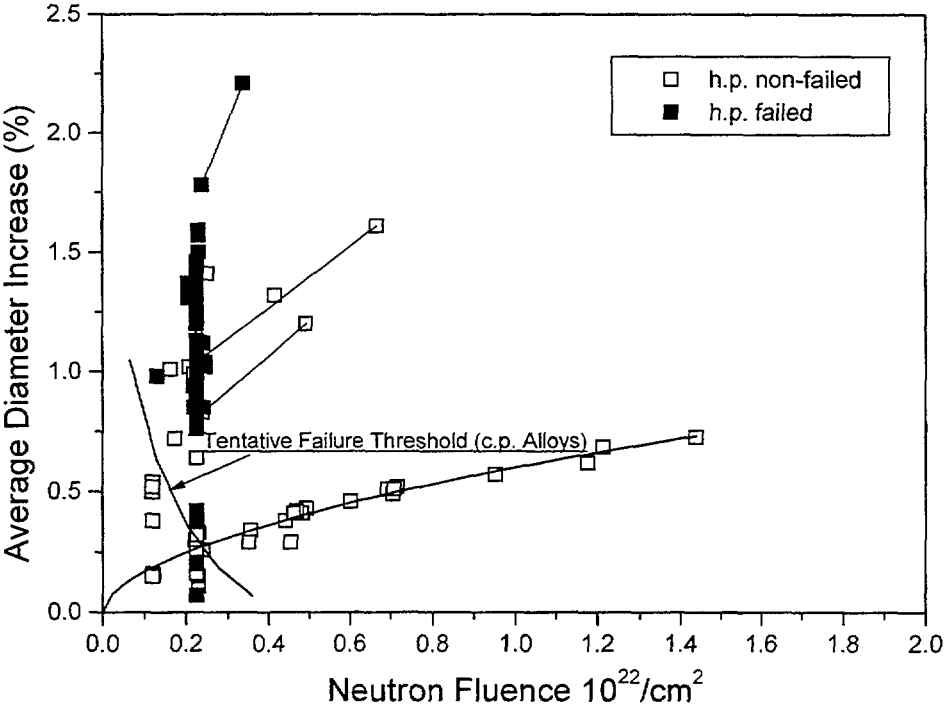

b) High purity alloys (not optimized condition)

FIG. 6. Map of experience with IASCC sensitive austenitic stainless steels

4.1. Slow strain rate (PWR RCCA with AgInCd absorber)

At low and medium neutron doses, the performance of RCCA with the slowly swelling AgInCd absorber is well in agreement with the conception of a „safe strain rate", which allows to cross over the failure threshold (see Fig. 6a). It is known, however, that also AgInCd can cause cracking of stainless steel cladding of PWR RCCA [2, 12, 13]. Such hairline fractures have been observed on a few control rods in one Siemens plant. The RCCAs containing single fractured rods were operated beyond the conservative design limit [8]. The problem was recognized in time by early examinations and, after 21 years of operation, the RCCA of that plant were replaced by new ones without any complication for reactor operation. The fractures occurred at very high neutron doses as indicated in Fig. 6a. Part of the diameter change measured in the fractured part of the rods is probably caused by crack opening. According to [2], crack width of such hairline cracks was between 0.1 and 0.2 mm which corresponds to 0.3 to 0.6% increase in diameter. Assuming similar behaviour and subtracting those values from the failure data would bring the RCCA failure range shown in Fig. 6a down in contact to the non-failure range. Hence, the data suggest that cracking may have occurred there despite of the slow straining rate applied by the AgInCd absorber.

According to present knowledge of the irradiation behaviour of AgInCd [8] swelling is linear with fluence. Based on the known creep properties of the cladding material the stress in the cladding can be calculated as function of neutron fluence and initial filling gap of the absorber (see 3.3). Fig. 7 shows the resulting stress histories of RCCA rods with various as fabricated gaps. When the gap is filled by absorber swelling and cladding creep, stress increases to a certain level and remains constant during further exposure under these assumptions. The maximum stress levels are well below the yield strength which increases with fluence. The maximum stress is the same for rods with small and nominal gap; gaps in the upper tolerance range would have avoided any stress. It is assumed that fractured rods had small initial gaps; the stress had lasted long time, therefore, until rupture occurred.

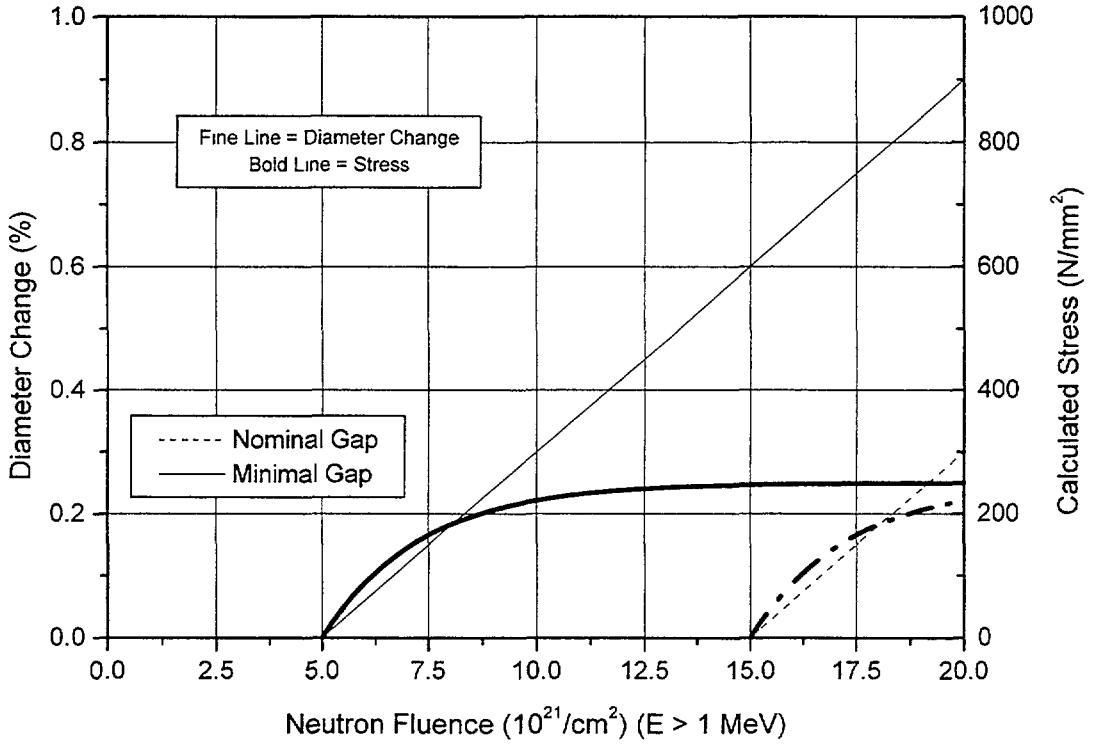

FIG. 7. Calculated stress history of a RCCA rod with AgInCd absorber

Presently, it is not exactly clear what mechanism caused fractures of RCCA cladding. The fracture mode of the Siemens RCCA was probably also intergranular, as found in examinations on fractured RCCA elsewhere [2, 12, 13]. Sipush et al [2] stated that austenitic stainless steel may

become susceptible to creep rupture due to radiation enhanced segregation of impurities to the grain boundaries. It is not clear if any corrosive attack by the water environment and, hence, IASCC plays a role in the fracture process at all.

In case of Siemens RCCA, fracture occurred only after favourably long life time when significant strain had been accumulated. Besides, some kind of creep rupture another possible explanation of the late fracturing might be an acceleration of clad straining at very high exposure. Irradiation of AgInCd results in building-up of Sn resulting in a) modification of the chemical composition due to neutron capture leading to expansion of the crystal lattice and b) formation of a second phase with lower density. Up to now, neither dimensional and density measurements on absorber materials [2, 8, 12, 13] nor crystallographic examinations [13] give any clear evidence of an increase in the swelling rate at high fluences due to influence of the second phase.

The dimensional data available up to now from Siemens RCCA do not indicate significant contribution of plastic deformation due to axial forces. This is concluded from the observation that the measured data are consistent with the assumption of linear absorber swelling in the range of experience up to $6x10^{22}$ cm^{-2} (E > 0.6 eV), see Fig. 8. Nevertheless, it can not be excluded that at very high exposures and for rods with unfavourable small gap size the rate of diameter change due to interaction with the AgInCd increases for reasons mentioned above.

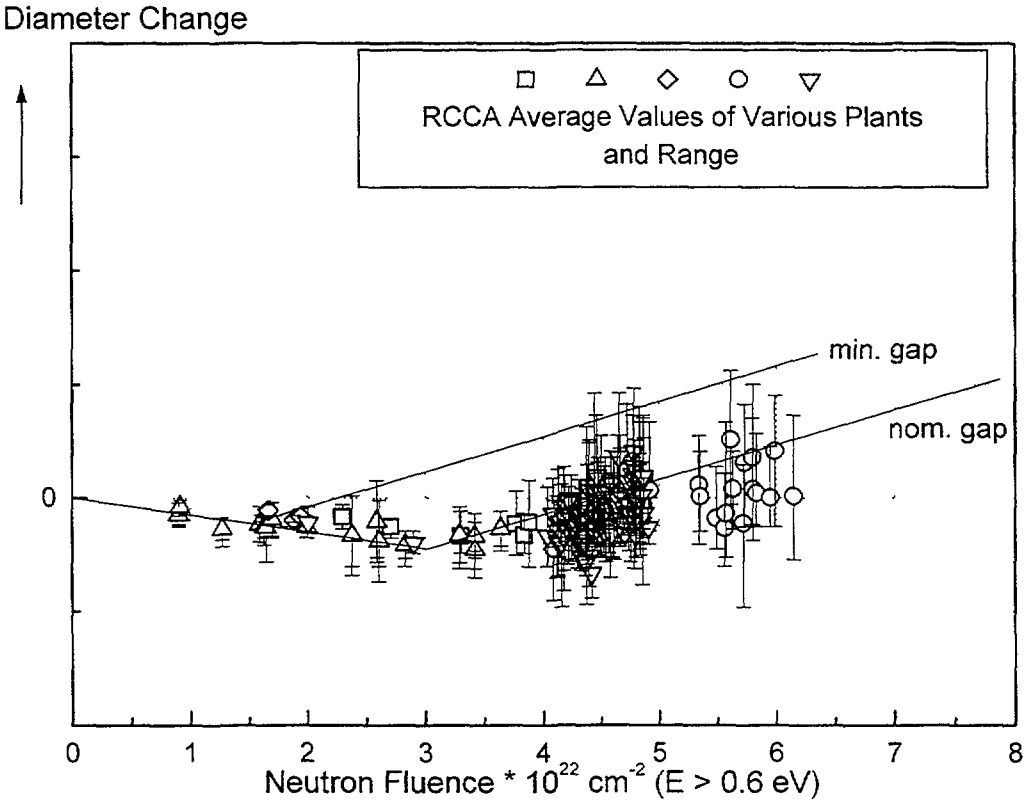

FIG. 8. Measured and calculated diameter changes of Siemens RCCA rods

For other RCCA designs and operating conditions, cladding fractures have been connected with enhanced diameter increase at the bottom of the absorber rod caused by axial forces due to rapid movement of RCCA („slumping"). This might have caused enhanced rate of diametral straining so that cladding fractures could occur at medium neutron doses (0.5 - $0.7x10^{22}cm^{-2}$, E > 1 MeV), already, and at low total strain, as reported [2, 13].

4.2. High strain rate (IASCC resistant materials for BWR application)

Requirements for BWR applications, mainly certain weight limits and required neutron worth, make it hard to design control rods without any B_4C. The high swelling rate of B_4C in the pellet or powder form as presently used leads to premature IASCC failure of cladding made from commercial purity alloys. EPRI/Siemens IASCC test programmes [4 - 6] have shown, that also with conventional high purity materials the failure threshold can be increased only slightly as indicated in Figure 6. In these programmes, however, appropriate microstructures were found which make austenitic stainless steels resistant against IASCC [7], as mentioned in 3.3. In Fig. 9, diameter changes measured on IASCC resistant cladding samples are plotted vs. neutron fluence. The data shown here come from PWR irradiation but are thought to be valid for BWR environments also, since it was found in the irradiation programmes that the differences between PWR and BWR environments did not influence the behaviour of high purity stainless steels under high neutron exposure.

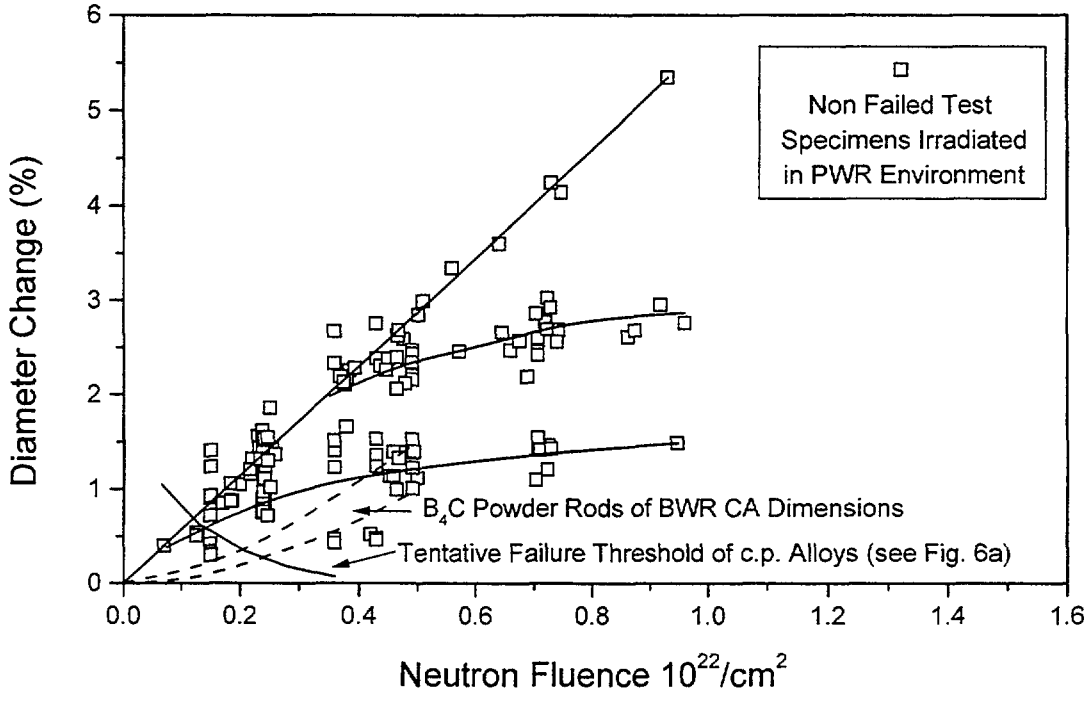

FIG. 9. Map of experience with IASCC resistant austenitic stainless steels irradiated in PWR irradiation tests. Range of diameter change for BWR control rod type test rods shown for comparison

To compare the experimental results of the improved alloys with the loads which are to be expected for BWR control rods in service, experimental data from another irradiation programme performed in a BWR with test rods having the original dimensions of B_4C rods in a BWR control assembly are shown in Fig. 9 also. The cladding of latter test rods was made from high purity Type 348 alloy, but not yet with optimum microstructure. So, the rods reached remarkable high neutron doses, but exhibited cladding cracks at end of life. At that time, the B^{10} burnout was 45% for the thin-wall clad rods and even 60% for the rods with the thicker wall. A prototype control assembly [14] made from the same alloy and having improved design features like Hf rods in the outermost positions of the blades, was operated successfully during seven years at maximum flux positions up to the high neutron dose of $3x10^{21}cm^{-2}$ (snvt) in the uppermost quarter.

The results show, that significant improvements of the performance of BWR control assemblies could be reached by appropriate choice of the material condition for the cladding of B_4C rods combined with a design using Hf absorber at the most exposed positions.

5. ELIMINATION OF CLADDING WEAR BY COATING

In several PWR plants fretting of the cladding due to vibrations of the absorber rods in the guide structure and the guide tubes of the fuel assemblies was observed. Criteria for maximum allowable wall thinning were established, and according to these criteria CA had to be replaced [e.g. 2, 8, 15]. To overcome this problem, coating of the cladding with hard layers was introduced. Siemens uses Cr_3C_2 coatings applied by a detonation gun process [8]. Other methods to protect the cladding from wear are Cr plating [16] or nitriding [15] of the cladding surface.

The experience with these surface treatments seems to be generally good [8, 15, 16]. Meanwhile, Cr_3C_2 coated RCCA were in service for up to 18 operational cycles without any indication of fretting attack.

6. SUMMARY

The various mechanisms which can cause mechanical failures of control rod cladding and limit the life time, are now rather well understood.

In PWRs, experience has shown that very long lifetime can be reached using AgInCd absorber in conventional stainless steel clad with appropriate design. Wear problems can be avoided if necessary by proper surface treatment.

Control rod design for BWRs apparently can not completely give up B_4C absorber, which is putting high demands upon the cladding material. There might exist a potential for further improvement by careful choice of cladding material condition with regard to IASCC resistance.

REFERENCES

[1] STRASSER, A.A., SHEPPARD, K.D., „Light water reactor reactivity control", Nucl. Energy 23 (1984) 169-178.

[2] SIPUSH, P.J., et al., „Life time of PWR silver-indium-cadmium control rods", EPRI-NP-4512 (1986).

[3] EICKELPASCH, N., et al., „BWR control rods - operational experience and post irradiation examinations", Nucl. Technol. 60 (1983) 362 ff.

[4] GARZAROLLI, F., et al., „Deformability of austenitic stainless steels and Ni-base alloys in the core of a boiling and a pressurized water reactor", 3rd Int. Symp. On Environmental Degradation of Materials in Nuclear Power Systems-Water Reactors (1987) 657-664.

[5] DEWES, P., et al., „Measurement of the deformability of austenitic stainless steels and Nickel-base alloys in light water reactor cores", ASTM STP 1210 (1993) 83-101.

[6] GARZAROLLI, F., et al., „Deformability of high purity stainless steels and Ni-base alloys in the core of a PWR", 6th Int. Symp. On Environmental Degradation of Materials in Nuclear Power Systems-Water Reactors (1993) 607-613.

[7] GARZAROLLI, F., et al., „In-reactor testing of IASCC resistant stainless steels", 7zh Int. Symp. On Environmental Degradation of Materials in Nuclear Power Systems-Water Reactors (1995) 1055-1065.

[8] HEINS, L., et al., „Design of control rods for pressurized water reactors with special consideration of absorber swelling and clad creep down", IAEA-TECDOC-813, Vienna (1995) 15-36.

[9] GARZAROLLI, F., et al., to be published.

[10] SCOTT, P., „A review of irradiation assisted stress corrosion cracking", J. of Nucl. Mat. 211 (1994) 101-122.

[11] GARZAROLLI , F., STEHLE, H., „Behaviour of core structural materials in light water cooled power reactors", IAEA-SM-288/24 (1986).

[12] MATSUOKA, T., et al., „Intergranular cracking in cladding tube of PWR RCCA rodlets", 6th Int. Symp. On Environmental Degradation of Materials in Nuclear Power Systems-Water Reactors (1993) 765-772.
[13] BOURGOIN, J., et al., „Contribution a la connaissance du comportement sous irradiation des crayons de grappes de commande", Proc. of Int. Symp. Fontevraud III (1994) 715-725.
[14] GROSS, H., et al., „The BWR Hybrid 4 control rod", Nucl. Eng. Des. 108 (1988) 433-436.
[15] HERTZ, D., PEYRAN, J.C., „La nitruration ionique remede a l'usure des crayons de grappes de commande", Proc. of Int. Symp. Fontevraud III (1994) 752-759.
[16] MOON, J.E., et al., „Improved control rod performance through design enhancements and operational wear management strategies", Proc. of Int. Symp. Fontevraud III (1994) 726-735.

BWR CONTROL BLADE REPLACEMENT STRATEGIES

M.W. KENNARD
Stoller Nuclear Fuel,
NAC International,
Pleasantville, New York,
United States of America

J.E. HARBOTTLE
Stoller Nuclear Fuel,
NAC International,
Thornbury, Bristol,
United Kingdom

Abstract

The reactivity control elements in a BWR, the control blades, perform three significant functions provide shutdown margin during normal and accident operating conditions, provide overall core reactivity control, and provide axial power shaping control As such, the blades are exposed to the core's neutron flux, resulting in irradiation of blade structural and absorber materials Since the absorber depletes with time (if B_4C is used, it also swells) and the structural components undergo various degradation mechanisms (e g , embrittlement, corrosion), the blades have limits on their operational lifetimes Consequently, BWR utilities have implemented strategies that aim to maximize blade lifetimes while balancing operational costs, such as extending a refuelling outage to shuffle high exposure blades This paper examines the blade replacement strategies used by BWR utilities operating in U S , Europe and Asia by assembling information related to the utility's specific blade replacement strategy, the impact the newer blade designs and changes in core operating mode were having on those strategies, the mechanical and nuclear limits that determined those strategies, the methods employed to ensure that lifetime limits were not exceeded during operation, and blade designs used (current and replacement blades)

1. VENDOR DESIGNS AND LIFETIME LIMITS

1.1. Overview

Definition of Terms

Several terms common to the discussion of control blade exposure and limits are defined below.

1) **Nuclear end of life** – the exposure corresponding to a 10% reduction in initial cold reactivity worth, $\Delta k/k$, averaged over any quarter axial segment of the blade.

2) **Quarter axial segment** – the significant control blade segment relative to the core cold axial power distribution.

3) **snvt** – smeared thermal neutron fluence based on the exposure of the four fuel assemblies adjacent to the control blade of interest, units of 10^{21} n/cm^2.

4) **Tip adder** – exposure increment applied to a blade fully withdrawn from the core (i.e., absorber tip located below the active fuel region) to account for B_4C swelling and absorber tube sensitization in the tip region as a consequence of thermal neutron leakage and fast neutron thermalization below the core region.

Background

The original equipment blade designs offered by the various vendors consisted of all B_4C absorber contained within commercial purity stainless steel materials although the designs varied slightly, with GE and Siemens encapsulating the boron carbide in sealed tubes while ABB-Atom loads the absorber into gun-drilled holes in the blade wings. The mechanical limits of these early designs were based on loads expected during normal operation and accident conditions and included criteria on wear, fatigue, seismic loadings, and internal pressure. The nuclear end of life for the GE original equipment blades was calculated to be 42% ^{10}B depletion.

With irradiation, it was quite apparent that mechanical limits could not be met by the early original equipment designs. In 1978, for example, GE observed absorber tube cracking and boron carbide washout in high exposure blades. The vendor determined that cracking and washout occurred at 50% local ^{10}B depletion (Siemens observed similar degradation at 1.6 snvt or ~40% local depletion). The mechanism was determined to be irradiation assisted stress corrosion cracking (IASSC) of the absorber tubes, and ligaments between the holes in the ABB-Atom design, with tubing stresses generated by B_4C swelling. Figure 1 provides the worth vs. depletion curves for GE original equipment blades for the cases where 1) the nuclear lifetime is limiting (42% ^{10}B depletion) and, 2) the mechanical lifetime is limiting due to washout of boron carbide (34% ^{10}B depletion).

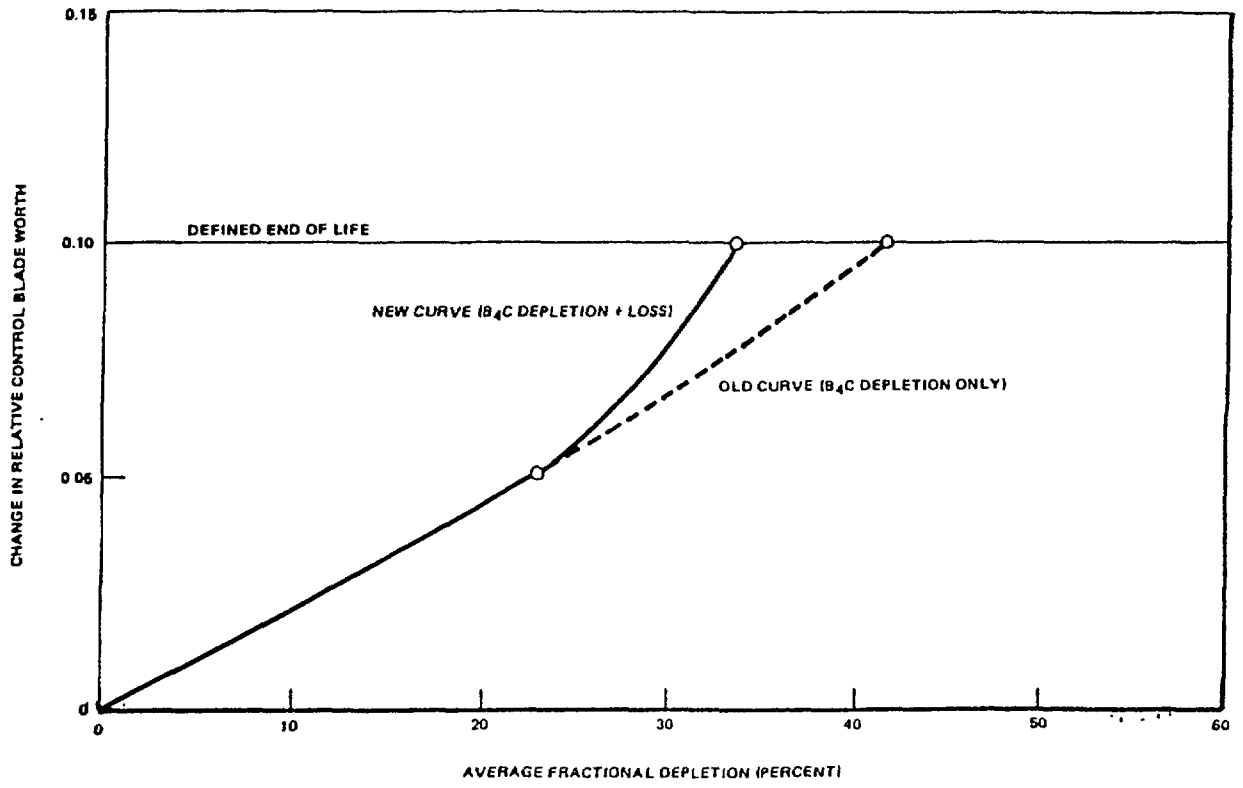

FIG. 1. Changes in relative blade worth as a function of fractional depletion (Reference: GE)

Subsequent to the observation of cracking and absorber washout in the early blade designs, the vendors have offered more and more advanced designs to first address blade integrity issues and secondly, to provide designs that could achieve higher exposures. Remedies included three major changes:

- use of high purity stainless steels for absorber tubes and wings, thereby improving material ductility and cracking thresholds;
- use of hafnium in the high duty blade areas (wing tip and outer edge) to reduce absorber swelling effects; and
- increased boron carbide loading effectively reducing the ^{10}B depletion rate and the attendant swelling rate.

Also included were low cobalt materials to reduce activation. The latest generation blades using these features have effectively tripled control blade lifetimes relative to the original equipment designs. Figure 2 graphically shows the exposure advantage of simply increasing B_4C loading in a given blade design.

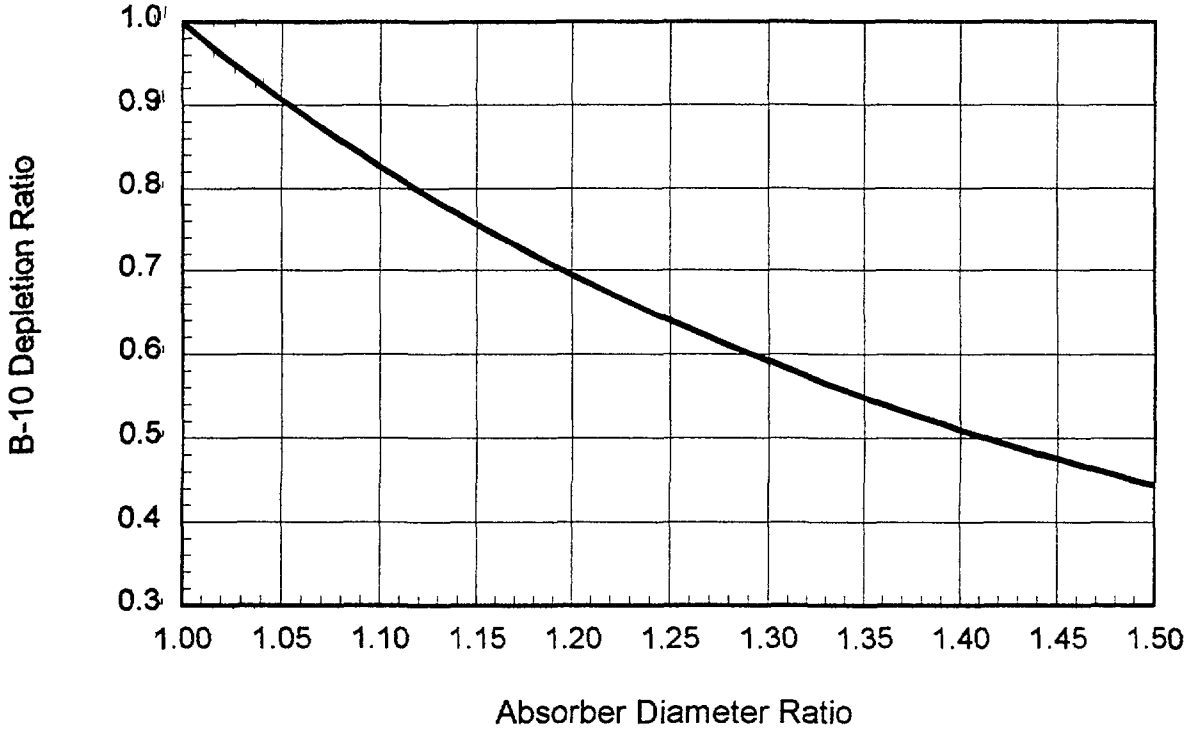

FIG. 2. Impact on depletion ratio of increasing absorber loading

Hafnium has been introduced into the designs in either plate or rod geometries, and in both cases, unclad. This is also true of the all hafnium Hitachi and Toshiba designs which are available with the absorber configured as either as full length plates or rods contained within a sheath similar to the GE Duralife series, for example. The exception is ABB-Atom, which maintains the solid stainless steel wing feature even in the hybrid configurations. In this case, solid hafnium rodlets and plugs are loaded into selected horizontal holes in each blade wing to provide the hafnium tip and edge regions, respectively.

Table I summarizes the blade designs offered by vendors. Note that Siemens does not actively market replacement control blades. Siemens will, however, provide blades if economical to do so.

1.2. ABB-Atom

The original equipment blade (CR-70) is an all-B_4C design wherein the boron carbide is loaded into holes bored horizontally into the 304 stainless steel wings. Like other vendors' designs, the CR-70 was susceptible to IASCC of the ligaments between the holes.

ABB-Atom introduced the CR-82 (hybrid with hafnium tip) in 1982 and the CR-85 (hybrid with hafnium tip and edge) in 1985. Although lifetimes were improved with the use of hafnium in the highest exposure regions of the designs, they are still prone to cracking as they use 304 SS as the blade wing material. In 1992, ABB-Atom introduced the CR-82M and CR-85M designs. These are similar to the CR-82 and CR-85 designs except that 316L is used for the wings and the absorber hole geometry has been modified. PIE examinations have confirmed improved in-reactor performance of 316L vs. 304. Note that all blades manufactured post-1992 use 316L for the wings.

ABB-Atom currently offers two additional designs, the CR-82M-1 and CR-85M-1. These are similar to the CR-82M and CR-85M designs, respectively, except for the absorber hole geometry which is consistent with that of the original CR-82 and CR-85 designs.

TABLE I. SUMMARY OF CONTROL BLADE FEATURES

Vendor	Blade Series	Absorber Type and Placem.			Comments
		TABLE I	Hf Tip	Hf Edge	
ABB	CR-70	X			Original equipment design
	CR-82	X	X		~Original equipment blade + Hf
	CR-82M	X	X		M series uses 316L, revised hole geometry
	CR-85	X	X	X	~Original equipment blade + Hf
	CR-85M	X	X	X	M series uses 316L, revised hole geometry
	CR-85M-1	X	X	X	CR-85 with 316L; used in Japan
GE	OE	X			Original equipment design
	D120	X			~Original equipment blade + HP304; susceptible to crevice corrosion
	D140	X	X		~Original equipment blade + HP304; susceptible to crevice corrosion
	D160	X		X	HP304 + Hf
	D190	X	X	X	HP304 + Hf
	D215	X	X	X	HP304 + Hf
	D230	X	X	X	HP304 + Hf
	Marathon	X	X	X	Rad Resist + Hf + new design abs. tubes
Siemens	OE	X			Original equipment design
	Hybrid-1	X		X	HP SS + Hf
	Hybrid-4	X	X	X	HP SS + Hf
Toshiba	OE	X			Original equipment design
	All-Hf		X	X	HP SS + All-Hf

The vendor has developed inspection-based guidelines addressing blade reuse and replacement that are a culmination of examinations performed to date. For U.S. utilities, the guidelines are relatively conservative. For example, for blades with 304SS wings which have reached an exposure of 3.0 snvt:

- visually inspect blade wings for cracks;
- discharge blade if cracked;
- if the blade is uncracked, reuse for one cycle and re-inspect applying the above criteria.

If the inspection at 3 snvt shows a blade to be uncracked, it can be shuffled to a shutdown bank. No further examinations are required. However, tip adders are recommended for evaluating CR-70 exposures.

For post-1992 blades using 316L, ABB-Atom recommends visual inspection of only the lead blades of each design. Currently, the CR-82M lead blades are in Unit R2. Inspections have identified limited cracking in two of the highest exposure blades which resided in high duty control cells for three cycles. Although the root cause analysis is not complete, the location of the cracks leads ABB-Atom to believe that the failure cause is manufacturing related.

Although guidelines for European utilities are similarly based on observations of cracking, there is a much larger experience base of operation with limited cracking. In some cases, utilities reload blades observed to have *minor* cracking for an additional cycle of operation.

Current replacements are primarily the CR-82M and CR-82M-1 designs.

1.3. General Electric

Table I provides a summary of the of the various blade designs offered by GE beginning with the original equipment blade offered in ~1960 to the most advanced, Marathon. One observes a progression in features based on the mechanical limitations identified in the original equipment, Duralife 120 and Duralife 140 designs. These advancements include high purity 304SS, redesigned handle-to-sheath and sheath-to-structure joints, and the use of hafnium absorber. The Duralife 200 series used higher B_4C loadings and the Marathon, a welded absorber design, to extend lifetimes even more.

Figure 3 provides the ^{10}B depletion rate curves, as a function of exposure in snvt, for two blades operated in a late generation BWR/5 plant. The original equipment blades have a 34% depletion limit based on cracking while the advanced design blades are limited to 58% ^{10}B depletion. Depletion rates differ because of the higher boron carbide loading in the advanced design blade. The 'real' lifetime advantage of the hybrid blade is the ratio of the EOL exposures in snvts, i.e. 4.39 ÷ 1.96 = 2.24.

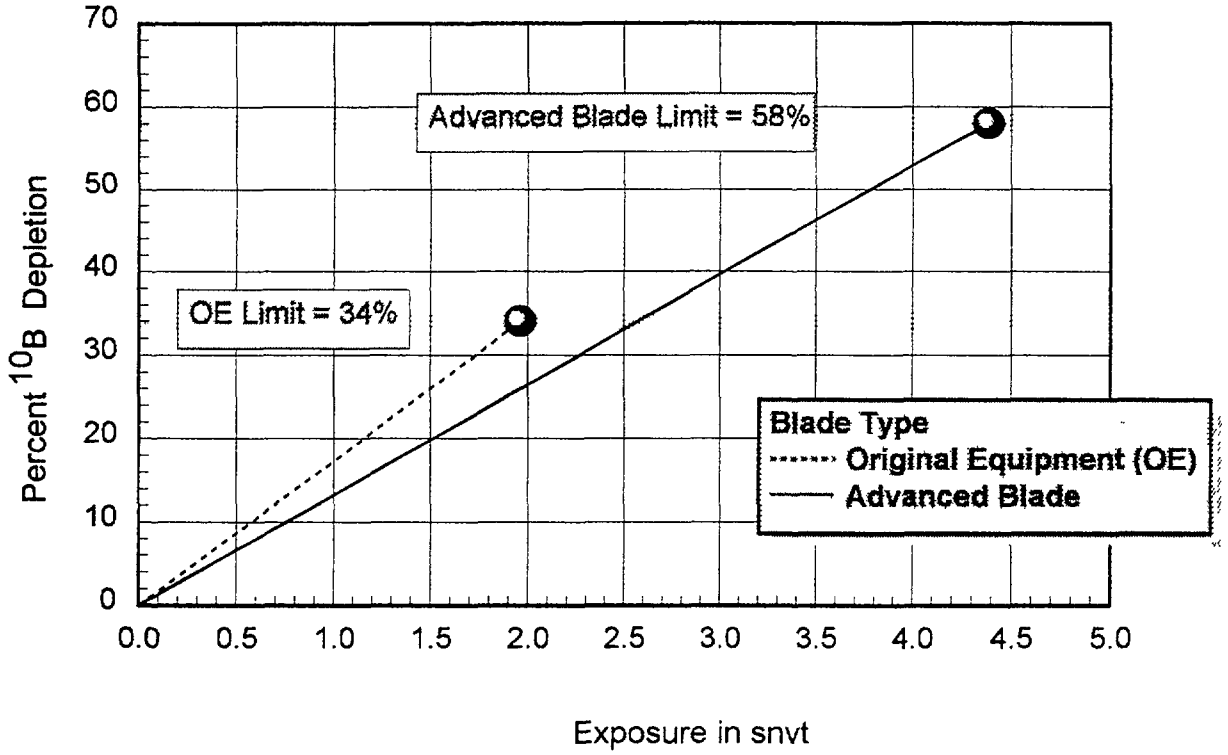

FIG. 3. Depletion rate and lifetime comparison, original equipment vs. advanced blade design

The original equipment, Duralife 120, and Duralife 140 designs (see Table I) have mechanical limits based on the observation of cracking. The Marathon design is limited mechanically by internal pressure at high exposures. The remaining designs have nuclear limits.

GE provides guidelines related to shuffling original equipment blades in Service Information Letter (SIL) 157 (similar guidelines are provided in SIL 579 for Duralife 120 and 140 designs):

- the exposure limit in terms of ^{10}B depletion is 34% peak quarter segment corresponding to ~2 snvt in a BWR/5 plant;
- if the exposure is less than 20% ^{10}B depletion, the blade can be moved to a new core position and remain there until its exposure reaches 34% at which time it must be discharged; and
- if the exposure is ≥20% and less than 34%, the blade may be shuffled but its residence time is limited, being the greater of:

- one cycle, or
- the equivalent number of cycles the blade would have remained in its prior position without exceeding the 34% limit.

This methodology introduced a 'phantom' exposure increment. That is, the exposure increment received in the new position was based on the exposure increment consistent with the prior core position. There are apparently no restrictions on shuffling advanced blade designs as long as nuclear and mechanical limits are met.

GE recommends tip adders for non-hafnium tip designs when placed in shutdown positions. Utilities have been reluctant to use them since 1) there were no requirements for their use, and 2) there was not a rigorous basis for the correlations.

1.4. Siemens

Siemens has long had a co-operative research and development program with GE. It is not surprising that the two vendors' designs are similar and share similar failure mechanisms (IASCC and crevice corrosion cracking). Based on absorber tube cracking observed in the original equipment blades in early cycles in several German BWR plants Siemens characterized the cracking phenomenon as a function of exposure (see Table II) and developed the following strategy for shuffling and replacement:

- original equipment blades can occupy high duty control cell positions to an exposure of ≤ 1.8 snvt projected EOL with subsequent discharge or movement to a core edge position;
- if the exposure is ≥1.4 snvt at beginning of cycle (BOC), the blade can be placed in any shutdown position; and
- if the exposure is ≥1.6 snvt at BOC, the blade can only be placed in a low duty shutdown position (not near core center).

TABLE II. SIEMENS ORIGINAL EQUIPMENT BLADE LIMITS

Characteristic	Local B-10 Depletion, %	% Nuclear Lifetime	Exposure, snvt
Begin cracking	30	37	~1.0
Begin TABLE I loss	40	49	~1.3
10% S/D margin reduction, B_4C + washout	54	66	~1.8
10% S/D margin reduction, B_4C without washout	82	100	~2.7

Original equipment blades are still used quite extensively in German reactors. The current advanced design offered is the Hybrid-4 blade (since ~1988) using high purity stainless steel, redesigned welds to minimize crevice corrosion, and hafnium at high duty blade tip and edge locations. The current limits are given in Table III (~BWR/6 plant design):

TABLE III. CURRENT BLADE LIMITS

Blade Design	Nuclear, snvt (%)	Mechanical, snvt (%)
Original equipment	3.2 (45)	~2.1 (~30)
Hybrid-4	5.3 (62)	≥4.0 (≥47)

The $\%^{10}B$ depletion values are peak segment average values. Operating experience supports blade exposures of more than 3.7 snvt as cracks have not been observed at these exposure levels.

2. UTILITY BLADE REPLACEMENT STRATEGIES

Data has been analyzed from a total of 23 utilities, operating 45 BWRs in the U.S., Europe, and the Far East, concerning their blade replacement strategies and operational limits. The responses are believed to be representative of the industry. The geographical breakdown of the utility companies consists of:

- 9 U.S. utilities (13 plants);
- 10 European utilities (19 plants); and
- 4 Far Eastern utilities (12 plants).

As summarized in Table IV, these represent BWR/2 to BWR/6 plant designs and GE, Siemens, and ABB-Atom NSSSs operated in control cell, conventional, and mono-sequence control cell modes. The table shows that the utilities have implemented a full range of blade designs, from all-B_4C to hybrid B_4C/hafnium to all-hafnium absorber materials.

2.1. Control Blade Shuffling Strategies

Frequency of Blade Shuffling

Table V summarizes blade shuffling activities performed by the responding utilities. More than one-half (58%) shuffle blades. Most obviously, this is to extend blade in-core residence times. Blades are generally moved from high duty positions (i.e., control cells in CCC cores) to shutdown positions where they remain withdrawn during operation. In such positions, the incremental exposure is negligible. Additionally, as noted by one utility, shuffling allows the high exposure but low cobalt blades to replace original equipment designs incorporating high cobalt materials.

Slightly less than one-half of the utilities do *not* shuffle blades, choosing instead to leave the blades in the same position from one cycle to the next. These utilities note that the life extension benefit is marginal, especially in light of the increased costs to shuffle blades which can only be done during a refuelling outage. One domestic utility estimates the cost to be as much as $10,000 per outage hour with it taking 4 to 8 hours to shuffle a pair of blades. With utilities moving to shorter and shorter outages, there is more pressure not to shuffle blades. Over the last 18 months in the U.S. there has been a 117% *increase* in the number of plants with outages of 40 days or less and a 93% *increase* in the number of plants with 50 day outages or less.

Shuffling Strategies

Vendors have a minor influence on the strategies implemented by utilities especially as the original equipment blades with their short mechanical lifetimes are replaced by hybrid blades incorporating advanced materials and absorbers. Siemens, for example, developed guidelines on where a blade could be placed based on its exposure level (see Table II) while GE proceduralized their guidelines in SIL 157 and SIL 579 for the original equipment and Duralife 120/140 series blades, respectively.

The strategies with the various designs are, of course, to move high burnup blades to low exposure regions and vice versa. The actual strategy depends primarily on design features C GE original equipment blades, for example, are still prone to B_4C swelling at blade tip positions even when fully withdrawn from the active core region in shutdown banks. This necessitates the use of 'phantom' exposures in subsequent cycles.

Figure 4 shows an example of the strategy used by Utility D for the end of cycle (EOC) 12 refueling outage at Unit D1. Four different types of moves were planned, the specific move depending on blade type and exposure:

Table IV. SUMMARY OF BWR PLANT FEATURES

Utility		Plant	NSSS Vendor	Plant Type	# Fuel Ass'ys	# Control Blades	Blade Types Currently Used	Operating Mode
USA	A	A1	GE	BWR/4	764	185	OE, D140, D215	CCC
	B	B1	GE	BWR/6	800	193	OE	CONV
		B2	GE	BWR/6	624	145	OE, CR82M	CONV
	C	C1	GE	BWR/2	560	137	OE, D160, D190, D230, M	CCC
	D	D1	GE	BWR/4	560	137	OE, D190, D230, M, CR82M	CCC
	E	E1	GE	BWR/2	532	129	OE, D190, D230	CONV
		E2	GE	BWR/5	764	185	OE, D190, D215, M	~CCC
	F	F1	GE	BWR/3	580	145	D140, CR82, CR82M, M	CCC
	G	G1	GE	BWR/4	560	137	OE, D190, D230	CONV
		G2	GE	BWR/4	560	137	OE, D190, D230, CR82	CONV
	H	H1	GE	BWR/4	764	185	OE, D160	CCC
		H2	GE	BWR/4	764	185	OE	CCC
	I	I1	GE	BWR/5	764	185	OE, D215	CCC
Europe	J	J1	KWU	N/A	592	145	OE, CR70, CR82, CR85	MSCC
	K	K1	GE	BWR/4	240	57	D230 + others	CCC
	L	L1	GE	BWR/6	648	149	OE, D230, CR85	CCC
	M	M1	KWU	N/A	532	129	OE, CR82, CR82M, CR85, M	MSCC
		M2	KWU	N/A	840	205	OE, CR82, CR82M, CR85, M	MSCC
	N	N1	GE	BWR/6	624	145	OE	CCC
	O	O1, O2	KWU	N/A	784	193	OE, Duralife series, M	CONV
	P	P1	KWU	N/A	592	145	OE, CR82, M	CCC
	Q	Q1, Q2	ABB	N/A	444	109	CR70, CR82, CR85	MSCC
		Q3, Q4, Q5	ABB	N/A	444-700	109-169	CR70, CR82, CR82M, M	MSCC
	R	R1, R2	ABB	N/A	500	121	CR70, CR82, CR82M, SR88	MSCC
	S	S1, S2, S3	ABB	N/A	676-700	161-169	CR70, CR82, CR82M, M	MSCC
Far East	T	T1, T2, T3, T4	GE	BWR/4, BWR/5	N/A	N/A	OE, all-Hf	CCC
	U	U1, U2	~GE	BWR/2, BWR/5	N/A	N/A	OE, CR85, CR85M1	CCC
	V	V1, V2	GE	BWR/4	408	97	OE, D215	CONV
		V3, V4	GE	BWR/6	624	145	OE, D230	CONV
	W	W1, W2	~GE	BWR/4	N/A	N/A	OE, all-Hf	CCC

OE = Original equipment **D140** = Duralife 140 **D160** = Duralife 160 **D190** = Duralife 190 **D215** = Duralife 215
D230 = Duralife 230 **M** = Marathon **CR70** = CR-70 **CR82** = CR-82 **CR82M** = CR-82M
CR85 = CR-85 **CR85M1** = CR-85M-1 **CCC** = control cell core **CONV** = conventional mode **MSCC** = mono-sequence control cell

Table V. CONTROL BLADE SHUFFLING - UTILITY RESPONSES

Utility		Shuffle Blades?	Comments
USA	A	Y	Shuffle to extend blade lifetimes
	B	N	Increases outage costs
	C	Y	Shuffle to extend blade lifetimes; high duty blades moved to shutdown positions
	D	Y	Shuffle to extend lifetimes & to replace high cobalt original equipment blades
	E	Y	Limited shuffling performed; extends lifetimes; blades moved from high duty positions to peripheral & core edge positions
	F	N	Increases outage costs
	G	N	Limited shuffling in past; used as a last resort
	H	N	Increases outage costs
	I	Y	Shuffle to extend blade lifetimes; high exposure blades moved to peripheral positions, peripheral blades moved to high duty positions
Europe	J	Y	Shuffle to extend blade lifetimes; high exposure blades moved to peripheral shutdown positions, shutdown blade moved to high duty positions
	K	Y	Shuffle to extend blade lifetimes; high exposure blades moved to peripheral shutdown positions, shutdown blades discharged
	L	N	Life extension is minimal; increases outage costs
	M	Y	Shuffle to extend blade lifetimes; high exposure blades moved to low duty shutdown positions
	N	Y	Shuffle to extend blade lifetimes
	O	N	Increases outage costs
	P	N	Increases outage costs
	Q	Y	Limited shuffling for life extension
	R	Y	Shuffle to extend blade lifetimes
	S	Y	Shuffle to extend blade lifetimes; typically move blades from control cells to shutdown positions
Far East	T	N	Life extension is minimal; replace with all-Hf designs
	U	N	Life extension is minimal
	V	Y	Shuffle to extend blade lifetimes
	W	N	Life extension is minimal; replace with all-Hf designs

- **Move A** – selected original equipment blades were moved to interior shutdown positions after having occupied shutdown positions near the core periphery for eight cycles;

- **Move B** – selected Marathons inserted at EOC 10 resided in shutdown positions for two cycles and were then moved into control cells;

- **Move C** – selected Duralife 230s inserted EOC 8 resided in control cell positions for four cycles and were then moved to shutdown positions; and

- **Move D** – selected Duralife 230s inserted EOC 9 resided in shutdown positions near the core periphery for three cycles and were then moved to control cell positions.

Examples typical of these moves are shown in Figure 4.

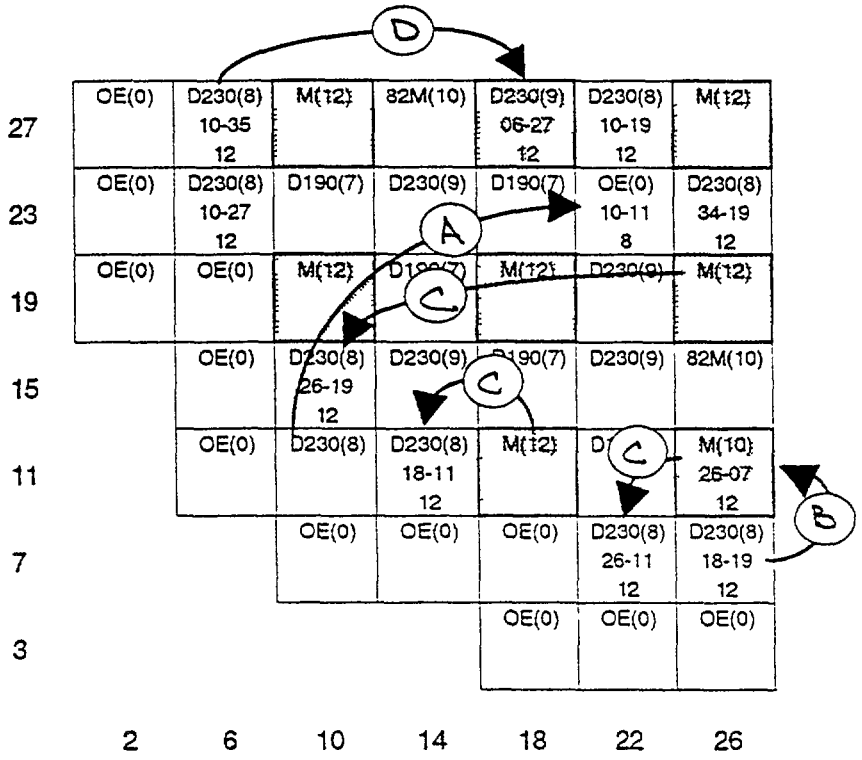

D230(8) 34-35 12 - Blade Type (Refueling Outage Loaded)
- Core Position Shuffled From
- Refueling Outage Shuffled

- Control Cell

Blade Type	Description
OE	Original Equipment
D190	Duralife 190
D230	Duralife 230
M	Marathon
82M	CR 82M

FIG 4 Planned blade shuffling for unit D1 at EOC 12

2.2. Control blade replacement strategies

Replacement Designs

Table VI provides a summary of the replacement blade designs used by the responding utilities and the calculational methods used to evaluate exposure. Quite apparent is the full range of replacement designs, from original equipment blades in three utilities to all-hafnium designs in several Far Eastern plants. The majority of utilities (87%) replace discharge blades with advanced designs incorporating improved structural steels and at least hafnium tips.

In the U.S., the majority of the utilities are using Duralife 190 and 200 series blades with hafnium tips and edges. Less common are Marathon designs and ABB-Atom's CR-82 and CR-82M designs. In Europe, most replacement blades are ABB-Atom's CR-82, CR-82M, and CR-85 designs

with GE providing a relatively small number of Duralife and Marathon blades. In the Far East, replacement designs incorporate either hafnium tips and edges (Duralife 200 series, CR-85, CR-85M-1) or are all-hafnium designs.

TABLE VI. CONTROL BLADE REPLACEMENT - UTILITY RESPONSES

Utility		Exposure Calculations	Tip Adders Used?	Replacement Designs
USA	A	-----	-----	D140, D215
	B	PowerPlex, 3D MONICORE	Y	OE, CR82M
	C	RODEX	Y	D160, D190, D230, M
	D	3D MONICORE	N	D190, D230, M, CR82M
	E	3D MONICORE	N	OE, D190, D215, D230, M
	F	-----	Y	D140, M, CR82, CR82M
	G	3D MONICORE	N	D160, D190, D230, CR82
	H	3D MONICORE	Y	OE, D160
	I	PowerPlex	N	D215
Europe	J	-----	-----	CR82, CR85
	K	-----	-----	D230
	L	Core Master/Presto	Y	D230, CR85
	M	-----	N	CR82, CR82M, CR85, M
	N	-----	-----	OE
	O	-----	-----	Duralife, M
	P	-----	-----	CR82, M
	Q	-----	-----	CR82, CR82M, CR85, M
	R	POLCA4	Y	CR82, CR82M
	S	-----	-----	CR82, CR82M, M
Far East	T	-----	-----	All-Hf
	U	3D MONICORE	N	CR85, CR85M1
	V	PowerPlex, 3D MONICORE	-----	D215, D230
	W	-----	N	All-Hf

As noted above, three utilities replace discharge blades with original equipment blades – Utilities E, H, and N. In these cases, the utilities have purchased (or received) the blades from canceled plants and use them as inventory for replacements. High cobalt pins and rollers are replaced in all cases to reduce primary system activation.

As these blades incorporate all-B_4C absorber, commercial purity steels, relatively high cobalt components, and geometries that promote coolant stagnation, they are prone to absorber tube cracking. Consequently, lifetimes are restricted by mechanical limits (exposures $\leq$34% B^{10} depletion) requiring that more blades be replaced over the life of the plant. This requires more handling of blades and the use of SIL 157 restrictions in shuffling. Additionally, the higher cobalt content relative to modern replacement designs increases primary system radiation fields.

In spite of these disadvantages, economic analyses tend to favor the use of the original equipment blades simply due to their extremely low price. In order to characterize the economic advantage of original equipment vs. advanced blades, we performed an analysis based on the following assumptions:

- the cost of the original equipment blades is $5,000 (replacement of high cobalt pins and rollers);

- the purchase price of a new advanced design blade is $75,000;
- nuclear lifetimes are 34% ^{10}B depletion (peak segment) for the original equipment blades, 54% for the advanced blades;
- disposal costs are $25,000 per blade;
- outage costs are $10,000 per hour;
- control cell core operation with typical blade exposure increments per cycle;
- no allowance for enhanced primary system radiation fields due to higher cobalt blade materials;
- no blade shuffling; and
- no escalation, future worth, etc. corrections.

Results are provided in Figures 5 and 6 through fifteen cycles of operation under these conditions.

Figure 5 shows the resulting blade replacement schedule. As one would expect, more original equipment blades are needed due simply to their shorter lifetimes. A total of 144 original blades are needed vs. 103 advanced design blades – an increase of 30%. Figure 6 provides the cumulative cost of using each blade type through EOC 15. Even with the larger number of blades needed and higher costs due to having to purchase and dispose of more blades, the economic advantage of the original equipment blades is substantial, with the cumulative EOC 15 cost being approximately 70% of that of the advanced blades. When averaged over the fifteen cycles, the cost advantage is about $300,000 per cycle.

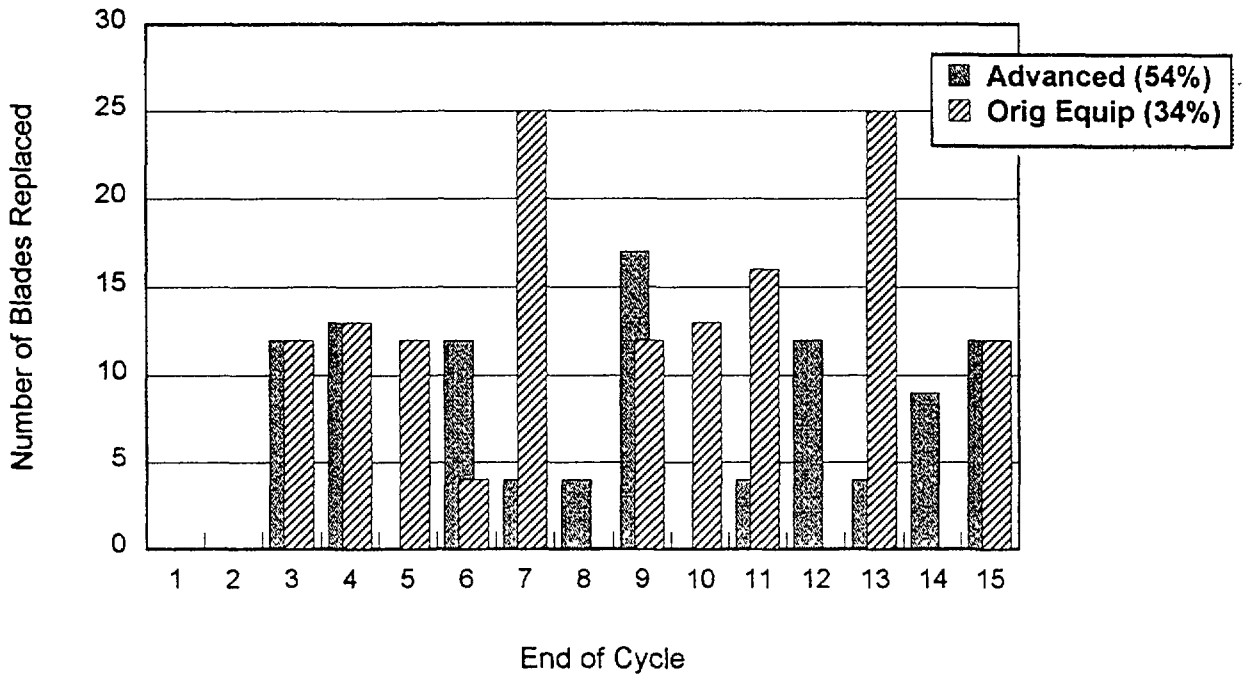

FIG 5. Impact of blade type on replacement schedule

Replacement Criteria – Utilities Using ABB-Atom Blades

The early blade designs incorporating 304SS for structural materials have lifetimes limited by IASCC. These are the CR-70, CR-82, and CR-85 series. The exposures to date of the advanced designs are not sufficient to determine if they are also limited by absorber integrity concerns.

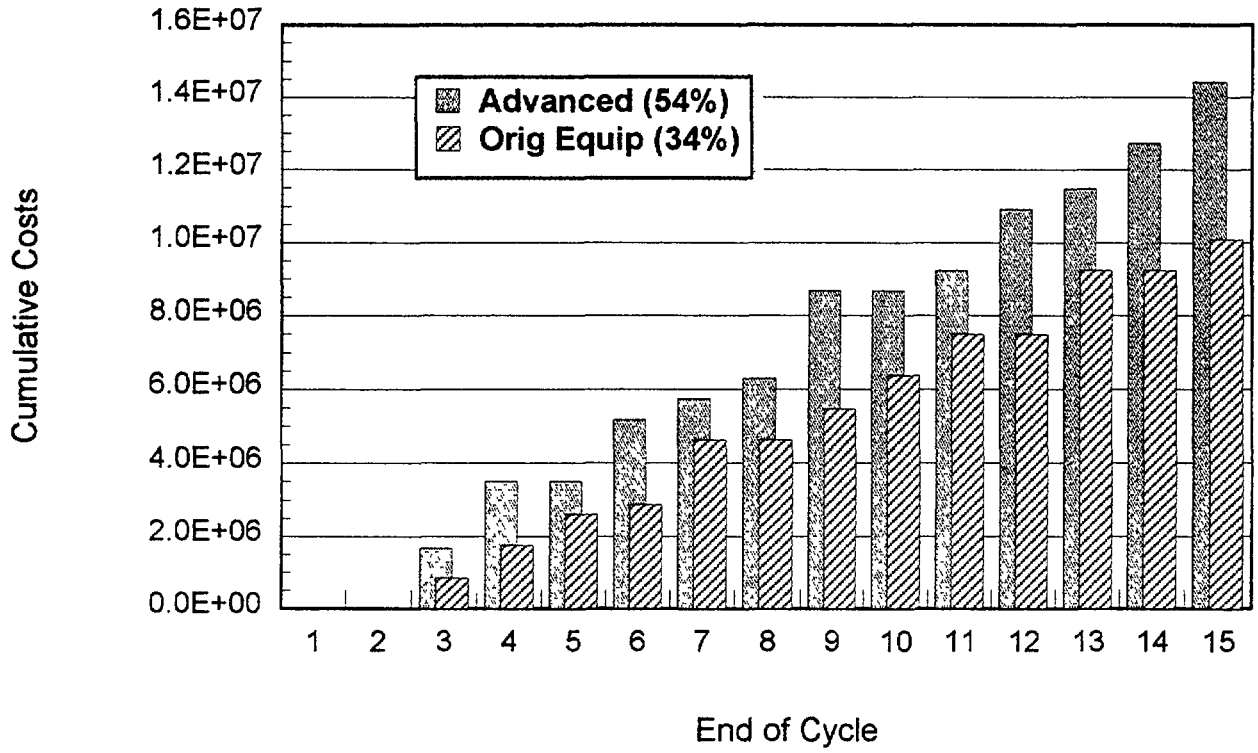

FIG. 6. Cumulative costs as a function of cycle completed

U.S. utilities have adopted ABB-Atom's guidelines and criteria related to blade replacement. As such, lead blades are inspected and discharged if cracks are observed.

European utilities, on the other hand, have adopted criteria that are, at times, more restrictive than those suggested by ABB-Atom. For example, Utility J has implemented limits of 1.9 snvt for CR-70s and a modest 3.0 snvt for the hybrid CR-82s and CR-85s. These are based on their own experiences of cracking in Unit J1.

The majority of other European utilities visually inspect blades on a frequent basis to assess cracking. A typical example is Utility S which operates several units in Sweden. The utility has developed exposure-related criteria for their units based on their experience with cracking in the CR-70 control blades. These criteria, noted below, apply specifically to the CR-70 blades and are recommended for the CR-82, CR-82M, and Marathon designs:

- blades with tip exposures exceeding 57% ^{10}B depletion shall be inspected before continued irradiation;
- blades with maximum quarter segment exposures above 18% ^{10}B depletion shall be inspected before continued service; and
- blades scheduled for control positions with quarter segment exposures in excess of 45% ^{10}B depletion shall be inspected before insertion in those positions (these particular blades are also inspected at EOC *after* their use in the control positions).

An additional criteria is applied to blades exposed in Units S1 and S2. Blades that are free of cracks with 1) tip exposures between 57% and 60% ^{10}B depletion, and 2) having a maximum quarter segment exposure below 18% ^{10}B depletion are allowed to continue operation for a maximum of two years in a shutdown position. These blades are, however, considered to be cracked during their second year of exposure with penalties applied in the shutdown margin evaluations.

Although most European utilities discharge blades when cracked, Utility S allows a cracked blade to be reinserted for an additional cycle only if it is moved to a shutdown position.

Replacement Criteria – Utilities Using GE Blades

With very few exceptions, vendor criteria and guidelines are implemented by U.S., European, and Far Eastern utilities. Inspections are not performed due to the presence of the sheath covering the absorber tubes. Blades are discharged when exposure limits are approached.

Two utilities have discharged blades well before their lifetimes. At EOC 2, Utility A discharged 165 original equipment blades and replaced them with Duralife 140s to reduce cobalt activation and, consequently, primary system radiation fields. Utility L, at EOC 3 in Unit L1, replaced 16 original equipment blades with Duralife 230s and CR-85s in order to quickly gain experience with hybrid designs.

Replacement Criteria – Utilities Using Siemens Blades

U.S. utilities responding to the survey have no experience with Siemens blades. Limits on original equipment blades used by European utilities vary from 1.6 snvt at Unit P1 to 2.7 snvt at Units M1 and M2. Referring to Table II, these limits approximate the 10% reduction in blade worth due to B_4C depletion plus washout (~1.8 snvt, BWR/2-5) and the 10% reduction in blade worth due only to B_4C depletion (~2.7 snvt, BWR/2-5).

Replacement Criteria – Utilities Using All-Hafnium Blades

All-hafnium blades are used in several Far Eastern plants. The utilities implement the vendor criteria and guidelines. Utility T limits original equipment (i.e., all B_4C designs) to $\leq$1.74 snvt due to cracking. All-hafnium blades are limited to $\leq$9.0 snvt at the top axial segment.

Use of Tip Adders

Nearly one-half of the responding utilities use tip adders to account for B_4C swelling and absorber tube sensitization occurring in the tip region of a blade when located in a shutdown position (i.e., fully withdrawn during operation). ABB-Atom and GE recommend that tip adders be used for all-B_4C blade designs. Tip adders are not needed for designs incorporating hafnium tips as hafnium experiences little swelling and growth during irradiation. With the exception of one utility, all responders still have original equipment blades under irradiation. Tip adders are typically on the order of 1 to 3% ^{10}B depletion per cycle. One U.S. utility uses 2% tip depletion per 10,000 MWd/st.

Reasons given for *not* using tip adders include:

- blades located on the core periphery receive effectively zero exposure;
- with operation in a conventional (i.e., sequence exchange) mode, all non-peripheral blades receive some exposure during the cycle and that exposure can be estimated and tracked;
- vendors do not *require* the use of tip adders;
- correlations for tip exposure are poorly benchmarked; and
- no trend has been observed in measured shutdown margin to indicate absorber loss.

Handle Embrittlement Issues

Although ABB-Atom and GE indicate that handle embrittlement is not a threat to blade integrity, several utilities have directly addressed this issue. Utility Q, in Units Q1 and Q2, discharges blades when they have reached a fluence of ~10^{22} n/cm^2 based on calculational methods. This corresponds to about 20 years residence time. Hot cell examinations have been performed on blades from Units Q3, Q4, and/or Q5 and from these some correlations were developed based on fast fluence. The utility replaces blades after 10 to 25 cycles of operation.

Blade Exposure Calculational Methods

Utilities use vendor correlations in calculating blade exposures. The methods consist of evaluating the exposures of the fuel assemblies adjacent to the blade of interest and converting the smeared thermal fluence (in snvt) to B^{10} depletion. Most utilities with GE NSSSs use 3D MONICORE from GE, or PowerPlex from Siemens, to estimate and trend blade exposures. Utilities with ABB NSSSs perform the exposure calculations using similar methods (i.e., COREMASER/PRESTO). In some instances, ABB-Atom performs the exposure evaluations for the utility.

The correlation between fluence in snvt and percent ^{10}B depletion is dependent on blade design (see, for example, Figure 3) and on the following factors:

- average void in the adjacent assemblies;
- design of the adjacent assemblies; and
- relationship between thermal fluence and core power.

The most sophisticated methods to date use correlations for the aforementioned factors, evaluating exposures in the four axial blade segments and blade tip (typically 6 in., 152 mm axial region).

3. CONCLUSIONS

On Shuffling

1) A total of 58% of the utilities shuffle blades at least on a limited basis, most often to extend lifetimes. Blades are generally moved from high duty positions (control cells, for example) to lower duty shutdown positions. One utility shuffles preferentially to positions occupied by *original equipment* blades to accelerate the removal of those blades containing high cobalt materials;

2) Slightly less than one-half of the utilities do *not* shuffle blades. Although blade lifetimes can be increased by moving them to low duty positions, shuffling increases outage costs through additional manpower and time requirements.

On Replacement Blade Designs

1) Utilities replace discharged blades with ones having a wide range of design features, from original equipment blades (similar to those they are discharging) at three utilities to all-hafnium designs used at two Far Eastern utilities. However, the majority of the utilities insert designs that employ at least crack-resistant structural materials and hafnium tips;

2) There tends to be a strong correlation between NSSS vendor and replacement blade supplier. Utilities with GE NSSSs (or NSSSs based on GE's designs) tend to load Duralife and/or Marathon designs while utilities with KWU and ABB NSSSs most often replace with ABB's designs (Siemens designs are essentially no longer available). However, it is quite apparent that both vendors are actively pursuing the replacement blade market and have been successful in loading their designs into the other vendor's NSSSs;

3) Three utilities have a large inventory of original equipment blades available from canceled plants that are used as replacements.

On Blade Replacement Strategies

1) Utilities Using ABB-Atom Blade Designs

- ABB-Atom recommends that utilities using 304SS blade designs (CR-70, CR-82, CR-85) begin inspecting blades at a peak segment exposure of 3 snvt;

- No specific mechanical limits have been established for blades using 316L wings i.e., CR-82M, CR-82-M-1, CR-85M, CR-85M-1. The strategy followed worldwide is that the lead blades are visually inspected each year. In this way, the observation of cracking will establish if the mechanical lifetimes are more limiting than the nuclear lifetimes.

2) Utilities Using GE Blades

- With few exceptions, vendor limits are implemented by utilities. Original equipment, Duralife 120, and Duralife 140 blades have a mechanical lifetime equivalent to 34% ^{10}B depletion due to absorber tube cracking and crevice corrosion. The Duralife 160 through 230 series, incorporating better materials, hafnium, and higher boron carbide loadings (Duralife 215 and 230), have resulted in an incremental improvement in lifetimes to a maximum of about three times that of the original equipment blade;

- Marathon designs are limited mechanically as a consequence of internal pressurization at high exposures due to helium generation from the (neutron, alpha) reaction with ^{10}B. The corresponding exposure limit is about 5.0 snvt;

3) Utilities Using Siemens Blades

- Designs offered by Siemens are similar to GE, so are susceptible to the same degradation phenomena. Although the nuclear limit for original equipment blades in BWR/2-5 series plants is 2.7 snvt (10% rod worth reduction due to B_4C depletion only), cracking begins at 1.0 snvt while B_4C loss is initiated at 1.3 snvt;

- Exposure limits employed by utilities using original equipment blades range from 1.6 snvt to 2.7 snvt;

- The Hybrid-4 design, incorporating hafnium, improved materials and design modifications, has a mechanical lifetime limit of ≥4.0 snvt. Lead blades have reached exposures of 3.7 snvt without indications of cracking.

On Tip Adders

- Nearly one-half of the responding utilities use tip adders to explicitly account for the exposure in the tip region of shutdown blades. Tip adders, used only for original equipment designs, range from 1 to 3% ^{10}B depletion per cycle;

- Reasons for *not* using tip adders are varied, but most common are 1) the vendor does not *require* them to be used, and 2) no trend is observed from BOC shutdown margin measurements to suggest absorber loss.

HIGH TEMPERATURE STUDY OF THE CONTROL ROD BEHAVIOUR UNDER ACCIDENT CONDITIONS

V. TROYANOV, A. POMESCHIKOV, V. SOUGONJAEV
Institute of Physics and Power Engineering,
Obninsk

V. PONOMARENKO, A. SCHEGLOV
Moscow Polimetal Plant,
Moscow

Russian Federation

Abstract

Control rod behaviour under accident conditions is considered. A comparative assessment of various types of absorbers is carried out in this respect. It was found that the best absorbers are dysprosium based absorbers. Dysprosium based control rods show no failure at temperatures below 1300°C. Boron based control rods may be liquefied at a temperature of 1150°C. Besides, the cladding may burst at lower temperature, due to the released helium. Experiments indicate that the absorber materials may initiate severe core damage under severe accidents. The beginning of core structure degradation is caused by the boron control rod liquefaction.

1. THE MAIN CORE DEGRADATION PROCESSES UNDER UNCONTROLLED TEMPERATURE INCREASE

The temperature range of core material liquefaction for WWER is between 650°C (melting point of burnable absorber based on aluminium, MPA) and 2700°C (melting point of uranium oxide and zirconium). This range may be divided conditionally to the low temperature range (not more 1500°C) and high temperature range (up to 2700°C). Let us consider the stainless steel melting point as the conditional border.

In the study considered the low temperature phenomena have been mostly analyzed. Just in this temperature range, the core degradation processes occur under severe accident conditions. These processes are fuel rod ballooning and failure, control rod failure and liquefaction, liquid eutectic formation, chemical interaction of differential types of materials, melt flow down, etc. Several schemes of core structure degradation are presented in chapter 2. These schemes are based on the experimental study of the phenomena analyzed.

2. EXPERIMENTAL STUDY OF THE CORE STRUCTURE DEGRADATION, ABSORBER CONCERN

2.1. Methodological approach

Contact interactions as well metallurgical liquefaction have been studied. Mock-ups of spacer grids, fuel rods, guide tubes have been used. Standard fuel, absorber and cladding materials have been applied for mock-up fabrication. A gamma facility and furnaces are used for testing. The gamma facility is a high temperature steam loop with steam pressure of 1 - 2 bar and test temperatures up to 1900°C. The temperature rise is approximately 1.5°C/sec. Mock-ups have been surveyed after testing and cutting and are examined metallographically by micro X-ray phase analysis. Mechanical material tensile testing has been carried out as well.

2.2. Fuel cladding/spacer grid interaction

A comparative assessment of the fuel cladding (FC) and spacer grid (SG) interactions in vacuum and in a steam environment has been done (see Table I).

TABLE I. FUEL ASSEMBLY DEGRADATION; INTERACTIONS OF THE FUEL RODS (FR) AND SPACER GRIDS (SG)

Temperature range, approximately °C	Phenomena
600-800	Fuel cladding ballooning
800-900	Fuel cladding failure Fission gas release Beginning of internal cladding oxidizing
1200 and higher	Cladding oxidizing acceleration Hydrogen release
1450	Melting of spacer grids Melt flow down Blockage formation
1900	Cladding melting

Remark no eutectic formations are observed up to stainless steel melting
FR cladding - Zr,1%Nb, Fuel - UO_2, SG - stainless steel

There are no visible interactions after 15 min testing at 980°C in vacuum. Metallography shows a 15-60 micrometer interaction layer. After 15 min testing at 1030°C in vacuum, the interaction zone is increased up to 25-360 micrometers in spite of the fact that no visible interactions are observed. At 1100°C and higher temperatures, significant interaction and liquefaction is observed. It was expected that liquefaction would happen approximately at 950°C, since the liquid eutectic temperature would be exceeded. Nevertheless, it did not happen, the initial oxide film on the zirconium cladding prevents it from liquefaction.

In the steam environment, the oxidation of zirconium is higher. A thick zirconium layer prevents the chemical interaction with steel up to 1500°C. This phenomenon is illustrated in Figs. 1 and 2.

2.3. Control rod cladding/absorber interaction

2.3.1. CRC/boron carbide

Pressurized mock-ups have been studied at a temperature range of 800-1200°C (see Table II).

TABLE II. FUEL ASSEMBLY DEGRADATION; INTERACTIONS OF BORON CARBIDE AND CONTROL ROD CLADDING GUIDE TUBE

Temperature range, approximately, °C	Phenomena
650 and higher	Diffusion of C and B into the cladding
800 and higher	Control Rod Cladding ballooning He released from B_4C Steel - B_4C interaction
1080 1174 1150 and higher	Ni/B eutectic formation Fe/B eutectic formation CR cladding liquefaction Guide tube liquefaction Melt flow down, blockage formation He released H2, CO, B203 released

Remark pressurized control rod cladding is not failed by the guide tube protection and guide tube strength
Control rod cladding - stainless steel, Guide tube - stainless steel

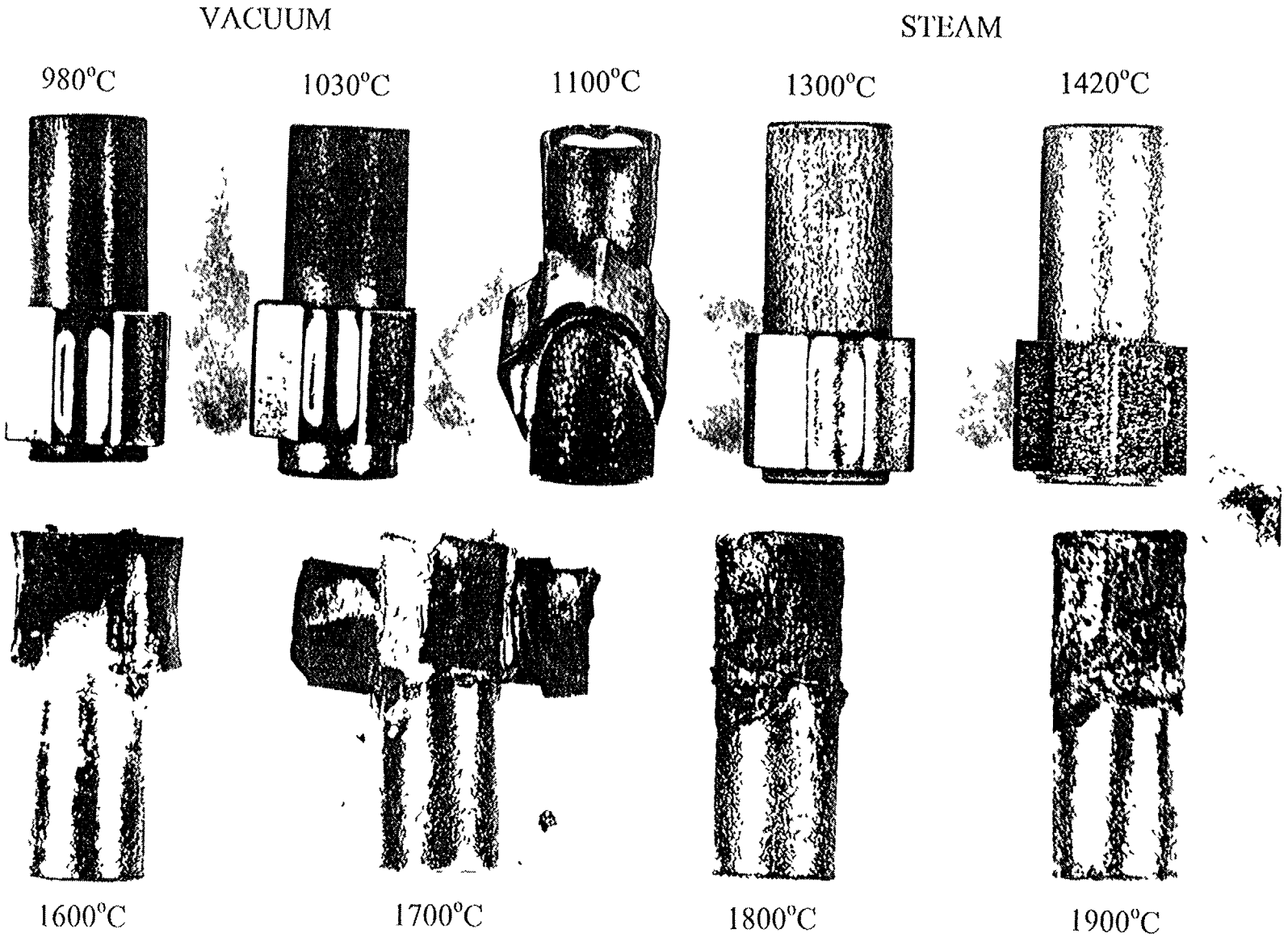

FIG 1 Spacer grid/fuel rod cladding interaction

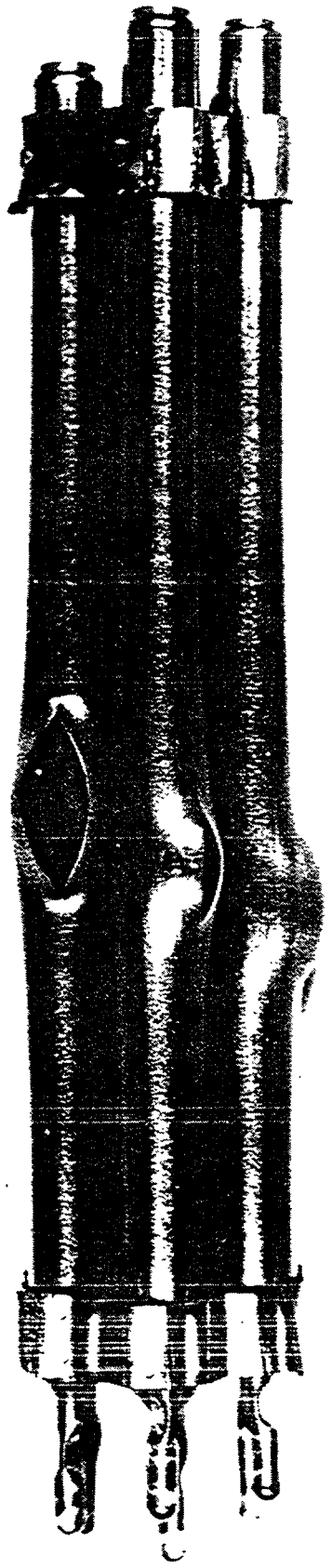

FIG. 2. Fuel assembly mock-up

There are no significant chemical interactions in the temperature range between 800-1150°C. This can be explained by the short period of temperature increase at the temperature rise rate of 1.5°C/sec. The beginning of liquefaction is observed at temperatures above 1150°C. Penetration of carbon and boron into the austenitic through diffusion is observed. Complex carbides type Me_7C_3 and borides type Me_2B is found. Fatal liquefaction occurs above 1200°C. Views of the mock-up are shown in Figs. 3-6, before and after testing at 1200°C and 1350°C.

2.3.2. CRC/dysprosium titanate

Non-pressurized mock-ups were tested at temperatures up to 1800°C (see Table III).

TABLE III. FUEL ASSEMBLY DEGRADATION; INTERACTIONS OF THE DYSPROSIUM TITANATE AND CONTROL ROD CLADDING GUIDE TUBE

Temperature range, approximately, °C	Phenomena
1200 and higher	Guide tube oxidizing acceleration
1450	Melting of the CR cladding Melt flow down within guide tubes No Di_2TiO_5 relocation due to its densification
1900	Guide tube material melting and flow down

Control rod cladding - NiCr alloy; Guide tube - Zr,1%Nb.

No significant chemical interaction has been observed up to 1400-1450°C. The views of mock-ups tested at 1200°C and 1400°C are shown in Fig. 7 and at 1800°C in Figs. 8-10.

2.4. Burnable absorber rod behaviour

The absorber alloy MPA is based on an aluminium/boron mixture. MPA is molten at temperatures higher than 650°C (see Table IV). The specific volume of MPA increases when melting by about 7%. The melt interacts with the zirconium cladding. Intermetallic compounds are formed, but the solubility of Al in Zr is not significant.

TABLE IV. FUEL ASSEMBLY DEGRADATION; BURNABLE ABSORBER ROD BEHAVIOUR

Temperature range, approximately, °C	Phenomena
650	MPA melting
650 and higher	Cladding - MPA melt interaction
700 and higher	Intermetallic compounds Zr/Al protect from further chemical interaction Cladding oxidizing
800 and higher	Cladding failure for pressurized BAR Molten absorber extraction and flow down **No failure for unpressurized BAR**

Burnable absorber - aluminium based boron alloy, MPA; Control rod cladding - Zr,1%Nb.
BAR - burnable absorber rod

The intermetallic layer is formed on the inner surface of the cladding. This is a barrier for further aluminium penetration into the cladding. The reaction rate depends on the diffusion through this layer. The fatal liquefaction of zirconium cladding does not occur. The failure of BAR cladding takes place for pressurized BARs only. For failed BARs, the gas pressure pushes the MPA melt through the hole and the melt flows down.

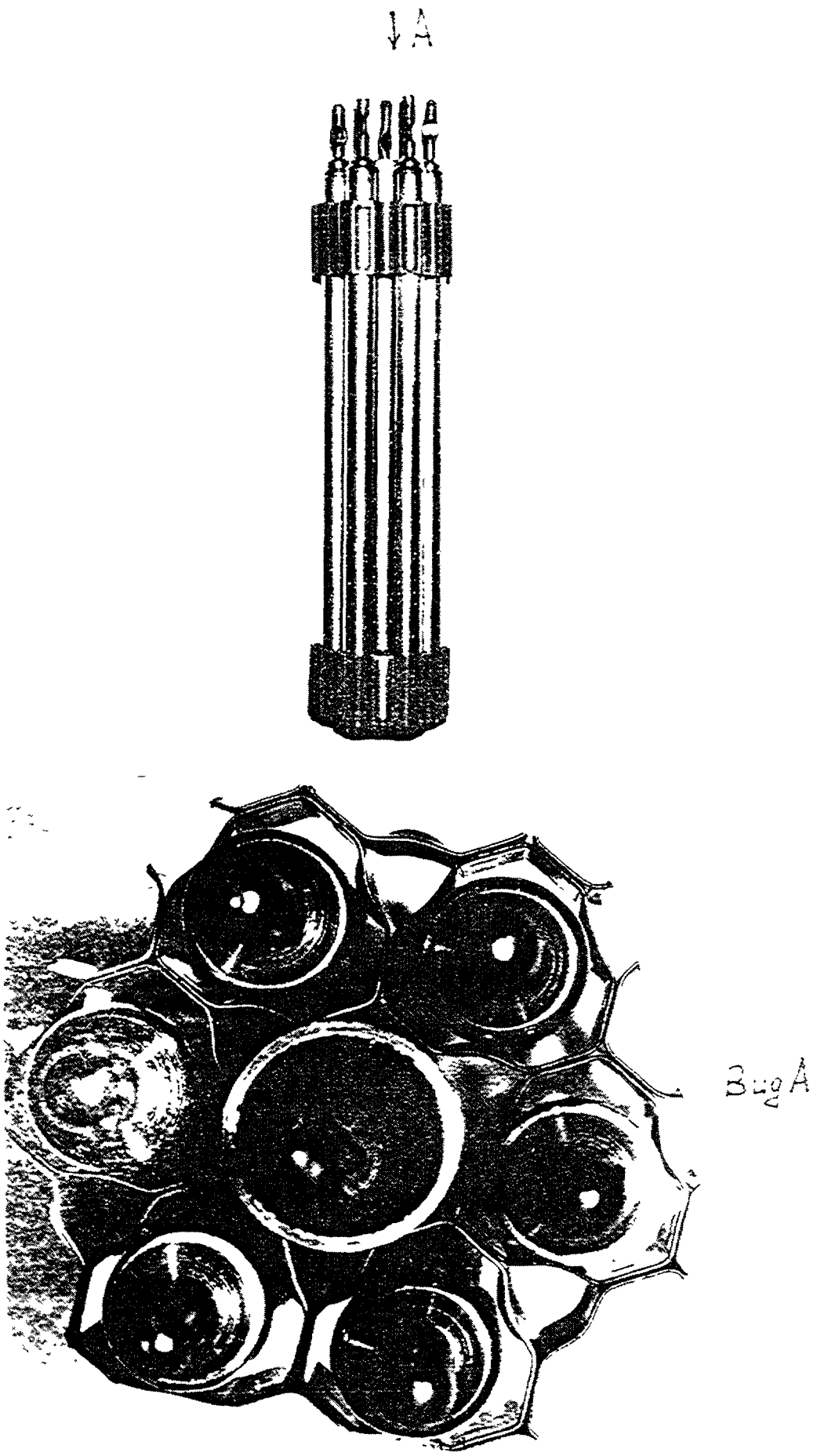

FIG. 3 Fuel assembly mock-up before testing

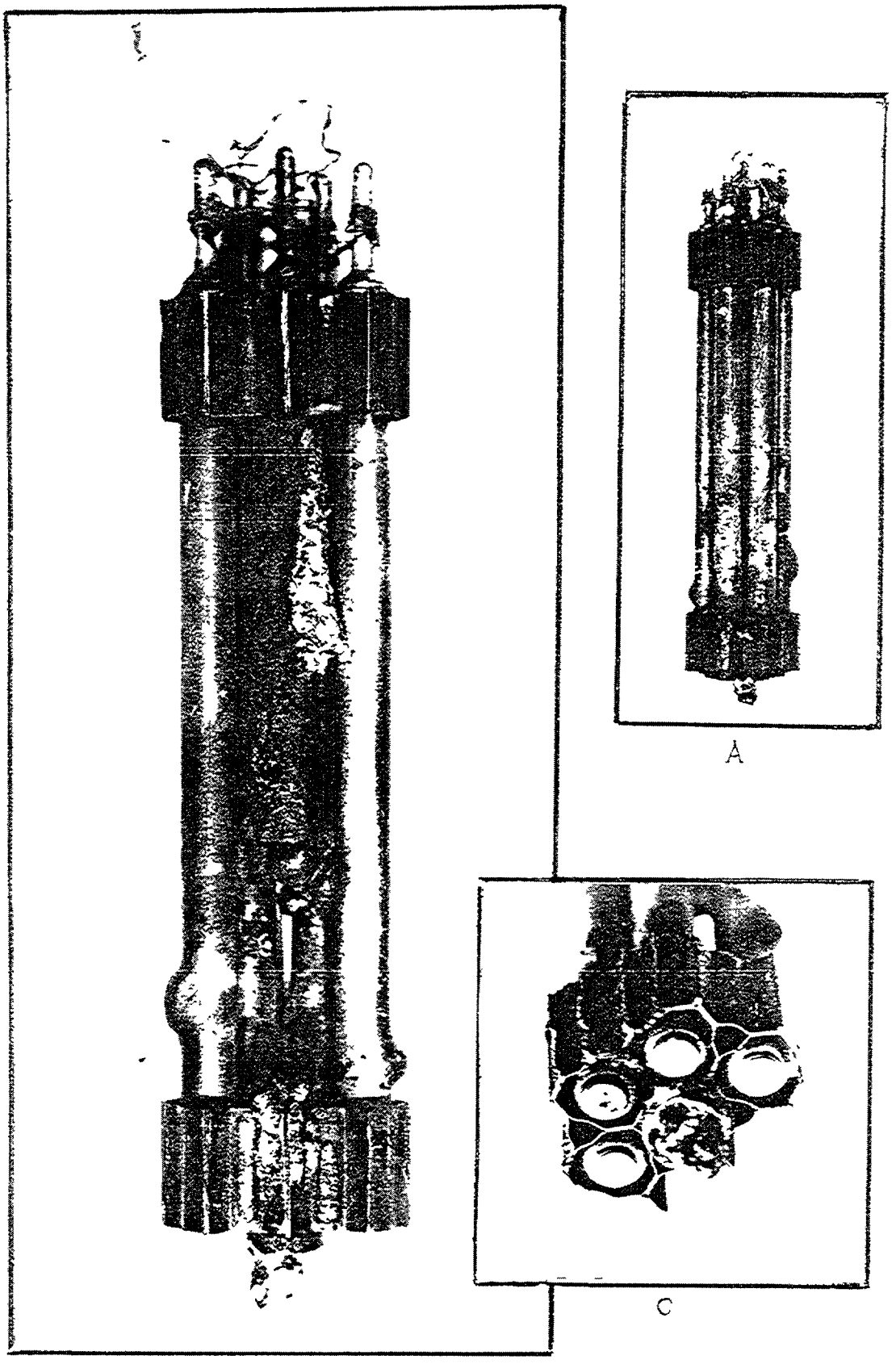

FIG 4 Boron contained mock-up after testing at 1200℃

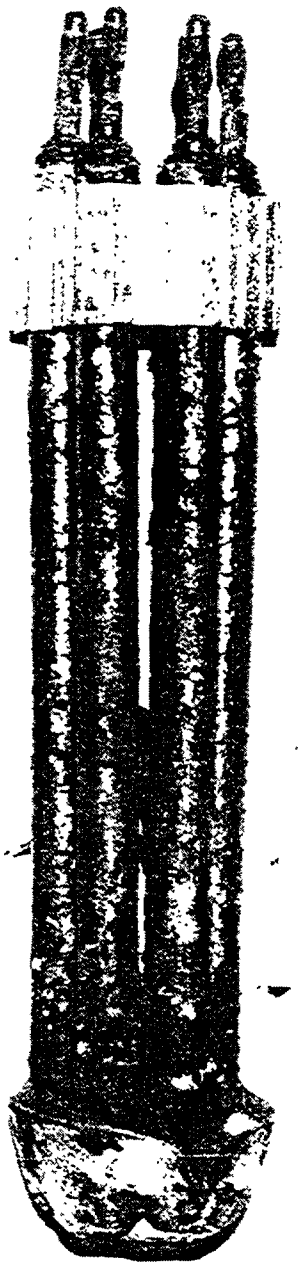

FIG. 5. Boron contained mock-up after testing at 1350 ℃

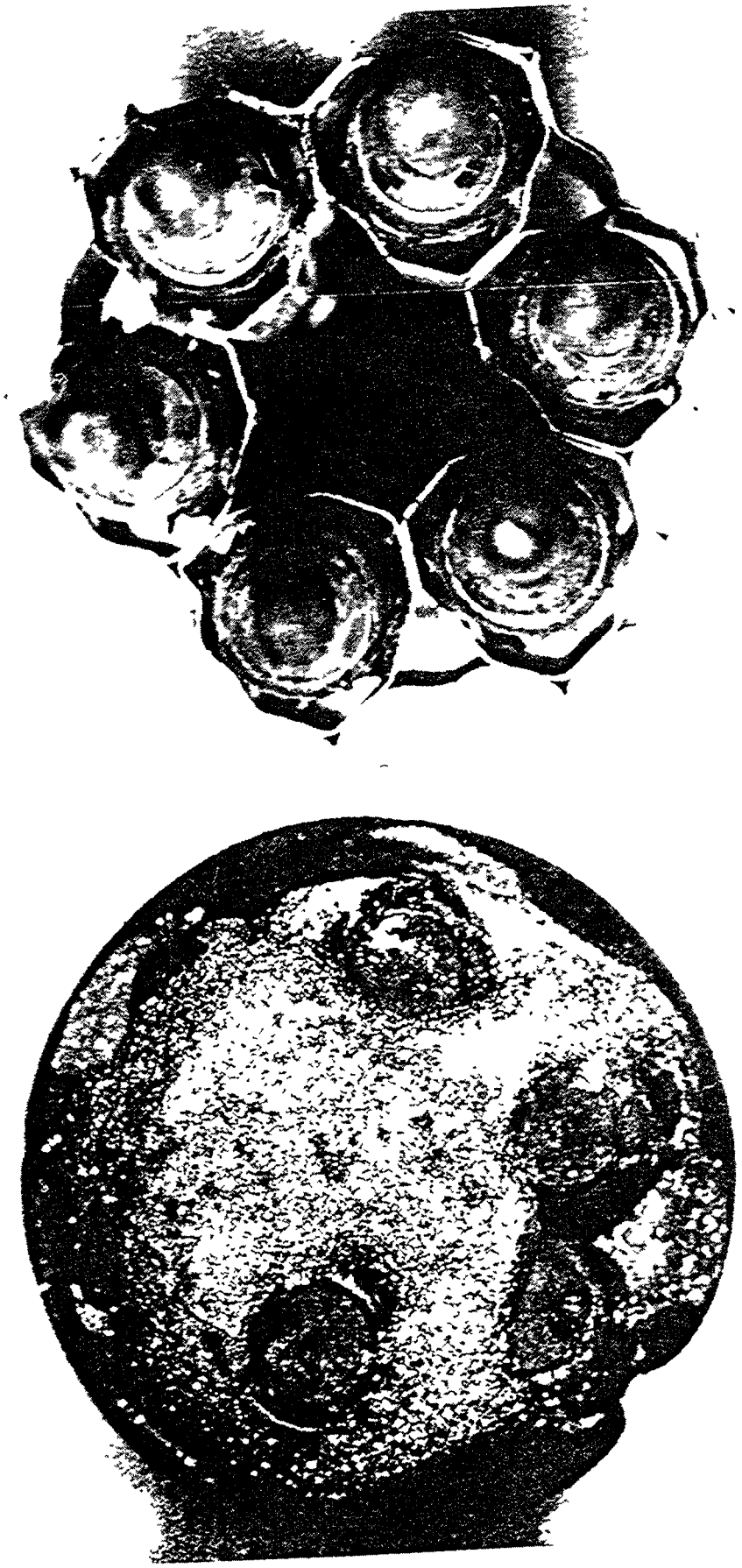

FIG. 6 Boron contained mock-up after testing at 1350 ℃

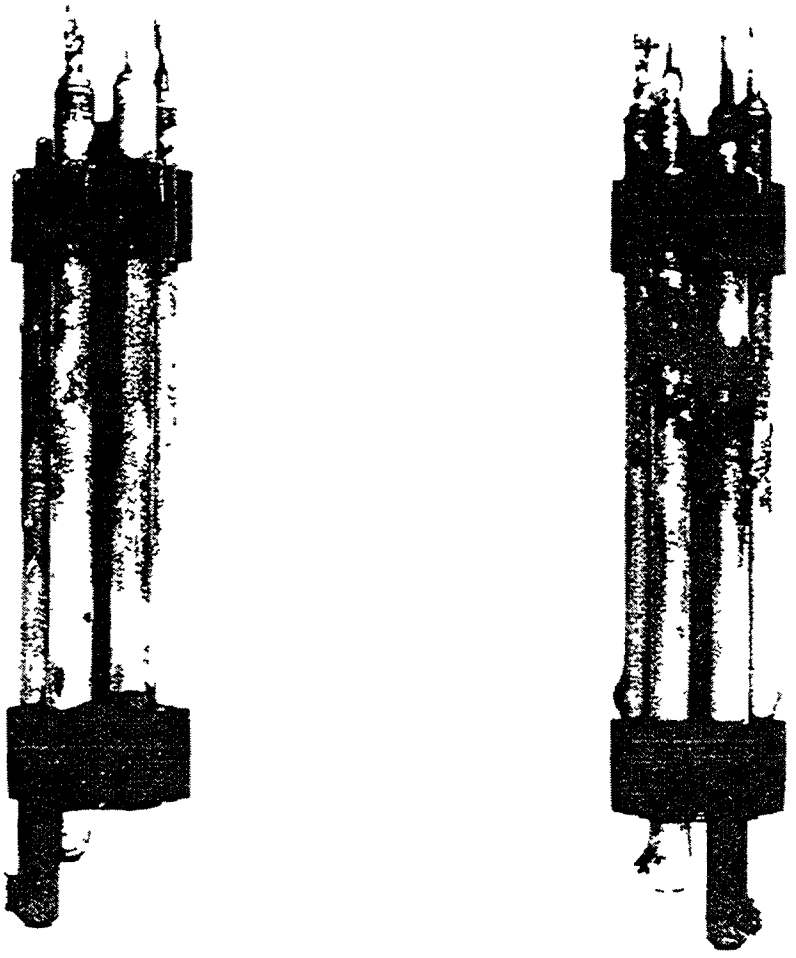

FIG 7 Dysprosium contained mock-up after testing at 1200°C (left) and 1400°C (right)

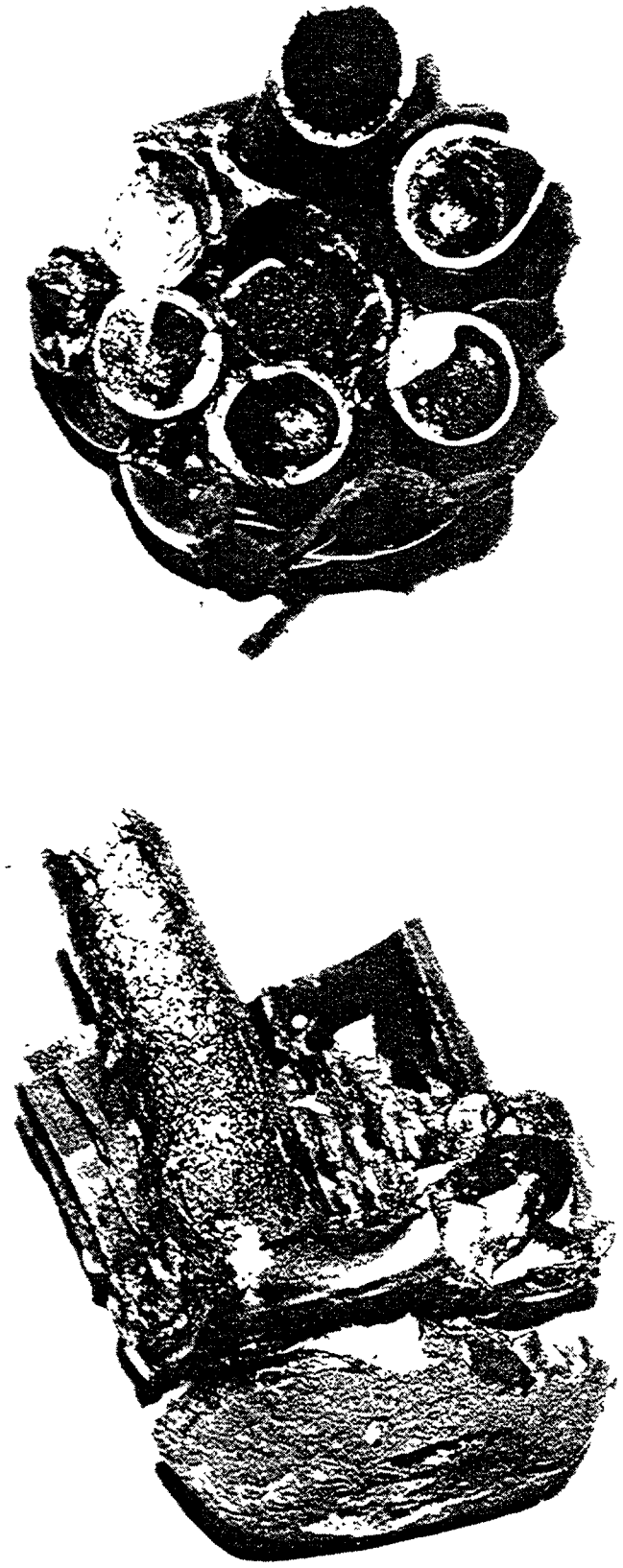

FIG. 8. Dysprosium contained mock-ups after testing at 1800°C

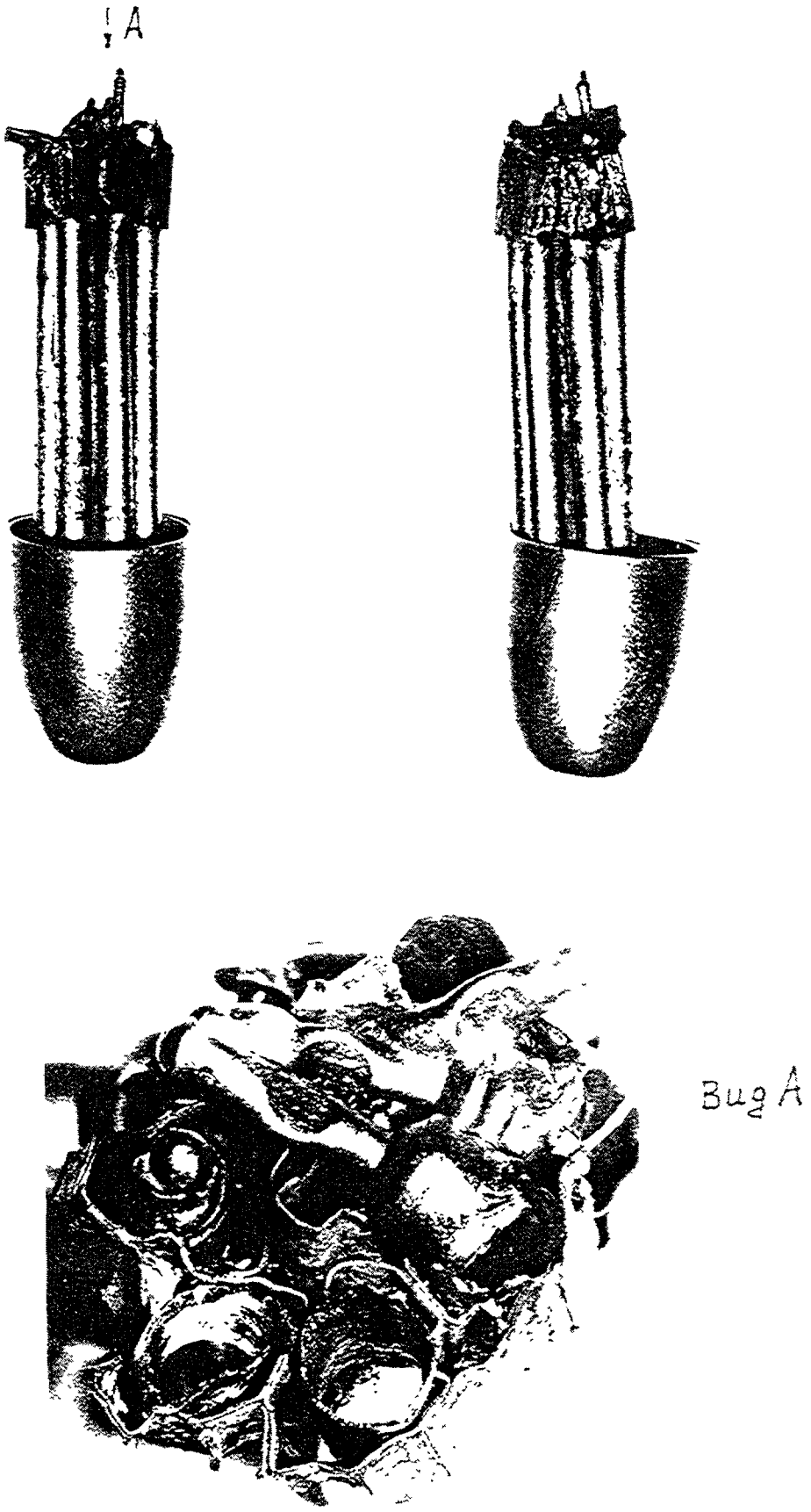

FIG. 9. Dysprosium contained mock-ups after testing at 1800 °C

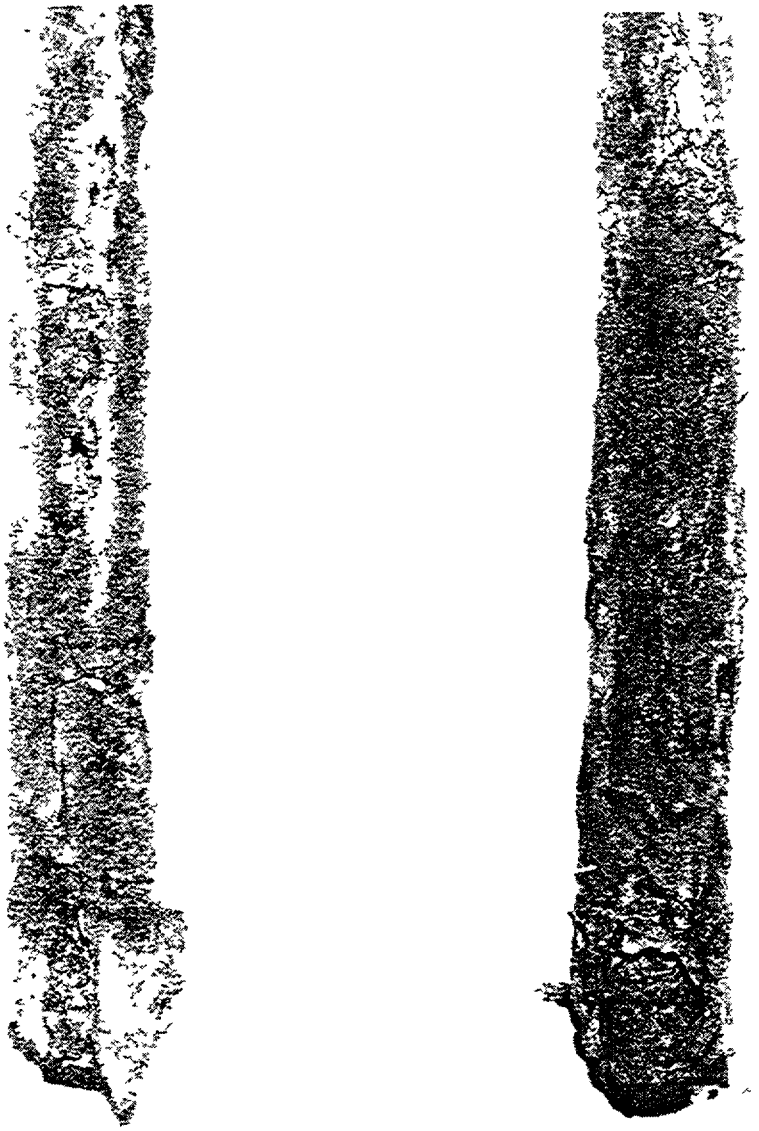

FIG 10 Dysprosium control rod after testing at 1800 ℃

SUMMARY

1. The liquefaction of boron absorber rods may happen between 1150-1200°C. It leads to liquid eutectic formations, flow down of melt and blockage formations mainly near the spacer grids.

2. Control rod liquefaction initiates core degradation in the melt formations observed. The temperature of absorber liquefaction is about 200°C less than fuel rod liquefaction.

3. Absorber relocation within the core may happen while the core structure is not destroyed.

4. Dysprosium absorbers are much more firm. Dysprosium absorber rods are not destroyed up to 1450°C. Only the bottom part of the absorber rods of the new Russian control rod design is made of dysprosium absorber.

5. It is supposed that under severe accident conditions, the control rods are inserted into the core. The most heated part of the core is the central cross-section. Thus, the unirradiated absorber is heated more.

Therefore, previous irradiation of absorbers before carrying out tests is not necessary for the above discussed experiments.

LIST OF PARTICIPANTS

Aden, V.G.	Ministry of Russian Federation for Atomic Energy, Moscow, Russian Federation
Afanasyev, A.	Ukraine State Department of Nuclear Power, Kiev, Ukraine
Andersson, T.	RTH, Väröbacka, Sweden
Bart, G.	Institut Paul Scherrer, Villigen PSI, Switzerland
Béchade, J.-L.	CEA/DTA/DECM/SRMA, Gif-sur-Yvette, France
Björnkist, L.	Vattenfall AB, Väröbacka, Sweden
Date, V.G.	Bhabha Atomic Research Centre, Trombay, Mumbai, India
Dewes, P.	Siemens AG, KWU, NBTW, Erlangen, Germany
ElSayed, A.	Atomic Energy Authority, Mugls El Shab-Cairo, Egypt
Harbottle, J.	Stoller Nuclear Fuel, Thornbury, Bristol, United Kingdom
Herter, P.	CEA, Centre d'Études de Saclay, Gif-sur-Yvette, France
Hinttala, J.	STUK, Radiation and Nuclear Safety Authority, Olkiluoto, Finland
Höglund, L.M.	Barsebäck Kraft AB, Löddeköpinge, Sweden
Jendrich, U.	Gesellschaft für Anlagen-und Reaktorsicherheit, (GRS)mbH, Cologne, Germany
Jonsson, T.	Studsvik Nuclear AB, Nyköping, Sweden
Kawashima, N.	Hitachi Engineering Co., Ltd, Ibaraki-ken, Japan
Kennard, M.W.	Stoller Nuclear Fuel, NAC International, New York, United States of America
Monchanin, M.	FRAMATOME, Lyon, France

Muttilainen, E.A.T.	Teollisuuden Voima Oy, Olkiluoto, Finland
Odeychuk, N.	Kharkov Institute of Physics and Technology, Kharkov, Ukraine
Poignet, B.	DRN/DER/SPRC, Saint-Paul-lez-Durances, France
Posselsky, V.B.	Ministry of Russian Federation for Atomic Energy, Moscow, Russian Federation
Rebensdorff, B.	ABB-ATOM/BU, Västeras, Sweden
Risovany, V.D.	Research Institute of Atomic Reactors, Dimitrovgrad, Ulyanovsk Region, Russian Federation
Ritchie, I.	International Atomic Energy Agency, Vienna
Sanovic, J.	Institute for Metal Structures, Ljubljana, Slovenia
Scheglov, A.	Moscow Polymetal Plant, Moscow, Russian Federation
Schulz, W.	Preussen Elektra Aktiengesellschaft, Hannover, Germany
Shoaib, K.A.	Permanent Mission of Pakistan to the IAEA, Vienna, Austria
Simeone, D.	CEA, Centre d'Études de Saclay, Gif-sur-Yvette, France
Troyanov, V.	Russian Federation of Atomic Energy Ministry, Obninsk, Kaluga Region, Russian Federation
Zakharov, A.	Research Institute of Atomic Reactors, Dimitrovgrad, Ulyanovsk Region, Russian Federation